Distribution Agreement

In presenting this thesis or dissertation as a partial fulfillment of the requirements for an advanced degree from Emory University, I hereby grant to Emory University and its agents the non-exclusive license to archive, make accessible, and display my thesis or dissertation in whole or in part in all forms of media, now or hereafter known, including display on the world wide web. I understand that I may select some access restrictions as part of the online submission of this thesis or dissertation. I retain all ownership rights to the copyright of the thesis or dissertation. I also retain the right to use in future works (such as articles or books) all or part of this thesis or dissertation.

Signature:

Michael R. Hollerbach	Date

Group IX Metal-Catalyzed C–H Activation Towards the Development of New Synthetic Strategies

By

Michael R. Hollerbach

Doctor of Philosophy

Chemistry

Simon B. Blakey, Ph.D.
Advisor

Frank E. McDonald, Ph.D.
Committee Member

William M. Wuest, Ph.D.
Committee Member

Accepted:

Kimberly J. Arriola, Ph.D.
Dean of the James T. Laney School of Graduate Studies

Date

Group IX Metal-Catalyzed C–H Activation Towards the Development of New Synthetic Strategies

By

Michael R. Hollerbach

B.S., College of Charleston, 2017

Advisor: Simon B. Blakey, Ph.D.

An abstract of
A dissertation submitted to the Faculty of the
James T. Laney School of Graduate Studies of Emory University
in partial fulfillment of the requirements for the degree of
Doctor of Philosophy
in Chemistry
2023

Abstract

Group IX Metal-Catalyzed C–H Activation Towards the Development of New Synthetic Strategies

By: Michael R. Hollerbach

Part 1 of this dissertation describes efforts leading to the development of a new class of chiral dienes, specifically C2 symmetric cyclooctadienes (CODs). Proven to be formidable ligands for asymmetric catalysis in recent years these ligands were limited to 1,5 disubstituted scaffolds historically. Through collaboration with the Davies Group at Emory University, previously unreported 3,7 disubstituted CODs were accessed in one step and subsequently diversified. The in-situ development of a homogeneous rhodium catalyst with these ligands for enantioselective $C_{(sp3)}$–H functionalization is described.

Part 2 of this dissertation addresses efforts to provide modern small molecule discovery with novel heterocyclic moieties for new cutting-edge agrochemicals and pharmaceuticals. Leveraging late-stage functionalization of C–H bonds has become increasingly powerful to target these moieties, however, non-directed activation of desired C–H bonds remain challenging. In response to this limitation, the design and use of directing groups has become extremely important despite their shortcomings. Previously, oxidative addition has been employed for directed annulations, but analogous reactivity with transmetallation has remained underexplored. Currently, we have developed new methodology to leverage transmetallation of boryl species to promote distal $C_{(sp^2)}$–H activation and subsequent functionalization.

Part 3 of this dissertation describes the effort of the Blakey Lab to adopt and pioneer new sustainable and green processes in the chemistry lab. Through continual commitment to reducing our environmental and carbon footprints, the Blakey lab has changed how we fundamentally operate day-to-day to lower or resource consumption and extend the life our consumables. This has led to several invaluable advancements in the understanding of energy consumption, water usage and waste production. Furthermore, quantitative data was collected to highlight the benefit for investing in new heat/stir plates and aluminum heating blocks.

Group IX Metal-Catalyzed C–H Activation Towards the Development of New Synthetic Strategies

By

Michael R. Hollerbach

B.S., College of Charleston, 2017

Advisors: Simon B. Blakey, Ph.D.

A dissertation submitted to the Faculty of the
James T. Laney School of Graduate Studies of Emory University
in partial fulfillment of the requirements for the degree of
Doctor of Philosophy
in Chemistry
2023

Acknowledgments

First and foremost, I would like to thank my mentor Dr. Simon B. Blakey for his continued support and trust over these past years. I have not only become a better chemist, but person under your mentorship these past 5 years. Furthermore, it has been a great honor to serve as a community member of the Blakey Lab and the Emory University Department of Chemistry. I would also like to thank my committee members, Dr. William M. Wuest and Dr. Frank E. McDonald for their continued guidance and support since arriving in the department. Throughout my time at Emory, my committee members and classroom Professors have served as a testament for true love of the chemistry and an inspiration for sharing that with younger generations through teaching, outreach, and mentorship. Additionally, I would like to thank my undergraduate advisor Dr. Timothy J. Barker who was instrumental in preparing me for graduate school and developing my lab hands.

I would also like to thank the members of the department that keep the wheels turning day in and day out. Without the help of Steve, Claire, and Edgar to keep my chemistry moving and making sure the resources needed arrived, I would have never completed the work I did. Additionally, thank you to Todd, Kira, Laura, and Ana for making sure the community was welcoming, the graduate student requirements were met, and the lights stayed on. To Jan, José, and Thomas, I thank you for always helping to maintain our lab and working to fix the many maintenance problems as we created, along with the early morning discussions. Additionally, I owe a huge debt of gratitude to Dr. Bing, Dr. Wu, Dr. Bacsa and Dr. Strobel for their help in characterization and data collection during my research. Patrick, Jayson, and Tim of the computer/electronics shops were also key in maintaining and fixing our instruments through blown capacitors and computer crashes. Finally, I would like to thank the community for their willingness to share chemicals, instruments, time, and brainpower. Many of my hardest challenges were solved

by the ideas shared in the hallways or at social gatherings in the department. To all the members of the Blakey Lab, past and present, thank you being a part of my journey and sharing the ups and downs with me. We have come along way as a lab since my arrival and as the Doc would say, “We’re at the tippity top of the mountain, but we’re really only halfway up.” I look forward to seeing the chemistry and community the Blakey lab continues to develop and foster at Emory over the coming years.

Lastly, I would like to thank my family and friends. I would not have been able to accomplish this without your support and guidance. It has truly meant everything to me that you have been tackling this challenge and life with me. I only hope that I can repay this kindness as life brings challenges and opportunities to your doorstep.

This dissertation is dedicated to the memory of Daniel Gentle. A best friend and gamer who will forever be missed. This Victory Royale is for you.

Daniel Shane "Bubba" Gentle

Jun 18, 2013 – Oct 9, 2022

Table of Contents

List of Figures

List of Schemes

List of Tables

Table of Abbreviations

Ac	Acetyl
Ar	Aryl
BINAP	2,2'-Bis(diphenylphosphino)-1,1'-binaphthalene
BINOL	1,1'-Bi-2-naphthol
BINOL-Cp	BINOL-derived cyclopentadienyl
Bn	Benzyl
Boc	*tert*-Butoxycarbonyl
BPE	1,2-Bis(dimethylphospholano)ethane
Bu	Butyl
Bz	Benzoyl
Cbz	Carboxybenzyl
COD	1,5-Cyclooctadiene
Cp	Cyclopentadienyl
Cp*	1,2,3,4,5-Pentamethylcyclopentadienyl
Cp^E	Functionalized cyclopentadienyl
Cp^XH	Functionalized cyclopentadiene
Cy	Cyclohexyl
DCE	1,2-Dichloroethane
d	Day
de	Diastereomeric excess
DET	Diethyltartarate
DFT	Density functional theory

DIPEA	Diisopropylamine (Hunig's base)
DMF	Dimethylformamide
Dppf	1,1'-Bis(diphenylphosphino)ferrocene
dr	Diastereomeric ratio
EDC	1-Ethyl-3-(3-dimethylaminopropyl)carbodiimide
EDCI	See EDC
ee	Enantiomeric excess
er	Enantiomeric ratio
Et	Ethyl
EWG	Electron-withdrawing group
FcCp	Ferrocene-derived cyclopenadienyl
Fmoc	Fluorenylmethyloxycarbonyl
hr	Hour
HFIP	1,1,1,3,3,3-Hexafluoro-2-propanol
HOBt	Hydroxybenzotriazole
HPLC	High-Performance Liquid Chromatography
^{i}Bu	*iso*-Butyl
Ind	Indenyl
IndH	Indene
^{i}Pr	*iso*-Propyl
KAIST	Korea Advanced Institute of Science and Technology
L	Ligand
LAH	Lithium aluminum hydride

M	Metal
*m*CPBA	*meta*-Chloroperbenzoic acid
Me	Methyl
min	Minute
Ms	Mesyl
MS	Molecular sieves
^{n}Bu	*n*-Butyl
NMM	*N*-methylmorpholine
^{n}Pr	*n*-Propyl
Ns	Nosyl
Nu	Nucleophile
OTf	Trifluoromethanesulfonate (triflate)
P orPG	Protecting group
Ph	Phenyl
Phth	Phthalimide
Pin	Pinacol
Piv	Pivaloyl
Pyr	Pyridine
R_L	Large R group
R_S	Small R group
^{s}Bu	*sec*-Butyl
TBDPS	*tert*-Butyldiphenylsilyl
TBS	*tert*-Butyldimethylsilyl

^{t}Bu	*tert*-Butyl
TEA	Triethylamine
Tf	Triflyl
TFA	Trifluoroacetic acid
TFE	2,2,2-Trifluoroethan-1-ol
THF	Tetrahydrofuran
TIPS	Triisopropylsilyl
TMP	2,2,6,6-Tetramethylpiperidinyl
TMS	Trimethylsilyl
Ts	Tosyl
X	Halide (generally): also, carbon or heteroatom

Part 1: Design and Application of Chiral Diene Systems via Iterative C–H Functionalization

Chapter 1: Historical Perspective, Synthesis, and Catalytic Application of Chiral Diene Ligands

1.1 Introduction to Chiral Olefins

In this chapter we will discuss the historical significance of chiral olefins and their importance as ligands for asymmetric catalysis. Specifically, we will focus on the design, synthesis, and use of modern chiral diene ligands. Furthermore, this chapter will investigate the current methods employed for enantio-enrichment of these ligands during or following synthesis systems with unique reactivity.

1.1.1 Brief History of Metal-Olefin Catalysis

Willy Marckwald's groundbreaking communication, *"Ueber asymmetrische Synthese"*, in 1904 opened the door to the most important aspect of organic chemistry in the last century.[1] His work on a brucine catalyzed decarboxylation of 2-ethyl-2-methylmalonic acid led to the enantioenriched butyric acid derivative. Following this advancement, the past century has seen a gold rush in the field of asymmetric catalysis and ligand design with chemists developing countless asymmetric methodologies and winning several Nobel prizes in Chemistry.[2] This understanding of asymmetric induction is a constantly evolving field, but over the years there have become several standout classes of ligands. While pnictogens based ligands have dominated the field overall, many other systems have been developed as well. BINOL, BINAP, TADDOL, SALEN

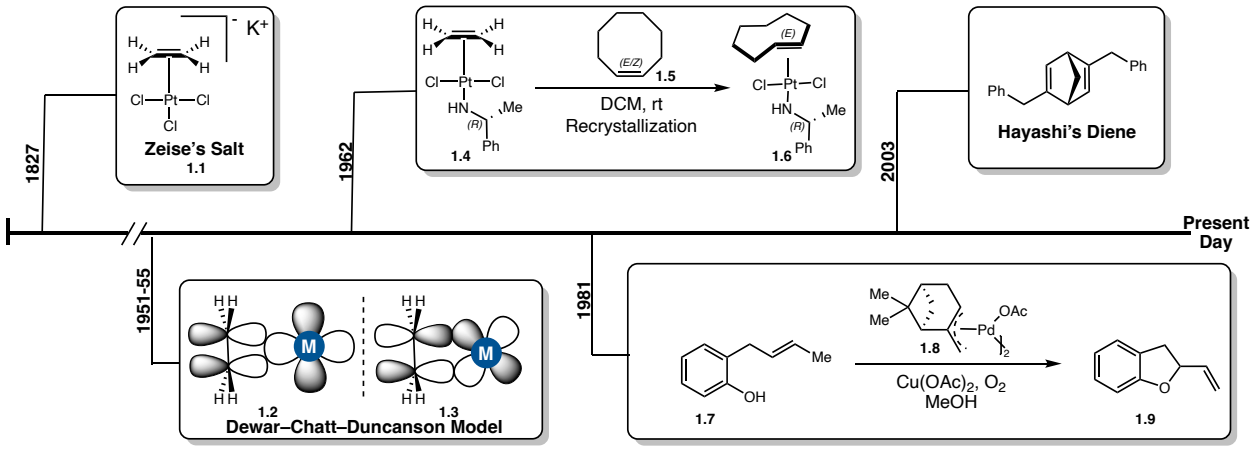

Figure 1. Important milestones in the development of chiral olefins for asymmetric catalysis.

and olefins represent just some of these non-pnictogen exclusive binding ligands developed in the past decades. Olefins, specifically chiral dienes, have risen to prominence in the last 20 years and lead to significant advances in the field of asymmetric catalysis.[3-5]

The first example of olefins used as a ligand in an organometallic complex was reported by William Christopher Zeise in 1827 (**Fig. 1**).[6] Zeise's accidental discovery, was aptly named Zeise's Salt **(1.1)**. The addition of $PtCl_4$ to refluxing ethanol resulted in the formation of $[(\eta^2\text{-}C_2H_4)PtCl_3]^-$ and further isolated as the potassium salt. This process leveraged the dehydration of ethanol, however modern processes utilize the pure ethylene gas commonly available from gas suppliers. Following the report of alkene ligands, the exact rational for their binding was unknown until 1951. The first half of the 1950s, Dewar, Chatt, and Duncanson each investigated the unique binding of alkenyl-transition metal complexes.[7,8] Their investigations lead to the Dewar–Chatt–Duncanson model that defines our current understanding of the ligand binding modes. The model states that the symmetrical π orbital of the alkene donates electron density into a d-orbital of the metal center **(1.2)**. Simultaneously, a different filled d-orbital of the metal donates electron density back into the π* antibonding orbital of the alkenes **(1.3)**. This specialized interaction, known as π backbonding, leads to a lengthened C–C bond and rehybridization of the sp^2 center to a sp^3 like carbon. *In-silico* studies have indicated that roughly a fourth of the binding energy displayed in these organometallic complexes is derived from the π backbonding.

Following the publication of the Dewar–Chatt–Duncanson model, the field continued to advance from simple alkenes to more complex systems. This led to the seminal publication by Cope in 1962 of the first chiral olefin complex **(1.6)**.[9] Cope utilized Zeise's salt with D-Phenethylamine to form the Pt-amino complex **(1.4)**. Following treatment with racemic

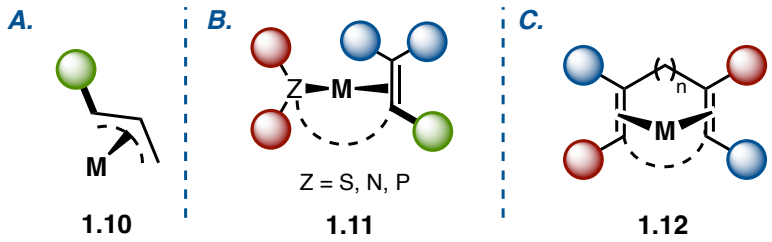

Figure 2. Common classes of chiral olefins.

cyclooctene **(1.5)**, the formation of planar chiral complexes allowed the selective recrystallization of the complexes bearing exclusively *(E)*-cyclooctene. The lack of free rotation in cyclooctene's alkyl chain allowed for Cope to release and characterize the pure *trans*-cyclooctene. Following this result, much of the work with chiral olefins followed in the same vein with metal-olefin complexes that included ligands bearing allylic **(1.10)**, alkene-heteroatom **(1.11)**, and diene **(1.12)** binding motifs (**Fig. 2**).[5] The use of monoterpene alkenes and dienes was prevalent throughout the second half of the 20th century, however the first asymmetric transformation utilized enantiopure α-pinene in 1981 (**Fig. 1**). Hosokawa and Murahashi introduced their Wacker-type oxidative cyclization with the chirality of α-pinene being utilized to induce enantiomeric excess and bound through a Pd–allyl type association **(1.8)**.[10] Finally two decades later, Hayashi disclosed the first chiral diene synthesis of a substituted bicyclo[2.2.1]hepta-2,5-diene **(Fig. 1)** and subsequent catalytic use in a rhodium centered, 1,4-addition of organoboron reagents to α,β-unsaturated ketones and esters.[11] This was quickly followed up by Carreira in 2004 with a novel bicylo[2.2.2] octa-2,5-diene for the kinetic resolution of allylic carbonates via iridium-centered allylic substitution. Carreira and coworkers then quickly followed up with a similar 1,4-addition of organoboron reagents to α, β-unsaturated ketones utilizing rhodium and a C_1-symmetric diene.[12] Following these two publications, the use of chiral dienes for asymmetric transition metal

catalyzed reactions reached a fever pitch and lead to the design of many new scaffolds and mechanistic studies of these systems.

1.1.2 Scaffolds and Their Peculiarities

In the first decade following Hayashi's disclosure[11], there were many scaffolds explored as both their native diene and with elaborate substitution (**Fig. 3**).[4,5] These substitutions were varied as chemist's sought to explore the steric, electronic, and bite angle effects of chiral dienes. The scaffolds first explored were that of bicyclo[2.2.1]hepta-2,5-diene [nbd] (**1.18**) and bicylo[2.2.2] octa-2,5-diene [bod] (**1.19**). Following these disclosures, the study of

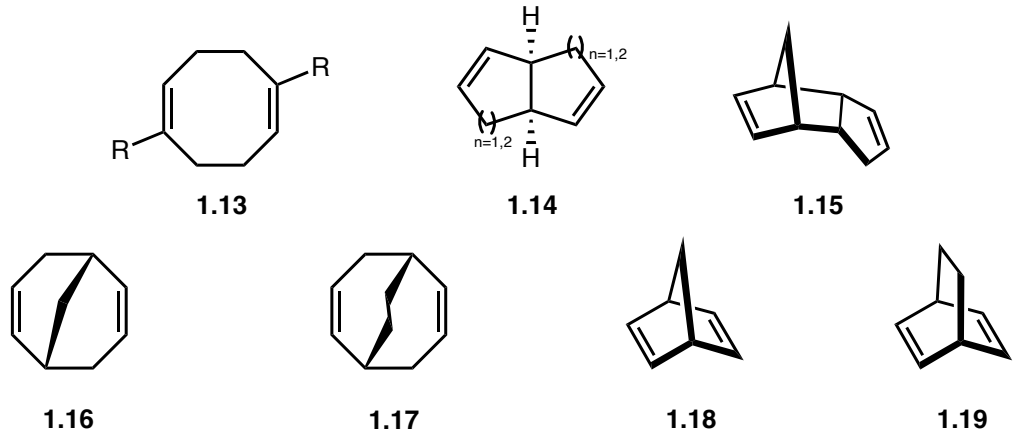

Figure 3. Historically utilized cyclic chiral diene scaffolds for ligand design.

bicyclo[3.3.1]nona-2,6-diene [bnd] (**1.16**), bicyclo[3.3.2]deca-2,6-diene [bdd] (**1.17**), and tetrafluorobenzobarrelene [tfb] were undertaken by Hayashi.[5,13] While Grützmacher, Du, Trauner, Xu, Lin, and Laschat all made critical contributions to the variety of scaffolds and their substitutions,[4] Hayashi and Carreira dominated this field following the disclosure of their use for asymmetric catalysis. While the variety of scaffolds was welcomed, the ligands were not as

interchangeable as previously theorized. The ligand systems showed notable nuance in reactivity and stereo-induction when used utilized across different transition metals and systems.

The investigations into the enantio-induction and rational design of new ligands were carried out on two fronts. The first was a glance into the coordination and stability of chiral dienes on transition metals, while the second investigated the spatial arrangement of the ligand during the enantiodetermining step. During the investigation of the ligand system itself, several key factors were noticed with regards to electronics influencing the π and π* orbitals, bite angle, and steric interactions about the diene.[4,14,15] Olefins have been shown to very reliant on back donation to stabilize the metal complex, especially when using electron-deficient alkenes.[16,17.] Utilizing $[Pt(PH_3)_2(L)]$ complexes, *in-silico* calculations indicated that intrinsic binding energy (ΔE_{int}) between the metal center and olefin did alter with substitutions leading to electron deficiency, but was much more tolerate to change that similar changes to phosphane ligands (**Table 1**). Despite

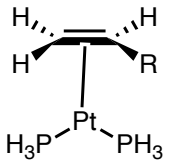

R	ΔE_{int}	D_e
H	-56.9	15.4
CN	-62.8	17.6
F	-58.9	11.9
NH_2	-54.7	6.6
OH	-53.9	9.9

Table 1. Pt-olefin complexes anylyzed for intrinsic binding and disassociation energies of substituted alkenes using *in-silico* calculations. (DFT, B3LYP, BS2). All values in kcal mol^{-1}.

there being minimal differences in the intrinsic binding energies, the adiabatic disassociation energies (D_e) told a more interesting story. This is accounted for by the previously mention elongation of the C–C alkene bond and rehybridization from sp^2 towards a sp^3 center bound to a transition metal. This led to several studies over the years in which ligand displacement of dienes was measured on different metal centers. One such set of equilibrium experiments was carried on rhodium metal and has acted as the guidance for their continued development (**Fig. 4**).[20] Recently, the equilibrium constants (K) were calculated with ratios determined using qNMR techniques and laid out the general hierarchy of chiral dienes.[4] These values indicate that the nbd (**1.18**) and bod (**1.19**) scaffolds represent the most favored ligands of the common scaffolds (**Fig 4.B**). While this is partially due to their lack of steric bulk about the olefins on the coordinating face, much of this arises from bite angle. These ligands both assume a 70º bite angle when coordinated to metal and this has been shown to be the optimal. Furthermore, the pyramidalization of the olefin carbons

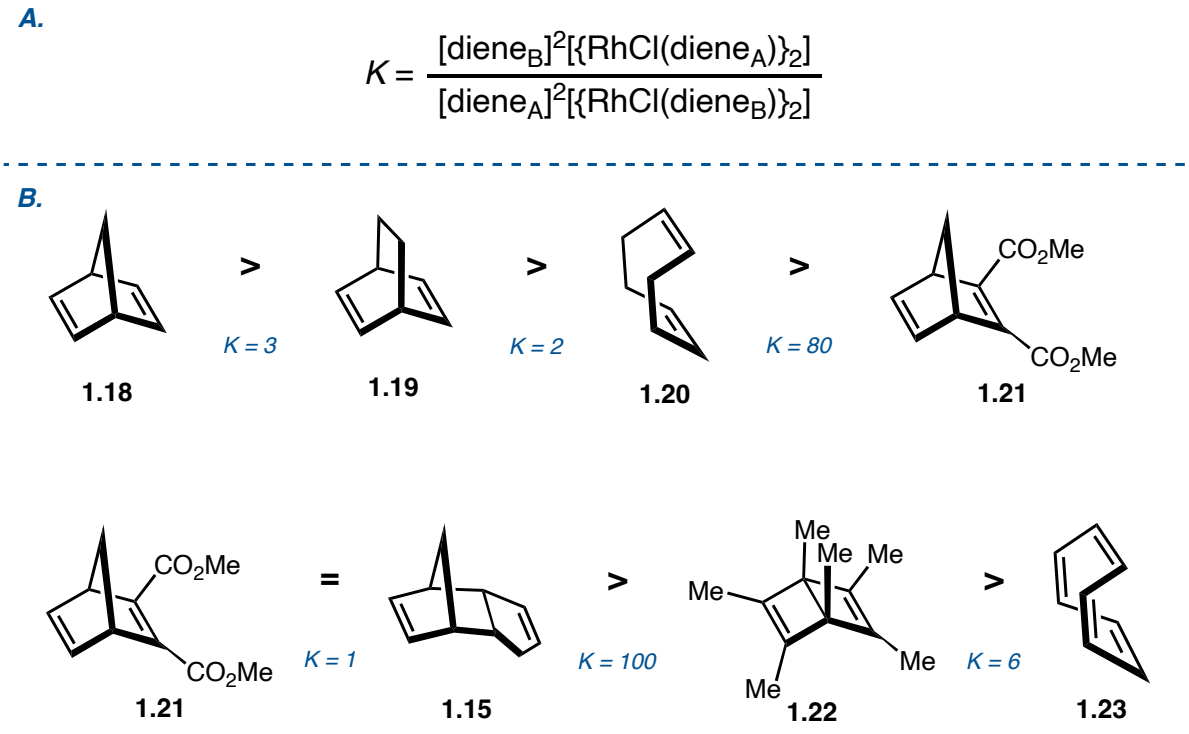

Figure 4. Stability of chiral diene ligands on rhodium with equilibrium constant *K* calculated from NMR studies.

leads to a lower π*LUMO and increases the magnitude of the backbonding.[14,21] When compared to the non-bridged cyclooctadiene [cod] (**1.20**), there is a slight favoritism for the bridged bicycles. Interestingly, a fully substituted olefin (**1.21**) shows a large *K* vs. cod (**1.20**) despite the trend indicated by the D_e in platinum-alkene studies (**Table 1**). This is most likely due to the steric encumbrance of the two methyl esters and illustrates the tightrope that must be walked between electronics and steric bulk. Finally, the unsymmetrical nature of (+)-Dcp (**1.15**) and the destabilizing electron donation of the methylated bicyclo[2.2.0]hexa-2,5-diene (**1.22**) lead them to be less stable as metal-diene complexes. This equilibrium scale has been extremely useful in helping to prepare new methodologies and allowing for ideal transition metal precatalysts to be identified prior to attempting an *in-situ* ligand swap.

In summary, the advent of enantioselective catalysis in 1904 has led to countless advancements over the past 120 years. These have had massive impacts on pharmaceutical, agrochemical, and the materials industries. While the methodologies have developed, so has the need for new classes of ligands that offer tuning of the metal center electronically and the spatial arrangement of approaching substrates/reactants. Chiral dienes have become one of the standout classes in these areas for their electronic tunability and numerous sites for steric groups to be attached. Despite the advantages, the field still suffers from issues with lengthy syntheses and stability issues with highly strained systems.

1.2 Accessibility and Application of Chiral Dienes in Asymmetric Catalysis

1.2.1 Selected Syntheses of Common Chiral Diene Scaffolds

As chiral dienes have found more usefulness in asymmetric catalysis, the syntheses of their ligands have also evolved to provide novel, highly tuned ligands. However, the incorporation of

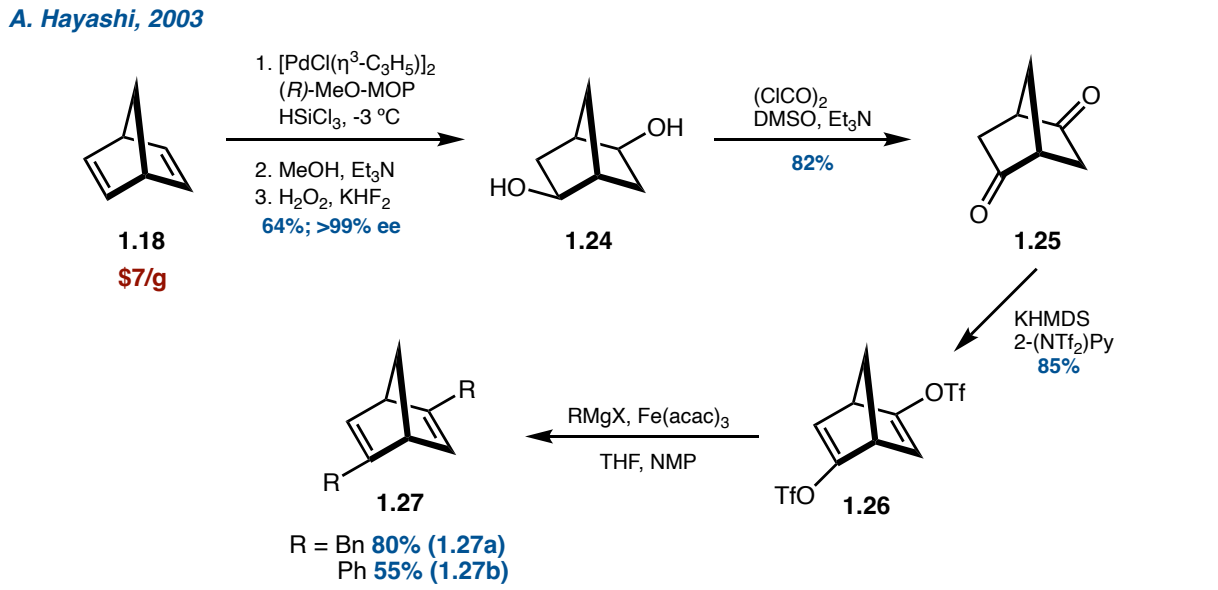

Scheme 1. Selected syntheses of Chiral Bicyclo[2.2.1]hepta-2,5-dienes for asymmetric catalysis.

these sterically congested and electronically tuned bicycles has remained a challenge. The major limitation of which is accessing the final enantiopure ligand. The initial nbd scaffold utilized by

Hayashi in his seminal publication, (*R,R*)-Bn-nbd (**1.27a**), required seven linear steps to the metal complex , six to the ligand, and relied on an asymmetric palladium reaction to set the stereochemistry (**Scheme 1.A**).[11] While the catalytic use of the *R*-MeO-MOP ligand in not inexpensive, the use of nbd (**1.18**) at $7/g makes this synthesis amenable. Following a global Swern oxidation, Hayashi was able to access the enantiopure 2,5-dione (**1.25**) which is utilized by others as a starting material. Following a vinylic triflation of both ketones (1.26), Hayashi and coworkers had access to a cross-coupling partner for either iron or palladium catalysis and could install a number of aryl and alkyl groups. This strategy only allows for disubstitution of the same group, but future synthesis operated with generation of a single ketone, protection, triflation and coupling in an iterative manner. The main issue with starting at the enantiopure 2,5-dione (**1.25**) is that it can be cost prohibitive at around $700/g. In 2010, Corey utilized chiral oxazaborolidine complex (**1.29**) to catalyze an asymmetric Diels-Alder reaction leading to highly enantiopure nbd framework **1.31** in excellent yields.[18] The alcohol was then capped with a protecting group or alkylated before use as a chiral diene ligand. Recently, Laschat and coworkers have shown a diastereoselective Diels−Alder reaction of cyclopentadiene with an oxazolidinone (**1.32**).[19] While oxazolidinones substituted with *gem*-dimethyl (**1.33a**) led to a moderate diastereomeric excess, the methylene variant was highly selective (**1.33b**). Laschat and coworkers were ultimately able to obtain the individual diastereomers through fractional recrystallization and utilize them. The syntheses shown are not all inclusive and for a review of other specialized examples can be found in the literature.[3-5,11]

While the above synthetic strategies represent the general thought process in construction of nbd (**1.18**) chiral dienes, the syntheses of bod scaffolds (**1.19**) are found to usually be very similar with respect to vinylic functionalization. The main differences are found in

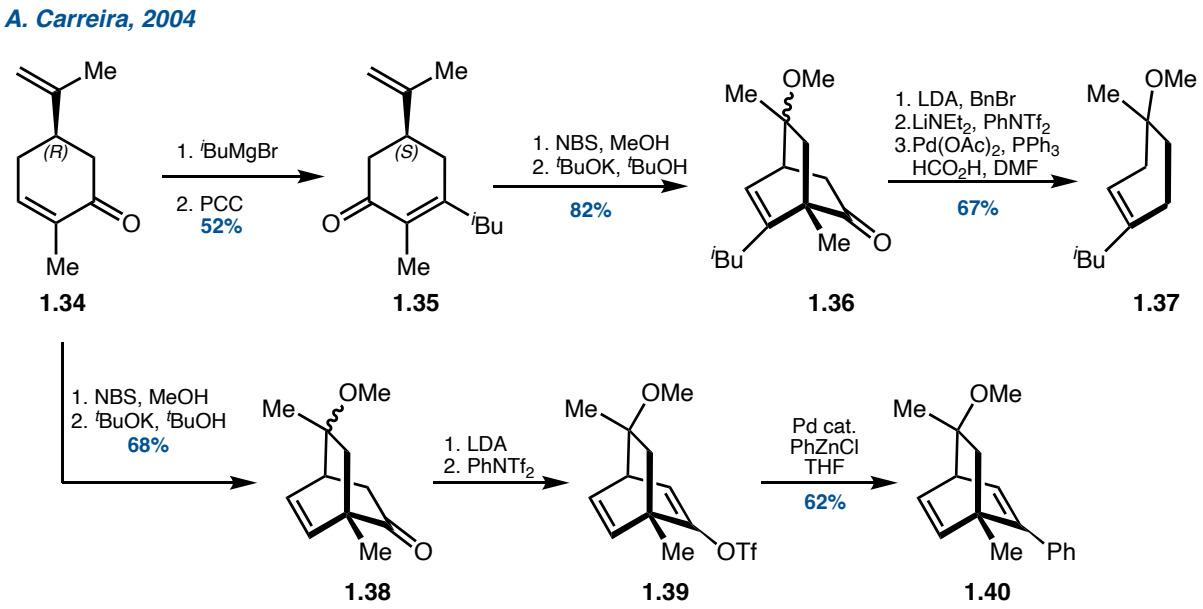

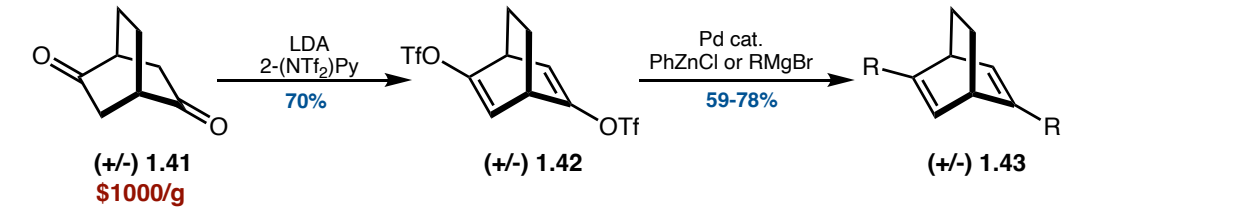

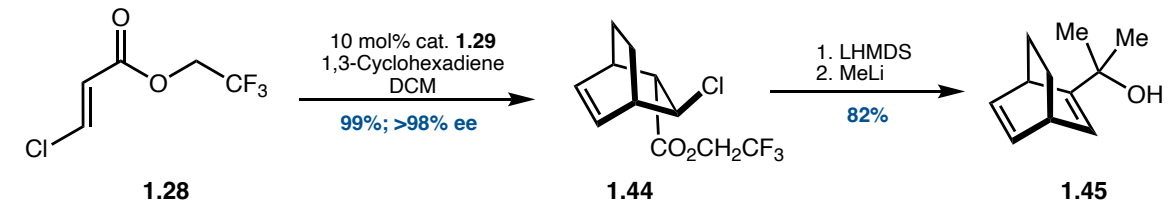

Scheme 2. Selected syntheses of Chiral Bicyclo[2.2.2]octa-2,5-dienes for asymmetric catalysis.

functionalization of the alkyl bridge and a tendency to functionalize at one or both bridgeheads. In Carreira's seminal kinetic resolution of allyl carbonates with an iridium-chiral diene system, the use of (-)-carvone (**1.34**) allowed to rapid access to the enantiopure chiral dienes in 5-7 linear steps (**Scheme 2.A**).[12,22,23] The initial route of Grignard addition and oxidation provided enone (**1.35**) in moderate yield. Following cyclization, the ketone enolate (**1.36**) was alkylated and the alkenyl

triflate was reduced via palladium to the corresponding alkene (**1.37**). This carvone method was also utilized to yield **1.40** through cyclization and triflation to provide **1.39**. Building on previous work, **1.39** was then cross coupled with organozinc reagents via palladium to provide the final ligand (**1.40**). Hayashi, in his pursuit of a bod (**1.19**) equivalent to his nbd (**1.18**) syntheses, utilized the same strategy as previously shown by his group in accessing the ketone before converting to the vinylic triflates and engaging organometallic reagents in a cross-coupling reaction **(Scheme 2.B**).[24] The difference in this disclosure was his use of the racemic ketone (**1.41**), costing $1000/gram, as a starting material and the lack of any stereoselective steps. This choice led to the use of preparatory HPLC separation on a chiral column but dramatically shortened the synthesis. In 2010, Corey also utilized his previous asymmetric Diels-Alder strategy with 1,3-cyclohexadiene and catalyst **1.29** to provide the monosubstituted chiral dienes (**1.45**) that required a capping of the alcohol prior to use in analogous fashion to the nbd scaffolds.[18] This again provided the chiral diene in excellent enantiomeric excess and yield with a short linear sequence.

While there are quite a few novel catalysts and scaffolds showcased in the literature, much of the chemistry was based on the more generalizable reactions showcased above. The trend in chiral diene syntheses was either that the scaffolds are built through an asymmetric cyclization, began with enantiomeric/diastereomerically pure starting materials, or are purified along the way by some method. In the future we will briefly touch on these methods of purifying enantiomers. For a more comprehensive list of ligands and syntheses currently in literature please use the chiral dienes reviews referenced.[3-5]

1.2.2 Methods Utilized to Acquire Enantiopure Ligands

While recent syntheses of chiral dienes have begun to rely more on asymmetric palladium catalysis to set ligand stereocenters, this remains an expensive challenge with the cost of exotic pnictogen based ligands. Many alternate routes to avoid these have been developed in recent years (**Figure 5**) The most promising has been the use of boron based ligands for asymmetric

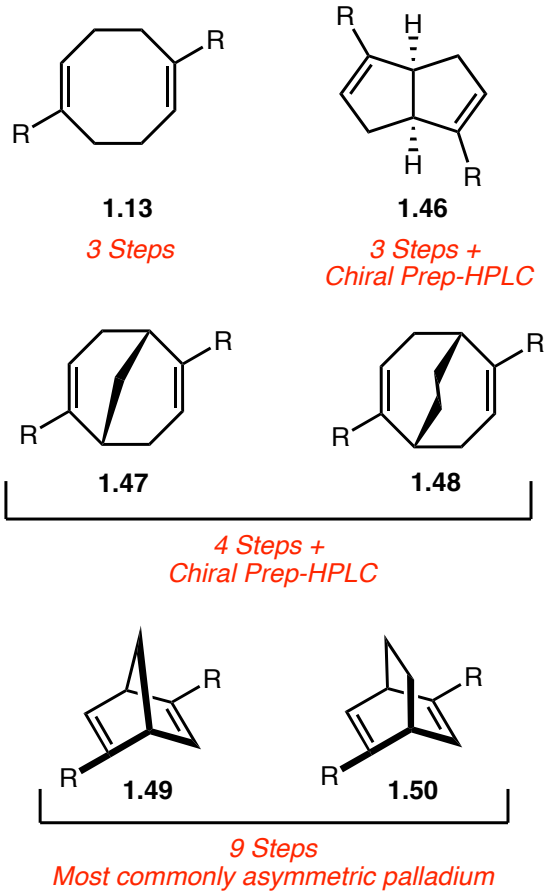

Figure 5. Chiral diene ligands and common purification route.

cyclization.[18,25] Additionally, the use of diastereoselective resolution during interim steps of the ligand design, or the use of a chiral hydrazine via condensation with the ketones or chiral diamines to separate while the ligand is on metal.[19,26,27] When the syntheses of the ligands are not amenable to any of the above methods, or the ligand is needed quickly, a brute force approach, through the

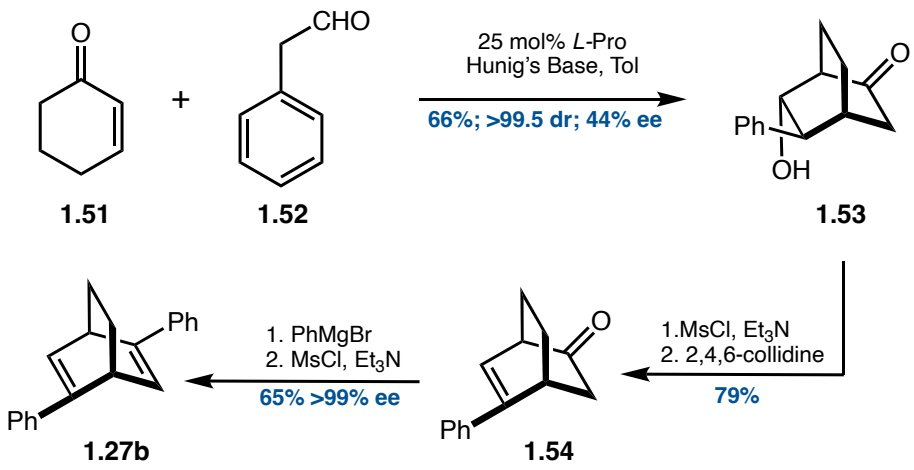

Scheme 3. Organocatalytic Michael addition-Aldol reaction utilizing *L*-Proline.

use of chiral prep-HPLC/SFC is relied upon at the most amenable step.[4-5,24] While racemic synthesis and mechanical separation sounds like the best method, the resolution is much more of an art than a basic science. Additionally, the equipment is very expensive to produce meaningful amounts of the ligands and is not ubiquitous throughout laboratories. With the advance in biocatalysis and kinetic resolution technologies, Carnell and coworker were able to utilize porcine pancreas lipase (PPL) to carry out a chemo-enzymatic kinetic resolution of the diketone intermediate in their specific ligand syntheses.[28,29] While there are many approaches to access the enantiopure/diasteromerically pure ligands, there has yet to be an excellent and cheap way to access this class to date. The most cost effective to date has come from the use of enantiopure terpenoids and a recent example of a Michael Addition-Aldol reaction utilizing *L*-Proline as an organocatalyst to access the C^2-symmetric bod scaffolds (**Scheme 3**).[30,31] As the community progresses the access to these chiral dienes has only become more facile. The hope is that in the near future, a highly robust and easily diversifiable strategy will be developed that can operate on many of the scaffold interchanably and without the need for expensive chiral ligands or added

steps to ensure high enantiopurity. This will allow the plethura of reactions that utlize chiral dienes to continue to expand and be more applicable to industrial needs at the kilo and tonne scales.

1.2.3 Selected Applications in Asymmetric Catalysis

The use of chiral dienes in asymmetric catalysis to build important motifs cannot be understated in importance. However, much of the work in this area has been driven by ligand design and recognition of existing limitations of those systems. Many of the transformations utilizing chiral diene ligands were previously accessible via other methods, however the chiral diene catalysis has become well known for generating high yields and excellent stereoselectivity. The use of group IX transition metals, excluding cobalt have been instrumental in this endeavor, particularly rhodium.[3-5] Iridium is the next most common metal, however there are some examples of ruthenium[32-34] and palladium[35-38] metal catalysts utilizing chiral dienes. This brief synopsis will mainly highlight the rhodium catalyzed reactions for sake of brevity.

A. Miyaura, 1997

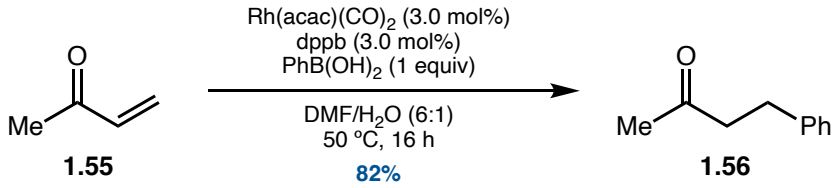

B. Hayashi, 1998

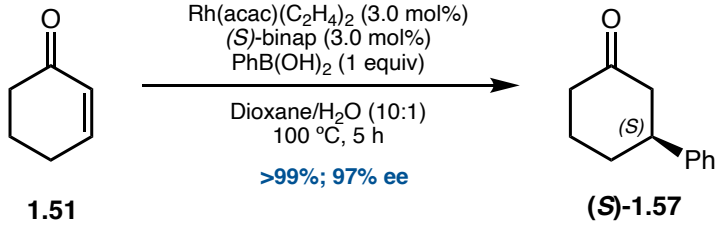

Scheme 4. Historical conjugate addition reactions that set the stage for chiral dienes.

When thinking about the most renowned reactivity of rhodium-chiral diene systems, the mind of any chemist is instantly drawn to 1,4-conjugate additions of arylboronic acids to enones. These α,β-unsaturated ketones were first arylated racemically by Miyaura in 1997 using rhodium

(**Figure 5**).[38] The next year, Hayashi introduced an enantioselective version with utilizing (*S*)-binap as the chiral ligand.[39] This group then quickly followed this up with a mechanistic study in 2002 and proposed a catalytic cycle.[40] Serendipitously, in this mechanistic study, the rate of rhodoarylation of the enone was found to be faster in the presence of cyclooctadiene over binap.

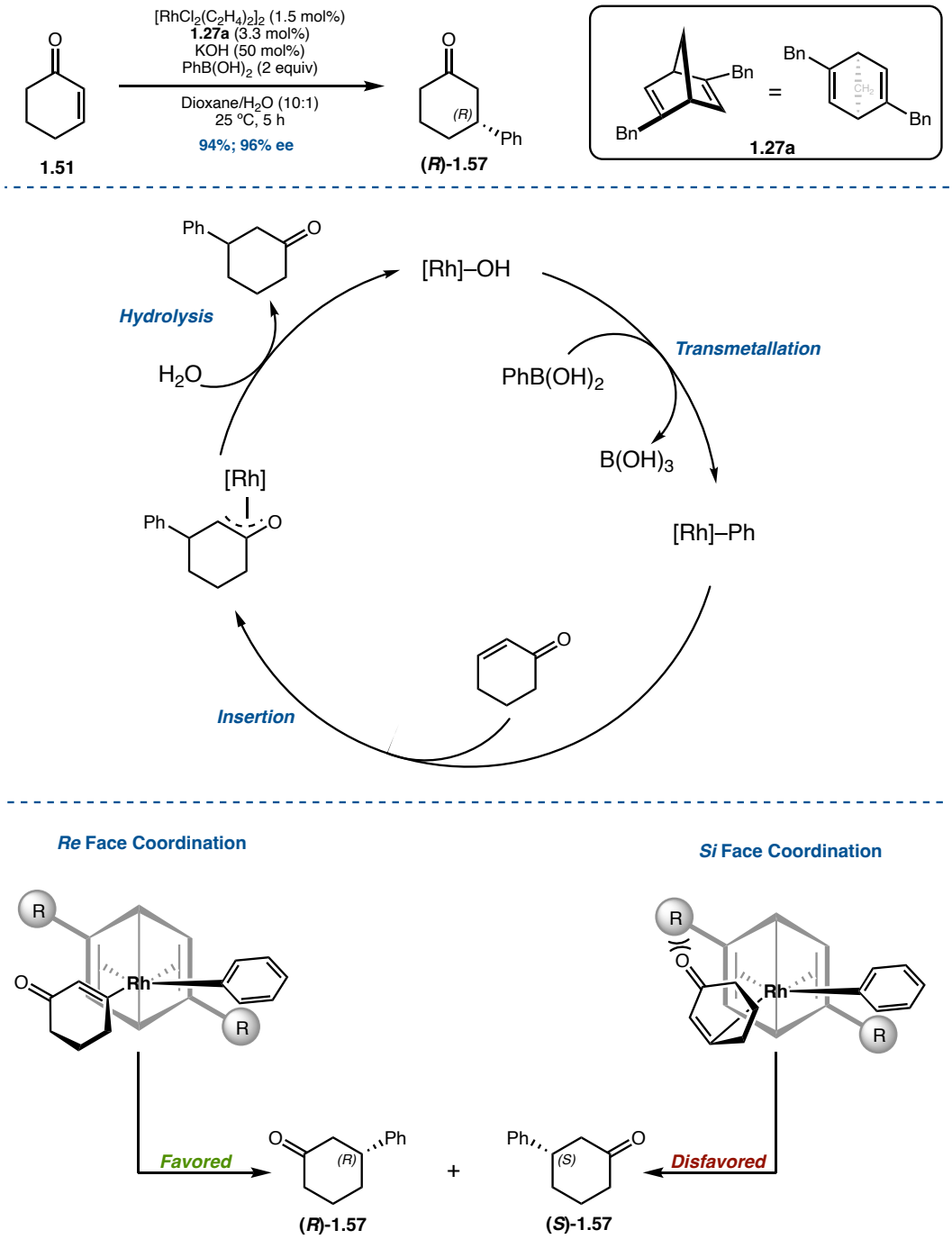

Figure 6. Catalytic cycle as described by Hayashi and the origin of enantioselectivity.

This small finding planted the seed for Hayashi's group to propose the idea of chiral dienes and within 2 two years capitalize on this mechanistic understanding.[11,41,42]

In Hayashi's seminal publication[11], the asymmetric 1,4-conjugate addition of a phenyl boronic acid to cyclohex-2-en-1-one (**1.51**), eventually named the Hayasyi-Miyaura reaction, led to the selective formation of arylated cyclic ketone **[(*R*)-1.57**] in excellent yields and high

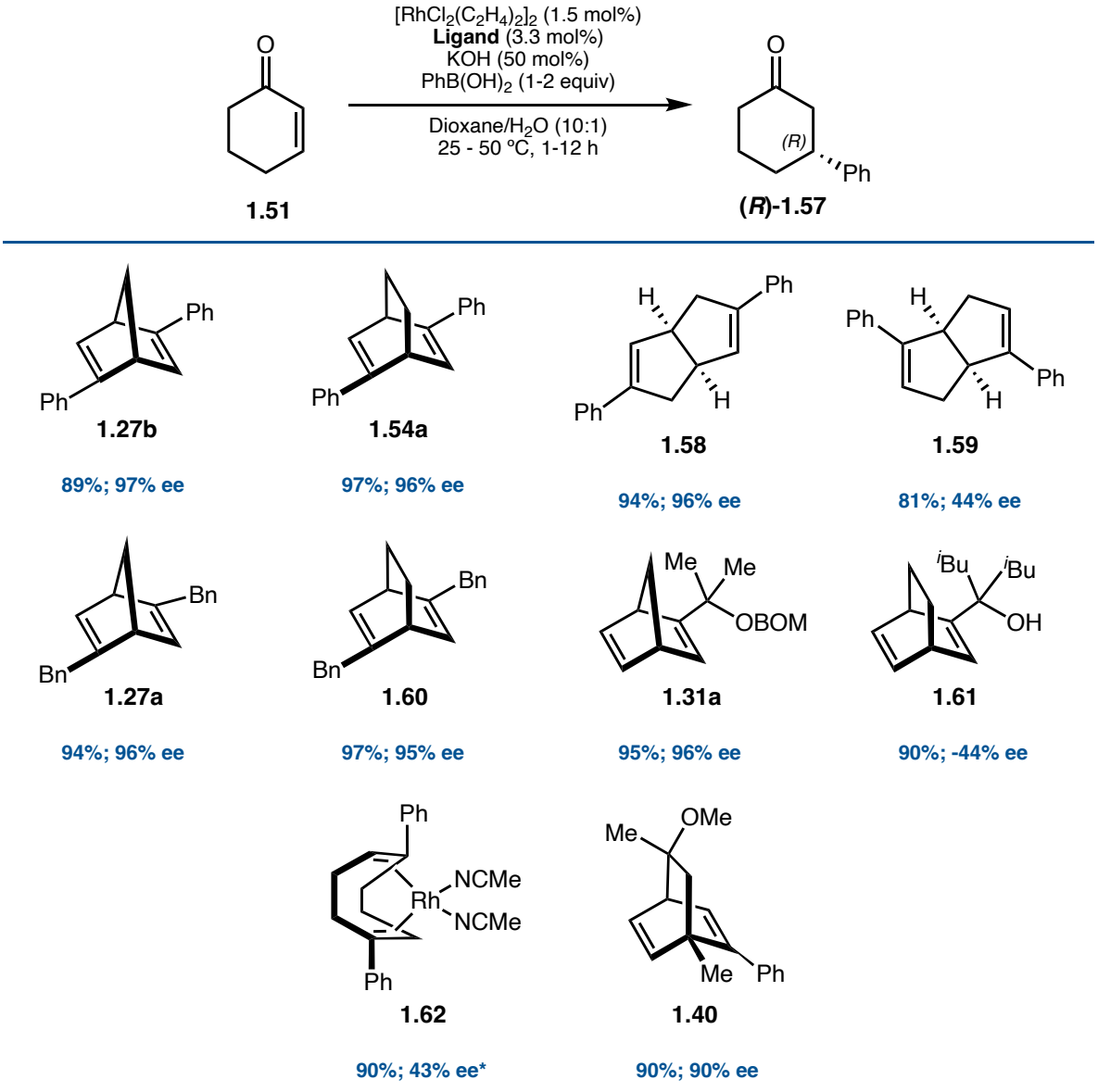

Scheme 5. Selected examples of chiral diene ligands catalyzing Hayashi's benchmark reaction. All utilized similar material loadings, temperatures and time. (*__1.62__ was loaded at 3 mol % Rh with no extra ligand.)

enantioselectivity (**Figure 6**). This transformation, which proceeded through the rate determining transmetallation of rhodium (I) hydroxide and subsequent addition to the olefin of the enone. The phenylrhodation then provides the coordinated product that is freed upon hydrolysis of the rhodium providing the product **[(*R*)-1.57**]. It is important to mention this catalytic cycle operates completely at rhodium(I) and illustrates no change in oxidation state of the metal. While the rate determining step is the transmetallation, the enantiodetermining step occurs during the coordination of the enone (**Figure 6**). As illustrated, the steric clash between the R group of the chiral diene disfavors the formation of **[(*S*)-1.57**]. While this illustrates the cyclic substrates, acyclic α, β-unsaturated carbonyl compounds function similarly with the R_{small} and R_{large} dictating the alignment. Finally, with this disclosure, Hayashi established the benchmark reaction for new chiral dienes to be tested against. This benchmark reaction has led to large amounts of data comparing rhodium-chiral diene catalysts' ability to perform these transformations with cyclo-(pent/hex/hept)-en-ones (**Scheme 5**).[5] As you can see by the data presented, the chiral diene scaffolds offer excellent yields and good to excellent enantioexcesses across the various scaffolds. The main shortcoming is the use of the cyclooctadiene scaffold (**1.62**) in which yield was maintained but stereoselectivity suffered greatly. While not shown, these methodologies were also quite effective in generating quaternary centers with alkyl substitutions at the 4-position of 1,4 cyclic and acyclic enones. Hirano and coworkers showed this can be predicted by observing the % buried volume ($\%V_{bur}$) of the catalyst and tuning the chiral dienes to allow for more sterically bulky substituents. The $\%V_{bur}$ of dienes currently disclosed range from 40.7% for bod (**1.19**) and tap out at ~57% for Ph2-bnd (**1.27b**).[43] Additionally, they looked at electronic parameters to help access the effect on reactivity. Through a combination of factors, Hirano laid out the groundwork for future rational design of ligands, however, to date, there has yet to be a publication that rationally designs a ligand through the use

of $\%V_{bur}$ such as we have seen in the phosphorous ligands' selection utilized in many palladium-catalyzed reactions.

While 1,4 conjugate additions are the main driving force behind chiral diene ligand design, the use has been extended to include quite a large variation in reactivity over the past two decades. Chiral dienes have been shown competent in 1,2-additions of imines/aldehydes and even 1,6-additions to α, β,γ,δ-unsaturated carbonyl compounds and enyamides.[11] The use of imine, sulfonyl and nitroalkenes have also been reported as well in the field. While the previous examples represent most of the field, the past five years have seen an expansion into carbene chemistry, amination, fluorination and coupling chemistry to provide axially chiral biaryl units. This has even led to an expansion of the transmetallation partners to other boron species and more tradition organometallic species such as organozinc. While many of these reactions are out of the scope of this dissertation, comprehensive reviews of reactions using chiral diene ligands is available.[3-5, 11]

1.3 Concluding Remarks

Chiral dienes have developed as a remarkable ligand family since the first disclosures by Hayashi and Carreira, however they still have a long journey ahead to make them amenable to industry and the broader academia. The main challenges for these systems are their ligand first development for specific transformations and their reliance on expensive metals (Rh, Ir, Ru, and Pd). Despite this shortcoming, the field continues to develop new and highly enantioselective methodologies with chiral dienes. This field continues to progress and with a breakthrough to more sustainable metals and simpler ligand syntheses, chiral dienes are poised to be as ubiquitous as phosphorus-based ligands in the field of asymmetric catalysis.

1.4 References

1. Marckwald. Über asymmetrische Synthese. *Ber. Dtsch. Chem. Ges.* **1904**, *37*, 349-354.

2. Trost, B. M. Asymmetric catalysis: An enabling science. *PNAS,* **2004,** *101,* 5348-5355.; Hughes, D. L. Asymmetric Organocatalysis in Drug Development—Highlights of Recent Patent Literature. *Org. Process Res. Dev.* **2018**, *22*, 574–584.; Wisniak, J. The History of Catalysis. From the Beginning to Nobel Prizes. *Educacíon Quimica,* 2010, *21*, 60-69.; Robertson, A. J. B. The Early History of Catalysis. *Platinum Metals Rev.*, **1975**, *19*, 64-66.

3. Johnson, J. B.; Rovis, T. More than Bystanders: The Effect of Olefins onTransition-Metal-Catalyzed Cross-Coupling Reactions. *Angew. Chem., Int. Ed.* **2008**, *47*, 840-871.

4. Defieber, C.; Grutzmacher, H.; Carreira, E. M. Chiral Olefins as Steering Ligands in Asymmetric Catalysis. *Angew. Chem., Int. Ed.* **2008**, *47*, 4482-4502.

5. Huang, Y.; Hayashi, T. Chiral Diene Ligands in Asymmetric Catalysis. *Chem. Rev.* **2022**, *122*, 14346−14404.

6. Zeise, W. C. Von der Wirkung zwischen Platinchlorid und Alkohol, und den dabei entstenhenden neuen Substanzen. *Poggendorffs Ann. Phys.* **1827**, *9*, 498-541.

7. Dewar, M. Bulletin de la Société Chimique de France **1951**, *18*, C79; Chatt, J.; Duncanson, L. A. Olefin co-ordination compounds. Part III. Infra-red spectra and structure: attempted preparation of acetylene complexes. *J. Chem. Soc*., **1953**, 2939-2947.; Chatt, J.; Duncanson, L. A.; Venanzi, L. M. Directing effects in inorganic substitution reactions. Part I. A hypothesis to explain the trans-effect. *J. Chem. Soc.*, **1955**, 4456-4460.

8. Mingos, M. P. A historical perspective on Dewar's landmark contribution to organometallic chemistry. *J. Organomet. Chem*. **2001**, *635*, 1–8.

9. Cope, A. C.; Howell, C. F.; Knowles, A. Resolution of trans-Cycloöctene; Confirmation of the Asymmetry of cis-trans-1,5-Cycloöctadiene. *J. Am. Chem. Soc.* **1962**, *84*, 3191-3192.

10. Hosokawa, T.; Uno, T.; Inui, S.; Murahashi, S.-I. Palladium (II)-catalyzed asymmetric oxidative cyclization of 2-allylphenols in the presence of copper(II) acetate and molecular oxygen. Study of the catalysis of the Wacker-type oxidation. *J. Am. Chem. Soc.* **1981**, *103*, 2318-2323.

11. Hayashi, T.; Ueyama, K.; Tokunaga, N.; Yoshida, K. A Chiral Chelating Diene as a New Type of Chiral Ligand for Transition Metal Catalysts: Its Preparation and Use for the Rhodium-Catalyzed Asymmetric 1,4-Addition. *J. Am. Chem. Soc.* **2003**, *125*, 11508-11509.

12. Fischer, C.; Defieber, C. Suzuki, T. Carreira, E. M. Readily Available [2.2.2]-Bicyclo-octadienes as New Chiral Ligands for Ir(I): Catalytic, Kinetic Resolution of Allyl Carbonates. *J. Am. Chem. Soc.* **2004**, *126*, 1628–1629.

13. Nishimura, T.; Kumamoto, H.; Nagaosa M.; Hayashi, T. The concise synthesis of chiral tfb ligands and their application to the rhodium-catalyzed asymmetric arylation of aldehydes. *Chem. Commun.*, **2009**, 5713–5715.

14. Hartley, F. R. Thermodynamic data for olefin and acetylene complexes of transition metals. *Chem. Rev.* **1973**, *73*, 163-189.

15. Tolman, C. A. Olefin complexes of nickel (0). III. Formation constants of (olefin)bis(tri-o-tolyl phosphite)nickel complexes. *J. Am. Chem. Soc.* **1974**, *96*, 2780-2789.

16. G. Frison, G.; Grützmacher, H. Coordinated olefins, H_2C-CHR, and phosphanes, PH_2R: a theoretical study of the R substituent effect. J. Organomet. Chem. 2002, 643, 285-291.

17. Esteruelas, M. E.; Oro, L. A. Iridium and rhodium complexes with tetrafluoro-benzobarrelene diolefins. *Coord. Chem. Rev.* **1999**, *193–195*, 557- 618.

18. Brown, M. K.; Corey, E. J. Catalytic Enantioselective Formation of Chiral-Bridged Dienes Which Are Themselves Ligands for Enantioselective Catalysis. *Org. Lett.* **2010**, *12*, 172−175.

19. Deimling, M.; Kirchhof, M.; Schwager, B.; Qawasmi, Y.; Savin, A.; Muhlhauser, T.; Frey, W.; Claasen, B.; Baro, A.; Sottmann, T.; Laschat, S. Asymmetric Catalysis in Liquid Confinement: Probing the Performance of Novel Chiral Rhodium-Diene Complexes in Microemulsions and Conventional Solvents. *Chem. Eur. J*. **2019**, *25*, 9464−9476.

20. Volger, H. C.; Gaasbeek, M. M. P.; Hogeveen, H.; Vrieze, K. Olefin coordination compounds of rhodium. V. Relative stabilities and rates of exchange of olefin complexes of rhodium(I). *Inorg. Chim. Acta* **1969**, *3*, 145-150.

21. Frenking, G.; Pidun, U. Ab initio studies of transition-metal compounds: the nature of the chemical bond to a transition metal. *J. Chem. Soc. Dalton Trans.* **1997**, 1653-1662.

22. Defieber, C.; Paquin, J.-F.; Serna, C.; Carreira, E. M. Chiral [2.2.2] Dienes as Ligands for Rh(I) in Conjugate Additions of Boronic Acids to a Wide Range of Acceptors. *Org. Lett*. **2004**, *6*, 3873−3876.

23. Paquin, J.-F.; Defieber, C.; Stephenson, C. R. J.; Carreira, E. M. Asymmetric Synthesis of 3,3-Diarylpropanals with Chiral Diene- Rhodium Catalysts. *J. Am. Chem. Soc.* **2005**, *127*, 10850−10851.

24. Otomaru, Y.; Okamoto, K.; Shintani, R.; Hayashi, T. Preparation of C2-Symmetric Bicyclo[2.2.2]octa-2,5-diene Ligands and Their Use for Rhodium-Catalyzed Asymmetric 1,4-Addition of Arylboronic Acids. *J. Org. Chem.* **2005**, *70*, 2503−2508.

25. Hatano, M.; Sakamoto, T.; Mizuno, T.; Goto, Y.; Ishihara, K. Chiral Supramolecular U-Shaped Catalysts Induce the Multiselective Diels-Alder Reaction of Propargyl Aldehyde. *J. Am. Chem. Soc.* **2018**,*140*, 16253−16263.

26. Tokunaga, N.; Otomaru, Y.; Ueyama, K.; Shintani, R.; Hayashi, T. C2-Symmetric Bicyclo[2.2.2]octadienes as Chiral Ligands: Their High Performance in Rhodium-Catalyzed Asymmetric Arylation of N-Tosylarylimines. *J. Am. Chem. Soc.* **2004**, *126*, 13584-13585.

27. Läng, F.; Breher, F.; Stein, D.; Grützmacher, H. Chiral Olefins as Steering Ligands: Syntheses of C1-Symmetric Dibenzo[a,e]cyclooctenes (^{R}dbcot). *Organometallics,* **2005**, *24*, 2997- 3007.

28. Luo, Y.; Carnell, A. J. Chemoenzymatic Synthesis and Application of Bicyclo[2.2.2]octadiene Ligands: Increased Efficiency in Rhodium-catalyzed Asymmetric Conjugate Additions by Electronic Tuning. *Angew. Chem., Int. Ed*. **2010**, *49*, 2750−2754.

29. Luo, Y.; Carnell, A. J. A practical chemo-enzymatic synthesis of homochiral bicyclo[2.2.2]octane-2,5-dione. *J. Org. Chem*. **2010**, *75*, 2057−2060.

30. Abele, S.; Inauen, R.; Spielvogel, D.; Moessner, C. Scalable Synthesis of Enantiomerically Pure bicyclo[2.2.2]octadiene Ligands. *J. Org. Chem.* **2012**, *77*, 4765−4773.

31. Brönnimann, R.; Chun, S.; Marti, R.; Abele, S. C1-Symmetric Bicyclo[2.2.2]octa-2,5-diene (bod*) Ligands in Rhodium-Catalyzed Asymmetric 1,4-Addition of Arylboronic Acids to Enones and 1,2-Addition to N-[(4-Nitrophenyl)sulfonyl]imines. *Helv. Chim. Acta,* **2012**, *95*, 1809−1817.

32. Hiroi, Y.; Komine, N.; Komiya, S.; Hirano, M. Asymmetric Cross-Dimerization between Methyl Methacrylate and Substituted Alkene by Ru(0)−Bicyclononadiene Complex. *Org. Lett.* **2013**, *15*,2486−2489.

33. Hiroi, Y.; Komine, N.; Komiya, S.; Hirano, M. Regio- and Enantioselective Linear Cross-Dimerizations between Conjugated Dienes and Acrylates Catalyzed by New Ru(0) Complexes. *Organometallics* **2014**, *33*, 6604−6613.

34. Hirano, M.; Machida, S.; Abe, R.; Mishina, T.; Komine, N.; Wu, H.-L. Cross-Dimerization of 2,5-Dihydrofuran with Conjugated Dienes Catalyzed by (Chiral Diene)ruthenium(0) Complexes and Origins of the Enantioselectivity. *Organometallics* **2021**, *40*, 3370−3388.

35. Zhang, S.-S.; Wang, Z.-Q.; Xu, M.-H.; Lin, G.-Q. Chiral Diene as the Ligand for the Synthesis of Axially Chiral Compounds via Palladium-Catalyzed Suzuki-Miyaura Coupling Reaction. *Org. Lett.* **2010**, *12*, 5546−5549.

36. He, X.; Zhang, S.; Guo, Y.; Wang, H.; Lin, G.-Q. Mechanistic Investigations of a Palladium-Diene Catalyzed Suzuki−Miyaura Cross-Coupling Reaction. *Organometallics* **2012***, 31*, 2945−2948.

37. Stokes, B. J.; Liao, L.; de Andrade, A. M.; Wang, Q.; Sigman, M. S. A Palladium-Catalyzed Three-Component-Coupling Strategy for the Differential Vicinal Diarylation of Terminal 1,3-Dienes. *Org. Lett*. **2014**, *16*, 4666−4669.

38. Sakai, M.; Hayashi, H.; Miyaura, N. Rhodium-Catalyzed Conjugate Addition of Aryl- or 1-Alkenylboronic Acids to Enones. *Organometallics* **1997**, *16*, 4229−4231.

39. Takaya, Y.; Ogasawara, M.; Hayashi, T.; Sakai, M.; Miyaura, N. Rhodium-Catalyzed Asymmetric 1,4-Addition of Aryl- and Alkenylboronic Acids to Enones. *J. Am. Chem. Soc.* **1998**, *120*, 5579−5580.

40. Hayashi, T.; Takahashi, M.; Takaya, Y.; Ogasawara, M. Catalytic Cycle of Rhodium-Catalyzed Asymmetric 1,4-Addition of Organoboronic Acids. Arylrhodium, Oxa-π-allylrhodium, and Hydroxorhodium Intermediates. *J. Am. Chem. Soc.* **2002**, *124*, 5052−5058.

41. Kina, A.; Iwamura, H.; Hayashi, T. A Kinetic Study on Rh/binap-catalyzed 1,4-Addition of Phenylboronic Acid to Enones: Negative Nonlinear Effect Caused by Predominant Homochiral Dimer Contribution. *J. Am. Chem. Soc.* **2006**, *128*, 3904−3905.

42. Kina, A.; Yasuhara, Y.; Nishimura, T.; Iwamura, H.; Hayashi, T. Kinetic Studies Prove High Catalytic Activity of a Diene-Rhodium Complex in 1,4-Addition of Phenylboronic acid to α,β-Unsaturated Ketones. *Chem. Asian J.* **2006**, *1*, 707−711.

43. Hirano, M.; Komine, N.; Arata, E.; Gridneva, T.; Hatori, A.; Kaizawa, N.; Kamakura, Y.; Kuramochi, A.; Kurita, S.; Machida, S.; Okada, H.; Sawasaki, A.; Uchino, T. Recent advances of achiral and chiral diene ligands in transition-metal catalyses. Tet. Lett. 2019, 60, 150924-150939.

Chapter 2: Leveraging C–H Functionalization for Synthesis of Chiral C_2 symmetric 1,5-Cyclootadienes (COD) Ligands[1*]

*Work was carried out in collaboration with Bowen Zhang and Huw M. L. Davies through the NSF Center for C-H Functionalization at Emory University.

2.1 Introduction to Chiral C_2 symmetric 1,5-COD Ligands

In this chapter we will discuss driving force behind the idea and subsequent elucidation of a novel class of chiral diene ligands. While this ligand was originally born out of an idea for a different project, we recognized that their creation could help advance the chiral diene space. Their original purpose will briefly be discussed, followed by the looking at the derivatization and subsequent effectiveness in a chiral diene benchmark reaction, the Hayasyi-Miyaura reaction.

2.1.1 Brief History of Blakey Lab Catalysis

The Blakey lab has long been interested in group IX metal catalysis of C–H bonds and the advantages it offers over requiring a functional group handle. In recent history, the lab has focused on rhodium and iridium catalysis of allylic substrates to allow for new, powerful methods for complex molecule synthesis.[2,3] While CH bonds were previously thought inert, transition metals have shown their capability to insert into these bonds. Allylic $C_{(sp^3)}$–H bonds are especially reactive towards these transition metals and form a stable η^3-π-allyl intermediate. The Blakey lab has spent considerable time developing new methods for C–N,[4,6-9] C–O,[5] and C–C[11] bond forming reactions as well as new catalysts. Following our mechanistic understanding of the allylic C–H functionalization chemistry,[10] Dr. Christopher Poff and Dr. Caitlin Farr, were able to develop a new rhodium catalyst that leveraged the planar chirality of a ligand, 2-Me-3-Ph-indene (**2.5**), to alter our mechanistic pathway and install amide moieties stereoselectively with high regioselectivity (**Scheme 1A**).[9] While these newly designed indenyl ligands were excellent in our methodologies and boasted an easily accessible synthetic route, the resolution of the planar chiral catalysts remained a challenge. While many attempts were made to resolve the catalytic enantiomers via diastereomeric transformations and stereospecific complexation, a solution

remained elusive. In order to prevent delays, the monomeric rhodium(I) catalyst (**2.6**) was ultimately purified by chiral prep-HPLC and then oxidized to the rhodium(III)-dimer [**2.7**] (**Scheme 1B**). Understanding that widespread use and commercialization of this catalyst was the final goal, new methods had begun to be investigated for the resolution of this compound. This led us to collaborate in the National Science Foundation Center for C–H Functionalization (NSF-CCHF) with the Davies group at Emory University, and specifically Dr. Bowen Zhang.

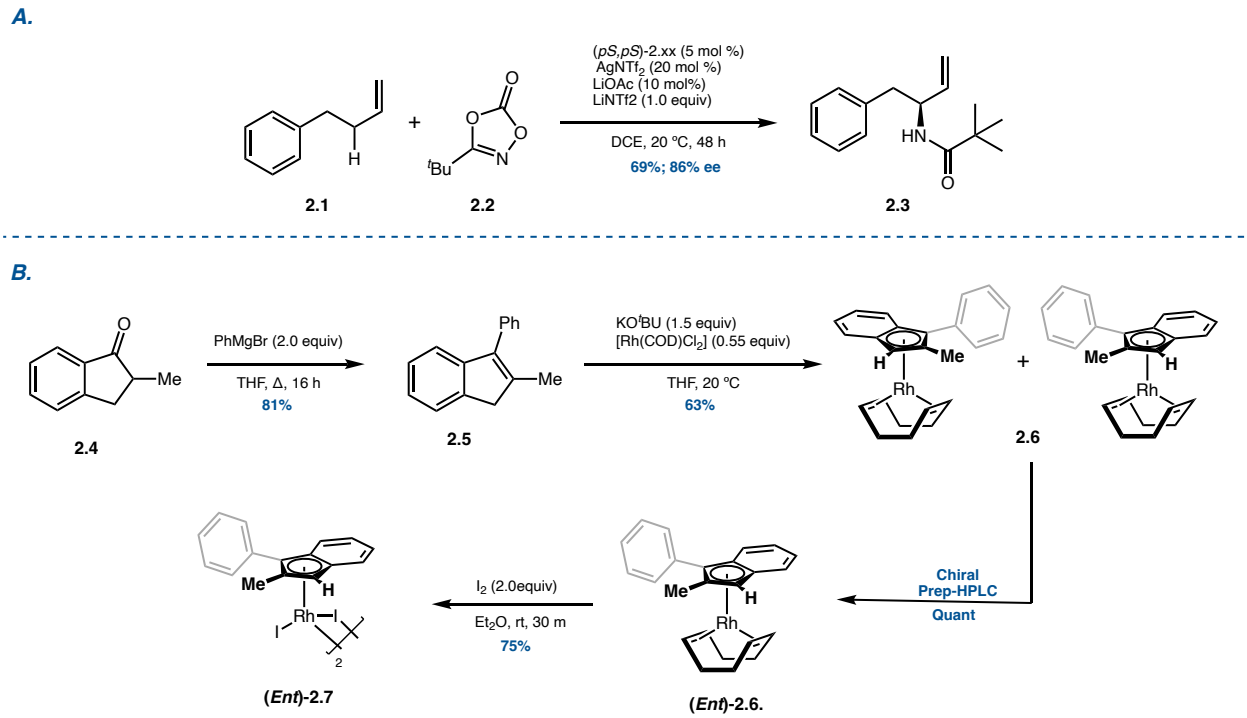

Scheme 1. A) Enantioselective amidation developed by the Blakey Lab. B) Indenyl ligand synthesis and catalyst resolution.

2.1.2 Collaboration on Novel C_1–Symmetric COD Compounds for Diastereomeric Resolution of Indenyl Catalysts

Chiral dienes were postulated to be an exceptional route for the diastereomeric resolution of the rhodium(I) catalysts (**2.6**) due to its use of COD as the spectator ligand in existing the synthesis. Despite this revelation, the cost of enantiopure dienes and their troublesome syntheses presented a challenge at the time that would merely add steps to the resolution or require chiral prep-HPLC at an earlier time. To combat this problem, the Davies group was approached about

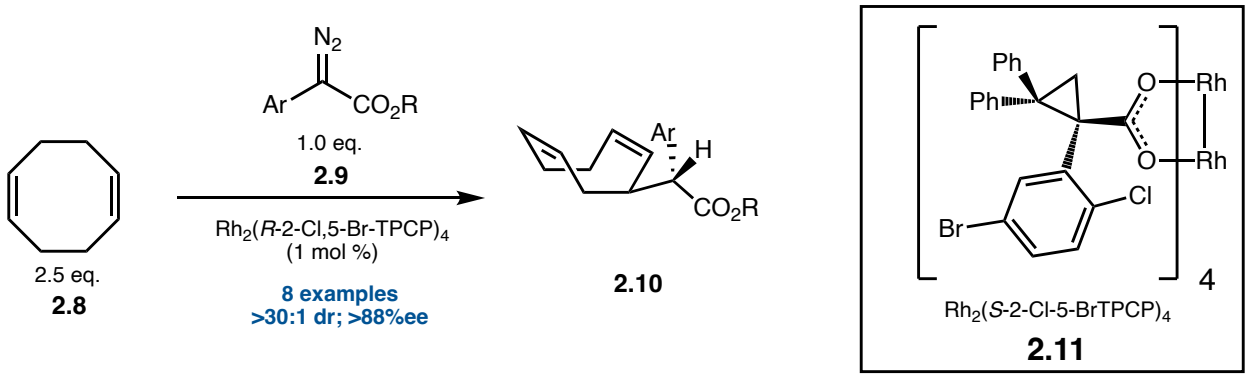

Scheme 2. Mono-allylic C–H functionilization of COD

the ability of their commercially available catalysts to selectively functionalize COD in a single step and allow for resolution in that manner. Davies and Zhang were able to test this hypothesis and show that they could indeed functionalize COD selectively (**Scheme 2**). The Rhodium(I) chiral COD complex was generated via ligand exchange from the chlorobis(ethylene)rhodium(I) dimer, ($[Rh(C_2H_4)_2Cl]_2$) was then subjected to the complexation procedure (**Scheme 3**) The initial testing by Dr. Caitlin Farr showed promising results in that diastereomers were formed following complexation, however this led to a litany of products that were unable to be isolated. Further

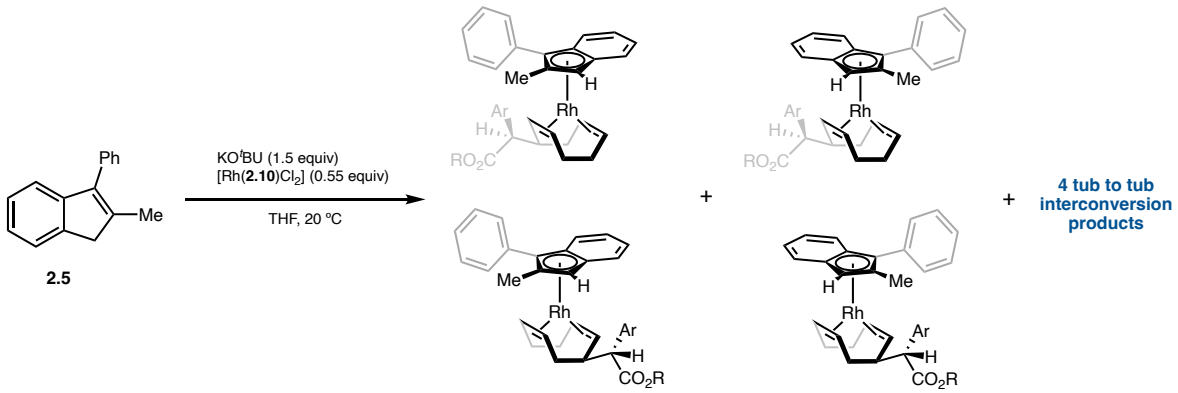

Scheme 3. Mono-allylic C–H functionalized C_1–symmetric COD following complexation.

investigation of the spectra and HPLC traces led to the realization that a C_1 chiral diene arising from mono-substitution would be too problematic to continue due to its ability to interconvert in-situ during complexation with metal, especially in the presence of heat. Leaning back into the literature, it was shown that the C_2–symmetric chiral dienes had a much larger barrier tub-to-tub interconversion (~30 kcal mol^{-1})[13] and would provide the same ligand therefore represented a promising target for the next iteration of testing.

2.2 Generation of Chiral C_2–symmetric 1,5-COD Ligands and Evaluation in Asymmetric Catalysis

2.2.1 Collaboration on Novel C_2–Symmetric COD Compounds for Diastereomeric Resolution of Indenyl Catalysts

Following a meeting with our collaborators, Dr. Bowen Zhang was able to further his methodology to generate the C_2 chiral diene and provide a chance at a more tenable resolution through alterations to the reagent and substrate equivalents (**Scheme 4A**). These ligands provided an answer to the issue of tub-to-tub conversion that the mono-substituted CODs potentially suffered from and dramatically simplified the theoretical conversion. Additionally, the ligands

were formed in good yield and excellent enantioselectivity due to the minor enantiomer of the mono-allylic product being further transformed into the *meso* diastereomer, an enrichment process

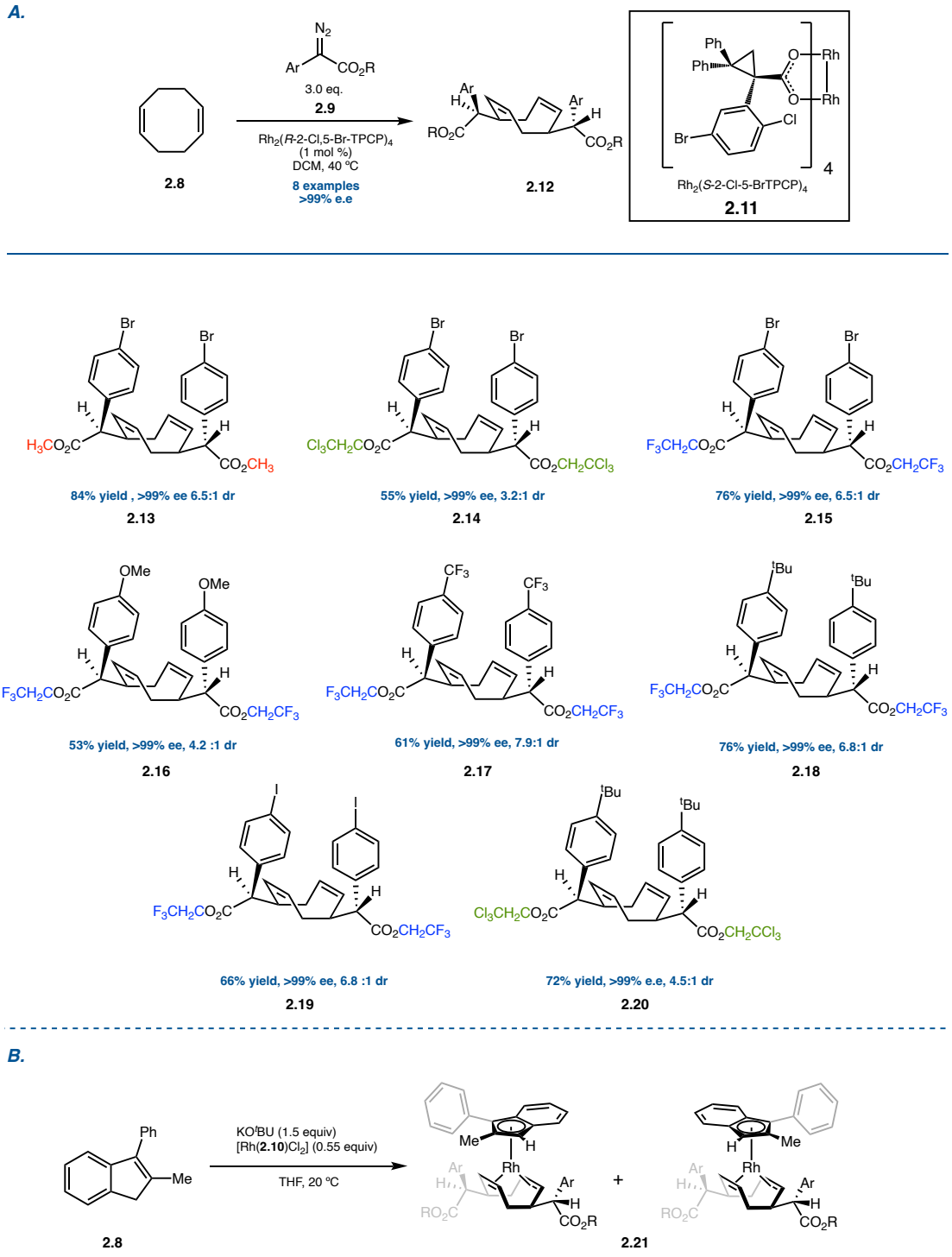

Scheme 4. Double-allylic C–H functionilization of COD to provide the C2-symmetric COD and diastereomers following complexation.

described by the Horeau Principle.[12] While diastereoselectivity was only moderate, Dr. Zhang was able to separate them with silver nitrate doped silica gel via column chromatography. Surprising, the regioselectivity of the second allylic position was exclusive to the desired product and is a testament to the Davies lab's ability to select key C–H bonds for functionalization. Following their isolation, they were again prepared via a ligand exchange with $[Rh(C_2H_4)_2Cl]_2$ and subjected to treatment of normal complexation procedures to provide two diastereomers [**2.21**] (**Scheme 4B**). While believed some complexation was observed, Dr. Caitlin Farr, Patrick Gross, and I all failed to isolate the desired diastereomers in this reaction. This is believed to be due to the stability issues of the Rh(I)-indenyl chiral COD complex. Following this, Patrick Gross revisited the chiral CODs under these conditions to attempt a ligand swap from COD to chiral C_2-symmetric COD (**2.15**), however the ligand equilibrium data in Chapter 1 (**Ch.1.Fig. 4**) clearly shows that this was an unfavorable reaction, albeit unknown at the time. Ultimately, the resolution via chiral C_2-symmetric COD was shelved, however the new class of ligands were an exciting advancement to the field and so testing on a Hayashi-Miyaura reaction began.

2.2.2 Evaluation of C_2–Symmetric COD Compounds in a Hayashi-Miyaura Reaction

The evaluation of these ligands for 1,4-conjugte addition began during my rotation in the Blakey lab in 2018. Utilizing the first C_2-symmetric COD (**2.14**) variant, we began screening conditions to determine the viability of this endeavor. Our initial testing showed moderate yield when compared to COD but poor enantioselectivity at 26% *ee* (**Scheme 5**). In a bid to optimize enantioselectivity, conditions such as solvent, water to solvent ratio and heating were explored. These changes deleteriously affected the yield and confirmed our suspicious that the selectivity was innate to the ligand. Finally, we settled on reaction conditions that were like those used

previously by many in the field. While we did notice an increase in yield with temperature increase on initial testing, reproducibility of results became problematic in heated systems. Furthermore,

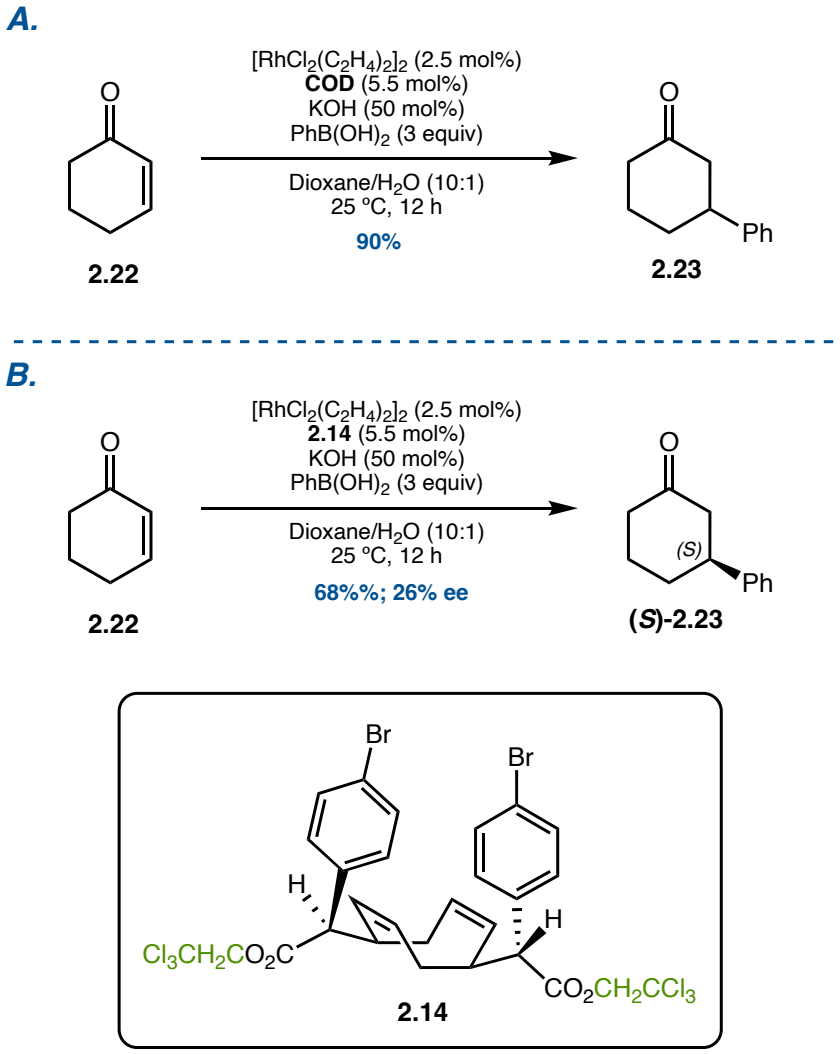

Scheme 5. Intial feasibility testing with 3,7 disubstituted CODs.

we chose to utilize three equivalents of phenyl boronic acid despite this being on the upper end of equivalents in Hayashi-Miyaura reactions. Finally with conditions in hand, we began to screen the first-generation ligands synthesis by Bow Zhang, consisting of the para-bromo aryls with substitutions of the ester functionality. The substitutions tested consisted of the methyl ester (**2.13**), trichloroethylester (**2.14**) and trifluoroethylester (**2.15**) (**Figure 1**). The results showed that while

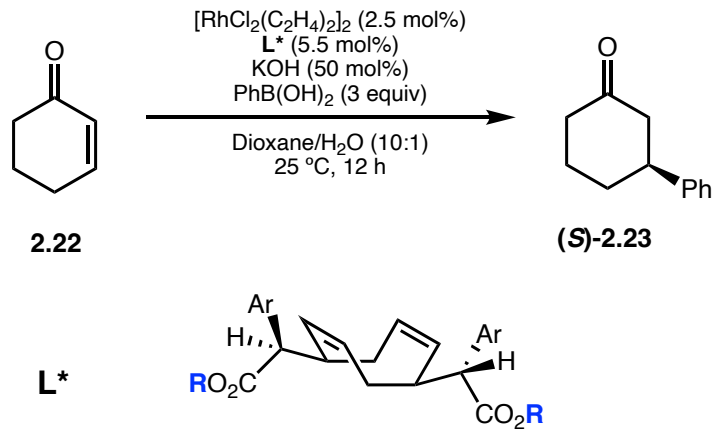

L*	Ar	R	yield, %	ee, %
2.13	*p*-BrC_6H_4	CH_3	67	39
2.14	*p*-BrC_6H_4	CH_2CCl_3	84	34
2.15	*p*-BrC_6H_4	CH_2CF_3	81	36
2.19	*p*-IC_6H_4	CH_2CF_3	~2	45
2.16	*p*-$OMeC_6H_4$	CH_2CF_3	68	30
2.17	*p*-$CF_3C_6H_4$	CH_2CF_3	60	33
2.20	*p*-$^tBuC_6H_4$	CH_2CF_3	45	22
2.24	*p*-BrC_6H_4	H	43	27

Figure 1. Screening of ester and aryl substitutions under optimized conditions.

the methyl ester (**2.13**) provided 39% *ee*, the yield suffered, and the decision was made to move forward with the trifluoroester (**2.15**) as it provided similar selectivity with an increase of ~15% yield. This then led us to probe the electronics of the aryl ring beta to the COD (**2.15-2.20**), but we found both a decrease and yield and selectivity in all cases but the para-iodophenyl (**2.19**). Despite

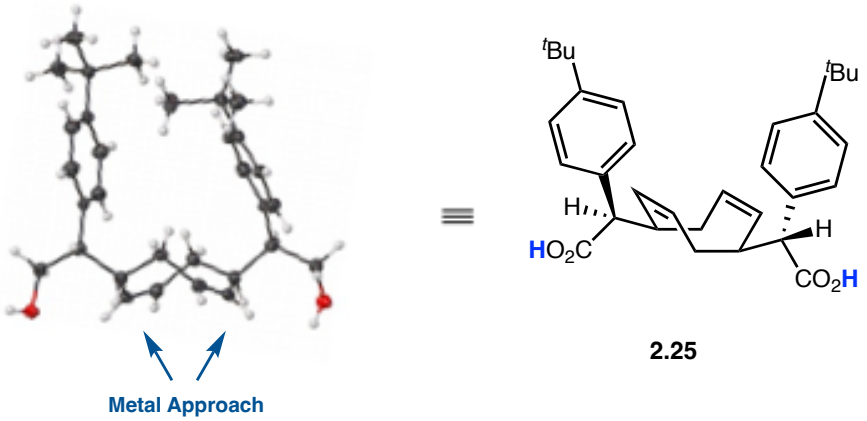

Figure 2. SCXRD of free ligand and hypothesis of metal binding approach

the slightly higher selectivity for the para-iodophenyl, the yield was dramatically lower due to potential side reactions between the rhodium and the iodine moiety. With this knowledge in hand, we chose to move forward with the para-bromo aryl ring, however we were unsure of how to proceed in the rational design of these ligands. For this we turned to Dr. John Bacsa, Emory's crystallographer, to help collect single crystal X-ray diffraction (SCXRD) of the free reduced ligand (**2.25)** and hopefully of the ligand bound to rhodium. While we were able to acquire a SCXRD of the free ligand, all attempts to generate diffracting crystals of the catalyst were unsuccessful (**Figure 2**). While the catalyst could be generated in refluxing toluene, the resulting product was an amorphous yellow powder. Further attempts to recrystallize led to only non-diffracting micro-crystal formation or glass. The final solvent system utilized to procure micro crystals of various ligands bound to rhodium was that of trifluoroethanol and trichloroethanol as the layered antisolvent. While at the time this was disheartening, the advent of Cryo-EM technology for small molecule absolute structural determination suggests if revisited, the structure could be determined.[14] Despite the lack of a catalyst structure, we felt confident that the free ligand

was poised in a similar manner and explained why our steric changes to the aryl ring (**2.20**) had not lead to any enrichment of the desired enantiomer [**(*S*)-2.23**]. To remedy this, we postulated that exploitation of TADDOL ligand design would be beneficial.[15.] We began by trying to utilize a double addition of various commercial and fresh aryl-Grignard reagents to the methyl ester, however no tertiary alcohol was formed and near quantitative return of starting material was

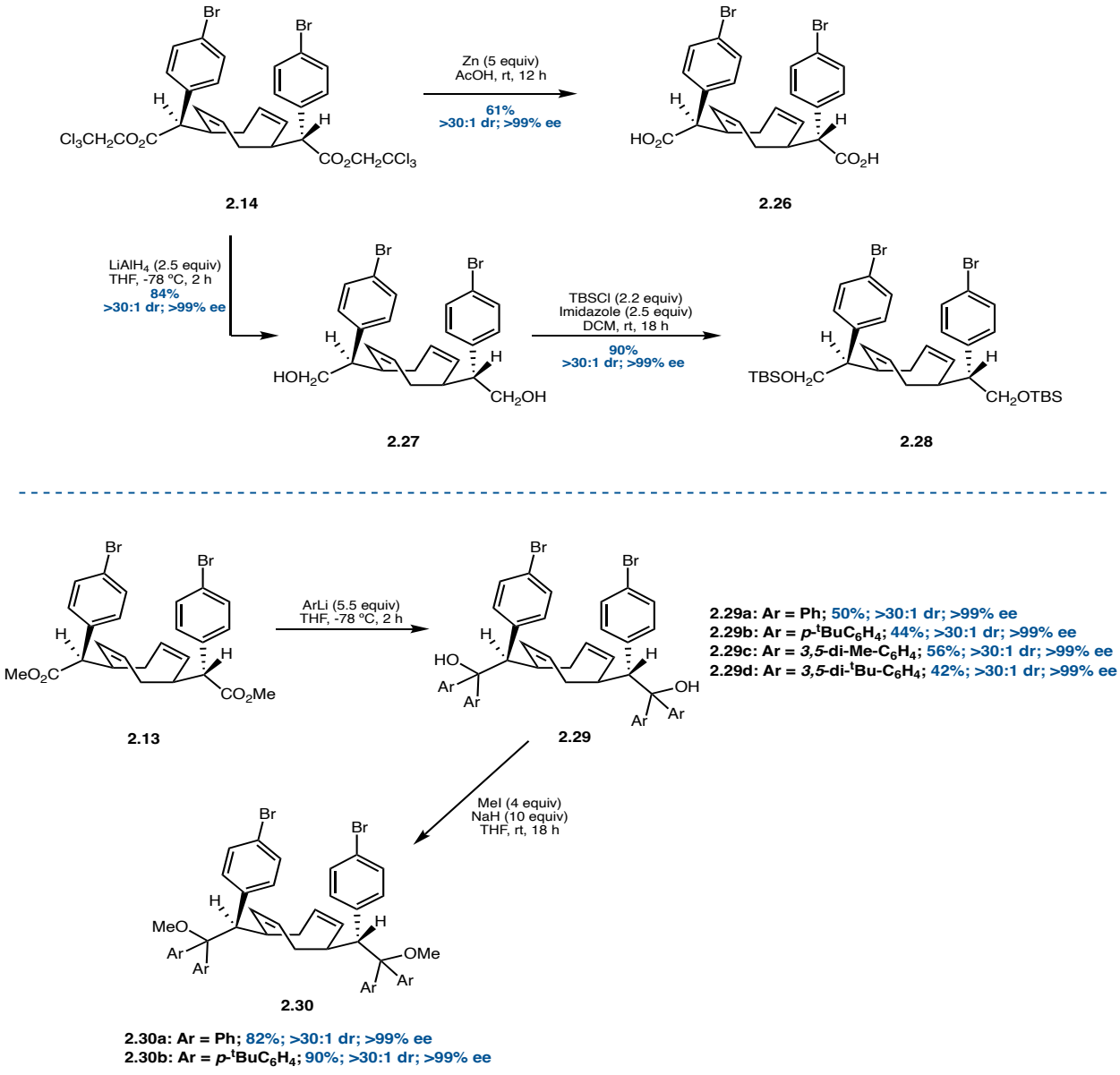

Scheme 6. Synthesis of the second generation of C_2-symmetric chiral COD ligands.

recovered. Luckily, the switch to fresh aryl-lithiates made *in-situ* led to the desired products with di-addition to both methyl esters at the beta position of the COD and providing the desired tertiary alcohol (**2.29a-d**) in moderate yields and retention of stereochemical information. Additionally, we generated the carboxylic acid (**2.26**), the free alcohol of the parent ligand (**2.27**), and the silyl

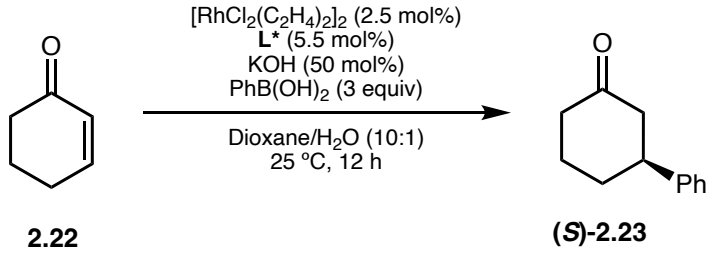

2.22 **(*S*)-2.23**

L*

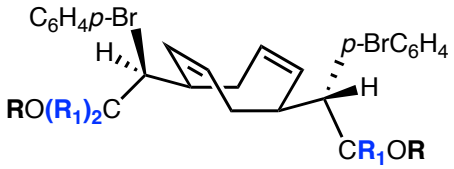

L*	R	R_1	yield, %	ee, %
2.27	H	H	61	26
2.28	TBS	H	78	53
2.29a	H	Ph	58	47
2.30a	CH_3	Ph	32	60
2.29b	H	*p*-^{t}BuC$_6$H$_4$	69	69
2.30b	CH_3	*p*-^{t}BuC$_6$H$_4$	81	59
2.29c	H	*3,5*-di-Me-C$_6$H$_4$	63	41
2.29d	H	*3,5*-di-^{t}Bu-C$_6$H$_4$	63	76

Figure 3. Screening of second generation derivatized ligands under optimized conditions.

ether (**2.28**) all in good to excellent yields without erosion of stereochemistry. Two of the arylated products were further diversified through methylation of the tertiary alcohol to the ether product (**2.30a-b**). With this diversified library in hand, we set about testing the enantio-inductive effect this second generation of ligands would have (**Figure 3**). While the yield fluctuated consistently between 60-80%, we were excited to see the enantioselectivity increasing as me modified the "beltline" of the chiral COD. This clearly indicated that we had found and were now influencing the steric environment that dictated *re/si* facial selectivity of the enone. While the primary alcohol (**2.27**) saw a loss in selectivity, the addition of a bulky silyl group (**2.28**) quickly recovered and increased the selectivity over 50% *ee* while maintaining moderate yields. Applying the TADDOL inspired chemistry saw that the di-addition of aryl groups to both sides led to an increase in selectivity that mirrored their increase in steric bulk (**2.29a-d**). Additionally, while methylation of the tertiary alcohol flanked by phenyl rings (**2.30a**) led to an increase in selectivity, this trend did not continue as we increased the steric bulk of the aryl rings (**2.30b**). Our hypothesis is that due to the increasing steric clashes of the tightly confined aryl rings, increased torsion of the rings begins to overwhelm the effect the small methyl group may be imparting. Finally, after viewing our data we determined that ligand (**2.29d**) was our optimal ligand by providing good yields and moderate enantioselectivity. With this result in hand, the decision was made to disclose this working 2019 without continuing onto a third generation.[1]

2.2.3 Evaluation of C_2–Symmetric COD Compounds in a α-Diazoester Insertion Reactions

Following the initial disclose of 3,7 disubstituted COD ligands, the ligands evaluated in a α-diazoester insertion reaction of benzofuranones. This reaction was reported by Wang and coworkers in late 2018 and utilized the diphenyl substituted nbd scaffold (**1.27b**) as its ligand

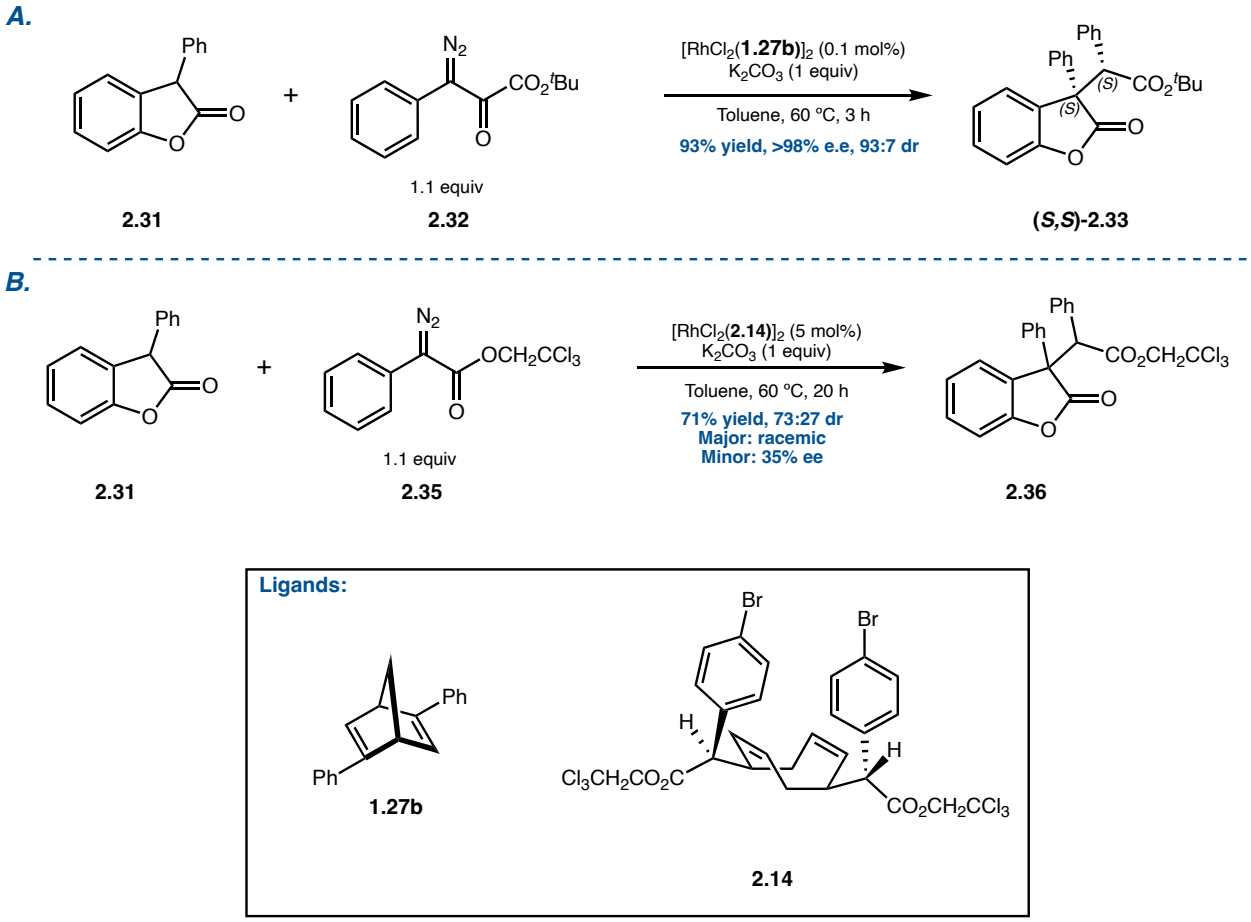

Scheme 7. Evaluation of α-diazoester insertion product using C_2-symmetric chiral COD ligands.

(**Scheme 7a**).[16] The initial investigation utilized the trichloroester ligand (**2.14**) and aimed to achieve the same high diastereo- and enantioselectivity as Wang and coworkers. In preparation for these experiments, the catalyst was prepared from $[Rh(C_2H_4)_2Cl]_2$ and isolated as a yellow powder as previously described. The 3-phenylbenzofuran-2(3H)-one (**2.31**) was then added to the reaction along with 2,2,2-trichloroethyl 2-diazo-2-phenylacetate (**2.35**) and catalyst. Despite our attempts at this reaction and good yields, the diastereomeric ratio remained moderate and the enantioselectivity poor (**Scheme 7b**). Additionally, the major diastereomer (**2.36**) was found to be racemic, and the minor enantiomer was the only product formed in enantiomeric excess. With a separate project having more interesting lead results, this preliminary study was handed off to

Bowen Zhang and the Davies group for further study as diazo insertions are one of their fortes, however they too were met with poor results and enantioinduction taking place solely on the minor diastereomer.

2.3 Concluding Remarks

Having successfully developed a new class of C_2-symmetric chiral diene ligands in a single, highly selective reaction utilizing the Davies labs catalyst, we were able to demonstrate the ability for 3,7-disubstituted CODs to be utilized in a benchmark asymmetric Hayashi-Miyaura reaction. While the final optimized ligand required an addition step, this chemistry represents a quick and facile way to access COD dienes for asymmetric catalysis. While further studies are not currently underway in either the Blakey or Davies labs, we hope that academia and industry will apply and improve upon our initial studies in the coming years.

2.4 References

1. Zhang, B., Hollerbach, M.R., Blakey, S.B., Davies, H.M.L. C–H Functionalization Approach for the Synthesis of Chiral C2-Symmetric 1,5-Cyclooctadiene Ligands. *Org. Lett.* **2019**, *21*, 9864-9868.

2. Nelson, T. A. F [†]; Hollerbach, [†]M. R.; Blakey, B. B. Allylic C–H Functionalization via Group 9 π-Allyl Intermediates. *Dalton Trans.* **2020**, *49*, 13928-13935. [†] Equally contributing authors.

3. Kazerouni, A. M.; McKoy, Q. A.; Blakey, B. B. Recent Advances in Oxidative Allylic C–H Functionalization via Group IX-Metal Catalysis. *Chem. Commun.* **2020**, *56*, 13287-13300.

4. Burman, J. S.; Blakey, S. B., Regioselective Intermolecular Allylic C−H Amination of Disubstituted Olefins via Rhodium/π-Allyl Intermediates. *Angew. Chem. Int. Ed*. **2017**, *56*,13666-13669.

5. Nelson, T. A. F.; Blakey, S. B., Intermolecular Allylic C−H Etherification of Internal Olefins. *Angew. Chem. Int. Ed*. **2018**, *57*, 14911-14915.

6. Burman, J. S.; Blakey, S. B., Regioselective Intermolecular Allylic C−H Amination of Disubstituted Olefins via Rhodium/π-Allyl Intermediates. *Angew. Chem. Int. Ed*. **2017**, *56*, 13666-13669.

7. Burman, J. S.; Harris, R. J.; Farr, C. M. B.; Bacsa, J.; Blakey, S. B., Rh(III) and Ir(III)Cp* Complexes Provide Complementary Regioselectivity Profiles in Intermolecular Allylic C–H Amidation Reactions. *ACS Catal*. **2019**, *9*, 5474-5479.

8. Kazerouni, A. M.; Nelson, T. A. F.; Chen, S. W.; Sharp, K. R.; Blakey, S. B., Regioselective Cp*Ir(III)-Catalyzed Allylic C–H Sulfamidation of Allylbenzene Derivatives. *J. Org. Chem*. **2019**, *84*, 13179-13185.

9. Farr, C. M. B.; Kazerouni, A. M.; Park, B.; Poff, C. D.; Won, J.; Sharp, K. R.; Baik, M.-H.; Blakey, S. B., Designing a Planar Chiral Rhodium Indenyl Catalyst for Regio- and Enantioselective Allylic C–H Amidation. *J. Am. Chem. Soc.* **2020**, *142*, 13996-14004.

10. Harris, R. J.; Park, J.; Nelson, T. A. F.; Iqbal, N.; Salgueiro, D. C.; Bacsa, J.; Macbeth, C. E.; Baik, M.-H.; Blakey, S. B., The Mechanism of Rhodium-Catalyzed Allylic C–H Amination. *J. Am. Chem. Soc.* **2020**, *142*, 5842-5851.

11. Unpublished work by Dr. Caitlin Farr in her thesis that can be found at Emory Theses and Dissertations Database. [https://etd.library.emory.edu/concern/etds/st74cr579?locale=en]

12. Davies, H. M. L.; Liao, K., Dirhodium tetracarboxylates as catalysts for selective intermolecular C–H functionalization. *Nat. Rev. Chem*. **2019**, *3*, 347-360.

13. Läng, F.; Breher, F.; Stein, D.; Grützmacher, H. Chiral Olefins as Steering Ligands: Syntheses of C1-Symmetric Dibenzo[*a,e*]-cyclooctenes (^{R}dbcot). *Organometallics* **2005**, *24*, 2997−3007.

14. Cabral, A., Cabral, J. E., & McNulty, R. Cryo-EM for small molecules. *Current Protocols*, **2022**, *2*, e632.

15. Seebach, D.; Beck, A. K.; Heckel, A. TADDOLs, Their Derivatives, and TADDOL Analogues: Versatile Chiral Auxiliaries. *Angew. Chem. Int. Ed*. **2001**, *40*, 92-138.

16. Liu, Y.; Zhou, C.; Xiong, M.; Jiang, J.; Wang, J. Asymmetric Rh(I)-Catalyzed Functionalization of the 3-C(sp3)-H Bond of Benzofuranones with α-Diazoesters. *Org. Lett.* **2018**, *20*, 5889−5893.

2.5 Experimental Section

2.5.1 General Information

All reactions were carried out under nitrogen atmosphere with anhydrous solvents in oven- or flame-dried glassware using standard Schlenk technique, unless otherwise stated. Anhydrous dichloromethane (DCM), diethyl ether (Et2O), tetrahydrofuran (THF), and toluene were obtained by passage through activated alumina using a Glass Contours solvent purification system. 1,4-dioxane was purchased from Dri-solv and sparged with nitrogen prior to use. Solvents for workup, extraction, and column chromatography were used as received from commercial suppliers without further purification. Unless otherwise reported, all catalysts were synthesized according to previously reported procedures by the Davies group. All other chemicals were purchased from Millipore Sigma, Strem Chemicals, Oakwood Chemicals, Alfa Aesar, Ambeed, or Combi-Blocks and used as received without further purification, unless otherwise stated.

^{1}H and 13C nuclear magnetic resonance (NMR) spectra were recorded on a Varian Inova 600 spectrometer (600 MHz 1 H, 151 MHz 13C), a Bruker 600 spectrometer (600 MHz 1 H, 151 MHz 13C), a Varian Inova 500 spectrometer (500 MHz 1 H, 126 MHz 13C), and a Bruker 400 spectrometer (400 MHz 1 H, 126 MHz 13C) at room temperature in $CDCl_3$ (dried over activated molecular sieves) with internal $CHCl_3$ as the reference (7.26 ppm for 1 H, 77.16 ppm for 13C), unless otherwise stated. Chemical shifts (δ values) were reported in parts per million (ppm) and coupling constants (J values) in Hz. Multiplicity was indicated using the following abbreviations: s = singlet, d = doublet, t = triplet, q = quartet, qn = quintet, m = multiplet, br = broad. High resolution mass spectra (HRMS) were obtained using a Thermo Electron Corporation Finigan LTQFTMS (at the Mass Spectrometry Facility, Emory University). High Pressure Liquid Chromatography (HPLC) was performed on an Agilent 1100 series HPLC utilizing CHIRALPAK

AD-H, AS-H, OD-H and OJ-H 4.6 x 150 mm analytical columns. Analytical thin layer chromatography (TLC) was performed on precoated glass-backed Silicycle SiliaPure® 0.25 mm silica gel 60 plates and visualized with UV light, ethanolic p-anisaldehyde, ethanolic bromocresol green, or aqueous potassium permanganate (KMnO4). Flash column chromatography was performed using Silicycle SiliaFlash® F60 silica gel (40- 63 μm) on a Biotage Isolera One system. Preparatory TLC was performed on precoated glass backed Silicycle SiliaPure® 1.0 mm silica gel 60 plates. We acknowledge the use of shared instrumentation provided by grants from the NIH and the NSF.

2.5.2 Procedures and Tabulated Data

General procedure for the diazo compound synthesis
Diazo compound **2-12** used in this work were pre-synthesized by group in storage following the general procedure below.

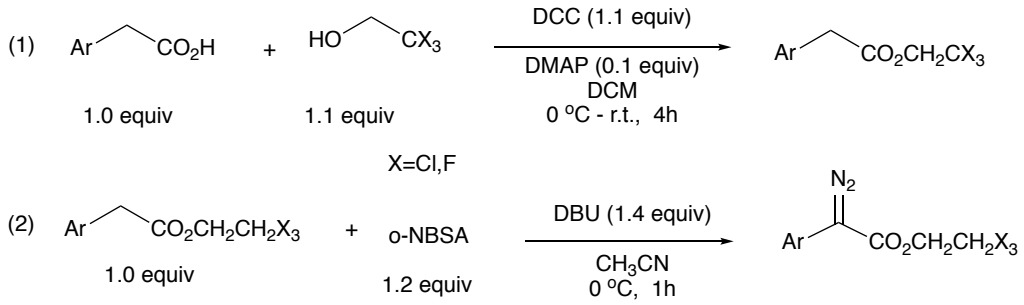

(1) Aryl acetic acid (1.0 equiv, 20 mmol) and 2,2,2-trihaloethanol (1.1 equiv, 22 mmol) were dissolved in 50 mL dichloromethane and stirred at 0 °C in ice/water bath. N,N'-Dicyclohexylcarbodiimide (DCC) (1.1 equiv. 22 mmol) was then added to the stirring solution carefully. Catalytic DMAP (0.1 equiv, 2.0 mmol) was then dissolved in 2 mL DCM and added to the solution. The white precipitation forms rapidly and the solution become milk color. The reaction was kept running for 4 h and warm to r.t. naturally. Filter and concentrate the solution give the crude ester product. Purify the ester with a quick silica plug (5% Et_2O/Pentane) and then

concentrate under vacuum, yielding the ester as colorless oil, which is directly used for the following diazo transfer step.

(2) Ester from step (1) (1.0 equiv, 10 mmol) and ortho-nitrobenzenesulfonyl azide (o-NBSA) (1.2 equiv, 12 mmol) were dissolved in 30 mL anhydrous CH_3CN. The solution was kept stirring at 0 °C and DBU (1.4 equiv, 14 mmol) was added dropwisely to the solution. The color of the solution gradually turned orange and it is quenched after 1 h by diluting with 100 mL Et_2O followed by adding 100mL NH_4Cl (sat.) solution. Extract the aqueous layer with Et_2O (30 mLx3), combined the organic layers and dry it over $MgSO_4$. Silica plug and concentrate give the crude diazo product as orange oil or solid. Further purification was done by flash column chromatography (2-5% Et_2O/Pentane)

General Procedure for mono-allylic-insertion

To a 16 mL glass reaction vial was added stir bar, 1,5-cyclooctadiene (COD) (0.75 mmol, 2.5 equiv, 81 mg/~0.1 mL) and Rh_2(*R*-2-Cl,5-BrTPCP)$_4$ (0.1 mol %). The vial was degassed and filled with Ar for several times. 2mL anhydrous DCM was then added to the vial and the solution was kept stirring at 0 °C for 5 min. Aryl diazo ester (0.3 mmol, 1.0 equiv) was dissolved in 4 mL DCM and added dropwisely to the vial over 3 h via syringe pump. The reaction was kept running for 2 h after the addition of diazo compound is finished. The solution was concentrated to give oil mixture and the crude ^{1}H NMR was obtained for dr analysis. Further purification was done by column chromatography (0.8-10% Et_2O in pentane depending on substrate), giving product as colorless oil.

General Procedure for bis-allylic-insertion

To a 16 ml glass reaction vial was added stir bar, 1,5-cyclooctadiene (COD) (0.3 mmol, 1.0 equiv, 32 mg) and Rh_2(2-Cl,5-BrTPCP)$_4$ (0.1 mol%). The vial was degassed and filled with Ar for several times. 2mL anhydrous DCM was then added to the vial and the solution was kept stirring at 40 °C for 5min. Aryl diazo ester (0.9 mmol, 3.0 equiv) was dissolved in 4ml DCM and added dropwisely to the vial over 3 h via syringe pump. The reaction was kept running for 2 h after the addition of diazo compound is finished. The solution was concentrated to give oil crude, ^{1}HNMR was obtained for dr analysis. Further purification was done by column chromatography (2-4% Et_2O in pentane) or 5% $AgNO_3$ on silica column chromatography (4-10% Et_2O in pentane), giving product as sticky oil or white solid.

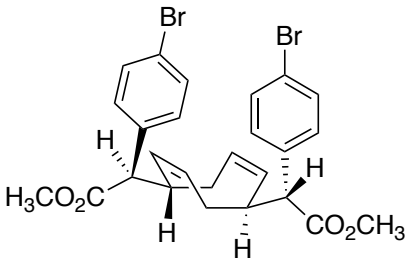

dimethyl 2,2'-((1S,2Z,5S,6Z)-cycloocta-2,6-diene-1,5-diyl)(2R,2'R)-bis(2-(4-bromophenyl)acetate) 2.13: Derived from the reaction of diazo **II** (0.9 mmol, 230 mg, 3.0 equiv) and COD (0.3 mmol, 32 mg, 1.0 equiv) following general procedure, major dr purified by normal column chromatography (6-8% Et_2O in pentane). Product: 141 mg, 84% yield; >99% ee.; dr = 6.5:1, white foam solid.

^{1}H NMR (600 MHz, $CDCl_3$) δ 7.44 (d, *J* = 8.5 Hz, 4H), 7.20 (d, *J* = 8.5 Hz, 4H), 5.44 (ddd, *J* = 11.6, 7.9, 6.0 Hz, 2H), 5.04 (dd, *J* = 11.6, 6.6 Hz, 2H), 3.67 (s, 6H), 3.41-3.35 (m, 2H), 3.37 (d, *J* = 2.8 Hz, 2H), 2.28 – 2.11 (m, 4H). ^{13}C NMR (151 MHz, $CDCl_3$) δ 173.25, 136.21, 131.62,

130.44, 130.38, 128.37, 121.50, 57.37, 52.15, 42.03, 32.66. IR: 2950, 1734, 1590, 1488, 1434, 1407, 1339, 1264, 1156, 1073, 1011, 908, 819 (cm^{-1}); HRMS-(APCI) m/z: found at 561.0275 [$(M+H)^+$: $[C_{26}H_{27}O_4Br_2]^+$ calculates to be 561.0271]; $[\alpha]^{20}_D$: -55.8° (c=1.00, $CHCl_3$); m.p. 66-70 °C

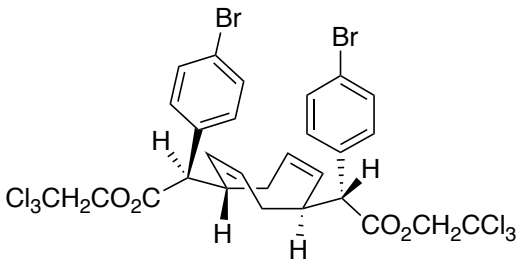

(2R,2'R)-bis(2,2,2-trichloroethyl) 2,2'-((1S,2Z,5S,6Z)-cycloocta-2,6-diene-1,5-diyl)bis(2-(4-bromophenyl)acetate) 2.14: Derived from the reaction of diazo **I** (0.9 mmol, 335 mg, 3.0 equiv) and COD (0.3 mmol, 32 mg, 1.0 equiv) following general procedure, major dr purified by normal column chromatography (2% Et_2O in pentane). Product: 152 mg, 55% yield; >99% ee.; dr = 3.2:1, white foam solid. A larger scale of reaction at COD (0.8 mmol, 86 mg) and diazo **3** (2.4 mmol, 3.0 equiv. 893 mg) was performed, given 340 mg product, 53% yield , >99% ee. dr = 3.2:1.

^{1}H NMR (600 MHz, $CDCl_3$) δ 7.51 – 7.41 (m, 4H), 7.26 – 7.23 (m, 4H), 5.51 – 5.41 (m, 2H), 5.04 (dd, *J* = 11.3, 7.9 Hz, 2H), 4.76 (d, *J* = 12.0 Hz, 2H, **H of CH_2 next to CCl_3**), 4.68 (d, *J* = 12.0 Hz, 2H, **H of CH_2 next to CCl_3**), 3.67 (qd, *J* = 10.1, 8.0, 5.4 Hz, 2H), 3.47 (d, *J* = 10.2 Hz, 2H), 2.47 – 2.36 (m, 2H), 2.14 (ddd, *J* = 15.9, 12.5, 8.0 Hz, 2H). ^{13}C NMR (151 MHz, $CDCl_3$) δ 170.81, 135.21, 131.79, 130.58, 129.95, 128.56, 121.94, 94.66, 74.30, 57.71, 41.11, 33.38. IR: 2924, 1750, 1489, 1408, 1371, 1262, 1216, 1136, 1074, 1012, 826, 762, 719 (cm^{-1}); HRMS-

(APCI) m/z: found at 792.8262 [$(M+H)^+$: $[C_{28}H_{25}O_4Br_2Cl_6]^+$ calculates to be 792.8245]; $[\alpha]^{20}_D$: +21.8° (c=1.00, $CHCl_3$); m.p. 48-52 °C

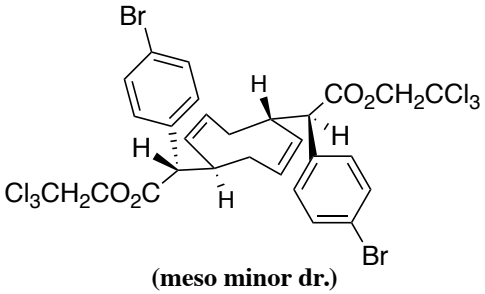

(meso minor dr.)

(2R,2'S)-bis(2,2,2-trichloroethyl) 2,2'-((1R,2Z,5S,6Z)-cycloocta-2,6-diene-1,5-diyl)bis(2-(4-bromophenyl)acetate) 2.14meso (meso minor dr): Originally isolated from the reaction that give **29**. Larger preparation is derived from mono insertion product **17** (0.4 mmol, 181 mg, 1.0 equiv) and diazo **I** (0.8 mmol, 298 mg, 2.0 equiv) following general procedure using the different enantiomer of catalyst. Purify this meso product with column chromatography (2% Et_2O in pentane). Product: 168 mg, 53% yield, white foam solid.

^1H NMR (600 MHz, $CDCl_3$) δ 7.48 – 7.43 (m, 4H), 7.26 – 7.22 (m, 4H), 5.57 (dtd, *J* = 10.7, 8.8, 1.8 Hz, 2H), 5.15 (dd, *J* = 11.7, 4.3 Hz, 2H), 4.79 (d, *J* = 12.0 Hz, 2H), 4.63 (d, *J* = 12.0 Hz, 2H), 3.62 (d, *J* = 10.8 Hz, 2H), 3.24 – 3.15 (m, 2H), 2.53 (ddd, *J* = 13.9, 9.1, 4.7 Hz, 2H), 2.46 – 2.35 (m, 2H). ^{13}C NMR (151 MHz, $CDCl_3$) δ 171.10, 135.26, 131.81, 130.89, 130.64, 127.33, 121.97, 94.63, 74.21, 56.04, 43.21, 30.23. IR: 2952, 2874, 1748, 1488, 1447, 1408, 1371, 1331, 1269, 1206, 1130, 1074, 1011 (cm^{-1}); HRMS-(APCI) m/z: found at 792.8262 [$(M+H)^+$: $[C_{28}H_{25}O_4Br_2Cl_6]^+$ calculates to be 792.8245]; m.p. 50-55 °C

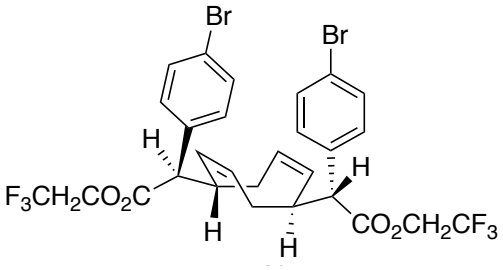

(2R,2'R)-bis(2,2,2-trifluoroethyl) 2,2'-((1S,2Z,5S,6Z)-cycloocta-2,6-diene-1,5-diyl)bis(2-(4-bromophenyl)acetate) 2.15: Derived from the reaction of diazo **III** (0.9 mmol, 290 mg, 3.0 equiv) and COD (0.3 mmol, 32 mg, 1.0 equiv) following general procedure, major dr purified by $AgNO_3$ column chromatography (4-8% Et_2O in pentane). Product: 160 mg, 76 % yield; >99% ee.; dr = 6.5:1, sticky oil to half solid.

^1H NMR (500 MHz, $CDCl_3$) δ 7.53 – 7.42 (m, 4H), 7.24 – 7.14 (m, 4H), 5.46 (ddd, *J* = 12.6, 7.9, 5.3 Hz, 2H), 5.04 (dd, *J* = 11.5, 7.3 Hz, 2H), 4.50 (ddd, *J* = 13.1, 8.7, 4.5 Hz, 2H, **H of CH_2 next to CF_3**), 4.44 (ddd, *J* = 12.7, 8.7, 4.5 Hz, 2H, **H of CH_2 next to CF_3**), 3.58 – 3.47 (m, 3H), 3.46 (d, *J* = 10.0 Hz, 2H), 2.25 (dt, *J* = 15.4, 4.6 Hz, 2H), 2.14 (ddd, *J* = 15.5, 12.0, 8.2 Hz, 2H). ^{13}C NMR (126 MHz, $cdcl_3$) δ 171.02, 134.97, 131.80, 130.36, 129.80, 128.54, 122.79 (q, J=277.7 Hz, **C of CF_3**), 121.97, 60.54 (q, J=36.6 Hz, **C of CH_2 next to CF_3**), 56.96, 41.60, 32.68. IR: 3017, 1753, 1489, 1408, 1282, 1168, 1138, 1074, 1012, 978, 817, 760, 644 (cm^{-1}); HRMS-(APCI) m/z: found at 694.9880 [$(M-H)^-$: $[C_{28}H_{23}O_4Br_2F_6]^+$ calculates to be 694.9873]; $[\alpha]^{20}_D$: -10.2° (c=1.00, $CHCl_3$);

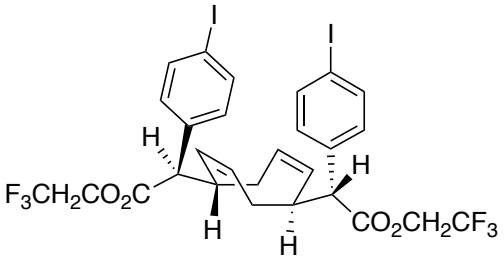

31

(2R,2'R)-bis(2,2,2-trifluoroethyl) 2,2'-((1S,2Z,5S,6Z)-cycloocta-2,6-diene-1,5-diyl)bis(2-(4-iodophenyl)acetate) 2.19: Derived from the reaction of diazo **IV** (0.9 mmol, 333 mg, 3.0 equiv) and COD (0.3 mmol, 32 mg, 1.0 equiv) following general procedure, major dr purified by $AgNO_3$ column chromatography (4-8% Et_2O in pentane). Product: 156 mg, 66 % yield; >99% ee.; dr = 6.8:1, white solid.

^{1}H NMR (600 MHz, $CDCl_3$) δ 7.68 – 7.64 (m, 4H), 7.08 – 7.05 (m, 4H), 5.46 (ddd, *J* = 12.4, 7.8, 5.4 Hz, 2H), 5.04 (dd, *J* = 11.5, 7.4 Hz, 2H), 4.50 (dq, *J* = 12.7, 8.4 Hz, 2H, **H of CH_2 next to CF_3**), 4.43 (dq, *J* = 12.7, 8.4 Hz, 2H, **H of CH_2 next to CF_3**), 3.55 – 3.47 (m, 2H), 3.44 (d, *J* = 10.0 Hz, 2H), 2.24 (dt, *J* = 15.3, 4.7 Hz, 2H), 2.14 (ddd, *J* = 15.6, 12.3, 8.2 Hz, 2H). ^{13}C NMR (151 MHz, $CDCl_3$) δ 171.02, 137.78, 135.66, 130.62, 129.83, 128.56, 122.81(q, J=277.7 Hz, **C of CF_3**), 93.61, 60.56 (q, J=36.7 Hz, **C of CH_2 next to CF_3**), 57.08, 41.57, 32.67. IR: 3017, 1752, 1485, 1405, 1281, 1168, 1138, 1063, 1007, 978, 815, 757, 644 (cm^{-1}); HRMS-(APCI) m/z: found at 792.9745 [$(M+H)^+$: $[C_{28}H_{25}O_4F_6I_2]^+$ calculates to be 792.9741]; $[\alpha]^{20}_D$: -7.1° (c=1.00, $CHCl_3$); m.p. 113-116 °C;

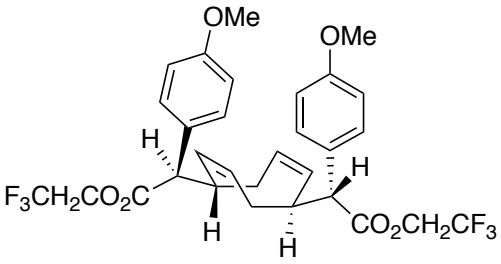

(2R,2'R)-bis(2,2,2-trifluoroethyl) 2,2'-((1S,2Z,5S,6Z)-cycloocta-2,6-diene-1,5-diyl)bis(2-(4-methoxyphenyl)acetate) 2.16: Derived from the reaction of diazo **V** (0.9 mmol, 247 mg, 3.0 equiv) and COD (0.3 mmol, 32 mg, 1.0 equiv) following general procedure, major dr purified by $AgNO_3$ column chromatography (4-8% Et_2O in pentane). Product: 96 mg, 53% yield; >99% ee.; dr = 4.2:1, white solid.

^{1}H NMR (600 MHz, $CDCl_3$) δ 7.26 – 7.23 (m, 4H), 6.90 – 6.83 (m, 4H), 5.45 (ddd, *J* = 12.1, 7.7, 5.1 Hz, 2H), 5.05 (dd, *J* = 11.5, 7.6 Hz, 2H), 4.49 (dq, *J* = 12.7, 8.4 Hz, 2H, **H of CH_2 next to CF_3**), 4.42 (dq, *J* = 12.7, 8.4 Hz, 2H, **H of CH_2 next to CF_3**), 3.80 (s, 6H), 3.63 – 3.52 (m, 2H), 3.44 (d, *J* = 10.3 Hz, 2H), 2.31 (dt, *J* = 15.4, 4.5 Hz, 2H), 2.19 (ddd, *J* = 15.7, 12.3, 8.1 Hz, 2H). ^{13}C NMR (151 MHz, $CDCl_3$) δ 171.78, 159.17, 130.32, 129.69, 128.18, 122.92 (q, J=277.7 Hz, **C of CF_3**), 114.06, 60.39 (q, J=36.6 Hz, **C of CH_2 next to CF_3**), 56.94, 55.21, 41.56, 32.93. IR: 2962, 2839, 1750, 1610, 1511, 1464, 1408, 1283, 1249, 1164, 1133, 1034, 977 (cm^{-1}); HRMS-(APCI) m/z: found at 601.2021 $[(M+H)^+$: $[C_{30}H_{31}O_6F_6]^+$ calculates to be 601.2029]; $[\alpha]^{20}_D$: -17.2° (c=1.00, $CHCl_3$); m.p. 89-93 °C

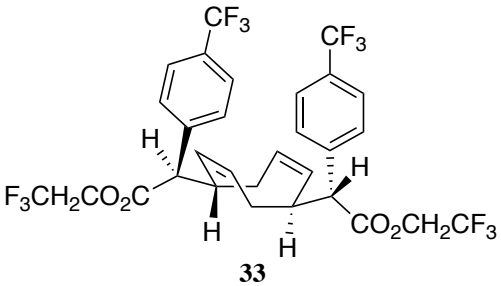

33

(2R,2'R)-bis(2,2,2-trifluoroethyl) 2,2'-((1S,2Z,5S,6Z)-cycloocta-2,6-diene-1,5-diyl)bis(2-(4-(trifluoromethyl)phenyl)acetate) 2.17: Derived from the reaction of diazo **VI** (0.9 mmol, 281 mg, 3.0 equiv) and COD (0.3 mmol, 32 mg, 1.0 equiv) following general procedure, major dr purified by $AgNO_3$ column chromatography (3-6% Et_2O in pentane). Product: 123 mg, 61 % yield; >99 % ee.; dr = 7.9:1, white solid.

^{1}H NMR (600 MHz, $CDCl_3$) δ 7.59 (d, *J* = 8.1 Hz, 4H), 7.45 (d, *J* = 8.1 Hz, 4H), 5.49 (ddd, *J* = 11.7, 8.0, 5.5 Hz, 2H), 5.06 (dd, *J* = 11.5, 7.0 Hz, 2H), 4.52 (dq, *J* = 12.7, 8.4 Hz, 2H, **H of CH_2 next to CF_3**), 4.44 (dq, *J* = 12.7, 8.4 Hz, 2H, **H of CH_2 next to CF_3**), 3.59 (d, *J* = 9.7 Hz, 2H), 3.58 – 3.50 (m, 3H), 2.25 (dt, *J* = 14.4, 4.3 Hz, 2H), 2.16 (ddd, *J* = 15.1, 11.6, 8.4 Hz, 2H). ^{13}C NMR (126 MHz, $cdcl_3$) δ 170.77, 139.84, 130.13 (q, J=32.5 Hz, **C on Ar ring next to CF_3**), 129.61, 129.14, 128.70, 125.57 (q, J=3.6 Hz, **C on Ar ring next to the 130.13 C**), 123.97 (q, J=272.3 Hz, **C of CF_3 on the Ar ring**), 122.74 (q, J=277.4 Hz, **C of CF_3 in the ester**), 60.60 (q, J=36.7 Hz, **C of CH_2 next to CF_3 in ester**), 57.22, 41.75, 32.52. IR: 3021, 1754, 1619, 1422, 1325, 1285, 1163, 1127, 1069, 1020, 979, 827, 723 (cm^{-1}); HRMS-(APCI) m/z: found at 677.1551 [$(M+H)^+$: $[C_{30}H_{25}O_4F_{12}]^+$ calculates to be 677.1556]; $[\alpha]^{20}_D$: -35.8° (c=1.00, $CHCl_3$); m.p. 96-101 °C

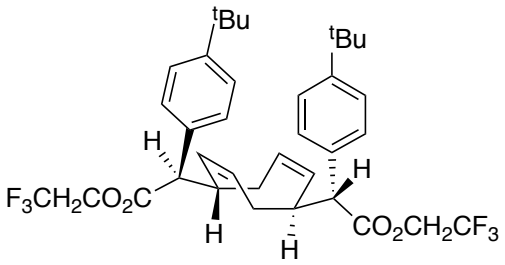

34

(2R,2'R)-bis(2,2,2-trifluoroethyl) 2,2'-((1S,2Z,5S,6Z)-cycloocta-2,6-diene-1,5-diyl)bis(2-(4-(tert-butyl)phenyl)acetate) 2.18: Derived from the reaction of diazo **VII** (0.9 mmol, 270 mg, 3.0 equiv) and COD (0.3 mmol, 32 mg, 1.0 equiv) following general procedure, major dr purified by $AgNO_3$ column chromatography (2-6% Et_2O in pentane). Product: 150 mg, 76 % yield; >99 % ee.; dr = 6.8:1, sticky oil to half solid.

^{1}H NMR (600 MHz, $CDCl_3$) δ 7.35 – 7.29 (m, 4H), 7.25 – 7.22 (m, 4H), 5.45 (ddd, *J* = 12.6, 7.6, 5.7 Hz, 2H), 5.07 (dd, *J* = 11.6, 7.2 Hz, 2H), 4.51 (dq, *J* = 12.7, 8.4 Hz, 2H, **H of CH_2 next to CF_3**), 4.37 (dq, *J* = 12.7, 8.4 Hz, 2H, **H of CH_2 next to CF_3**), 3.53 (m, 2H), 3.48 (d, *J* = 10.2 Hz, 2H), 2.33 – 2.19 (m, 4H), 1.30 (s, 18H). ^{13}C NMR (101 MHz, $CDCl_3$) δ 171.75, 150.59, 132.91, 130.36, 128.24, 128.08, 125.53, 122.90 (q, J=277.6 Hz, **C of CF_3**), 60.36 (q, J=36.5 Hz, **C of CH_2 next to CF_3**), 57.18, 41.59, 34.47, 32.56. IR: 2965, 1753, 1509, 1408, 1365, 1283, 1167, 1134, 1065, 1019, 978, 842, 823 (cm^{-1}); HRMS-(APCI) m/z: found at 653.3066 [$(M+H)^+$: $[C_{36}H_{43}O_4F_6]^+$ calculates to be 653.3060]; $[\alpha]^{20}_D$: -31.0° (c=1.00, $CHCl_3$);

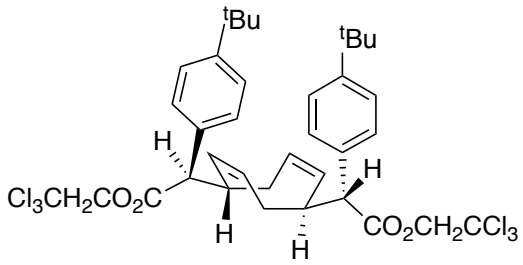

35

(2R,2'R)-bis(2,2,2-trichloroethyl) 2,2'-((1S,2Z,5S,6Z)-cycloocta-2,6-diene-1,5-diyl)bis(2-(4-(tert-butyl)phenyl)acetate) 2.20: Derived from the reaction of diazo **XII** (0.9 mmol, 315 mg, 3.0 equiv) and COD (0.3 mmol, 32 mg, 1.0 equiv) following general procedure, major dr purified by normal column chromatography (4-8% Et_2O in pentane). Product: 231 mg, 72 % yield; >99 % ee.; dr = 4.5:1, white foam solid. (Single crystal structure obtained for the reduction product of this compound.)

^{1}H NMR (600 MHz, $CDCl_3$) δ 7.36 – 7.27 (m, 9H), 5.46 (ddd, *J* = 11.9, 7.2, 4.9 Hz, 2H), 5.08 (dd, *J* = 11.6, 7.5 Hz, 2H), 4.73 (d, *J* = 12.0 Hz, 3H, **H of CH_2 next to CCl_3**), 4.69 (d, *J* = 12.0 Hz, 3H, **H of CH_2 next to CCl_3**), 3.78 – 3.68 (m, 2H), 3.50 (d, *J* = 10.5 Hz, 2H), 2.52 – 2.44 (m, 2H), 2.22 (ddd, *J* = 15.8, 12.2, 7.9 Hz, 2H), 1.31 (s, 18H). ^{13}C NMR (151 MHz, $CDCl_3$) δ 171.56, 150.60, 133.19, 130.53, 128.47, 128.12, 125.53, 94.82, 74.25, 58.00, 41.03, 34.51, 33.43, 31.32. IR: 2963, 1749, 1516, 1461, 1366, 1269, 1200, 1131, 1058, 915, 827, 771, 721 (cm^{-1}); HRMS-(APCI) m/z: found at 749.1296 [$(M+H)^+$: $[C_{36}H_{43}O_4Cl_6]^+$ calculates to be 749.1287]; $[\alpha]^{20}_D$: +10.2° (c=1.00, $CHCl_3$); m.p. 72-77 °C

Derivatization for Bis-insertion C2 symmetric chiral COD ligand

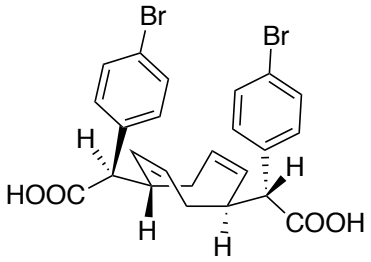

(2R,2'R)-2,2'-((1S,2Z,5S,6Z)-cycloocta-2,6-diene-1,5-diyl)bis(2-(4-bromophenyl)acetic acid) 2.26: Bis-insertion compound **2.14** (0.053 mmol, 41.9 mg, 1.0 equiv.) was dissolved in 1 mL AcOH. Zn powder (34.4 mg, 10 equiv.) was added to the solution, and the suspension was kept stirring overnight. Crude material was obtained by filtration and concentration under reduced pressure. Further column chromatography (50% Et_2O in pentane with 0.5% AcOH) gave pure product as white powder 17.2 mg, 61% yield.

^{1}H NMR (600 MHz, $CDCl_3$) δ 7.46 (d, *J* = 8.3 Hz, 4H), 7.23 (d, *J* = 8.6 Hz, 4H), 5.58 – 5.37 (m, 2H), 5.18 – 4.99 (m, 2H), 3.44 (d, *J* = 9.5 Hz, 2H), 3.40 – 3.25 (m, 2H), 2.49 – 2.31 (m, 2H), 2.32 – 2.21 (m, 2H). ^{13}C NMR (151 MHz, $CDCl_3$) δ 178.89, 135.49, 131.75, 130.45, 130.30, 128.50, 121.83, 57.01, 42.16, 31.86, 20.58. IR: 2921, 2851, 1725, 1488, 1409, 1263, 1098, 1012, 800, 730 (cm^{-1}); HRMS-(APCI) m/z: found at 530.9817 [$(M-H)^-$: $[C_{24}H_{21}O_4Br_2]^-$ calculates to be 530.9812]; $[\alpha]^{20}_D$: -14.0° (c=1.00, acetone); m.p. > 200 °C

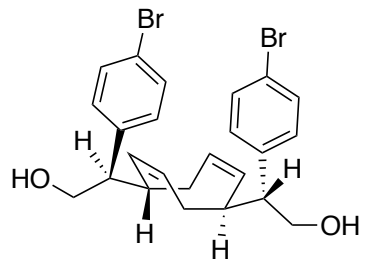

(2R,2'R)-2,2'-((1S,2Z,5S,6Z)-cycloocta-2,6-diene-1,5-diyl)bis(2-(4-bromophenyl)ethan-1-ol) 2.27: Bis-insertion compound **2.14** (0.065 mmol, 51.9 mg, 1.0 equiv.) was dissolved in 1 mL anhydrous THF, and the solution was cooled to -78 °C. $LiAlH_4$ (1.0 M THF solution) (0.18 mL, 2.5 equiv.) was slowly added to the stirring solution. The reaction was kept running for 2 h at -78 °C, then raised to r.t. for 15 min and quenched with 1mL sodium potassium tartrate solution(saturated) and 1.0 mL HCl(1.0 M). The organic phase was extracted with Et_2O multiple times, combined and dried over $MgSO_4$. Crude material was obtained through filtration and concentration under reduced pressure. Further column chromatography (60% Et_2O in pentane) gave pure product 27.5 mg as white powder, 84% yield.

^1H NMR (600 MHz, $CDCl_3$) δ 7.40 (d, *J* = 8.5 Hz, 4H), 6.94 (d, *J* = 8.4 Hz, 4H), 5.54 (ddd, *J* = 11.4, 9.0, 7.4 Hz, 2H), 5.32 (dd, *J* = 11.4, 6.3 Hz, 2H), 3.83 (dq, *J* = 7.5, 4.1, 3.5 Hz, 4H), 2.73 (dp, *J* = 11.8, 5.7 Hz, 4H), 1.72 (ddd, *J* = 12.2, 7.1, 4.9 Hz, 2H), 1.64 (dt, *J* = 13.2, 6.8 Hz, 2H). ^{13}C NMR (151 MHz, $CDCl_3$) δ 138.44, 131.18, 130.69, 129.52, 129.48, 120.73, 64.44, 53.00, 41.08, 31.63. IR: 3342 (broad OH), 3006, 2930, 2874, 1488, 1408, 1105, 1073, 1027, 1007, 819, 754 (cm^{-1}); HRMS-(APCI) m/z: found at 505.0376 $[(M+H)^+ : [C_{24}H_{27}O_2Br_2]^+$ calculates to be 505.0372]; $[\alpha]^{20}_D$: -129.2° (c=1.00, $CHCl_3$); m.p. 69-73 °C

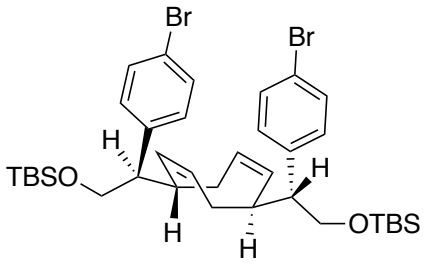

(1Z,3S,5Z,7S)-3,7-bis((R)-1-(4-bromophenyl)-2-((tert-butyldimethylsilyl)oxy)ethyl)cycloocta-1,5-diene 2.28: The di-ol starting material **2.27** (0.063

mmol, 31.7 mg, 1.0 equiv.) was dissolved in 1 mL DCM, and the solution was cooled to 0 °C. Imidazole (0.158 mmol, 10.8 mg, 2.5 equiv.) and TBSCl (0.139 mmol, 21.0 mg, 2.2 equiv.) was added to the solution, and the solution was kept stirring overnight. Crude material was obtained by filtration and concentration under reduced pressure. Further column chromatography gave pure product as white solid. 42.0 mg, 90% yield.

^{1}H NMR (600 MHz, $CDCl_3$) δ 7.33 (d, *J* = 8.4 Hz, 4H), 6.92 (d, *J* = 8.4 Hz, 4H), 5.54 (ddd, *J* = 11.3, 8.7, 7.0 Hz, 2H), 5.32 (dd, *J* = 11.4, 7.1 Hz, 2H), 3.76 (dd, *J* = 10.0, 7.2 Hz, 2H), 3.70 (dd, *J* = 10.0, 6.0 Hz, 2H), 2.93 (dq, *J* = 12.6, 6.2 Hz, 2H), 2.59 (q, *J* = 6.4 Hz, 2H), 1.79 (dt, *J* = 12.2, 6.0 Hz, 2H), 1.61 (td, *J* = 14.0, 9.2 Hz, 2H), 0.84 (s, 18H), -0.03 (s, 6H), -0.04 (s, 6H). ^{13}C NMR (151 MHz, $CDCl_3$) δ 139.82, 130.72, 130.67, 129.92, 129.47, 120.14, 64.52, 52.96, 39.99, 32.09, 25.86, 18.21, 0.00, -5.50. IR: 3008, 2953, 2928, 2885, 2856, 1488, 1471, 1408, 1361, 1254, 1097, 1074, 1010 (cm^{-1}); HRMS-(APCI) m/z: found at 733.2095 [$(M+H)^+$: $[C_{36}H_{55}O_2Br_2Si_2]^+$ calculates to be 733.2102]; $[\alpha]^{20}_D$: -109.0° (c=1.00, $CHCl_3$); m.p. 67-69 °C

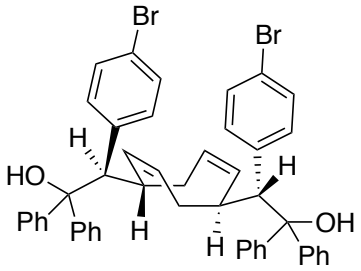

(2R,2'R)-2,2'-((1S,2Z,5S,6Z)-cycloocta-2,6-diene-1,5-diyl)bis(2-(4-bromophenyl)-1,1-diphenylethan-1-ol) 2.29a: The bis-insertion compound **2.14** (0.756 mmol, 380 mg, 1.0 equiv) was dissolved in 4 mL anhydrous THF. The solution was kept stirring under Ar at -78 °C. PhLi (1.9 M purchased from Sigma Aldrich) in THF 2.6 mL was slowly added to the stirring solution over 30 min. The reaction was maintained at -78 °C for 3 h. After that, the solution was diluted

with 4 mL Et_2O and quenched with HCl (1.0 M). The organic layer was extracted 3 times with Et_2O (1 mL), combined and dried over $MgSO_4$. Flash cotton pipette (a layer of silica) plug and concentration under reduced pressure gave crude sticky oil. Flash column chromatography (15% Et_2O/pentane) for the crude to remove nonpolar impurity and gave greenish yellow solid. Pure product was further obtained through recrystallization with ether/pentane system (40 °C cool to 0 °C) as white solid, 275mg, 50% yield.

^1H NMR (600 MHz, $CDCl_3$) δ 7.55 (dd, *J* = 8.4, 1.1 Hz, 4H), 7.33 (t, *J* = 7.8 Hz, 4H), 7.24 – 7.19 (m, 6H), 7.18 – 7.14 (m, 4H), 7.11 – 6.99 (m, 8H), 6.93 (t, *J* = 7.3 Hz, 2H), 5.48 (dd, *J* = 11.3, 7.2 Hz, 2H), 5.45 – 5.36 (m, 2H), 3.58 (d, *J* = 3.3 Hz, 2H), 2.67 (s, 2H), 2.66 – 2.54 (m, 2H), 1.46 – 1.32 (m, 4H). ^{13}C NMR (151 MHz, $CDCl_3$) δ 146.72, 146.05, 136.94, 133.10, 130.23, 130.04, 129.81, 128.54, 127.76, 126.76, 126.11, 125.42, 125.11, 120.34, 81.42, 58.20, 40.19, 33.32. IR: 3586(Broad), 3057, 3021, 2974, 2868, 1597, 1488, 1447, 1157, 1112, 1075, 1068, 1010 (cm^{-1}); HRMS-(ESI) m/z: found at 843.1261 [$(M+Cl)^-$: $[C_{48}H_{42}O_2Br_2Cl]^-$ calculates to be 843.1246]; $[\alpha]^{20}_D$: -94.3° (c=1.00, $CHCl_3$); m.p. > 200 °C

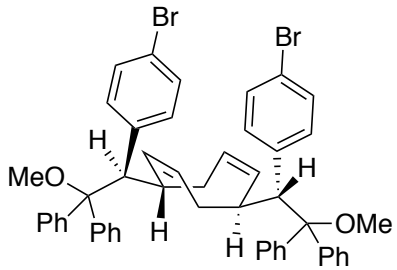

(1Z,3S,5Z,7S)-3,7-bis((R)-1-(4-bromophenyl)-2-methoxy-2,2-diphenylethyl)cycloocta-1,5-diene 2.30a: The di-ol starting material **2.29a** (59.7 mg, 0.074 mmol, 1 equiv) was dissolved in 1.5 mL anhydrous DCM. NaH (17.8 mg, 60% wt in mineral oil, 0.74 mmol, 10 equiv) was added

into the solution, and the suspension was kept stirring at 0 °C. CH_3I (52.5 mg, 0.37 mmol, 5 equiv) was then added to the solution. The reaction was let warm up to r.t. naturally and run overnight. After that, the reaction was quenched with NH_4Cl(saturated) and extracted with Et_2O multiple times. The organic layer was combined and dried over $MgSO_4$. Crude material was obtained through filtration and concentration under reduced pressure. Further column chromatography gave pure product as white solid 50.8 mg, 82% yield.

^1H NMR (600 MHz, $CDCl_3$) δ 7.27 (s, 10H), 7.24 (d, *J* = 8.6 Hz, 4H), 7.22 – 7.11 (m, 10H), 6.80 (d, *J* = 7.8 Hz, 4H), 5.09 – 4.97 (m, *J* = 7.9 Hz, 4H), 3.32 (d, *J* = 4.1 Hz, 2H), 2.78 (s, 6H), 2.64 – 2.44 (m, 2H), 1.37 – 1.29 (m, 2H), 1.18 (td, *J* = 13.8, 7.6 Hz, 2H). ^{13}C NMR (126 MHz, $CDCl_3$) δ 141.29, 137.95, 133.89, 130.74, 129.57, 128.95, 127.97, 127.48, 127.38, 127.35, 127.16, 120.08, 87.29, 60.76, 52.53, 40.52, 34.10, 29.70. IR: 3021, 2929, 2826, 1488,1446, 1407, 1193, 1074, 1010, 828, 756, 729, 702 (cm^{-1}); HRMS-(APCI) m/z: found at 871.1572 [$(M+Cl)^-$: $[C_{50}H_{46}O_2Br_2Cl]^-$ calculates to be 871.1559]; $[\alpha]^{20}_D$: -75.7° (c=1.00, $CHCl_3$); m.p. 91-96 °C

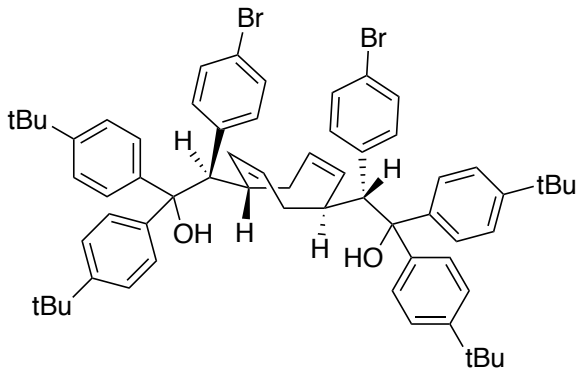

(2R,2'R)-2,2'-((1S,2Z,5S,6Z)-cycloocta-2,6-diene-1,5-diyl)bis(2-(4-bromophenyl)-1,1-bis(4-(tert-butyl)phenyl)ethan-1-ol) 2.29b: The bis-insertion compound **2.14** (0.1 mmol, 56.0 mg, 1.0 equiv.) was dissolved in 1 mL anhydrous THF, and the solution was cooled to -78 °C. ^{t}BuPhLi solution (prepared from Li and 4-^{t}BuPhBr, 0.94 M) (0.6 mL, 5.5 equiv.) was added to the stirring

solution, and the reaction was let run for 2 h at -78 °C. After that, the reaction was quenched with NH_4Cl (saturated) 1 mL , HCl (1.0 M) 1 mL and extracted with Et_2O multiple times. The organic phase was combined, dried over $MgSO_4$, filtered and concentrated to obtain crude material. Further column purification (5-8% Et_2O in pentane) gave pure product as white powder 43.5 mg, 42% yield.

^1H NMR (600 MHz, $CDCl_3$) δ 7.44 (d, *J* = 8.6 Hz, 4H), 7.32 (d, *J* = 8.5 Hz, 4H), 7.16 (d, *J* = 8.7 Hz, 4H), 7.11 (d, *J* = 8.8 Hz, 4H), 7.03 (d, *J* = 8.8 Hz, 8H), 5.52 (dd, *J* = 11.3, 7.2 Hz, 2H), 5.46 – 5.35 (m, 2H), 3.51 (d, *J* = 3.3 Hz, 2H), 2.67 (s, 2H), 2.56-2.60 (m, 2H), 1.36 – 1.31 (m, 4H), 1.30 (s, 18H), 1.15 (s, 18H). ^{13}C NMR (151 MHz, $CDCl_3$) δ 149.24, 148.64, 143.59, 143.29, 137.25, 133.14, 130.06, 129.71, 125.25, 125.12, 124.81, 124.57, 120.13, 81.20, 58.51, 40.33, 34.35, 34.12, 33.20, 31.35, 31.17. IR: 3580, 2962, 2867, 1509, 1487, 1404, 1363, 1269, 1109, 1076, 1010, 909, 839 (cm^{-1}); HRMS-(APCI) m/z: found at 1050.4424 [$(M+NH_4)^+$: $[C_{64}H_{78}O_2NBr_2]^+$ calculates to be 1050.4394]; $[\alpha]^{20}_D$: -98.5° (c=1.00, $CHCl_3$); m.p. > 200 °C

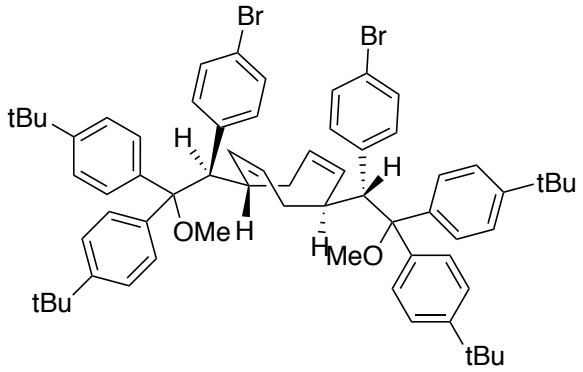

(1Z,3S,5Z,7S)-3,7-bis((R)-1-(4-bromophenyl)-2,2-bis(4-(tert-butyl)phenyl)-2-methoxyethyl)cycloocta-1,5-diene 2.30b: The di-ol starting material **2.29b** (37.9 mg, 0.037 mmol, 1 equiv) was dissolved in 1.5 mL anhydrous DCM. NaH (15 mg, 60% wt in mineral oil,

0.37 mmol, 10 equiv) was added into the solution, and the reaction was kept stirring at 0 °C. CH_3I (20.8 mg, 0.148 mmol, 4 equiv) was then added to the solution and the reaction was let warm up to r.t. overnight. After that, the reaction was quenched with NH_4Cl(saturated) 1 mL and extracted with Et_2O multiple times. The organic layer was combined and dried over $MgSO_4$, filtered and concentrated to yield crude material. Further column chromatography purification gave pure product 33.2 mg, 90% yield.

^{1}H NMR (600 MHz, $CDCl_3$) δ 7.28 (d, *J* = 8.7 Hz, 4H), 7.24 (dd, *J* = 8.8, 1.8 Hz, 9H), 7.09 (d, *J* = 8.8 Hz, 4H), 6.95 (d, *J* = 8.7 Hz, 8H), 5.12 (qd, *J* = 11.6, 7.0 Hz, 4H), 3.15 (d, *J* = 2.4 Hz, 2H), 2.82 (s, 6H), 2.29 – 2.19 (m, 2H), 1.30 (s, 18H), 1.24 (s, 18H), 1.11 – 0.95 (m, 4H). ^{13}C NMR (151 MHz, $CDCl_3$) δ 149.94, 149.56, 139.54, 138.40, 137.95, 134.15, 130.42, 129.68, 129.57, 128.41, 128.22, 124.35, 123.90, 119.99, 87.70, 60.93, 52.92, 41.22, 34.39, 34.30, 33.07, 31.37, 31.25. IR: 2962, 2903, 2868, 1508, 1486, 1403, 1363, 1271, 1110, 1083, 1011, 966, 833 (cm^{-1}); HRMS-(APCI) m/z: found at 1083.4276 $[(M+Na)^+$: $[C_{66}H_{78}O_2Br_2Na]^+$ calculates to be 1083.4261]; $[\alpha]^{20}_D$: -132.7° (c=1.00, $CHCl_3$); m.p. 159-163 °C

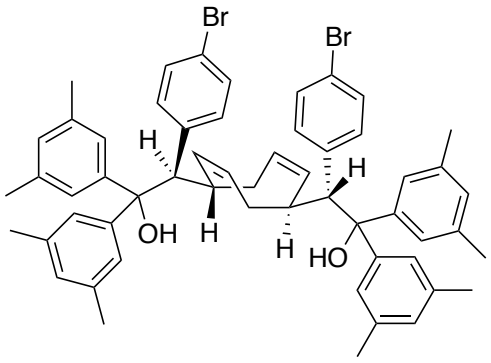

(2R,2'R)-2,2'-((1S,2Z,5S,6Z)-cycloocta-2,6-diene-1,5-diyl)bis(2-(4-bromophenyl)-1,1-bis(3,5-dimethylphenyl)ethan-1-ol) 2.29c: Bis-insertion ester **2.14** (0.1 mmol, 56.0 mg, 1.0

equiv.) was dissolved in 1 mL anhydrous THF, and the solution was cooled to -78 °C. 3,5-diMePhLi solution (prepared from Li and 3,5-di-Methyl-4-Br-benzene, 0.73 M) (0.75 mL, 5.5 equiv.) was slowly added to the stirring solution, and the reaction was let run for 2 h at -78 °C. After that, the reaction was quenched with NH_4Cl (saturated) 1 mL, HCl (1.0 M) 1mL and extracted with Et_2O multiple times. The organic phase was combined, dried over $MgSO_4$, and concentrated to give crude material. Further column purification (2-5% Et_2O in pentane) gave pure product as white solid 52.1 mg, 56% yield.

^1H NMR (600 MHz, $CDCl_3$) δ 7.16 (d, *J* = 8.7 Hz, 4H), 7.13 (s, 4H), 7.11 – 6.98 (m, 4H), 6.82 (d, *J* = 7.7 Hz, 6H), 6.56 (s, 2H), 5.51 (dd, *J* = 11.4, 7.1 Hz, 2H), 5.44 – 5.33 (m, 2H), 3.51 (d, *J* = 3.2 Hz, 2H), 2.54 – 2.49 (m, 2H), 2.50 (s, 2H), 2.29 (s, 12H), 2.10 (s, 12H), 1.38 – 1.27 (m, 4H). ^{13}C NMR (151 MHz, $CDCl_3$) δ 146.75, 146.21, 137.70, 137.40, 136.92, 133.13, 130.09, 130.03, 129.69, 128.33, 127.73, 123.38, 122.84, 120.11, 81.28, 58.39, 40.38, 33.36, 21.69, 21.45. IR: 3586, 2007, 2916, 1597, 1487, 1408, 1376, 1216, 1157, 1111, 1075, 1010, 843 (cm^{-1}); HRMS-(APCI) m/z: found at 920.2830 [(M) : $[C_{56}H_{58}O_2Br_2]$ calculates to be 920.2809]; $[\alpha]^{20}_D$: -121.0° (c=1.00, $CHCl_3$); m.p. 140-144 °C

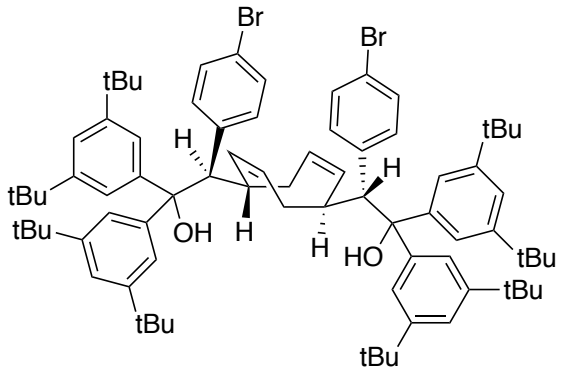

(2R,2'R)-2,2'-((1S,2Z,5S,6Z)-cycloocta-2,6-diene-1,5-diyl)bis(2-(4-bromophenyl)-1,1-bis(3,5-di-tert-butylphenyl)ethan-1-ol) 2.29d: Bis-insertion ester **2.14** (0.1 mmol, 56.0 mg, 1.0 equiv.) was dissolved in 1 mL anhydrous THF, and the solution was cooled to -78 °C. 3,5-ditBuPhLi solution (prepared from Li and 3,5-di-tBu-4-Br-benzene, 1.1 M) (0.5 mL, 5.5 equiv.) was slowly added to the stirring solution, and the reaction was let run for 4 h at -78 °C. After that, the reaction was quenched with NH_4Cl (saturated) 1 mL, HCl (1.0 M) 1mL. The organic phase was extracted with Et_2O multiple times, combined, dried over $MgSO_4$, and concentrated to give crude material. Further column purification (0-2% Et_2O in pentane) gave pure product as white solid 55.3 mg, 44% yield.

^{1}H NMR (600 MHz, $CDCl_3$) δ 7.42 (d, *J* = 1.7 Hz, 4H), 7.25 (t, *J* = 1.7 Hz, 2H), 7.11 (d, *J* = 8.7 Hz, 4H), 6.96 (dd, *J* = 13.7, 1.7 Hz, 10H), 5.46 (dd, *J* = 11.4, 6.7 Hz, 2H), 5.43 – 5.37 (m, 2H), 3.36 (d, *J* = 3.2 Hz, 2H), 2.60 – 2.53 (m, 2H), 2.55 (s, 2H), 1.44 – 1.32 (m, 4H), 1.30 (s, 36H), 1.09 (s, 36H). ^{13}C NMR (151 MHz, $CDCl_3$) δ 150.17, 149.36, 145.00, 144.92, 137.31, 133.18, 130.16, 129.82, 129.59, 120.30, 120.23, 120.20, 120.02, 119.79, 82.28, 60.07, 40.76, 34.95, 34.70, 33.53, 31.55, 31.29. IR: 3609, 2962, 2904, 2866, 1598, 1487, 1477, 1393, 1362, 1248, 1109, 1076, 1011, 879 (cm^{-1}); HRMS-(APCI) m/z: found at 1279.6415 [$(M+Na)^+$: $[C_{80}H_{106}O_2Br_2Na]^+$ calculates to be 1279.6452] $[\alpha]^{20}_D$: -35.8° (c=1.00, $CHCl_3$); m.p. 128-131 °

General Procedure for conjugate addition test (Arylation of cyclohex-2-enone)

To an oven dried 4 mL vial with a stir bar was weighed di-μ-chlorotetraethylene dirhodium (0.025 equiv) and cyclooctadiene derived ligand (0.055 equiv). The vial was wrapped with Teflon™ thread tape, fitted with a septum cap and the atmosphere was exchanged for a dry N_2

atmosphere (3 cycles, 1 minute per cycle). Dry, nitrogen sparged 1,4-dioxane (1.8 mL) was then added to the vial and placed on a preheated hotplate at 50 °C to stir for 20 minutes under N_2. Aqueous potassium hydroxide (0.18 mL, 56.1 mg/mL, 0.50 equiv, sparged with N_2) was added to the reaction vial via syringe and allowed to stir for an additional 10 minutes at temperature. The vial was opened for addition of solid phenylboronic acid (3 equiv), then quickly resealed and the headspace was purged under positive pressure with addition of a vent needle for 1 minute. To the vial was added cyclohex-2-enone (0.2 mmol, 1 equiv) via syringe and the vial was fitted with a N_2 balloon and allowed to stir at temperature for 12 hours. The reaction was removed from heat, allowed to cool, and diluted with diethyl ether and passed through a silica plug. The combined organics were dried over sodium sulfate and concentrated under reduced pressure. The crude mixture was then purified by flash chromatography on silica gel in a gradient of Hexanes: EtOAc (97:3 → 90:10) to afford the pure 3-phenylcyclohexan-1-one. Spectra agreed with published results (*J. Am. Chem. Soc.* **2008**, *130*, 7, 2172–2173).

Part 2: Applications of Transmetallation in Group IX Metal Catalysis

Chapter 3: Introduction to Traceless C–H Directing Groups

3.1 Introduction to Directed Metal C–H Functionalization

In this chapter we will discuss introduce metal directed C–H functionalization, the importance of directing groups, their uses, and limitations. Specifically, we will focus on the design, synthesis, and use of traceless directing groups in modern transition metal catalyzed reactions. Furthermore, this chapter will serve to outline the state of art methods in the field of traceless directing groups.

3.1.1 Brief History of Directed Metal C–H Functionalization

The widespread inclusion of heterocyclic moieties in popular agrochemicals and pharmaceuticals is indicative of the current leanings in modern small molecule discovery.[1] While the number of these heterocyclic molecules have increased exponentially, the synthetic techniques employed to access these scaffolds remains somewhat stagnant. This reliance on linear synthesis from acyclic precursors with preinstalled functionality severely restricts the ability for quick

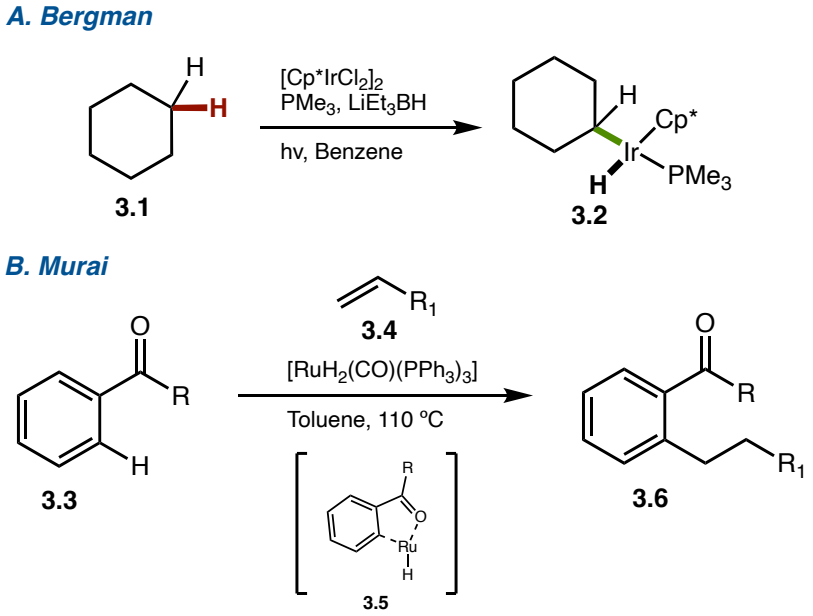

Scheme 1. Historical perspective of modern C–H functionalization's beginnings and the advancement to directed C–H activation strategies employed today.

diversification of these heterocycles. In response to these limitations, late-stage functionalization of C–H bonds has become increasingly relied on over the past several decades, however, non-directed activation of a desired C–H bond remains a challenge.[2] The beginning of this modern gold rush in C–H bond activation is normally credited to Bergman[3a] and Graham[3b] for their independent work utilizing iridium(I) pentamethylcyclopentadiene complexes to functionalize saturated hydrocarbons in 1982 (**Scheme 1.A**). Shortly thereafter in 1993, Murai and coworkers disclosed the seminal study on transition-metal catalyzed directed C–H activation. The group utilized an *ortho*-ketone functionality to direct ruthenium into the adjacent aryl C–H and utilize simple alkenes as an alkylating reagent (**Scheme 1.B**).[3c] Following this disclosure, many groups began utilizing an adjacent directing group (DG), generally consisting of a Lewis basic moiety, to serve as an internal metal coordination site that generated a metallocycle intermediate with improved stability.[2] Jin-Quan Yu and Guangbin Dong, among many others, have developed a vast number of methods for directed C–H functionalization,[2] however the chemistry still suffers from unwanted functionality, the DG, being present in the final molecule. Fortuitously, the increased interest in C–H functionalization over the last 60 years has led to the development of a range of new DGs with various modifications to promote facile removal, use, and/or atom economy.[4] When comparing the new classes of DGs, they offer a rough division into three classes: 1. Permanent Directing Groups; 2. Transient Directing Groups; 3. Traceless Directing Groups. While all of these offer the molecular foreman to construct their desired functionality, the choice must be weighed on a molecule-to-molecule basis due to the group's inherent limitations.

Diving deeper, the term "permanent" DG applies to functionality placed onto the molecule prior to the directed metalation step and remains following the desired functionalization (**Figure 1.A**). These groups are irremovable during the reaction or one that requires extra synthetic steps

A. Permanent Directing Groups

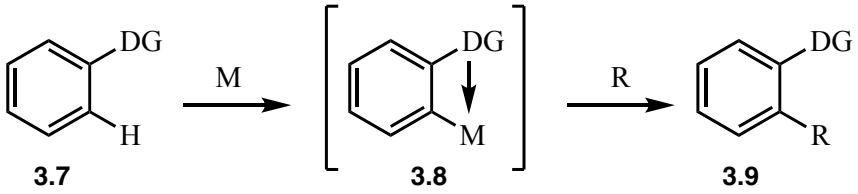

3.7 **3.8** **3.9**

B. Transient Directing Groups

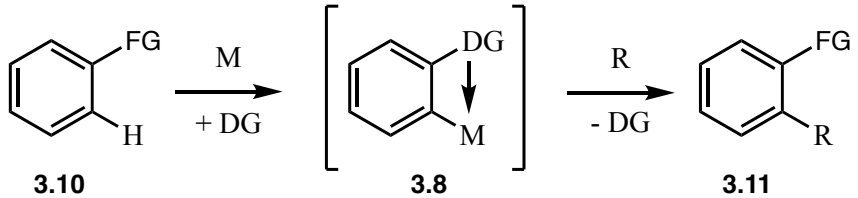

3.10 **3.8** **3.11**

C. Traceless Directing Groups

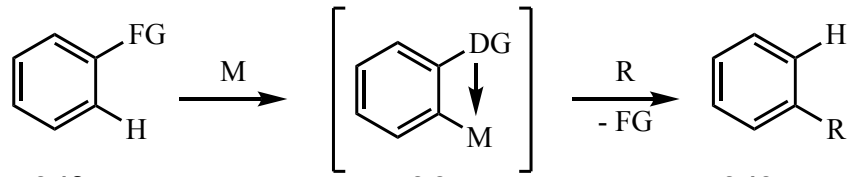

3.12 **3.8** **3.13**

Figure 1. Directing groups methodology commonly encountered in transition catalyzed C–H functionalization.

to remove following the functionalization. Permanent DGs encompass of wide variety of monodentate and bidentate functionalities to include some of the more common ones such as ketones, esters, amides, 2-pyridyl, and 8-aminoquinolone derived amides.[4] Despite the vast array of transformations relying on permanent DGs, their usefulness is limited in industrial applications due to the need for your molecular scaffold to incorporate/tolerate the DG moiety in the final structure. Additionally, the typical removal conditions are sometimes quite harsh and will not tolerate much of the desired functionality prevalent in compounds today.[4b-c] In response to these limitations, researchers began developing transient DGs through the use of easily reversible reactions *in-situ*.

Transient DGs leverage the reversibility of processes such as condensations[5] or phosphorylation[6] to allow for formation of a DG *in-situ* and then subsequently be removed during the workup (**Scheme 1.B**). This strategy allows for more manageable functional groups such as aldehydes, ketones, and phenols to be converted into highly Lewis basic functionalities during the reaction but return as useful synthetic handles for the following steps.[7] While this strategy has significantly increased the usefulness of DG chemistry, the need to ablate/convert an unwanted functional group in following steps still leaves something to be desired in new methodologies. Significant care must be taken in these catalytic reactions due to the ability for the free functionality, of the substrate and/or the pre-complexed directing group from errant, irreversible coordination of the transition metal. The academe's call for better methods with more atom economic processes is slowly being met with the development of a new class of DG chemistry, traceless DGs.

Traceless DGs are defined by their ability to promote metal engagement and then to facilitate the desired distal C–H functionalization before being ablated during the reaction (**Figure 1.C**). The functional groups most prevalent in the emerging field have been carboxylic acids[8,9], halogens [10-13], and boron[14,15], however carboxylic acids are the current field leader due to the ability to leave a free C–H bond following decarboxylation. Additionally, the access to carboxylic acids of relevant substrates, paired with its robust methods have led to significant advances in the field. Despite this inequity, the availability and prevalence of halogenated/borylated substrates has increased substantially with industry's reliance on cross-coupling methods for the rapid development of complex motifs. In the past two decades, the power of halogenated substrates to promote oxidative addition of a transition metal, followed by subsequent C–H insertion, and reductive elimination has become quite useful in intramolecular and domino annulation

strategies.[11-13] This oxidative addition strategy, first disclosed by Ames[16] and Dyker[17,18], served as inspiration for Baudouin and coworkers as they began to showcase the wide utility of this strategy for traceless DG annulation chemistry via palladium metal (**Figure 1.A**).[19] Despite this methodology proving quite effective, the next logical on-ramp to these catalytic cycles, transmetallation, has not been pursued adequately to date.

3.2 Current Directing Groups Strategy in C–H Functionalization

3.2.1 Permanent Directing Groups and Their Removal

The discovery of directed C–H functionalization and by extension, permanent directing groups is attributed to Murahasi in 1955 in which he published a cobalt catalyzed, ortho insertion of carbon monoxide, into an aryl C–H of azobenzene and aldimine.[20] This directly led to the

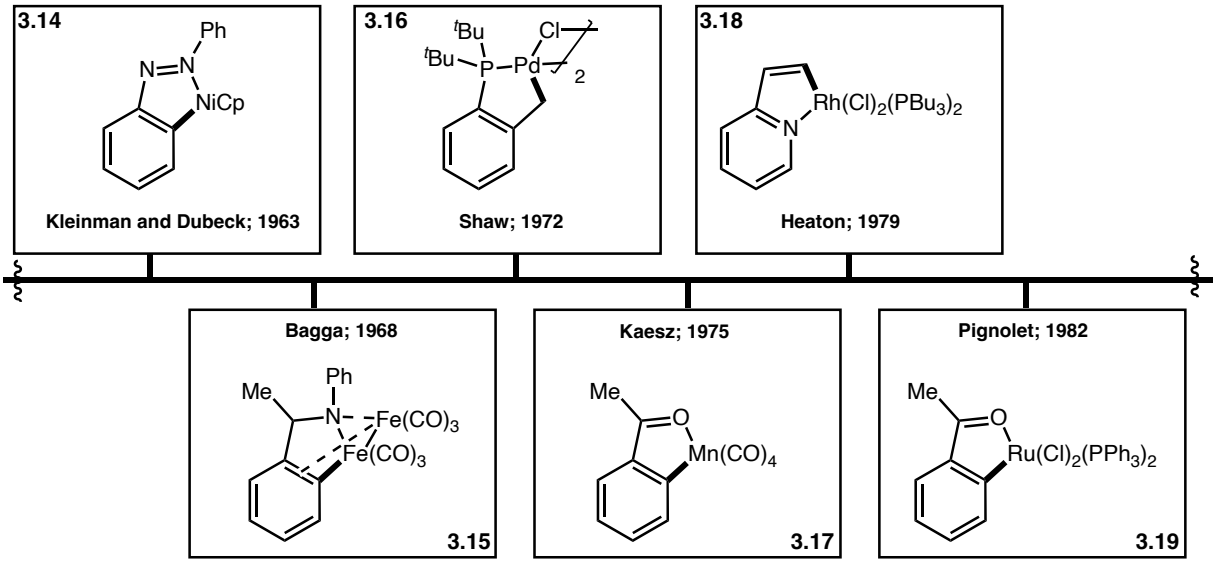

Figure 2. Brief timeline of pioneering work on stochiometric C–H functionalization utilizing permanent directing groups to access cyclometalated intermediates of transition metals.

widespread investigation by several scientists during the mid-20th century on stochiometric complexes that mirrored the unique metallocycle intermediate observed by Murahashi (**Figure 2**).[21] It is interest to note that the catalytic method predated the stochiometric studies by nearly a

decade and required a further decade to return to highly developed catalytic methods once more. The stochiometric complexes did provide key insights into the formation and control of metallocycles formed via C–H activation as they allowed for the determination of regioselectivity and evaluation of the Lewis basic moieties to chelate the metal. From these studies arose not only monodentate directing groups but also poly-dentate, specifically bidentate metal binders.[21] Additionally, the wide applicability of C–H activation by first row and second row transition metals via directed metal insertion served as a fortuitous sign for future developments.

The development of the permanent directing group by researchers as the time was counter intuitive to traditional transition metal catalysis methodology. The avoidance of highly Lewis basic moieties and metal chelators was often practiced, preventing catalyst poisoning or generation of off-cycle metal species. Additionally, the use of directing groups required appropriate ligand selection about the metal to allow for the open coordination site and appropriate movement of the C–H bond. Traditionally this movement occurs via four historically utilized mechanistic pathways: 1. Oxidative Addition; 2. Electrophilic; 3. σ-bond metathesis; 4. 1,2-addition.[22] In much of the group IV chemistry presented in this thesis, the electrophilic pathway is utilized via a subcategory known as concerted metalation deprotonation (CMD). This pathway generally utilizes a carboxylate ligand, such as a acetate or benzoate, to assist in an intramolecular deprotonation while maintaining the metal oxidation state prior to the C–H activation. The protonated carboxylate can then exit the catalytic cycle and serve as a proton reservoir and/or be deprotonated to regenerate the carboxylate ligand for reentry to the catalytic cycle. While mechanistically this requires the catalyst to interact with just the desired C–H bond, the inclusion of these directing groups proved pivotal for efficacious and selective C–H functionalization.

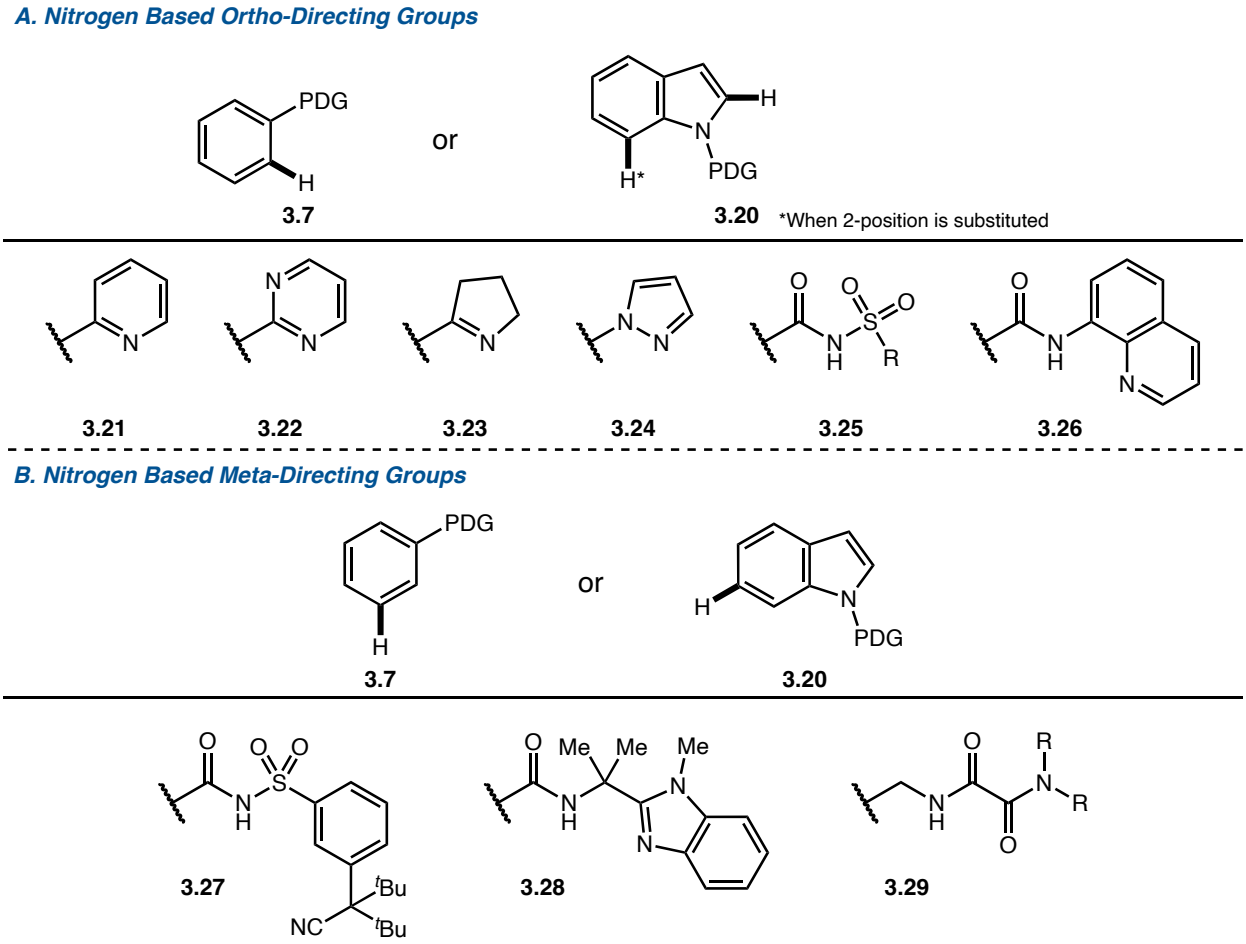

Figure 3. Selected examples of the more prevalent nitrogen based permanent directing groups to promote regioselective metal catalyzed C–H activation.

The moieties most often chosen for these directing group methodologies utilizes aptly positioned carbonyl, silyl, nitrogen, sulfur and phosphorous to name several. However, the majority of the field is dominated by nitrogen based directing groups installed via amides, nitriles, imines, nitrogen heterocycles or a combination of several for bidentate chelation. Generally, nitrogen in the -3 oxidation state is preferred like those listed above, however the -2 oxidation states of hydrazine/hydrazone and -1 oxidation state of azo/hydroxylamine are also utilized. The pendant directing group then relies on its linker length to provide the most favorable chelation structure with the metal to position it in proximity to the desired distal C–H. This is illustrated wonderfully through the use of 2-substituted pyridines (**3.21**) and 8-aminoquinoline amides (**3.26**)

to provide the ortho-substituted arene or 2-substituted indole (**Figure 3.A**). Likewise, the use of longer tethers and distant nitrile in (**3.27**) allows for the functionalization of *meta*-positions or even the 6-position of the indole. It should be noted that many of the longer tethers rely on the Thorpe Ingold effect to help pre-position the directing group in its chelated shape as illustrated by the *gem*-dimethyl in **3.28.** While these methods are varied in type of permanent directing group, they are very efficacious in the delivering the desired functionalization despite their shortcomings with later removal of the directing group.[21,23-24]

The removal of permanent directing groups has been mirroring the evolution of C–H functionalization methodology since the mid-20th century discovery of this powerful transformation.[20-22] Disappointingly, these removal methodologies still require promiscuous reductive, oxidative and/or strongly basic conditions to return the group to desired functional groups for further scaffold modifications.[23] Utilizing indole scaffolds **3.30** and **3.31** as an example, the removal of the directing groups was carried out mostly via hydrolysis or "quaternization and thiol/alcoholysis" (**Scheme 2**). Additionally, reagents like $NaBH_4$ can be utilized but have unintended effects like the reduction of the indole to indane. Other nitrogen based directing groups

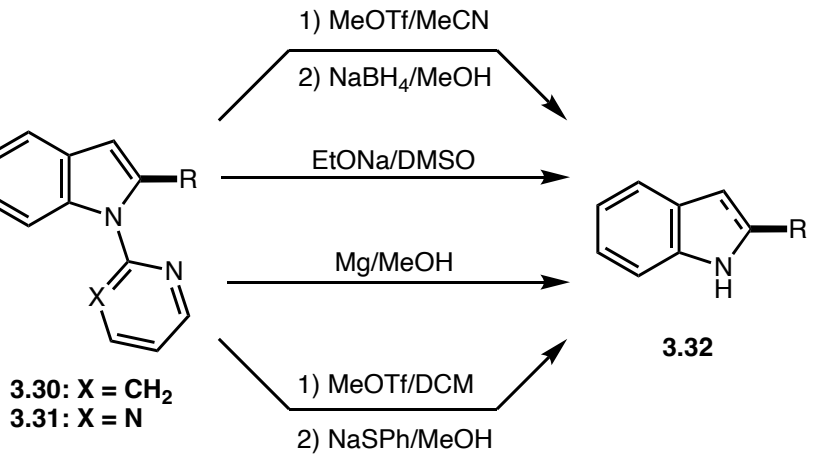

Scheme 2. Conditions for the removal of pyridine and pyrazine directing groups.

like sulfonyls were removed via samarium iodide, manganese (III) acetate dihydrate, magnesium metal, Red-Al® or sodium napthalide.[23] While these are very effective for the removal of sulfonyls, they are quite promiscuous when it comes to chemo/regioselectivity and typically preclude late-stage C–H functionalization of complex scaffolds. Amide, urea, and carboxamide directing groups were implemented more recently and offer much milder cleavage conditions while also allowing for access to desirable functionality. In the case of 8-aminoquinoline (AQ), this can be converted to carboxylic acids or esters with acid or base mediated lysis. Acidolysis is more preferential due to its ability to prevent epimerization in the case of sp^3 attached amide directing groups. Despite this, the fact remains that strong acid/base and high temperatures are quite detrimental to many functional groups and bathing a scaffold in concentrated acid or strong base is the textbook example of a non-chemoselective methodology.[25] Additionally, the AQ group can be converted to the free amide via ozonolysis and ammonium hydroxide or the directing group can be fully substituted with the use of a Boc protecting group to allow for further conversion.

The Boc protected AQ group can be converted into the functional groups mentioned earlier but also allow access to primary alcohols following lithium aluminum hydride ($LiAlH_4$) or lithium

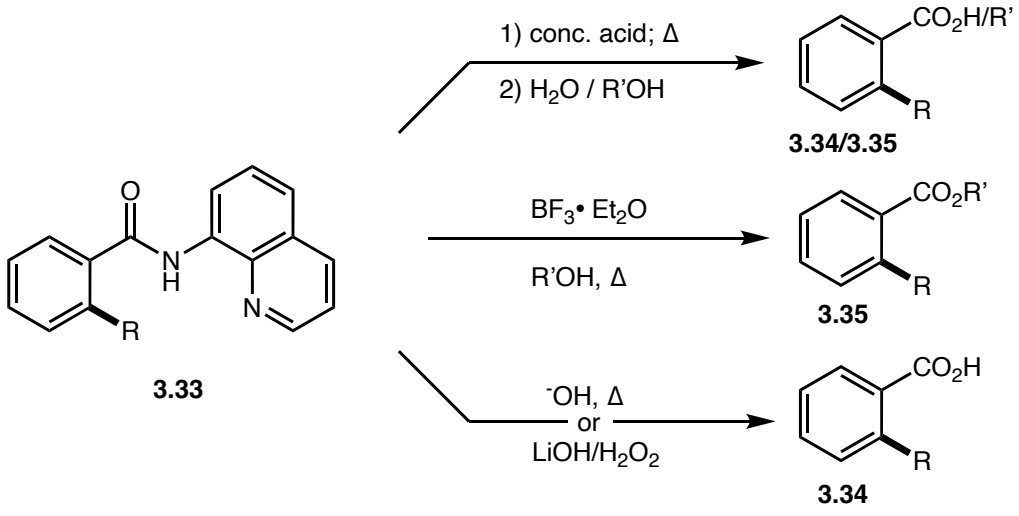

Scheme 3. Conditions for the removal of 8-aminoquinoline directing group.

aluminum borohydride ($LiBH_4$) treatment. Additionally, the aldehyde is within reach utilizing a zirconium sandwich catalyst [Cp_2 Zr(H)Cl] or large excesses of DIBAL at cryogenic temperatures.[25] While the majority of the permanent directing group are still utilizing nitrogen, there are more bespoke directing group methods that utilize various other heteroatoms that can be investigated in the following reviews.[21-25] The use of carboxylic acids as permanent and transient directing groups will be touched upon in a later section.

3.2.2 Transient Directing Group Strategy and Pitfalls

The limitations of permanent directing groups and their need for removal following the desired C–H functionalization led to the need for a better method and serendipitously, Jun and

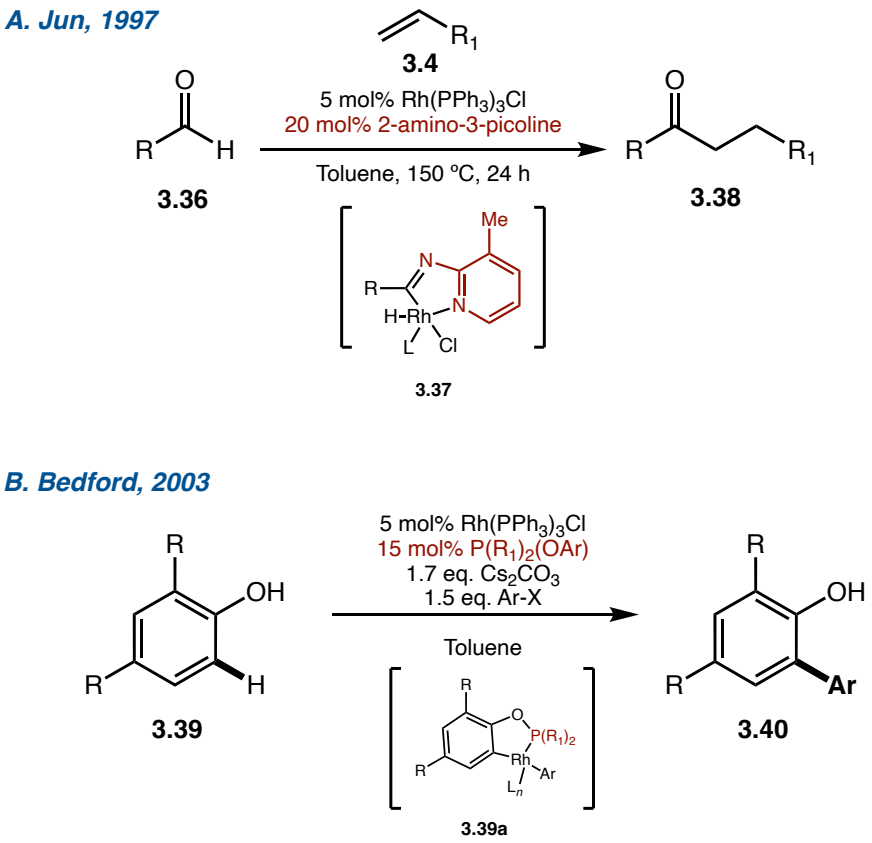

Scheme 4. Pioneering work on transient directing groups in the field of C–H functionalization.

coworkers discovered this when they added a 2-amino-3-picoline to rhodium catalyzed hydroacylation (**Scheme 4.A**).[26] The authors correctly postulated that the aldehyde was condensing with the free amino group and directing the Wilkinson's catalyst into the aldehyde and forming the rhodacycle (**3.37**). Several year later, a phosphinite additive proved beneficial to the *ortho*-arylation of phenols through the reversible transesterification of the substrate (**Scheme 4.B**).[27-29] Bedford and coworkers correctly hypothesized that this would allow the previously disfavored 4-membered metallocycle of the phenol to expand to a more favorable 5-membered system. Despite these early reports the advancements in transient directing group strategy have mainly been to tailor the additive to the substrate class to achieve the desired site selectivity.

While these two systems are more than two decades old, the transient directing group strategy remains very much concentrated around the functionality presented above. The use of condensation reactions by in large dominates this field and has migrated into the use of canonical and non-canonical amino acids to provide readily available stereocenters for enantioselective methods development or preorganization of the metallocycle.[27-31] Glycine, and *tert*-leucine are the more commonly utilized amino acids during methodology development. In the case of methodologies that are racemic or utilize a different means of enantioinduction, substituted anilines, alkyl-diamines and amino substituted heteroarenes provides robust and facile transient directing groups for condensations with carbonyls. In the case of primary, secondary, or aromatic alcohols, the directing groups tend to function via transesterification of another alcohol or a phosphorous containing additive, traditionally phosphinite. Continual development of this strategy has led to both more selective directing groups but also to functionalization at more distal C–H bonds than previously seen. Additionally, the design of newer transient directing group strategies and the repurposing of older chemistry has allowed this field to continue to blossom. Dong and

coworkers leverage a secondary amine, 7-azaindoline, to generate the enamine *in-situ* allowing for a more acidic $C_{(sp^2)}$–H bond that undergoes metal activation (Scheme 5.A).[32-33] A second example of repurposed chemistry was published by the Lautens group expanding upon the previously reported Catellanì reaction. While this reaction does require a permanent directing group for the first palladation, the subsequent coordination and migratory insertion of the strained alkene, norbornene, acts a transient group to offer *meta*-functionalization before β-hydride elimination of the palladium-norbornene (**Scheme 5.B**).[34-36] This strained alkene strategy has recently seen a resurgence do to a 2013 report published by Dong and coworkers that utilize aryl halides and *N*-benzoyloxyamines to develop a ortho amination.[37] Coincidentally, this report combines both a traceless halide directing group, which will be discussed later, and the transient strained alkene.

Like the Dong amination, a second transient directing group also blurs the lines between permanent, transient, and traceless. This is caried out by the carboxylation of a carbon or nitrogen in the substrate with CO_2 and subsequently leveraged by the metal to direct into a distal C–H bond (**Scheme 5.C**).[28,38] Specifically, in this instance, the carbonylation *ortho* to the phenol allows for the *meta*-functionalization and subsequent decarboxylation. The carboxylation reaction may or may not take place in the same step and therefore could be viewed differently system to system. Despite how this is classified, it serves as a basis for the traceless directing group strategies in which carboxylic acids are utilized and then ablated in the same transformative process.

Additionally, a fourth sub-genre of transient directing groups breaks the mold like the above examples. These are the non-covalent transient directing groups that utilize electrostatic, hydrogen or coordinate bonding to deliver the desired C–H activation. These groups are referred to as "transient directing mediators" and have been demonstrated high levels of conversion and enantioselectivity in the literature.[27] One such example by Kuninobu, Kanai and coworkers,

A. Enamine Transient Directing Group

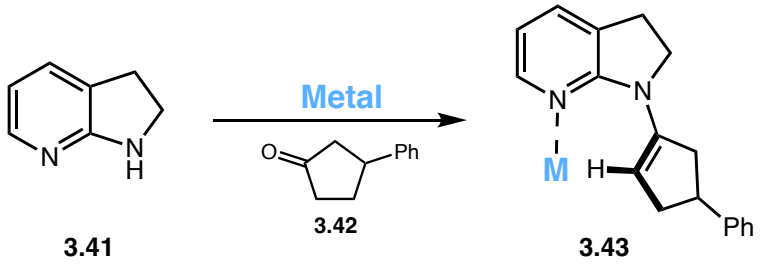

3.41 3.42 3.43

B. Cattellani Type Reaction: Transient Directing Group

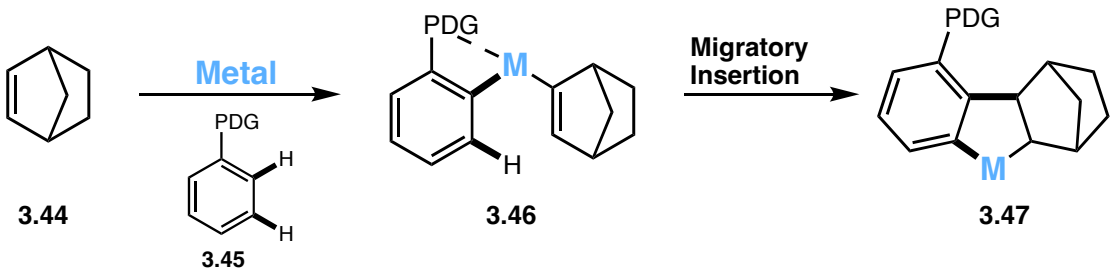

3.44 3.45 3.46 3.47

C. Carbon Dioxide as a Transient Directing Group

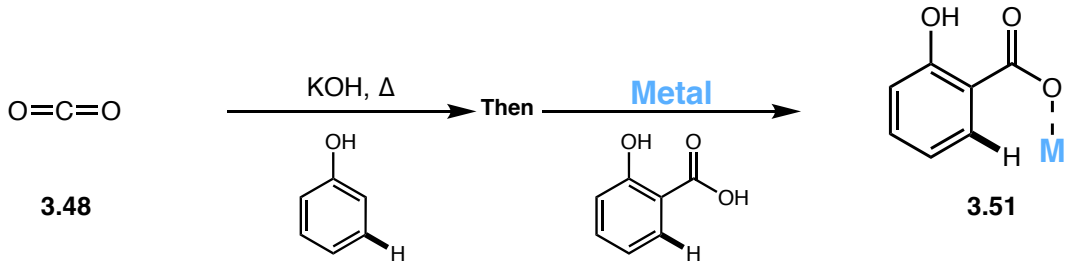

3.48 3.49 3.50 3.51

D. Transient Directing group that Utilizes Intermolecular hydrogen bonding

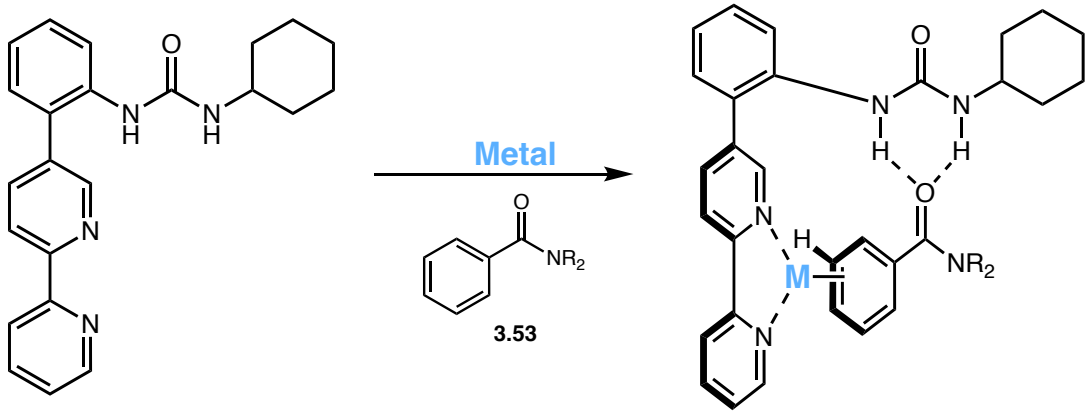

3.52 3.53 3.54

Scheme 5. Less developed methods used in transient directing group strategy for placing the metal in proximity to distal C–H bonds.

utilizes a urea/bipyridyl structure to position the metal and substrate inside a pocket for a *meta*-selective borylation (**Scheme 5.D**).[39] While these systems are highly selective for their desired substrates, the coming years will see a larger incorporation of various transition metals and more widely applicable systems as the number of researchers in this area increases.

While the use of transient directing groups has widely advanced the area of C–H functionalization, the heavy reliance on imine and phosphinite chemistry has served as barrier to further exploration. This requirement for sensitive oxygenated functional groups is convenient when the native group is useful in later transformations, however, still leads to an extra step when ablation is required. Furthermore, the various other methods are very substrate dependent and have yet to offer a widely applicable system across transition metals and coupling/addition partners outside of the traditional inter/intramolecular C–C, C–N, C–B, and C–O bond forming reactions of C–H functionalization. This gap in the literature is where traceless directing groups have begun to make a mark for themselves.

3.2.3 Traceless Directing Group Strategy and Current State of the Art

Traceless directing groups are a new strategy that rose out of the desire for atom economy, reduced step counts and unfavorable chemoselectivity issues discussed with permanent and transient directing groups. While this field is still emerging since the early 21st century, several criteria have been established to help define traceless directed C–H functionalization methods. Paul and coworkers beautifully laid these out and are as follows: "(i) during functionalization, the directing group should be regarded as stable and reversibly coordinated with the metal center, (ii) the directing group should assist C–H functionalization and thereafter be removed in a single step and (iii) the directing group should not constitute a part of the target molecule".[40] This boils down

A. Goosen, 2007

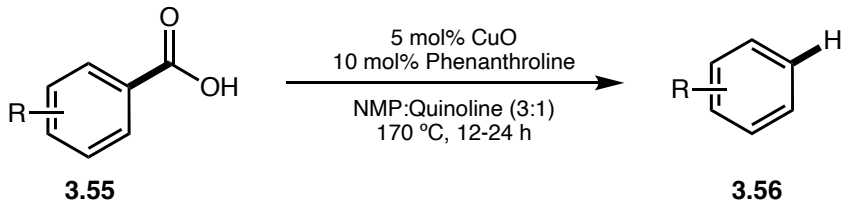

3.55 **3.56**

B. Daugulis, 2007

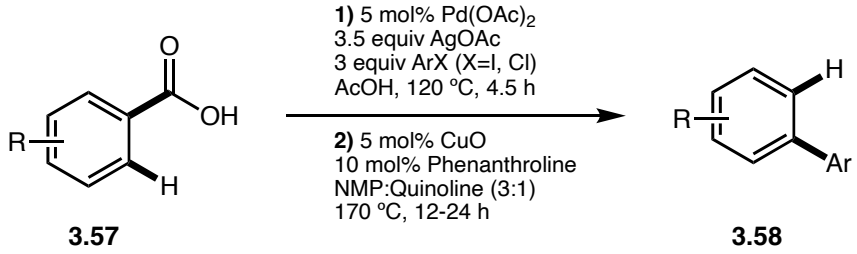

3.57 **3.58**

C. Miura, 2008

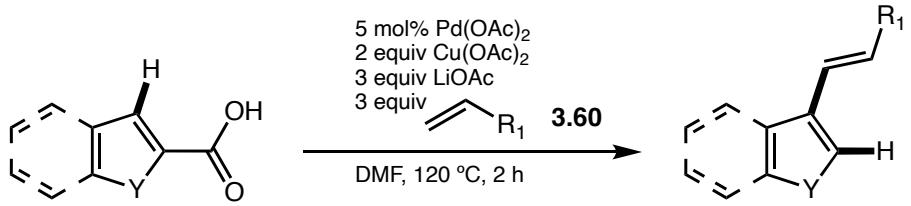

Y = NR, O, S Y = NR, O, S

3.59 **3.61**

Scheme 6. Seminal work in the development of traceless directing group chemistry and its application with carboxylic acids.

to the overarching theme that functional groups inherent to the compound actively assist in carrying out the transition metal catalyzed transformation and then are ablated in a one pot approach to the desired product. While the criteria laid out above are very cut and dry in text, their application is much harder to apply when looking at the academic body of work in this area. While some confusion remains around what functional groups are in fact a considered the "gold standard" traceless directing group. Historically speaking, this has pointed to carboxylic acids due to their wide natural and commercial availability. In fact, the chemistry surrounding metal catalyzed proto-

decarboxylation is quite robust and led to the first reports where the term "traceless directing group" was employed to describe the C–H functionalization. The work done by Gooßen[41] and Su[42] on proto-decarboxylation by copper catalysis and the mechanism by which *ortho*-substituents decrease the barrier to decarboxylation by destabilizing steric interaction and via metal transition state stabilization of the decarboxylation (**Scheme 6.A**). This mechanistic information was finally acted upon by Daugulis and coworkers[44] in which a benzoic acid was arylated with aryl halides and palladium catalysis before being decarboxylated in a second step via Gooßen's copper oxide conditions (**Scheme 6.B**).[41] This two-step system set the stage for a race to find the best one pot reaction for carboxylic direct C–H functionalization. This accolade was later bestowed upon Miura and coworkers in 2008 in which the 3-position vinylation of heteroarenes and decarboxylation of the 2-position occurred in a one pot reaction sequentially, avoiding proto-decarboxylation of the starting material (**Scheme 6.C**).[45.] Following this report the decade following saw a huge increase in the use of carboxylic acids as a traceless directing group in the field of C–H functionalization largely around $C_{(sp^2)}$–H activation but also beginning to branch into some $C_{(sp^3)}$–H activation as well.[43] Additionally, aldehyde, amide, α-imino oxy acid, *N*-oxide, nitroso, and silyl groups were shown to participate in traceless C–H functionalization as the field has progressed in the intervening years.[40] Characteristically, the use of halides and boronates intramolecularly is absent in many, if not most, of the reports about traceless directing group strategy, despite predating the often referenced seminal work in the field.

Prior to the work on decarboxylative C–H functionalization, the use of halides for intramolecular cyclization had been previously investigated quite extensively at the turn of the century but was known and forgotten many years earlier.[19] While some may question the classification of halides as traceless directing groups, remembering the broad principles for

A. Ames, 1982

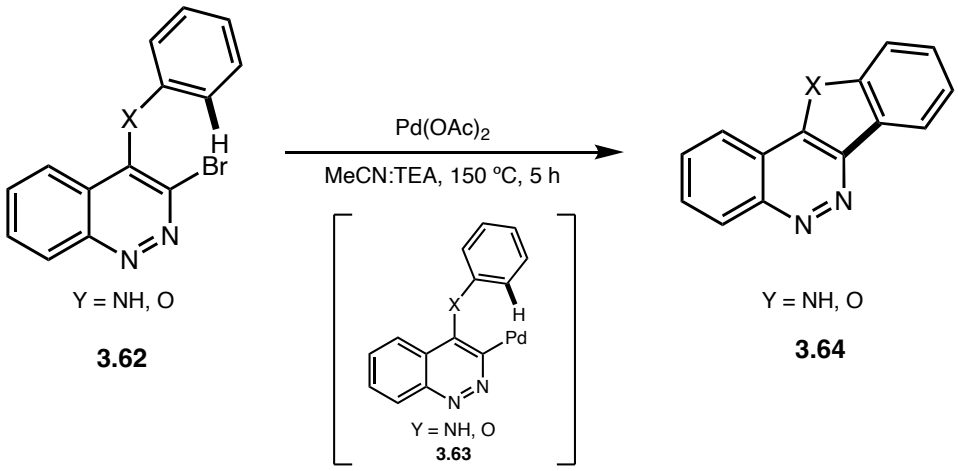

B. Dyker, 1992

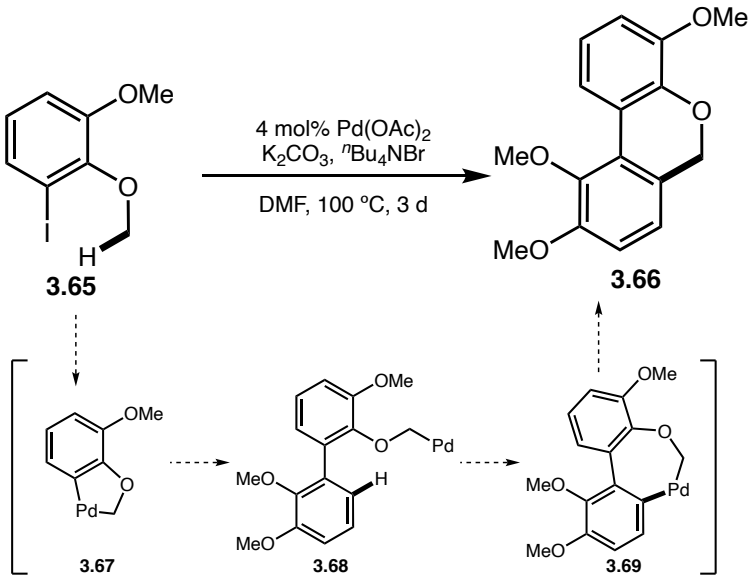

C. Baudoin, 2003

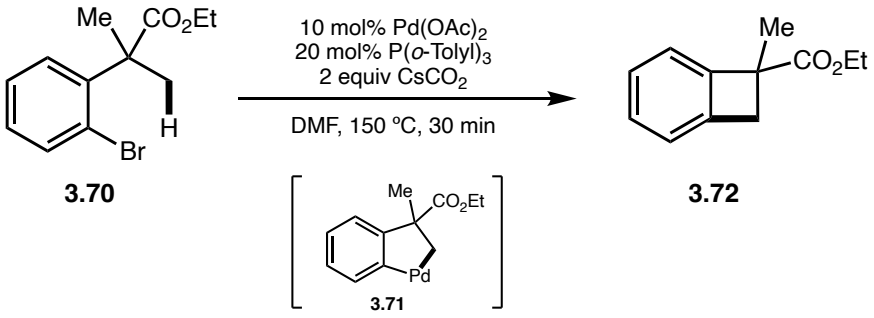

Scheme 7. Seminal work in the development of halides as a traceless directing group for C–H annnulation reactions.

traceless directing groups from above can help clarify. During C–H functionalization the following criteria should be met:

1. The group is stable and coordinated with the metal center.
2. The assists in C–H functionalization and then is ablated in a single step.
3. The group should not constitute a part of the product.[40]

As stated earlier, Ames[16] published a paper describing this transformation with $C_{(sp^2)}$–H activation in 1982 (**Scheme 7.A**), and Dyker[17] published a similar method for $C_{(sp^3)}$–H activation a decade later (**Scheme 7.B**). While there were various reports of similar $C_{(sp^2)}$–H activation in the literature[46], it wasn't until 2003 that this method was serendipitously reinvigorated by an unpredicted side product isolated by Baudoin and coworkers during work on dehydrogenation towards the synthesis of antimitotic bridged biaryl compounds (**Scheme 7.C**).[8,19] Following these reports, Fagnou and coworkers began exploring this area in 2004 with new high turnover variations of the previously described Ames arylation.[47] Before Fagnou's untimely passing in 2009 from H_1N_1, the "Fagnou Factory" and Baudoin groups published heavily in the area of halide traceless directing groups. In 2006, Fagnou and coworkers published an intermolecular variation of their chemistry however the conditions relied on swamping the catalyst with 10 equivalents of starting material and occurred without a directing aspect to the metal initialed by the halide metal interaction thus violating the second principle listed above.[48] Despite the large amount of work in this area, the analogous reaction with transmetallation reagents had not been described in the literature.

A thorough search of the literature turned up only several examples describing traceless directing groups with boron, furthermore only one containing transmetallation. The first report by Smith III and coworkers from 2013 offers a C–H functionalization via a traceless directing group

A. Smith III, 2013 (incorrectley labelled traceless)

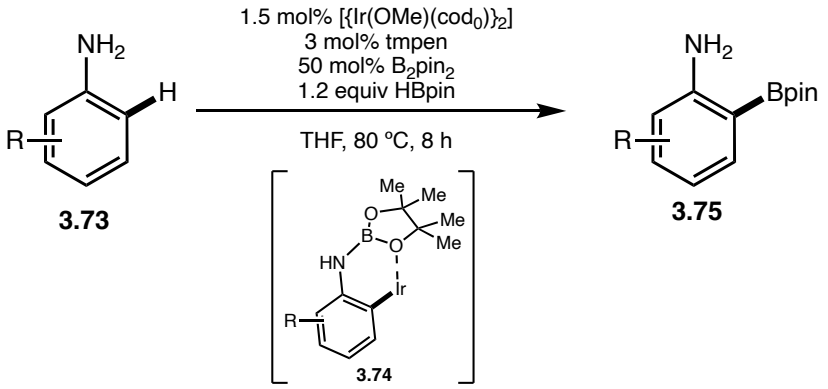

B. Ackermann, 2019

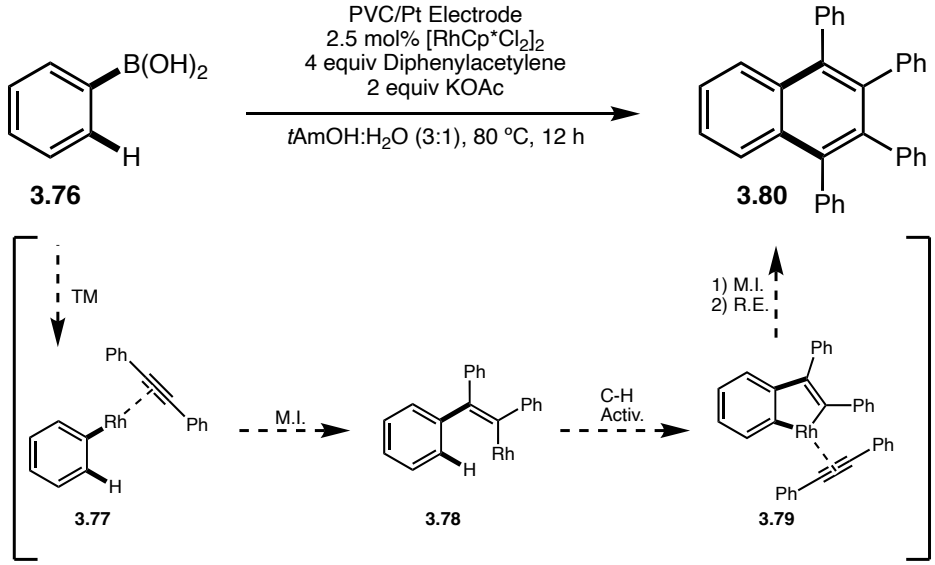

Scheme 8. Early in the development of boron and transmetallation based traceless directing groups for C–H functionalization.

utilizing boron, however this paper actually describes a transient directing group that is formed during the reaction and subsequently removed (**Scheme 8.A**).[14] The borylation on the amine leads to a handle that directs the iridium into the *ortho*-C–H and borylates that position before returning to the free amine upon workup. The second example is by Ackermann and coworkers in 2019 and reports on an electrochemical and an analogous copper oxidized rhodium annulation for access to

highly aromatic materials.[15] Ackermann's strategy was the first example in which the metal was directed the substrate via transmetallation (**3.77**), however it relied on a migratory insertion of diphenylacetylene to first elongate the carbon chain bearing Rh (**3.78**) before placing the metal in position to the ortho-C–H and allow for the formation of the desired rhodacycle(**3.79**). A second migratory insertion of diphenylacetylene to form the 7-membered rhodacycle then allowed for reductive elimination to free the desired tetraphenylnapthalene (**3.80**) in high yields. While this first example of boron as a traceless transmetallation directing group succeeded, it left much to be desired as this strategy moved forward. In short, the need to truncate this process to coordination of the metal, followed by immediate distal C–H activation was highly desired.

3.3 Concluding Remarks

C–H functionalization utilizing directing groups has developed into a remarkably powerful strategy since the first disclosures by Murahasi in the mid-20th century, however they still prove to be one of the best methods available for selective C–H activation. Their development from permanent to transient and now onto traceless directing groups have continued to benefit the academic/industrial community with enhanced atom economy, lower linear step counts, and chemo/regioselectivity at every turn. Despite their shortcomings, the field continues to develop new and highly selective methodologies with all three of these classes of directing groups. Recent advances in traceless directing groups via oxidative addition have leveraged the powerful metallocycle intermediates, yet the analogous transmetallation methodology has yet to be realized in its full potential. The application of this new traceless directing group methodology is an exciting prospect to keep an eye on despite being in its infancy at this time.

3.4 References

1. Katritzky, A.R. Introduction: Heterocycles. *Chem. Rev.* **2004**, *104*, 2125-2126.

2. a) Crabtree, R.H.; Lei, A. Introduction: CH Activation. *Chem. Rev.* **2017**, *117*, 8481-8482. **b)** Davies, H.M.L.; Morton, D. Recent Advances in C–H Functionalization. *J. Org. Chem.* **2016**, *81*, 343-350. **c)** Mural, K.; Machado, L.A.; Carvalho, R. L.; Pedrosa, L.F.; Mukherjee, R.; Da Silva Jr., E.; Maiti, D. Decoding Directing Groups and Their Pivotal Role in C H Activation. *Chem. Eur. J.* **2021**, *27*, 12453-12508

3. a) Janowicz, A. H.; Bergman, R. G. Carbon–hydrogen activation in saturated hydrocarbons: direct observation of M + R−H → M(R)(H). *J. Am. Chem. Soc.* **1982**, *104*, 352–354. **b)** Hoyano, J. K.; Graham, W. A. G. Oxidative addition of the carbon–hydrogen bonds of neopentane and cyclohexane to a photochemically generated iridium(I) complex. *J. Am. Chem. Soc.***1982**, **104** 3723–3725. **c.)** Murai, S.; Kakiuchi, F.; Sekine, S.; Tanaka, Y.; Kamatani, A.; Sonoda, M.; Chatani, N. Efficient catalytic addition of aromatic carbon-hydrogen bonds to olefins. *Nature* **1993**, *366*, 529–531.

4. a) Sambiagio, C.; Schonbaurer, D.; Bliek, R.; Dao-Huy, T.; Pototschnig, G.; Schaaf, P.; Wiesinger, T.; Zia, M. F.; Wencel-Delord, J.; Besset, T.; Maes, B.; Schnürch, M. A comprehensive overview of directing groups applied in metal-catalysed C–H functionalization chemistry." *Chem. Soc. Rev*. **2018**, *47*, 6603-6743. **b)** Verho, O.; Lati, M. P. Oschmann, M. A Two-Step Procedure for the Overall Transamidation of 8-Aminoquinoline Amides Proceeding via the Intermediate N-Acyl-Boc-Carbamates. *J. Org. Chem.* **2018**, *83*, 4464-4476. **c)** Zhang, Z.; Li, X. Song, M.; Wan, Y. Zheng, D.; Zhang, G.; Chen, G. Selective Removal of Aminoquinoline Auxiliary by IBX Oxidation. *J. Org. Chem.* **2019**, *84*, 12792-12799.

5. St. John-Campbell, S.; Bull, J.A. Transient imines as 'next generation' directing groups for the catalytic functionalisation of C–H bonds in a single operation. *Org. Biomol. Chem.* **2018**, *16*, 4582-4595.

6. Xu, X.; Luo, J. Transition-metal-catalyzed Directing Group-Assisted C–H Activation of Phenols. *ChemSusChem* **2019**, *12*, 4601-4616.

7. Gandeepan, P.; Ackermann, L. Transient Directing Groups for Transformative C–H Activation by Synergistic Metal Catalysis. *Chem* **2018**, *4*, 199-222.

8. Font, M.; Quinbell, J.; Perry, G.; Larrosa, I. The use of carboxylic acids as traceless directing groups for regioselective C–H bond functionalisation. *Chem. Commun*. **2017**, *53*, 5584-5597.

9. Simonetti, M.; Larrosa, I. Good things come in threes. *Nature Chem.* **2016**, *8*, 1086-1088.

10. Andries-Ulmer, A.; Brunner, C.; Rehbein, J.; Gulder, T. Fluorine as a Traceless Directing Group for the Regiodivergent Synthesis of Indoles and Tryptophans. *J. Am. Chem. Soc.* **2018**, *140*, 13034-1304.

11. Baudoin, O.; Herrbach, A.; Guéritte, F. The palladium-catalyzed C–H activation of benzylic gem-dialkyl groups. *Angew. Chem. Int. Ed.* **2003**, *42*, 5736-5740.

12. Kefalidis, C. E.; Davi, M.; Holstein, P. M.; Clot, E.; Baudoin, O. Mechanistic study on the selectivity of olefin vs. cyclobutene formation by palladium(0)-catalyzed intramolecular C(sp3)–H activation. *J. Org. Chem*. **2014**, *79*, 11903-11910.

13. Rocaboy, R.; Dailler, D.; Baudoin, O. A Four-Step Synthesis of (±)-γ-Lycorane via Pd^0-Catalyzed Double $C(sp^2)$–H/$C(sp^3)$–H Arylation. *Org. Lett.* **2018**, *20*, 772-775.

14. Kong, W. L.; Finger L. H.; Oliveira, J. C. A.; Ackermann, L. Rhodaelectrocatalysis for Annulative C−H Activation: Polycyclic Aromatic Hydrocarbons through Versatile Double Electrocatalysis. *Angew. Chem. Int. Ed.* **2019**, *58*, 6342-6346.

15. Preshlock, S.; Plattner, D.; Maligres, P.; Krska, S.; Maleeczka Jr., R.; Smith III, M. A Traceless Directing Group for C–H Borylation. *Angew. Chem. Int.* **2013**, *52*, 12915-12919.

16. Ames, D. E.; Bull, D. Some Reactions of 3-Halogenocinnolines Catalysed by Palladium Compounds. *Tetrahedron* **1982**, *38*, 383−387.

17. Dyker, G. Palladium-Catalyzed C−H Activation of Methoxy Groups: a Facile Synthesis of Substituted 6H-Dibenzo[b,d]pyrans. *Angew. Chem., Int. Ed. Engl.* **1992**, *31*, 1023−1025.

18. Dyker, G. Palladium-Catalyzed C−H Activation at Methoxy Groups for Cross- Coupling Reactions: a New Approach to Substituted Benzo[b]furans. *J. Org. Chem.* **1993**, *58*, 6426−6428.

19. Baudoin, O. Ring Construction by Palladium(0)-Catalyzed C(sp3)−H Activation. *Acc. Chem. Res.* **2017**, *50*, 1114−1123.

20. a.) Murahashi, S. Synthesis of Phthalimidines from Schiff Bases and Carbon Monoxide. J. Am. Chem. Soc. 1955, 77, 6403−6404. **b.)** Murahashi, S.; Horiie, S. The Reaction of Azobenzene and Carbon Monoxide. J. Am. Chem. Soc. 1956, 78, 4816−4817.

21. a.) Rej, S.; Ano, Y.; Chatani, N. Bidentate Directing Groups: An Efficient Tool in C–H Bond Functionalization Chemistry for the Expedient Construction of C–C Bonds. *Chem. Rev*. **2020**, *120*, 1788−1887. **b.)** Liu, B.; Romine, A.M.; Rubel, C.Z.; Engle, K.M.; Shi, B.-F. Transition-metal-catalyzed, coordination-assisted functionalization of nonactivated C(sp^3)–H bonds. *Chem. Rev.* **2021**, *121*, 14957–15074. C.) Woźniak, L.; Tan, J.-F.;

Nguyen, Q.-H.; Madron du Vigne, A.; Smal, V.; Cao, Y.-X.; Cramer, N. Catalytic enantioselective functionalizations of C–H bonds by chiral iridium complexes. *Chem. Rev.* **2020**, *120*, 10516–10543.

22. Altus, K.M., Love, J.A. The continuum of carbon–hydrogen (C–H) activation mechanisms and terminology. *Commun. Chem.* **2021**, 4, 173-184 (2021).

23. Carvalho, R.L.; Almeida, R.G.; Murali, K.; Machado, L.A.; Pedrosa, L.F.; Dolui, P.; Maiti, D.; da Silva Júnior, E.N. Removal and modification of directing groups used in metal-catalyzed C–H functionalization: The magical step of conversion into 'conventional' functional groups. *Org. Biomol. Chem.* **2021**, *19*, 525–547.

24. Wang, X.; Lu, M.-Z.; Loh, T.-P. Transition-Metal-Catalyzed C–C Bond Macrocyclization via Intramolecular C–H Bond Activation. *Catalysts* **2023**, *13*, 438-461.

25. Fitzgerald, L.S.; O'Duill, M.L. A Guide to Directing Group Removal: 8-Aminoquinoline. *Chem. Eur. J*. **2021**, *27*,8411–8436.

26. Jun,C.-H.; Lee,H.; Hong,J.-B. Chelation-Assisted Intermolecular Hydroacylation: Direct Synthesis of Ketone from Aldehyde and 1-Alkene. *J.Org.Chem*.**1997**, *62*, 1200−1201.

27. Jacob, C.; Maes, B. U. W.; Evano, G. Transient Directing Groups in Metal Organic Cooperative Catalysis. *Chem. Eur. J.* **2021**, *27*, 13899–13952.

28. Gandeepan, P.; Ackermann, L. Transient Directing Groups for Transformative C–H Activation by Synergistic Metal Catalysis. *Chem*, **2018**, *4*, 199-222.

29. Zhao, Q.; Poisson, T.; Pannecoucke, X.; Besset, T. The Transient Directing Group Strategy: A New Trend in Transition Metal-Catalyzed C–H Bond Functionalization. *Synthesis* **2017**, *49*, 4808-4826.

30. Lapuh, M. I.; Mazeh, S.; Besset, T. Chiral Transient Directing Groups in Transition-Metal-Catalyzed Enantioselective C−H Bond Functionalization. *ACS Catal*. **2020**, *10*, 12898-12919.

31. Rasheed, O. K.; Sun, B. Advances in Development of C–H Activation/Functionalization Using a Catalytic Directing Group. *ChemistrySelect* **2018**, *3*, 5689–5708.

32. Mo, F.; Dong, G. Regioselective ketone-alkylation with simple olefins via dual activation. *Science* **2014**, *345*, 68–72.

33. Lim, H. N.; Dong, G. Catalytic intramolecular ketone alkylation with olefins by dual activation. *Angew. Chem. Int. Ed.* **2015**, 54, 15294–15298.

34. Della, N.; Fontana, M.; Motti, E.; Catellani, M. Pd/Norbornene: a winning combination for selective aromatic functionalization via CH bond activation. *Acc. Chem. Res*. **2016**. *49*, 1389–1400.

35. Lautens, M.; Piguel, S. A new route to fused aromatic compounds by using a palladium-catalyzed alkylation-alkenylation sequence. *Angew. Chem. Int. Ed*. **2000**, *39*, 10451046.

36. Catellanì, M.; Motti, E.; Della Ca', N. Catalytic sequential reactions involving palladacycle-directed aryl coupling steps. *Acc. Chem. Res.***2008**, *41*,1512–1522.

37. Dong, Z.; Dong, G. Ortho vs ipso: site-selective Pd and norbornene-catalyzed arene CH amination using aryl halides. *J. Am. Chem. Soc*. **3013**, *135*,18350–18353.

38. Drapeau, M. P.; Gooßen, L. J. Carboxylic Acids as Directing Groups for C–H Bond Functionalization. *Chem. Eur. J.* **2016**, *22*, 18654 – 18677.

39. Kuninobu, Y.; Ida, H.; Nishi, M.; Kanai, M. A meta-selective C–H borylation directed by a secondary interaction between ligand and substrate *Nat. Chem.* **2015**, *7*, 712–717.

40. Rani, G.; Luxami, V. Paul, K. Traceless directing groups: a novel strategy in regiodivergent C–H functionalization.

41. Gooßen, L. J.; Thiel, W. R.; Rodríguez, N.; Linder, C.; Melzer, B. Copper-Catalyzed Protodecarboxylation of Aromatic Carboxylic Acids. *Adv. Synth. Catal*., **2007**, *349*, 2241–2246.

42. Xue, L.; Su, W.; Lin, Z. Mechanism of silver- and copper-catalyzed decarboxylation reactions of aryl carboxylic acids. *Dalton Trans*. **2011**, *40*, 11926–11936.

43. Font, M.; Quibell, J. M.; Perry, G. J. P.; Larrosa, I. The use of carboxylic acids as traceless directing groups for regioselective C–H bond functionalization. *Chem. Commun.,* **2017**, *53*, 5584-5597.

44. Chiong, H. A.; Pham, Q-N.; Daugulis, O. Two Methods for Direct *ortho*-Arylation of Benzoic Acids. *J. Am. Chem. Soc.* **2007**, *129*, 9879-9884.

45. Maehara, A.; Tsurugi, H.; Satoh, T.; Miura, M. Regioselective C−H Functionalization Directed by a Removable Carboxyl Group: Palladium-Catalyzed Vinylation at the Unusual Position of Indole and Related Heteroaromatic Rings. *Org. Lett.* **2008**, *10*, 1159-1162.

46. Hassa, J.; Svignon, M.; Gozzi, C.; Schultz, E.; Lemaire, M. Aryl−Aryl Bond Formation One Century after the Discovery of the Ullmann Reaction. *Chem. Rev*. **2002**, *102*,1359–1470.

47. Campeau, L-C.; Parisien, M. Leblanc, M.; and Fagnou, K. Biaryl Synthesis via Direct Arylation: Establishment of an Efficient Catalyst for Intramolecular Processes. *J. Am. Chem. Soc.* **2004**, *126*, 9186–9187.

48. Campeau, L-C.; Fagnou, K. Palladium-catalyzed direct arylation of simple arenes in synthesis of biaryl molecules. *Chem. Commun*., **2006**, 1253-1264.

Chapter 4: Leveraging α-Amino Boron Species for the Synthesis 1,2-Dihydroquinolines Scaffolds via C–H Annulation

4.1 Introduction to Transmetallation as a C–H Functionalization Strategy for Annulation

In this chapter we will discuss the development of a boron starting material from commercially available anilines and subsequent traceless directed, C–H annulation, of 3,4-disubstituted 1,2-dihydroquinolines with regiospecificity. Subsequently, this project led to the generation of new methodology for α-amino boron species, their preparation from commercial feedstocks and use as a traceless directing group. Additionally, this directed C–H annulation strategy expanded the scope of traceless directing methodology to include the direct use of transmetallation. Finally, this research was concluded through the regioselective access to a privileged dihydroquinoline scaffold offering unique opportunities to academics and industrial scientists alike for future compound development.

4.1.1 Initial Investigations into Transmetallation Directed C–H Functionalization

Following the 2019 disclosure by Ackermann and coworkers detailed in the previous chapter[1], we set out to design a model system to leverage the potential of their disclosure. Looking at the chemical oxidation conditions presented in the paper, we were able to determine the most plausible mechanism for the transformation (**Scheme 1. A**). The first goal we set out to achieve in our model system, was to determine if the initial elongation of the rhodium via migratory insertion (**4.2→4.3**) was necessary to maintain reactivity. We hypothesized that the stability of the 5-membered rhodacycle (**4.4**) was the driving force behind the sequence of these events. To test this hypothesis, we studied the overarching features of a model system that would adequately answer the experimental question. We settled on two plausible precursor structures that would both funnel into the anticipated metallocycle (**4.8**), however would approach from two fundamentally different

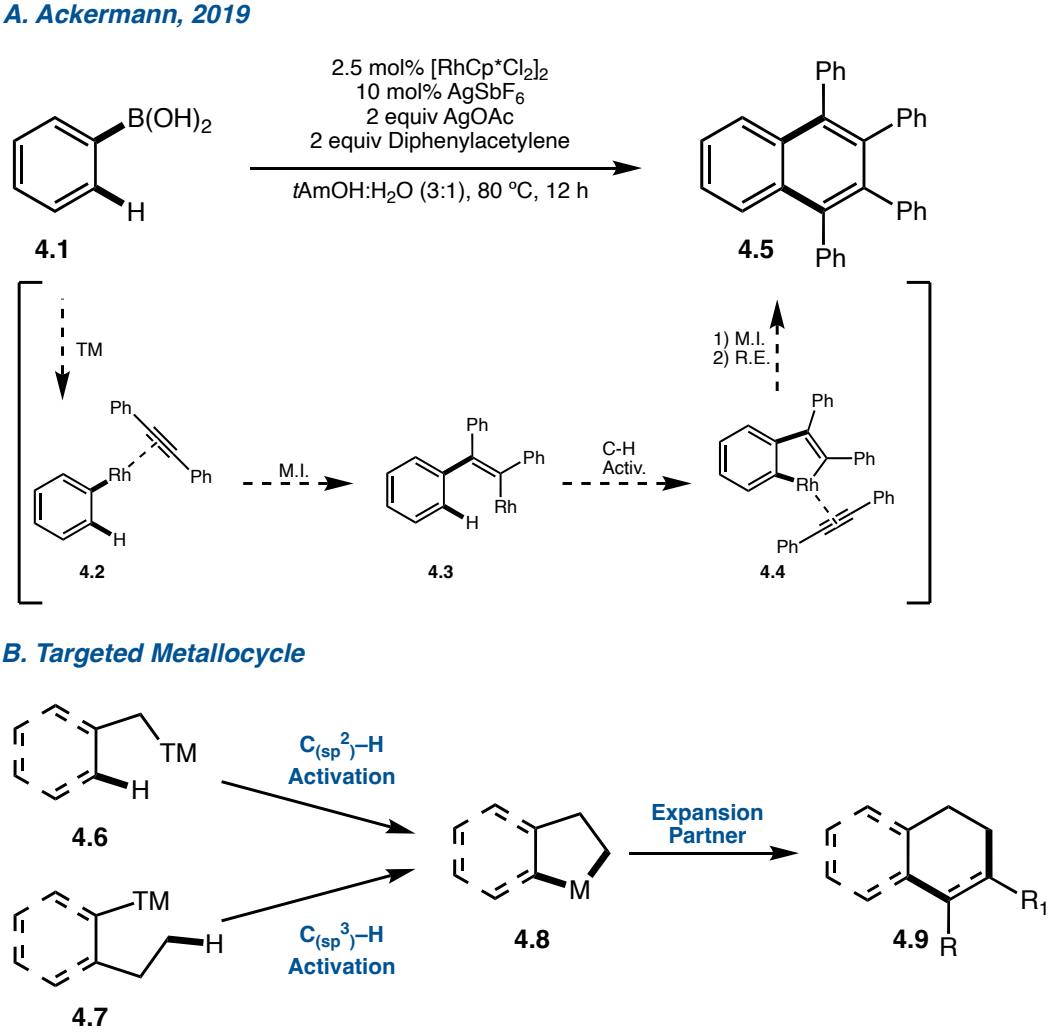

Scheme 1. Ackermann's chemical conditions for the C–H annulation of tetraphenlynapthalenethat led to the design of a hypothesis that the mettallocycle would allow for a convergent intermediate to would allow for succesful design of annulation methodology.

forms of transmetallation and C–H activation (**Scheme 1.B**). The first route envisioned (**4.6→4.8**), utilized a benzylic boron species for transmetallation, before $C_{(sp^2)}$–H activation led to the desired metallocycle. The second route (**4.7→4.8**) would utilize aryl boronic species to transmetallate then undergo $C_{(sp^3)}$–H activation before again providing **4.8**. When comparing the two pathways, it was obvious that the $C_{(sp^2)}$–H was an easier bond to functionalize, however my previous work with benzyl boronic species had illustrated the highly stable nature of these compounds.[2-4] Avoiding

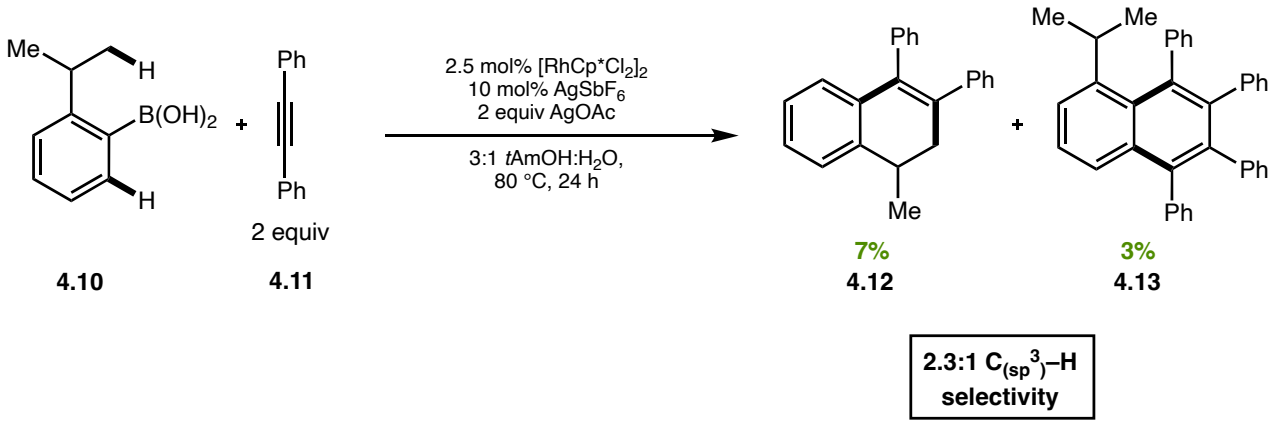

Scheme 2. Model study to determine the selectivity between migratoy insertion versus the formation of the rhodocycle.

the need for forcing conditions at an early stage, the decision was made to utilize the more commercially available aryl boronic species and slightly less acidic (reactive) $C_{(sp^3)}$–H. With these goals in mind, the commercially available aryl boronic acid (**4.10**) was chosen as the initial testing substrate. The decision to utilize an *ortho*-isopropyl group served as a good balance between providing the most chance of a $C_{(sp^3)}$–H to be in proximity to the metal, while avoiding the steric encumbrance of a *tert*-butyl moiety. Upon reacting **4.10** under the previously reported conditions, there was very little conversion of the starting material to the desired products and moderate amounts of protodeborylation due to basic aqueous conditions at high temperature.[5] Despite these findings, two compounds were isolated in 10% total yield from this reaction that corresponded with the $C_{(sp^3)}$–H (**4.12**) and the $C_{(sp^2)}$–H (**4.13**) products. Delightfully, this model system illustrated a 2.3:1 chemoselectivity for the formation of the rhodacycle prior to migratory insertion. With this information in hand, our hypothesis that accessing the metallocycle via a poised system was possible, and in fact favored. While excited about our formation of the 1-methyl-3,4-diphenyl-1,2-dihydronaphthalene (**4.12**), it was apparent that this C–C bond forming reaction was not innovative enough, even if we controlled the stereochemistry of the 1-position with our

enantioselective indenyl catalysts.[6] With this in mind, we revisited our model systems and devised a new group of substrates that would allow us to access pharma-relevant heterocyclic cores abundant in pharmacophores and industrial chemicals.

4.1.2 Early Development and Testing of α-Amino Boronic Acid Esters

The initial results of the model system, coupled with our excitement to access heterocyclic moieties led us to begin our initial investigation with alkylamines and moving on into alcohols and thiols once a reliable method had been developed (**Scheme 3.A**). As a secondary objective, we designed a system in which the C–H bond would be more reactive than the previously hypothesized benzyl boronic species. The boronic acid or acid ester would now be alkyl and alpha

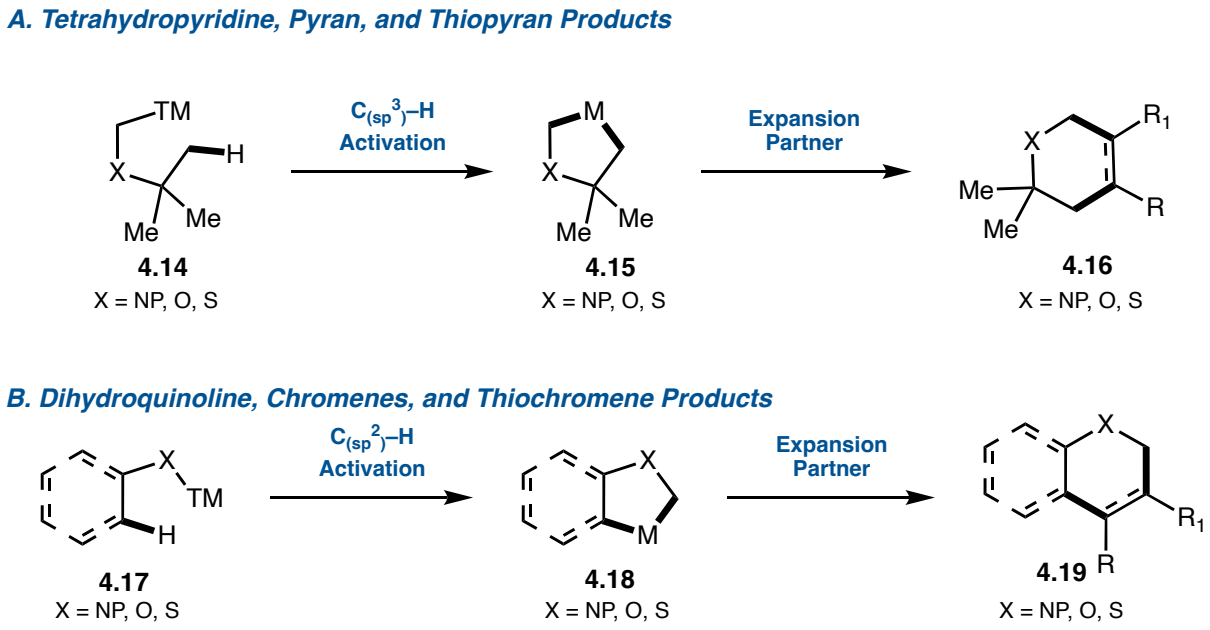

Scheme 3. Synthetic plan to access valuable heterocycles utilizing transmetallation to direct C–H functionalization.

to a heteroatom, thus rendering it more reactive to transmetallation than the carbon counterpart (**Scheme 3.B**). Our first optimization substrate chosen was *tert*-butyl amine due to its nine $C_{(sp^3)}$–

H bonds that existed at the site of functionalization. While previously we had avoided *tert*-butyl due to steric concerns, this system lacked the rigid planarity of a benzene ring. Additionally, the protecting group of the nitrogen had to be chosen as the free amine would be a liability for both the transition metal and potential intramolecular activation of the empty p-orbital at boron.

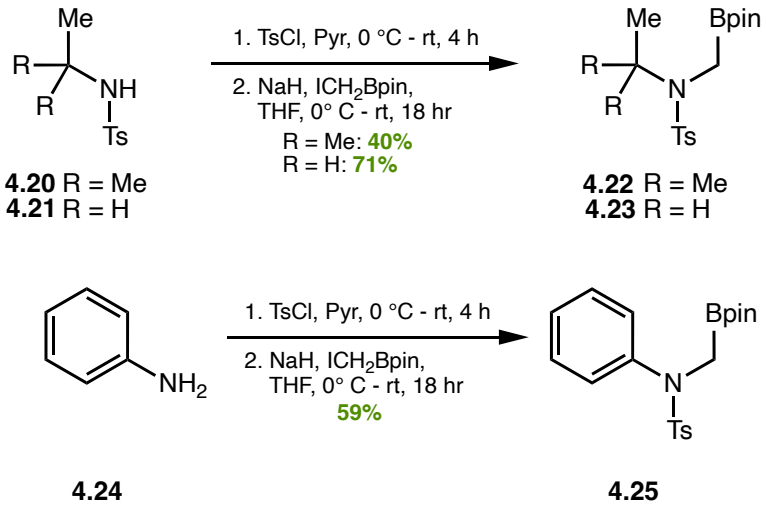

Scheme 4. Initial preparation route to α-amino boronic acid ester for testing.

Furthermore, the nitrogen needs a protecting group that decreases its Lewis basicity and avoids moieties known to participate in directed C–H functionalization. With these limitations in mind and the desire for a robust group, we chose the sulfonamide family and tosyl specifically, to leverage its stability at elevated temperature. Commercially available alkylamines (**4.20**, **4.21**) and aniline (**4.24**) were protected under basic condition with tosyl chloride, purified, and alkylated with iodomethylboronic acid pinacol ester over two steps to provide the bench stable boryl species (**4.22, 4.23, 4.25**) in moderate to good yields. The alkyalation was evaluated with several bases to include KOtBu, nBuLi, and tertiary amines, however, NaH (60% dispersion in oil) provided the most consistent and unadulterated conversion to the α-amino boronic acid ester. With these compounds in hand, we subjected it to the same conditions previously utilized in **Scheme 2** and

saw no reactivity with the alkylamine derived species (**4.22** or **4.23**). However, a 6% yield of the corresponding 1,2-dihydroquinoline product arising from $C_{(sp^2)}$–H functionalization of the aniline derivative (**4.25**) was observed. This motivated us to undertake a screening campaign to quickly optimize common parameters of the reaction, however the aryl region of the proton NMR was

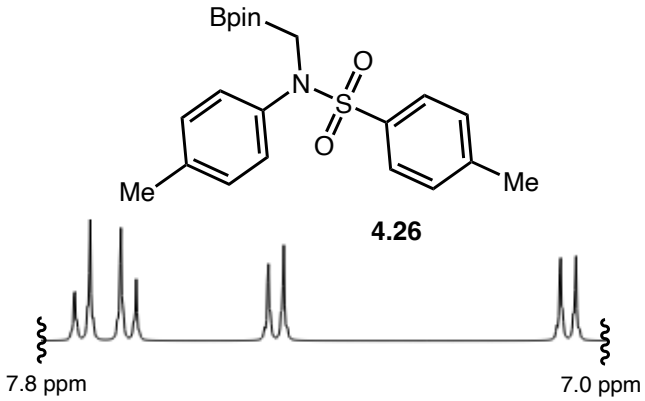

Figure 1. Substrate selection for two-dimensional screening based on aryl ^{1}H NMR signals.

overcomplicated by the large amount aryl C–H signals so the substrate was altered to assist with screening by internal standard. The decision was made to utilize *p*-toluidine as the commercially available precursor due to the high symmetry afforded by the compound's (**4.26**) aryl-^{1}H NMR signals (**Figure 1**) and by the ease with which we could determine desymmetrization arising from $C_{(sp^2)}$–H functionalization. The reagent (**4.26**) was synthesized by the above method on gram-scale and isolated in 67% yield over two steps as a bench stable powder for use in optimization studies.

Initially, the optimization began with the screening of various oxidants and AgOAc and $Cu(OAc)_2$ were both found to be competent, however the Blakey lab has seen silver loadings present challenges in the past with Rh(III) catalysis and therefore avoid super stochiometric loadings whenever possible. As a result, we began the 2D screening with copper acetate and an increased temperature of 100 ºC to maximize chances of conversion. During solvent screening of various mixtures of degassed neat solvent and water (degassed), a trend was seen in which the

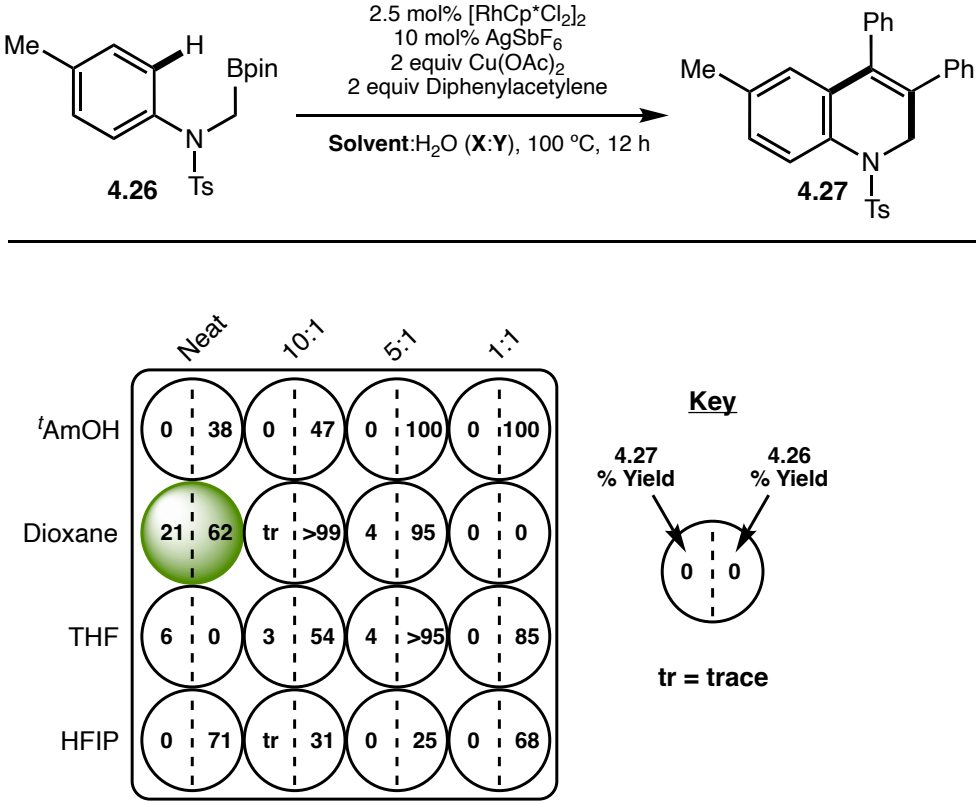

Scheme 5. Two-dimensional screening with internal standard. Yields based on integration of ^{1}H NMR signals following workup.

inclusion of water at low levels allowed the consumption of starting material but rarely converted to the desired product (**Scheme 5**). The major byproduct observed during these experiments was methylated sulfonamide arising from the protodeborylation of **4.26**. Serendipitously, the use of neat dioxane led to conversion of the starting material, while also preventing the formation of the prototdeborylated byproduct. Studies involving various metals (Rh, Co, Ir), addition of CMD promoting carboxylates ($^-$OAc, $^-$OBz, $^-$OPiv, $^-O_2$CAdamantyl), and their cation (Li^+, Cs^+, H^+) illustrated that only Rh(III) and the carboxylic acid were competent in the system. The use of 10% AcOH additive led to an increase of 7% in overall yield while still avoiding the conversion of starting material to *N*-methyl sulfonamide. Further screening led us to benzoic acid and $Cu(OAc)_2$ as the best combination of additives and oxidant (**Scheme 6**). This combination not only provided

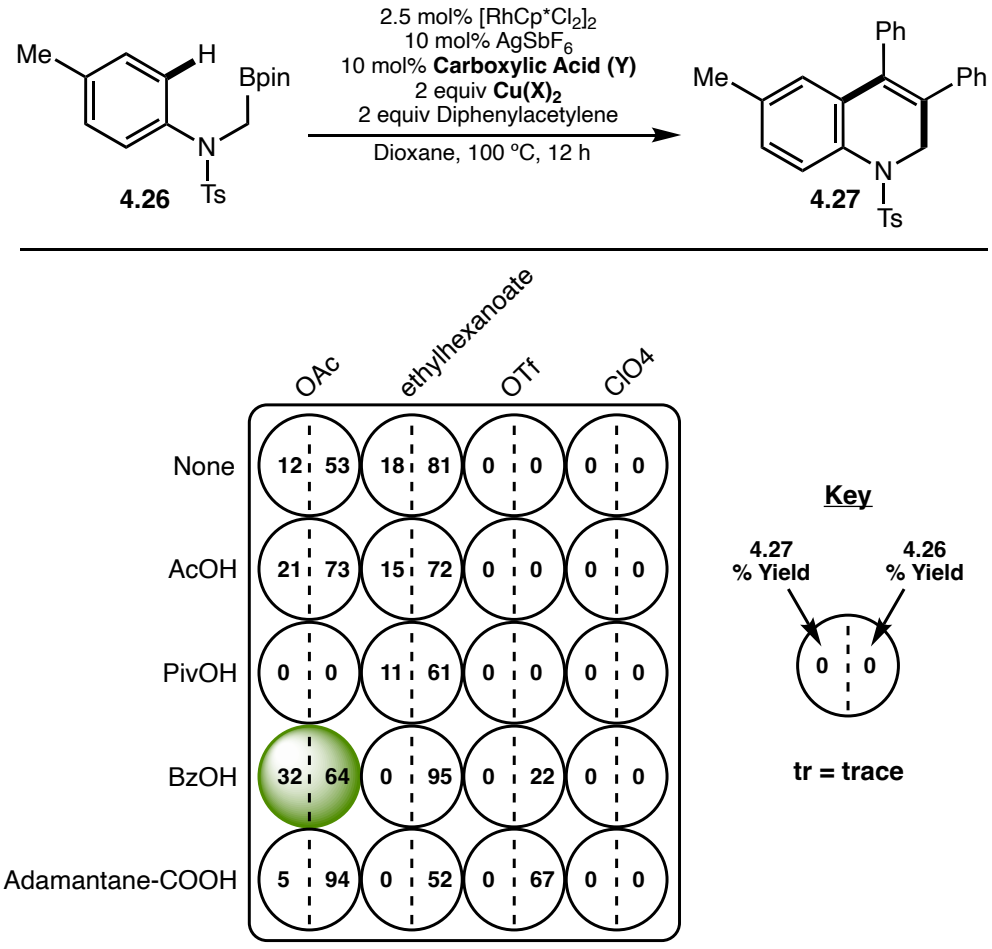

Scheme 6. Two-dimensional screening with internal standard. Yields based on integration of ^{1}H NMR signals following workup.

better conversion, but the mass balance was beneficial for continued optimization studies. Benzoic acid derivatives were then screened to determine if the pKa of the benzoate played an important role in the conversion of starting material (**4.26**) to product (**4.27**). *Para*-substituted benzoic acid derivatives were screened (-CF_3; -H; -^{t}Bu; -OMe; -NMe_2) and 4CF_3-benzoic acid, the most stable carboxylate, was shown as the most efficacious for the conversion of starting material. Following this discovery, the temperature was raised to 120 °C and the catalyst loading to 5 mol% [RhCp*Cl_2]$_2$. This newly optimized system was able to achieve 48% conversion to product (**4.27**) and a 7% yield of a detosylated/aromatized quinoline (**4.28**) [**Scheme 7**]. Subsequent work on this

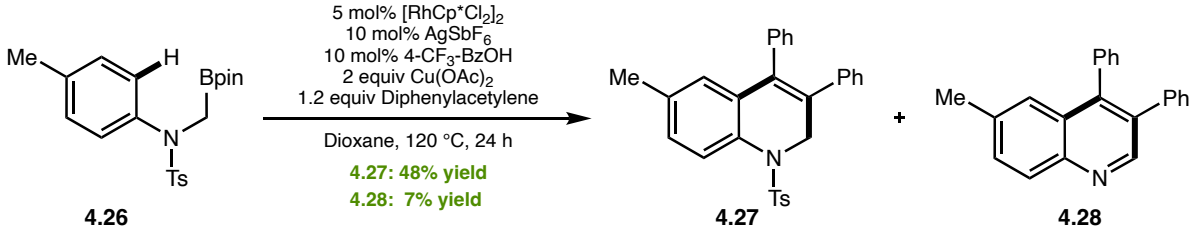

Scheme 7. Final conditions following the two-dimensional screening campaign.

reaction revealed a plateau had been reached as the conversion to product refused to increase above the ~50% mark. Examining the system mechanistically led us to the belief that the quinoline byproduct (**4.28**) may be poisoning our catalyst and preventing the rhodium from re-engaging the next molecule of substrate. This postulation arose due to the presence of the quinoline's (**4.28**) Lewis basic nitrogen and its ability to direct C–H functionalization as described in Chapter 3. To test this hypothesis, a series of experiments were carried out utilizing the standard conditions (**Scheme 8**). The first experiment was catalyst doping, in which an addition catalytic equivalent of

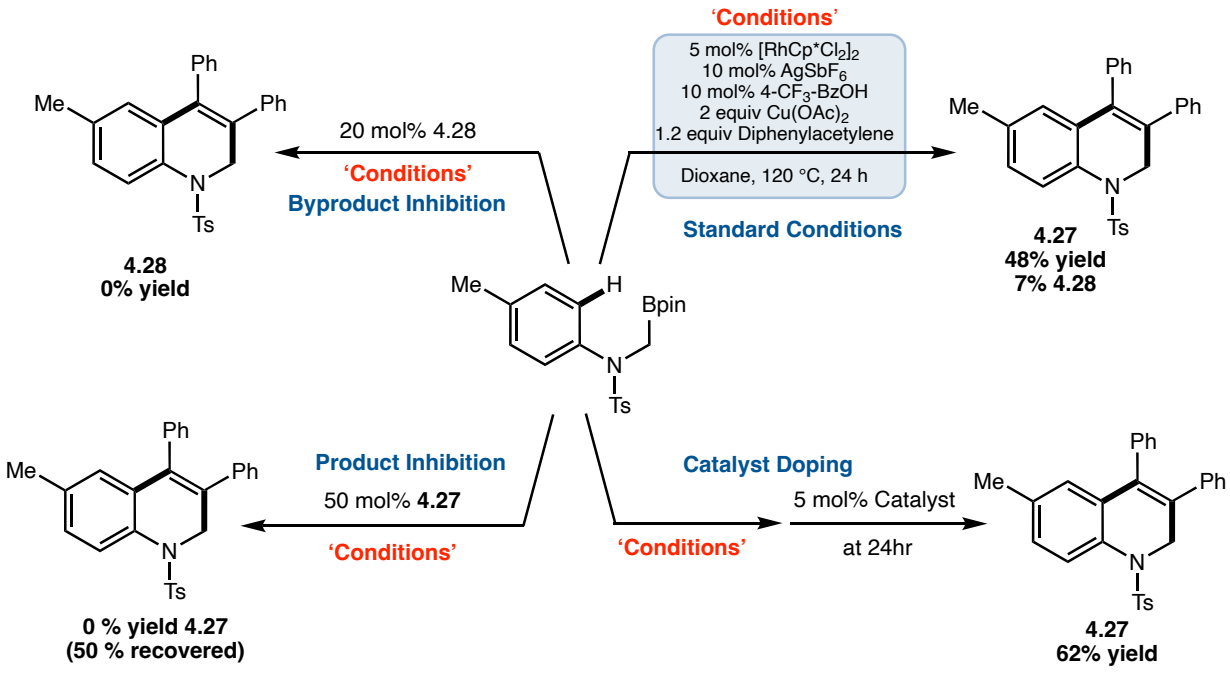

Scheme 8. Mechanistic experiments to determine if catalyst death/poisoning is the issue causing the plateau in yield.

pre-stirred [RhCp*Cl_2]$_2$ and $AgSbF_6$ for dehalogenation were added in an aliquot of dioxane. The result of this addition was a rescuing of the reaction and addition conversion of (**4.27**) by ~15%. With the experimental evidence clearly pointing to some agent acting to shutdown catalysis, we began to probe whether this could be attributed to product and/or byproduct inhibition. When the reaction was doped with 50% of the isolated product (**4.27**), we saw a return of the same percentage with no additional conversion. When the reaction was doped with 20 mol% of the quinoline byproduct (**4.28**), twice the rhodium loading, the reaction was completely inhibited. With these results in hand, we were able to draw the conclusion that the aromatization of 1,2-dihydroquinoline was resulting in a Lewis basic poison that chelated and removed the rhodium from our productive cycle. Equipped with this knowledge, we set out to determine the cause of detosylation observed in the 1,2-dihydroquinoline products and subsequent catalysis poisoning. We were acutely aware that our reaction was taking place in a highly basic environment due to the excess of acetate and elevated temperatures. Additionally, the *in-situ* formation of the quinoline was observed in the NMR samples of chloroform treated with KCarb and molecular sieves, albeit at a slower rate. The base mediated tosyl deprotection and aromatization was then confirmed in a 61% yield by treatment of 1,2-dihydroquinoline (**4.27**) with excess KO^{t}Bu in dioxane at 80 ºC to provide quinoline (**4.28**).

Following this investigation, we were able to propose a catalytic cycle and our byproduct formation (**Scheme 9**). The [RhCp*Cl_2]$_2$ is dehalogenated via silver from $AgSbF_6$ to lower the induction time to on cycle. At this point (**Complex I**), the Rh (III) catalyst engages the substrate and undergoes transmetallation to form **Complex II** and utilizes a carboxylate ligand to perform CMD on the *ortho*-C($_{sp^2}$)–H. The coordination of migratory insertion partner, diphenylacetylene in this example, forms **Complex III,** the 5-membered rhodacycle. Formal migratory insertion of

the alkyne generates the high energy 7-membered rhodacycle, **Complex IV**, which quickly undergoes reductive elimination to the desired product with Rh(I) coordinated (**Complex V**). Disassociation of the Rh(I) and oxidation by two equivalents of copper acetate return the catalyst to **Complex I** and turnover the cycle. As the product accumulates and is exposed to free acetate ligand and heat, the base-promoted aromatization occurs and produces the quinoline that begins to chelate and siphon off rhodium from the active cycle.

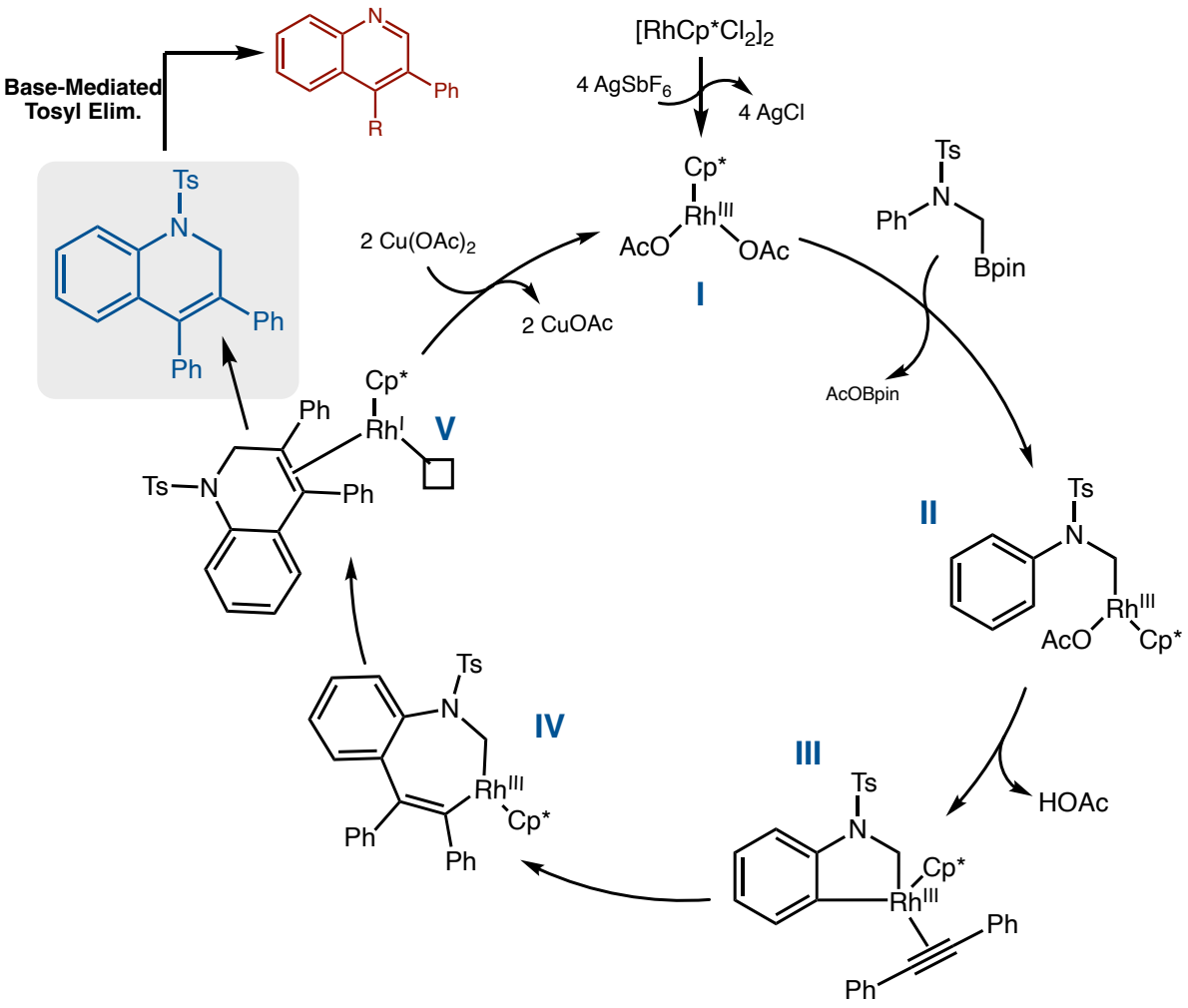

Scheme 9. Proposed catalytic cycle and off-pathway formation of quinoline byproduct

The discovery and development of this transmetallation traceless directing group chemistry required many variables of optimization to achieve a competent system. Despite our initial challenges this system proved to be highly consistent, and we hoped that the yield would improve as we explored additional substrates and migratory insertion partners. With that goal in mind, we set out to determine the limitations of the current system over a broad range of aryl α-amino boronic acids and insertion partners.

4.2 Exploration of Expansion Partners and Further Development of Aryl α-Amino Boronic Species

4.2.1 Screening for Competence of Migratory Insertion Partners

Looking to determine the scope of compounds that could participate in migratory insertion, several typical partners were selected from commercial sources (**4.27a-e; h-k**) and two made via known procedures in a single step (**4.27f-g**) [**Scheme 10**]. The use of electron withdrawing esters on the alkyne completely turned off reactivity, as did the terminally protected alkyne (**4.27a-c)**. Despite this, the inclusion of an alkyl substituent opposite the aryl unit, provided slightly lower reactivity, but saw regioselective insertion that exclusively provided the aryl moiety at the *beta*-carbon of the 1,2-dihydroquinoline (**4.27d-f)**. The use of styrene and 1,2-disubstituted aryl alkenes were also met with no reactivity in this system to our surprise (**4.27h-i**). Finally, the incorporation of phenyl allene (**4.27g**), styrene (**4.27j**), and benzonitrile (**4.27k**) were not acceptable in this methodology. With the results of this screen in hand, we limited our migratory insertion partners to aryl alkynes and avoided the use of strongly electron withdrawing groups at the other end. The current hypothesis for the shutdown seen with the ester bearing alkynes is a belief that the electron withdrawing groups remove too much electron density from the alkyne and thus lead to a poor π-

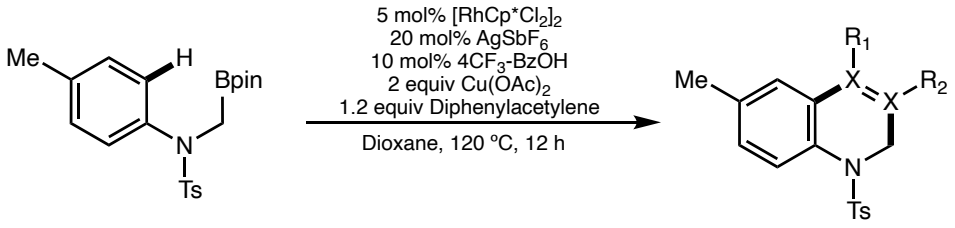

4.26

4.27 a-k
X = C, NH

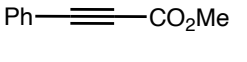

4.27a

0% yield

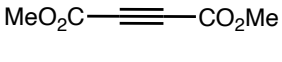

4.27b

0% yield

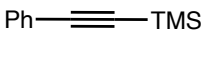

4.27c

0% yield

4.27d

29 % yield
>20:1 r.r.

4.27e

22 % yield
>20:1 r.r.

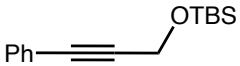

4.27f

32 % yield
>20:1 r.r.

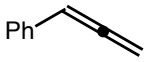

4.27g

0% yield

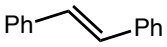

4.27h

0% yield

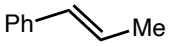

4.27i

0% yield

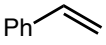

4.27j

0% yield

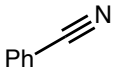

4.27k

0% yield

Scheme 10. Scope of migratory insertion partners tested for reactivity.

acid that cannot coordinate effectively to the rhodium metal prior to insertion. Further computational studies and mechanistic investigations will need to be undertaken to test this hypothesis and help elucidate the underlying reasons.

4.2.2 Generation of α-Amino Boronic Species and Evaluation in Optimized Conditions

Following our screening campaign of insertion partners, we began to validate the tolerance of our α-amino boronic species. This was step was to determine if we were limited to tosyl sulfonamide. We began by preparing variously protected anilines to include *N*-Boc, *N*-TMS, *N*-TCBoc, *N*-CBZ, and *N*-Benzoyl, however the alkylation with iodomethylboronic acid pinacol ester failed with each of these. The isolated reaction product was usually the *N*-methyl tertiary amine pointing to stability issues allowing protodeborylation to occur. This was not without precedent though as Molander and coworkers had previously prepared the N-Boc-α-amino species and quickly converted it to the BF_3K salt due to bench/purification stability issues.[7] Additionally, Marder and coworkers also found the 2-amino pyridine variant with α-methine or pseudo-quaternary center required -70 ºC storage in the glovebox to prevent degradation.[8] The substrate

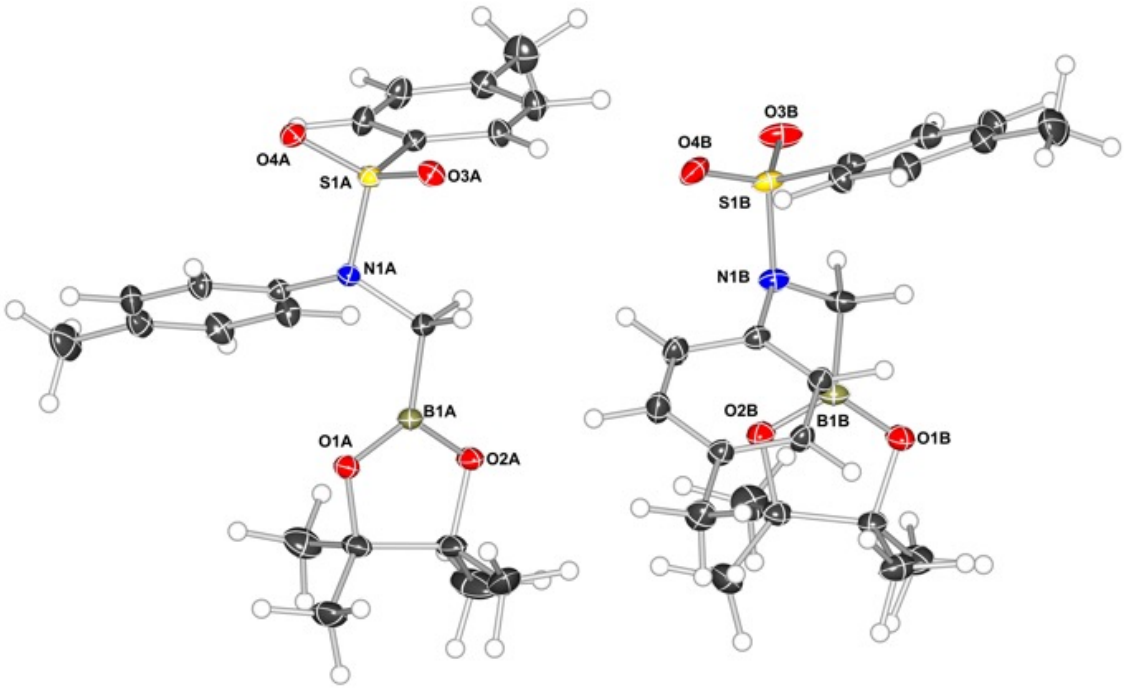

Figure 2. SCXRD of (4-Me)-Ph-α-amino boronic acid pinacal ester. Observed as two different configurations in one cell and no signs of intramolecular stabilization were detected.

we developed was found to be bench stable and unlike Marder's, did not rely on intramolecular bonding to stabilize the pyridine as indicated by our crystal structure of **4.26** (**Figure 2**)The one avenue we failed to explore was the alkyl masked aniline due to the previous evidence of Lewis basicity interference with the catalyst. This remains an unexplored area that could be very beneficial for the formation of tricyclic systems as experimentation with carbon substitutions at the α-position progress.

Armed with this knowledge, we were able to move forward in obtaining a boryl scope. The plan was to study the limitations of the system on both aryl and heteroaryl systems. This required probing the steric and electronic effects of the α-amino boronic acid esters, as well as determining the overall stability of these complexes. We began this by examining the effect of substituents around the aryl ring at the *ortho*- (**4.29a-e**), *meta*-(**4.29f-j**), and *para*- (**4.29k-r**) positions (**Scheme 11**). Additionally, we looked at multiple substitutions of the aryl ring at the *meta*- and *para*-positions (**4.29s-x**), for changes in regioselectivity of the $C_{(sp^2)}$–H selectivity of the rhodium catalyst. Throughout the development of these substrates, the yields were consistently 50-80% over two steps and showed little impact on the formation of the α-amino boronic acid pinacol esters. The exception of which is the 4-nitroaniline (**4.29p**), where the highly crystalline nature of the products caused significant issues and losses during workup and purification. Furthermore, this method was applicable to various aminopyridines (**4.30a-c**) with only a slight degradation in yield over two steps and arising from lower conversion during alkylation.

Following some initial testing with the *para*-substituted α-amino boronic acid pinacol esters, we determined that the 4-CF_3 substrate (**4.29o**) would be utilized for additional optimization studies utilizing ^{19}F NMR with internal standards and would be the substrate utilized to explore alkyne diversity. Therefore, a large-scale reaction of **4.29o** was conducted utilizing only

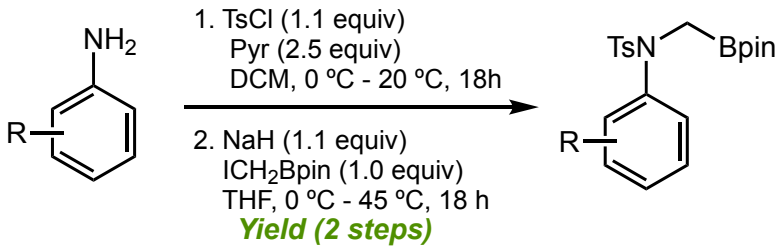

4.29 R = **a: 2-Me: 71%** **b: 2-^{i}Pr: 79%** **c: 2-^{t}Bu: 60%** **d: 2-CF_3: 74%** **e: 2-F: 62%** **f: 3-OMe: 60%** **g: 3-OPh: 56%** **h: 3-Me: 64%** **i: 3-F:72%** **j: 3-CF_3: 63%** **k: 4-OMe: 54%** **4.26: 4-Me: 65%** **4.25: 4-H: 77%** **l: 4-F: 78%** **m: 4-Ph: 66%** **n: 4-Br: 72%** **o: 4-CF_3: 64%** **p: 4-NO_2: 38%** **q: 4-vinyl: 53%** **r: 4-CO_2Me: 57%** **s: 3,5-OMe: 55%** **t: 3,5-Me: 67%** **u: 3,5-CF_3: 72%** **v: 3,4,5-Me: 59%** **w: 3CF_3-4Br: 57%** **y: 3CF_3-4Me: 75%** **x: 3,4-dioxole: 56%**

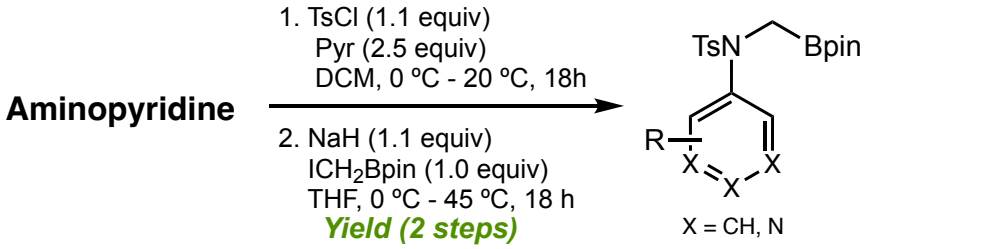

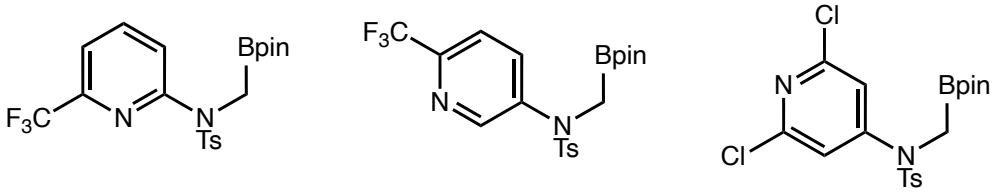

4.30a **47%** **4.30b** **62%** **4.30c** **43%**

Scheme 11. Scope of α-aminoboronic acid pinocol ester partners developed to test reactivity.

triggeration/recrystallization and a comparable yield of 62% was obtained providing nearly 10 g of material. Further diversification of the α-amino boronic acid pinacol esters will be covered in a later section.

4.2.3 Revisiting Optimization of The Rhodium Catalyzed System Prior to Implementation

During the development of this project, the 2020 COVID lockdown and several other pauses occurred between the initial optimization screening and development of the method. In order to determine the optimal conditions were already in hand, a second optimization screen was carried out with a new substrate (**4.29o**) which allowed for rapid determination of crude yields by ^{19}F NMR with α,α,α-trifluorotoluene as the internal standard. During the rescreening we revisited many of the conditions from earlier, as well as some new modifications to the system. While revisiting competent metal catalysts, we saw that CoCp* and IrCp* (**Scheme 12; Entry 3-4**) derivatives still showed no sign of reactivity, however $RhCp^E$ (**Scheme 12; Entry 2**) was able to generate product albeit in a lower yield. Additionally, the use of other Rh(III) catalysts (RhInd*, $RhCp^{tBu}$) not shown here were able to catalyze the transformation but in very low yields. Revisiting the addition of carboxylic acids saw that 4CF3-BzOH acid remained the most capable by a margin of ~30% (**Scheme 12; Entry 5-7**). The molar percentage of benzoic acid derivative was also found to be very important as the yield decreased as the equivalents rose above a 1:1 ratio with Rh metal (**Scheme 12; Entry 8-9**). Fluctuations in heating continued to show that 120 ºC was the optimal temperature and lower temperature suffered from lack of transmetallation, and high temperatures led to facile decomposition of the boronic acid pinacol ester moiety (**Scheme 12; Entry 10-12**). Furthermore, the removal of $Cu(OAc)_2$ in favor of silver oxidants or other Cu^{2+} lead to a shutdown in reactivity that showed stochiometric conversion to rhodium loading at best (**Scheme 12; Entry 13-18**). One bespoke oxidant of note is the inclusion of $Cu(4CF_3\text{-}BzO)_2$ [**4.31**], as this was utilized to lower the basicity of the overall system utilizing the additive (**Figure 3**). The system was unable to perform even when acetate was doped back in and further confirmed our determination of a 1:1 molar ratio of the additive to rhodium. Finally, modification of the tosyl protecting group to that

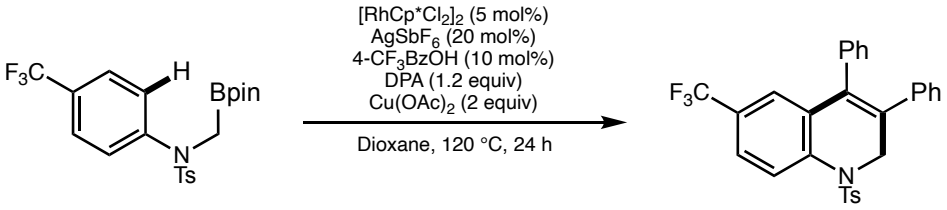

Entry	Deviation from Std. Cond.	Yield by ^{19}F NMR (isol.)
1	**None**	**76% (73%)**
2	$[RhCp^{E}Cl_2]_2$ (5 mol%) as catalyst	32%
3	$[IrCp^*Cl_2]_2$ (5 mol%) as catalyst	0 %
4	$[CoCp^*(CO)I_2]$ (10 mol%) as catalyst	0 %
5	AcOH in place of 4-CF_3BzOH	46 %
6	PivOH in place of 4-CF_3BzOH	21 %
7	BzOH in place of 4-CF_3BzOH	35%
8	20 mol% 4-CF_3BzOH	50 %
9	50 mol% 4-CF_3BzOH	37 %
10	80 °C	9 %
11	100 °C	52 %
12	140 °C	40 %
13	AgOAc in place of $Cu(OAc)_2$	>5 %
14	AgOBz in place of $Cu(OAc)_2$	>5 %
15	$Cu(OTf)_2$ in place of $Cu(OAc)_2$	Trace
16	Cu(ethylhexonoate)$_2$ in place of $Cu(OAc)_2$	14 %
17	$Cu(acac)_2$ in place of $Cu(OAc)_2$	>5 %
18	Cu(4-CF_3-BzOH)$_2$ **[4.31]** in place of $Cu(OAc)_2$	7 %
19	Mesylated instead of Tosyl protected SM **[4.32]**	83 % (81%)
20	Nosylated instead of Tosyl protected SM **[4.33]**	78 % (68 %)

Scheme 12. Optimization table following rescreening relevant conditions with optimal substrate.

of mesyl and nosyl showed great promise, however both groups were more readily eliminated to provide the quinoline and suffered from shorter lifetime of the final compounds (**Scheme 12;**

Entry 19-20). With the confirmation of our optimal system in hand, we began to turn our eye toward the scope of this reaction in terms of both the α-amino boronic acid pinacol esters and the alkyne migratory insertion partners.

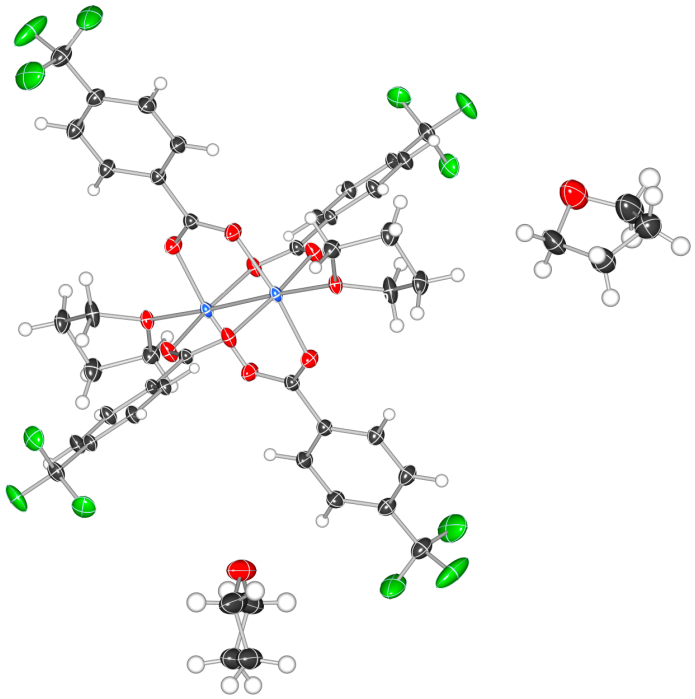

Figure 3. SCXRD of Cu(4CF_3-BzO)$_2$ as a paddle wheel dimer with two THF molecules as co-crystallized. Due to copper interfering with the NMR, we confirmed the identity with crystallography.

4.3 Evaluating the Scope of This Methodology and Inherit Limitations of the System

4.3.1 Scope of Aryl α-Amino Boronic Acid Pinacol Esters with Diphenylacetylene

Methodology development relies on the scientist reporting the new method to adequately screen the electronic and steric parameters that may upset the transformation. This crucial information will help to guide others in academia and industry as they pursue different or more

challenging substrates on the utility of a new method and its adaptability. In keeping with this standard, the first exploration of scope focused on the use of the substituted α-amino boryl species (**4.29a-x; 4.30a-c**) to determine their efficacy in this method. We began by screening the *ortho*-substituents and found that steric hinderance *ortho*- to the amine shut down reactivity of the system in the case of these systems (**Scheme 13: Entry 4.34a-e**). Additional work was done to determine if the tosyl group was causing this issue, however test reactions with the mesyl variants also showed limited to no reactivity. Exploration at the *meta*-position more fruitful in our investigation due to the presence of regioselectivity for the least sterically encumbered product leaving the substituent at the 7-position of the dihydroquinoline scaffold (**Scheme 13: Entry 4.34h-j**). Interestingly, ethereal linkages lead to a regiomeric ratio of ~1.6:1 for the 5-position in all cases despite the size of the attached carbon moiety (**Scheme 13: Entry 4.34f-g**). While we are uncertain

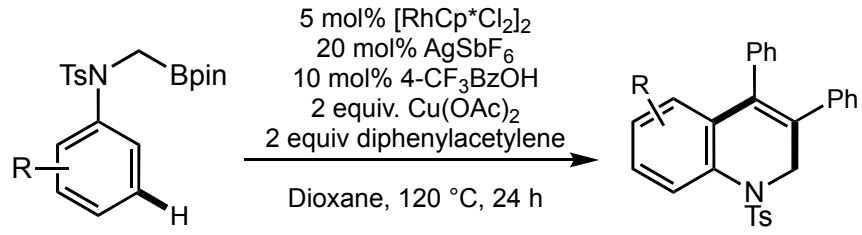

4.25; 4.26; 4.29a-x → **4.27; 4.34a-x; 4.35**

4.34 R =

a: 2-Me: 13%*
b: 2-^{i}Pr: 9%*
c: 2-^{t}Bu: 0%
d: 2-CF3: 6%*
e: 2-F: n.d.
f: 3-OMe: 60%,1.5:1 rr
g: 3-OPh: 63%,1.7:1 rr
h: 3-Me: 36%, >20:1 rr
i: 3-F: n.d.
j: 3-CF_3: 54%, >20:1 rr
k: 4-OMe: 27%
4.27: 4-Me: 78%
4.35: 4-H: 72%
l: 4-F: 38%
m: 4-Ph: 61%
n: 4-Br: 59%
o: 4-CF_3: 73%
p: 4-NO_2: 42%
q: 4-vinyl: 53%
r: 4-CO_2Me: 63%
s: 3,5-OMe: 42%
t: 3,5-Me: 0%
u: 3,5-CF_3: 0%
v: 3,4,5-Me: 0%
w: 3CF_3-4Br: 75%, >20:1 rr
y: 3CF_3-4Me: 74%, >20:1 rr
x: 3,4-dioxole: 41%,1.6:1 rr

* = ^{1}H NMR yield

Scheme 13. Scope of 1,2-dihydroquinoline products with substitution at the α-aminoboronic acid pinocol ester partner.

as to the exact reasoning for this inversion, the current hypothesis is that there is some form of coordination occurring to drastically reverse the normal selectivity and override steric influences. While sterics were a large consideration due to desymmetrization of the products, the *para*-substituents were studied more for their electronic influences. There were no clear electronic trends that could be drawn from the observed data as the yields were very stead in the 50-80% range across the group (**Scheme 13: Entry 4.27; 4.34k-r; 4.35**). It is of note that the 4-OMe (**4.34k**), 4-F (**4.34l**) and 4-NO_2 (**4.34p**) substitutions all suffered from low yields despite repeated experiments and currently is unexplained. Following the mono-substituted studies, we turned our attention to di- and tri- substitutions but found that the 3,5-substitution pattern only worked with -OMe groups (**Scheme 13: Entry 4.34s-v**). Presently, we believe this is due to the small steric α-value of methoxy but may be related to the coordination hypothesized above.[9] Finally, we tested out the 3,4-disubstitution pattern and were delighted to observe high regioselectivity for the meta substituent in the 7-postion, except for the dioxolane (**Scheme 13: Entry 4.34w-x**). In the case of the dioxolane (**4.34x**), we again observed the sterics being overridden and the 5,6- bridged position being the major regioisomer.

4.3.2 Scope of (Hetero)Aryl α-Amino Boronic Acid Pinacol Esters with Diphenylacetylene

Evaluation of heteroaryl moieties in this reaction was conducted through the application of differently substituted aminopyridines. Due to the concern of Lewis basic pyridyl nitrogen, the substitution of electron withdrawing groups was utilized ortho to the nitrogen in all three test substrates (**4.30a-c**). Unsurprisingly, conversion to the 1,2-dihydro-1,8-naphthyridine (**4.36a**) was low yielding due to the competing 5-membered rhodacycle with the aromatic nitrogen. This however was not the case in the 3-amino (**4.30b**) and 4-amino (**4.30c**) variants, as the nitrogen is

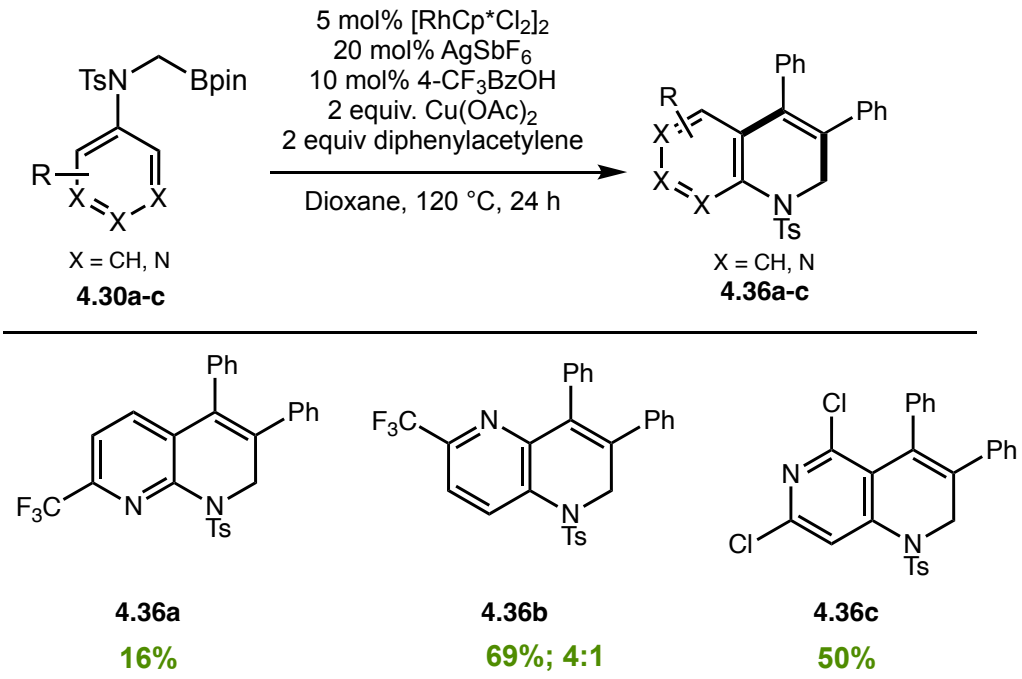

Scheme 14. Scope of heteroaryl α-aminoboronic acid pinocol ester partners developed to test reactivity.

further away and the metallocycle is significantly less favored. There was a good yield and moderate regioselectivity for the 1,2-dihydro-1,5-naphthyridine (**4.36b**) in a 4:1 ratio between the 2-position and the 4-position. This is to be expected at the reactivity of pyridine positions is known to be 2 > 4 > 3 in two-electron, metal catalyzed reactions such as this one. The 2,6-dichloro-4-amino substrate also achieved moderate yield of the desired 1,2-dihydro-1,6-naphthyridine (**4.36c**). While there are limitations on the use of heteroaryl species, this serves to inform the community that these previously difficult scaffolds are attainable but require careful planning to avoid unchecked Lewis basicity and regioselectivity issues.

With all these results in hand, we were able to move forward with the alkyne scope. It is of note that we chose to move forward with (4-CF_3)-Ph α-amino boronic acid pinacol (**4.29o**) over 4-Me (**4.26**) as the initial studies indicated this substrate performed better with the diverse alkynyl partners. As a word of caution, this decision, while great for yields, was severely problematic due

to the fluorine-carbon splitting observed in ^{13}C NMR. While highly regioselective compounds were easily characterized by high field NMR, inseparable mixtures of regioisomers were problematic due to the overlapping signals and large quartet *J* values.

4.3.3 Scope of (Hetero)Aryl Alkynes with (4-CF_3)-Ph α-Amino Boronic Acid Pinacol Ester

Evaluation of alkyne partners for the annulation reaction began with looking at substituted (hetero)aryl rings to probe any electronic nuances of the migratory insertions. This was first undertaken by looking at bis-substituted alkynes with electron withdrawing and donating groups at the *para*-position (**Scheme 15: Entry 4.38a-c**). While all the substrates provided good yields, the 4-OMe bis-substitution (**4.38c**) did led to a 5-10% decrease in total product. In a bid to leverage this small difference, we designed a push-pull like system in which one ring was electron withdrawing and the other donating (**4.37d**). This system provided the highest overall yield but only provided 1.7:1 regioselectivity with the electron donating ring installed at the site of C–H functionalization (**4.38d**). Further studies utilizing pyrrole and pyridine heteroaryl alkynes juxtaposed by a phenyl (**4.37e-f**) led to a significant decrease in yield but maintained comparable regioselectivity at a ratio of ~2:1 (**4.38e-f**). While the decrease in yield was significant, these scaffolds had previously been unknown and showcase the wide applicability of this system to tolerate differently substituted (hetero)aryl alkynes. Building off this promising start, we began to look at singly substituted aryl alkynes in a hope that further diversification would be possible.

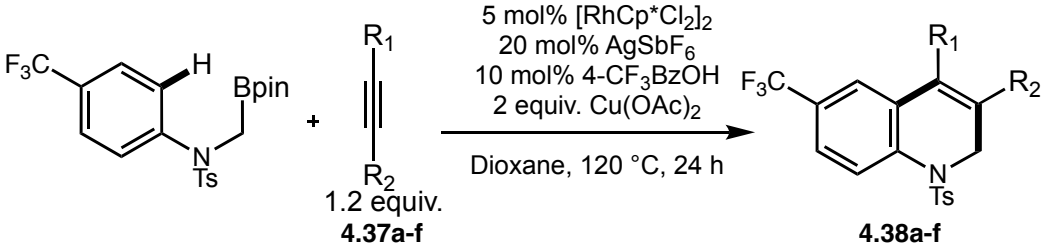

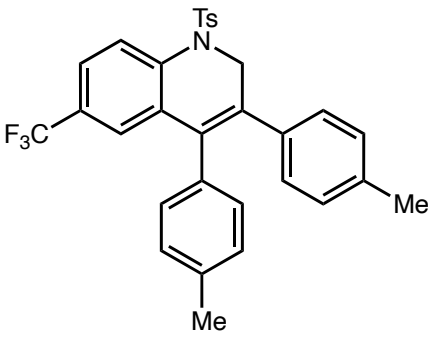

4.38a
72%

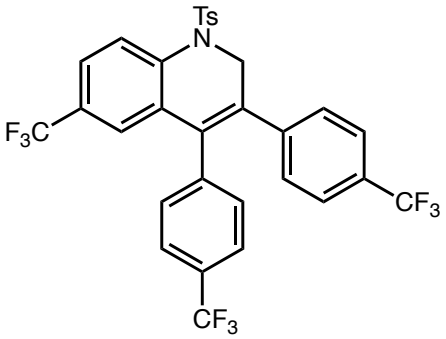

4.38b
78%

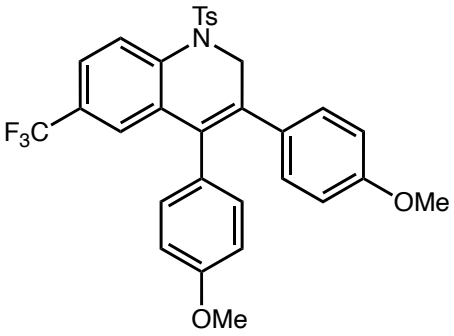

4.38c
67%

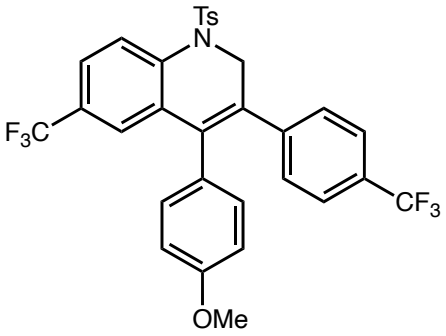

4.38d
80%; 1.7:1

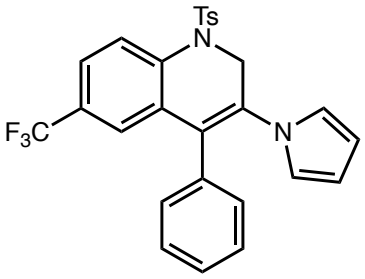

4.38e
28%; 1.7:1

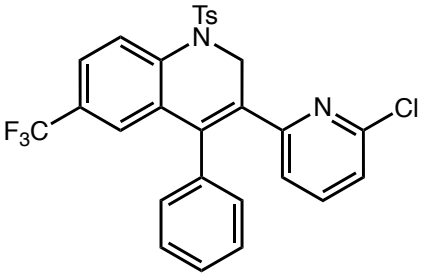

4.38f
49%; 2.1:1

Scheme 15. Scope of heteroaryl alkyne insertion partners.

4.3.4 Scope of Alkyl- Aryl Alkynes with (4-CF_3)-Ph α-Amino Boronic Acid Pinacol Ester

When choosing alkynes for the scope, we sought to find interesting moieties that would leverage the previously observed regioselectivity. Additionally, we strived to include functionality that could be expanded upon in subsequent step as needed to build interesting scaffolds without the substitutions being deemed merely as accoutrement. We began by reinvestigating the previously competent alkynes from our initial screening (**Scheme 10**). Despite the lower yields with the 4-Me substituted substrate (**4.26**), we found that the 4-CF_3 substrate (**4.29o**) provided us with good yields and a retention of excellent regioselectivity. Phenyl alkyne substituted with methyl (**4.40a**), ethyl (**4.40b**), and cyclopropyl (**4.40c**) at the terminal carbon provided yields more than 65% and retained complete selectivity for placing the alkyl group next to the site of C–H activation (**Scheme 16**). Furthermore, silyl protected propargyl alcohols were tolerated when TIPS (**4.40d**) was used as a protecting group. The use of TBS (**4.40d**) saw a sharp drop in desired product due to the desilylative conditions of the reaction with less robust groups. It is of note that the byproduct of the reaction was the free alcohol 1,2-dihydroquinoline. The retention of stereochemistry on the propargyl alcohol (**4.40e**) also provided mechanistic evidence that the alkyne was not going through an allene prior to or during C–H functionalization. Finally, a phthalimide protected amino acid derivative, arising from homopropargylamine, was also competent in this reaction providing modest yield and excellent selectivity. This was an exciting result as non-canonical amino acids have become very useful in pharmaceuticals and biotherapies in recent years. An additional biorelevant molecule was utilized, however in the case of a sugar (acetate protected tetrahydro-

2H-pyran derivative on 3-phenylproparyl alcohol) we were only able to observe the regioselectivity (18:1) by NMR due to separation issues.

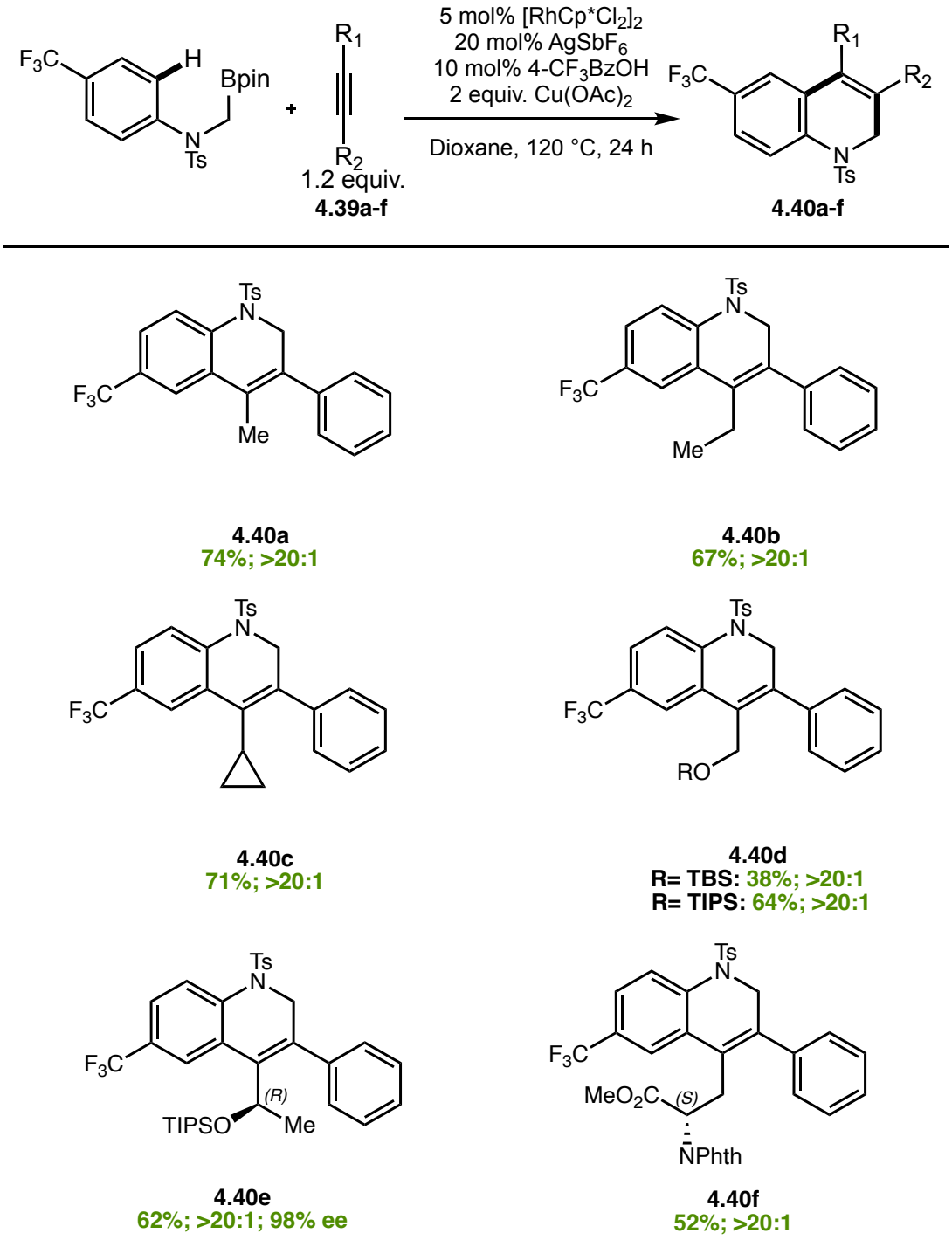

Scheme 16. Scope of alkyl-aryl alkyne insertion partners.

With the promising results of this study, we turned our attention toward the viability of heteroaryl-alkyl alkynes to determine if they too would be competent expansion partners. Sadly, the results seemed extremely dependent on the heteroaryl substitution present (**Scheme 17**). In the case of a 2-substituted pyridine, the yield of **4.42a** was marginal but retained excellent regioselectivity. 2-substituted thiophene provided good yield and excellent selectivity (**4.42b**), yet the 3-substituted furan (**4.42c**) suffered from a significant loss in yield. Furthermore, the 5-

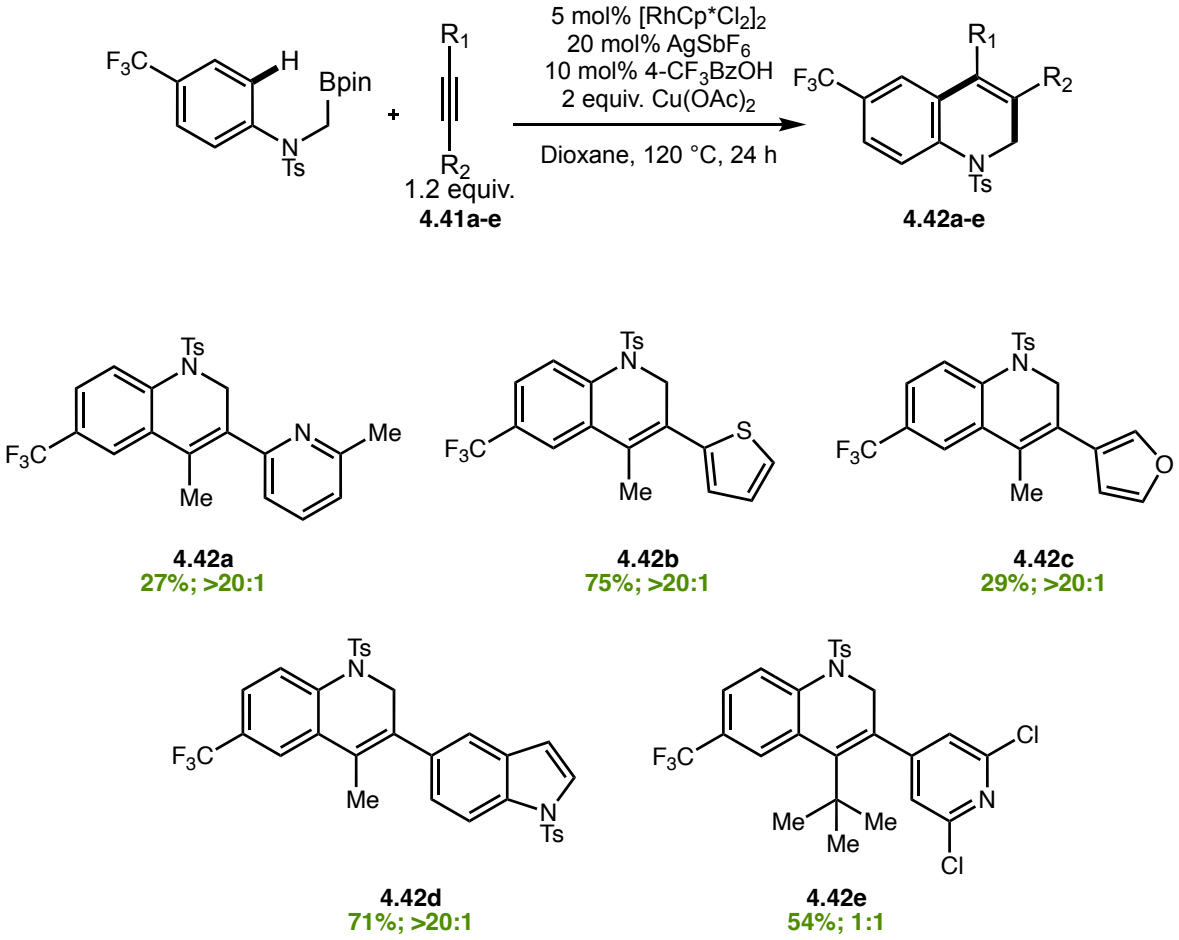

Scheme 17. Scope of alkyl-heteroaryl alkyne insertion partners.

substituted, tosyl protected indole behaved as previous aryl rings had to provide **4.42d** with excellent selectivity and good yield. In a final bid to include pyridine, the 2,6-dichloro-4-(3,3-dimethylbut-1-yn-1-yl)pyridine (**4.41e**) was able to provide the product (**4.42d**) in modest yield

but 1:1 selectivity. This departure from the usual >20:1 selectivity was baffling at first, however the α-value of a *tert*-butyl group is >4.5 while the pyridine can be estimated close to phenyl at 3.0.[9] The tert-butyl group is significantly larger than the methyl, methylene, and methine centers utilized earlier as these only have an α-value of 1.8 to 2.3, and therefore steric hindrance at the benzylic position is not unreasonable.[9] Following the completion of this heteroaryl-alkyl scope, we believed that enough substrate diversity had been illustrated for this methodology and began compiling the necessary data to complete the story. The main issue we encountered, was that variability of the alkyne and its regioselectivity had led to a highly acidic proton at the benzylic/α-amino methylene that rendered some of these compounds unstable and prone to tosyl-elimination/aromatization. In some cases, this occurred while NMRs were being taken and in other cases the product was stable for months. While we have no way to predict this stability, it is paramount to treat these 1,2-dihydroquinoline products as unstable until evidence points to otherwise. Due to this we explored what options were available to functionalize the products into more stable pool of diversifiable intermediates.

4.3.5 Diversification of 1,2-Dihydroquinolines and Further Experiments

The desire to convert these products into various products arises from the need to utilize these scaffolds as core molecules for the construction of larger systems. To prove the utility of this building block, we began by assessing the most common modifications available through changes in oxidation state. This required us to first carry out a gram scale reaction of our methodology and

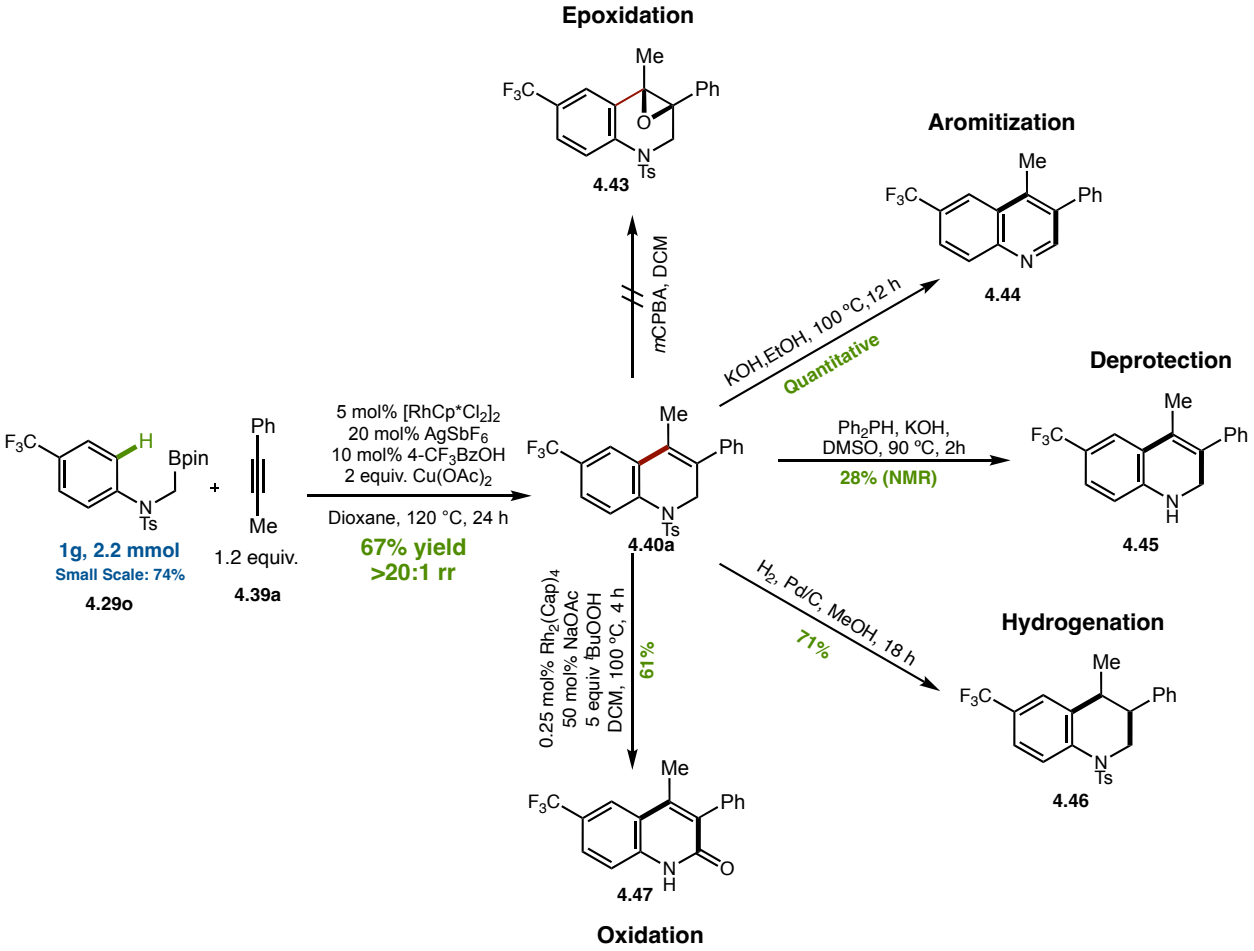

Scheme 18. Gram scale reaction and diversification of **4.40a**.

this provided us with ample material for future studies. It is of note that the gram scale reaction provided 4.40a in similar yield and selectivity as the smaller reaction previously despite being scaled by a factor of twenty-two. The first two studies undertaken were the aromatization and hydrogenation of the 1,2-dihydroquinoline (**4.40a**). The base mediated tosyl elimination with KOH in ethanol provided the quinoline (**4.44**) in quantitative yield. These conditions were superior to the previously utilized KO*t*Bu in THF discussed previously which provided only ~70% conversion. The hydrogenation to provide the 1,2,3,4-tetrahydroquinoline (**4.46**) utilized 5% Pd/C under an atmosphere of hydrogen gas to provide a 71% yield at room temperature. These conditions were very mild and near quantitative conversion is conceivable with the inclusion of

heat, pressure, and/or more reactive catalysts. We began looking at various ways of oxygenating the substrate and began first with a focus on forming the fully substituted oxirane (**4.43**). Despite our attempts with various conditions using *m*CPBA and H_2O_2, in all cases the 1,2-dihydroquinoline (**4.40a**) was destroyed. While this was disheartening, there remain avenues for the access to these oxiranes. One such possibility is the use of propargyl alkyne followed by a Sharpless epoxidation or trying a larger suite of more exotic peroxides/peroxyacids. Undeterred by the oxirane attempts, we turned our eyes towards lactamization of **4.40a**. Our first attempts with SeO_2 were unsuccessful, however the use of Doyle's dirhodium catalyst, $Rh_2(Cap)_4$, offered immediate conversion to the lactam (**4.47**).[10] Unpredictably, the detosylation of the amide to provide the secondary nitrogen was carried out during the reaction eliminating the need for a second step to deprotect. Finally, we turned our attention to deprotection of **4.40a** to provide the free secondary amine. Various methods were employed to remove the tosyl group, to include sodium naphthalenide, TfOH,[11] and phosphines.[12] In all cases, the desulfonation and workup provided us with the quinoline (**4.44**) upon isolation. The method by Yang and coworkers with diphenyl phosphine was the only reaction that showed the desired product (**4.45**) in 28% NMR yield when an aliquot was taken during the reaction. At completion, the product obtained was solely the quinoline (**4.44**). Despite these setbacks we decided to move on as clearly serious optimization and/or advancement in the field desulfonylation of these substrates is required.

With the diversification complete, we turned our attention towards several other reactions to complete the investigation of this methodology. The most important of which was the determination of the reversibility of the $C_{(sp^2)}$–H activation. To accomplish this with our substrates we developed several deuterated analogues of our starting materials to study hydrogen incorporation at the position ortho to the amine. To deconvolute our signals, the decision was made

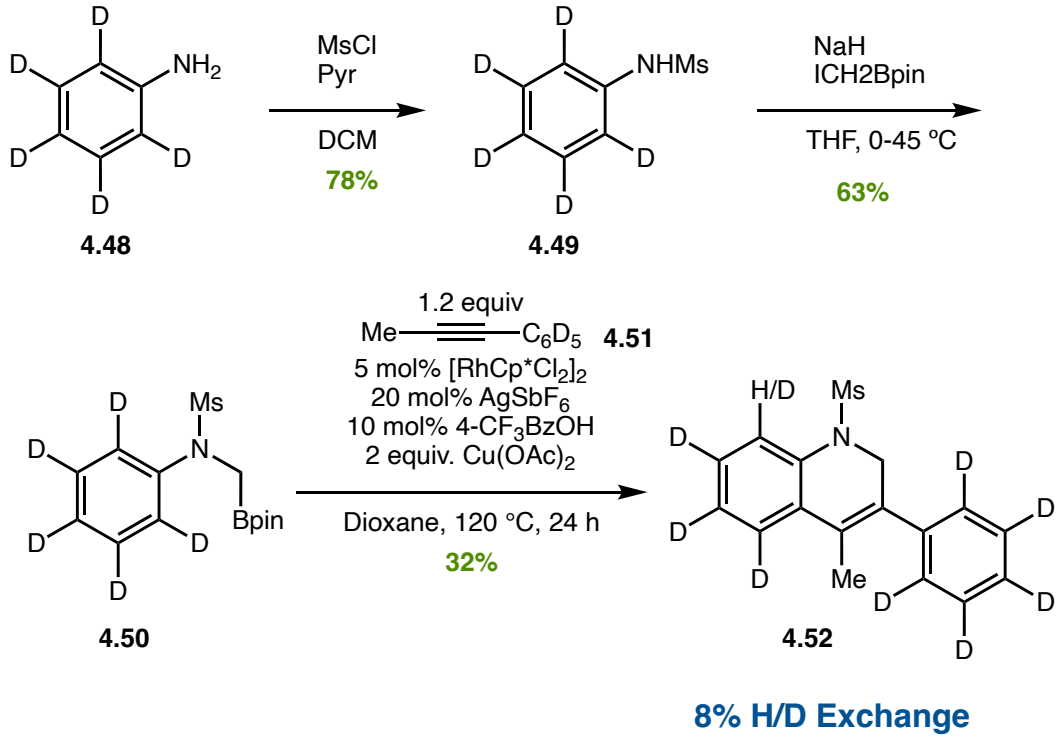

Scheme 19. Determination of reversibility via hydrogen/deuterium incorporation experiments.

to utilize the mesylate protecting group on the starting material (**4.50**) and a fully deuterated phenyl on the alkyne (**4.51**). Upon subjection to the reaction conditions, we observed a 32% of **4.52** overall yield with excellent regioselectivity as expected (**Scheme 19**). The ^{1}H NMR did show 8% hydrogen incorporation at the 4-position of **4.52** which is indicative of reversibility at the C–H activation step. While 8% seems insignificant, the total pool of available hydrogen from the reaction mixture was 10% due to the prescence of the 4-CF_3-BzOH additive. With these results in hand and an excess of **4.50**, we also utilized KIE to gain some initial rate determinations (**Scheme 20**).[13] To accomplish this, we utilized reaction quenching at initial timepoints of 30, 120, and 240 minutes to approximate the initial slope of the reaction. Our findings pointed to an experimental

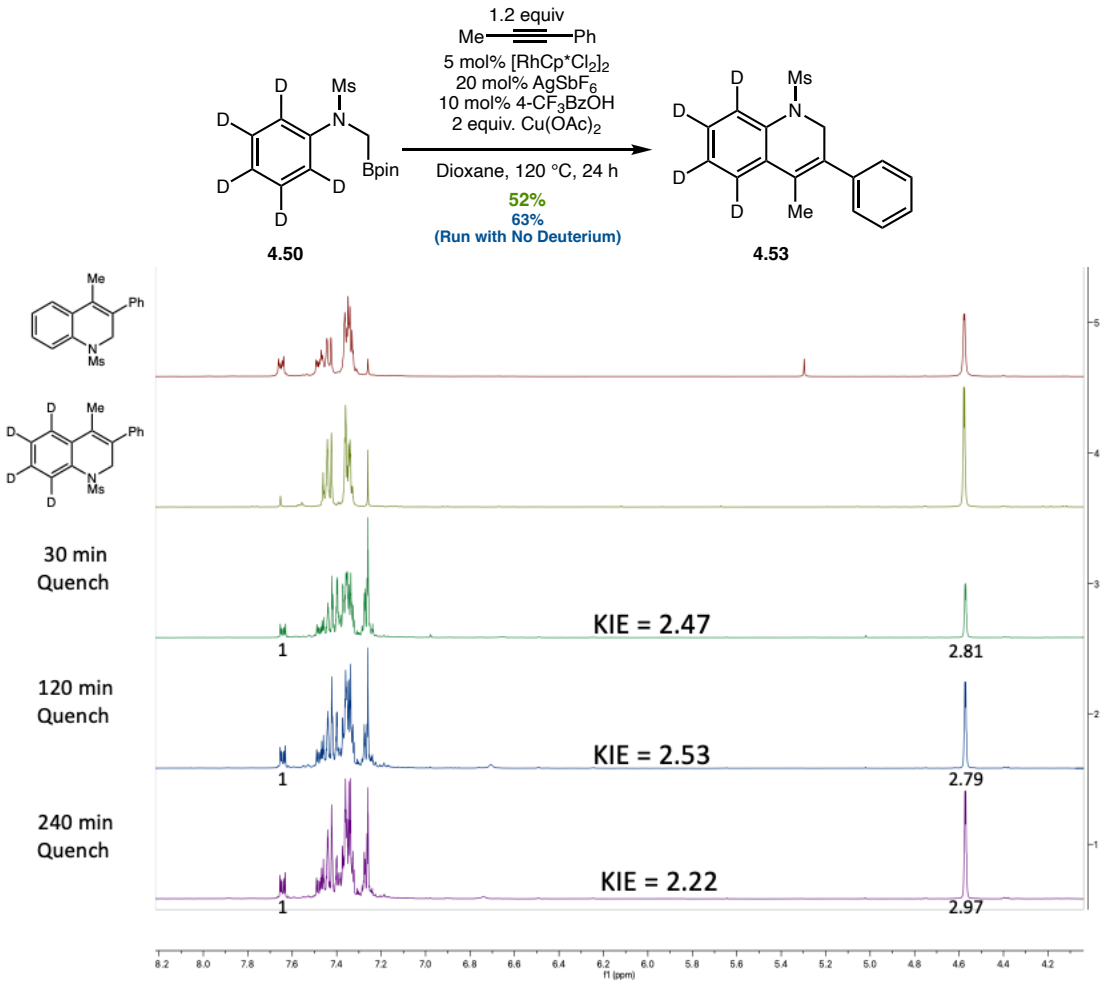

Scheme 20. Determination of initial rate through KIE experiments and ^{1}H NMR.

initial rate of ~2.5 which fits squarely within the window of a rate we expect to find. Further computational investigation and detailed kinetic experiments will be required to confirm this and determine exact values. We hope that following the disclosure of this methodology that other academics with expertise in this area would be interested to collaborate on these studies.

4.4 Concluding Remarks

Having successfully developed a new method for the use of transmetallation reagents for C–H annulation, we were able to demonstrate the utility of (hetero)aryl α-amino boronic acid pinacol

esters and alkynes to be utilized towards the production of 1,2-dihydroquinolines in moderate to good yield and excellent regioselectivity. Previously these scaffolds were readily approached via intramolecular allylic amination and elimination of O-leaving groups at the 4 position.[14] This generally limited the availability of non-cyclic 3,4 disubstitutions in the literature. While the final methodology leaves some to be desired, this chemistry represents a first of its kind approach to C–H functionalization via transmetallation and immediately followed by C–H functionalization. While this disclosure in preparation will mark the end of this project, we hope that industry and academia will leverage our work to continue expanding the scope of traceless directing groups, transmetallation reagents, and other uses for the newly disclosed α-amino boryl species.

4.5 References

1. Kong, W. L.; Finger L. H.; Oliveira, J. C. A.; Ackermann, L. Rhodaelectrocatalysis for Annulative C−H Activation: Polycyclic Aromatic Hydrocarbons through Versatile Double Electrocatalysis. *Angew. Chem. Int. Ed.* **2019**, *58*, 6342-6346.

2. Hollerbach, M.R.; Barker, T. J. Chemoselective Benzylation of Aldehydes Using Lewis Base Activated Boronate Nucleophiles. *Organometallics*, **2018**, *37*,1425-1427.

3. Hollerbach, M.R.; Hayes, J.C.; Barker, T. J. Benzylation of Imines with Activated Boronate Nucleophiles. *Eur. J. Org. Chem*. **2019**, *7*, 1646-1648.

4. Hayes, J.C.; Hollerbach, M.R.; Barker, T. J. Nucleophilic addition of benzylboronates to activated Ketones. *Tet. Lett*. **2020**, *61*, 151505.

5. Cox, P. A.; Reid, M.; Leach, A. G.; Campbell, A. D.; King, E. J.; Lloyd-Jones, G. C. Base-Catalyzed Aryl-$B(OH)_2$ Protodeboronation Revisited: From Concerted Proton Transfer to Liberation of a Transient Aryl Anion. *J. Am. Chem. Soc.* **2017,** *139*, 13156-13165.

6. Farr, C. M. B.; Kazerouni, A. M.; Park, B.; Poff, C. D.; Won, J.; Sharp, K. R.; Baik, M.-H.; Blakey, S. B., Designing a Planar Chiral Rhodium Indenyl Catalyst for Regio- and Enantioselective Allylic C–H Amidation. *J. Am. Chem. Soc.* **2020**, *142*, 13996-14004.

7. Molander, G. A.; Shin, I. Potassium Boc-Protected Secondary Amino methyl trifluoroborates: Synthesis and Suzuki Miyaura Cross-Coupling Reactions. *Org. Lett.* **2012**, *14*, 4458-4461.

8. Ming, W.; Liu, X.; Friedrich, A.; Krebs, J.; Marder, T.B. The Borono−Strecker Reaction: Synthesis of α-Aminoboronates via a Multicomponent Reaction of Carbonyl Compounds, Amines, and B2pin2. *Org. Lett.***2020**, *22*, 365-370.

9. Muller, P. Glossary of terms used in physical organic chemistry (IUPAC Recommendations 1994). *Pure and Applied Chemistry*. **1994**, *66* (5): 1077–1184.

10. Yu, Y.; Humeidi, R.; Alleyn, J. R.; Doyle, M. P. Catalytic Allylic Oxidation of Cyclic Enamides and 3,4-Dihydro-2H-Pyrans by TBHP. *J. Org. Chem.* **2017**, *82*, 8506−8513.

11. Javorskis, T.; Orentas, E. Chemoselective Deprotection of Sulfonamides Under Acidic Conditions: Scope, Sulfonyl Group Migration, and Synthetic Applications. *J. Org. Chem*. **2017**, *82*, 13423−13439.

12. Li, C.; Huang, Y.; Cao, S.; Luo, Y.; Zhang, Y.; Yang, G. A robust and facile method for desulfonation to amines. *Org. Chem. Front*. **2021**, *8*, 6182–6186.

13. Baldwin, J.E.; Gallagher, S.S.; Leber, P.A.; Raghavan, A.S.; Shukla, R. Deuterium Kinetic Isotope Effects and Mechanism of the Thermal Isomerization of Bicyclo[4.2.0]oct-7-eneto1,3-Cyclooctadiene. *J. Org. Chem*. **2004**, *69*, 7212-7219.

14. a) Zhang, Z.; Zeng, X.; Xie, D., Chen, D.; Ding, L.; Wang, A.; Yang, L.; Zhong, G.; N-Heterocyclic Carbene-Catalyzed Activation of Esters of N-Hydroxyphthalimide: A Highly Enantioselective Route to Chiral Dihydropyridinones Bearing an All Carbon Quaternary Stereogenic Center. *Org. Lett.*, **2015**, *17*, 5052-5055. b) Chen, S.; Hao, L.; Zhang, Y.; Tiwari, B.; Chi, Y.R. Asymmetric Access to the Smallest Enolate Intermediate via Organocatalytic Activation of Acetic Ester. *Org. Lett*., **2013**, *15*, 5822-5825. c) Case, F. H. Substituted 1,10-Phenanthrolines. I. The Synthesis of Certain Mono- and Polymethyl-1,10-phenanthrolines. *J. Am. Chem. Soc.* **1948**, *70*, 3994–3996. d) Arcadi, A.; Calcaterra, A.; Fabrizi, G.; Fochetti, A.; Goggiamani, A.; Iazzetti, A.; Marrone, F.; Marsicano, V.; Mazzoccanti, G.; Serraiocco, A. Synthesis of 4-Substituted-1,2-Dihydroquinolines by Means of Gold-Catalyzed Intramolecular Hydroarylation Reaction of *N*-Ethoxycarbonyl-*N*-Propargylanilines. *Molecules* **2021**, *26*, 3366-3368. e) Tabassum, R.; Ashfaq, M.Oku, H. Development of an efficient, one-pot, multicomponentprotocol for synthesis of 8-hydroxy-4-phenyl-1,2-dihydroquinoline derivatives. *J. Heterocyclic Chem*. **2021**, *58*, 534–547

4.6 Experimental Section

4.6.1 General Information

All reactions were carried out under nitrogen atmosphere with anhydrous solvents in oven-or flame-dried glassware using standard Schlenk technique, unless otherwise stated. Anhydrous dichloromethane (DCM), diethyl ether (Et_2O), tetrahydrofuran (THF), and toluene were obtained by passage through activated alumina using a Glass Contours solvent purification system. Dioxane was dried and deoxygenated by sodium/benzophenone still and used freshly distilled. Solvents for workup, extraction, and column chromatography were used as received from commercial suppliers without further purification. All chemicals were purchased from Sigma-Aldrich, Strem Chemicals, Oakwood Chemicals, Alfa-Aesar, Ambeed, or Fluka and used as received without further purification, unless otherwise stated. ^{1}H and ^{13}C nuclear magnetic resonance (NMR) spectra were recorded on a Varian Inova 600 spectrometer (600 MHz ^{1}H, 151 MHz ^{13}C), a Bruker 600 spectrometer (600 MHz ^{1}H, 151 MHz ^{13}C), a Varian Inova 500 spectrometer (500 MHz ^{1}H, 126 MHz ^{13}C), and a Varian Inova 400 spectrometer (400 MHz ^{1}H, 126 MHz ^{13}C) at room temperature in $CDCl_3$ with internal $CHCl_3$as the reference (7.26 ppm for ^{1}H, 77.16 ppm for ^{13}C), unless otherwise stated. Chemical shifts (δ values) were reported in parts per million (ppm) and coupling constants (Values) in Hz. Multiplicity was indicated using the following abbreviations: s = singlet, d = doublet, t = triplet, q = quartet, qn = quintet, m = multiplet, br = broad. High resolution mass spectra (HRMS) were obtained using a Thermo Electron Corporation Finigan LTQFTMS (at the Mass Spectrometry Facility, Emory University). High Pressure Liquid Chromatography (HPLC) was performed on an Agilent 1100 series HPLC utilizing CHIRALPAK AD-H, AS-H, OD-H and OJ-H 4.6x 150 mm analytical columns. Analytical thin layer chromatography (TLC) was performed on precoated glass-backed Silicycle SiliaPure® 0.25 mm silica gel 60 plates and visualized with UV light, ethanolic p-anisaldehyde, or aqueous potassium permanganate (KMnO4). Flash column chromatography was performed using Silicycle SiliaFlash® F60 silica gel (40-63 μm) on a Biotage Isolera One system. Preparatory TLC

was performed on precoated glass backed Silicycle SiliaPure® 1.0 mm silica gel 60 plates. We acknowledge the use of shared instrumentation provided by grants from the NIH and the NSF.

4.6.2 Procedures and Tabulated Data

General Procedure 1 (GP1) for Sulfamidation of Primary Amines:

A flame dried 2-neck round bottom flask with stir bar was charged with amine (1.0 equiv.) and placed under N_2 atmosphere (3 x 1 min/cycle). The flask was solvated with anhydrous DCM (0.2M) and placed in a 0 ˚C ice bath under a positive stream of N_2. The TsCl (1.1 equiv.) was added under positive stream of N_2 and the reaction. Anhydrous pyridine (2.2 equiv.; 3.2 if amine was HCl Salt) was added was allowed to stir at 0 ˚C for an additional 30 min. The reaction was then brought to room temperature and allowed to stir for 18 hours.

Aryl substrate workup: The reaction was suspended in 1M HCl and then extracted with DCM times. The combined organic layer was further washed with saturated aqueous $CuSO_4$ (1x) to remove excess pyridine, DI H2O (1x), and then brine (1x). The organic layer was then dried over sodium sulfate and concentrated. The residue was then either recrystallized via triggeration in Et_2O:Pentane or purified by column chromatography in EtOAc: Hex (90:10 → 80:20) in cases of an oil. Triggerated solids were confirmed by NMR and used in the next reaction without further purification.

Heteroaryl substrate workup: Basified with 3M NaOH and extracted with DCM three times. Organic layer was discarded, and water layer was acidified to pH 3 with conc. HCl while stirring. Flask was allowed to cool down in fridge for 1 hour and then filtered through a glass frit and triturated with pentanes before drying under vacuum.

General Procedure 2 (GP2) for *N*-Alkylation of Sulfonamides:

An oven dried round bottom with stir bar was charged with a 60% dispersion of NaH in mineral oil (1.1 equiv.) and placed under N_2 atmosphere (3 x 1 min/cycle). A second oven dried vial was loaded with sulfonamide (1.1 equivalent) and placed under N_2 atmosphere (3 x 1 min/cycle) before being solvated with a minimal amount of anhydrous THF. The round bottom was then solvated with anhydrous THF (0.1 M) and allowed to stir vigorously to suspend NaH. Slow addition of the sulfonamide solution forms a dense precipitate in solution that is allowed to stir for 1 hour (sonication may be required in some cases to break large clumps and regain stirring prior to next step). The 2-(iodomethyl)-4,4,5,5-tetramethyl-1,3,2-dioxaborolane (1.0 equiv.) is added to the round bottom via syringe and then the reaction is heated at 40 ˚C for 18 hours. Following the return to room temperature, the reaction is quenched with saturated aqueous NH_4Cl and extracted thrice with DCM. The combined DCM pulls were then dried over sodium sulfate and concentrated on a rotary-evaporator. The residue was recrystallized via triggeration in Et_2O:Pentane or purified on silica gel flash chromatography in Pentane: Acetone (95:5 →85:15) to afford the desired product.

(Note: The α-aminoboronic ester products slowly degrade on silica and alumina, thus they require quick purifications. Acetone prevents streaking found with other solvents.)

General Procedure 3 (GP2) for C–H annulation:

An oven dried vial with stir bar was charged with $[RhCp^*Cl_2]_2$ (5 mol %), $AgSBF_6$ (20 mol %), *p*-trifluoromethyl-benzoic acid (10 mol %), and copper (II) acetate (2.0 equiv.) in a glovebox under N_2 atmosphere. A second vial was charged with the boryl species (1.0 equiv.) and the alkyne (1.2 equiv.) The second vial was then solvated with freshly distilled anhydrous dioxane (0.02 M) and the contents added to the reaction vial under N_2 before being washed with dioxane a second time. The reaction vial was then sealed with Teflon tape, followed by electrical tape. The reaction vial is then placed in a heating block at 120 ˚C and stirred vigorously for 24 hours. Following the return to room temperature, the reaction is transferred to a larger vial with minimal Et_2O and concentrated on a rotary evaporator to dryness. The reaction is then resuspended in Et_2O, sonicated for 1 minute or

until all residue is free of the glass. The organic layer is passed through a celite filter to remove particulates with diethyl ether before being transferred into a separatory funnel with sat. aq. $NaHCO_3$ and extracted with Et_2O (3x). The combined organic layers are washed with DI H_2O, dried over sodium sulphate, filtered, and concentrated by rotary evaporator under reduced pressure. The solid residue was purified on silica gel flash chromatography to afford the desired product with Hexanes:EtOAc (100:0→85:15). Products have various level of storage stability and are prone to aromatization.

General Triggeration procedure:

A 250 mL RBF was loaded with the crude material in a minimum amount of ether and pentane was added until cloudiness was observed. An additional aliquot of ether was added to clarify the solution and then the flask was placed on a rotary evaporator. The flask was rotated rapidly outside the water bath while vacuum was applied until a dense precipitate was seen. The flask was then filtered through a glass frit and the solid triturated with cold pentanes. The procedure was repeated with the mother liquor. The solid was then collected and dried under vacuum overnight.

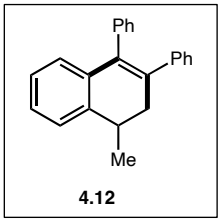

4.12

Following a known procedure[3], 1-methyl-3,4-diphenyl-1,2-dihydronaphthalene was recovered as a white residue in 7% yield following silica gel chromatography in 9:1 Hex:EtOAc. ^{1}H NMR (600 MHz, cdcl3) δ 7.54 – 7.49 (m, 1H), 7.35 – 7.29 (m, 3H), 7.27 – 7.15 (m, 3H), 7.10 (dt, J = 7.7, 1.3 Hz, 1H), 7.05 – 7.00 (m, 2H), 6.94 – 6.79 (m, 2H), 6.52 – 6.44 (m, 2H), 3.99 (d, J = 12.8 Hz, 1H), 3.53 (d, J = 12.2 Hz, 1H), 3.21 (q, J = 6.9 Hz, 1H), 0.45 (d, *J* = 6.8, 1.7 Hz, 3H). Nominal MS: Calculated for $C_{23}H_{20}$ (Mass + H): 297.16 Found: 267.117

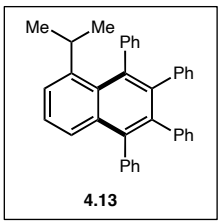

4.13

Following a known procedure[3], 5-isopropyl-1,2,3,4-tetraphenylnaphthalene was recovered as a white residue in 3% yield following silica gel chromatography in 9:1 Hex:EtOAc. ^{1}H NMR (600 MHz, cdcl3) δ 7.66 – 7.62 (m, 1H), 7.50 (ddd, J = 14.5, 7.9, 1.4 Hz, 2H), 7.42 – 7.34 (m, 2H), 7.26 – 7.19 (m, 5H), 7.14 – 7.07 (m, 4H), 6.74 – 6.70 (m, 2H), 2.86 (q, J = 6.7 Hz, 1H), 0.94 (d, J = 6.7 Hz, 6H).

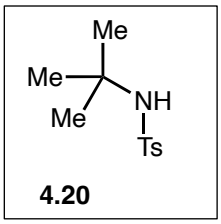

4.20

***N*-(*tert*-butyl)-4-methylbenzenesulfonamide** was obtained by known literature procedure and matched the reported known spectral data.[1]

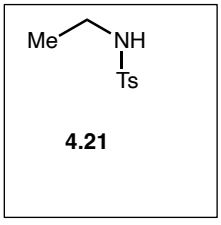

4.21

***N*-ethyl-4-methylbenzenesulfonamide** was obtained by known literature procedure and matched the reported known spectral data.[2]

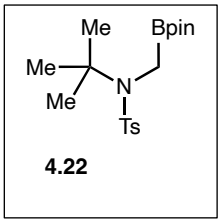

4.22

Following GP2, N-(tert-butyl)-4-methyl-N-((4,4,5,5-tetramethyl-1,3,2-dioxaborolan-2-yl)methyl)benzenesulfonamide was isolated as an off-white powder in 55% yield, 374 mg. ^{1}H NMR (600 MHz, cdcl3) δ 8.41 (m, 2H), 7.71 (m, 2H), 3.33 (s, 1H), 2.86 (s, 3H), 1.72 (s, 12H).

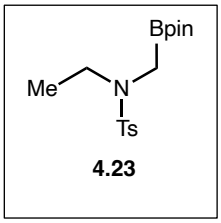

4.23

Following GP2, N-ethyl-4-methyl-N-((4,4,5,5-tetramethyl-1,3,2-dioxaborolan-2-yl)methyl)benzenesulfonamide was isolated as an tan powder in 83% yield. ^{1}H NMR (500 MHz, cdcl3) δ 7.72 (d, J = 8.3 Hz, 2H), 7.29 (d, J = 7.9 Hz, 2H), 3.16 (q, J = 7.2 Hz, 2H), 2.66 (s, 2H), 2.41 (s, 3H), 1.26 (s, 12H), 1.06 (t, J = 7.2 Hz, 3H).

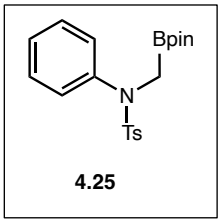

4.25

Following GP2, 4-methyl-*N*-phenyl-*N*-((4,4,5,5-tetramethyl-1,3,2-dioxaborolan-2-yl)methyl)benzenesulfonamide, was isolated as an white solid in 80% yield, 982 mg. ^{1}H NMR (400 MHz, $CDCl_3$) δ 7.37 (d, *J* = 8.3 Hz, 2H), 7.26 – 7.15 (m, 5H), 7.09 – 7.02 (m, 2H), 3.15 (s, 2H), 2.39 (s, 3H), 1.02 (s, 12H).^{13}C NMR (101 MHz, $CDCl_3$) δ 143.48, 142.05, 132.68, 129.20, 128.55, 128.36, 127.23, 127.15, 84.08, 24.49, 21.63. ^{11}B NMR (128 MHz, $CDCl_3$) δ 31.55. HRMS (+ p APCI) calculated for $C_{20}H_{27}O_4N^{10}B^{32}S$ [M+H] calculated for 387.17847, found 387.17849.

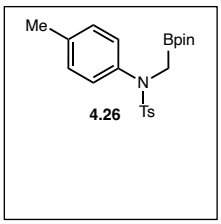

Following GP2, 4-methyl-*N*-((4,4,5,5-tetramethyl-1,3,2-dioxaborolan-2-yl)methyl)-*N*-(*p*-tolyl)benzenesulfonamide, was isolated as an white solid in 79% yield. ^{1}H NMR (400 MHz, $CDCl_3$) δ 7.39 (d, *J* = 8.3 Hz, 2H), 7.20 (d, *J* = 8.0 Hz, 2H), 7.05 – 7.00 (m, 2H), 6.93 (d, *J* = 8.4 Hz, 2H), 3.12 (s, 2H), 2.39 (s, 3H), 2.30 (s, 3H), 1.04 (s, 12H). ^{13}C NMR (101 MHz, $CDCl_3$) δ 143.37, 139.43, 137.03, 132.83, 129.18, 128.42, 127.09, 84.06, 24.52, 21.64, 21.14. ^{11}B NMR (128 MHz, $CDCl_3$) δ 31.77. HRMS (+ p APCI) calculated for $C_{21}H_{29}O_4N^{10}B^{32}S$ [M+H] calculated for 401.19412, found 401.19418.

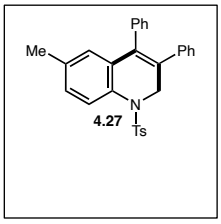

Following GP3 (0.1 mmol scale), 6-methyl-3,4-diphenyl-1-tosyl-1,2-dihydroquinoline, was isolated as a white solid in 78% yield. ^{1}H NMR (400 MHz, $CDCl_3$) δ 7.71 – 7.66 (m, 1H), 7.35 – 7.29 (m, 2H), 7.22 – 7.08 (m, 8H), 6.94 (ddd, *J* = 8.0, 1.8, 0.8 Hz, 1H), 6.71 – 6.63 (m, 2H), 6.58 (d, *J* = 7.9 Hz, 1H), 6.47 – 6.40 (m, 2H), 4.85 (s, 2H), 2.45 (s, 3H), 2.43 (s, 3H).^{13}C NMR (101 MHz, $CDCl_3$) δ 143.43, 138.70, 138.25, 137.27, 136.33, 134.56, 133.94, 130.50, 130.16, 129.60, 129.13, 127.93, 127.91, 127.78, 127.62, 127.54, 127.47, 127.05, 126.89, 126.54, 50.64, 21.47, 21.42. HRMS (+ p APCI) calculated for $C_{29}H_{26}O_2N^{32}S$ [M+H] calculated for 452.1679, found 452.1680.

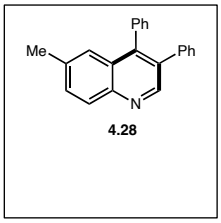

4.28

Following GP3, 6-methyl-3,4-diphenylquinoline was isolated as a white residue in 7% yield following silica gel chromatography in 9:1 Hex:EtOAc. ^{1}H NMR (399 MHz, cdcl3) δ 8.93 (s, 1H), 8.08 (d, J = 8.6 Hz, 1H), 7.55 (dd, J = 8.6, 1.9 Hz, 1H), 7.43 (s, 1H), 7.38 – 7.32 (m, 3H), 7.25 – 7.08 (m, 5H), 2.44 (s, 3H).

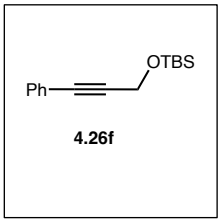

4.26f

***tert*-butyldimethyl((3-phenylprop-2-yn-1-yl)oxy)silane** was obtained by known literature procedure and matched the reported known spectral data.[3]

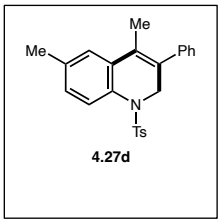

4.27d

Following GP3, 4,6-dimethyl-3-phenyl-1-tosyl-1,2-dihydroquinoline was isolated as a white residue in 29% yield following silica gel chromatography in 9:1 Hex:EtOAc. ^{1}H NMR (400 MHz, $cdcl_3$) δ 7.64 (d, *J* = 8.1 Hz, 2H), 7.37 (t, *J* = 7.4 Hz, 2H), 7.30 (d, *J* = 7.3 Hz, 2H), 7.25 (d, *J* = 8.2 Hz, 1H), 7.18 – 7.09 (m, 3H), 7.06 – 6.98 (m, 2H), 4.54 (s, 2H), 2.39 (s, 3H), 2.29 (s, 3H), 1.59 (s, 3H).

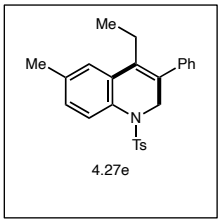

4.27e

Following GP3, 4-ethyl-6-methyl-3-phenyl-1-tosyl-1,2-dihydroquinoline was isolated as a white residue in 22% yield following silica gel chromatography in 9:1 Hex:EtOAc. ^{1}H NMR (400 MHz, cdcl$_3$) δ 7.70 (d, *J* = 8.1 Hz, 2H), 7.35 (d, *J* = 8.1, 2H), 7.30 (d, *J* = 8.0 Hz, 2H), 7.19 – 7.02 (m, 3H), 6.98 – 6.92 (m, 3H), 4.56 (s, 2H), 2.39 (s, 3H), 2.34 (s, 3H), 2.21 (q, *J* = 7.4 Hz, 2H), 0.41 (t, *J* = 7.5 Hz, 3H).

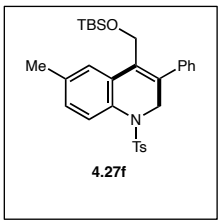

4.27f

Following GP3, 4-(((tert-butyldimethylsilyl)oxy)methyl)-6-methyl-3-phenyl-1-tosyl-1,2-dihydroquinoline was isolated as a white residue in 32% yield following silica gel chromatography in 9:1 Hex:EtOAc. ^{1}H NMR (500 MHz, cdcl3) δ 8.20 (d, J = 8.6 Hz, 2H), 7.51 – 7.41 (m, 2H), 7.42 – 7.33 (m, 3H), 7.16 – 7.06 (m, 2H), 7.02 (ddd, J = 7.7, 5.0, 2.9 Hz, 3H), 4.78 (d, J = 1.7 Hz, 2H), 4.10 (s, 2H), 2.57 (s, 3H), 2.37 (s, 3H), 0.86 (s, 9H), 0.70 (s, 6H).

Tosylated Compunds:

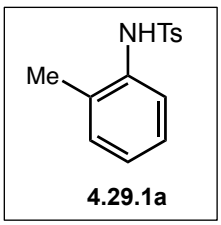

4.29.1a

Following GP1, 4-methyl-*N*-(*o*-tolyl)benzenesulfonamide, was isolated as a white solid in 67% yield and matched the reported known spectral data.[4]

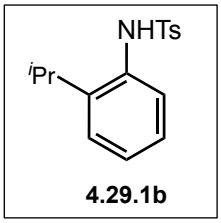

4.29.1b

Following GP1, *N*-(2-isopropylphenyl)-4-methylbenzenesulfonamide, was isolated as a white solid in 58% yield and matched the reported known spectral data.[4]

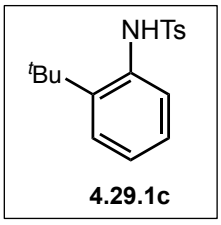

4.29.1c

Following GP1, *N*-(2-(*tert*-butyl)phenyl)-4-methylbenzenesulfonamide, was isolated as a white solid in 71% yield and matched the reported known spectral data.[5]

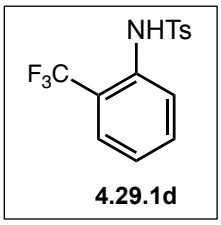

4.29.1d

Following GP1, 4-methyl-*N*-(2-(trifluoromethyl)phenyl)benzenesulfonamide, was isolated as a tan solid in 60% yield and matched the reported known spectral data.[6]

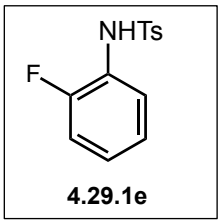

4.29.1e

Following GP1, *N*-(2-fluorophenyl)-4-methylbenzenesulfonamide, was isolated as a yellow solid in 76% yield and matched the reported known spectral data.[7]

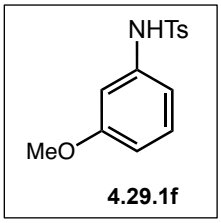

4.29.1f

Following GP1, *N*-(3-methoxyphenyl)-4-methylbenzenesulfonamide, was isolated as a white solid in 71% yield and matched the reported known spectral data.[8]

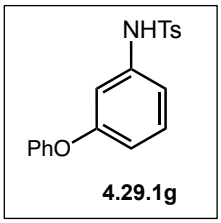

4.29.1g

Following GP1, 4-methyl-*N*-(3-phenoxyphenyl)benzenesulfonamide, was isolated as a white solid in 88% yield and matched the reported known spectral data.[9]

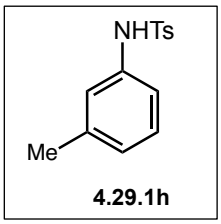

4.29.1h

Following GP1, 4-methyl-*N*-(*m*-tolyl)benzenesulfonamide, was isolated as a tan solid in 75% yield and matched the reported known spectral data.[10]

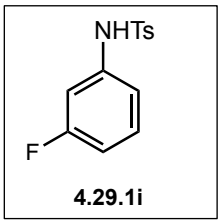

4.29.1i

Following GP1, *N*-(3-fluorophenyl)-4-methylbenzenesulfonamide, was isolated as a light-yellow solid in 93% yield and matched the reported known spectral data.[11]

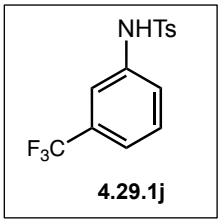

Following GP1, 4-methyl-*N*-(3-(trifluoromethyl)phenyl)benzenesulfonamide, was isolated as a off-white solid in 78% yield and matched the reported known spectral data.[12]

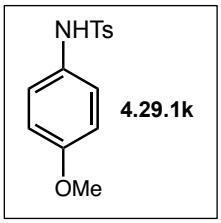

Following GP1, *N*-(4-methoxyphenyl)-4-methylbenzenesulfonamide, was isolated as a white solid in 75% yield and matched the reported known spectral data.[10]

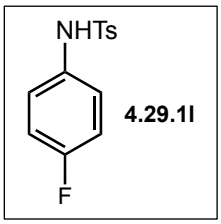

Following GP1, *N*-(4-fluorophenyl)-4-methylbenzenesulfonamide, was isolated as a light-yellow solid in 87% yield and matched the reported known spectral data.[13]

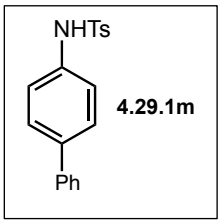

Following GP1, *N*-([1,1'-biphenyl]-4-yl)-4-methylbenzenesulfonamide, was isolated as a white solid in 82% yield and matched the reported known spectral data.[14]

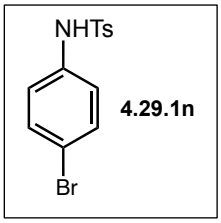

Following GP1, *N*-(4-bromophenyl)-4-methylbenzenesulfonamide, was isolated as a off-white solid in 90% yield and matched the reported known spectral data.[15]

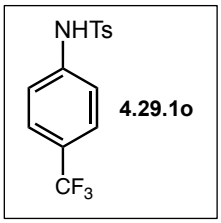

Following GP1, 4-methyl-*N*-(4-(trifluoromethyl)phenyl)benzenesulfonamide, was isolated as a white solid in 88% yield and matched the reported known spectral data.[14]

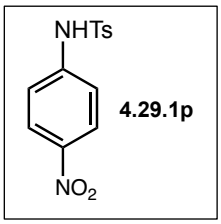

Following GP1, 4-methyl-*N*-(4-nitrophenyl)benzenesulfonamide, was isolated as an orange solid in 44% yield and matched the reported known spectral data.[10]

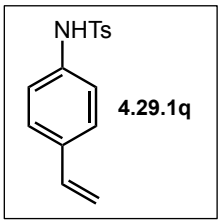

Following GP1, 4-methyl-*N*-(4-vinylphenyl)benzenesulfonamide, was isolated as an clear oil in 93% yield and matched the reported known spectral data.[16]

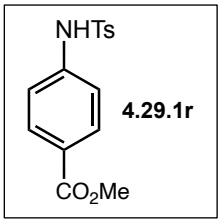

Following GP1, methyl 4-((4-methylphenyl)sulfonamido)benzoate, was isolated as an off-white solid in 92% yield and matched the reported known spectral data.[16]

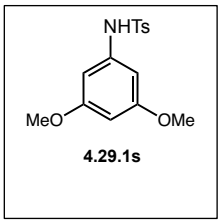

Following GP1, *N*-(3,5-dimethoxyphenyl)-4-methylbenzenesulfonamide, was isolated as a white solid in 70% yield and matched the reported known spectral data.[14]

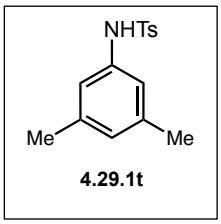

Following GP1, *N*-(3,5-dimethylphenyl)-4-methylbenzenesulfonamide, was isolated as a white solid in 85% yield and matched the reported known spectral data.[14]

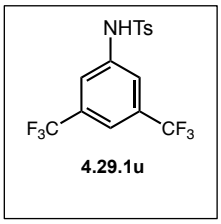

Following GP1, *N*-(3,5-bis(trifluoromethyl)phenyl)-4-methylbenzenesulfonamide, was isolated as a light-yellow solid in 82% yield and matched the reported known spectral data.[17]

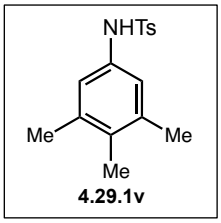

Following GP1, 4-methyl-*N*-(3,4,5-trimethylphenyl)benzenesulfonamide, was isolated as an off-white solid in 83% yield and matched the reported known spectral data.[18]

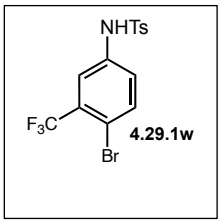

Following GP1, *N*-(4-bromo-3-(trifluoromethyl)phenyl)-4-methylbenzenesulfonamide, was isolated as a white solid in 94% yield. ^{1}H NMR (400 MHz, $CDCl_3$) δ 7.73 – 7.66 (m, 2H), 7.59 (d, *J* = 8.6 Hz, 1H), 7.36 (d, *J* = 2.7 Hz, 1H), 7.33 – 7.29 (m, 2H), 7.18 (dd, *J* = 8.6, 2.7 Hz, 1H), 6.76 (s, 1H), 2.43 (s, 3H).^{19}F NMR (376 MHz, $CDCl_3$) δ -63.08. HRMS (+ p APCI) calculated for $C_{14}H_{12}O_2N^{79}BrF_3{}^{32}S$ [M+H] calculated for 393.97187, found 393.97222.

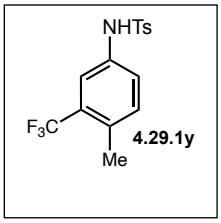

Following GP1, 4-methyl-*N*-(4-methyl-3-(trifluoromethyl)phenyl)benzenesulfonamide, was isolated as a white solid in 85% yield. ^{1}H NMR (600 MHz, $CDCl_3$) δ 7.71 – 7.66 (m, 2H), 7.29 (d, *J* = 2.5 Hz, 2H), 7.25 – 7.23 (m, 2H), 7.18 (dd, *J* = 8.3, 2.4 Hz, 1H), 7.13 (d, *J* = 8.3 Hz, 1H), 2.38 (s, 6H). ^{13}C NMR (151 MHz, $CDCl_3$) δ 144.41, 135.80, 134.63, 133.65, 133.04, 129.94, δ 129.70 (q, *J* = 30.3 Hz), 127.41, 124.64, 123.88 (q, *J* = 273.9 Hz), 123.09, 119.05 (q, *J* = 5.8 Hz). 21.66, δ 18.82

(q, J = 2.5 Hz). ^{19}F NMR (565 MHz, $CDCl_3$) δ -62.09. HRMS (+ p APCI) calculated for $C_{15}H_{15}O_2NF_3{}^{32}S$ [M+H] calculated for 330.07701, found 330.07689.

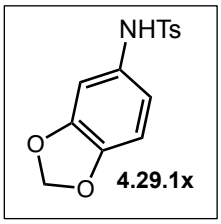

Following GP1, *N*-(benzo[*d*][1,3]dioxol-5-yl)-4-methylbenzenesulfonamide, was isolated as a white solid in 65% yield and matched the reported known spectral data.[19]

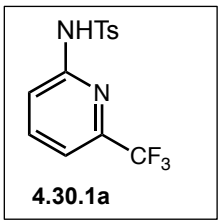

Following GP1, 4-methyl-*N*-(6-(trifluoromethyl)pyridin-2-yl)benzenesulfonamide, was isolated as a tan solid in 81% yield. ^{1}H NMR (400 MHz, $CDCl_3$) δ 8.42 (d, J = 2.4 Hz, 1H), 8.02 – 7.85 (m, 1H), 7.82 – 7.69 (m, 3H), 7.60 (d, J = 8.5 Hz, 1H), 7.39 – 7.21 (m, 2H), 2.42 (s, 3H).^{19}F NMR (376 MHz, $CDCl_3$) δ -67.38 HRMS (+ p APCI) calculated for $C_{13}H_{12}O_2N_2F_3{}^{32}S$ [M+H] calculated for 317.05661, found 317.05702.

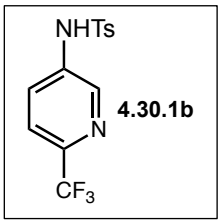

Following GP1, 4-methyl-*N*-(6-(trifluoromethyl)pyridin-3-yl)benzenesulfonamide, was isolated as a white-tan solid in 82% yield and matched the reported known spectral data.[20]

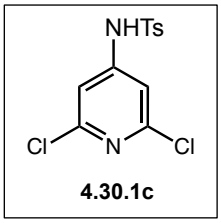

4.30.1c

Following GP1, 4*N*-(2,6-dichloropyridin-4-yl)-4-methylbenzenesulfonamide, was isolated as a white solid in 62% yield. ^{1}H NMR (400 MHz, $CDCl_3$) δ 7.91 – 7.73 (m, 2H), 7.56 (s, 1H), 7.42 – 7.30 (m, 2H), 6.97 (s, 2H), 2.44 (s, 3H). ^{13}C NMR (101 MHz, $CDCl_3$) δ 151.47, 147.89, 145.69, 134.87, 130.37, 127.31, 110.75, 21.68. HRMS (+ p APCI) calculated for $C_{19}H_{24}O_4N_2{}^{10}B^{35}Cl_2{}^{32}S$ [M+H] calculated for 456.09577, found 456.09614.

Borylated Compounds:

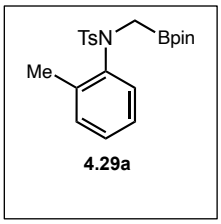

4.29a

Following GP2, 4-methyl-*N*-((4,4,5,5-tetramethyl-1,3,2-dioxaborolan-2-yl)methyl)-*N*-(*o*-tolyl)benzenesulfonamide, was isolated as a white amorphous solid in 67% yield. ^{1}H NMR (400 MHz, $CDCl_3$) δ 7.60 – 7.41 (m, 2H), 7.28 – 7.20 (m, 3H), 6.95 (tdd, J = 7.3, 1.7, 0.7 Hz, 1H), 6.40 (dd, J = 7.9, 1.3 Hz, 1H), 3.47 (d, J = 15.1 Hz, 1H), 2.81 (d, J = 15.1 Hz, 1H), 2.52 (s, 3H), 2.42 (s, 3H), 1.02 (s, 6H), 0.90 (s, 6H). ^{13}C NMR (101 MHz, $CDCl_3$) δ 143.38, 140.79, 140.76, 133.29, 131.10, 129.17, 128.68, 127.86, 126.15, 125.71, 84.26, 83.88, 24.60, 24.44, 24.14, 21.58, 18.96. ^{11}B NMR (128 MHz, $CDCl_3$) δ 31.91.

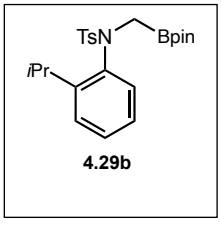

4.29b

Following GP2, *N*-(2-isopropylphenyl)-4-methyl-*N*-((4,4,5,5-tetramethyl-1,3,2-dioxaborolan-2-yl)methyl)benzenesulfonamide, was isolated as a off-white solid in 70% yield. ^{1}H NMR (400 MHz, $CDCl_3$) δ 7.60 – 7.44 (m, 2H), 7.35 (dd, *J* = 7.9, 1.6 Hz, 1H), 7.27 – 7.24 (m, 2H), 7.22 (td, *J* = 7.6, 1.4 Hz, 1H), 6.93 (ddd, *J* = 8.0, 7.3, 1.6 Hz, 1H), 6.42 (dd, *J* = 8.0, 1.4 Hz, 1H), 3.78 (hept, *J* = 6.9 Hz, 1H), 3.44 (d, *J* = 15.5 Hz, 1H), 2.85 (d, *J* = 15.4 Hz, 1H), 2.43 (s, 3H), 1.40 (d, *J* = 6.5 Hz, 0H), 1.33 – 1.22 (m, 6H), 1.05 (s, 6H), 0.92 (s, 6H). ^{13}C NMR (101 MHz, $CDCl_3$) δ 150.49, 143.35, 139.60, 133.08, 129.10, 128.96, 128.09, 127.18, 125.74, 125.35, 84.25, 83.88, 77.24, 27.61, 24.54, 24.50, 24.43, 24.16, 23.58, 21.55. ^{11}B NMR (128 MHz, $CDCl_3$) δ 31.74.

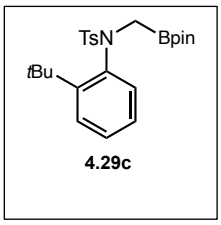

4.29c

Following GP2, *N*-(2-(*tert*-butyl)phenyl)-4-methyl-*N*-((4,4,5,5-tetramethyl-1,3,2-dioxaborolan-2-yl)methyl)benzenesulfonamide, was isolated as a white solid in 71% yield. ^{1}H NMR (400 MHz, $CDCl_3$) δ 7.59 – 7.54 (m, 2H), 7.30 – 7.26 (m, 2H), 7.19 (ddd, *J* = 8.3, 7.1, 1.5 Hz, 1H), 6.89 (ddd, *J* = 8.0, 7.1, 1.6 Hz, 1H), 6.24 (dd, *J* = 8.0, 1.5 Hz, 1H), 3.34 (d, *J* = 15.1 Hz, 1H), 2.83 (d, *J* = 15.1 Hz, 1H), 2.44 (s, 3H), 1.60 (s, 9H), 1.07 (s, 6H), 0.96 (s, 6H). ^{11}B NMR (128 MHz, $CDCl_3$) δ 31.99.

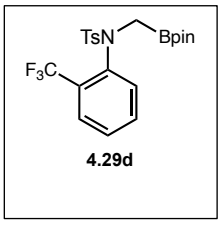

4.29d

Following GP2, 4-methyl-*N*-((4,4,5,5-tetramethyl-1,3,2-dioxaborolan-2-yl)methyl)-*N*-(2-(trifluoromethyl)phenyl)benzenesulfonamide, was isolated as a yellow solid in 66% yield. ^{1}H NMR (400 MHz, $CDCl_3$) δ 7.74 – 7.65 (m, 1H), 7.65 – 7.60 (m, 2H), 7.47 – 7.36 (m, 2H), 7.32 – 7.27 (m, 2H), 7.06 – 6.91 (m, 1H), 3.32 (d, *J* = 15.7 Hz, 1H), 3.00 (d, *J* = 15.7 Hz, 1H), 2.44 (s, 3H), 1.05 (s,

6H), 0.97 (s, 6H). ^{13}C NMR (101 MHz, $CDCl_3$) δ 139.82 (d, *J* = 1.6 Hz), 134.13, 131.17 (q, *J* = 30.2 Hz), 129.46, 128.44, 127.96 (q, *J* = 4.6 Hz), 123.41 (q, *J* = 274.1 Hz), 84.01, 24.63, 24.42, 21.68. ^{19}F NMR (376 MHz, $CDCl_3$) δ -58.42. ^{11}B NMR (128 MHz, $CDCl_3$) δ 31.48.

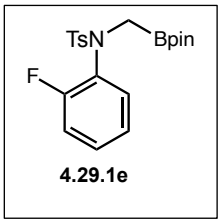

4.29.1e

Following GP2, *N*-(2-fluorophenyl)-4-methyl-*N*-((4,4,5,5-tetramethyl-1,3,2-dioxaborolan-2-yl)methyl)benzenesulfonamide, was isolated as a yellow solid in 76% yield. ^{1}H NMR (400 MHz, $CDCl_3$) δ 7.55 (d, *J* = 8.2 Hz, 2H), 7.34 – 7.20 (m, 4H), 7.16 – 7.04 (m, 1H), 7.04 – 6.95 (m, 1H), 3.28 (d, *J* = 1.7 Hz, 2H), 2.44 (s, 3H), 1.12 – 0.98 (m, 12H). ^{13}C NMR (101 MHz, $CDCl_3$) δ 160.94, 158.42, 143.49, 134.15, 131.66, 129.39 (d, *J* = 8.2 Hz), 129.32, 128.93, 128.82, 123.93 (d, *J* = 3.7 Hz), 116.45, 116.25, 83.99, 24.43, 21.60. ^{19}F NMR (376 MHz, $CDCl_3$) δ -117.51. ^{11}B NMR (128 MHz, $CDCl_3$) δ 31.70.

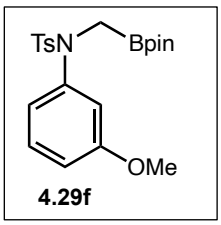

4.29f

Following GP2, *N*-(3-methoxyphenyl)-4-methyl-*N*-((4,4,5,5-tetramethyl-1,3,2-dioxaborolan-2-yl)methyl)benzenesulfonamide, was isolated as a white solid in 83% yield. ^{1}H NMR (400 MHz, $CDCl_3$) δ 7.41 (d, 2H), 7.21 (d, 2H), 7.11 (td, *J* = 7.9, 0.8 Hz, 1H), 6.79 – 6.71 (m, 2H), 6.56 (ddd, *J* = 8.0, 1.9, 1.0 Hz, 1H), 3.74 (s, 3H), 3.13 (s, 2H), 2.39 (s, 3H), 1.06 (s, 12H). ^{13}C NMR (101 MHz, $CDCl_3$) δ 159.55, 143.43, 143.23, 132.65, 128.97, 128.32, 118.61, 113.42, 113.01, 84.03, 55.38, 24.46, 21.56. ^{11}B NMR (128 MHz, $CDCl_3$) δ 32.01.

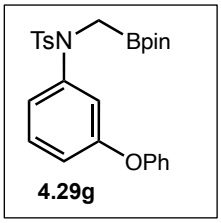

4.29g

Following GP2, 4-methyl-*N*-(3-phenoxyphenyl)-*N*-((4,4,5,5-tetramethyl-1,3,2-dioxaborolan-2-yl)methyl)benzenesulfonamide, was isolated as a white solid in 64% yield. ^{1}H NMR (400 MHz, $CDCl_3$) δ 7.50 – 7.41 (m, 2H), 7.38 – 7.30 (m, 2H), 7.26 – 7.19 (m, 3H), 7.16 – 7.08 (m, 1H), 6.98 – 6.93 (m, 2H), 6.90 (dddd, *J* = 8.0, 4.9, 2.2, 0.9 Hz, 2H), 6.76 (t, *J* = 2.2 Hz, 1H), 3.14 (s, 2H), 2.42 (s, 3H), 1.12 (s, 12H). ^{13}C NMR (101 MHz, $CDCl_3$) δ 157.07, 156.83, 143.48, 143.42, 132.95, 129.70, 129.33, 129.18, 128.21, 123.39, 122.10, 118.74, 117.60, 117.57, 84.05, 24.51, 21.52. ^{11}B NMR (128 MHz, $CDCl_3$) δ 31.47.

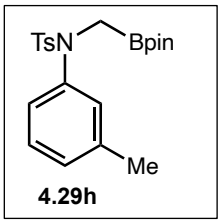

4.29h

Following GP2, 4-methyl-*N*-((4,4,5,5-tetramethyl-1,3,2-dioxaborolan-2-yl)methyl)-*N*-(*m*-tolyl)benzenesulfonamide, was isolated as a tan solid in 85% yield. ^{1}H NMR (400 MHz, $CDCl_3$) δ 7.42 (d, *J* = 8.3 Hz, 2H), 7.23 (dt, *J* = 8.0, 0.7 Hz, 2H), 7.12 (t, *J* = 7.8 Hz, 1H), 7.06 – 7.01 (m, 1H), 6.97 (dd, *J* = 1.5, 0.8 Hz, 1H), 6.85 – 6.75 (m, 1H), 3.16 (s, 2H), 2.42 (s, 3H), 2.29 (d, *J* = 0.8 Hz, 3H), 1.06 (s, 12H). ^{13}C NMR (101 MHz, $CDCl_3$) δ 143.28, 141.93, 138.31, 132.88, 129.05, 128.35, 128.23, 128.21, 127.79, 123.77, 83.96, 24.43, 21.54, 21.25. ^{11}B NMR (128 MHz, $CDCl_3$) δ 31.39.

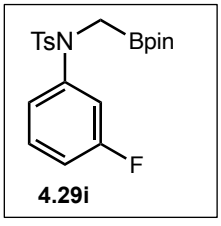

4.29i

Following GP2, *N*-(3-fluorophenyl)-4-methyl-*N*-((4,4,5,5-tetramethyl-1,3,2-dioxaborolan-2-yl)methyl)benzenesulfonamide, was isolated as a light-yellow solid in 77% yield. ^{1}H NMR (400 MHz, $CDCl_3$) δ 7.42 – 7.37 (m, 2H), 7.20 (dd, *J* = 14.1, 7.9 Hz, 3H), 6.92 (tdd, *J* = 8.3, 2.5, 1.0 Hz, 1H), 6.89 – 6.82 (m, 2H), 3.14 (s, 2H), 2.40 (s, 3H), 1.06 (s, 12H). ^{13}C NMR (101 MHz, $CDCl_3$) δ 159.78 (d, *J* = 253.4 Hz), 143.59, 134.25, 131.76, 129.49 (d, *J* = 8.2 Hz), 129.42, 129.03, 128.92, 128.13, 124.03 (d, *J* = 3.7 Hz), 116.45 (d, *J* = 20.3 Hz), 84.09, 24.53, 21.70. ^{19}F NMR (376 MHz, $CDCl_3$) δ -112.16. ^{11}B NMR (128 MHz, $CDCl_3$) δ 31.94.

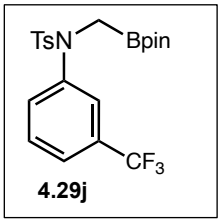

4.29j

Following GP2, 4-methyl-*N*-((4,4,5,5-tetramethyl-1,3,2-dioxaborolan-2-yl)methyl)-*N*-(3-(trifluoromethyl)phenyl)benzenesulfonamide, was isolated as an off-white solid in 78% yield. ^{1}H NMR (400 MHz, $CDCl_3$) δ 7.48 (dtd, *J* = 7.4, 1.7, 0.8 Hz, 1H), 7.41 (dt, *J* = 8.1, 0.7 Hz, 1H), 7.39 – 7.34 (m, 3H), 7.24 – 7.18 (m, 2H), 3.18 (s, 2H), 2.41 (s, 3H), 1.02 (s, 12H). ^{13}C NMR (101 MHz, $CDCl_3$) δ 144.07, 142.85, 132.35, 131.25, 131.02 (q, *J* = 32.7 Hz), 129.45, 129.19, 128.30, 123.79 (dq, *J* = 7.4, 3.8 Hz), 123.71 (q, *J* = 272.3 Hz), 84.29, 24.51, 21.67. ^{19}F NMR (376 MHz, $CDCl_3$) δ -62.75. ^{11}B NMR (128 MHz, $CDCl_3$) δ 31.46.

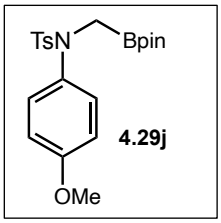

4.29j

Following GP2, *N*-(4-methoxyphenyl)-4-methyl-*N*-((4,4,5,5-tetramethyl-1,3,2-dioxaborolan-2-yl)methyl)benzenesulfonamide, was isolated as a white solid in 72% yield. ^{1}H NMR (400 MHz, $CDCl_3$) δ 7.42 (d, *J* = 8.3 Hz, 2H), 7.27 – 7.17 (m, 2H), 6.99 (d, *J* = 9.0 Hz, 2H), 6.78 (d, *J* = 9.0 Hz,

2H), 3.80 (s, 3H), 3.15 (s, 2H), 2.43 (s, 3H), 1.07 (s, 12H). ^{13}C NMR (101 MHz, $CDCl_3$) δ 158.53, 143.30, 134.68, 132.72, 129.12, 128.59, 128.38, 113.60, 83.99, 77.26, 55.45, 24.48, 21.57. ^{11}B NMR (128 MHz, $CDCl_3$) δ 32.07. HRMS (+ p APCI) calculated for $C_{21}H_{29}O_5N^{10}B^{32}S$ [M+H] calculated for 417.18903, found 417.18904.

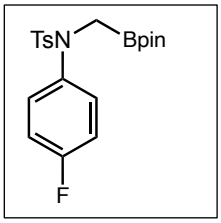

Following GP2, N-(4-fluorophenyl)-4-methyl-N-((4,4,5,5-tetramethyl-1,3,2-dioxaborolan-2-yl)methyl)benzenesulfonamide, was isolated as a yellow solid in 90% yield. ^{1}H NMR (400 MHz, $CDCl_3$) δ 7.38 (d, *J* = 8.3 Hz, 2H), 7.22 (d, *J* = 7.8 Hz, 2H), 7.06 – 6.98 (m, 2H), 6.93 (dd, *J* = 9.1, 8.2 Hz, 2H), 3.13 (s, 2H), 2.40 (s, 3H), 1.05 (s, 12H). ^{13}C NMR (101 MHz, $CDCl_3$) δ 161.55 (d, *J* = 246.9 Hz), 143.71, 138.00 (d, *J* = 3.1 Hz), 132.49, 129.34, 129.15 (d, *J* = 8.6 Hz), 128.39, 115.38 (d, *J* = 22.6 Hz), 84.19, 24.55, 21.67. ^{19}F NMR (376 MHz, $CDCl_3$) δ -114.39. ^{11}B NMR (128 MHz, $CDCl_3$) δ 31.66. HRMS (+ p APCI) calculated for $C_{20}H_{26}O_4N^{10}BF^{32}S$ [M+H] calculated for 405.16905, found 405.16915.

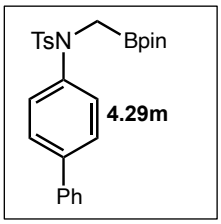

Following GP2, *N*-([1,1'-biphenyl]-4-yl)-4-methyl-*N*-((4,4,5,5-tetramethyl-1,3,2-dioxaborolan-2-yl)methyl)benzenesulfonamide, was isolated as a white solid in 81% yield. ^{1}H NMR (400 MHz, $CDCl_3$) δ 7.56 (d, *J* = 7.0 Hz, 2H), 7.49 (d, *J* = 8.5 Hz, 2H), 7.46 – 7.40 (m, 4H), 7.39 – 7.32 (m, 1H), 7.22 (d, *J* = 7.8 Hz, 2H), 7.15 (d, *J* = 8.6 Hz, 2H), 3.19 (s, 2H), 2.41 (s, 3H), 1.05 (s, 12H). ^{13}C NMR (101 MHz, $CDCl_3$) δ 143.48, 141.27, 140.28, 139.84, 132.67, 129.20, 128.85, 128.35, 127.50,

127.44, 127.11, 127.02, 84.08, 77.26, 24.44, 21.58. ^{11}B NMR (128 MHz, $CDCl_3$) δ 32.56. HRMS (+ p APCI) calculated for $C_{26}H_{31}O_4N^{10}B^{32}S$ [M+H] calculated for 463.20977, found 463.20978.

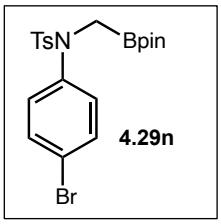

Following GP2, *N*-(4-bromophenyl)-4-methyl-*N*-((4,4,5,5-tetramethyl-1,3,2-dioxaborolan-2-yl)methyl)benzenesulfonamide, was isolated as a off-white solid in 80% yield. ^{1}H NMR (400 MHz, $CDCl_3$) δ 7.38 (dd, *J* = 8.6, 4.9 Hz, 4H), 7.22 (d, *J* = 8.0 Hz, 2H), 6.95 (d, *J* = 8.8 Hz, 2H), 3.12 (s, 2H), 2.40 (s, 3H), 1.06 (s, 12H). ^{13}C NMR (101 MHz, $CDCl_3$) δ 143.82, 141.26, 132.44, 131.70, 129.40, 128.86, 128.35, 120.85, 84.27, 24.57, 21.69. ^{11}B NMR (128 MHz, $CDCl_3$) δ 31.56.

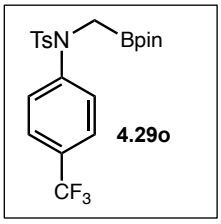

Following GP2, 4-methyl-*N*-((4,4,5,5-tetramethyl-1,3,2-dioxaborolan-2-yl)methyl)-*N*-(4-(trifluoromethyl)phenyl)benzenesulfonamide, was isolated as a light tan to yellowish solid in 73% yield. ^{1}H NMR (400 MHz, $CDCl_3$) δ 7.52 (dt, *J* = 8.3, 0.8 Hz, 2H), 7.38 (d, *J* = 8.3 Hz, 2H), 7.26 – 7.18 (m, 4H), 3.18 (s, 2H), 2.41 (s, 3H), 1.04 (s, 12H). ^{13}C NMR (151 MHz, $CDCl_3$) δ 145.51, 143.99, 132.63, 129.50, 128.94 (q, *J* = 32.7 Hz), 128.25, 127.18, 125.70 (q, *J* = 3.7 Hz), 124.03 (q, *J* = 272.0 Hz), 84.32, 24.52, 21.67. ^{19}F NMR (376 MHz, $CDCl_3$) δ -62.44. ^{11}B NMR (128 MHz, $CDCl_3$) δ 32.20. HRMS (+ p APCI) calculated for $C_{21}H_{26}O_4N^{10}BF_3{}^{32}S$ [M+H] calculated for 455.16585, found 455.16609.

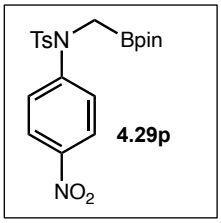

Following GP2, 4-methyl-*N*-(4-nitrophenyl)-*N*-((4,4,5,5-tetramethyl-1,3,2-dioxaborolan-2-yl)methyl)benzenesulfonamide, was isolated as a light orange solid in 86% yield. ^{1}H NMR (400 MHz, $CDCl_3$) δ 8.16 – 8.10 (m, 2H), 7.40 – 7.35 (m, 2H), 7.30 – 7.26 (m, 2H), 7.25 – 7.21 (m, 2H), 3.21 (s, 2H), 2.40 (s, 3H), 1.07 (s, 12H). ^{13}C NMR (101 MHz, $CDCl_3$) δ 148.16, 145.75, 144.39, 132.45, 129.66, 128.07, 126.67, 124.04, 84.51, 24.61, 21.71. ^{11}B NMR (128 MHz, $CDCl_3$) δ 31.95. HRMS (+ p APCI) calculated for $C_{20}H_{26}O_6N_2{}^{10}B^{32}S$ [M+H] calculated for 432.16355, found 432.16374.

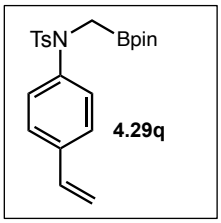

Following GP2, 4-methyl-*N*-((4,4,5,5-tetramethyl-1,3,2-dioxaborolan-2-yl)methyl)-*N*-(4-vinylphenyl)benzenesulfonamide, was isolated as an clear oil in 57% yield. ^{1}H NMR (400 MHz, $CDCl_3$) δ 7.43 (d, 2H), 7.31 (d, 2H), 7.23 (d, 2H), 7.05 (d, 2H), 6.69 (dd, J = 17.6, 10.9 Hz, 1H), 5.73 (dd, J = 17.6, 0.9 Hz, 1H), 5.27 (dd, J = 10.9, 0.9 Hz, 1H), 3.17 (s, 2H), 2.42 (s, 3H), 1.08 (s, 12H). ^{13}C NMR (101 MHz, $CDCl_3$) δ 143.53, 141.61, 136.40, 136.19, 132.86, 129.28, 128.42, 127.22, 126.35, 114.38, 84.18, 24.58, 21.68. ^{11}B NMR (128 MHz, $CDCl_3$) δ 31.53. HRMS (+ p APCI) calculated for $C_{22}H_{29}O_4N^{10}B^{32}S$ [M+H] calculated for 413.19412, found 413.19418.

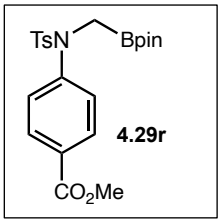

Following GP2, methyl 4-((4-methyl-*N*-((4,4,5,5-tetramethyl-1,3,2-dioxaborolan-2-yl)methyl)phenyl)sulfonamido)benzoate, was isolated as an off-white solid in 62% yield. ^{1}H NMR (400 MHz, $CDCl_3$) δ 7.93 (d, *J* = 8.7 Hz, 2H), 7.36 (d, *J* = 8.3 Hz, 2H), 7.18 (t, *J* = 8.7 Hz, 4H), 3.91 (s, 3H), 3.19 (s, 2H), 2.39 (s, 3H), 1.05 (s, 12H). ^{13}C NMR (101 MHz, $CDCl_3$) δ 166.69, 146.45, 143.90, 132.65, 130.04, 128.35, 128.22, 126.42, 84.31, 52.34, 24.59, 21.68. ^{11}B NMR (128 MHz, $CDCl_3$) δ 32.24. HRMS (+ p APCI) calculated for $C_{22}H_{29}O_6N^{10}B^{32}S$ [M+H] calculated for 445.18395, found 445.18418.

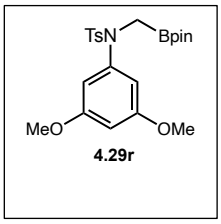

Following GP2, *N*-(3,5-dimethoxyphenyl)-4-methyl-*N*-((4,4,5,5-tetramethyl-1,3,2-dioxaborolan-2-yl)methyl)benzenesulfonamide, was isolated as a off-white solid in 79% yield. ^{1}H NMR (400 MHz, $CDCl_3$) δ 7.50 – 7.42 (m, 2H), 7.25 – 7.16 (m, 2H), 6.32 (t, *J* = 2.3 Hz, 1H), 6.27 (d, *J* = 2.3 Hz, 2H), 3.70 (s, 6H), 3.11 (s, 2H), 2.40 (s, 3H), 1.09 (s, 12H). ^{13}C NMR (101 MHz, $CDCl_3$) δ 160.49, 144.07, 143.52, 133.19, 129.24, 105.45, 99.92, 84.16, 55.58, 24.65, 21.65. ^{11}B NMR (128 MHz, $CDCl_3$) δ 31.49. HRMS (+ p APCI) calculated for $C_{22}H_{31}O_6N^{10}B^{32}S$ [M+H] calculated for 447.1996, found 447.20024.

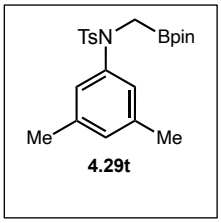

4.29t

Following GP2, *N*-(3,5-dimethylphenyl)-4-methyl-*N*-((4,4,5,5-tetramethyl-1,3,2-dioxaborolan-2-yl)methyl)benzenesulfonamide, was isolated as a white solid in 79% yield. ^{1}H NMR (400 MHz, $CDCl_3$) δ 7.41 (d, *J* = 8.3 Hz, 2H), 7.20 (d, *J* = 8.0 Hz, 2H), 6.84 – 6.80 (m, 1H), 6.70 – 6.63 (m, 2H), 3.10 (s, 2H), 2.39 (s, 3H), 2.20 (s, 6H), 1.03 (s, 12H). ^{13}C NMR (101 MHz, $CDCl_3$) δ 143.33, 141.87, 138.04, 132.96, 129.06, 128.75, 128.45, 124.89, 83.99, 24.49, 21.62, 21.24. ^{11}B NMR (128 MHz, $CDCl_3$) δ 31.73. HRMS (+ p APCI) calculated for $C_{16}H_{27}O_4N^{10}B^{32}S$ [M+H] calculated for 447.1996, found 339.17847.

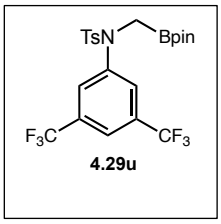

4.29u

Following GP2, *N*-(3,5-bis(trifluoromethyl)phenyl)-4-methyl-*N*-((4,4,5,5-tetramethyl-1,3,2-dioxaborolan-2-yl)methyl)benzenesulfonamide, was isolated as a light yellow, amorphous solid in 88% yield. ^{1}H NMR (400 MHz, $CDCl_3$) δ 7.73 (tt, *J* = 1.6, 0.8 Hz, 1H), 7.55 – 7.51 (m, 2H), 7.46 – 7.34 (m, 2H), 7.33 – 7.09 (m, 2H), 3.21 (s, 2H), 2.42 (s, 3H), 1.04 (s, 12H). ^{13}C NMR (101 MHz, $CDCl_3$) δ 144.58, 144.08, 132.47, 132.07 (q, *J* = 33.7 Hz), 129.68, 128.23, 127.62 (dt, *J* = 4.3, 2.2 Hz), 123.01 (q, *J* = 272.9 Hz), 120.53 (q, *J* = 3.9 Hz), 84.51, 24.54, 21.64. ^{19}F NMR (376 MHz, $CDCl_3$) δ -63.04. ^{11}B NMR (128 MHz, $CDCl_3$) δ 31.68.

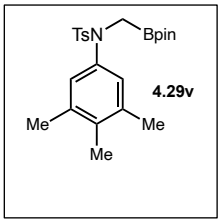

Following GP2, 4-methyl-*N*-((4,4,5,5-tetramethyl-1,3,2-dioxaborolan-2-yl)methyl)-*N*-(3,4,5-trimethylphenyl)benzenesulfonamide, was isolated as an off-white solid in 71% yield. ^{1}H NMR (600 MHz, $CDCl_3$) δ 7.48 – 7.39 (m, 2H), 7.25 – 7.13 (m, 2H), 6.70 (s, 2H), 3.09 (d, *J* = 1.6 Hz, 2H), 2.41 (d, *J* = 1.5 Hz, 3H), 2.17 (d, *J* = 2.3 Hz, 6H), 2.11 (d, *J* = 1.5 Hz, 3H), 1.05 (d, *J* = 1.6 Hz, 12H). ^{13}C NMR (151 MHz, $CDCl_3$) δ 143.08, 138.86, 136.47, 134.00, 133.38, 128.96, 128.43, 126.23, 83.87, 24.44, 21.52, 20.45, 15.09.

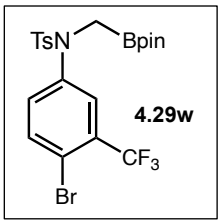

Following GP2, *N*-(4-bromo-3-(trifluoromethyl)phenyl)-4-methyl-*N*-((4,4,5,5-tetramethyl-1,3,2-dioxaborolan-2-yl)methyl)benzenesulfonamide, was isolated as a white solid in 61% yield. ^{1}H NMR (400 MHz, $CDCl_3$) δ 7.60 (d, *J* = 8.6 Hz, 1H), 7.40 (d, *J* = 8.3 Hz, 2H), 7.25 (d, *J* = 8.1 Hz, 2H), 7.18 (dd, *J* = 8.6, 2.6 Hz, 1H), 3.15 (s, 2H), 2.42 (s, 3H), 1.06 (s, 12H). ^{13}C NMR (101 MHz, $CDCl_3$) δ 144.30, 141.77, 135.18, 132.42, 131.85, 130.44 (q, *J* = 31.7 Hz), 129.60, 128.25, 126.43 (q, *J* = 5.5 Hz), 122.54 (q, *J* = 273.6 Hz), 118.09 (q, *J* = 1.7 Hz), 84.45, 24.58, 21.69. ^{19}F NMR (376 MHz, $CDCl_3$) δ -62.96. ^{11}B NMR (128 MHz, $CDCl_3$) δ 31.63. HRMS (+ p APCI) calculated for $C_{21}H_{25}O_4N^{10}B^{79}BrF_3{}^{32}S$ [M+H] calculated for 533.07636, found 533.07714.

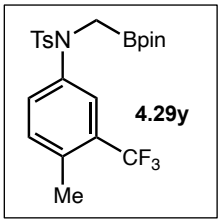

Following GP2, 4-methyl-*N*-(4-methyl-3-(trifluoromethyl)phenyl)-*N*-((4,4,5,5-tetramethyl-1,3,2-dioxaborolan-2-yl)methyl)benzenesulfonamide, was isolated as a white solid in 88% yield. ^{1}H NMR (400 MHz, $CDCl_3$) δ 7.39 (d, *J* = 8.3 Hz, 2H), 7.25 – 7.20 (m, 3H), 7.19 (d, *J* = 2.0 Hz, 1H), 3.14 (s, 2H), 2.44 (d, *J* = 1.8 Hz, 3H), 2.41 (s, 3H), 1.04 (s, 12H). ^{13}C NMR (101 MHz, $CDCl_3$) δ 143.93, 140.04, 135.67 (d, *J* = 2.0 Hz), 132.58, 132.24, 130.81, 129.41, 129.08 (q, *J* = 30.4 Hz), 128.34, 124.53 (q, *J* = 5.7 Hz), 124.09 (q, *J* = 273.9 Hz), 84.26, 24.53, 21.60, 19.06 (q, *J* = 2.1 Hz). ^{19}F NMR (376 MHz, $CDCl_3$) δ -62.00. ^{11}B NMR (128 MHz, $CDCl_3$) δ 32.19. HRMS (+ p APCI) calculated for $C_{22}H_{28}O_4N^{10}BF_3^{32}$ [M+H] calculated for 469.1815, found 469.1820.

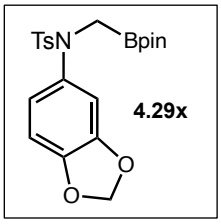

Following GP2, *N*-(benzo[*d*][1,3]dioxol-5-yl)-4-methyl-*N*-((4,4,5,5-tetramethyl-1,3,2-dioxaborolan-2-yl)methyl)benzenesulfonamide, was isolated as a white solid in 65% yield. ^{1}H NMR (400 MHz, $CDCl_3$) δ 7.44 (d, *J* = 8.3 Hz, 2H), 7.22 (dd, *J* = 8.6, 0.7 Hz, 2H), 6.68 (d, *J* = 2.2 Hz, 1H), 6.62 (d, *J* = 8.3 Hz, 1H), 6.38 (dd, *J* = 8.3, 2.2 Hz, 1H), 5.94 (s, 2H), 3.09 (s, 2H), 2.40 (s, 3H), 1.07 (s, 12H). ^{13}C NMR (101 MHz, $CDCl_3$) δ 147.43, 146.69, 143.54, 136.02, 129.26, 128.43, 109.58, 107.47, 101.55, 84.12, 24.57, 21.65. ^{11}B NMR (128 MHz, $CDCl_3$) δ 31.67. HRMS (+ p APCI) calculated for $C_{22}H_{28}O_4N^{10}BF_3^{32}$ [M+H] calculated for 431.1683, found 431.1688.

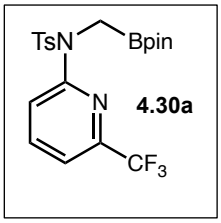

Following GP2, 4-methyl-*N*-((4,4,5,5-tetramethyl-1,3,2-dioxaborolan-2-yl)methyl)-*N*-(6-(trifluoromethyl)pyridin-2-yl)benzenesulfonamide, was isolated as a tan solid in 58% yield. ^{1}H NMR (600 MHz, $CDCl_3$) δ 7.97 (d, J = 8.4 Hz, 1H), 7.82 (ddd, J = 8.4, 7.6, 0.8 Hz, 1H), 7.47 – 7.38 (m, 3H), 7.24 – 7.17 (m, 2H), 3.35 (s, 2H), 2.38 (s, 3H), 1.06 (s, 12H). ^{13}C NMR (151 MHz, $CDCl_3$) δ 154.27, 145.85 (q, J = 35.2 Hz), 144.13, 138.39, 133.61, 129.46, 127.68, 122.86, 121.08 (q, J = 274.2 Hz), 116.65 (q, J = 2.9 Hz), 83.87, 24.53, 21.53. ^{19}F NMR (565 MHz, $CDCl_3$) δ -67.86. ^{11}B NMR (128 MHz, $CDCl_3$) δ 32.40. HRMS (+ p APCI) calculated for $C_{20}H_{25}O_4N_2{}^{10}BF_3{}^{32}S$ [M+H] calculated for 456.1611, found 456.1617.

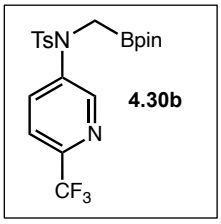

Following GP2, 4-methyl-*N*-((4,4,5,5-tetramethyl-1,3,2-dioxaborolan-2-yl)methyl)-*N*-(6-(trifluoromethyl)pyridin-3-yl)benzenesulfonamide, was isolated as a white solid in 76% yield. ^{1}H NMR (600 MHz, $CDCl_3$) δ 8.34 (d, J = 2.5 Hz, 1H), 7.73 – 7.68 (m, 1H), 7.61 (dd, J = 8.4, 0.7 Hz, 1H), 7.44 – 7.37 (m, 2H), 7.26 (d, 2H), 3.24 (s, 2H), 2.41 (s, 3H), 1.05 (s, 12H). ^{13}C NMR (151 MHz, $CDCl_3$) δ 147.66, 145.81 (q, J = 35.0 Hz), 144.54, 141.43, 135.66, 132.48 (d, J = 2.2 Hz), 129.85, 128.07, 121.06 (d, J = 7.0 Hz), 120.26 (q, J = 2.6 Hz), 84.57, 24.56, 21.68. ^{19}F NMR (565 MHz, $CDCl_3$) δ -67.61. ^{11}B NMR (128 MHz, $CDCl_3$) δ 31.53. HRMS (+ p APCI) calculated for $C_{20}H_{25}O_4N_2{}^{10}BF_3{}^{32}S$ [M+H] calculated for 456.1611, found 456.1610.

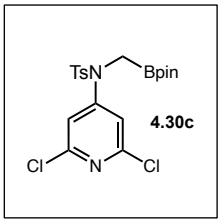

Following GP2, *N*-(2,6-dichloropyridin-4-yl)-4-methyl-*N*-((4,4,5,5-tetramethyl-1,3,2-dioxaborolan-2-yl)methyl)benzenesulfonamide, was isolated as a white solid in 69% yield. ^{1}H NMR (600 MHz, $CDCl_3$) δ 7.55 – 7.48 (m, 2H), 7.30 – 7.26 (m, 2H), 7.12 (s, 2H), 3.25 (s, 2H), 2.42 (s, 3H), 1.16 (s, 12H). ^{13}C NMR (151 MHz, $CDCl_3$) δ 153.21, 150.71, 144.92, 133.04, 130.09, 129.88, 127.68, 116.70, 116.66, 84.76, 24.58, 21.63. ^{11}B NMR (128 MHz, $CDCl_3$) δ 31.92. HRMS (+ p APCI) calculated for $C_{19}H_{24}O_4N_2{}^{10}B^{35}Cl_2{}^{32}S$ [M+H] calculated for 456.0958, found 456.0961.

1,2-dihydroquinoline Products:

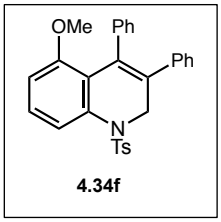

4.34f

Following GP3, 5-methoxy-3,4-diphenyl-1-tosyl-1,2-dihydroquinoline, was isolated as a white solid in 60% yield, 1.5:1 r.r.

Major: ^{1}H NMR (600 MHz, $CDCl_3$) δ 7.59 (dd, *J* = 8.2, 1.1 Hz, 1H), 7.42 (d, *J* = 2.7 Hz, 1H), 7.37 – 7.33 (m, 2H), 7.32 – 7.29 (m, 3H), 7.17 – 7.13 (m, 1H), 7.00 – 6.91 (m, 2H), 6.67 – 6.63 (m, 3H), 6.56 – 6.51 (m, 2H), 6.44 – 6.38 (m, 2H), 4.84 (s, 2H), 3.90 (s, 3H), 2.41 (s, 3H).

Minor: ^{1}H NMR (600 MHz, $CDCl_3$) δ 7.59 (dd, *J* = 8.2, 1.1 Hz, 1H), 7.13 – 7.08 (m, 9H), 7.06 – 7.00 (m, 1H), 6.71 – 6.65 (m, 2H), 6.58 (d, *J* = 8.7 Hz, 1H), 6.29 (dt, *J* = 7.1, 1.3 Hz, 2H), 4.73 (s, 2H), 3.16 (s, 3H), 2.39 (s, 3H).

^{13}C NMR (151 MHz, $CDCl_3$) δ 159.07, 156.58, 143.41 (d, *J* = 5.5 Hz), 139.89, 138.72, 138.68, 137.25, 136.95, 136.72, 136.17, 135.92, 133.66, 132.10, 130.71, 130.40, 129.21, 129.05, 128.60, 128.22, 127.88, 127.85, 127.72, 127.69, 127.66, 127.55, 127.51, 127.48, 126.98, 126.93, 126.67, 126.65, 125.82, 125.75, 122.10, 119.04, 113.23, 111.65, 110.73, 55.60, 55.43, 50.95, 50.60, 21.41.

HRMS (+ p APCI) calculated for $C_{29}H_{26}O_3N^{32}S$ [M+H] calculated for 468.16279, found 468.16407.

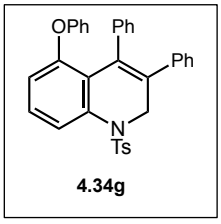

4.34g

Following GP3, 8-isopropyl-3,4-diphenyl-1-tosyl-1,2-dihydroquinoline, was isolated as a white solid in 63% yield, 1.7:1 r.r.

Major: ^{1}H NMR (400 MHz, $CDCl_3$) δ 7.54 (d, *J* = 2.6 Hz, 1H), 7.43 – 7.35 (m, 6H), 7.20 – 7.13 (m, 5H), 6.72 – 6.67 (m, 2H), 6.65 (d, *J* = 8.7 Hz, 1H), 6.50 – 6.43 (m, 2H), 6.34 – 6.25 (m, 1H), 6.24 – 6.17 (m, 1H), 4.88 (s, 2H), 2.45 (d, *J* = 2.6 Hz, 5H).

Minor: ^{1}H NMR (400 MHz, $CDCl_3$) δ 7.80 (dd, *J* = 8.1, 1.2 Hz, 1H), 7.48 (dd, *J* = 4.9, 1.9 Hz, 1H), 7.13 – 7.03 (m, 10H), 6.96 – 6.87 (m, 2H), 6.88 – 6.80 (m, 3H), 6.80 – 6.75 (m, 2H), 6.59 – 6.51 (m, 2H), 4.82 (s, 2H), 2.44 (s, 3H).^{13}C NMR (101 MHz, $CDCl_3$) δ 156.87, 156.82, 156.70, 152.46, 143.86, 143.75, 138.74, 138.72, 137.50, 137.25, 136.80, 136.39, 136.19, 133.70, 132.52, 132.36, 131.81, 131.21, 130.73, 130.58, 130.03, 129.56, 129.50, 129.40, 129.35, 129.25, 129.07, 128.79, 128.25, 128.17, 128.15, 128.13, 128.03, 127.96, 127.77, 127.73, 127.31, 127.18, 127.08, 127.04, 126.23, 125.18, 123.94, 122.68, 122.27, 119.59, 119.26, 117.24, 116.94, 116.81, 77.36, 51.03, 50.66, 31.74, 29.85, 22.80, 21.65, 21.64, 14.27. HRMS (+ p APCI) calculated for xx [M+H] calculated for xx, found xx.

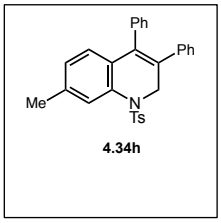

4.34h

Following GP3, 7-methyl-3,4-diphenyl-1-tosyl-1,2-dihydroquinoline, was isolated as a white solid in 36% yield, >20:1 r.r. ^{1}H NMR (400 MHz, $CDCl_3$) δ 7.71 – 7.66 (m, 1H), 7.35 – 7.29 (m, 2H), 7.22 – 7.08 (m, 8H), 6.94 (ddd, *J* = 8.0, 1.8, 0.8 Hz, 1H), 6.71 – 6.63 (m, 2H), 6.58 (d, *J* = 7.9 Hz, 1H), 6.47 – 6.40 (m, 2H), 4.85 (s, 2H), 2.45 (s, 3H), 2.43 (s, 3H). ^{13}C NMR (101 MHz, $CDCl_3$) δ 143.43, 138.70, 138.25, 137.27, 136.33, 134.56, 133.94, 130.50, 130.16, 129.60, 129.13, 127.93, 127.91, 127.78, 127.62, 127.54, 127.47, 127.05, 126.89, 126.54, 50.64, 21.47, 21.42. HRMS (+ p APCI) calculated for $C_{29}H_{26}O_2N^{32}S$ [M+H] calculated for 452.1679, found 452.1680.

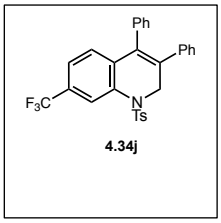

4.34j

Following GP3, 3,4-diphenyl-1-tosyl-7-(trifluoromethyl)-1,2-dihydroquinoline, was isolated as a white solid in 56% yield, >20:1 r.r. ^{1}H NMR (400 MHz, $CDCl_3$) δ 8.11 (d, *J* = 1.8 Hz, 1H), 7.44 – 7.22 (m, 4H), 7.23 – 7.07 (m, 7H), 6.78 (dd, *J* = 8.2, 1.0 Hz, 1H), 6.72 – 6.59 (m, 2H), 6.47 – 6.31 (m, 2H), 4.89 (s, 2H), 2.42 (s, 3H). ^{13}C NMR (101 MHz, $CDCl_3$) δ 138.10, 136.51, 136.10, 135.98 (d, *J* = 1.5 Hz), 135.13, 133.38, 133.24, 129.86 (q, *J* = 32.9 Hz), 128.39, 128.09, 127.91, 127.67, 127.18, 124.30 (q, *J* = 4.0 Hz), 124.13 (q, *J* = 133.1), 123.30 (q, *J* = 3.8 Hz), 50.46, 21.63. ^{19}F NMR (376 MHz, $CDCl_3$) δ -62.43. HRMS (+ p APCI) calculated for $C_{29}H_{23}O_2NF_3{}^{32}S$ [M+H] calculated for 506.1396, found 506.1403.

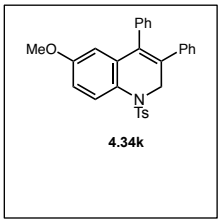

4.34k

Following GP3, 6-methoxy-3,4-diphenyl-1-tosyl-1,2-dihydroquinoline, was isolated as a white solid in 27% yield. ^{1}H NMR (400 MHz, $CDCl_3$) δ 7.76 (d, *J* = 8.8 Hz, 1H), 7.28 (d, *J* = 8.3 Hz, 2H), 7.17 – 7.06 (m, 8H), 6.87 (dd, *J* = 8.8, 2.9 Hz, 1H), 6.71 – 6.60 (m, 2H), 6.42 – 6.34 (m, 2H), 6.19 (d, *J* = 2.9 Hz, 1H), 4.83 (s, 2H), 3.67 (s, 3H), 2.42 (s, 3H). ^{13}C NMR (101 MHz, $CDCl_3$) δ 158.01, 143.46, 138.58, 136.89, 136.09, 133.97, 133.92, 131.34, 130.49, 129.18, 128.31, 127.99, 127.89, 127.83, 127.71, 127.55, 127.18, 127.08, 112.61, 112.54, 77.25, 55.37, 50.70, 29.73, 21.50. HRMS (+ p APCI) calculated for $C_{29}H_{26}O_3N{}^{32}S$ [M+H] calculated for 468.1628, found 468.1633.

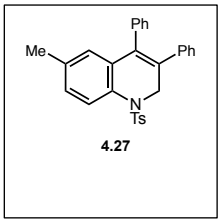

4.27

Following GP3, 6-methyl-3,4-diphenyl-1-tosyl-1,2-dihydroquinoline, was isolated as a white solid in 78% yield. ^{1}H NMR (400 MHz, $CDCl_3$) δ 7.71 – 7.66 (m, 1H), 7.35 – 7.29 (m, 2H), 7.22 – 7.08 (m, 8H), 6.94 (ddd, *J* = 8.0, 1.8, 0.8 Hz, 1H), 6.71 – 6.63 (m, 2H), 6.58 (d, *J* = 7.9 Hz, 1H), 6.47 – 6.40 (m, 2H), 4.85 (s, 2H), 2.45 (s, 3H), 2.43 (s, 3H). ^{13}C NMR (101 MHz, $CDCl_3$) δ 143.43, 138.70, 138.25, 137.27, 136.33, 134.56, 133.94, 130.50, 130.16, 129.60, 129.13, 127.93, 127.91, 127.78, 127.62, 127.54, 127.47, 127.05, 126.89, 126.54, 50.64, 21.47, 21.42. HRMS (+ p APCI) calculated for $C_{29}H_{26}O_2N^{32}S$ [M+H] calculated for 452.1679, found 452.1680.

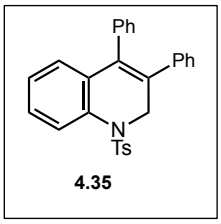

4.35

Following GP3, 3,4-diphenyl-1-tosyl-1,2-dihydroquinoline, was isolated as a white solid in 72% yield. ^{1}H NMR (400 MHz, $CDCl_3$) δ 7.84 (dd, *J* = 8.0, 1.3 Hz, 1H), 7.35 – 7.27 (m, 3H), 7.17 – 7.08 (m, 9H), 6.71 – 6.61 (m, 3H), 6.44 – 6.37 (m, 2H), 4.86 (s, 2H), 2.41 (s, 3H). ^{13}C NMR (101 MHz, $CDCl_3$) δ 143.54, 138.57, 137.08, 136.20, 134.59, 133.93, 132.80, 130.81, 130.51, 129.17, 128.78, 128.00, 127.88, 127.84, 127.61, 127.15, 127.06, 126.70, 126.68, 50.52, 21.50. HRMS (+ p APCI) calculated for $C_{28}H_{24}O_2N^{32}S$ [M+H] calculated for 438.1522, found 438.1521.

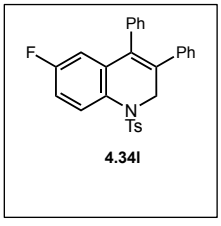

4.34l

Following GP3, 6-fluoro-3,4-diphenyl-1-tosyl-1,2-dihydroquinoline, was isolated as a light-yellow solid in 38% yield. ^{1}H NMR (400 MHz, $CDCl_3$) δ 7.83 (dd, *J* = 8.8, 5.3 Hz, 1H), 7.38 – 7.28 (m, 5H), 7.26 – 7.10 (m, 9H), 7.04 (ddd, *J* = 8.8, 7.9, 2.9 Hz, 1H), 6.79 – 6.58 (m, 2H), 6.54 – 6.29 (m, 3H), 4.88 (s, 2H), 2.45 (s, 3H). ^{13}C NMR (101 MHz, $CDCl_3$) δ 162.3, 159.9, 136.42, 135.93, 134.73 (d, *J* = 8.3 Hz), 132.06, 130.41, 130.37, 129.28, 128.88 (d, *J* = 8.5 Hz), 128.20, 127.88 (d, *J* = 8.0 Hz), 127.65, 127.40 (d, *J* = 8.8 Hz), 114.71 (d, *J* = 22.9 Hz), 113.23 (d, *J* = 24.4 Hz), 50.59, 21.52. ^{19}F NMR CPD (376 MHz, CDCl3) δ -113.98. HRMS (+ p APCI) calculated for $C_{28}H_{23}O_2NF^{32}S$ [M+H] calculated for 456.1428, found 456.1432.

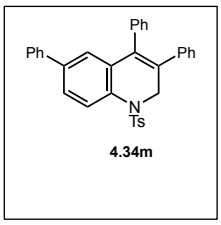

4.34m

Following GP3, 3,4,6-triphenyl-1-tosyl-1,2-dihydroquinoline, was isolated as a white solid in 61% yield. ^{1}H NMR (400 MHz, $CDCl_3$) δ 7.91 (d, *J* = 8.3 Hz, 1H), 7.57 (dd, *J* = 8.3, 2.1 Hz, 1H), 7.43 – 7.31 (m, 7H), 7.21 – 7.07 (m, 8H), 6.91 (d, *J* = 2.1 Hz, 1H), 6.70 – 6.59 (m, 2H), 6.50 – 6.42 (m, 2H), 4.88 (s, 2H), 2.41 (s, 3H). ^{13}C NMR (101 MHz, $CDCl_3$) δ 143.71, 140.35, 139.52, 138.74, 137.04, 136.42, 134.14, 134.05, 133.18, 131.31, 130.65, 129.38, 128.90, 128.19, 128.04, 127.98, 127.75, 127.59, 127.56, 127.38, 127.23, 127.09, 126.75, 125.35, 50.71, 21.62. HRMS (+ p APCI) calculated for $C_{20}H_{28}O_8N_6{}^{32}S$ [M+H] calculated for 512.16838, found 512.16813.

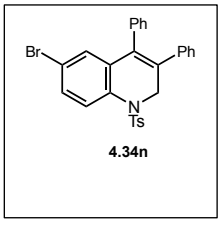

4.34n

Following GP3, 6-bromo-3,4-diphenyl-1-tosyl-1,2-dihydroquinoline, was isolated as a white solid in 59% yield. ^{1}H NMR (400 MHz, $CDCl_3$) δ 7.71 (d, *J* = 8.6 Hz, 1H), 7.43 (dd, *J* = 8.6, 2.3 Hz, 1H),

7.35 – 7.27 (m, 2H), 7.23 – 7.01 (m, 8H), 6.78 (d, J = 2.3 Hz, 1H), 6.72 – 6.57 (m, 2H), 6.47 – 6.33 (m, 2H), 4.84 (s, 2H), 2.43 (s, 3H). ^{13}C NMR (101 MHz, $CDCl_3$) δ 143.95, 138.30, 136.41, 136.17, 134.80, 133.78, 132.36, 130.96, 130.50, 129.49, 128.86, 128.38, 128.04, 127.95, 127.70, 127.50, 120.56, 50.52, 21.64. HRMS (+ p APCI) calculated for $C_{28}H_{21}O_2N^{79}Br^{32}S$ [M+H] calculated for 514.04709, found 514.04707.

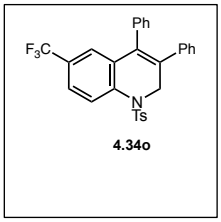

4.34o

Following GP3, 3,4-diphenyl-1-tosyl-6-(trifluoromethyl)-1,2-dihydroquinoline, was isolated as a white solid in 73% yield. ^{1}H NMR (400 MHz, $CDCl_3$) δ 7.96 (dd, J = 8.4, 1.0 Hz, 1H), 7.56 (ddd, J = 8.4, 2.2, 0.8 Hz, 1H), 7.34 – 7.27 (m, 2H), 7.23 – 7.04 (m, 8H), 6.93 (d, J = 2.0 Hz, 1H), 6.72 – 6.56 (m, 2H), 6.48 – 6.36 (m, 2H), 4.88 (s, 2H), 2.42 (s, 3H). ^{19}F NMR (376 MHz, $CDCl_3$) δ -62.49. ^{13}C NMR (101 MHz, $CDCl_3$) δ 147.38, 144.02, 140.71, 138.06, 136.09, 133.58, 133.25, 133.12, 132.63, 132.47, 130.32, 130.25, 129.84, 129.78, 129.43, 129.19, 129.15, 129.10, 128.98, 128.91, 128.43, 128.34, 128.03, 127.95, 127.79, 127.76, 127.66, 127.48, 127.43, 127.40, 126.12, 124.59, 124.56, 123.96, 123.54, 123.50, 50.30, 21.50, 21.38. HRMS (+ p APCI) calculated for $C_{29}H_{23}O_2NF_3{}^{32}S$ [M+H] calculated for 506.13961, found 506.14067.

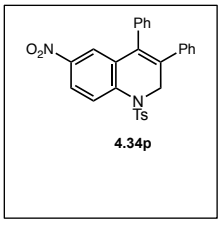

4.34p

Following GP3, 6-nitro-3,4-diphenyl-1-tosyl-1,2-dihydroquinoline, was isolated as a yellow solid in 42% yield. ^{1}H NMR (400 MHz, $CDCl_3$) δ 8.16 (dd, J = 8.8, 2.6 Hz, 1H), 8.01 (d, J = 8.8 Hz, 1H), 7.56 (d, J = 2.6 Hz, 1H), 7.36 – 7.30 (m, 2H), 7.20 – 7.10 (m, 7H), 6.73 – 6.63 (m, 2H), 6.50 – 6.39

(m, 2H), 4.91 (s, 2H), 2.42 (s, 3H). ^{13}C NMR (101 MHz, $CDCl_3$) δ 146.02, 144.48, 140.37, 137.83, 136.07, 135.75, 133.83, 133.25, 132.86, 130.34, 129.69, 128.71, 128.16, 128.10, 127.89, 127.63, 127.47, 122.77, 121.87, 50.41, 21.65. HRMS (+ p APCI) calculated for $C_{28}H_{23}O_4N_2{}^{32}S$ [M+H] calculated for 483.1373, found 483.1375.

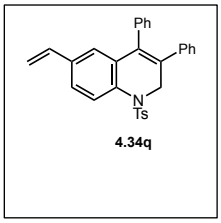

4.34q

Following GP3, 3,4-diphenyl-1-tosyl-6-vinyl-1,2-dihydroquinoline, was isolated as a white solid in 53% yield. ^{1}H NMR (400 MHz, $CDCl_3$) δ 7.81 (d, *J* = 8.3 Hz, 1H), 7.41 (dd, *J* = 8.5, 2.1 Hz, 1H), 7.33 – 7.28 (m, 2H), 7.20 – 7.14 (m, 2H), 7.14 – 7.07 (m, 6H), 6.69 – 6.62 (m, 3H), 6.53 (dd, *J* = 17.6, 10.9 Hz, 1H), 6.46 – 6.36 (m, 2H), 5.55 (dd, *J* = 17.6, 0.8 Hz, 1H), 5.16 (dd, *J* = 10.9, 0.8 Hz, 1H), 4.84 (s, 2H), 2.41 (s, 3H). ^{13}C NMR (101 MHz, $CDCl_3$) δ 143.68, 138.71, 137.04, 136.40, 136.22, 136.01, 134.00, 132.90, 131.16, 130.65, 128.15, 128.03, 127.97, 127.73, 127.34, 125.40, 124.98, 114.44, 50.67, 21.62. HRMS (+ p APCI) calculated for $C_{22}H_{29}O_4N^{10}B^{32}S$ [M+H] calculated for 413.19412, found 413.19418.

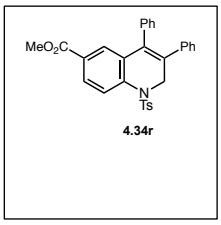

4.34r

Following GP3, methyl 3,4-diphenyl-1-tosyl-1,2-dihydroquinoline-6-carboxylate, was isolated as a white solid in 63% yield. ^{1}H NMR (400 MHz, $CDCl_3$) δ 7.98 (dd, *J* = 8.4, 2.0 Hz, 1H), 7.92 (dd, *J* = 8.4, 0.5 Hz, 1H), 7.38 (d, *J* = 1.9 Hz, 1H), 7.33 – 7.27 (m, 2H), 7.19 – 7.10 (m, 8H), 6.70 – 6.62 (m, 2H), 6.47 – 6.34 (m, 2H), 4.87 (s, 2H), 3.82 (s, 3H), 2.40 (s, 3H). ^{13}C NMR (101 MHz, CDCl3) δ

166.48, 128.25, 128.02, 127.91, 127.87, 127.50, 127.45, 127.31, 126.90, 52.23, 50.38, 21.51. HRMS (+ p APCI) calculated for $C_{30}H_{26}O_4N^{32}S$ [M+H] calculated for 496.1577, found 496.1582.

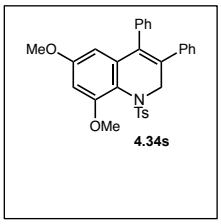

4.34s

Following GP3, 6,8-dimethoxy-3,4-diphenyl-1-tosyl-1,2-dihydroquinoline, was isolated as a white solid in 42% yield. ^{1}H NMR (400 MHz, $CDCl_3$) δ 7.40 – 7.33 (m, 2H), 7.17 (d, *J* = 2.5 Hz, 1H), 7.14 – 7.10 (m, 2H), 7.10 – 7.05 (m, 3H), 7.05 – 7.00 (m, 1H), 7.00 – 6.93 (m, 2H), 6.56 – 6.50 (m, 2H), 6.33 – 6.27 (m, 2H), 6.26 (d, *J* = 2.5 Hz, 1H), 4.72 (s, 2H), 3.92 (s, 3H), 3.14 (s, 3H), 2.39 (s, 3H). ^{13}C NMR (101 MHz, $CDCl_3$) δ 160.04, 157.63, 143.51, 140.02, 138.97, 138.01, 136.72, 132.13, 129.28, 128.71, 128.36, 127.98, 127.58, 127.54, 126.99, 126.46, 115.64, 102.82, 98.89, 55.74, 55.35, 51.26, 21.52. HRMS (+ p APCI) calculated for $C_{30}H_{28}O_4N^{32}S$ [M+H] calculated for 498.1734, found 498.1735.

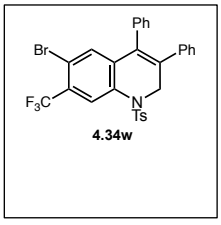

4.34w

Following GP3, 6-bromo-3,4-diphenyl-1-tosyl-7-(trifluoromethyl)-1,2-dihydroquinoline, was isolated as a white solid in 75% yield, >20:1 r.r.. ^{1}H NMR (600 MHz, $CDCl_3$) δ 8.17 (s, 1H), 7.37 – 7.33 (m, 2H), 7.26 – 7.22 (m, 1H), 7.22 – 7.12 (m, 7H), 6.99 (s, 1H), 6.71 – 6.63 (m, 2H), 6.46 – 6.38 (m, 2H), 4.89 (s, 2H), 2.46 (s, 3H). ^{13}C NMR (151 MHz, $CDCl_3$) δ 144.11, 137.59, 136.95, 135.53, 134.70 (d, *J* = 2.5 Hz), 133.71, 132.08, 130.15, 129.92, 129.50, 128.41, 127.94, 127.79 (d, *J* = 2.2 Hz), 127.67, 127.44, 126.61 (d, *J* = 5.6 Hz), 125.29 – 119.55 (m), 50.19, 21.44. ^{19}F NMR (565

MHz, $CDCl_3$) δ -62.33. HRMS (+ p APCI) calculated for $C_{29}H_{22}O_2N^{79}BrF_3{}^{32}S$[M+H] calculated for 584.05012, found 584.04979.

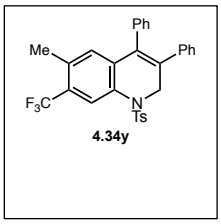

4.34y

Following GP3, 6-methyl-3,4-diphenyl-1-tosyl-7-(trifluoromethyl)-1,2-dihydroquinoline, was isolated as a white solid in 74% yield, >20:1 r.r. ^{1}H NMR (600 MHz, $CDCl_3$) δ 8.07 (s, 1H), 7.33 – 7.28 (m, 2H), 7.23 – 7.16 (m, 2H), 7.18 – 7.09 (m, 8H), 6.68 – 6.61 (m, 2H), 6.55 (s, 1H), 6.45 – 6.38 (m, 2H), 4.85 (s, 2H), 2.42 (s, 3H), 2.31 (q, *J* = 1.8 Hz, 3H). ^{13}C NMR (151 MHz, $CDCl_3$) δ 143.78, 138.13, 136.43, 136.13, 135.39, 134.82, 133.36, 133.05, 132.38, 130.37, 130.06, 129.76, 129.36, 128.20, 127.91, 127.81, 127.60, 127.46, 124.79 (q, *J* = 5.8 Hz), 126.85 – 121.29 (m), 50.42, 29.71, 21.49, 19.17 (d, *J* = 2.3 Hz). ^{19}F NMR (565 MHz, $CDCl_3$) δ -61.47. HRMS (+ p APCI) calculated for $C_{30}H_{25}O_2NF_3{}^{32}S$ [M+H] calculated for 520.15526, found 520.15526.

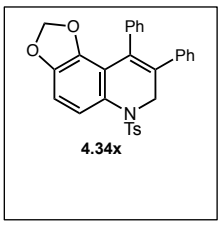

4.34x

Following GP3, 8,9-diphenyl-6-tosyl-6,7-dihydro-[1,3]dioxolo[4,5-*f*]quinoline, was isolated as a tan solid in 41% yield, 1.6:1 r.r. Major: ^{1}H NMR (400 MHz, $CDCl_3$) δ 7.41 (d, *J* = 8.3 Hz, 2H), 7.22 – 7.17 (m, 1H), 7.16 – 7.10 (m, 5H), 7.07 – 7.00 (m, 2H), 6.82 (d, *J* = 8.4 Hz, 1H), 6.64 – 6.60 (m, 2H), 6.41 – 6.34 (m, 2H), 6.00 (s, 1H), 5.60 (s, 2H), 4.81 (s, 2H), 2.45 (d, *J* = 3.2 Hz, 3H). ^{13}C NMR (101 MHz, $CDCl_3$) δ 146.79, 143.80, 143.57, 138.39, 137.25, 136.38, 130.60, 130.44, 129.82, 129.67, 129.31, 129.16, 128.96, 128.86, 128.63, 128.05, 128.00, 127.89, 127.77, 127.74, 127.37,

127.07, 126.90, 126.10, 116.11, 107.36, 101.15, 77.25, 51.05, 21.53. HRMS (+ p APCI) calculated for $C_{29}H_{24}O_4N^{32}S$ [M+H] calculated for 482.14206, found 482.14231.

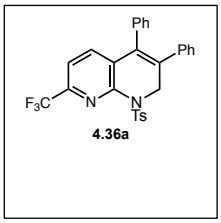

4.36a

Following GP3, 3,4-diphenyl-1-tosyl-7-(trifluoromethyl)-1,2-dihydro-1,8-naphthyridine, was isolated as a white solid in 16% yield. ^{1}H NMR (400 MHz, $CDCl_3$) δ 8.53 (d, *J* = 8.2 Hz, 1H), 8.10 (d, *J* = 8.3 Hz, 2H), 7.83 (d, *J* = 8.3 Hz, 1H), 7.80 – 7.71 (m, 2H), 7.45 (dd, *J* = 5.1, 1.8 Hz, 3H), 7.33 (ddd, *J* = 8.9, 2.5, 1.3 Hz, 3H), 7.08 – 7.02 (m, 3H), 7.00 (dd, *J* = 6.6, 3.0 Hz, 3H), 5.07 (s, 2H), 2.40 (s, 3H).

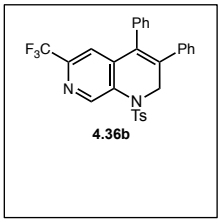

4.36b

Following GP3, 3,4-diphenyl-1-tosyl-6-(trifluoromethyl)-1,2-dihydro-1,7-naphthyridine, was isolated as a white solid in 69% yield, 4:1 r.r. Major: ^{1}H NMR (600 MHz, $CDCl_3$) δ 8.25 (dd, *J* = 8.3, 0.7 Hz, 1H), 7.59 (d, *J* = 8.3 Hz, 1H), 7.38 – 7.34 (m, 2H), 7.19 – 7.11 (m, 5H), 7.10 – 7.04 (m, 2H), 6.88 – 6.73 (m, 2H), 6.64 – 6.50 (m, 2H), 4.88 (s, 2H), 2.38 (s, 3H). ^{13}C NMR (151 MHz, $CDCl_3$) δ 150.28, 145.27 (q, *J* = 35.2 Hz), 138.11, 137.51, 135.73, 134.24, 133.91, 121.24 (q, *J* = 274.3 Hz), 118.89, 49.94, 21.49. ^{19}F NMR (565 MHz, $CDCl_3$) δ -67.72. Minor: ^{1}H NMR (600 MHz, $CDCl_3$) δ 9.11 (s, 1H), 7.38 – 7.32 (m, 2H), 7.26 – 7.22 (m, 1H), 7.21 – 7.13 (m, 6H), 6.94 (d, *J* = 0.6 Hz, 1H), 6.71 – 6.62 (m, 2H), 6.49 – 6.39 (m, 2H), 4.92 (s, 2H), 2.43 (s, 3H). ^{13}C NMR (151 MHz, $CDCl_3$) δ 148.01, 145.69 (q, *J* = 34.8 Hz), 144.43, 140.17, 137.33, 137.14, 135.64, 134.64,

132.87, 131.59, 130.00, 129.59, 128.61, 128.25, 128.09 (d, J = 3.1 Hz), 127.65, 127.38, 121.26 (q, J = 274.0 Hz), 116.58 (d, J = 3.0 Hz), 50.20, 21.45. ^{19}F NMR (565 MHz, $CDCl_3$) δ -67.64. HRMS (+ p APCI) calculated for $C_{28}H_{22}O_2N_2F_3{}^{32}S$ [M+H] calculated for 507.13486, found 507.13503.

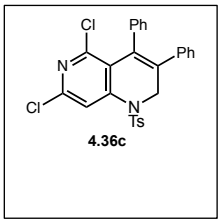

4.36c

Following GP3, 5,7-dichloro-3,4-diphenyl-1-tosyl-1,2-dihydro-1,6-naphthyridine, was isolated as a white solid in 50% yield. ^{1}H NMR (600 MHz, $CDCl_3$) δ 7.94 (s, 1H), 7.47 – 7.42 (m, 2H), 7.22 – 7.18 (m, 3H), 7.18 – 7.15 (m, 2H), 7.15 – 7.13 (m, 1H), 7.08 (dd, J = 8.5, 7.0 Hz, 2H), 6.68 – 6.51 (m, 2H), 6.51 – 6.29 (m, 2H), 4.77 (s, 2H), 2.43 (s, 3H). ^{13}C NMR (151 MHz, $CDCl_3$) δ 148.38, 148.29, 147.79, 144.82, 137.79, 136.34, 134.74, 130.60, 129.88, 128.11, 127.99, 127.89, 127.77, 127.48, 125.54, 118.62, 50.44, 21.55. HRMS (+ p APCI) calculated for $C_{27}H_{21}O_2N_2{}^{35}Cl_2{}^{32}S$ [M+H] calculated for 507.06953, found 507.06988.

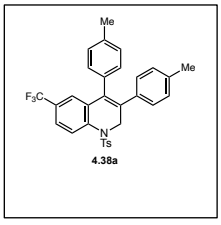

4.38a

Following GP3, 3,4-di-*p*-tolyl-1-tosyl-6-(trifluoromethyl)-1,2-dihydroquinoline, was isolated as a white solid in 72% yield. ^{1}H NMR (400 MHz, $CDCl_3$) δ 7.96 (dd, J = 8.5, 0.9 Hz, 1H), 7.66 – 7.51 (m, 1H), 7.39 – 7.25 (m, 4H), 7.19 – 7.11 (m, 2H), 7.01 – 6.91 (m, 5H), 6.65 – 6.53 (m, 2H), 6.41 – 6.24 (m, 2H), 4.86 (s, 2H), 2.44 (s, 3H), 2.31 (d, J = 9.3 Hz, 6H). ^{19}F NMR (376 MHz, $CDCl_3$) δ -62.43.

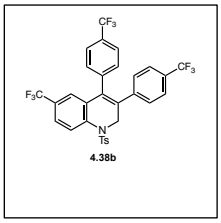

Following GP3, 1-tosyl-6-(trifluoromethyl)-3,4-bis(4-(trifluoromethyl)phenyl)-1,2-dihydroquinoline, was isolated as a white solid in 78% yield. ^{1}H NMR (400 MHz, $CDCl_3$) δ 8.03 (d, *J* = 8.4 Hz, 1H), 7.66 (dd, *J* = 8.5, 2.1 Hz, 1H), 7.46 (t, *J* = 8.0 Hz, 4H), 7.37 – 7.30 (m, 2H), 7.25 – 7.15 (m, 2H), 6.86 (d, *J* = 2.1 Hz, 1H), 6.81 – 6.71 (m, 2H), 6.64 – 6.54 (m, 2H), 4.90 (s, 2H), 2.47 (s, 3H). ^{19}F NMR (376 MHz, $CDCl_3$) δ -62.54, -62.68, -62.80. HRMS (+ p APCI) calculated for $C_{31}H_{21}O_2NF_9{}^{32}S$ [M+H] calculated for 642.11438, found 642.11393.

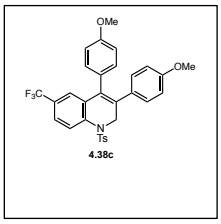

Following GP3, 3,4-bis(4-methoxyphenyl)-1-tosyl-6-(trifluoromethyl)-1,2-dihydroquinoline, was isolated as a white solid in 67% yield. ^{1}H NMR (400 MHz, $CDCl_3$) δ 7.93 (d, *J* = 8.3 Hz, 1H), 7.58 – 7.49 (m, 1H), 7.31 – 7.26 (m, 2H), 7.15 – 7.05 (m, 2H), 6.95 (d, *J* = 2.1 Hz, 1H), 6.72 – 6.64 (m, 4H), 6.64 – 6.55 (m, 2H), 6.38 – 6.29 (m, 2H), 4.82 (s, 2H), 3.78 (d, *J* = 2.9 Hz, 6H), 2.40 (s, 3H). ^{19}F NMR (376 MHz, $CDCl_3$) δ -62.43. HRMS (+ p APCI) calculated for $C_{31}H_{27}O_4NF_3{}^{32}S$ [M+H] calculated for 566.16074, found 566.15923.

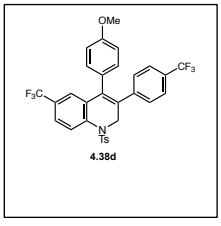

Following GP3, 4-(4-methoxyphenyl)-1-tosyl-6-(trifluoromethyl)-3-(4-(trifluoromethyl)phenyl)-1,2-dihydroquinoline, was isolated as a white solid in 80% yield, 1.7:1 r.r. ^{1}H NMR (600 MHz, $CDCl_3$) δ 7.97 (d, *J* = 8.4 Hz, 1H), 7.57 (dd, *J* = 8.5, 2.1 Hz, 1H), 7.43 (d, *J* = 8.0 Hz, 2H), 7.33 – 7.28 (m, 2H), 7.15 (d, *J* = 8.0 Hz, 2H), 6.81 (d, *J* = 2.1 Hz, 1H), 6.69 – 6.64 (m, 2H), 6.62 – 6.53 (m, 3H), 4.85 (s, 2H), 3.77 (s, 3H), 2.43 (s, 3H). ^{13}C NMR (151 MHz, $CDCl_3$) δ 159.01, 144.06, 140.51, 137.51, 136.11, 133.37, 132.64, 130.82, 129.80, 129.38, 129.17, 129.00 – 128.21 (m), 126.62, 126.37, 125.42 (q, *J* = 3.8 Hz), 125.04 – 124.35 (m), 123.25 – 122.63 (m), 113.59, 55.22, 50.31, 21.53. ^{19}F NMR (565 MHz, $CDCl_3$) δ -62.52, -62.60. HRMS (+ p APCI) calculated for $C_{31}H_{24}O_3NF_6{}^{32}S$ [M+H] calculated for 604.13756, found 604.13689.

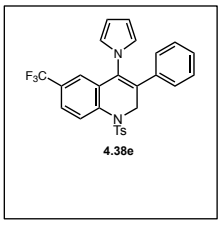

4.38e

Following GP3, 3-phenyl-4-(1*H*-pyrrol-1-yl)-1-tosyl-6-(trifluoromethyl)-1,2-dihydroquinoline, was isolated as a white solid in 28% yield. Major: ^{1}H NMR (600 MHz, $CDCl_3$) δ 7.56 (ddd, *J* = 8.4, 2.1, 0.7 Hz, 1H), 7.31 – 7.26 (m, 2H), 7.25 – 7.19 (m, 4H), 7.16 – 7.12 (m, 2H), 6.93 (d, *J* = 2.1 Hz, 1H), 6.48 – 6.42 (m, 2H), 6.11 (td, *J* = 2.2, 1.5 Hz, 2H), 6.07 – 5.98 (m, 2H), 4.85 (s, 2H), 2.40 (s, 3H). ^{19}F NMR (376 MHz, $CDCl_3$) δ -62.53. Minor: ^{1}H NMR (600 MHz, $CDCl_3$) δ 8.02 – 7.90 (m, 2H), 7.62 (ddd, *J* = 8.4, 2.2, 0.7 Hz, 1H), 7.31 – 7.27 (m, 2H), 7.25 – 7.20 (m, 2H), 7.13 – 7.09 (m, 2H), 6.81 (d, *J* = 2.1 Hz, 1H), 6.58 – 6.52 (m, 2H), 6.11 (td, *J* = 2.2, 1.5 Hz, 2H), 5.85 (s, 2H), 4.97 (s, 2H), 2.41 (s, 3H). ^{19}F NMR (376 MHz, $CDCl_3$) δ -62.59. ^{13}C NMR (151 MHz, $CDCl_3$) δ 144.37, 144.29, 137.81, 136.35, 135.68, 135.47, 135.11, 134.21, 132.40, 130.50, 130.48, 129.14 (q, *J* = 26.8 Hz), 128.95 (q, *J* = 23.7 Hz), 127.28, 127.27, 126.41, 125.60 (q, *J* = 3.7 Hz), 124.49 (q, *J* = 270.94 Hz), 124.32 (q, *J* = 3.7 Hz), 123.64 (q, *J* = 258.5 Hz)123.29 (q, *J* = 3.8 Hz), 121.40, 121.26 (q, *J* =

3.8 Hz), 119.80, 109.88, 109.54, 49.87, 48.36, 21.52, 21.49. HRMS (+ p APCI) calculated for $C_{27}H_{22}O_2N_2F_3{}^{32}S$ [M+H] calculated for 495.1348, found 495.1352.

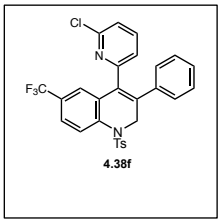

4.38f

Following GP3, 4-(6-chloropyridin-2-yl)-3-phenyl-1-tosyl-6-(trifluoromethyl)-1,2-dihydroquinoline, was isolated as a white solid in 49% yield, 2.1:1 r.r. Major: ^{1}H NMR (600 MHz, $CDCl_3$) δ 7.97 (d, *J* = 8.2 Hz, 1H), 7.61 (ddd, *J* = 8.4, 2.1, 0.7 Hz, 1H), 7.37 – 7.27 (m, 2H), 7.30 – 7.28 (m, 1H), 7.26 – 7.12 (m, 3H), 7.13 – 7.02 (m, 3H), 6.96 – 6.90 (m, 1H), 6.61 – 6.29 (m, 2H), 5.90 (dd, *J* = 7.7, 0.8 Hz, 1H), 5.00 (s, 2H), 2.39 (s, 3H).Minor: ^{1}H NMR (600 MHz, $CDCl_3$) δ 7.97 – 7.94 (m, 2H), 7.60 – 7.57 (m, 2H), 7.36 (d, *J* = 8.3 Hz, 2H), 7.30 – 7.28 (m, 3H), 7.19 – 7.16 (m, 3H), 6.77 – 6.71 (m, 2H), 6.09 (dd, *J* = 7.5, 0.9 Hz, 1H), 4.81 (s, 2H), 2.38 (s, 3H).^{13}C NMR (151 MHz, $CDCl_3$) δ 156.66, 156.36, 151.18, 144.13, 144.01, 138.88, 138.64, 137.57, 137.22, 136.58, 136.31, 136.22, 135.84, 132.47, 131.26, 131.17, 130.91, 130.38, 129.98, 129.82, 129.45, 129.04, 128.80, 128.57, 128.44, 128.34, 128.26, 127.64, 127.46, 127.30, 127.08, 125.64 (q, *J* = 3.7 Hz), 125.10 (q, *J* = 3.7 Hz), 124.73, 124.23, 124.14 (q, *J* = 3.9 Hz), 123.21, 123.11 (d, *J* = 3.9 Hz), 122.92, 122.74, 122.55, 50.05, 48.68, 21.64, 21.60.^{19}F NMR (565 MHz, $CDCl_3$) δ -62.49 – -62.55 (bs). HRMS (+ p APCI) calculated for $C_{28}H_{21}O_2N_2{}^{35}ClF_3{}^{32}S$ [M+H] calculated for 541.0960, found 541.0968.

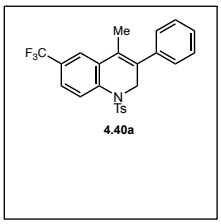

4.40a

Following GP3, 4-methyl-3-phenyl-1-tosyl-6-(trifluoromethyl)-1,2-dihydroquinoline, was isolated as a white solid in 74% yield, >20:1 r.r. ^{1}H NMR (400 MHz, $CDCl_3$) δ 7.90 (dd, *J* = 8.3, 0.9 Hz, 1H), 7.64 – 7.57 (m, 1H), 7.50 (d, *J* = 2.1 Hz, 1H), 7.46 – 7.39 (m, 2H), 7.39 – 7.30 (m, 3H), 7.11 (ddt, *J* = 13.7, 6.7, 1.2 Hz, 4H), 4.62 (q, *J* = 1.6 Hz, 2H), 2.35 (s, 3H), 1.72 (t, *J* = 1.7 Hz, 3H). ^{19}F NMR (376 MHz, $CDCl_3$) δ -62.31. HRMS (+ p APCI) calculated for $C_{24}H_{21}O_2NF_3{}^{32}S$ [M+H] calculated for 444.12396, found 444.12449.

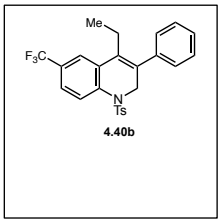

4.40b

Following GP3, 4-ethyl-3-phenyl-1-tosyl-6-(trifluoromethyl)-1,2-dihydroquinoline, was isolated as a white solid in 67% yield, >20:1 r.r. ^{1}H NMR (400 MHz, $CDCl_3$) δ 7.94 (dd, *J* = 8.5, 0.9 Hz, 1H), 7.58 (dd, *J* = 8.7, 2.1 Hz, 1H), 7.48 (d, *J* = 2.3 Hz, 1H), 7.42 – 7.29 (m, 5H), 7.14 (d, *J* = 8.1 Hz, 2H), 6.99 – 6.88 (m, 2H), 4.61 (s, 2H), 2.37 (s, 3H), 2.27 (d, *J* = 7.5 Hz, 2H), 0.46 (t, *J* = 7.5 Hz, 3H). ^{19}F NMR (376 MHz, $CDCl_3$) δ -62.35. HRMS (+ p APCI) calculated for $C_{28}H_{21}O_2N_2{}^{35}ClF_3{}^{32}S$ [M+H] calculated for 541.0960, found 541.0968.

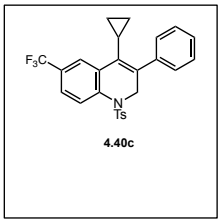

4.40c

Following GP3, 4-cyclopropyl-3-phenyl-1-tosyl-6-(trifluoromethyl)-1,2-dihydroquinoline, was isolated as a white solid in 71% yield, >20:1 r.r. ^{1}H NMR (600 MHz, $CDCl_3$) δ 7.88 (d, *J* = 8.3 Hz, 1H), 7.85 (d, *J* = 2.1 Hz, 1H), 7.57 (dd, *J* = 8.5, 2.1 Hz, 1H), 7.43 – 7.36 (m, 4H), 7.36 – 7.32 (m, 1H), 7.31 – 7.26 (m, 2H), 7.05 – 6.99 (m, 2H), 4.64 (d, *J* = 2.2 Hz, 2H), 2.28 (s, 3H), 1.51 (dqt, *J* = 7.8, 5.5, 2.8 Hz, 1H), 0.63 – 0.36 (m, 2H), -0.83 (td, *J* = 6.0, 4.4 Hz, 2H).^{13}C NMR (151 MHz,

$CDCl_3$) δ 144.07, 137.58, 137.47, 137.30, 135.78, 134.11, 130.74, 129.18, 129.13, 128.09, 127.97, 126.91, 126.86, 124.03 (q, *J* = 3.7 Hz), 123.93 (q, *J* = 271.1 Hz), 122.37 (q, *J* = 3.9 Hz), 50.35, 21.36, 9.77, 8.81. ^{19}F NMR (565 MHz, $CDCl_3$) δ -62.35. HRMS (+ p APCI) calculated for $C_{26}H_{23}O_2NF_3{}^{32}S$ [M+H] calculated for 470.1396, found 470.1403.

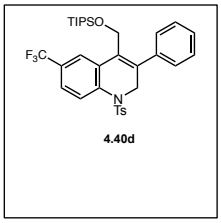

4.40d

Following GP3, 3-phenyl-1-tosyl-6-(trifluoromethyl)-4-(((triisopropylsilyl)oxy)methyl)-1,2-dihydroquinoline, was isolated as a white solid in 64% yield, >20:1 r.r. ^1H NMR (600 MHz, $CDCl_3$) δ 8.73 (s, 1H), 7.94 (d, *J* = 8.5 Hz, 1H), 7.57 (d, *J* = 8.3 Hz, 1H), 7.34 (dt, *J* = 12.0, 6.7 Hz, 3H), 7.30 – 7.24 (m, 2H), 7.15 (d, *J* = 7.9 Hz, 2H), 6.76 (d, *J* = 7.0 Hz, 2H), 4.85 (d, *J* = 6.5 Hz, 1H), 4.82 (d, *J* = 17.2 Hz, 1H), 4.40 (d, *J* = 17.0 Hz, 1H), 2.39 (s, 3H), 0.89 (d, *J* = 6.5 Hz, 3H), 0.79 (dd, *J* = 16.7, 7.2 Hz, 19H), 0.75 – 0.67 (m, 4H). ^{13}C NMR (151 MHz, $CDCl_3$) δ 143.99, 138.74, 138.23, 136.73, 132.46, 129.85, 129.41, 128.52, 128.22, 128.00, 127.12, 125.29, 125.26, 125.24, 125.19, 124.42, 124.40, 123.39, 66.85, 49.84, 29.85, 23.02, 21.62, 17.81, 12.08. ^{19}F NMR (565 MHz, $CDCl_3$) δ -62.40. HRMS (+ p APCI) calculated for $C_{33}H_{41}O_3NF_3{}^{32}S^{28}Si$ [M+H] calculated for 616.25266, found 616.2523.

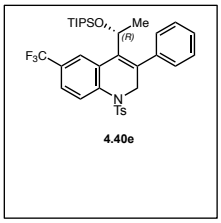

4.40e

Following GP3, (*R*)-3-phenyl-1-tosyl-6-(trifluoromethyl)-4-(1-((triisopropylsilyl)oxy)ethyl)-1,2-dihydroquinoline, was isolated as a white solid in 62% yield, >20:1 r.r.' 98% e.e. ^1H NMR (600

MHz, $CDCl_3$) δ 8.75 (d, *J* = 2.2 Hz, 1H), 7.96 (dd, *J* = 8.5, 0.9 Hz, 1H), 7.64 – 7.55 (m, 1H), 7.42 – 7.33 (m, 3H), 7.31 (d, *J* = 8.3 Hz, 2H), 7.20 – 7.14 (m, 2H), 6.79 (d, *J* = 7.2 Hz, 2H), 4.88 (q, *J* = 6.6 Hz, 1H), 4.84 (d, *J* = 17.1 Hz, 1H), 4.42 (d, *J* = 17.1 Hz, 1H), 2.42 (s, 3H), 0.92 (d, *J* = 6.5 Hz, 3H), 0.83 (d, *J* = 7.2 Hz, 9H), 0.80 (d, *J* = 7.2 Hz, 9H), 0.77 – 0.70 (m, 3H). ^{13}C NMR (151 MHz, $CDCl_3$) δ 143.83, 138.61, 138.10, 136.61, 133.11, 132.32, 129.45, 128.38, 128.07, 127.28, 125.11 (q, *J* = 3.9 Hz), 124.27 (q, *J* = 3.7 Hz), 124.15 (q, *J* = 272.4 Hz), 66.72, 49.71, 22.89, 21.48, 17.70 (d, *J* = 8.3 Hz), 11.94. ^{19}F NMR (565 MHz, $CDCl_3$) δ -62.41. HRMS (+ p APCI) calculated for $C_{34}H_{43}O_3NF_3{}^{32}SSi$ [M+H] calculated for 630.2685, found 630.2694.

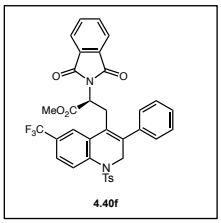

4.40f

Following GP3, methyl (*S*)-2-(1,3-dioxoisoindolin-2-yl)-3-(3-phenyl-1-tosyl-6-(trifluoromethyl)-1,2-dihydroquinolin-4-yl)propanoate, was isolated as a white solid in 52% yield, >20:1 r.r. ^{1}H NMR (400 MHz, $CDCl_3$) δ 7.83 – 7.74 (m, 1H), 7.73 – 7.64 (m, 5H), 7.52 (ddd, *J* = 8.4, 2.1, 0.8 Hz, 1H), 7.44 – 7.36 (m, 2H), 7.23 – 7.17 (m, 2H), 7.11 – 6.98 (m, 3H), 6.74 – 6.67 (m, 2H), 4.58 (dd, *J* = 9.8, 3.0 Hz, 1H), 4.50 – 4.43 (m, 2H), 3.65 (s, 3H), 3.38 (dd, *J* = 15.3, 9.8 Hz, 1H), 3.27 (dd, *J* = 15.3, 3.0 Hz, 1H), 2.41 (s, 3H). ^{13}C NMR (101 MHz, $CDCl_3$) δ 138.51, 137.84, 137.00, 136.49, 133.98, 131.61, 130.25, 129.68, 128.58, 127.75, 127.33, 127.18, 126.67, 125.85, 125.24, 124.84 (d, *J* = 3.7 Hz), 123.57, 123.48, 120.76 (d, *J* = 3.9 Hz), 52.99, 50.87, 50.00, 26.47, 21.62.

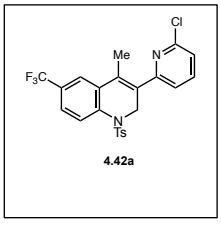

4.42a

Following GP3, 27, was isolated as a white solid in 27% yield, >20:1 r.r. ^{1}H NMR (400 MHz, $CDCl_3$) δ 7.90 (dd, *J* = 8.4, 1.0 Hz, 1H), 7.68 – 7.60 (m, 2H), 7.50 (d, *J* = 2.0 Hz, 1H), 7.42 – 7.36 (m, 2H), 7.26 (dd, *J* = 8.0, 0.8 Hz, 2H), 7.06 – 7.00 (m, 2H), 6.99 (dd, *J* = 7.6, 0.8 Hz, 1H), 4.76 (q, *J* = 1.6 Hz, 2H), 2.29 (s, 3H), 1.75 (t, *J* = 1.6 Hz, 3H).

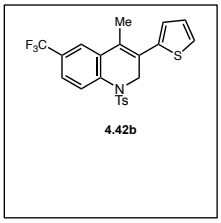

4.42b

Following GP3, 4-methyl-3-(thiophen-2-yl)-1-tosyl-6-(trifluoromethyl)-1,2-dihydroquinoline, was isolated as a white solid in 75% yield, >20:1 r.r. ^{1}H NMR (400 MHz, $CDCl_3$) δ 7.86 (dd, *J* = 8.3, 1.0 Hz, 1H), 7.58 (ddd, *J* = 8.3, 2.1, 0.8 Hz, 1H), 7.45 (d, *J* = 2.1 Hz, 1H), 7.41 (dd, *J* = 5.1, 1.1 Hz, 1H), 7.27 – 7.21 (m, 3H), 7.11 (dd, *J* = 5.1, 3.6 Hz, 1H), 7.04 (dd, *J* = 3.6, 1.1 Hz, 1H), 7.03 – 6.98 (m, 2H), 4.64 (q, *J* = 1.6 Hz, 2H), 2.29 (s, 3H), 1.81 (d, *J* = 3.1 Hz, 3H). ^{13}C NMR (101 MHz, $CDCl_3$) δ 143.95, 139.88, 137.94 (q, *J* = 1.4 Hz), 135.34, 133.88, 129.28 (q, *J* = 32.6 Hz), 129.15, 127.80, 127.50, 127.44, 127.14, 127.11, 124.47 (q, *J* = 3.8 Hz), 124.11 (q, *J* = 272.3 Hz), 121.48 (q, *J* = 3.8 Hz), 50.56, 21.58, 15.25.^{19}F NMR (376 MHz, $CDCl_3$) δ -62.35. HRMS (+ p APCI) calculated for $C_{22}H_{19}O_2NF_3{}^{32}S_2$ [M+H] calculated for 450.0804, found 450.0806.

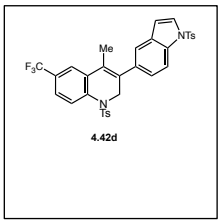

4.42d

Following GP3, 4-methyl-1-tosyl-3-(1-tosyl-1*H*-indol-5-yl)-6-(trifluoromethyl)-1,2-dihydroquinoline, was isolated as a white solid in 71% yield, >20:1 r.r. ^{1}H NMR (600 MHz, $CDCl_3$) δ 8.02 – 7.95 (m, 1H), 7.89 (d, *J* = 8.3 Hz, 1H), 7.87 – 7.82 (m, 2H), 7.64 (d, *J* = 3.7 Hz, 1H), 7.60 (dd, *J* = 8.4, 2.1 Hz, 1H), 7.49 (d, *J* = 2.1 Hz, 1H), 7.32 (ddd, *J* = 13.2, 7.5, 1.4 Hz, 4H), 7.29 – 7.24

(m, 2H), 7.07 (ddd, *J* = 15.0, 8.5, 1.3 Hz, 3H), 6.69 (dd, *J* = 3.7, 0.8 Hz, 1H), 4.60 (d, *J* = 1.8 Hz, 2H), 2.41 (s, 3H), 2.35 (s, 3H), 1.71 (d, *J* = 1.7 Hz, 3H). ^{13}C NMR (151 MHz, $CDCl_3$) δ 145.25, 143.86, 137.91, 135.79, 135.26, 134.14, 134.00, 133.48, 133.22, 130.74, 130.06, 129.89, 129.13, 128.83, 128.61, 127.24, 127.12, 126.94, 126.88, 126.78, 125.89, 125.13, 124.92, 124.27, 124.24, 121.48, 121.07, 121.04, 119.84, 113.39, 108.76, 50.37, 21.65, 21.48, 14.60. ^{19}F NMR (565 MHz, $CDCl_3$) δ -62.34.

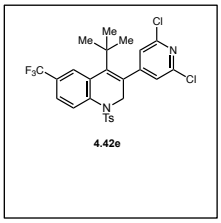

4.42e

Following GP3, 4-(*tert*-butyl)-3-(2,6-dichloropyridin-4-yl)-1-tosyl-6-(trifluoromethyl)-1,2-dihydroquinoline, was isolated as a white solid in 54% yield, 1:1 r.r. ^{1}H NMR (400 MHz, $CDCl_3$) δ 7.95 (d, *J* = 8.4 Hz, 1H), 7.89 – 7.81 (m, 2H), 7.57 (qd, *J* = 5.5, 2.1 Hz, 4H), 7.33 – 7.24 (m, 5H), 7.21 (d, *J* = 8.3 Hz, 2H), 6.98 (s, 2H), 6.66 (d, *J* = 2.0 Hz, 1H), 6.40 (s, 2H), 4.53 (s, 2H), 4.21 (s, 2H), 2.47 (s, 3H), 2.39 (s, 3H), 2.03 (s, 2H), 0.94 (s, 10H), 0.90 (s, 10H). ^{13}C NMR (101 MHz, $CDCl_3$) δ 155.02, 152.39, 150.79, 150.47, 144.67, 144.59, 139.27, 139.26, 137.08, 137.06, 136.79, 135.00, 132.99, 131.69, 129.94, 129.50, 128.89, 127.76, 127.60, 127.44, 127.33, 126.62, 126.23, 125.75, 125.21, 124.98, 124.95, 124.87, 124.60, 124.57, 124.53, 124.49, 124.28, 124.24, 124.20, 124.16, 122.70, 122.50, 122.06, 122.02, 121.98, 121.95, 52.52, 47.08, 37.22, 32.89, 30.50, 21.66, 21.48, 21.05, 14.20. ^{19}F NMR (376 MHz, $CDCl_3$) δ -62.43. HRMS (+ p APCI) calculated for $C_{26}H_{23}Cl_2F_3N_2O_2{}^{32}S$[M+H] calculated for 555.0884, found 555.0903.

Diversification:

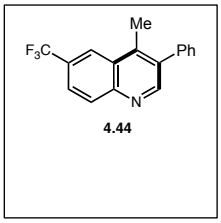

4.44

A 5 mL vial with stir bar was loaded with KOH (2.5 equiv.) and **4.40a** (1 equiv.). The vial was sealed and solvated with absolute ethanol before being heated at 100 ºC for 12 h. The reaction was quenched by pouring into water and extracted with ether (3x). The combined organics were washed with DI water (1x), dried over Na2SO4, filtered, and concentrated in vacuo. Silica gel chromatography in Hex:EtOAc 95:5 provided 4-methyl-3-phenyl-6-(trifluoromethyl)quinoline isolated as a off-white solid in >99% yield. ^{1}H NMR (400 MHz, $CDCl_3$) δ 8.93 (s, 1H), 8.43 (s, 1H), 8.28 (d, *J* = 8.8 Hz, 1H), 7.93 (dd, *J* = 8.8, 2.0 Hz, 1H), 7.59 – 7.52 (m, 2H), 7.52 – 7.46 (m, 1H), 7.45 – 7.37 (m, 2H), 2.72 (s, 3H). ^{13}C NMR (101 MHz, $CDCl_3$) δ 153.66, 148.08, 141.88, 138.00, 131.27, 129.98, 128.80, 128.32 – 119.85 (m), 124.76 (q, *J* = 3.1 Hz), 122.49 (q, *J* = 4.4 Hz), 15.84. ^{19}F NMR (376 MHz, $CDCl_3$) δ -62.09. HRMS (+ p APCI) calculated for $C_{17}H_{13}NF_3$ [M+H] calculated for 288.09946, found 288.09879.

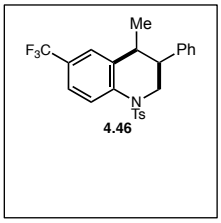

4.46

Adapted from a known procedure[21], 4-methyl-3-phenyl-1-tosyl-6-(trifluoromethyl)-1,2,3,4-tetrahydroquinoline, was isolated by column chromatography (Hex: EtOAc 95:5) as a oil in 71% yield. ^{1}H NMR (400 MHz, $CDCl_3$) δ 8.07 (d, *J* = 8.8 Hz, 1H), 7.67 – 7.56 (m, 2H), 7.47 (dd, *J* = 8.8, 2.3 Hz, 1H), 7.40 – 7.30 (m, 4H), 7.27 (d, *J* = 7.9 Hz, 3H), 7.12 – 6.88 (m, 2H), 4.44 (ddd, *J* = 12.7, 4.2, 1.2 Hz, 1H), 3.90 (dd, *J* = 12.7, 11.8 Hz, 1H), 3.09 (dt, *J* = 11.8, 4.4 Hz, 1H), 2.43 (s, 3H), 0.77 (d, *J* = 7.2 Hz, 3H). ^{13}C NMR (101 MHz, $CDCl_3$) δ 144.31, 139.42, 138.85, 135.79, 134.96, 129.89, 128.63, 127.47, 127.14, 125.99 (d, *J* = 3.9 Hz), 126.20 – 125.27 (m), 123.89 (d, *J* = 3.7 Hz), 122.64,

45.87, 41.20, 37.71, 21.59, 16.97. ^{19}F NMR (376 MHz, $CDCl_3$) δ -62.11. HRMS (+ p APCI) calculated for $C_{24}H_{23}O_2NF_3{}^{32}S$ [M+H] calculated for 446.13961, found 446.13884.

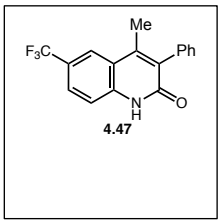

4.47

Adapted from a known procedure[22], 4-methyl-3-phenyl-6-(trifluoromethyl)quinolin-2(1*H*)-one, was isolated by column chromatography [EtoAc: Hexane (0-10% EtOAc)] as a white solid in 61% yield. ^{1}H NMR (400 MHz, $CDCl_3$) δ 8.91 (s, 1H), 8.40 (s, 1H), 8.25 (d, *J* = 8.8 Hz, 1H), 7.90 (dd, *J* = 8.8, 2.0 Hz, 1H), 7.57 – 7.50 (m, 2H), 7.50 – 7.44 (m, 1H), 7.43 – 7.36 (m, 2H), 2.70 (s, 3H). ^{13}C NMR (101 MHz, $CDCl_3$) δ 153.69, 148.10, 141.84, 138.01, 135.80, 131.30, 129.97, 128.79, 128.52, 128.13, 127.38, 124.74 (q, *J* = 3.1 Hz), 125.85 – 119.73 (m), 122.48 (q, *J* = 4.4 Hz), 29.85, 15.83. ^{19}F NMR (376 MHz, $CDCl_3$) δ -62.09. HRMS (+ p APCI) calculated for $C_{17}H_{13}ONF_3$ [M+H] calculated for 304.09438, found 304.09396.

References:

1. Lu, L.; Chen, C.; Jiang, H.; Yin, B. Three-Component Ring-Opening Reactions of Cyclic Ethers, α-Diazo Esters, and Weak Nucleophiles under Metal-Free Conditions. *J. Org. Chem*. **2018**, *83*, 14385-14395.

2. Zeng,X.; Tu,Y.; Zhang, Z.; You, C.; Wu, J.; Ye, Z.; Zhao, J. Transition-Metal-Free One-Step Synthesis of Ynamides. *J. Org. Chem*. **2019**, *84*, 4458−4466.

3. Kong,W.L.; Finger L.H.; Oliveira, J.C.A.; Ackermann, L. Angew. Chem. Int. Ed. 2019, 58, 6342-6346.

4. Liang, S.; Jensen, M. P. Half-Sandwich Scorpionates as Nitrene Transfer Catalysts. *Organometallics* 2012, 31, 23, 8055–8058.

5. Buckingham, F.; Calderwood, S.; Checa B., Keller, T.; Tredwell, M.; Collier, T. L.; Newington, I. M.; Bhall, R.; Glasser, M.; Gouverneur V. Oxidative fluorination of N-arylsulfonamides. *Journal of Fluorine Chemistry **2015**, 180*, 33–39.

6. Laha, J. K.; Jethava, K. P.; Dayal, N. Palladium-Catalyzed Intramolecular Oxidative Coupling Involving Double C(sp2)–H Bonds for the Synthesis of Annulated Biaryl Sultams. *J. Org. Chem.* 2014, 79, 17, 8010–8019.

7. Albanese, D.; Landini, D.; Lupi, V.; Penso, M. Straightforward Synthesis of 2-Substituted 3,4-Dihydro-2H-1,4-benzoxazines under Solid−Liquid Phase Transfer Catalysis Conditions. *Ind. Eng. Chem. Res.* **2003**, *42*, 680–686.

8.Hermann, J. M.; Unterherer, M.; Jügenliemk, G.; Heilmann, J.; Ko2nig, B. Synthesis of Phenyl-1-benzoxepinols Isolated from Butcher's Broom and Analogous Benzoxepines. *Eur. J. Org. Chem*. **2014**, 3170–3181.

9. Naidoo, J., Bemben, C. J.; Allwein, S. R.; Liang, J.; Pieper, A. A.; Ready, J. M. Development of a scalable synthesis of P7C3-A20, a potent neuroprotective agent. *Tett. Lett.* **2013**, *54*, 4429-4431.

10. Hosseinzadeh, R.; Tajbakhsh, M.; Mohadjerani, M.; Alikarma, M. Copper-catalysed *N*-arylation of arylsulfonamides with aryl bromides and aryl iodides using KF/Al_2O_3 . *J. Chem. Sci.* **2010**, *122*, 143–148.

11. Lakrout, S.; K'tir, H.; Amira, A.; Berredjem, M.; Aouf, N-E. A simple and eco-sustainable method for the sulfonylation of amines under microwave-assisted solvent-free conditions. *RSC Adv.* **2014**, *4*, 16027-16032.

12. Li, X.; Chen, F.; Lu, G-P. Fe-based metal-organic frameworks for the synthesis of N-arylsulfonamides via the reactions of sodium arylsulfinates or arylsulfonyl chlorides with nitroarenes in water. *Tett. Lett.* ***2018***, *59*, 4226-4230.

13. Park, K. K.; Lee, J. J.; Ryu, J. Photo-Fries rearrangement of N-arylsulfonamides to aminoaryl sulfone derivatives. *Tetrahedron* **2003**, *59*, 7651-7659.

14. Lee, D.; Chang, S. Direct C□H Amidation of Benzoic Acids to Introduce meta- and para-Amino Groups by Tandem Decarboxylation. *Chem. Eur. J.* **2015**, *21*, 5364–5368.

15. Yudasaka, M.; Shimbo, D.; Maruyama, T.; Tada, N.; Itoh, A. Synthesis, Characterization, and Reactivity of an Ethynyl Benziodoxolone (EBX)–Acetonitrile Complex. *Org. Lett.* **2019**, *21*, 4, 1098–1102.

16. Shi, G.; Gadhe, C. G.; Park, S-W.; Kim, K. S.; Kang, J.; Seema, H., Singh, J.; Cho J. Novel Ionophores with 2n-Crown-n Topology: Anion Sensing via Pure Aliphatic C–H···Anion Hydrogen Bonding. *Org. Lett.* **2014**, *16*, 2, 334–337.

17. Phetsang, W.; Chaturongakul, S.; Jiarpinitnun, C. Electron-withdrawing substituted benzenesulfonamides against the predominant community-associated methicillin-resistant *Staphylococcus aureus* strain USA300. *Monatshefte für Chemie* **2013**, *144*, 461–471.

18. Beringer, F. M.; Ugelow, I. The Aromatization and Rearrangement of Cyclic Ketones. IV. Substituted Acetanilides from Cyclohexenone Oximes. *J. Am. Chem. Soc.* **1953**, *75*, 2635–2639.

19. Sanchez-Cantalejo, F.; Priest, J. D.; Davies, P. W. A Gold Carbene Manifold to Prepare Fused γ-Lactams by Oxidative Cyclisation of Ynamides. *Chem. Eur. J.* **2018**, *24*, 17215–17219.

20.Xhu, C.; Kale, P.; Yue, H.; Rueping, M. Redox-Neutral Cross-Coupling Amination with Weak N-Nucleophiles: Arylation of Anilines, Sulfonamides, Sulfoximines, Carbamates, and Imines via Nickelaelectrocatalysis. *JACS Au* **2021**, *1*, 1057–1065.

21. Ghosh, N.; Nayak, S.; Sahoo, A. K. Gold(I)-Catalyzed 6-endo-Dig Hydrative Cyclization of an Alkyne-Tethered Ynamide: Access to 1,6-Dihydropyridin-2(3H)ones. *Chem. Eur. J.* **2013**, *19*, 9428–9433.

22. Yu, Y.; Humedi, R., Alleyn, J. R.; Doyle, M. P. Catalytic Allylic Oxidation of Cyclic Enamides and 3,4-Dihydro-2H-Pyrans by TBHP. *J. Org. Chem*. **2017**, *82*, 8506−8513.

Chapter 5: Developing a Scalable and Chromatography-Free Route Towards a Safe 1,2-Carboamidation Substrate for Peptide Macrocyclization

5.1 Introduction to 1,2-Carboamidation Methodology and Transfer Substrate Development

In this chapter, we will discuss the progress towards a scalable and chromatography-free route to the amidation of tyrosine. Previous attempts utilized an unstable and temperamental compound known as MSH. Though a new route to the tyrosine carboamidation reaction was established, the route suffered from low yields and the need for column chromatography at every step. Optimization of this route for scalability and ease of access were undertaken to provide material for further investigations. This work was conducted in collaboration with Dr. Chris Poff and Sophia Xu, a former undergraduate in the Blakey lab.

5.1.1 Brief History of the Blakey Lab's Cobalt Catalyzed 1,2-Carboamidation of Acrylamides

Dr. Chris Poff began his work on developing a new methodology for the 1,2-carboamidation of acrylamides with the desire to develop a cobalt catalyst with our 2-Me, 3-phenyl indenyl platform. This would allow access to enantioselective macrocyclization strategies as the methodology unfolded. Despite his best attempts, this catalyst platform remained out of reach and continues too today. Dr. Poff then turned his attention to the 1,2-carboamidation literature where Glorius had disclosed a cobalt system with acrylates[1] and Liu a rhodium system with acrylamides.[2]

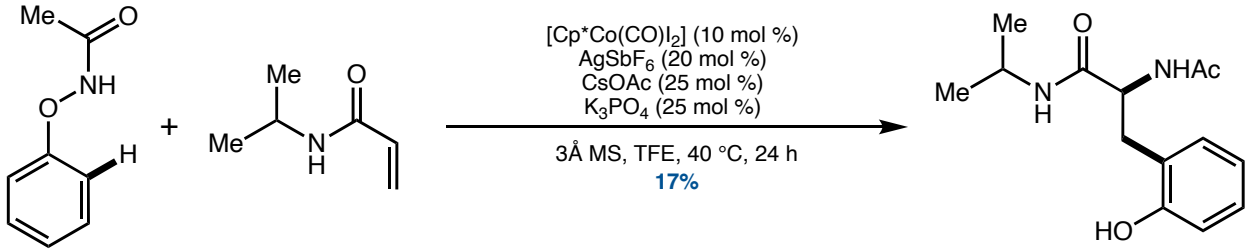

5.1 **5.2** **5.3**

Scheme 1. Dr. Poff's initial model system for cobalt-catalyzed 1,2-carboamidation of acrylamides.

Drawing from these reports, Dr. Poff was able to develop an initial model system that allowed for cobalt catalysis and broad acrylamide 1,2-carboamidation (**Scheme 1**). Dr. Poff was able to show that phenoxyactamide (**5.1**) and isopropyl acrylamide (**5.2**) were able to generate the desired product (**5.3**) with low yields under the previously disclosed Glorius conditions.[1] Despite this promising result, the target of the Blakey Lab had always been macrocyclic peptides via this strategy. Therefore Dr. Poff developed a new model system utilizing tyrosine as the carboamidation reagent. Following a brief optimization, Dr. Poff was able to determine optimal

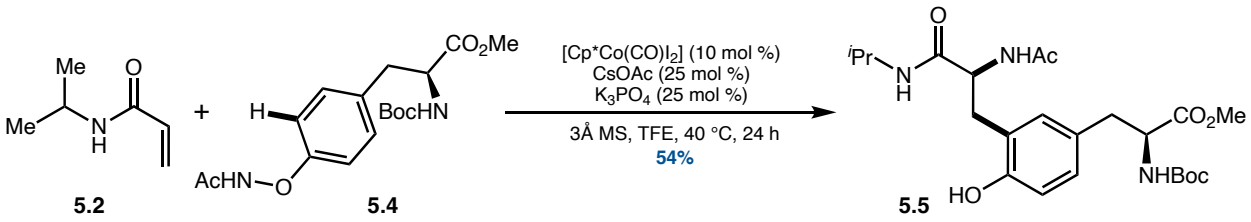

Scheme 2. Dr. Poff's optimized conditions for cobalt-catalyzed 1,2-carboamidation of the peptide model system.

conditions for the transformation on the peptide model system. Notably, this was removal of the $AgSbF_6$ that increased reactivity substantially and provided the *meta*-functionality of the protected tyrosine (**Scheme 2**). Further studies showed that this method could function intermolecularly between two amino acids in comparable yields as well. With the methodology showing promise, and an undergraduate, Sophia Xu, prepared linear peptide precursors for macrocyclization studies. The need arose for large quantities of the tyrosine carboamidation reagent to be produced in compliance with the needs of the Solid Phase Peptide Synthesis (SPPS) system.

5.1.2 Preparation of the Tyrosine 1,2-Carboamidation Substrate

The development of the tyrosine 1,2-carboamidation reagent began following known procedures utilized for phenoxyacetamides substrates seen in the literature.[1-2] This route utilizes the Chan-Evans-Lam reaction with phenylboronic acid and *N*-hydroxyphthalimide to introduce the key N–O bond required as the internal oxidant. Deprotection of the phthalimide with hydrazine monohydrate and acylation then provide the desired product in moderate to good yields.[3-4] Despite their efficacy on phenolic substrates, the Chan-Evans-Lam coupling failed to deliver the tyrosine product (**5.4**) in all attempts from protected amino acid derivatives. To rectify this supply issue, Dr. Poff turned to the literature and discovered a known process for the formation of the Boc-Tyr(ONAc)-OMe (**5.4**) from the protected amino acid directly (**Scheme 3**).[4-5] This process utilized

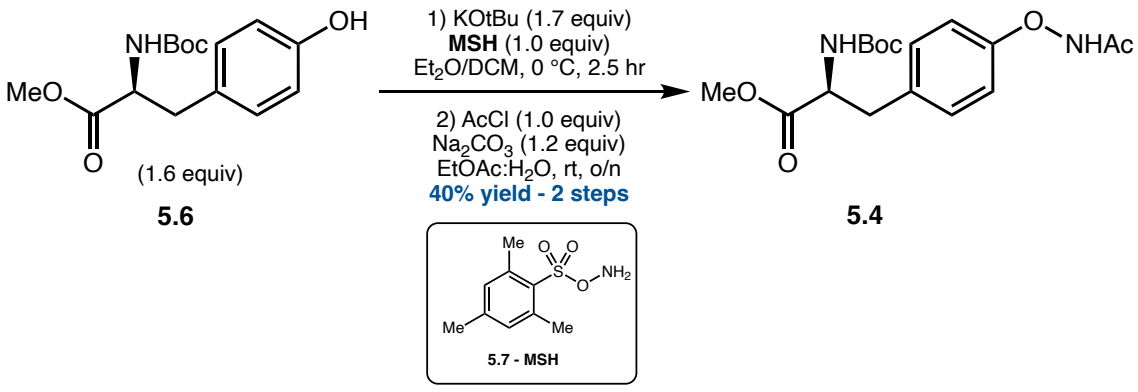

Scheme 3. Known route for access to Boc-Tyr(ONAc)-OMe.

a very reactive aminating reagent known as MSH (**5.7**). During this time both Dr. Poff and myself were making and utilizing MSH (**5.7**) for the amination of alcohols for $C_{(sp^2)}$–H and $C_{(sp^3)}$–H functionalization methodologies. While MSH (**5.7**) was an identified explosive/deflagration substance,[6] proper protocols in the storage and handling of the substance had been taken in accordance with the literature. These included the use of proper PPE, blast shields, cold storage,

crystal size management, separate storage, and plastic containers. Despite these safety measures in place, a multi-gram amount of the (**5.7**) violently deflagrated in the chemical fridge. The cause of the incident was later determined to be most likely attributed to larger than desired crystal sizes due to an increase in the scale of the reaction/triggeration steps previously utilized. Following this, the lab decided that the compound was not something we should continue working with or allow our undergrad Sophia Xu to handle. Consequently, Dr. Poff undertook a new synthetic route to access the desired substrate (**5.4**).

Drawing from the synthesis of phenoxyacetamides, Dr. Poff was able to convert Boc-Tyr-OMe into the boryl species through palladium catalysis in the hopes of leveraging the Chan-Evans-Lam (**Scheme 4**.**A**). Dr. Poff was in fact able to convert Boc-Tyr-OMe (**5.6**) into the triflate and use palladium catalysis to borylate the substrate in 2 steps with an 84% yield following column chromatography. Attempts to utilize the copper-catalyzed Chan-Evans-Lam with the Boc-Phe(4-

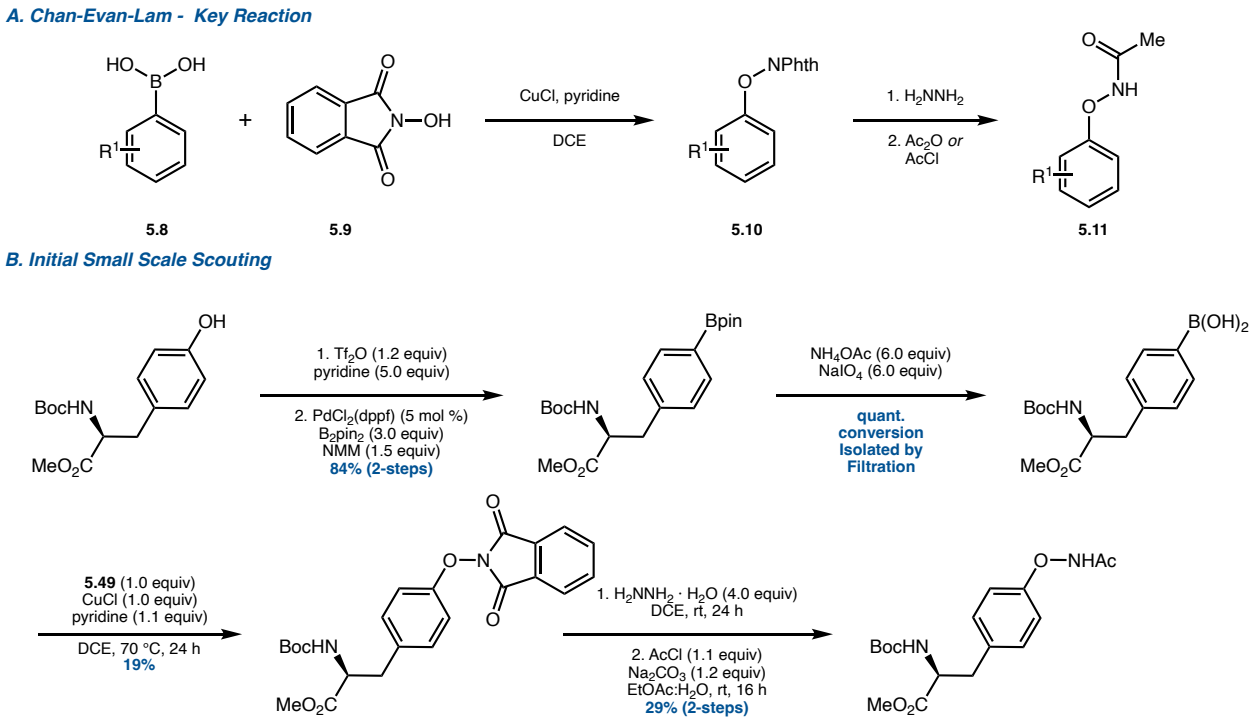

Scheme 4. New route for safer access to Boc-Tyr(ONAc)-OMe without aminating reagents.

Bpin)-OMe (**5.12**) offered no reactivity and thus the conversion to the Boc-Phe[4-B(OH)$_2$]-OMe (**5.13**) was deemed necessary. While various attempts were made to convert the pinacol ester to the acid, the oxidative method was deemed the most efficacious due to the acid-labile Boc protecting group. Additionally, the quantitative yield and ease of purification via filtration was deemed superior to the need for a more atom economic process. The subsequent Chan-Evans-Lam supplied **5.14** in a disapprovingly low yield following chromatography and the deprotection/acylation provided the desired Boc-Tyr(ONAc)-OMe (**5.4**) in a yield complementary to the literature. Due to the demand of the substrate and the departure from lab of Dr. Poff, we began a campaign to increase the yields of this linear synthesis and optimize the route for chromatography free purification where possible.

Sophia Xu began optimization of the Chan-Evan-Lam reaction, and I undertook the supply of the Boc-Phe[B(OH)$_2$]-OMe (**5.13**) precursor. Beginning with the triflation, the impurity following the concentration of this step was pyridine **(Scheme 5)**. The addition of three washes of saturated aqueous copper (II) sulfate and an additional dH$_2$O was able to provide the product free

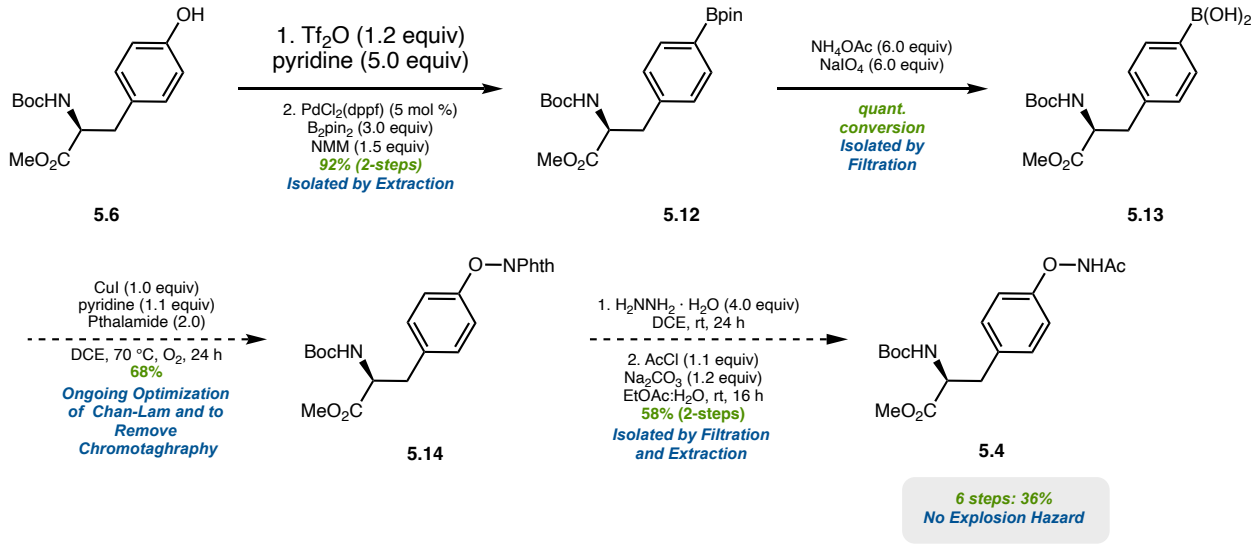

Scheme 5. Decagram scale route for safer access to Boc-Tyr(ONAc)-OMe without aminating reagents.

of pyridine and immediately usable in the palladium borylation with minimal losses. While attempts to borylate with $B_2(OH)_4$ directly were unsuccessful, the observed reactivity of by Dr. Poff with B_2Pin_2 was able to be purified via filtration through celite, extraction and concentration at elevated temperatures under reduced pressure allowing for a two-step yield of 92% with no chromatography. The conversion of the pinacol ester (**5.12**) to the boronic acid (**5.13**) was carried out via ammonium acetate and sodium periodate in super stochiometric amounts (6.0 equivalents each) to provide quantitative conversion. In one instance, the conversion was incomplete following workup and subjugation of the material to these conditions a second time provided the desired conversion. With ~8 grams of material supplied; Sophia Xu undertook a large screening campaign for the optimization of the Chan-Evans-Lam coupling under my mentorship.

The optimization of the Chan-Evans-Lam coupling looked at various copper sources, bases, oxidants, equivalents, and temperatures (**Scheme 6**). Through her investigations, she found that pyridine and pure oxygen at 70 ºC were the best combination for conversion (**Scheme 6, Entry 2**) with a yield of 28%. This was increased to 55% conversion when the copper catalyst was changed to CuI, a previously rare choice for Chan-Evans-Lam couplings (**Scheme 6, Entry 11**). Further modifications of the *N*-hydroxypthamide equivalents to double the initial amount led to the highest yield of 64% (**Scheme 6, Entry 13**). This reaction was also extremely clean and easily purified by column chromatography following workup. Through careful study of crude NMRs and isolation of the byproduct, we were able to determine the impurity by comparison to literature compounds and identified it as Boc-Phe(4-I)-OMe at about 8%. A subsequent gram scale reaction of this optimized methodology provided the desired Boc-Tyr(ONPhth)-OMe (**5.14**) in 68% yield with chromatography required to remove the iodinated phenylalanine. The product (**5.14**) was then carried through the final two steps and isolated by chromatography as the desired Boc-Tyr(ONAc)-

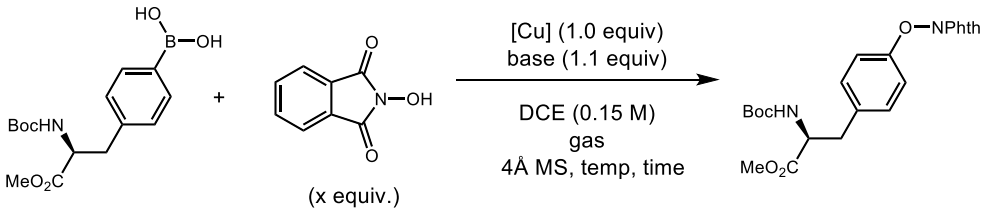

Entry	[Cu]	x	Gas	Base	Temp (°C)	Time (hr)	Yield □%□
1	CuCl	1.0	air	pyridine	70	24	17
2	CuCl	1.0	O_2	pyridine	70	24	28
3	CuCl	1.0	O_2	lutidine	70	24	22
4	CuCl	1.0	O_2	DMAP	70	24	27
5	CuCl	1.0	O_2	Et_3N	70	24	10
6	CuCl	1.0	O_2	DIPEA	70	24	14
7	CuCl	1.0	O_2	pyridine (1.0 equiv) + DMAP (20 mol%)	70	24	25
8	$Cu(OAc)_2$	1.0	O_2	pyridine	70	24	17
9	CuBr	1.0	O_2	pyridine	70	24	35
10	CuBr·SMe_2	1.0	O_2	pyridine	70	24	29
11	CuI	1.0	O_2	pyridine	70	24	55
12	CuI	1.5	O_2	pyridine	70	24	43
13	CuI	2.0	O_2	pyridine	70	24	64
14	CuI	2.5	O_2	pyridine	70	24	48
15	CuI	3.0	O_2	pyridine	70	24	52
16	CuI	2.0	O_2	pyridine	80	24	43
17	CuI	2.0	O_2	pyridine	60	24	47
18	CuI	2.0	O_2	pyridine	40	24	3
19	CuI	2.0	O_2	pyridine	70	48	58

Scheme 6. Optimization of the Chan-Evans-Lam by Sophia Xu.

OMe (**5.4**) in 58% yield. This new linear sequence can provide the Boc-Tyr(ONAc)-OMe (**5.4**) in 6 linear steps with a 36% overall yield and no use of explosive precursors.

5.1.3 Remaining Challenges for the Tyrosine 1,2-Carboamidation Substrate

While the current system functions as desired the last three steps have yet to optimized on the decagram scale. The remaining challenges are the purification of the **5.14** reaction mixture, as it still requires column chromatography for the removal of the iodinated byproduct and testing the hydrazine deprotection and acylation on a larger scale. Additionally, this reaction uses elevated temperature and pure oxygen which is less than ideal for scalability due to risk of fire in the flammable dichloroethane solvent that cannot be discounted. For this reason, I was able to develop a SOP with Emory's EHSO department for the safe use of pure oxygen atmospheres at elevated temperatures in flammable solvents for this methodology. The conversion to a 95/5 mix of nitrogen/oxygen that is currently seen in industrial scale reactions is an improvement that would help immensely with the safety of this methodology. In addition to fire risk, the use of high temperatures, metal catalyst and oxygen present the possibility for the formation of vinyl chloride via dehydrochlorination of 1,2-DCE.[9] This is further converted into the oxirane by cytochrome P450 and is a known mutagen or if burned can form dioxins in the environment.[10] Furthermore,

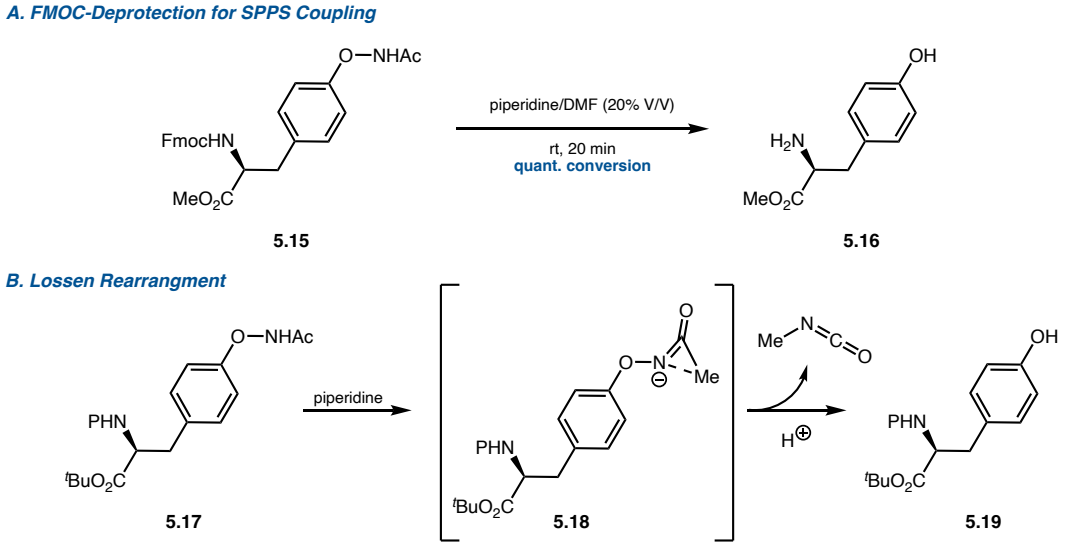

Scheme 7. Rearrangement of FMoc substrate upon treatment with deprotection conditions.

the design of an FMoc-Tyr(ONAc)-OMe (**5.15**) was undertaken to allow the use of this non-canonical amino acid on the SPPS, however, the SPPS deprotection conditions afforded exclusively the deprotected Tyr-OMe (**5.16**) as the major product (**Scheme 7.A**). Through sure persaverance in scouring the literature, Sophia Xu was able to find precedent for this rearrangment and determined we were seeing a Lossen type rearrangment to cleave the N–O bond (**Scheme 7.B**). Interstingly, the $C_{(sp^3)}$–H methodology of these reagents had been facing this problem for

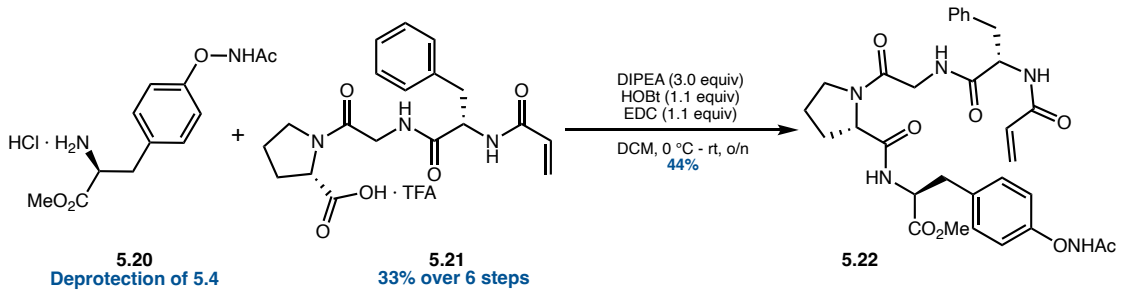

Scheme 8. Amide coupling of Tyr(ONAc)-OMe to linear peptide for macrocylization studies.

several weeks and upon discovery of this mechanism was able to be diagnosed as the major problem plaguing that methodology as return of the alcohol was being seen during acylation. In response to this limitation, Sophia Xu was able to procure the HCL salt of **5.4** (**5.20**) and succesfully couple the amine to the linear peptide developed on resin in the SPPS (**Scheme 8**). This allowed for initial testing of the cobalt catalyzed intermolecular macrocyclization conditions developed by Dr. Poff on an intramolecular system. While the macrocycle has yet to be formed, this is a project that is ongoing in the Blakey lab.

5.2 Concluding Remarks

Over the course of this project, Dr. Poff was able to develop a 1,2-carboamidation strategy for acrylamides with the aim of transitioning it to macrocyclization of linear peptides. Successful

studies in both intermolecular 1,2-carboamidation for acrylamides and peptide like moieties showcase the need for a safe and reliable route for Tyr(ONAc) on scale. While the previous route utilized an explosive aminating reagent, MSH, Dr. Poff was able to demonstrate an alternate route utilizing a Chan-Evans-Lam reaction. Following the elucidation of this low yielding route, Sophia Xu and I were able to optimize the route for scalability and chromatography free purification where possible, to provide 36% over 6 steps. This directly led to an increase of nearly 10-fold in yield over the initial route (3.9% over 6 steps) and was analogous to the 41% yield provided by the MSH over 2 steps. Presently, this project is ongoing in several directions to include the investigation of macrocyclization, acrylamide functionalization, and adaption of the reagent to SPPS friendly coupling conditions.

5.4 References

1. Lerchen, A.; Knecht, T.; Daniliuc, C. G.; Glorius, F. Unnatural Amino Acid Synthesis Enabled by the Regioselective Cobalt(III)-Catalyzed Intermolecular Carboamination of Alkenes. *Angew. Chem. Int. Ed.* **2016**, *55*, 15166–15170.

2. Hu, Z.; Tong, X.; Liu, G. Rhodium(III) Catalyzed Carboamination of Alkenes Triggered by C−H Activation of N-Phenoxyacetamides under Redox-Neutral Conditions. *Org. Lett.* **2016**, *18*, 1702–1705.

3. Liu, G.; Shen, Y.; Zhou, Z.; Lu, X. Rhodium(III)-Catalyzed Redox-Neutral Coupling of N-Phenoxyacetamides and Alkynes with Tunable Selectivity. *Angew. Chem. Int. Ed.* **2013**, *52*, 6033–6037.

4. Petrassi, H. M.; Sharpless, K. B.; Kelly, J. W. The Copper-Mediated Cross-Coupling of Phenylboronic Acids and N-Hydroxyphthalimide at Room Temperature: Synthesis of Aryloxyamines. *Org. Lett.* **2001**, *3*, 139–141

5. Li, B.; Lan, J.; Wu, D.; You, J. Rhodium(III)-Catalyzed Ortho -Heteroarylation of Phenols through Internal Oxidative C–H Activation: Rapid Screening of Single-Molecular White-Light-Emitting Materials . *Angew. Chem. Int. Ed.* **2015**, *54*, 14008–14012.

6. Yan, D.; Wang, G.; Xiong, F.; Sun, W. Y.; Shi, Z.; Lu, Y.; Li, S.; Zhao, J. A Selenium-Catalysed Para-Amination of Phenols. *Nat. Commun.* **2018**, *9*, 1–9.

7. Bernardes, G. J. L.; Chalker, J. M.; Errey, J. C.; Davis, B. G. Facile Conversion of Cysteine and Alkyl Cysteines to Dehydroalanine on Protein Surfaces: Versatile and Switchable Access to Functionalized Proteins. *J. Am. Chem. Soc.* **2008**, *130*, 5052–5053.

8. Jašíková, L.; Hanikýřová, E.; Škríba, A.; Jašík, J.; Roithová, J. Metal-Assisted Lossen Rearrangement. *J. Org. Chem.* **2012**, *77*, 2829–2836.

9.Lee, S.; Yoon, W.; Ji, J.; Ahn, H. Complete oxidation of 1,2-dichloroethane over highly efficient Cu/Al-Ti composite metal oxide catalyst. Journal of Environmental Chemical Engineering 2022, 10, 108325-108332.

10. CAS. “The Science behind Dioxins, Vinyl Chloride, and Proven Remediations.” *CAS*, **2023**. www.cas.org/resources/cas-insights/safety/science-behind-dioxins-vinyl-chloride-and-provenremediations#:~:text=Dioxins%20are%20environmental%20contaminants%20consisting,byproduct%20of%20burning%20vinyl%20chloride.

5.5 Experimental Section

5.5.1 General Information

All reactions were carried out under nitrogen atmosphere with anhydrous solvents in oven- or flame-dried glassware using standard Schlenk technique, unless otherwise stated. Anhydrous dichloromethane (DCM), diethyl ether (Et2O), tetrahydrofuran (THF), and toluene were obtained by passage through activated alumina using a Glass Contours solvent purification system. 2,2,2-trifluoroethanol was distilled over calcium hydride (CaH_2) and stored over activated molecular sieves. Solvents for workup, extraction, and column chromatography were used as received from commercial suppliers without further purification. Unless otherwise reported, compounds **5.4,**[1] and $[Cp^*Co(CO)I_2]$[2] were synthesized according to previously reported procedures. All other chemicals were purchased from Millipore Sigma, Strem Chemicals, Oakwood Chemicals, Alfa Aesar, or Combi-Blocks and used as received without further purification, unless otherwise stated.

^{1}H and 13C nuclear magnetic resonance (NMR) spectra were recorded on a Varian Inova 600 spectrometer (600 MHz 1 H, 151 MHz 13C), a Bruker 600 spectrometer (600 MHz 1 H, 151 MHz 13C), a Varian Inova 500 spectrometer (500 MHz 1 H, 126 MHz 13C), and a Bruker 400 spectrometer (400 MHz 1 H, 126 MHz 13C) at room temperature in CDCl3 (dried over activated molecular sieves) with internal CHCl3 as the reference (7.26 ppm for 1 H, 77.16 ppm for 13C), unless otherwise stated. Chemical shifts (δ values) were reported in parts per million (ppm) and coupling constants (J values) in Hz. Multiplicity was indicated using the following abbreviations: s = singlet, d = doublet, t = triplet, q = quartet, qn = quintet, m = multiplet, br = broad. High resolution mass spectra (HRMS) were obtained using a Thermo Electron Corporation Finigan LTQFTMS (at the Mass Spectrometry Facility, Emory University). High Pressure Liquid Chromatography (HPLC) was performed on an Agilent 1100 series HPLC utilizing CHIRALPAK

AD-H, AS-H, OD-H and OJ-H 4.6 x 150 mm analytical columns. Analytical thin layer chromatography (TLC) was performed on precoated glass-backed Silicycle SiliaPure® 0.25 mm silica gel 60 plates and visualized with UV light, ethanolic p-anisaldehyde, ethanolic bromocresol green, or aqueous potassium permanganate (KMnO4). Flash column chromatography was performed using Silicycle SiliaFlash® F60 silica gel (40- 63 μm) on a Biotage Isolera One system. Preparatory TLC was performed on precoated glass backed Silicycle SiliaPure® 1.0 mm silica gel 60 plates. We acknowledge the use of shared instrumentation provided by grants from the NIH and the NSF.

5.5.2 Procedures

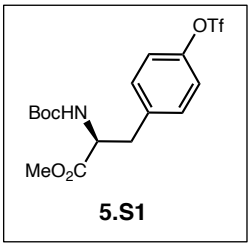

5.S1

Methyl (*S*)-2-((tert-butoxycarbonyl)amino)-3-(4-(((trifluoromethyl_sulfonyl_oxe)phenyl)proponate (5.S1) – To a flame-dried 250 mL RBF equipped with a stir bar was added Boc-Tyr-OMe (10.0 g, 33.9 mmol, 1.0 equiv) before sealing with a rubber septum and exchanging the atmosphere with nitrogen. The Boc-Tyr-OMe was dissolved in DCM (60.0 mL, 0.35 M total concentration) and pyridine (13.4 g, 169.5 mmol, 5.0 equiv) was added before the reaction was cooled to 0 °C in a ice/water bath. Tf_2O (9.56 g, 40.7 mmol, 1.2 equiv) was added to the reaction flask and allowed to stir at 0 °C under a balloon of nitrogen. After 1 hour, the reaction was diluted with DCM (150.0 mL) and washed with DI H_2O (1500.0 mL), 1N NaOH (150.0 mL), saturated Cu_2SO_4 (3 x 150.0 mL), DI H_2O (1500.0 mL), and brine (150.0 mL). The organic layer was dried over Na_2SO_4, filtered to remove the drying agent, and concentrated *in vacuo* to afford **5.S1** (14.0 g, 97% yield) as a clear oil. **^{1}H NMR** (500 MHz, $CDCl_3$) δ 7.25 – 7.16 (m, 4H), 5.02 (d, *J* = 8.2

Hz, 1H), 4.60 (q, *J* = 6.8 Hz, 1H), 3.71 (s, 3H), 3.17 (dd, *J* = 13.9, 5.8 Hz, 1H), 3.04 (dd, *J* = 13.9, 6.6 Hz, 1H), 1.41 (s, 12H).[3]

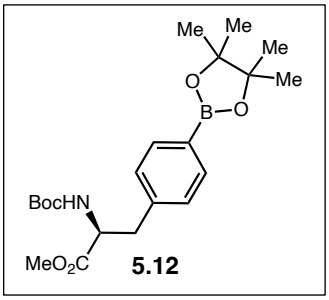

5.12

Methyl (*S*)-2-((tert-cutoxycarbonyl)amino)-3-(4-(4,4,5,5-tetramethyl-1,3,2-dioxaborolan-2-yl)phenyl)propanoate (5.12) – To a 500 mL RBF equipped with a stir bar was added **5.S1** (14.0 g, 32.0 mmol, 1.0 equiv) and $PdCl_2$(dppf) (1.17 g, 1.6 mmol, 5 mol %) before sealing with a rubber septum and exchanging the atmosphere with nitrogen. The solids were then dissolved in 1,4-dioxane (100.0 mL, 0.32 M total concentration), and *N*-methylmorpholine (4.8551 g, 48.0 mmol, 1.5 equiv) and pinacol borane (24.4 g, 96.0 mmol, 3.0 equiv) were added. The reaction was placed into a pre-heated 70 °C heating block and allowed to stir under a balloon of nitrogen. After 16 hours, the reaction was cooled to room temperature, filtered over a pad of celite. The organic layer was dried over Na_2SO_4, filtered to remove the drying agent, and concentrated *in vacuo* at 50 C to afford **5.12** (12.3 g, 95% yield) as a pale-yellow oil. **^{1}H NMR** (500 MHz, $CDCl_3$) δ 7.73 (d, *J* = 7.9 Hz, 2H), 7.12 (d, *J* = 7.6 Hz, 2H), 4.94 (d, *J* = 8.5 Hz, 1H), 4.58 (d, *J* = 7.3 Hz, 1H), 3.70 (s, 3H), 3.10 (qd, *J* = 13.8, 5.9 Hz, 2H), 1.42 (s, 10H), 1.34 (s, 12H).[3]

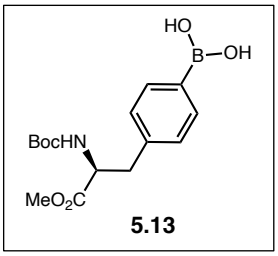

5.13

(*S*)-(4-(2-((tert-butoxycarbonyl)amino)-3-methoxy-3-oxopropyl)phenyl)boronic acid (5.12) – To a 1000 mL flame-dried RBF equipped with a stir bar was added NH_4OAc (14.1 g, 182.4 mmol, 6.0 equiv) and $NaIO_4$ (39.0 g, 182.4 mmol, 6.0 equiv) before sealing with a rubber septum and exchanging the atmosphere with nitrogen. **5.12** (12.3 g, 30.4 mmol. 1.0 equiv)

was dissolved in acetone (50 mL) and added to the reaction flask followed by additional acetone (200.0 mL) and DI H_2O (120.0 mL). The reaction stirred at room temperature under a balloon of nitrogen for 48 hours before being diluted with Et_2O (250.0 mL) and filtered through a pad of celite. The solvent was removed *in vacuo* to afford **5.13** (9.8 g, >99% yield) as a white solid. **^{1}H NMR** (500 MHz, $CDCl_3$) δ 7.99 (d, *J* = 7.3 Hz, 2H), 7.18 (t, *J* = 7.9 Hz, 2H), 5.01 (d, *J* = 8.3 Hz, 1H), 4.69 – 4.54 (m, 2H), 3.72 (s, 3H), 3.29 – 2.90 (m, 2H), 1.42 (s, 9H).[3]

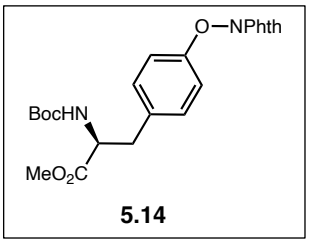

5.14

Methyl (*S*)-2-((tert-butoxycarbonyl)amino)-3-(4-((1,3-dioxoisointolin-2-yl)oxy)phenyl)propanoate (5.14) – To a flame-dried 100 mL RBF equipped with a stir bar, added **5.13** (1.0 g, 3.1 mmol, 1.0 equiv), activated 4Å molecular sieves (751 mg, 250 mg/mmol), *N*-hydroxyphthalimide (1.0 g, 6.2 mmol, 2.0 equiv), and CuI (0.59 g, 3.1 mmol, 1.0 equiv). The mixture was dissolved in 1,2-DCE (20.0 mL) and pyridine (0.270 g, 3.4 mmol, 1.1 equiv). The reaction was sparged with O_2 for 15 minutes prior to heating. The reaction was heated to 70 °C and allowed to stir under a balloon of O2. After 24 hours, the reaction was cooled to room temperature concentrated onto celite. The mixture was concentrated *in vacuo* and purified by flash chromatography on silica (30% EtOAc in hexanes) to afford **5.14** (0.93 g, 68% yield) as an white foam. **^{1}H NMR** (600 MHz, $CDCl_3$) δ 7.91 (dd, *J* = 5.4, 3.1 Hz, 2H), 7.83 – 7.78 (m, 2H), 7.15 – 7.07 (m, 4H), 4.95 (d, *J* = 8.3 Hz, 1H), 4.55 (q, *J* = 6.6 Hz, 1H), 3.70 (s, 3H), 3.09 (dd, *J* = 14.0, 5.8 Hz, 1H), 3.02 (dd, *J* = 14.0, 6.1 Hz, 1H), 1.41 (s, 9H). **^{13}C NMR** (151 MHz, $CDCl_3$) δ 172.27, 163.06, 158.15, 155.19, 135.05, 132.60, 130.74, 128.93, 124.13, 114.87, 80.17, 54.47, 52.42, 37.59, 28.42. **HRMS** (-APCI) calculated for $C_{23}H_{23}O_7N_2$ $[M-H]^-$ 439.1511, found 439.1514.

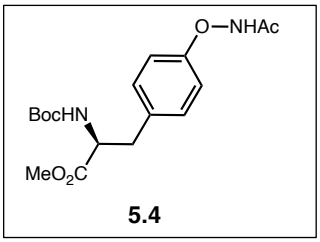

5.4

Methyl (*S*)-3-(4-(acetamidooxy)phenyl)-2-((tert-butoxycarbonyl)amino)propanoate (5.4) – To a 50 mL oven-dried RBF equipped with a stir bar under a nitrogen atmosphere was added a solution of **5.14** (0.93 g, 2.11 mmol, 1.0 equiv) in DCM (20.0 mL, 0.1 M). Hydrazine hydrate (0.423 g, 8.44 mmol, 4.0 equiv) was added and the reaction stirred at room temperature under a balloon of nitrogen. After 24 hours, $MgSO_4$ was added and the reaction continued to stir at room temperature. The reaction was filtered over celite and the solid washed with DCM (50.0 mL) and EtOAc (50.0 mL) before solvent removal *in vacuo*. To a 100 mL oven-dried reaction vial equipped with a stir bar, added Na_2CO_3 (0.0276 g, 2.53 mmol, 1.2 equiv) before sealing and exchanging the atmosphere with nitrogen. The crude material from the first step was dissolved in EtOAc (7 mL) and the solution added to the reaction flask followed by DI H_2O (3 mL). Acetyl chloride (0.182 g, 2.32 mmol, 1.1 equiv) was added and the reaction allowed to stir at room temperature under a balloon of nitrogen. After 16 hours, the reaction was quenched with saturated $NaHCO_3$ (50 mL). The aqueous layer was extracted with EtOAc (3 x 50 mL) and the combined organic layers dried over $MgSO_4$, filtered, and concentrated *in vauco*. Purification by flash chromatography on silica afforded **5.4** (431 mg, 58% yield) as a white solid. **^{1}H NMR** (400 MHz, $CDCl_3$) δ 7.20 – 6.91 (m, 4H), 4.96 (s, 1H), 4.54 (d, *J* = 7.4 Hz, 1H), 3.71 (s, 3H), 3.06 – 2.97 (m, 2H), 2.08 (s, 3H), 1.41 (s, 9H).[1]

5.5.3 Supplementary References

1. a) Li, B.; Lan, J.; Wu, D.; You, J. Rhodium(III)-Catalyzed ortho- Heteroarylation of Phenols through Internal Oxidative C–H Activation: Rapid Screening of Single-Molecular White-Light-Emitting Materials. *Angew. Chem. Int. Ed.* **2015**, *54*, 14008-14012. b) Yan, D.; Want, G.; Xiong, F.; Sun, W. Y.; Shi, Z.; Lu, Y.; Li, S.; Zhao, J. A Selenium-Catalysed Para-Amination of Phenols. *Nat. Commun.* **2018**, *9*, 1-9.

2. Sun, B.; Yoshino, T.; Matsunaga, S.; Kanai, M. A Cp*CoI_2-dimer as a precursor for cationic Co(III)-catalysis: Application to C–H phosphoramidation of indoles. *Chem. Commun.* **2015**, *51*, 4659-4661.

3. Feng, Z.; Min, Q,-Q.; Xiao, Y.-L.; Zhang, B.; Zhang, X. Pallatium-Catalyzed Difluoroalkylaiton of Aryl Boronic Acids: A New Method for the Synthesis of Aryldifluoromethylated Phosphonates and Carboxylic Acid Derivatives. *Angew. Chem. Int. Ed.* **2014**, *53*, 1669-1673.

Part 3: Implementation of Green Chemistry Lab Principles

Chapter 6: Advancing the Green Lab's Directive at Emory University in the Blakey Lab

6.1 Introduction to Green Lab Initiatives in the Blakey Lab

In this chapter we will discuss the driving force behind the implementation of Green Lab principles in the Blakey Lab. While this move to greener processes was born out of an institutional grant program, the Blakey Lab has made many changes over the years to implement energy, water, and waste conservation measures. While relatively small changes on the scale of Emory University and chemistry, we continue to strive to limit our environmental and carbon footprints while serving as an example and resource to help others do the same.

6.1.1 Brief History of Blakey Lab Green Lab Initiatives

Development of greener chemical transformations and better lab sustainability has been an ongoing challenge laid out to scientists throughout the field for more than 30 years.[1-3] Where previously the chemical processes have been based solely on cost, safety, and accessibility, the collective census of scientists have agreed that sustainability should be included in this list with equal importance. While these seem mutually exclusive, many publications have shown great advancements in the methodology by developing a greener method.[1] So much research has begun to fill this area, that the major publishers have all added a suite of journals focused on green chemistry, processes, and equipment to their stables. My Green Lab, a nonprofit devoted to sustainable laboratory work and education, began its mission in 2013 to help spread awareness and serve as a resource for laboratories worldwide.[4] Emory University's own Office of Sustainability Initiatives (OSI) also opened a Green Lab program in 2016 with a mission akin to that of My Green Lab. The Blakey Lab has been a diligent participant of the OSI Green Labs program since 2016 and maintained bronze and increased to gold status as the years have progressed. Initially led by Dr. Jacob Burman and Dr. Taylor Farmer Nelson, the green initiatives and lab compliance has

been driven by Dr. Chris Poff, Eleda Plouch, Keili Diaz, and me. Over the years we have made many changes to the lab to foster greener equipment, processes, and methodologies. Initially in 2017 the lab began running equipment on surge protectors to prevent vampire loads when off and built a trolley pump to eliminate the need for water aspirators in the hoods. These additions allowed us to drastically cut down on water usage during filtrations and low-pressure vacuum manipulations. The following year we received a grant to convert our oil bath heating mantles to aluminum block mantles. These were more efficacious especially in running large numbers of reactions at once. While these purchases were funded by Green Incentives grants, the lab was also making strides of its own to modernize equipment, waste streams, and inventory management. The conversion of several old chemical fridges into one larger, more energy efficient refrigerator was undertaken by the lab. Additionally, the freezer was defrosted yearly and had the coils cleaned to maximize energy efficiency. Waste streams were subdivided to better regulate the inclusion of P-waste and reactive chemicals in separate smaller reservoirs to eliminate the need for incineration of large volumes of traditional waste. Furthermore, Dr. Chris Poff and I completely reengineered the inventory management system with the help of a French company, Find Molecule, to better track and locate chemicals within the lab. As a testament to this change, the previously weeklong inventory process (>4000 unique bottles) has been slimmed down to less than one day and has an error rate of less than 3% as determined by missing and misplaced chemicals. This has also greatly reduced the overordering and expiring of chemicals in the lab. While the benefit of this implemented system took nearly three years to fully realize, it has made a lasting impact by decreasing shipping waste and chemical waste. While these measures were very beneficial, the lab knew we could continue to improve in our processes and even track usage data associated with the changes.

6.1.2 Identification and Implementation of Water, Acetone, and Glass Sustainability

In 2020, the Dr. Taylor Farmer-Nelson and myself identified our current largest source of waste to be from glassware cleaning and coauthored a grant to address this. The process of cleaning glassware for research requires multiple rinses of tap water, soap, DI water and acetone. The use of environmentally toxic acids and bases are sometimes required for hard to clean glassware (i.e., large flasks with small openings). Our goal was to reduce the overall usage of water, acetone and harsh chemicals during the cleaning and drying of our glassware.

Prior to our initiative, glassware, including test tubes, was handwashed following a general SOP that includes several acetone washes, soap washes, scrubs and rinses, followed by an additional acetone rinse for adequate drying without water scaling. This current method, common throughout almost every chemistry lab, requires about 20 gallons of water to handwash 30 pieces of glassware.[5] In our lab, a typical student cleans between 60 to 70 pieces of glassware per week (excluding test tubes) which equates to ~40 gal/lab member. When considering the average number of lab members, 12, that quickly equated to 480 gal/week and almost 25,000 gal/yr of water used exclusively for cleaning glassware by hand.

Additionally, acetone is used during the rinsing and drying process which generates waste that must be disposed of by EHSO through a third-party vendor. The subsequent waste is treated as hazardous material and requires transportation and careful disposal using incineration that wastes unnecessary energy. The typical lab member utilizes ~2.5 L of acetone to clean and dry glassware per week which equates to 30 L/wk across the entire lab and ~1,600 L/yr for the purpose of handwashing glassware. In some circumstances, when glassware has tough residue, is too large for scrub brushes to reach, or has narrow openings, the use of harsh, environmentally toxic chemical baths must be used to clean them. These range from soaking glassware in a strong acid

or base mixed with isopropanol to the direct application of strong acids and/or peroxides. Not only do these processes create hazardous waste requiring disposal, but they place an increased risk on the lab members as well.

Glassware washers, when loaded properly, use less water than handwashing and will dry the glassware reducing the need for an additional acetone rinse. The glassware washers that are available are large enough to supply the entire lab with clean glassware and can wash 44 pieces of everyday glassware in one cleaning cycle. The glassware washer we acquired is highly efficient and uses 4.5 gal/cycle of tap water and 1.6 gal/cycle of DI water. This total water usage of 6.1 gal/cycle is a significant decrease from the previous water consumption. Each lab member produces enough glassware per week to require ~1.4 cycles/week and across the lab that equates to 2 cycles/day using a total of ~86 gal/wk or ~4,500 gal/yr. This would represent an 82% decrease in water usage for the purpose of hand washing common glassware. Additionally, this would decrease the acetone required by eliminating the portion used in rinsing the clean glassware (~0.8 L/wk). This would reduce the use of acetone to 1.7 L/wk which corresponds to ~20L/wk or 1,060 L/yr and represents a 33% reduction in acetone that would normally exit in our waste stream. While water conservation is easily calculated, the downstream energy and cost savings associated with the reduction of our waste are not, but they do represent an important part of creating a more sustainable lab.

In addition to washing everyday glassware, our lab decided long ago that we would recycle disposable test tubes to decrease our glass waste which ends up in landfills, as it cannot legally be recycled. Sadly, test tubes are prone to cracking, chipping and/or shattering during the handwashing process. Every time a rack of 72 test tubes is washed, there are several that are lost due to these rough cleaning conditions. Furthermore, smaller test tubes are thrown out if unable to

get clean due to inability to clean them properly due to small opening. While this seems minor, our lab members use and clean ~3 racks/day (216 tubes) which quickly equates to significant loses. To remedy this, we have utilized the glassware washer to wash test tubes, extending their lifetime and eliminating the need to dispose of small tubes. While we cannot recycle the test tubes that break, we have successfully limited the number that we dispose of on a yearly basis and the waste of cleaning them.

During the implementation of this project, COVID protocols were enacted at many levels of the University, and this severely hampered our ability to accurately quantify the number of consumables and waste being generated. Sadly, the water savings cannot be calculated due to the buildings system yet. Qualitatively though, the glassware washer has made a large impact on the cleaning and preservation of test tubes. The machine is regularly run 2-3 times per day with 5-15 racks (300-1,000 test tubes per load) and other glassware. Additionally, there are very rarely any circumstances where tubes break during the washing cycle, apart from the occasional uncoordinated lab member loading and unloading.

6.2 Further Implementation of Aluminum Heating Blocks for Energy Savings

6.2.1 Increasing Overall Usage of Energy Efficient Heating Methods

Previously, we committed the lab to being oil bath free to reduce the risk oil waste, lower our fire risk, and save energy used to heat large mineral oil baths. We acquired some of these aluminum blocks/metal heating devices in a previous grant written by Dr. Jacob Burman, “Blakey Lab Goes Green 2.0: Heating Oil Alternatives”. They have worked exceptionally well for the lab and have made large impacts to the workflow (**Figure 1**). Unsurprisingly, as the lab has grown (from 8 to14 people), so has the need to heat reactions. In response to this need, and the

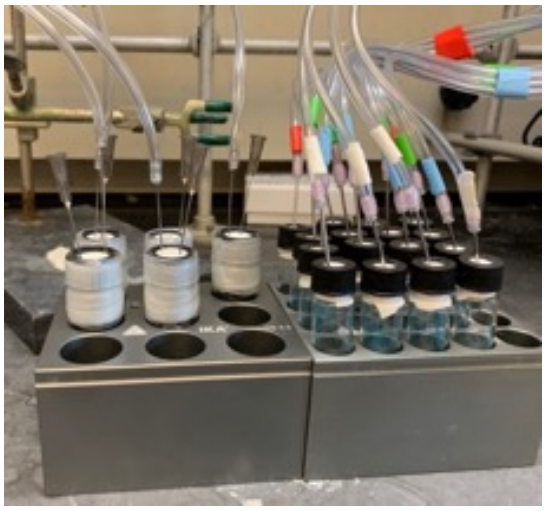

Figure 1. Two of the Blakey Lab dry heating blocks showcasing the ability to run large numbers of reactions efficiently.

commitment we made to abolishing oil baths, many have taken to using sand baths to heat reactions/groups of reactions when aluminum blocks are not available. While environmentally this is superior to oil from a disposal standpoint, the energy required to heat a glass dish containing 2-3 lbs. of sand is quite demanding. Furthermore, we are heating these sand baths from 60-180ºC for 12 to 24 hours inside a hood with 100 CFM exhaust fans. To say this current method is energy intensive would be an understatement. Taking these factors into account, the lab identified our heating processes as the largest source of wasted energy that has not been addressed to date.

Implementation of this project was straightforward as the lab had intimate knowledge of the capabilities and applications these systems provided by our previous incentives grant. Furthermore, the addition of these heating blocks will allow the use of sand baths to be limited to only extremely high heat reactions (>260ºC) or in the case of specific safety concerns, both of which are rare. The pairing of these blocks with our high efficiency stir plates (26 out of the 32 stir plates meet this criteria) allow for minimization of heat loss and less kW/h and led directly to less CO_2 emissions. Additionally, two Kill-A-Watt meters allowed us to compare our systems and

determine quantitatively our energy decrease. This data generation will help direct the OSI in future policy for new and existing labs on campus.

We believe this study will continue to help lessen the carbon footprint of the Blakey Lab and future labs to come, while also meeting several of the UN's goals for sustainable development.[6] Finally, the implementation of this project led to the end of inefficient sand baths in our lab, a decrease in reaction-time-to-heat (less kW/h used) and a lower overall usage (kW/h) throughout the lab for heating. The secondary achieved was to derive real-life data of the electricity usage and savings with aluminum heating blocks to inform future policy regarding laboratory reaction heating.

6.2.2 Data Collection and Interpretation

The experiment was setup utilizing the three stir plates commonly found in our lab and other labs on Emory's campus. We chose to us a Heidolph Hei-temp, IKA RCT digital and Chemglass RCT plate for these studies. These were paired with a 500 mL round bottom flask heating block and air-cooled Findenser (**Figure 2**). The experiment also utilized 1 kg of sand in a glass crystallization

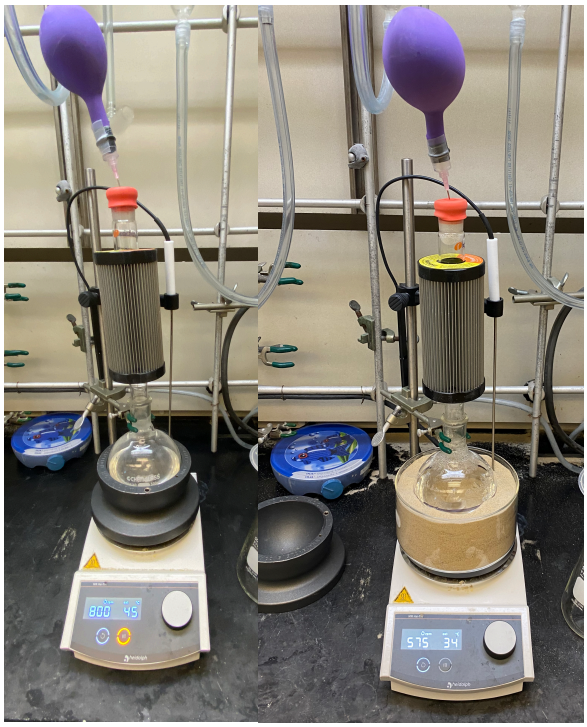

Figure 2. Experimental setup showing the comparison of both the aluminum heating mantle and the sand bath.

dish filled to the level of liquid in the flask. The choice of solvent was 250mL of water and this was brought to reflux at 100 ºC for various lengths of time. The energy consumed by these reactions was monitored with Kill-A-Watt devices that track the amount of energy passing through the device. The measurements were recorder at 4 h, 8 h, 12 h, 24 h and 48 h. These values were then compared against one another and against the control of merely stirring.

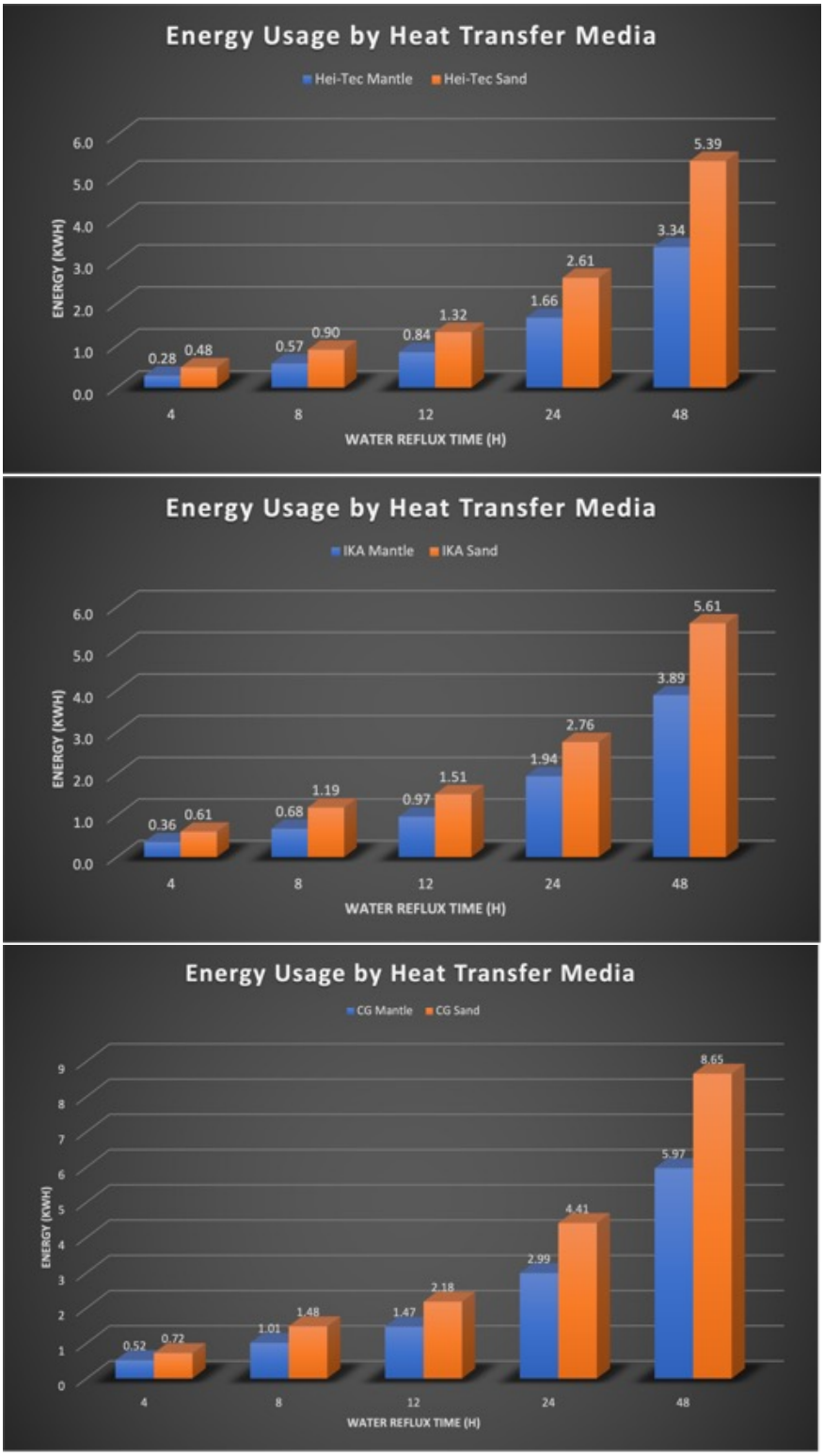

Figure 3. Graphs of Energy Usage by Heat Transfer Media

between the two heating methods (**Figure 3**). The results showed that at the 24-hour mark, the difference in energy usage was roughly 1-1.5 kW/h across the three plates in favor of the aluminum heating block. This savings in energy correlates to 1.5-2.2 lbs. of CO_2 per day by switching to more efficient heating blocks. These results are shown graphically in **Figure 4** and illustrate the potential

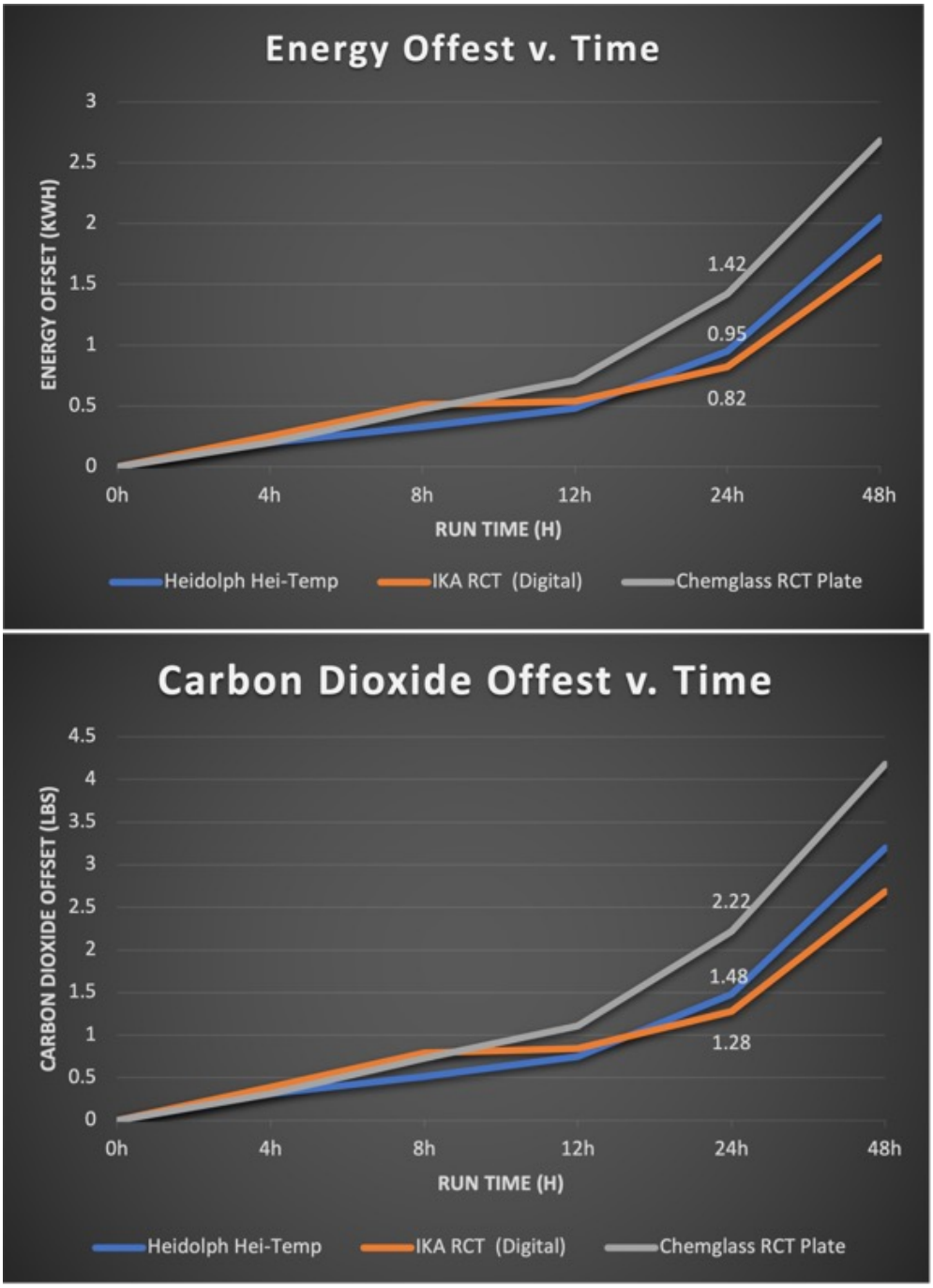

Figure 4. Graphs of Energy and Carbon Offset over time.

for saving across the lab. We also looked at the predictability of these system over 28 days and compared this to experimental findings. Over the 4 weeks of heating with the Heidolph Hei-temp and the Chemglass RCT, we found that the experimental and predicted values of energy usage had an average of 2% difference. This was excellent as it validated our ability to predict the overall energy consumption of the stir plates and indicated a constant value of energy usage despite variable environmental conditions.

Following the completion of this data collection, Heidolph representatives approached the lab for a copy of the raw data to analyze. Additionally, this study was shared with a Harvard researcher who is attempting to implement more efficient chemistry practices in their department and the Emory OSI representatives. Owing to the interest in this study, data from heating by oil bath, standard practice in many labs, should be added to this data to fully gauge the effectiveness of aluminum heating blocks and their ability to offset carbon emissions through energy reduction. With this added information, I believe that the work could be disclosed for the community in *ACS Sustainable Chemistry & Engineering* or a similar journal.

6.3 Concluding Remarks

The Blakey labs continued commitment to creating a greener, more sustainable lab environment has been ongoing for years. This dedication has been continued by Eleda Plouch and Keili Diaz as they were awarded a grant for a more energy efficient photochemical reactor this past year. Additionally, in recognition of the lab's continued efforts, The Emory OSI honored Simon Blakey as the 2023 Faculty Sustainability Innovator for being "a leader in campus lab sustainability for many years." This recognition just further highlights the need for continued innovation and sustainability in the Blakey Lab. Finally, the lessons learned from the Blakey Lab and others has led to a Sustainability Initiative group led by Hannah Gold, Caroline McCormick,

and Eleda Plouch to bring all of the chemistry department under the OSI Green Labs certification and look for further ways to foster green and/or sustainable chemistry from the administrative level through the individual labs.

6.4 References

1. Krishna N. Ganesh, K. N.; Zhang, D.; Miller, S. J. Rossen, K.; Chirik, P. J.; Kozlowski, M. C.; Zimmerman, J. B.; Brooks, B. W.; Savage, P. E.; Allen, D. T.; Voutchkova-Kostal, A. M. Green Chemistry: A Framework for a Sustainable Future. *Org. Process Res. Dev.* **2021***, 25,* 1455–1459.

2. Aparecida de Marco, B.; Rechelo, B. S.; Tótoli, E. G.; Kogawa, A. C.; Salgado; H. R. N. Evolution of green chemistry and its multidimensional impacts: A review. *Saudi Pharmaceutical Journal.* **2019**, *27,* 1–8.

3. Martinez, J.; Cortés, J. F.; Miranda, R. Green Chemistry Metrics, A Review. *Processes* **2022**, *10*, 1274-1301.

4. My Green Lab (501c). *My Green Lab*, **2013**, www.mygreenlab.org/.

5. Environmental Protection Agency. *EPA WaterSense: Laboratories*. EPA. **2019**, https://www.epa.gov/watersense/types-facilities#Laboratories.

6. United Nations. *THE 17 GOALS.* Department of Economic and Social Affairs: Sustainable Development. **2019,** https://sdgs.un.org/goals.

6.5 Experimental Section

General procedure for measurement of energy usage.

The selected heat/stir plate was placed in the hood at a central position and loaded with either the 500 mL RBF aluminum heating block or crystallization dish with ¼" of sand in the bottom. A flask clamp was then fitted to hold a 250 mL RBF with stir bar in the heating block or resting on the sand. A Class A graduated cylinder was then used to measure and add 250.0 mL of water to the RBF. The remaining 1kg of sand was then added to bring the layer of sand equal to the water level. The RBF was then fitted with a 24/40 Findenser and the condenser was secured at the top with a clamp to maintain vertical reflux. A septum and air filled balloon was then attached to the system at the top. The Kill-A-Watt measurement device was placed into the outlet and the plate plugged into its outlet. The stir plate was then set to 1000 RPM and 100 ºC. Measurements were recorded using the timer function and kW/h consumption meter of the Kill-A-Watt at 4 h, 8 h, 12 h, 24 h, 48 h and 672 h (28 days).

1 kg Sand (kWh)						
	0h	**4h**	**8h**	**12 h**	**24h**	**48h**
Heidolph Hei-Temp	0	0.48	0.90	1.32	2.61	5.39
IKA RCT (Digital)	0	0.61	1.19	1.51	2.76	5.61
Chemglass RCT Plate	0	0.72	1.48	2.18	4.41	8.65

Heating Mantle (kWh)						
	0h	**4h**	**8h**	**12h**	**24h**	**48h**
Heidolph Hei-Temp	0	0.28	0.57	0.84	1.66	3.34
IKA RCT (Digital)	0	0.36	0.68	0.97	1.94	3.89
Chemglass RCT Plate	0	0.52	1.01	1.47	2.99	5.97

Stirring RT (kWh)						
	0h	**4h**	**8h**	**12h**	**24h**	**48h**
Heidolph Hei-Temp	0	0.02	0.04	0.06	0.13	0.26
IKA RCT (Digital)	0	0.01	0.03	0.05	0.11	0.23
Chemglass RCT Plate	0	0.02	0.04	0.06	0.13	0.27

∆ RT v. 100 ºC* (kWh)						
	0h	**4h**	**8h**	**12h**	**24h**	**48h**
Heidolph Hei-Temp	0	0.26	0.53	0.78	1.53	3.08
IKA RCT (Digital)	0	0.35	0.65	0.92	1.83	3.66
Chemglass RCT Plate	0	0.5	0.97	1.41	2.86	5.7
***Compared to Heating Mantle**						

Energy Offset (kWh)						
	0h	**4h**	**8h**	**12h**	**24h**	**48h**
Heidolph Hei-Temp	0	0.20	0.33	0.48	0.95	2.05
IKA RCT (Digital)	0	0.25	0.51	0.54	0.82	1.72
Chemglass RCT Plate	0	0.20	0.47	0.71	1.42	2.68

Offset (lbs. CO2)						
	0h	**4h**	**8h**	**12h**	**24h**	**48h**
Heidolph Hei-Temp	0	0.31	0.51	0.75	1.48	3.20
IKA RCT (Digital)	0	0.39	0.80	0.84	1.28	2.68
Chemglass RCT Plate	0	0.31	0.73	1.11	2.22	4.18
				1kW = 1.56 lbs CO2		Via: EPA

Long Term Projections					
		days (672 h)	**Usage (kwh)**	**CO2 (lbs)**	**% Difference**
Chemglass HM 100ºC	**Actual**	28	82.94	129.3864	1%
Chemglass HM 100ºC	**Predicted**	28	83.72	130.6032	
Heidolph rt stir	**Actual**	28	3.76	5.8656	3%
Heidolph rt stir	**Predicted**	28	3.64	5.6784	

Supplemental Characterization

Chapter 2: HPLC Traces

HPLC analysis for conjugate addition test (column: OJH_30min_1ml/min _1%)

1. test with 1,5-Cyclooctadiene (racemic reaction)

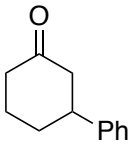

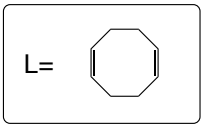

Signal 1: DAD1 C, Sig=210,4 Ref=off

Peak #	RetTime [min]	Type	Width [min]	Area [mAU*s]	Height [mAU]	Area %
1	15.493	VB	0.3441	3389.26660	149.71777	50.1511
2	18.915	BB	0.4216	3368.83813	122.95934	49.8489

Totals : 6758.10474 272.67712

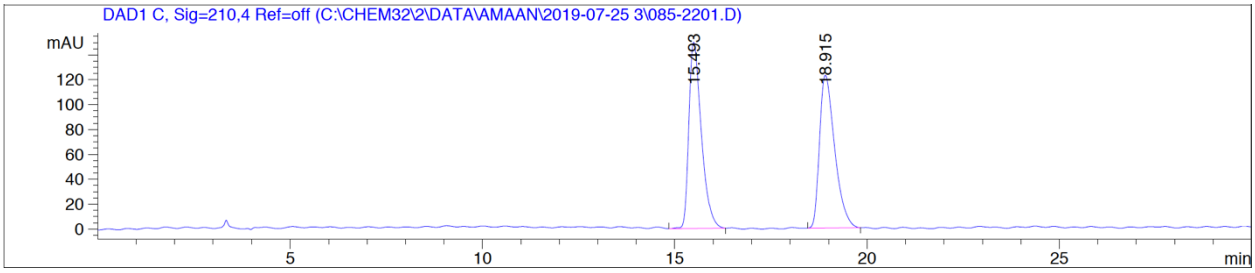

2. test with C2-symmetric chiral COD ligands and their derivatives

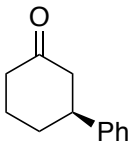

(1). L=2.13, 39% ee.

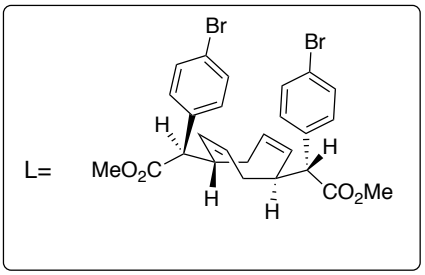

Signal 2: DAD1 C, Sig=210,4 Ref=off

Peak #	RetTime [min]	Type	Width [min]	Area [mAU*s]	Height [mAU]	Area %
1	15.289	VB	0.3740	1.20196e4	497.26553	30.7100
2	18.298	BB	0.5639	2.71193e4	757.13055	69.2900
Totals :				3.91388e4	1254.39609	

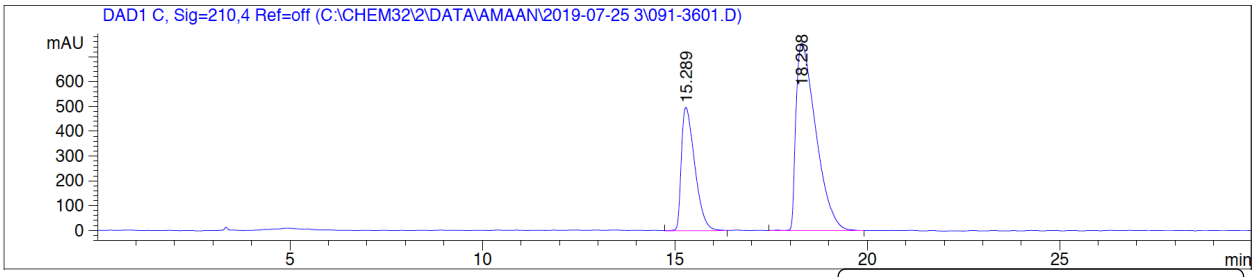

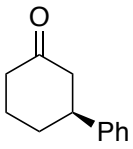

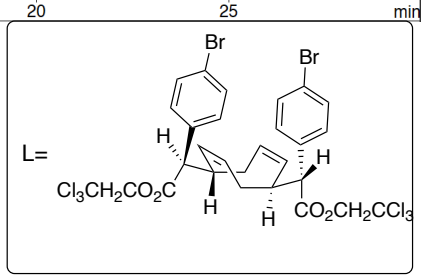

(2). L=2.14, 34% ee.

Signal 1: DAD1 C, Sig=210,4 Ref=off

Peak #	RetTime [min]	Type	Width [min]	Area [mAU*s]	Height [mAU]	Area %
1	15.450	BB	0.3744	1.46869e4	602.50049	32.7329
2	18.630	BB	0.5526	3.01820e4	837.23248	67.2671
Totals :				4.48690e4	1439.73297	

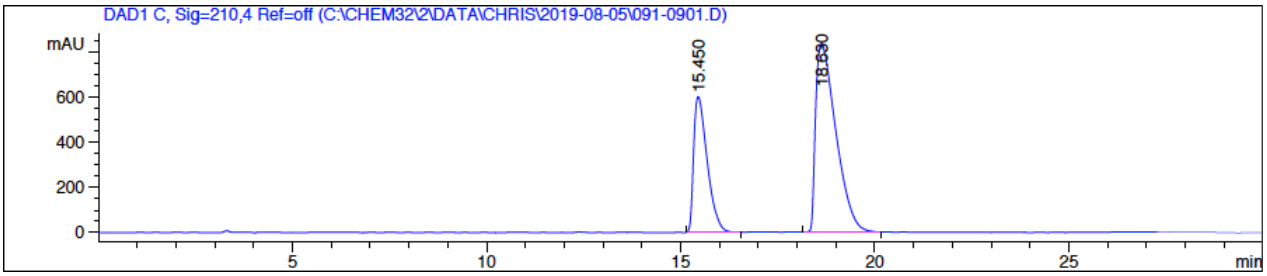

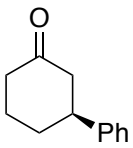

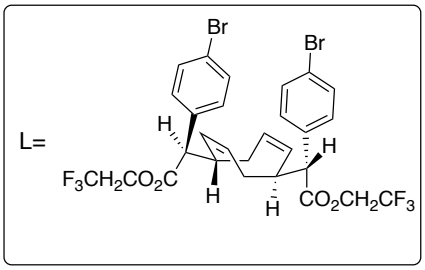

(3). L=2.15, 36% ee.

Signal 1: DAD1 C, Sig=210,4 Ref=off

Peak #	RetTime [min]	Type	Width [min]	Area [mAU*s]	Height [mAU]	Area %
1	15.412	BB	0.3902	1.58306e4	623.60895	32.2460
2	18.445	BB	0.5778	3.32627e4	882.38849	67.7540

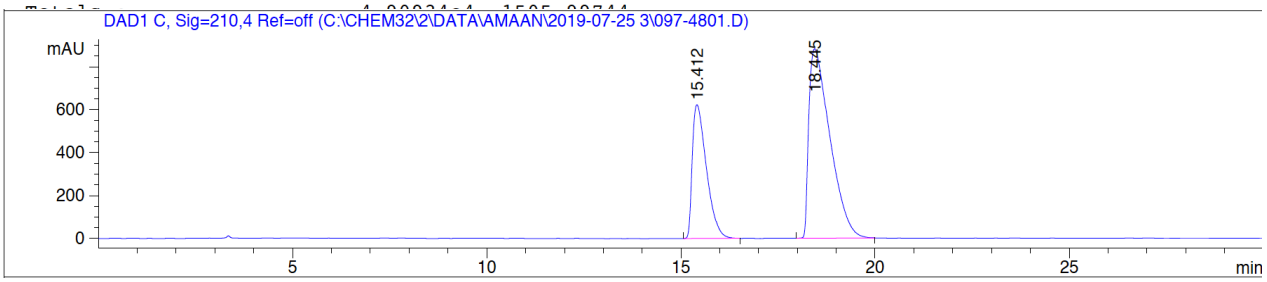

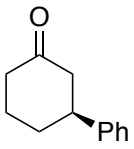

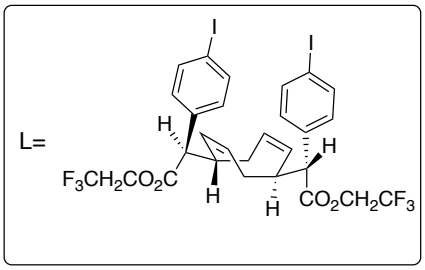

(4). L=2.19, 45% ee.

Signal 1: DAD1 C, Sig=210,4 Ref=off

Peak #	RetTime [min]	Type	Width [min]	Area [mAU*s]	Height [mAU]	Area %
1	15.590	BB	0.3171	329.31805	15.67247	27.6779
2	18.876	BB	0.3805	860.50415	34.32642	72.3221
Totals :				1189.82220	49.99889	

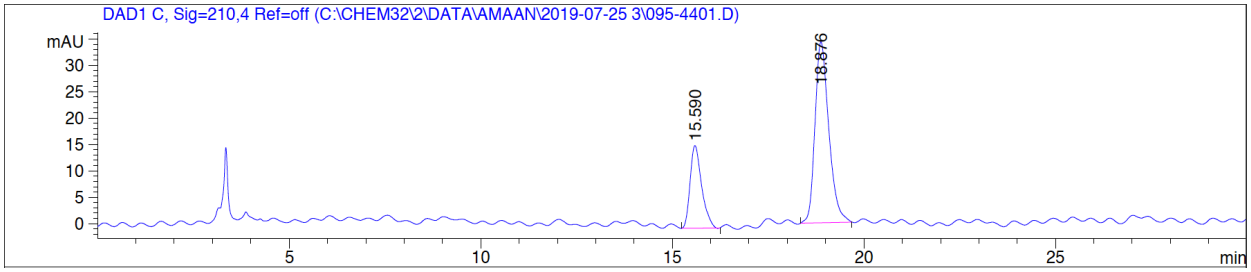

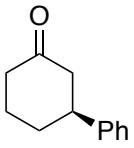

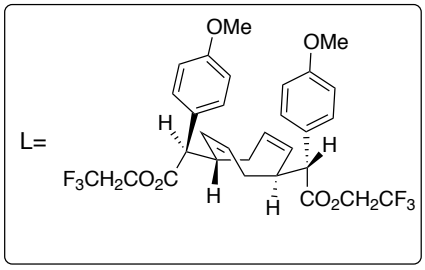

(5). L=2.16, 30% ee.

Signal 1: DAD1 C, Sig=210,4 Ref=off

Peak #	RetTime [min]	Type	Width [min]	Area [mAU*s]	Height [mAU]	Area %
1	15.384	BB	0.3969	1.98576e4	770.04730	35.1377
2	18.369	BB	0.5576	3.66560e4	968.45874	64.8623

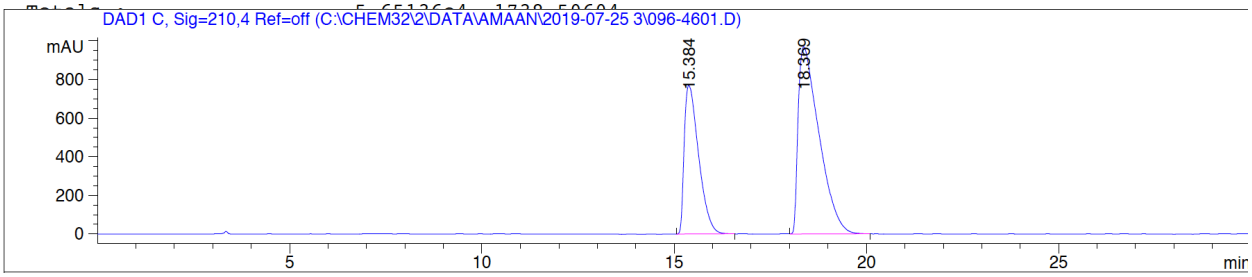

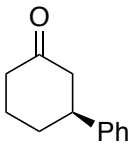

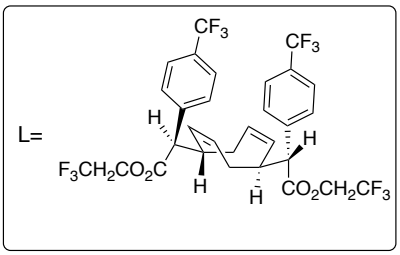

(6). L=2.17, 33% ee.

Signal 1: DAD1 C, Sig=210,4 Ref=off

Peak #	RetTime [min]	Type	Width [min]	Area [mAU*s]	Height [mAU]	Area %
1	15.319	BB	0.3681	1.16148e4	483.75128	33.6101
2	18.342	BB	0.5086	2.29427e4	681.73700	66.3899
Totals :				3.45575e4	1165.48828	

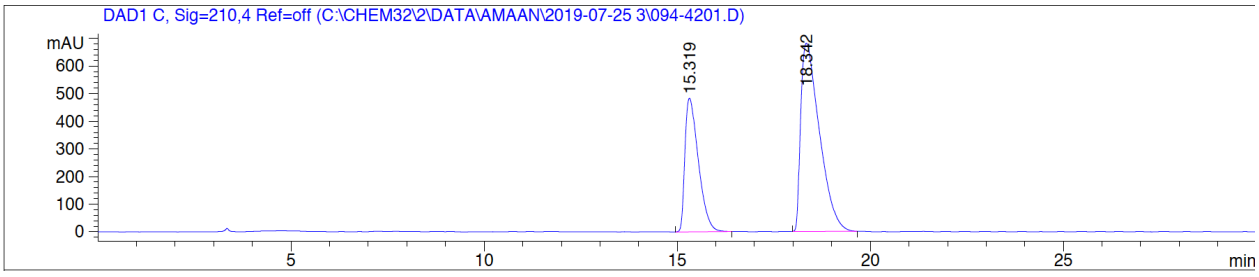

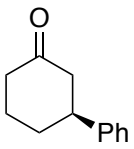

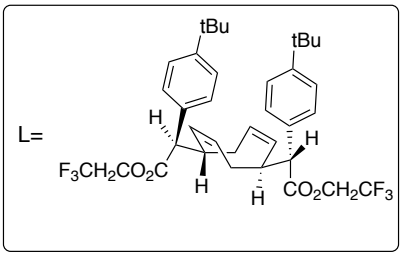

(7). L=2.18, 22% ee.

Signal 1: DAD1 C, Sig=210,4 Ref=off

Peak #	RetTime [min]	Type	Width [min]	Area [mAU*s]	Height [mAU]	Area %
1	15.610	BB	0.4381	2.67188e4	949.94879	39.1501
2	18.772	BB	0.5890	4.15284e4	1037.52234	60.8499
Totals :				6.82472e4	1987.47113	

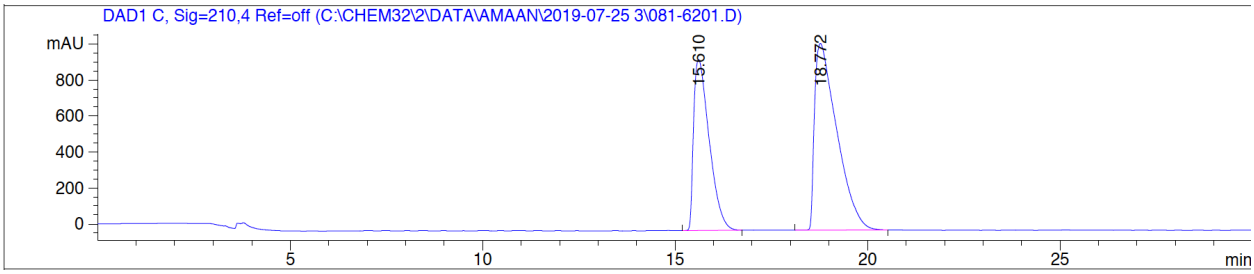

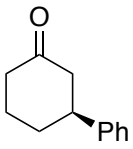

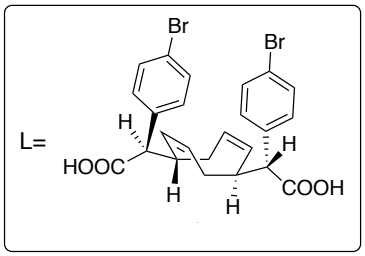

(9). L=2.26, 27% ee.

Signal 1: DAD1 C, Sig=210,4 Ref=off

Peak #	RetTime [min]	Type	Width [min]	Area [mAU*s]	Height [mAU]	Area %
1	15.292	BB	0.3646	8040.54785	341.64832	36.5930
2	18.450	BB	0.4848	1.39324e4	440.72278	63.4070
Totals :				2.19729e4	782.37109	

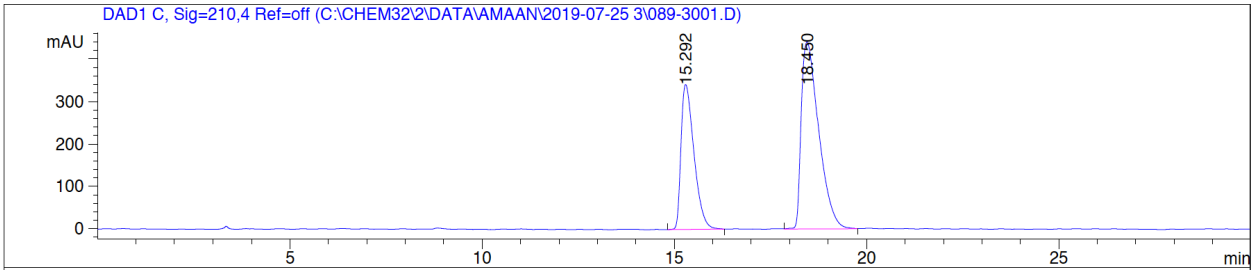

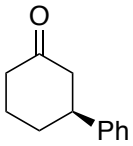

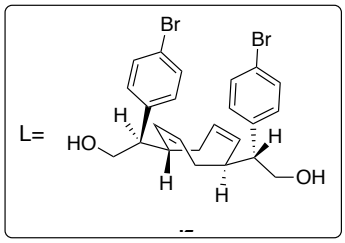

(8). L=2.27, 26% ee.

Signal 1: DAD1 C, Sig=210,4 Ref=off

Peak #	RetTime [min]	Type	Width [min]	Area [mAU*s]	Height [mAU]	Area %
1	15.293	BB	0.3648	9337.66113	396.40738	36.7708
2	18.398	BB	0.4906	1.60566e4	500.13208	63.2292

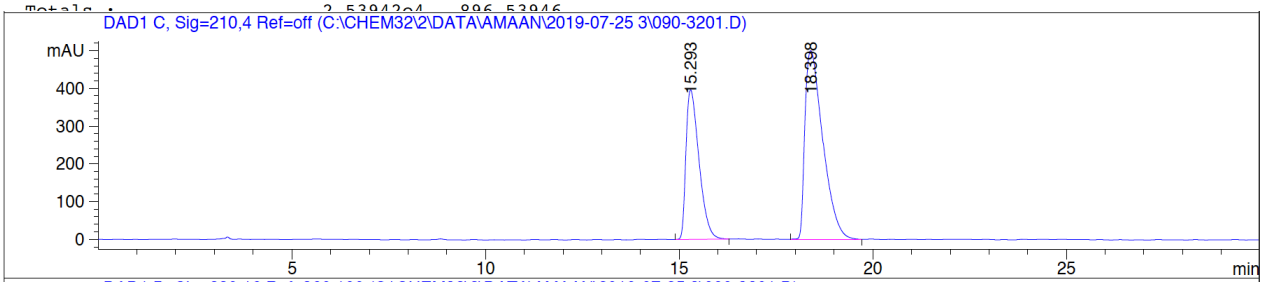

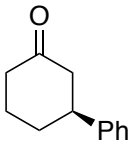

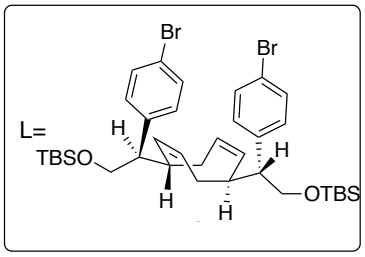

(12). L=2.28, 53% ee.

Signal 1: DAD1 C, Sig=210,4 Ref=off

Peak #	RetTime [min]	Type	Width [min]	Area [mAU*s]	Height [mAU]	Area %
1	15.304	BB	0.3619	1.01920e4	434.13281	23.5753
2	18.193	BB	0.5715	3.30398e4	897.48987	76.4247

Totals : 4.32319e4 1331.62268

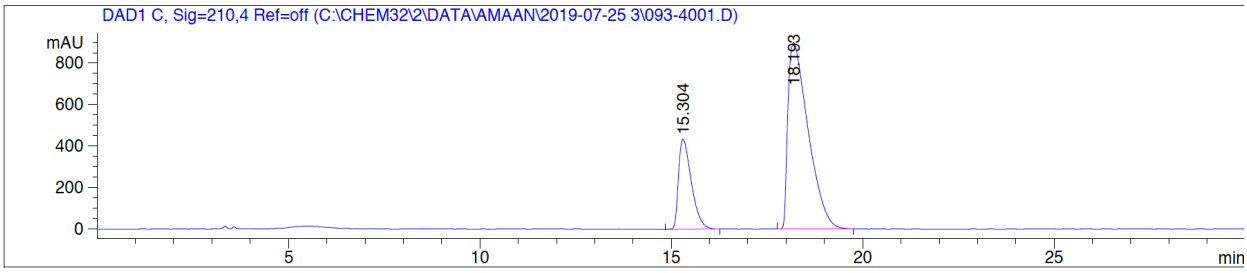

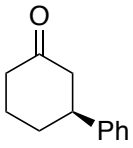

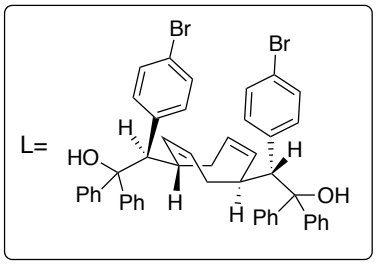

(10). L=2.29a, 47% ee.

Signal 1: DAD1 C, Sig=210,4 Ref=off

Peak #	RetTime [min]	Type	Width [min]	Area [mAU*s]	Height [mAU]	Area %
1	15.551	BB	0.3571	529.52753	22.13255	26.4121
2	18.953	VB	0.4298	1475.34106	52.82749	73.5879
Totals :				2004.86859	74.96004	

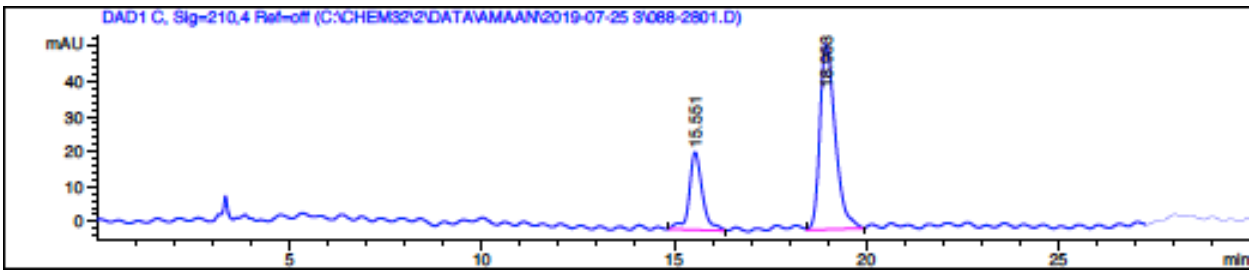

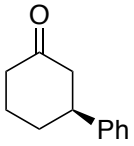

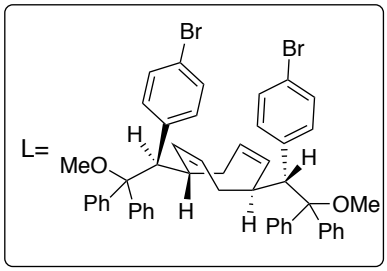

(11). L=2.30a, 60% ee.

Signal 1: DAD1 C, Sig=210,4 Ref=off

Peak #	RetTime [min]	Type	Width [min]	Area [mAU*s]	Height [mAU]	Area %
1	16.694	BB	0.3768	1534.34827	60.72484	19.8006
2	20.110	BB	0.4812	6214.63330	199.64850	80.1994
Totals :				7748.98157	260.37334	

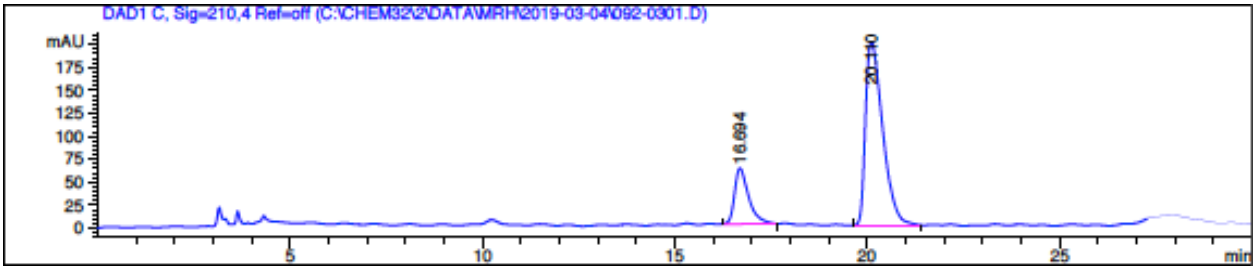

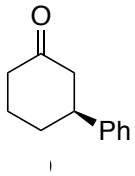

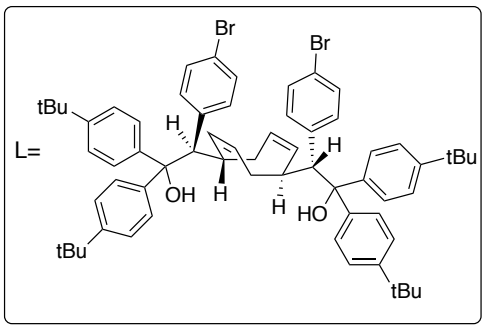

(13). L=2.29b, 69% ee.

Signal 1: DAD1 C, Sig=210,4 Ref=off

Peak #	RetTime [min]	Type	Width [min]	Area [mAU*s]	Height [mAU]	Area %
1	15.430	VB	0.3499	6226.05908	273.17520	15.2606
2	18.297	BB	0.5817	3.45722e4	917.27521	84.7394
Totals :				4.07982e4	1190.45041	

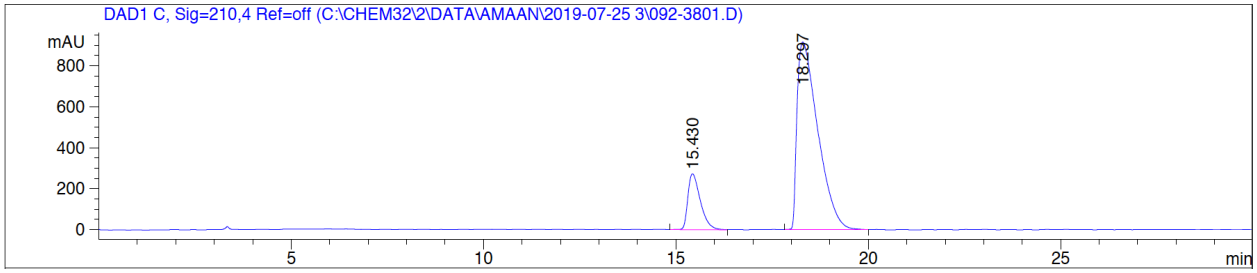

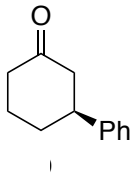

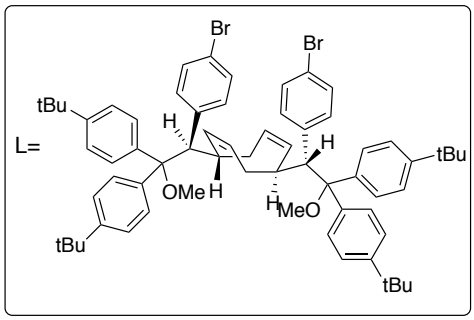

(14). L=2.30b, 59% ee.

Signal 1: DAD1 C, Sig=210,4 Ref=off

Peak #	RetTime [min]	Type	Width [min]	Area [mAU*s]	Height [mAU]	Area %
1	15.151	BB	0.3686	1.14708e4	480.38049	20.4964
2	17.951	VB	0.5870	4.44942e4	1130.92139	79.5036
Totals :				5.59650e4	1611.30188	

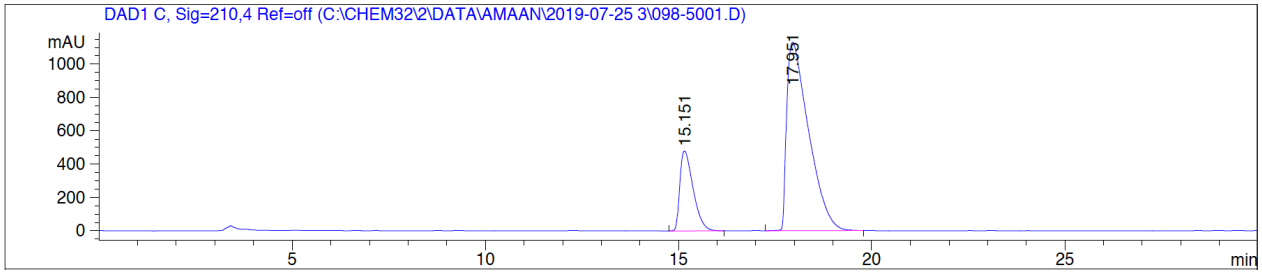

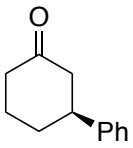

50

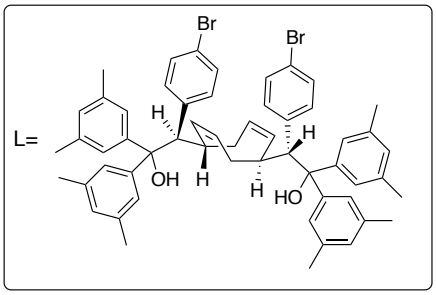

(15). L=2.29c, 41% ee.

```
Signal 1: DAD1 C, Sig=210,4 Ref=off

Peak RetTime Type  Width     Area      Height     Area
  #   [min]        [min]   [mAU*s]     [mAU]       %
----|-------|----|-------|----------|----------|--------|
   1  15.587 BB    0.3432 3716.06152  164.74695  29.6503
   2  18.804 VB    0.4713 8816.89844  291.16553  70.3497

Totals :                  1.25330e4   455.91248
```

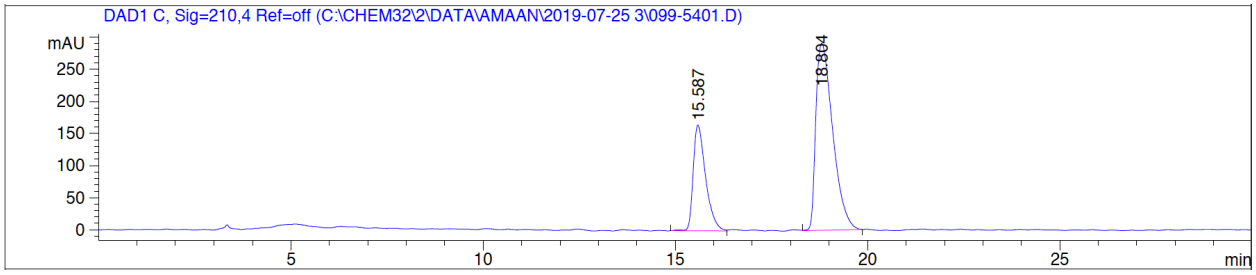

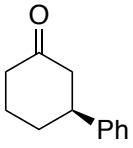

)

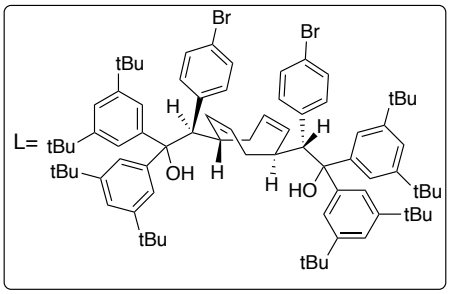

(15). L=2.29d, 76% ee.

```
Signal 1: DAD1 C, Sig=210,4 Ref=off

Peak RetTime Type  Width     Area      Height     Area
  #   [min]        [min]   [mAU*s]     [mAU]       %
----|-------|----|-------|----------|----------|--------|
   1  15.450 BB    0.3402 4872.13184  220.15059  11.9691
   2  18.223 BB    0.5714 3.58338e4   964.50671  88.0309

Totals :                  4.07059e4   1184.65730
```

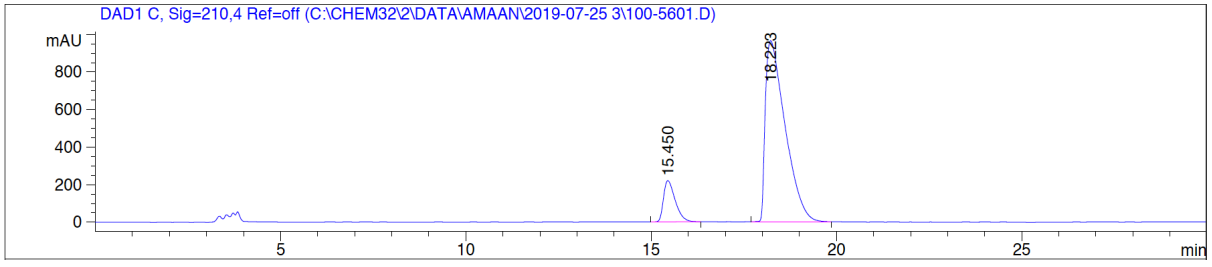

Chapter 4: Spectra and Crystallography

4.6.1

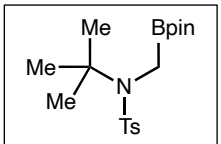
Me
Bpin
Me
N
Me
Ts

4.22

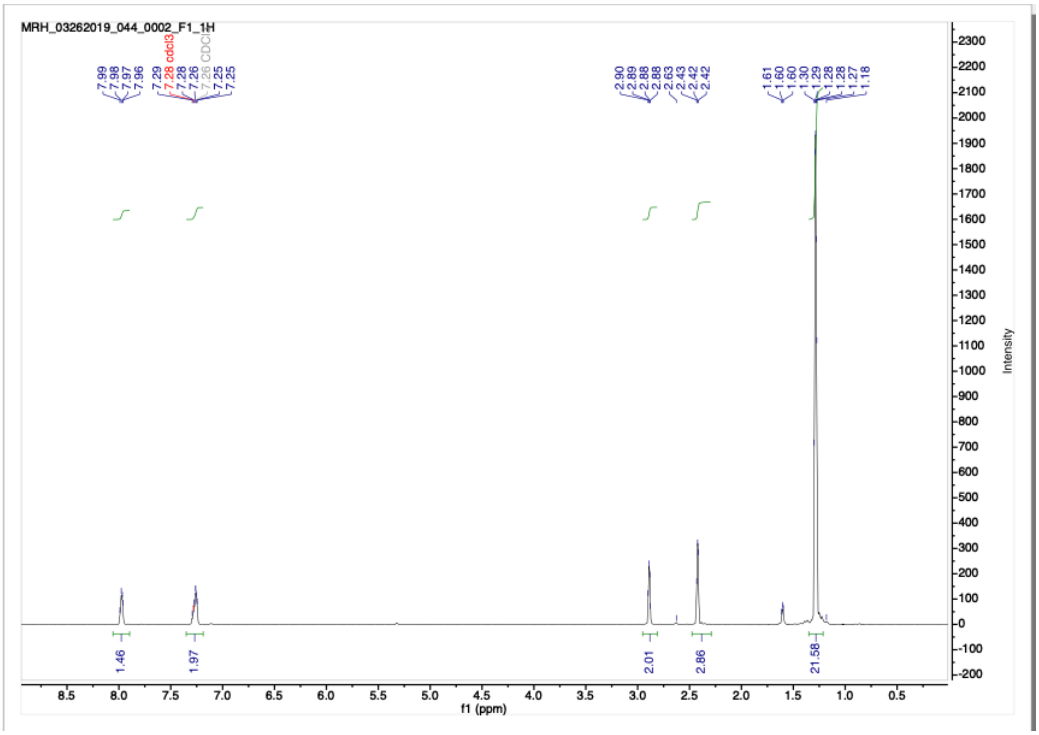
MRH_03262019_044_0002_F1_1H
7.99
7.98
7.97
7.96
7.29
7.28 cdcl3
7.28
7.26
7.25 CDCl3
7.25
7.25
2.90
2.89
2.88
2.88
2.43
2.42
2.42
1.61
1.60
1.60
1.30
1.29
1.28
1.28
1.27
1.18
1.46
1.97
2.01
2.86
21.58
f1 (ppm)
Intensity

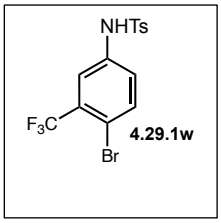
NHTs
F3C
Br
4.29.1w

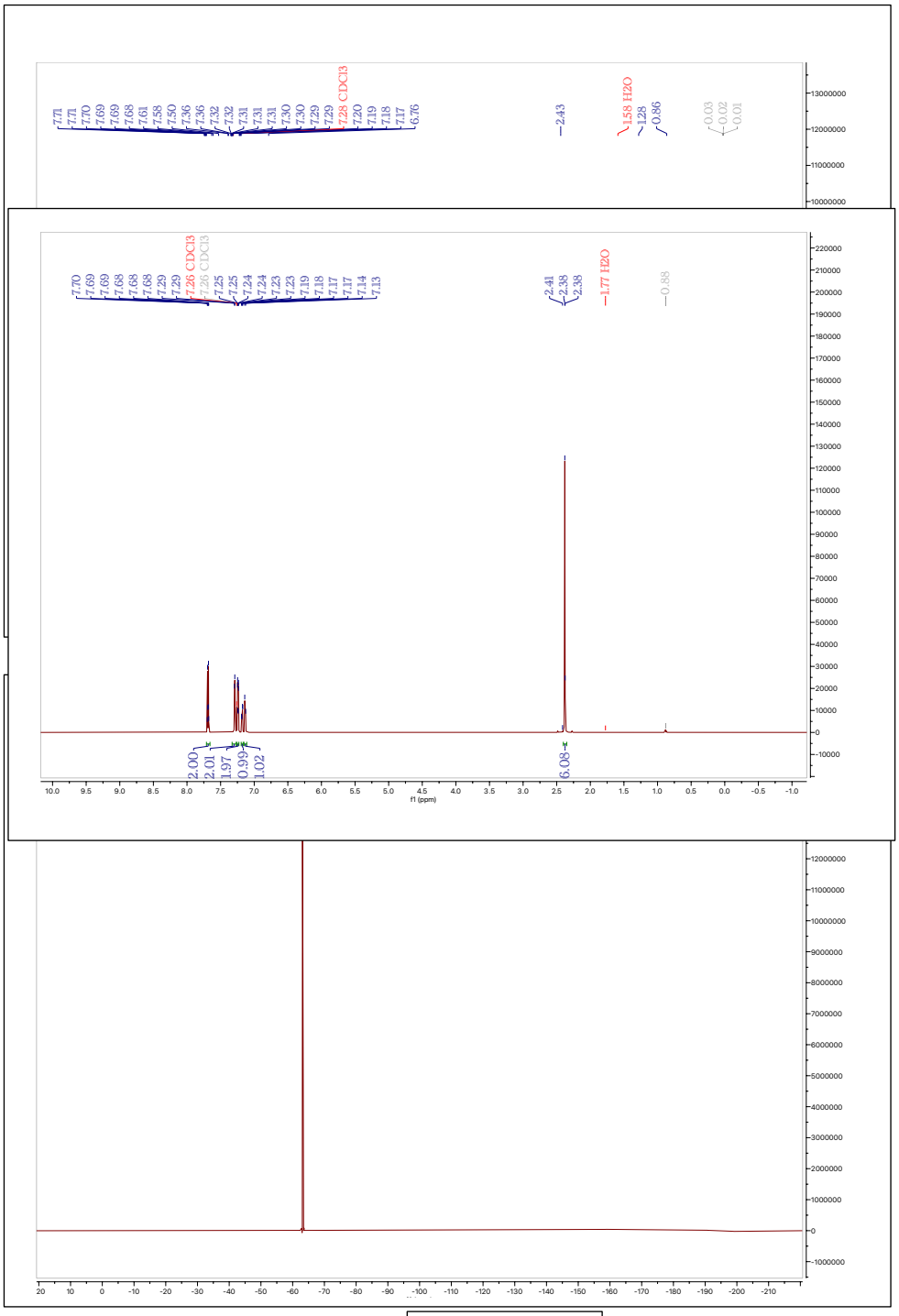
7.71
7.71
7.70
7.69
7.69
7.68
7.61
7.58
7.50
7.36
7.36
7.32
7.32
7.31
7.31
7.31
7.30
7.30
7.29
7.29
7.28 CDCl3
7.20
7.19
7.18
7.17
6.76
2.43
1.58 H2O
1.28
0.86
0.03
0.02
0.01
7.70
7.69
7.69
7.68
7.68
7.68
7.29
7.29
7.26 CDCl3
7.26 CDCl3
7.25
7.25
7.24
7.24
7.23
7.23
7.19
7.18
7.17
7.17
7.14
7.13
2.41
2.38
2.38
1.77 H2O
0.88
2.00
2.01
1.97
0.99
1.02
6.08
f1 (ppm)

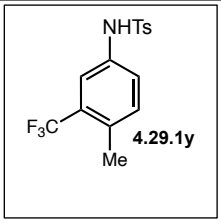
NHTs
F3C
Me
4.29.1y

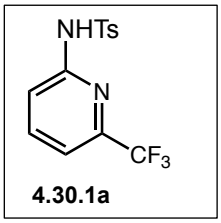
NHTs
N
CF3

4.30.1a

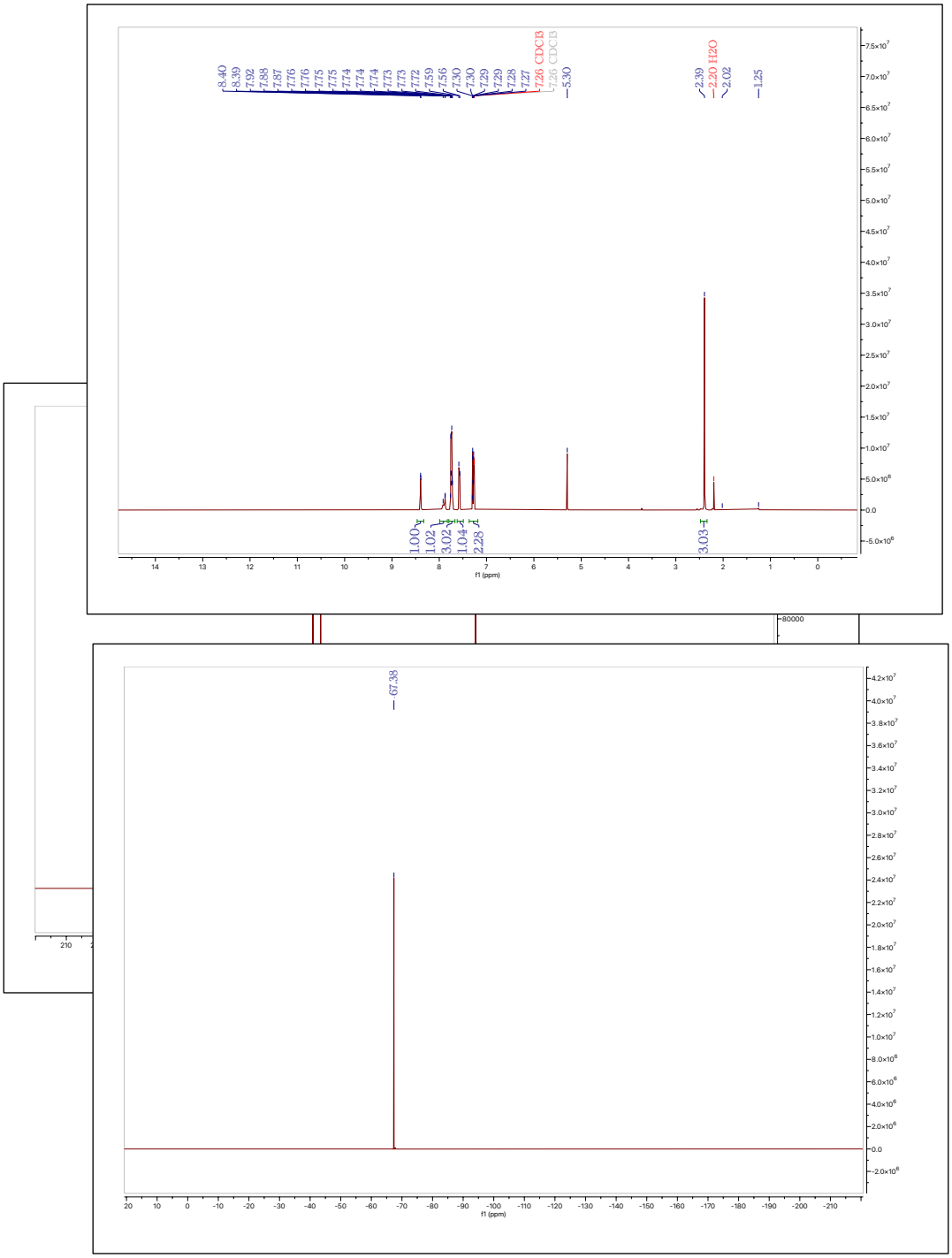
8.40
8.39
7.92
7.88
7.87
7.76
7.76
7.75
7.75
7.74
7.74
7.74
7.73
7.73
7.72
7.59
7.56
7.30
7.30
7.29
7.29
7.28
7.27
7.26 CDCl3
7.26 CDCl3
5.30
2.39
2.20 H2O
2.02
1.25
1.00
1.02
3.02
1.04
2.28
3.03
f1 (ppm)
67.38
f1 (ppm)

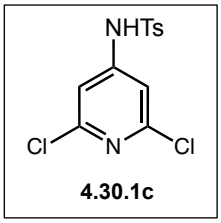
NHTs
Cl
N
Cl

4.30.1c

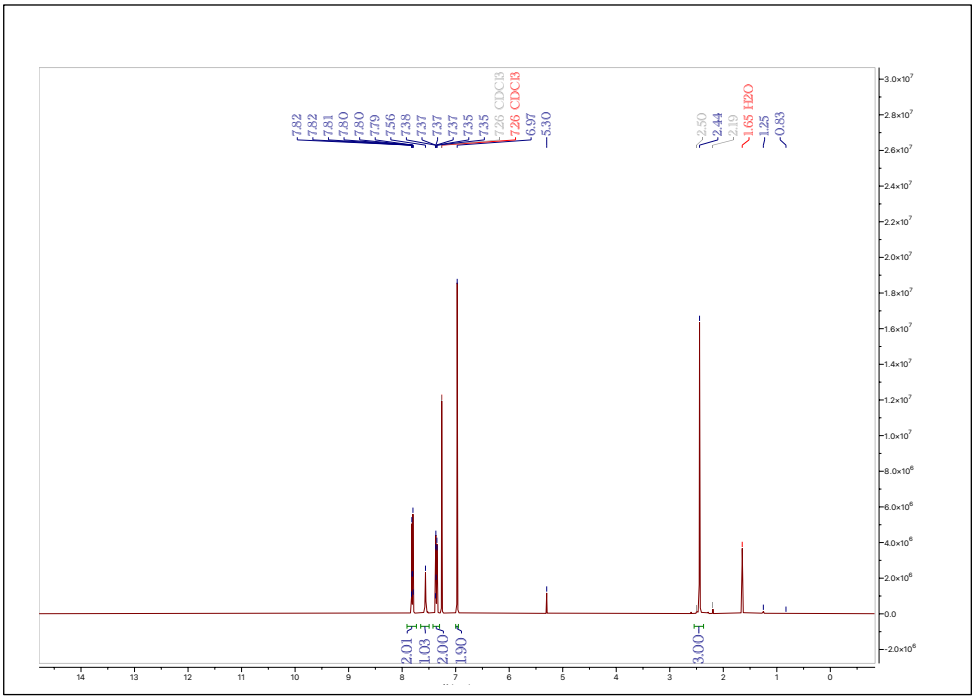
7.82
7.82
7.81
7.80
7.80
7.79
7.56
7.38
7.37
7.37
7.37
7.35
7.35
7.26 CDCl3
7.26 CDCl3
6.97
5.30
2.50
2.44
2.19
1.65 H2O
1.25
0.83
2.01
1.03
2.00
1.90
3.00

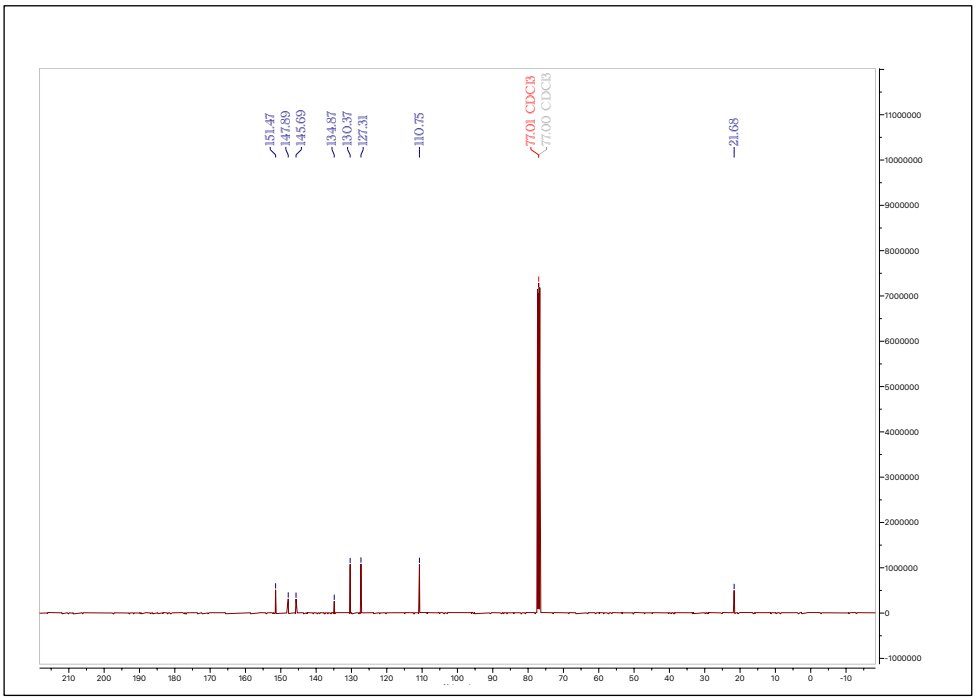
151.47
147.89
145.69
134.87
130.37
127.31
110.75
77.01 CDCl3
77.00 CDCl3
21.68

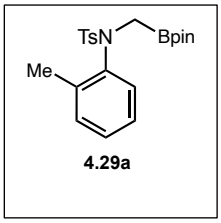
TsN
Bpin
Me

4.29a

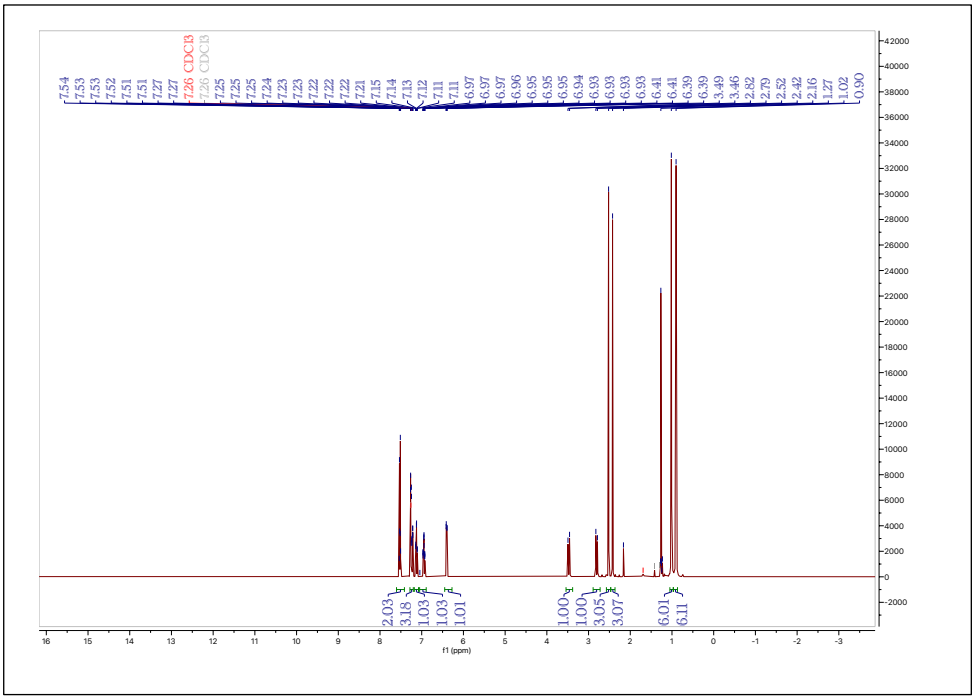
7.54
7.53
7.53
7.52
7.51
7.51
7.27
7.27
7.26 CDCl3
7.26 CDCl3
7.25
7.25
7.25
7.24
7.23
7.23
7.22
7.22
7.22
7.21
7.15
7.14
7.13
7.12
7.11
7.11
6.97
6.97
6.97
6.96
6.95
6.95
6.95
6.94
6.93
6.93
6.93
6.93
6.41
6.41
6.39
6.39
3.49
3.46
2.82
2.79
2.52
2.42
2.16
1.27
1.02
0.90
2.03
3.18
1.03
1.03
1.01
1.00
1.00
3.05
3.07
6.01
6.11
f1 (ppm)

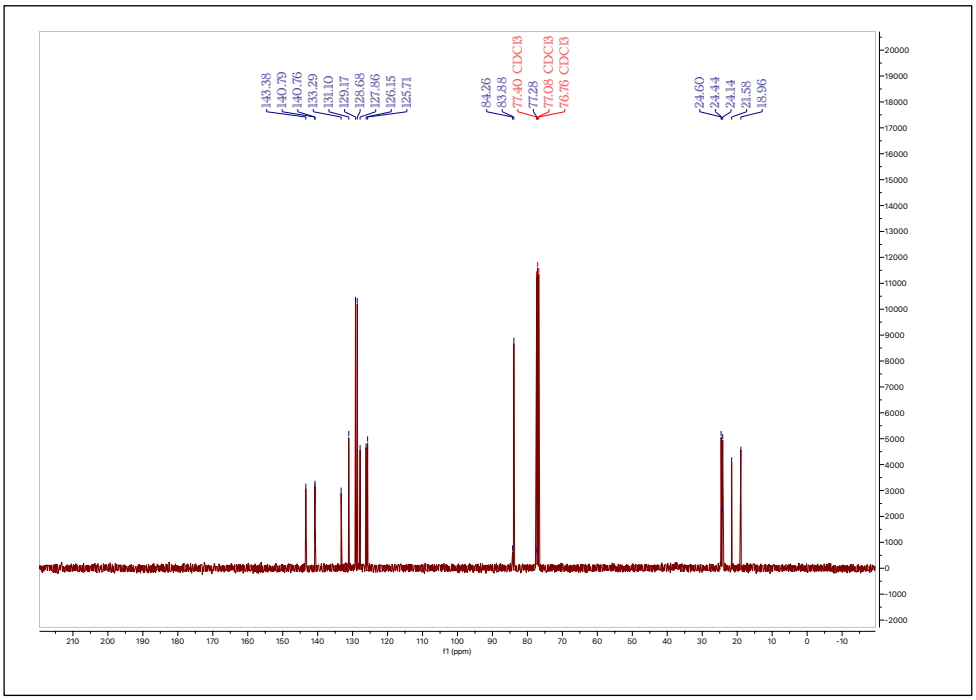
143.38
140.79
140.76
133.29
131.10
129.17
128.68
127.86
126.15
125.71
84.26
83.88
77.40 CDCl3
77.28
77.08 CDCl3
76.76 CDCl3
24.60
24.44
24.14
21.58
18.96
f1 (ppm)

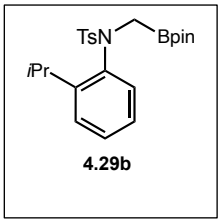
TsN
Bpin
iPr

4.29b

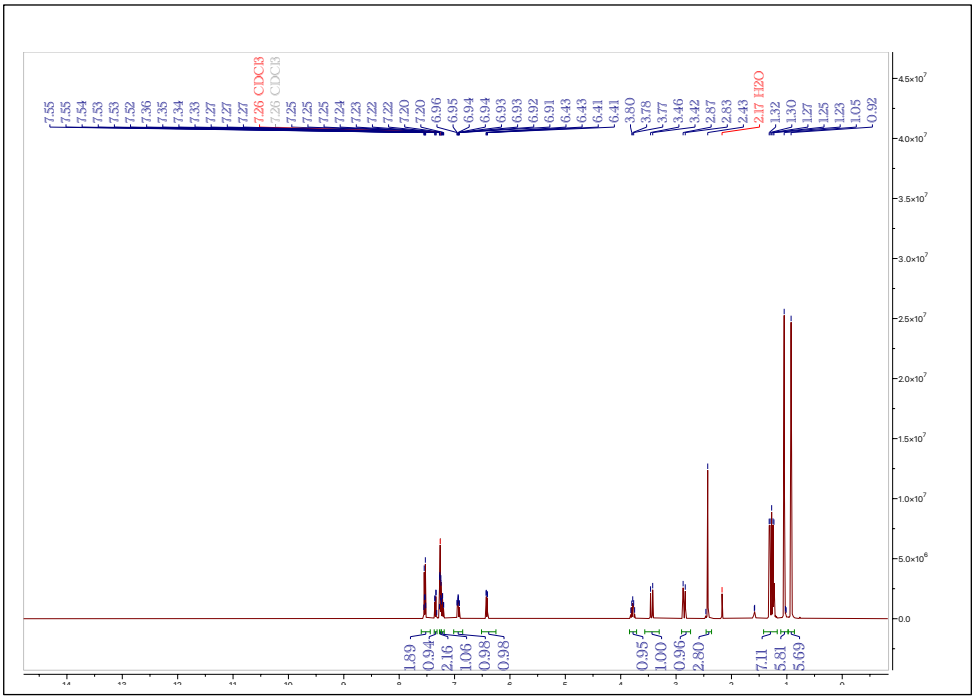
7.55
7.55
7.54
7.53
7.53
7.52
7.36
7.35
7.34
7.33
7.27
7.27
7.27
7.26 CDCl3
7.26 CDCl3
7.25
7.25
7.25
7.24
7.23
7.22
7.22
7.20
7.20
6.96
6.95
6.94
6.94
6.93
6.93
6.92
6.91
6.43
6.43
6.41
6.41
3.80
3.78
3.77
3.46
3.42
2.87
2.83
2.43
2.17 H2O
1.32
1.30
1.27
1.25
1.23
1.05
0.92
1.89
0.94
2.16
1.06
0.98
0.98
0.95
1.00
0.96
2.80
7.11
5.81
5.69

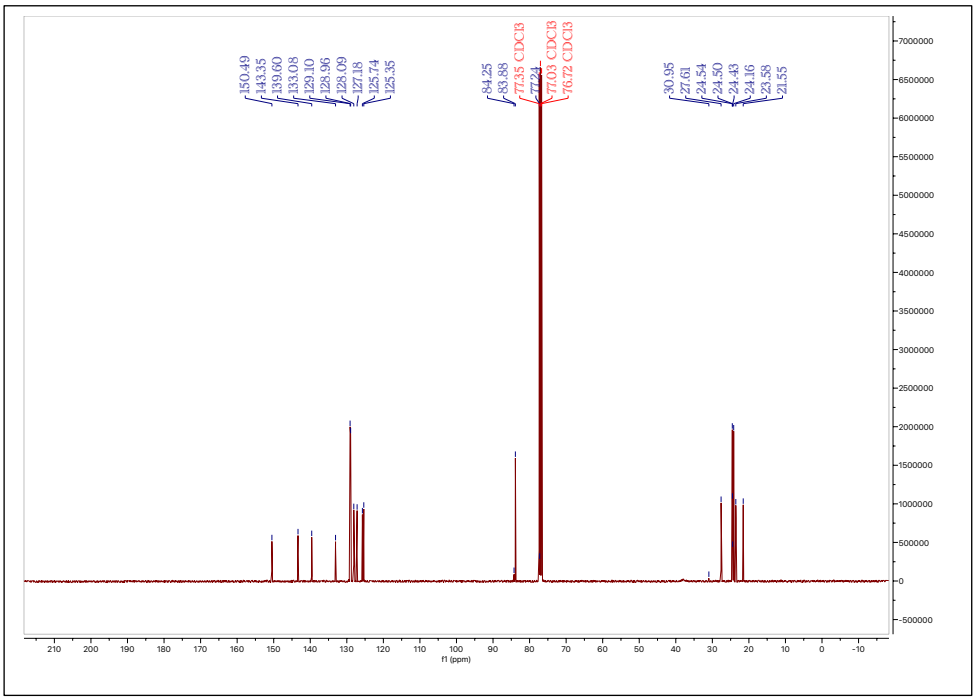
150.49
143.35
139.60
133.08
129.10
128.96
128.09
127.18
125.74
125.35
84.25
83.88
77.35 CDCl3
77.23
77.03 CDCl3
76.72 CDCl3
30.95
27.61
24.54
24.50
24.43
24.16
23.58
21.55
f1 (ppm)

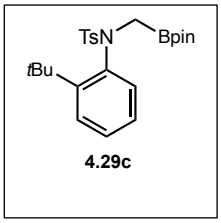
TsN
Bpin
tBu

4.29c

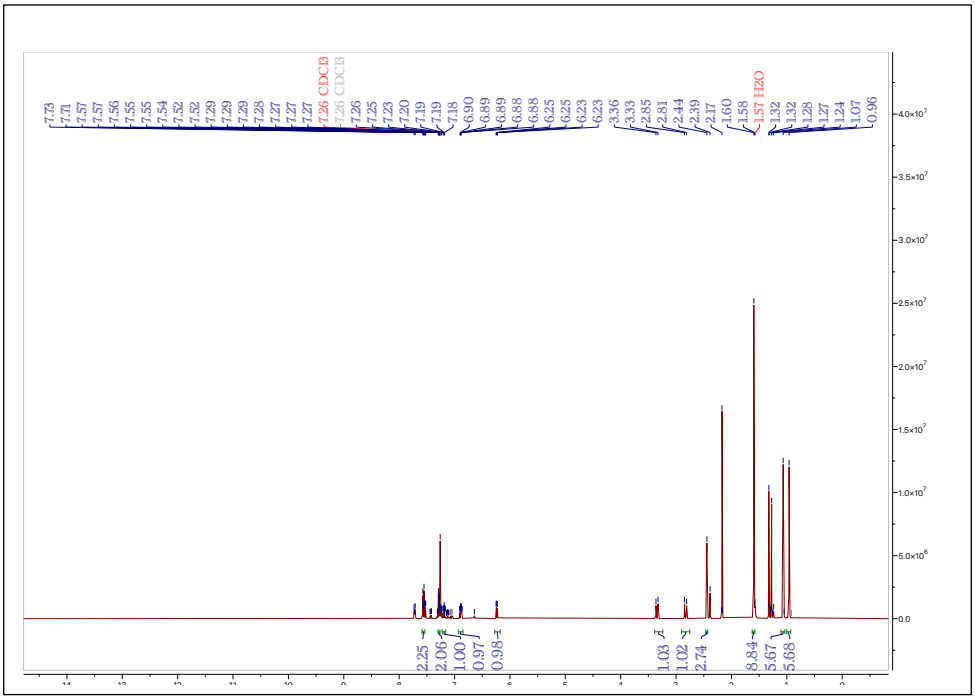
7.73
7.71
7.57
7.57
7.57
7.56
7.55
7.55
7.54
7.52
7.52
7.29
7.29
7.29
7.28
7.27
7.27
7.27
7.27
7.26 CDCl3
7.26 CDCl3
7.26
7.25
7.23
7.20
7.19
7.19
7.18
6.90
6.89
6.89
6.88
6.88
6.25
6.25
6.23
6.23
3.36
3.33
2.85
2.81
2.44
2.39
2.17
1.60
1.58
1.57 H2O
1.32
1.32
1.28
1.27
1.24
1.07
0.96
2.25
2.06
1.00
0.97
0.98
1.03
1.02
2.74
8.84
5.67
5.68

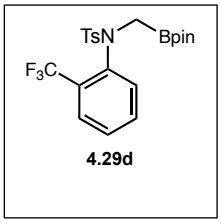

4.29d

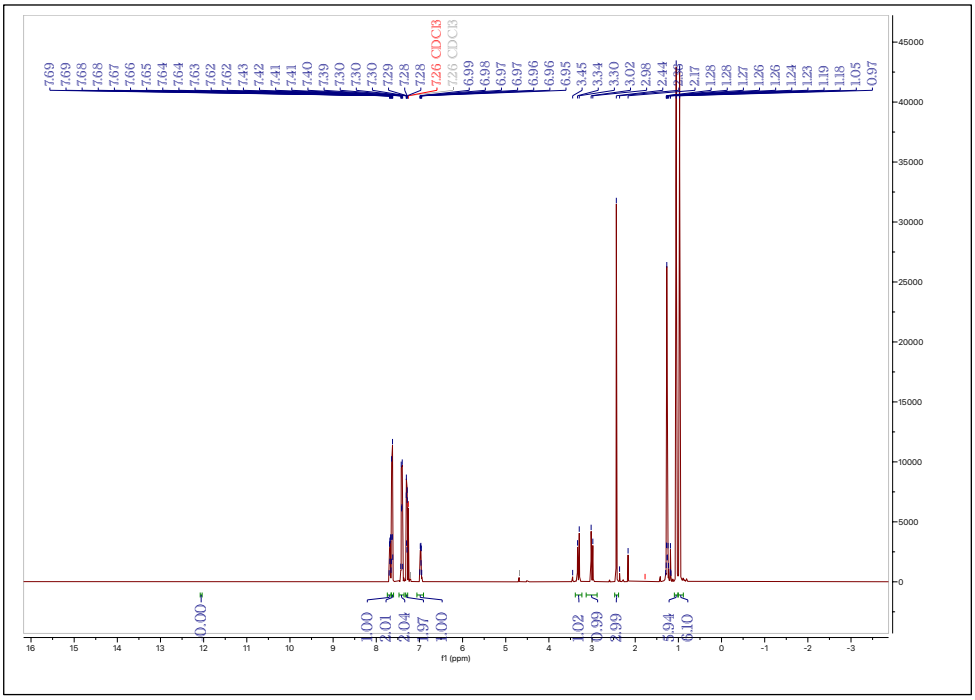

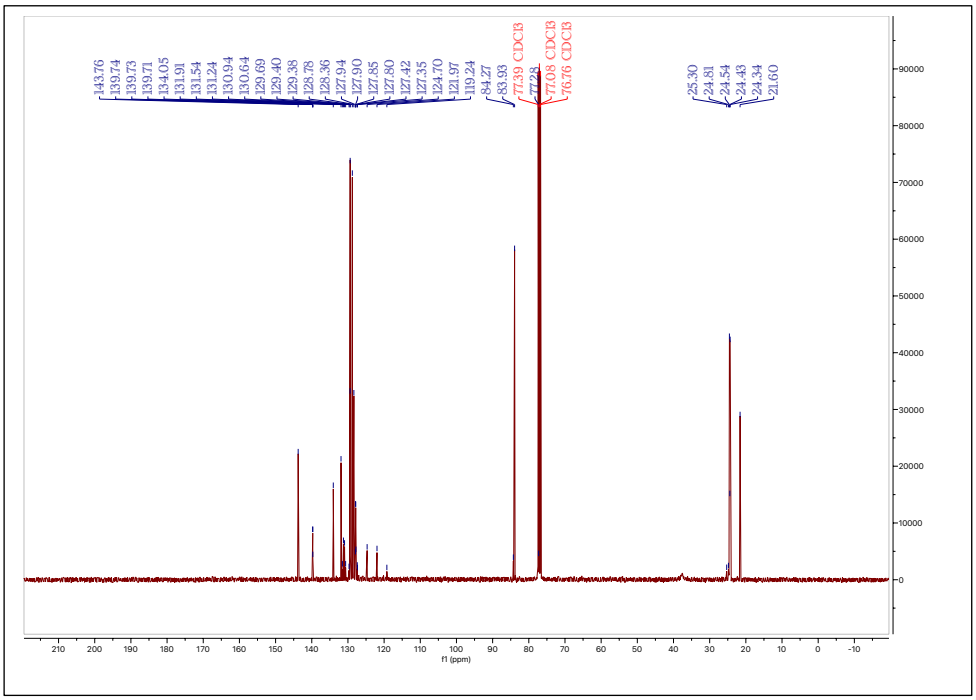

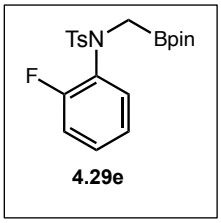
TsN
Bpin
F

4.29e

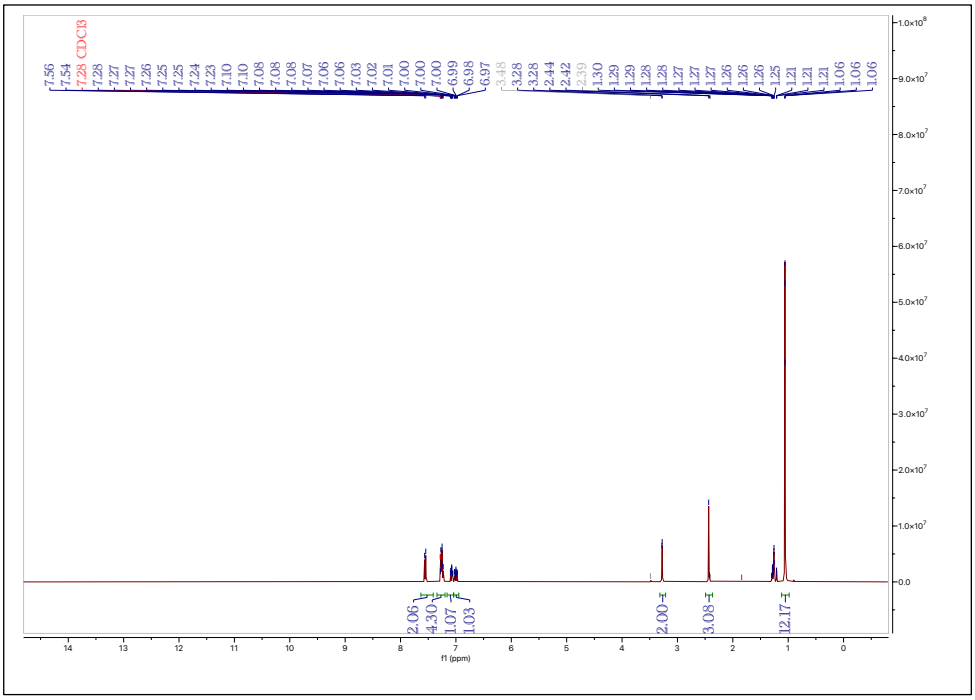
7.56
7.54
7.28 CDCl3
7.28
7.27
7.27
7.26
7.25
7.25
7.24
7.23
7.10
7.08
7.08
7.08
7.07
7.06
7.06
7.03
7.02
7.01
7.00
7.00
7.00
6.99
6.98
6.97
3.48
3.28
3.28
2.44
2.42
2.39
1.30
1.29
1.29
1.28
1.27
1.27
1.27
1.26
1.26
1.26
1.25
1.21
1.21
1.21
1.06
1.06
1.06
2.06
4.30
1.07
1.03
2.00
3.08
12.17
f1 (ppm)

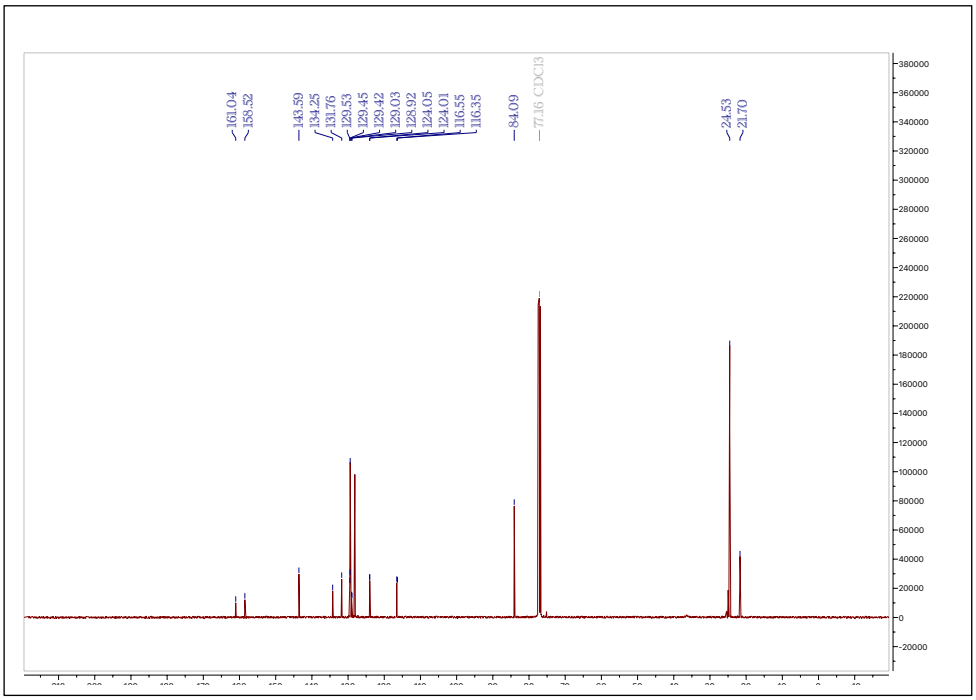
161.04
158.52
143.59
134.25
131.76
129.53
129.45
129.42
129.03
128.92
124.05
124.01
116.55
116.35
84.09
77.16 CDCl3
24.53
21.70

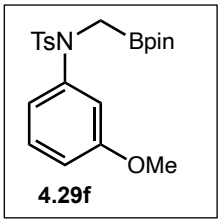
TsN
Bpin
OMe

4.29f

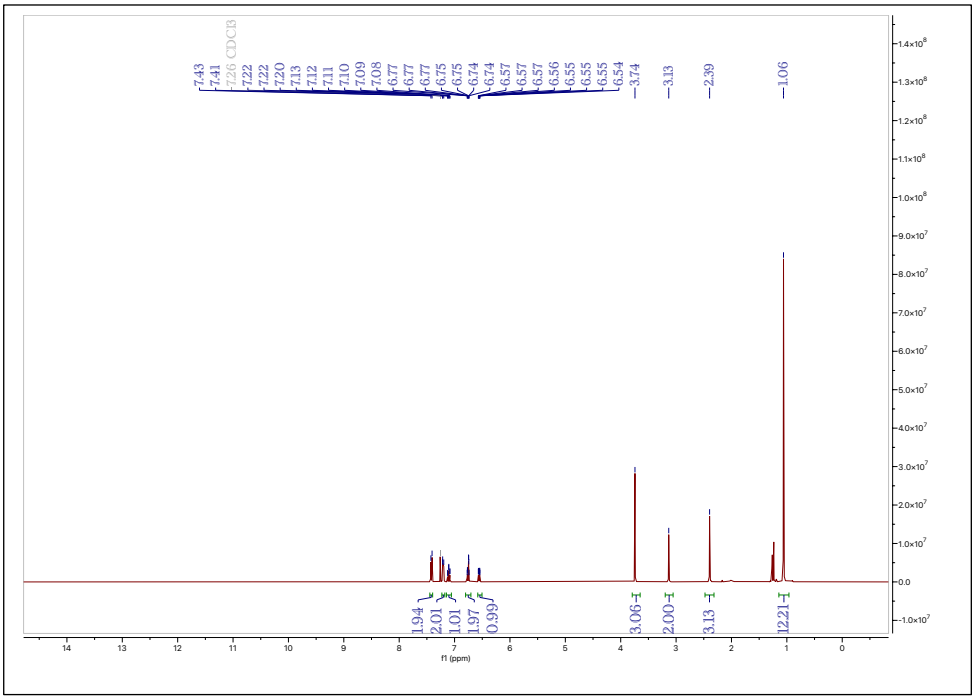
7.43
7.41
7.26 CDCl3
7.22
7.22
7.20
7.13
7.12
7.11
7.10
7.09
7.08
6.77
6.77
6.77
6.75
6.75
6.74
6.74
6.57
6.57
6.57
6.56
6.55
6.55
6.55
6.54
3.74
3.13
2.39
1.06
1.94
2.01
1.01
1.97
0.99
3.06
2.00
3.13
12.21
f1 (ppm)

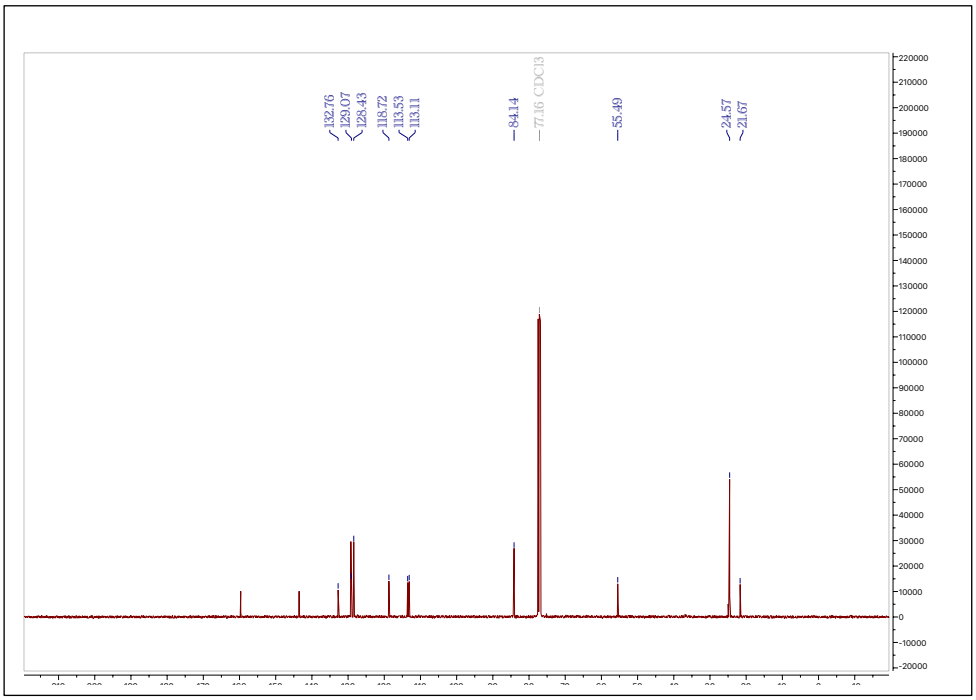
132.76
129.07
128.43
118.72
113.53
113.11
84.14
77.16 CDCl3
55.49
24.57
21.67

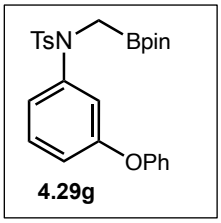
TsN
Bpin
OPh

4.29g

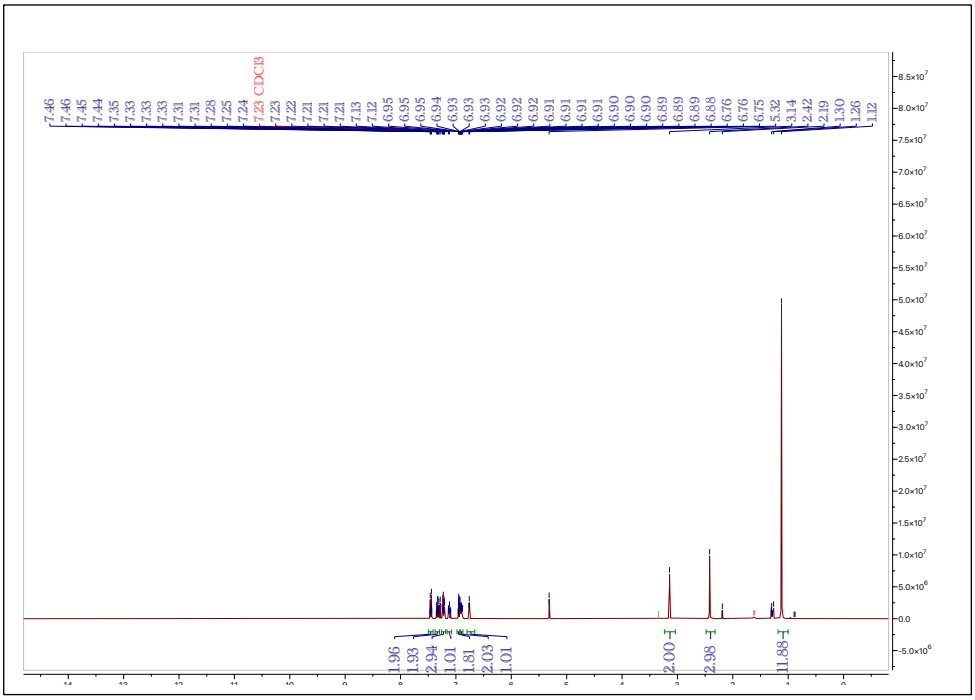
7.46
7.46
7.45
7.44
7.35
7.33
7.33
7.33
7.31
7.31
7.28
7.25
7.24
7.23 CDCl3
7.23
7.22
7.21
7.21
7.21
7.13
7.12
6.95
6.95
6.95
6.94
6.93
6.93
6.93
6.92
6.92
6.92
6.91
6.91
6.91
6.91
6.90
6.90
6.90
6.89
6.89
6.89
6.88
6.76
6.76
6.75
5.32
3.14
2.42
2.19
1.30
1.26
1.12
1.96
1.93
2.94
1.01
1.81
2.03
1.01
2.00
2.98
11.88

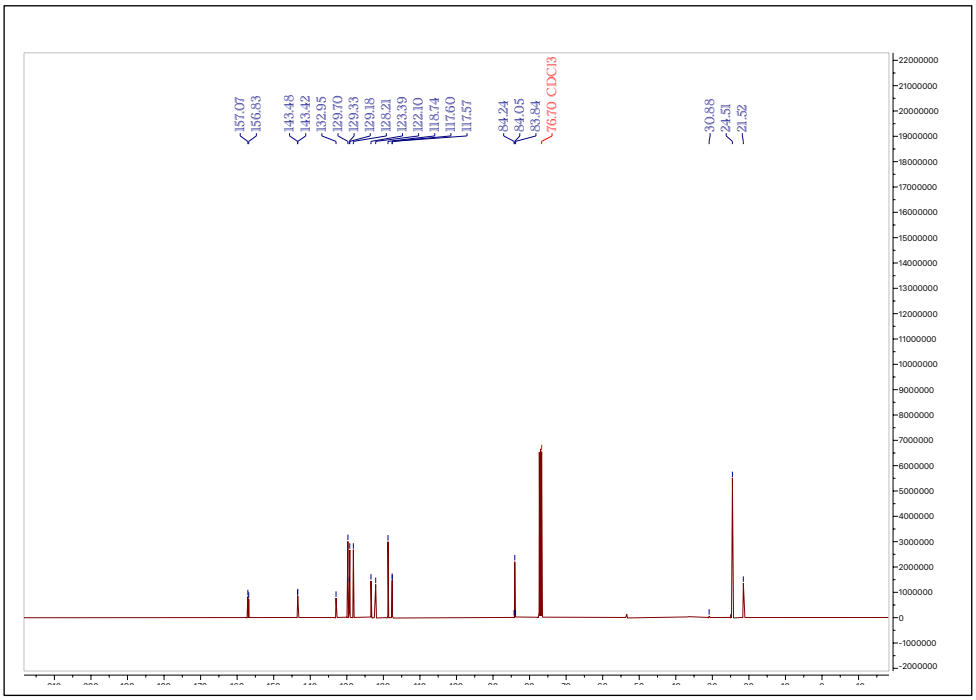
157.07
156.83
143.48
143.42
132.95
129.70
129.33
129.18
128.21
123.39
122.10
118.74
117.60
117.57
84.24
84.05
83.84
76.70 CDCl3
30.88
24.51
21.52

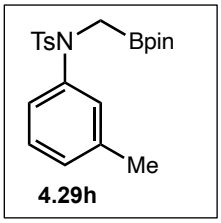
TsN
Bpin
Me

4.29h

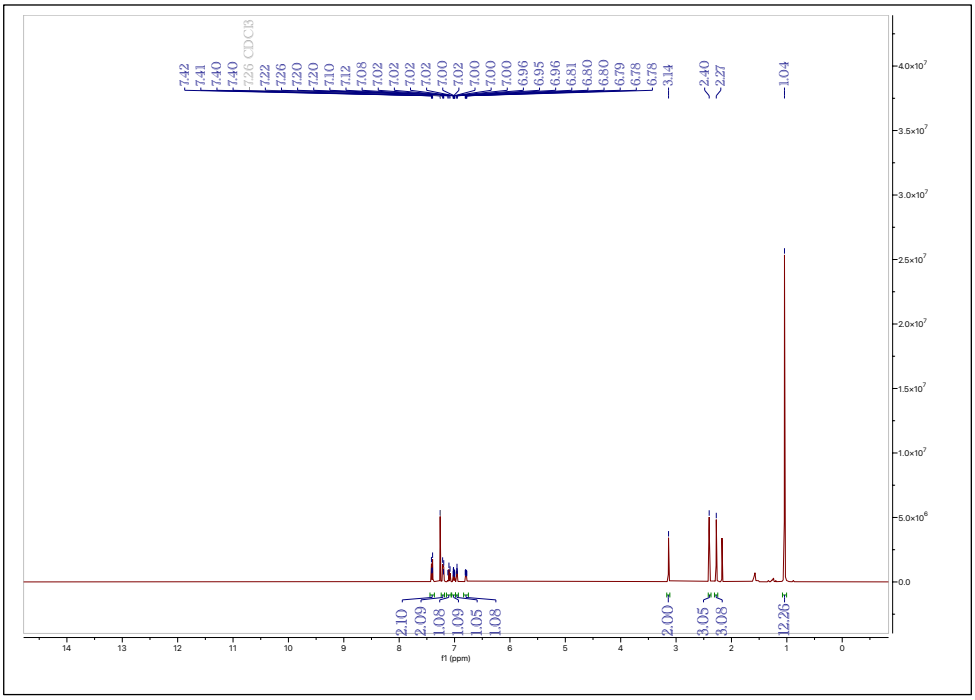
7.42
7.41
7.40
7.40
7.26 CDCl3
7.22
7.26
7.20
7.20
7.10
7.12
7.08
7.02
7.02
7.02
7.02
7.00
7.02
7.00
7.00
7.00
6.96
6.95
6.96
6.81
6.80
6.80
6.79
6.78
6.78
3.14
2.40
2.27
1.04
2.10
2.09
1.08
1.09
1.05
1.08
2.00
3.05
3.08
12.26
f1 (ppm)

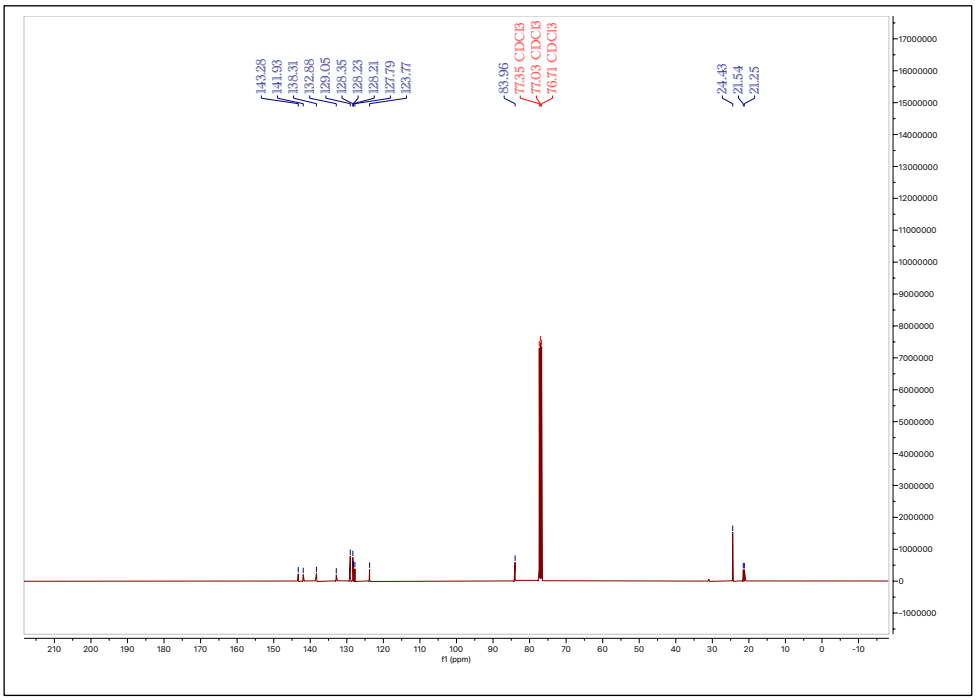
143.29
141.93
138.31
132.88
129.05
128.35
128.23
128.21
127.79
123.77
83.96
77.35 CDCl3
77.03 CDCl3
76.71 CDCl3
24.43
21.54
21.25
f1 (ppm)

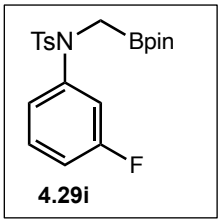
TsN
Bpin
F

4.29i

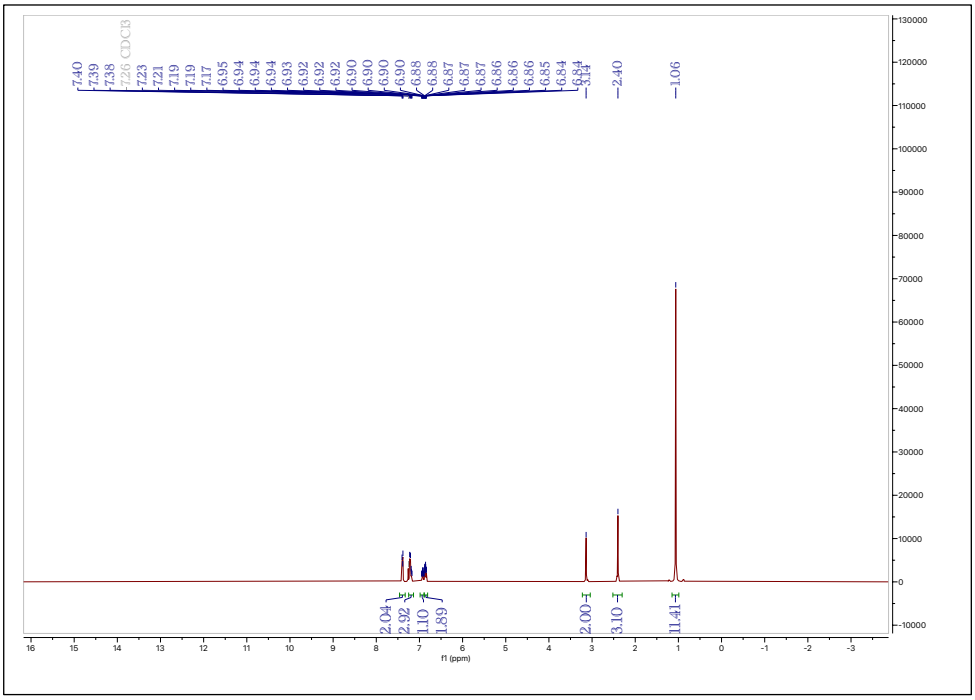
7.40
7.39
7.38
7.26 CDCl3
7.23
7.21
7.19
7.19
7.17
6.95
6.94
6.94
6.94
6.93
6.92
6.92
6.92
6.90
6.90
6.90
6.90
6.88
6.88
6.87
6.87
6.87
6.86
6.86
6.86
6.85
6.84
6.84
3.44
2.40
1.06
2.04
2.92
1.10
1.89
2.00
3.10
11.41
f1 (ppm)

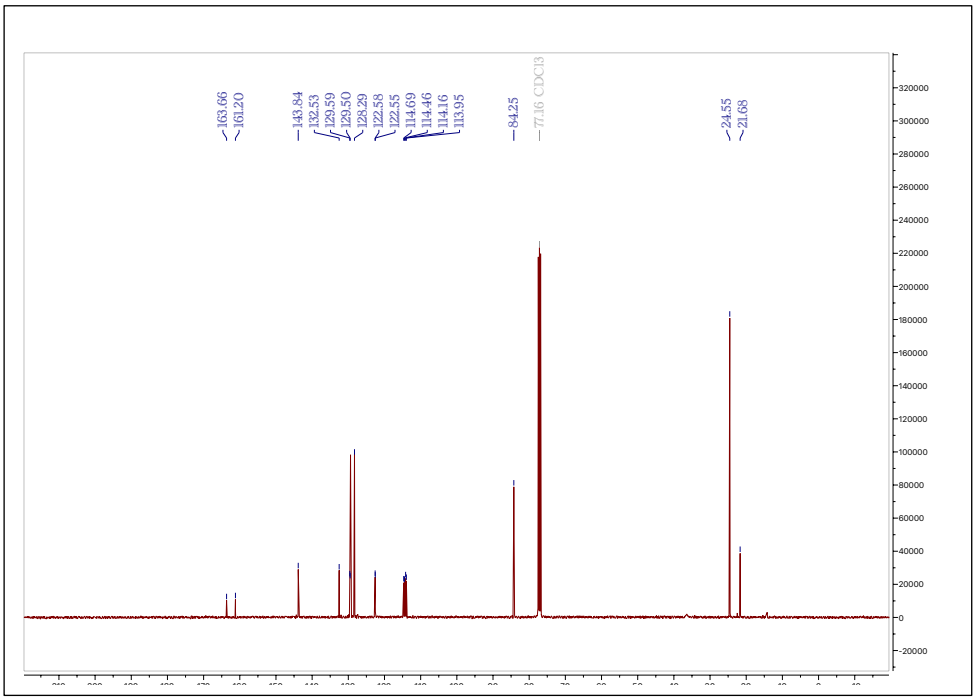
163.66
161.20
143.84
132.53
129.59
129.50
128.29
122.58
122.55
114.69
114.46
114.16
113.95
84.25
77.16 CDCl3
24.55
21.68

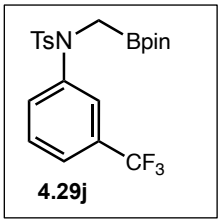
TsN
Bpin
CF3

4.29j

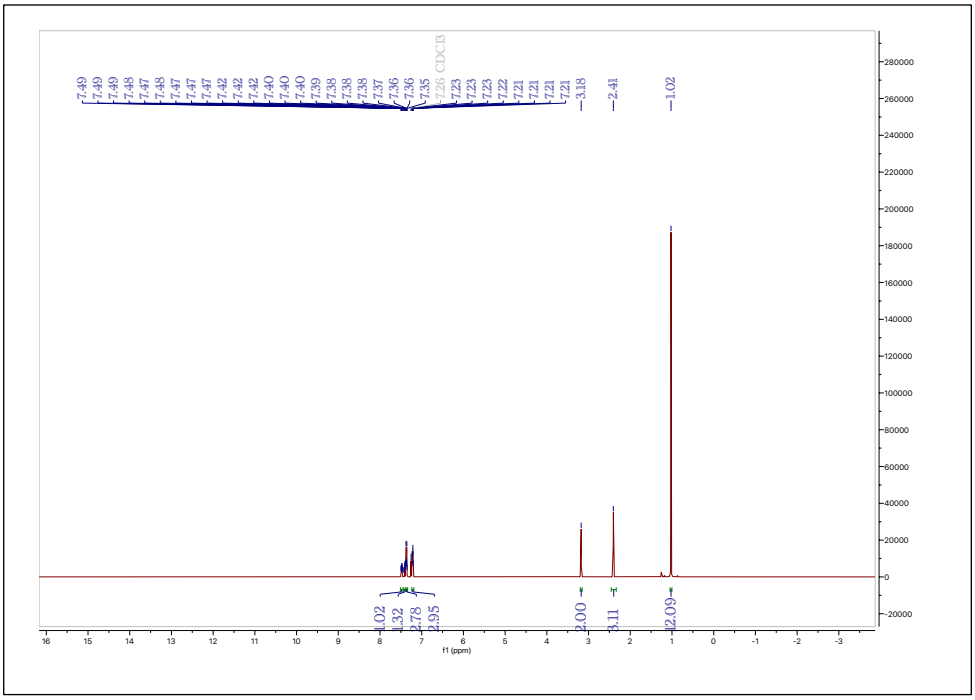
7.49
7.49
7.49
7.48
7.47
7.48
7.47
7.47
7.47
7.42
7.42
7.42
7.40
7.40
7.40
7.39
7.38
7.38
7.38
7.37
7.36
7.36
7.35
7.26 CDCl3
7.23
7.23
7.23
7.22
7.21
7.21
7.21
7.21
3.18
2.41
1.02
1.02
1.32
2.78
2.95
2.00
3.11
12.09
f1 (ppm)

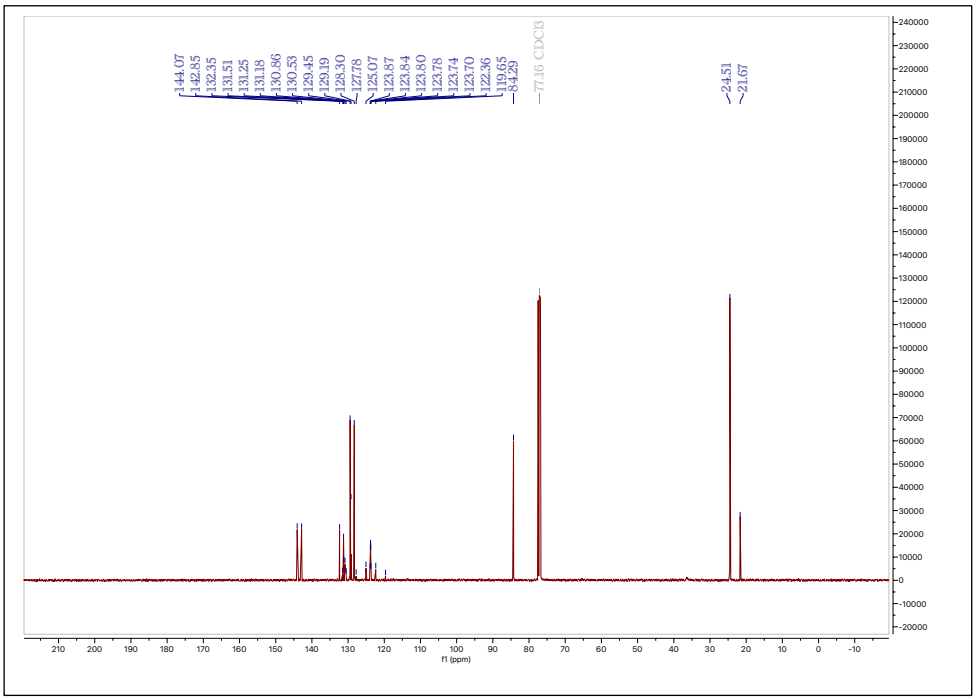
144.07
142.85
132.35
131.51
131.25
131.18
130.86
130.53
129.45
129.19
128.30
127.78
125.07
123.87
123.84
123.80
123.78
123.74
123.70
122.36
119.65
84.29
77.16 CDCl3
24.51
21.67
f1 (ppm)

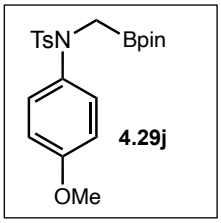
TsN
Bpin
4.29j
OMe

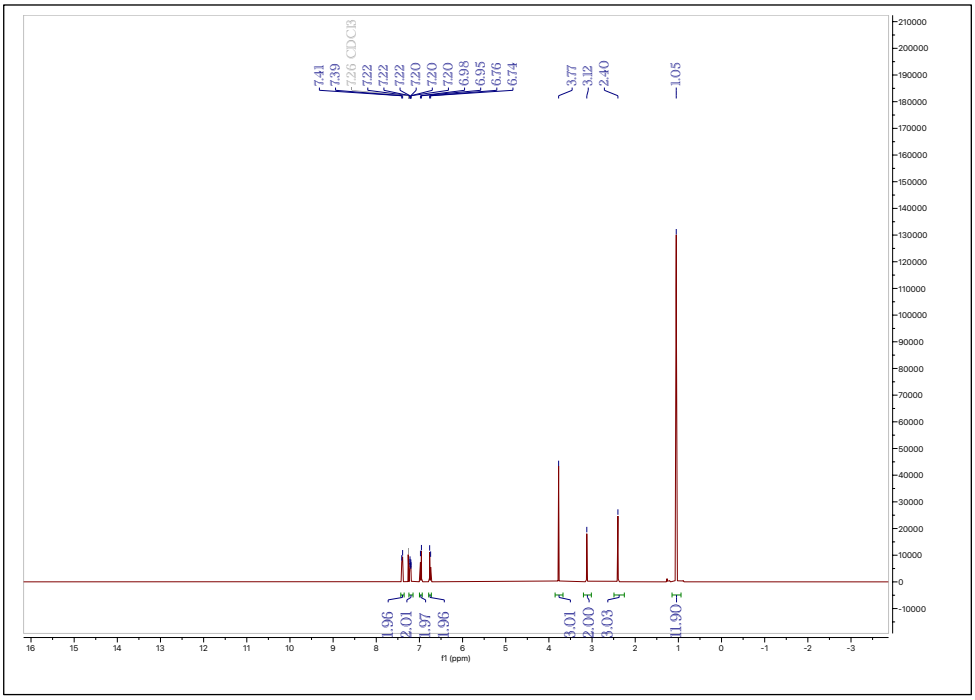
7.41
7.39
7.26 CDCl3
7.22
7.22
7.22
7.20
7.20
7.20
6.98
6.95
6.76
6.74
3.77
3.12
2.40
1.05
1.96
2.01
1.97
1.96
3.01
2.00
3.03
11.90
f1 (ppm)

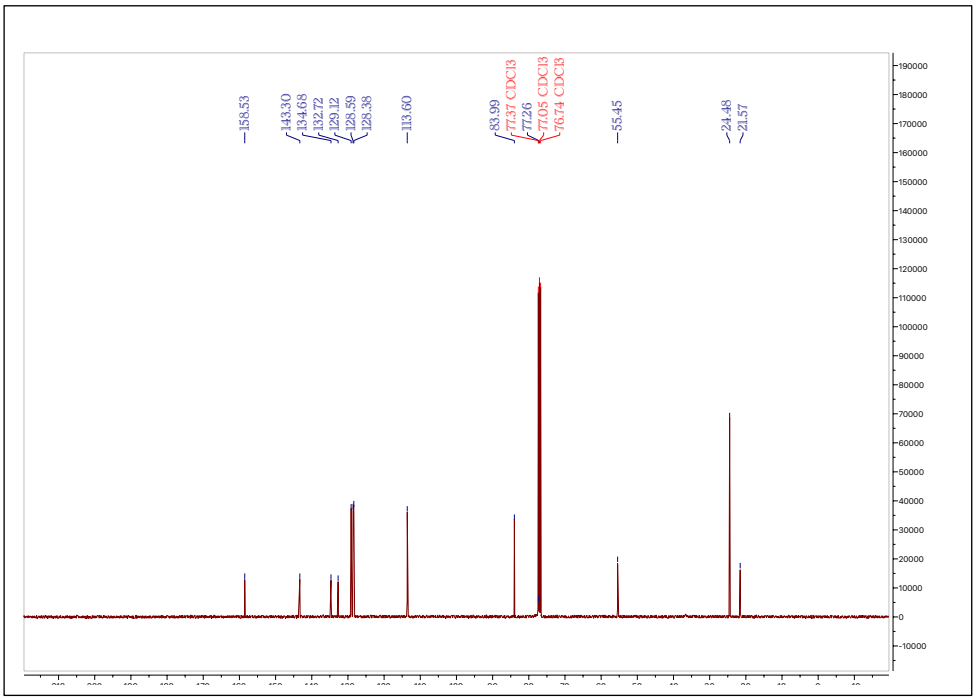
158.53
143.30
134.68
132.72
129.12
128.59
128.38
113.60
83.99
77.37 CDCl3
77.26
77.05 CDCl3
76.74 CDCl3
55.45
24.48
21.57

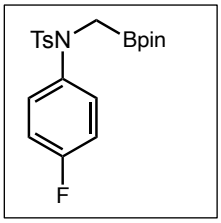
TsN
Bpin
F

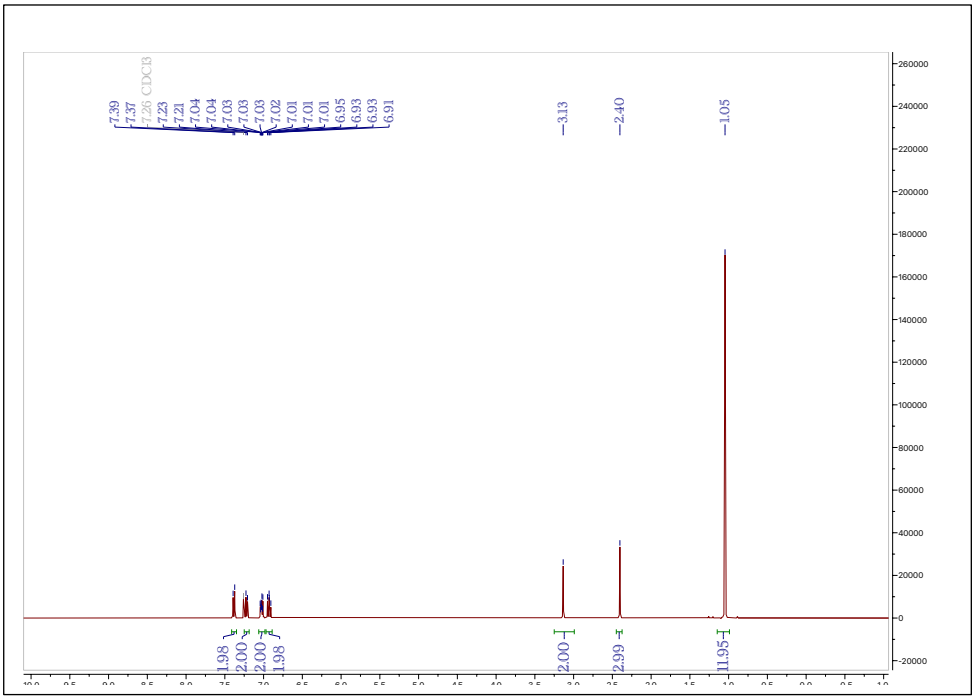
7.39
7.37
7.26 CDCl3
7.23
7.21
7.04
7.04
7.03
7.03
7.03
7.02
7.01
7.01
7.01
6.95
6.93
6.93
6.91
3.13
2.40
1.05
1.98
2.00
2.00
1.98
2.00
2.99
11.95

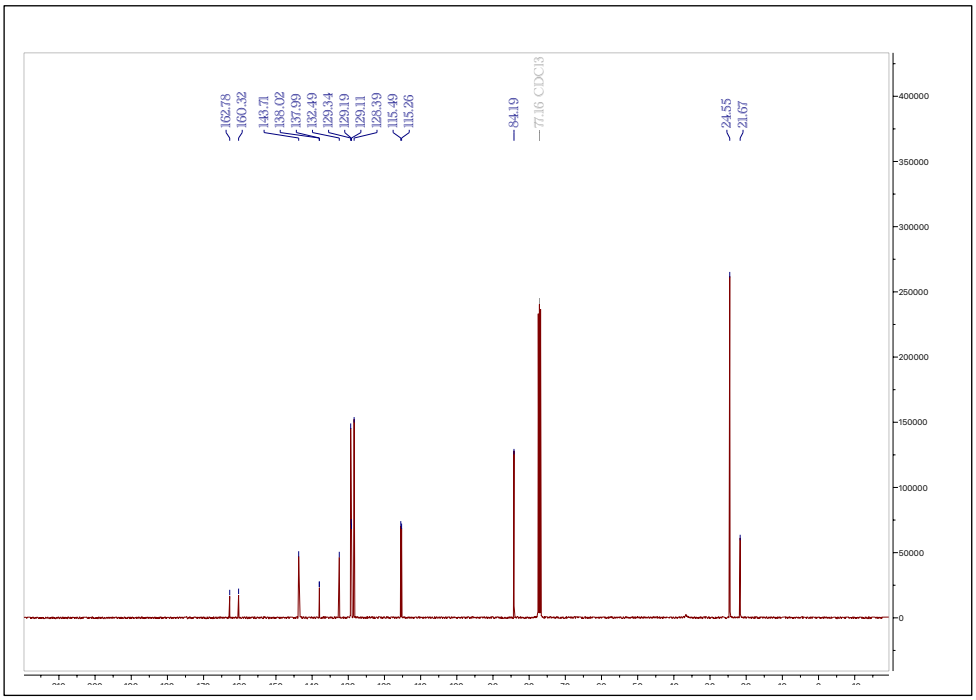
162.78
160.32
143.71
138.02
137.99
132.49
129.34
129.19
129.11
128.39
115.49
115.26
84.19
77.16 CDCl3
24.55
21.67

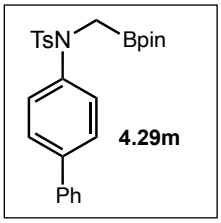
TsN
Bpin
4.29m
Ph

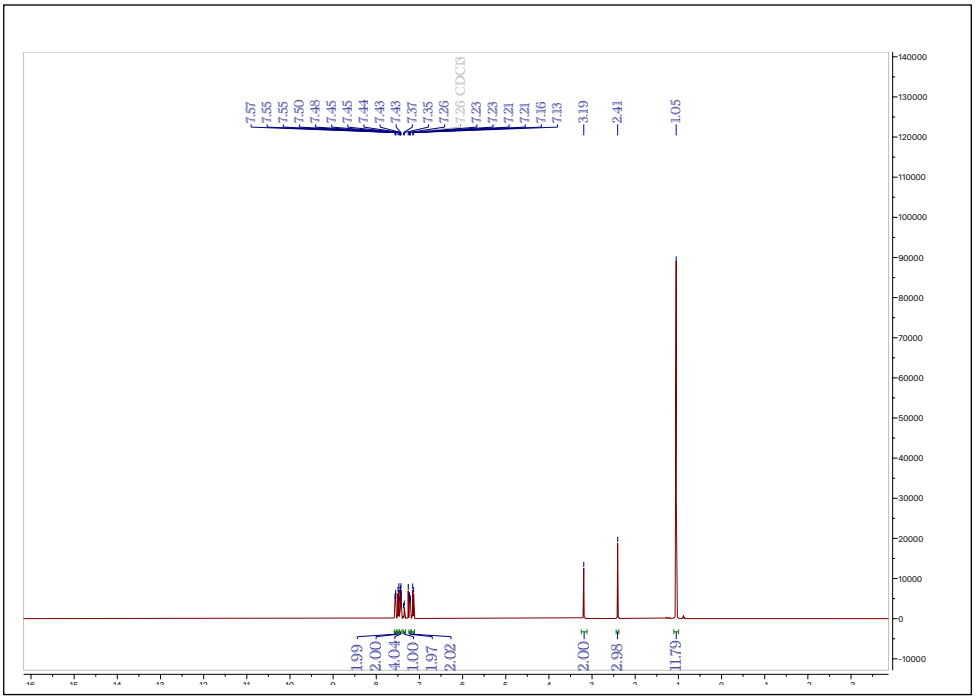
7.57
7.55
7.55
7.50
7.48
7.45
7.45
7.44
7.43
7.43
7.37
7.35
7.26
7.26 CDCl3
7.23
7.23
7.21
7.21
7.16
7.13
3.19
2.41
1.05
1.99
2.00
4.04
1.00
1.97
2.02
2.00
2.98
11.79

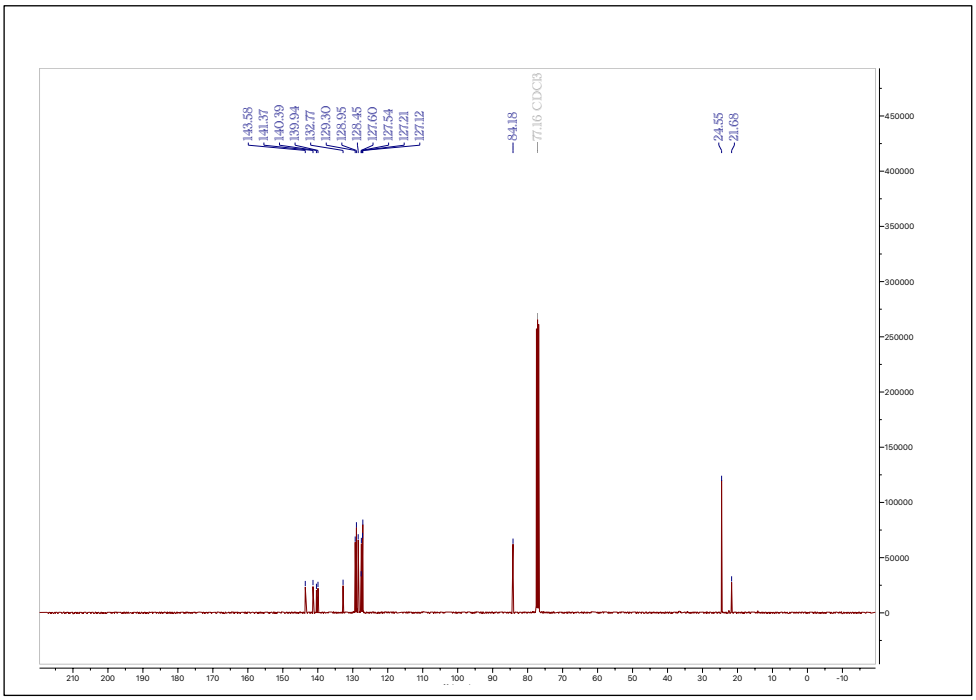
143.58
141.37
140.39
139.94
132.77
129.30
128.95
128.45
127.60
127.54
127.21
127.12
84.18
77.16 CDCl3
24.55
21.68

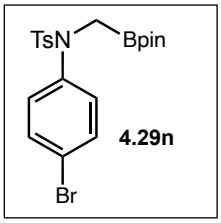
TsN
Bpin
Br

4.29n

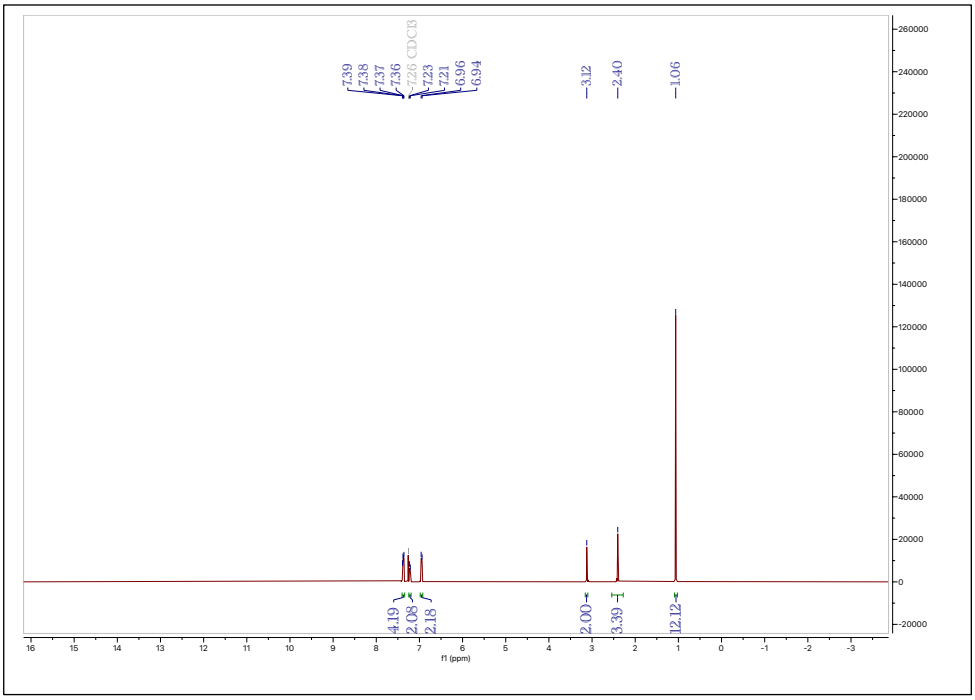
7.39
7.38
7.37
7.36
7.26 CDCl3
7.23
7.21
6.96
6.94
3.12
2.40
1.06
4.19
2.08
2.18
2.00
3.39
12.12
f1 (ppm)

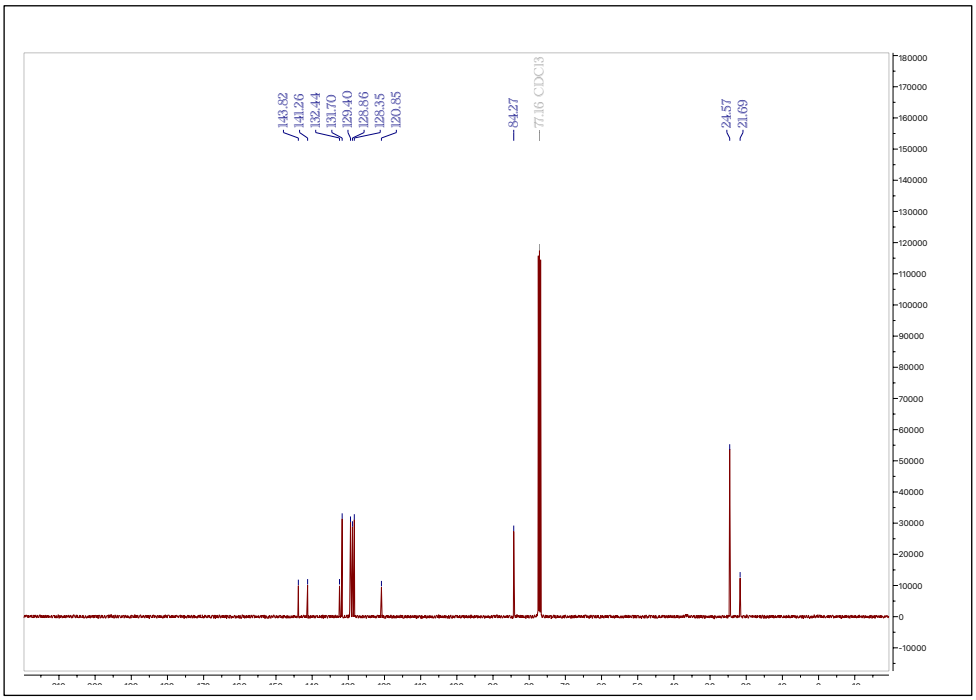
143.82
141.26
132.44
131.70
129.40
128.86
128.35
120.85
84.27
77.16 CDCl3
24.57
21.69

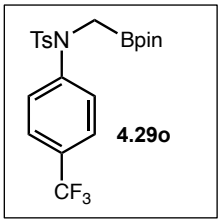
TsN
Bpin
4.29o
CF3

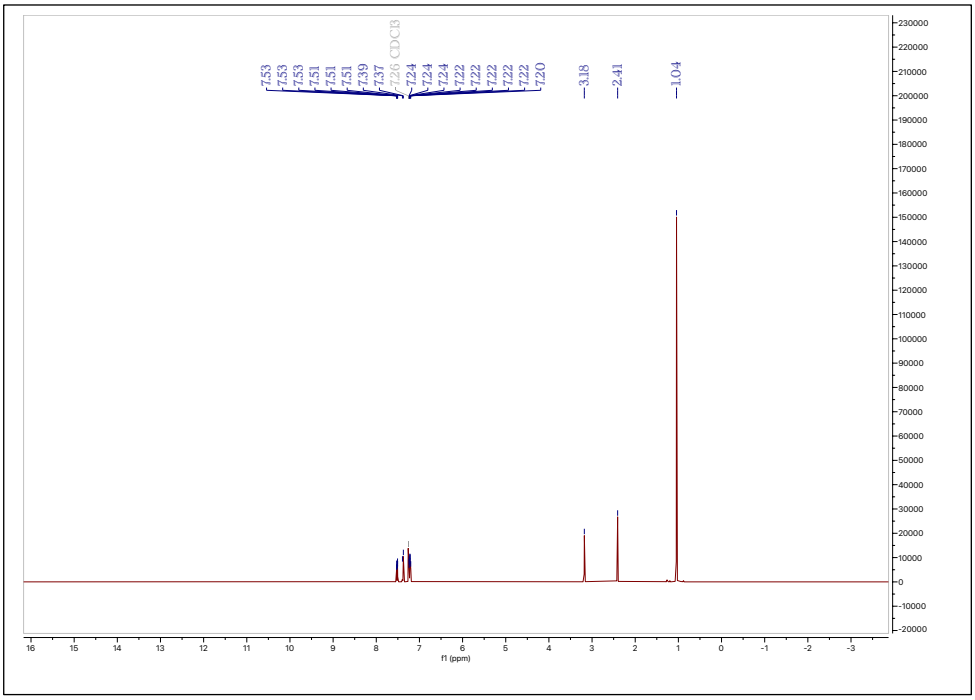
7.53
7.53
7.53
7.51
7.51
7.51
7.39
7.31
7.26 CDCl3
7.24
7.24
7.24
7.22
7.22
7.22
7.22
7.20
3.18
2.41
1.04
f1 (ppm)

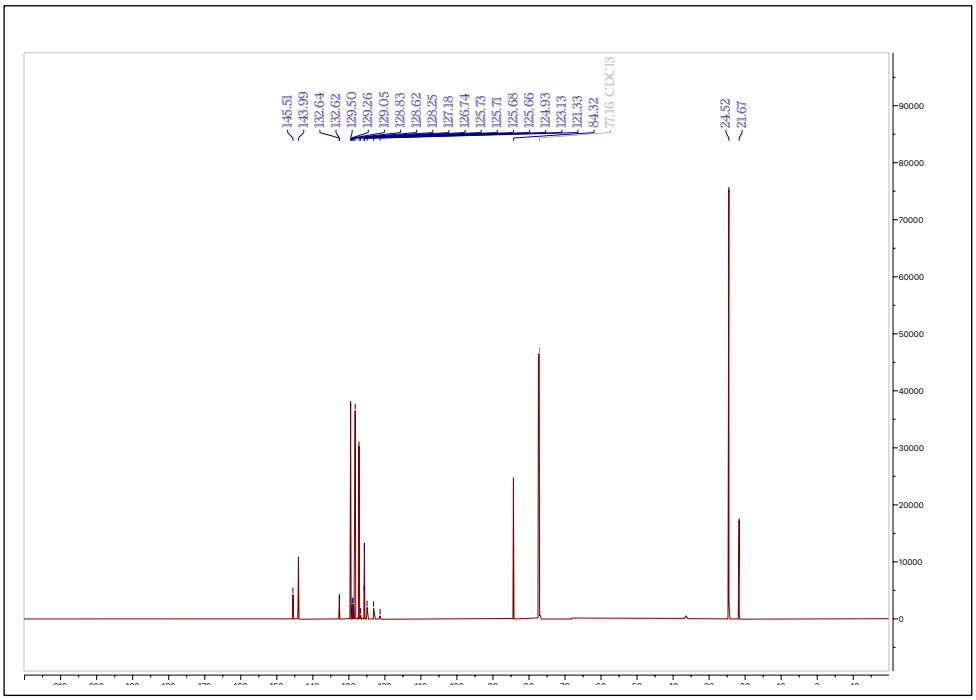
145.51
143.99
132.64
132.62
129.50
129.26
129.05
128.83
128.62
128.25
127.18
126.74
125.73
125.71
125.68
125.66
124.93
123.13
121.33
84.32
77.16 CDCl3
24.52
21.67

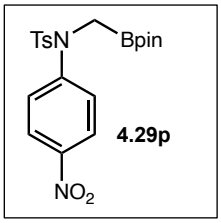
TsN
Bpin
4.29p
NO2

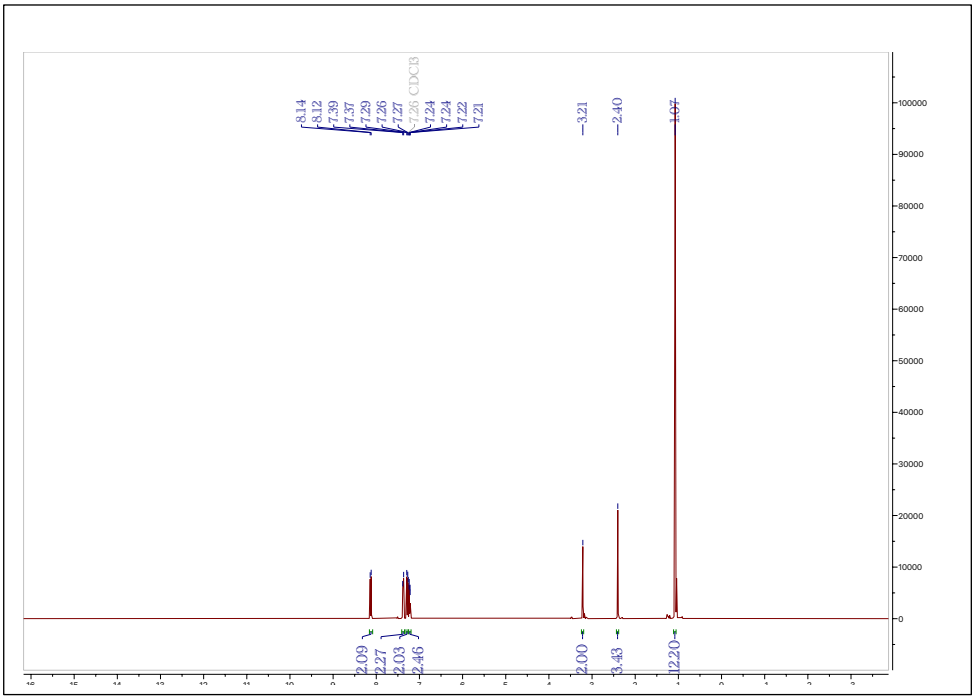
8.14
8.12
7.39
7.37
7.29
7.26
7.27
7.26 CDCl3
7.24
7.24
7.22
7.21
3.21
2.40
1.07
2.09
2.27
2.03
2.46
2.00
3.43
12.20

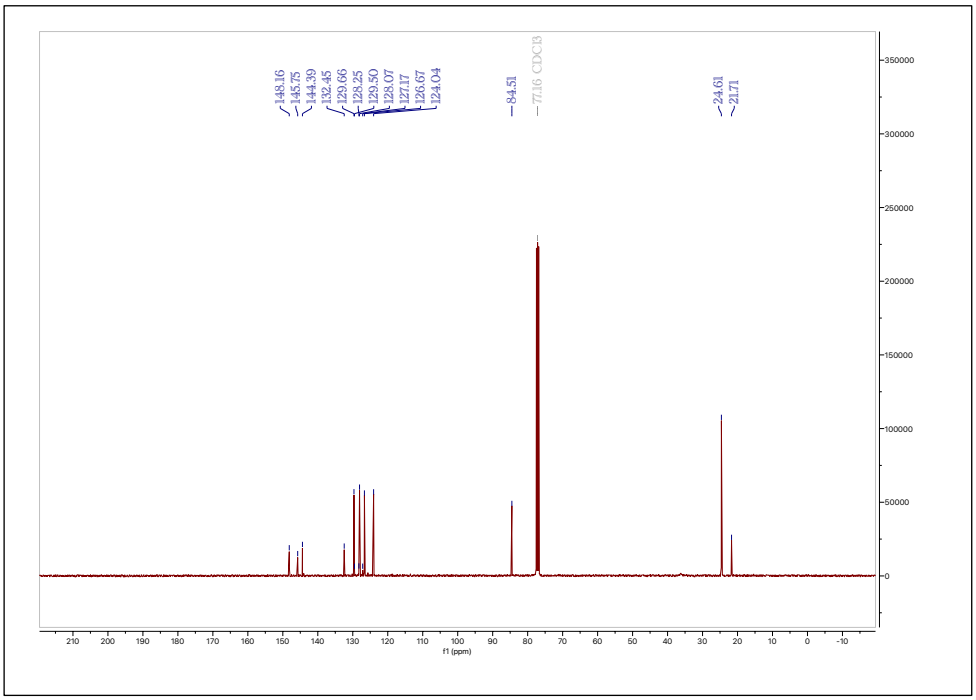
148.16
145.75
144.39
132.45
129.66
128.25
129.50
128.07
127.17
126.67
124.04
84.51
77.16 CDCl3
24.61
21.71
f1 (ppm)

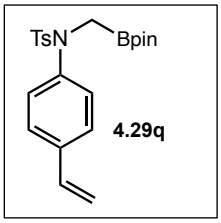
TsN
Bpin
4.29q

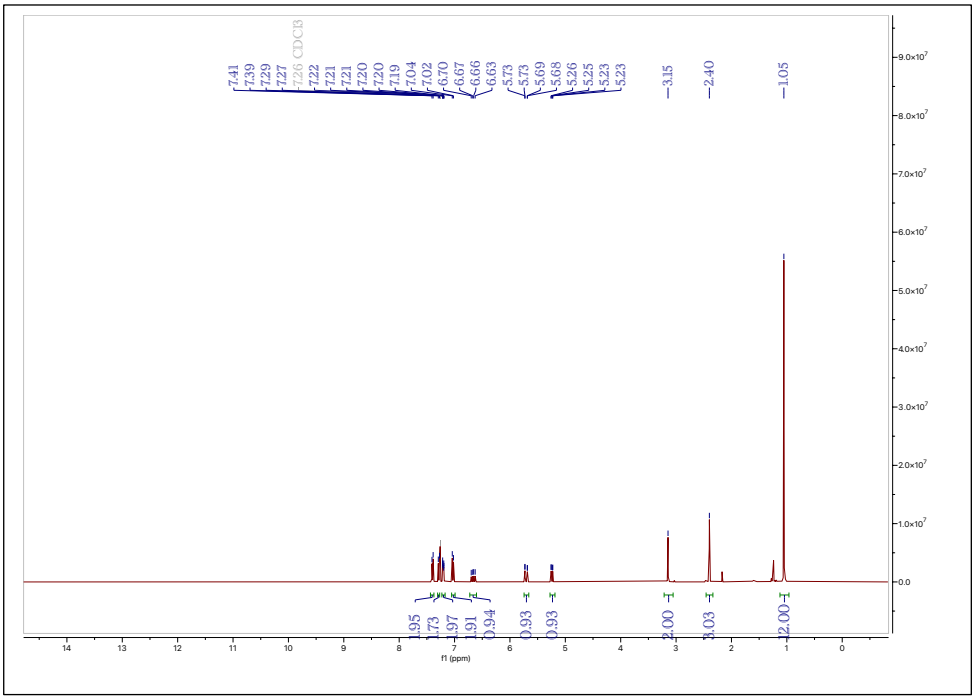
7.41
7.39
7.29
7.27
7.26 CDCl3
7.22
7.21
7.21
7.20
7.20
7.19
7.04
7.02
6.70
6.67
6.66
6.63
5.73
5.73
5.69
5.68
5.26
5.25
5.23
5.23
3.15
2.40
1.05
1.95
1.73
3.97
1.91
0.94
0.93
0.93
2.00
3.03
12.00
f1 (ppm)

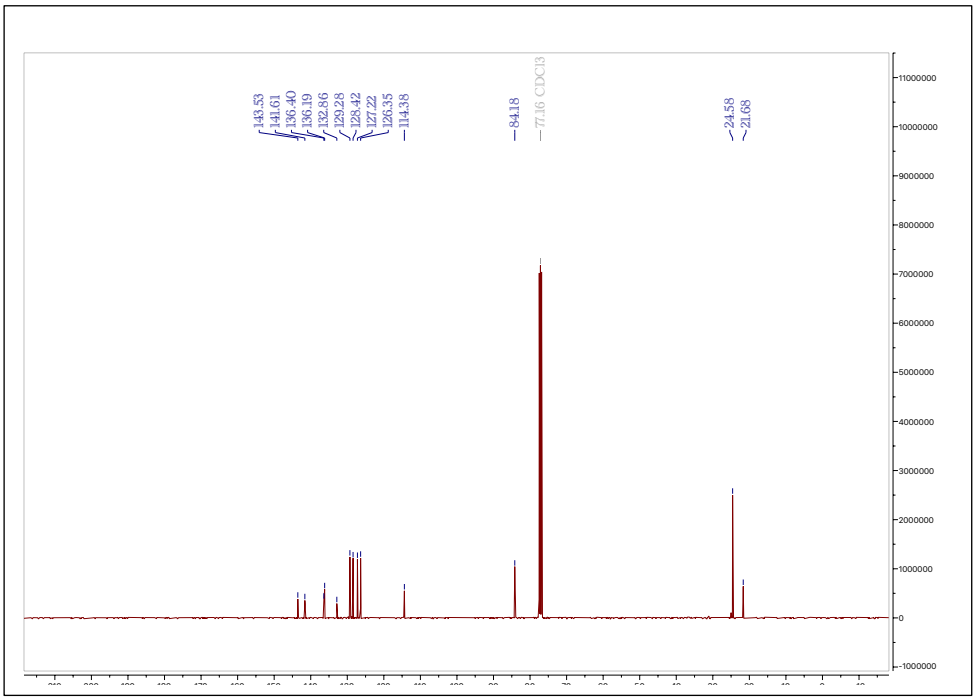
143.53
141.61
136.40
136.19
132.86
129.28
128.42
127.22
126.35
114.38
84.18
77.16 CDCl3
24.58
21.68

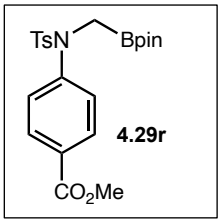
TsN
Bpin
4.29r
CO2Me

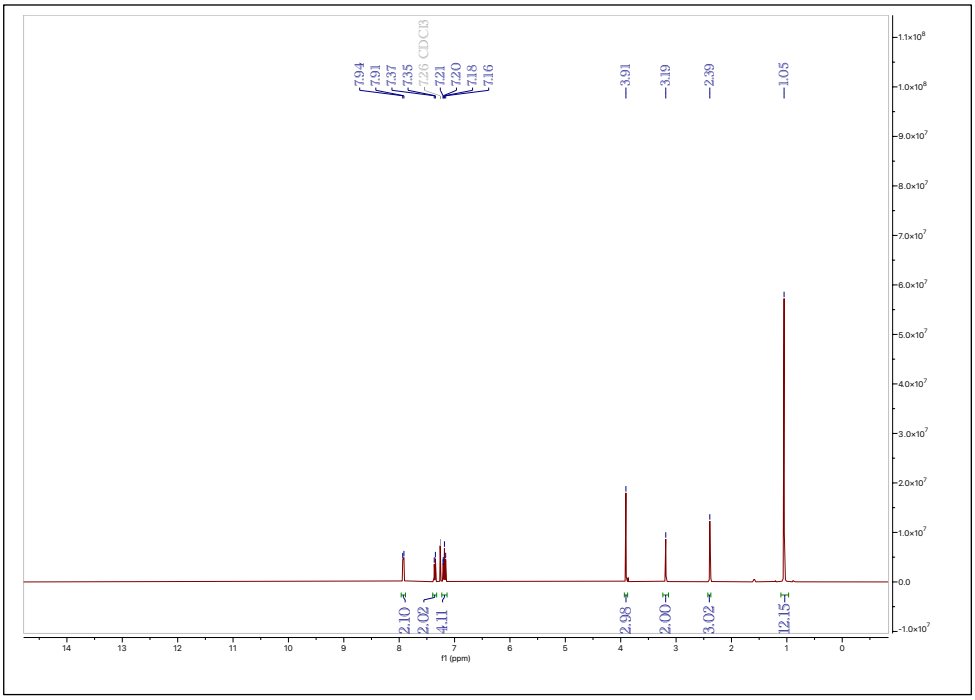
7.94
7.91
7.37
7.35
7.26 CDCl3
7.21
7.20
7.18
7.16
3.91
3.19
2.39
1.05
2.10
2.02
4.11
2.98
2.00
3.02
12.15
f1 (ppm)

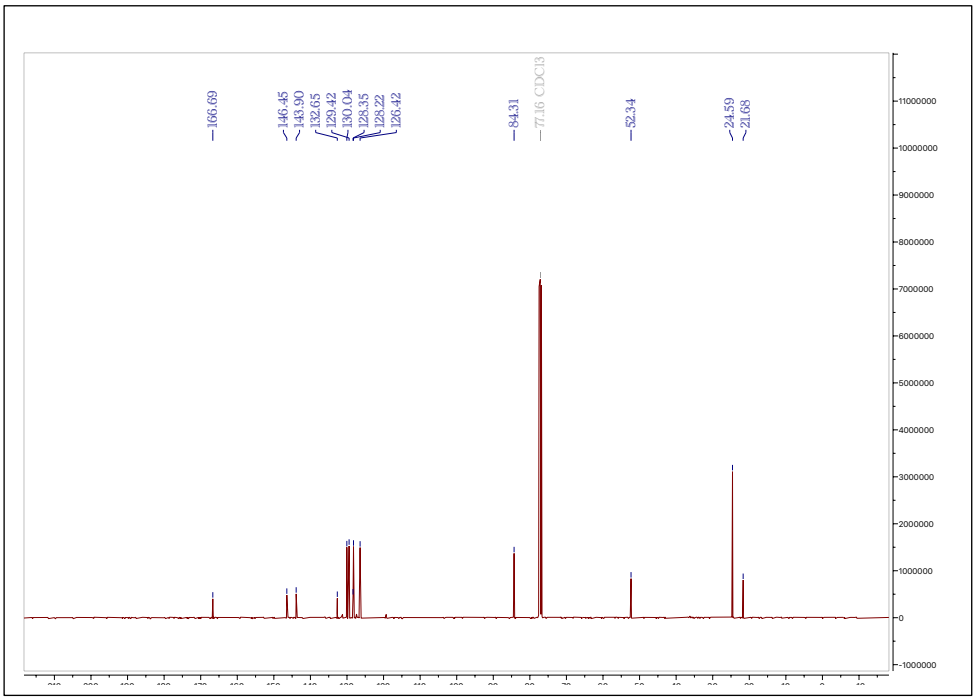
166.69
146.45
143.90
132.65
129.42
130.04
128.35
128.22
126.42
84.31
77.16 CDCl3
52.34
24.59
21.68

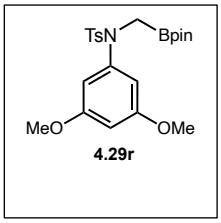
TsN
Bpin
MeO
OMe

4.29r

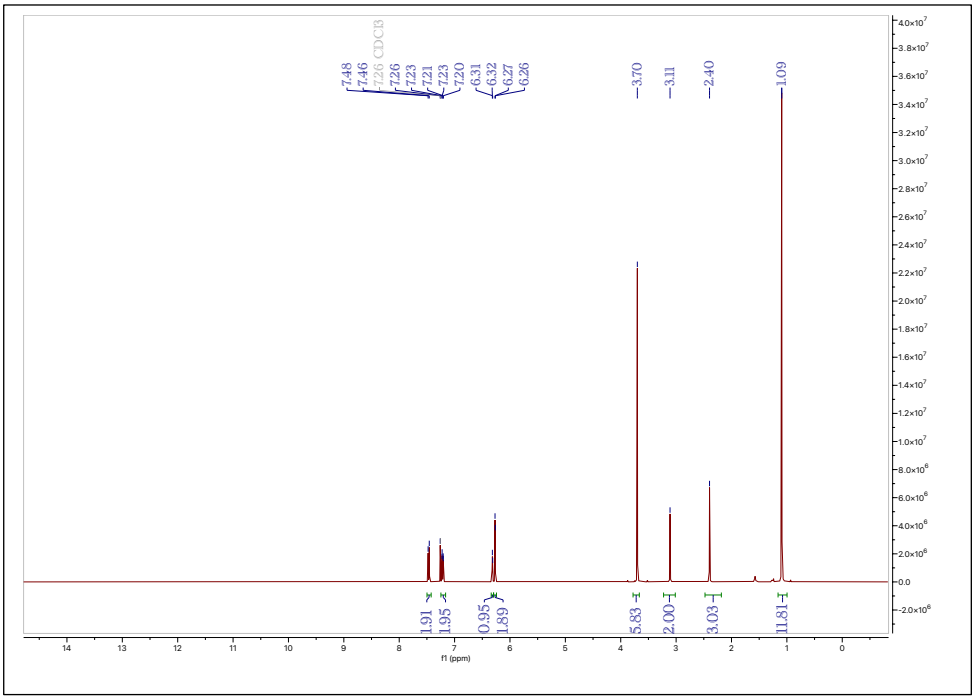
7.48
7.46
7.26 CDCl3
7.26
7.23
7.21
7.23
7.20
6.31
6.32
6.27
6.26
3.70
3.11
2.40
1.09
1.91
1.95
0.95
1.89
5.83
2.00
3.03
11.81
f1 (ppm)

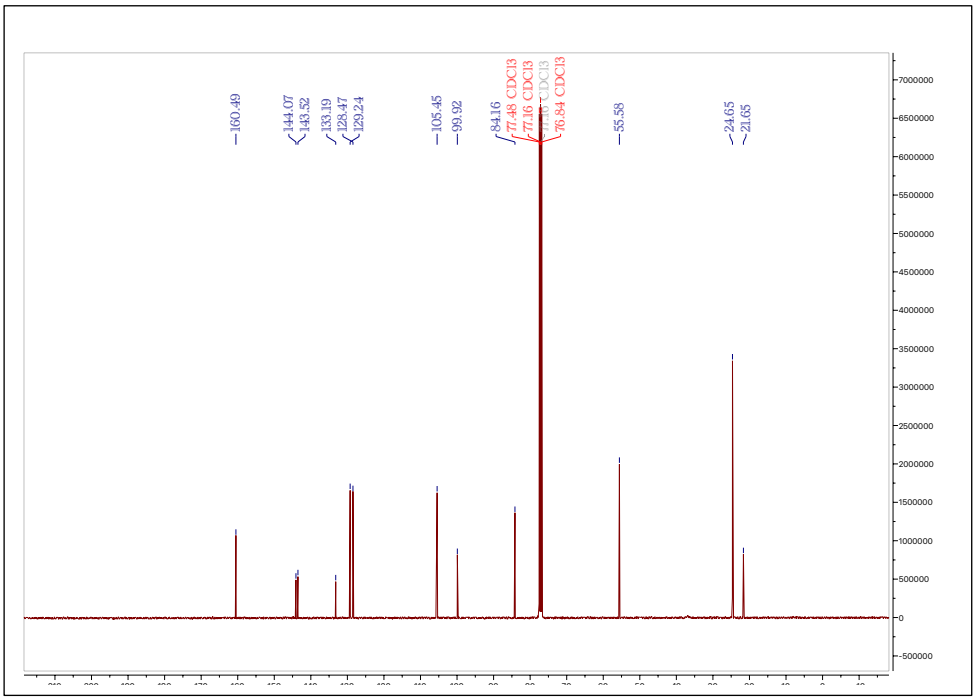
160.49
144.07
143.52
133.19
128.47
129.24
105.45
99.92
84.16
77.48 CDCl3
77.16 CDCl3
76.84 CDCl3
55.58
24.65
21.65

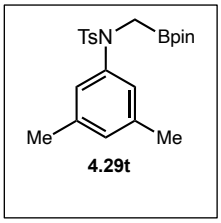
TsN
Bpin
Me
Me

4.29t

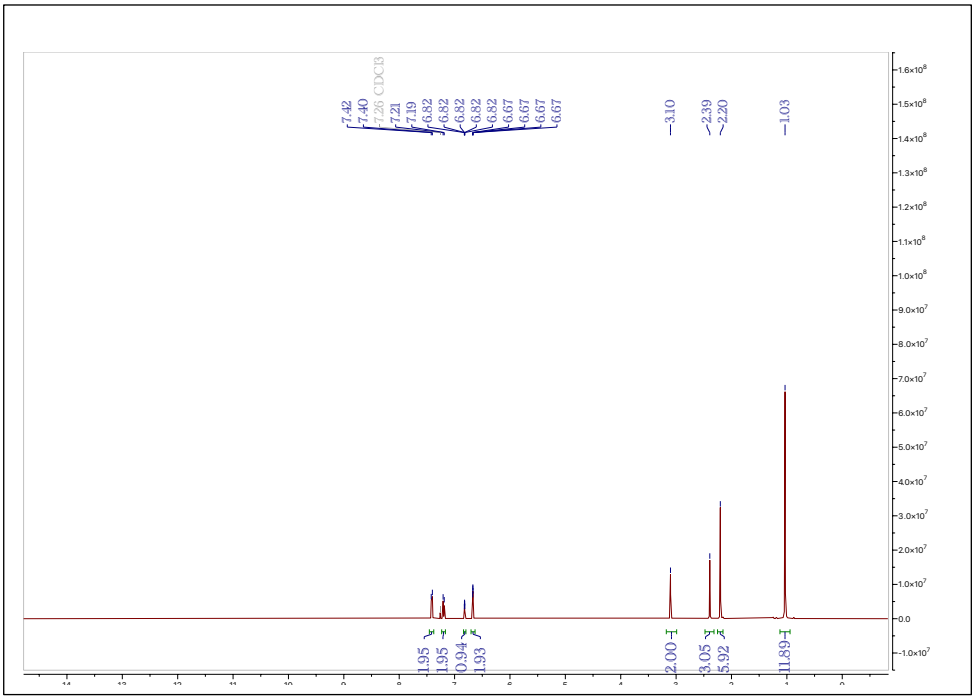
7.42
7.40
7.26 CDCl3
7.21
7.19
6.82
6.82
6.82
6.82
6.82
6.67
6.67
6.67
6.67
3.10
2.39
2.20
1.03
1.95
1.95
0.94
1.93
2.00
3.05
5.92
11.89

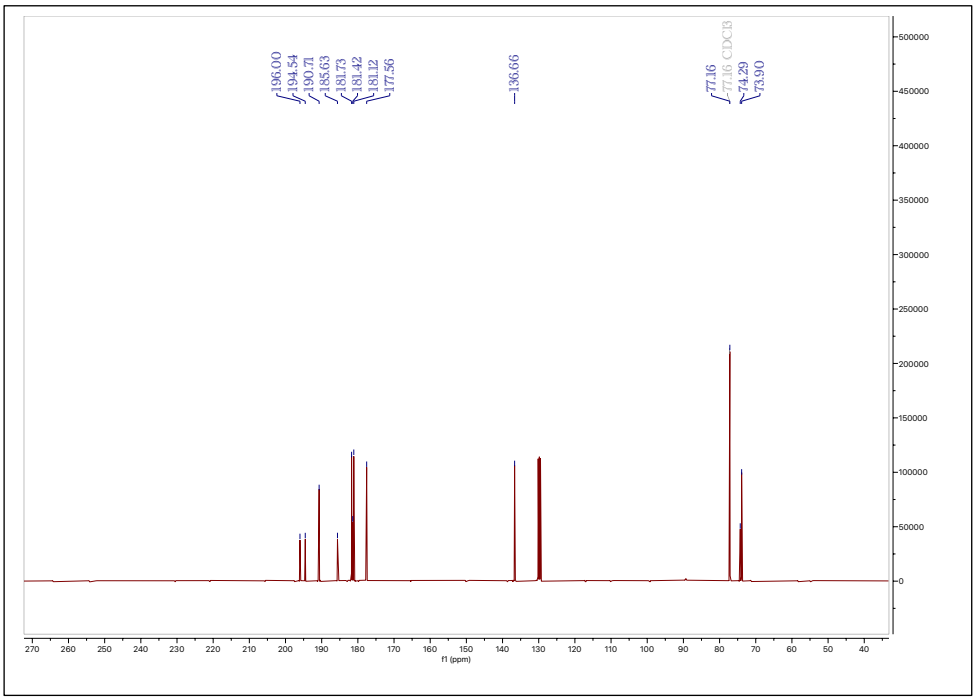
196.00
194.54
190.71
185.63
181.73
181.42
181.12
177.56
136.66
77.16
77.16 CDCl3
74.29
73.90
f1 (ppm)

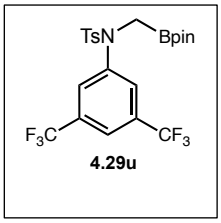
TsN
Bpin
F3C
CF3

4.29u

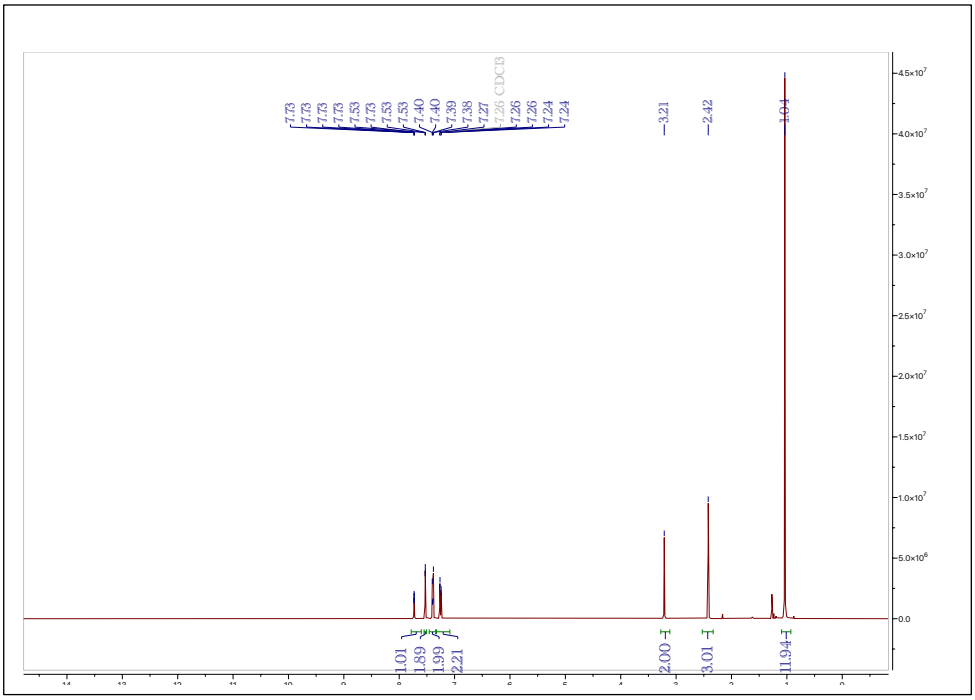
7.73
7.73
7.73
7.73
7.53
7.73
7.53
7.53
7.40
7.40
7.39
7.38
7.27
7.26 CDCl3
7.26
7.26
7.24
7.24
3.21
2.42
1.04
1.01
1.89
1.99
2.21
2.00
3.01
11.94

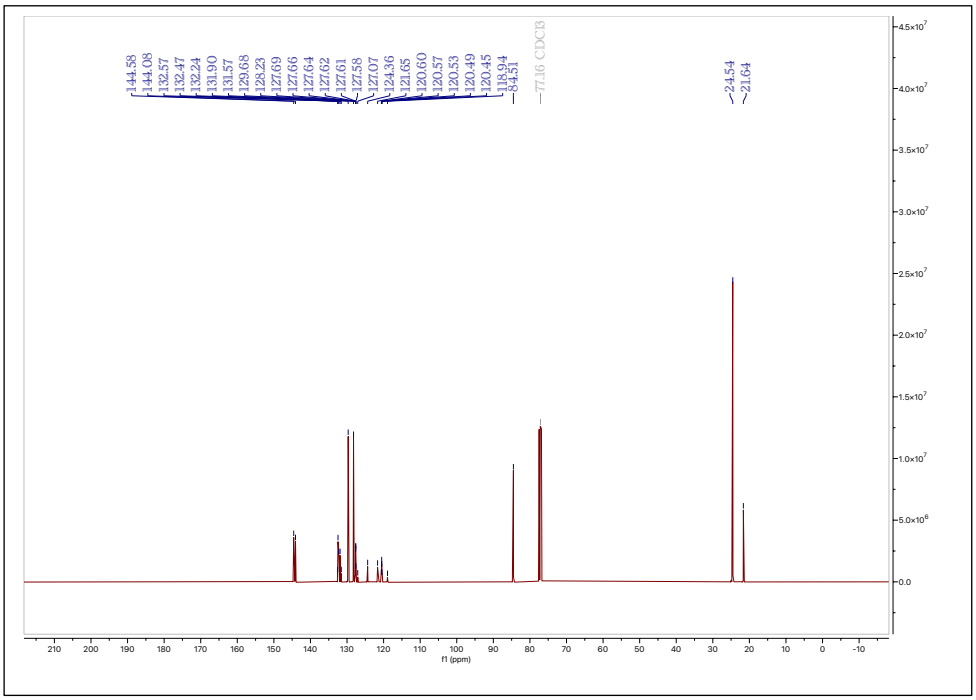
144.58
144.08
132.57
132.47
132.24
131.90
131.57
129.68
128.23
127.69
127.66
127.64
127.62
127.61
127.58
127.07
124.36
121.65
120.60
120.57
120.53
120.49
120.45
118.94
84.51
77.16 CDCl3
24.54
21.64
f1 (ppm)

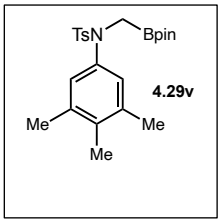
TsN
Bpin
4.29v
Me
Me
Me

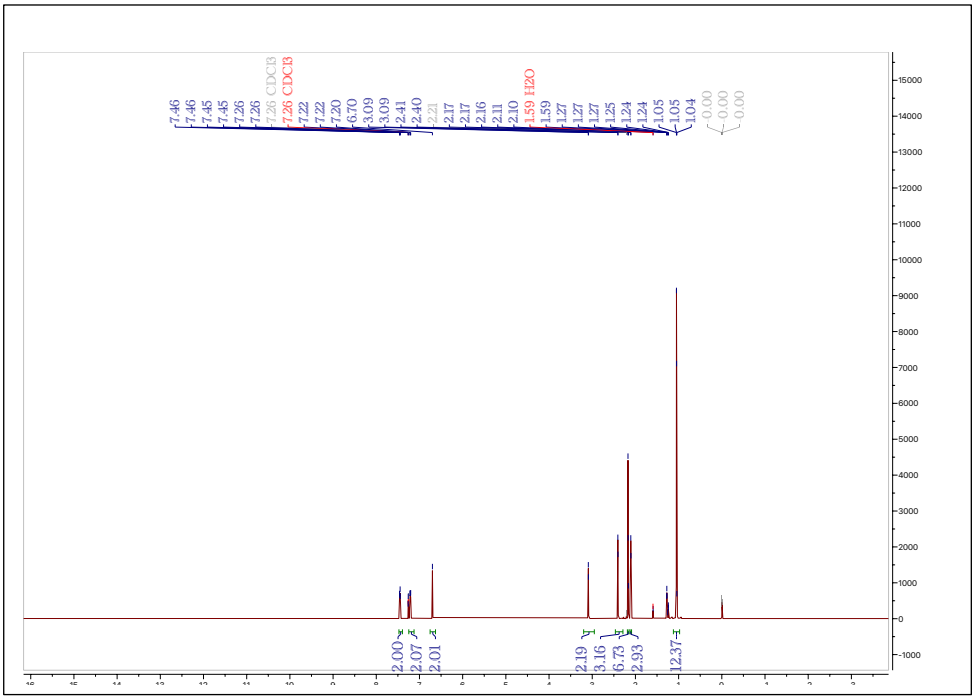
7.46
7.46
7.45
7.45
7.26
7.26
7.26 CDCl3
7.26 CDCl3
7.22
7.22
7.20
6.70
3.09
3.09
2.41
2.40
2.21
2.17
2.17
2.16
2.11
2.10
1.59 H2O
1.59
1.27
1.27
1.27
1.25
1.24
1.24
1.05
1.05
1.04
0.00
0.00
0.00
2.00
2.07
2.01
2.19
3.16
6.73
2.93
12.37

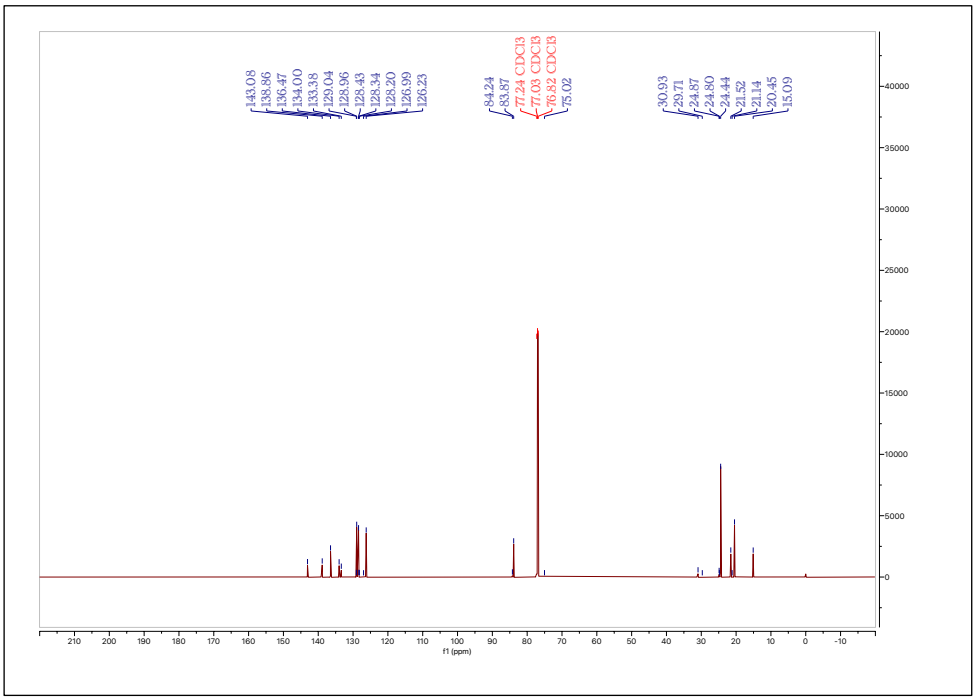
143.08
138.86
136.47
134.00
133.38
129.04
128.96
128.43
128.34
128.20
126.99
126.23
84.24
83.87
77.24 CDCl3
77.03 CDCl3
76.82 CDCl3
75.02
30.93
29.71
24.87
24.80
24.44
21.52
21.14
20.45
15.09
f1 (ppm)

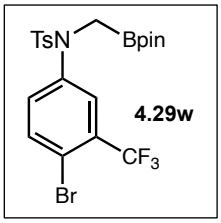
TsN
Bpin
4.29w
CF3
Br

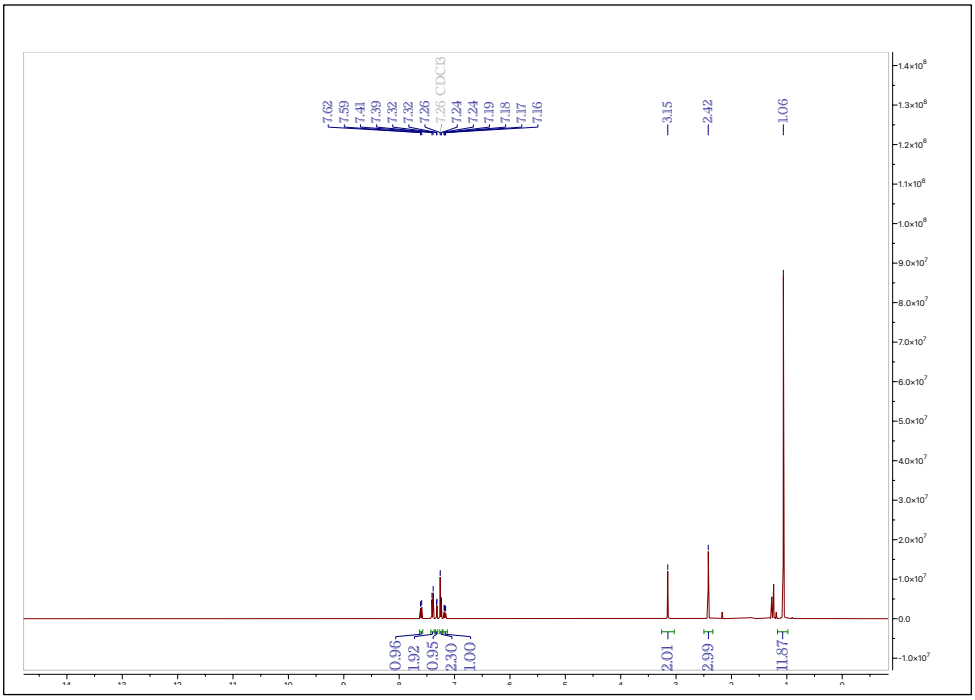
7.62
7.59
7.41
7.39
7.32
7.32
7.26
7.26 CDCl3
7.24
7.24
7.19
7.18
7.17
7.16
3.15
2.42
1.06
0.96
1.92
0.95
2.30
1.00
2.01
2.99
11.87

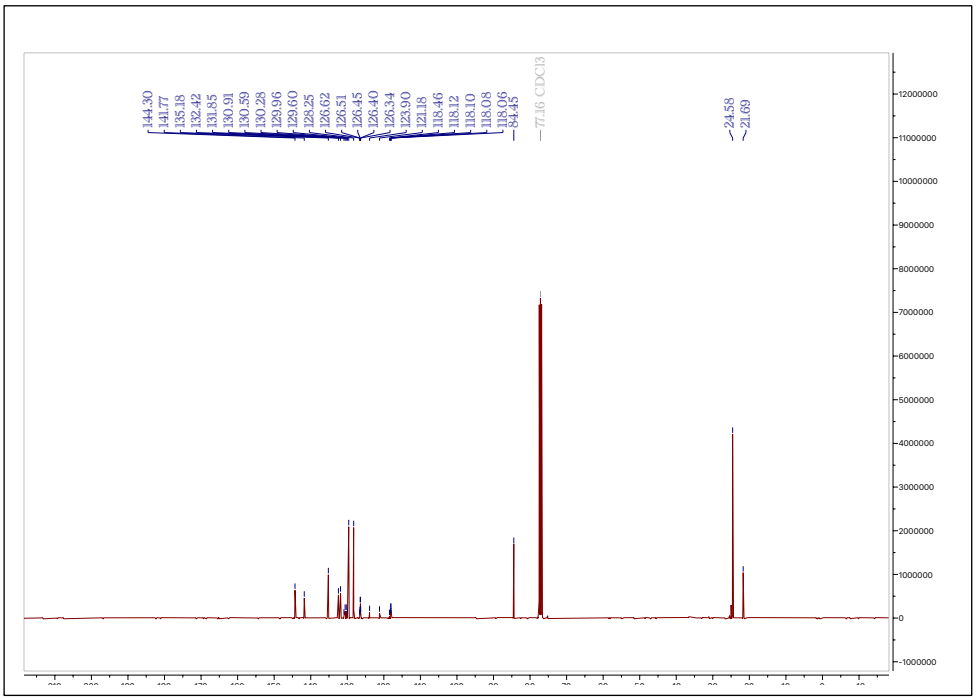
144.30
141.77
135.18
132.42
131.85
130.91
130.59
130.28
129.96
129.60
128.25
126.62
126.51
126.45
126.40
126.34
123.90
121.18
118.46
118.12
118.10
118.08
118.06
84.45
77.16 CDCl3
24.58
21.69

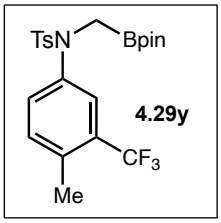
TsN
Bpin
4.29y
CF3
Me

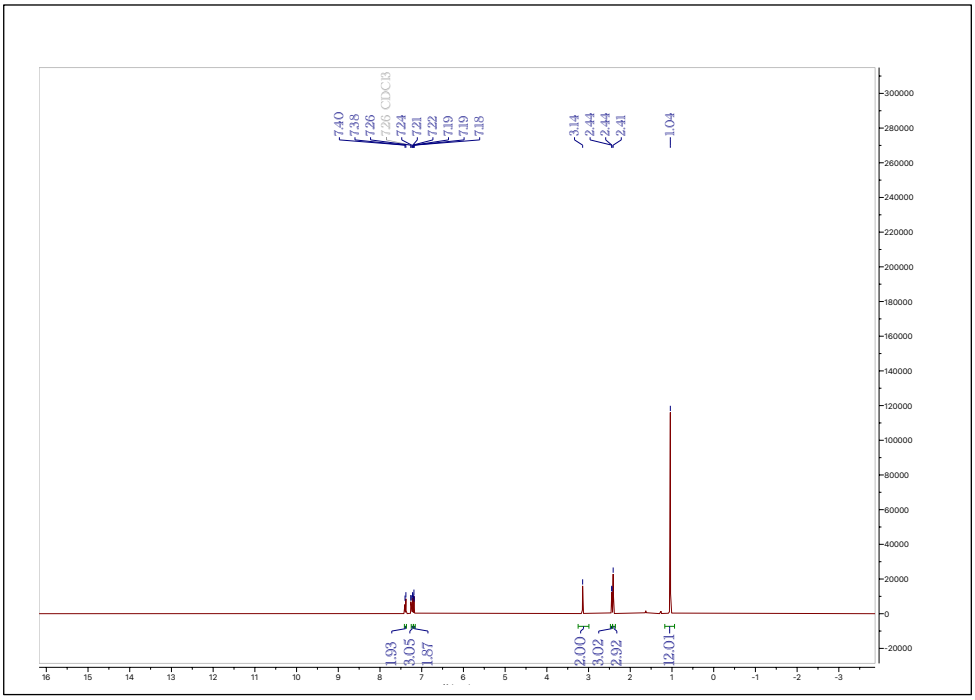
7.40
7.38
7.26
7.26 CDCl3
7.24
7.21
7.22
7.19
7.19
7.18
3.14
2.44
2.44
2.41
1.04
1.93
3.05
1.87
2.00
3.02
2.92
12.01

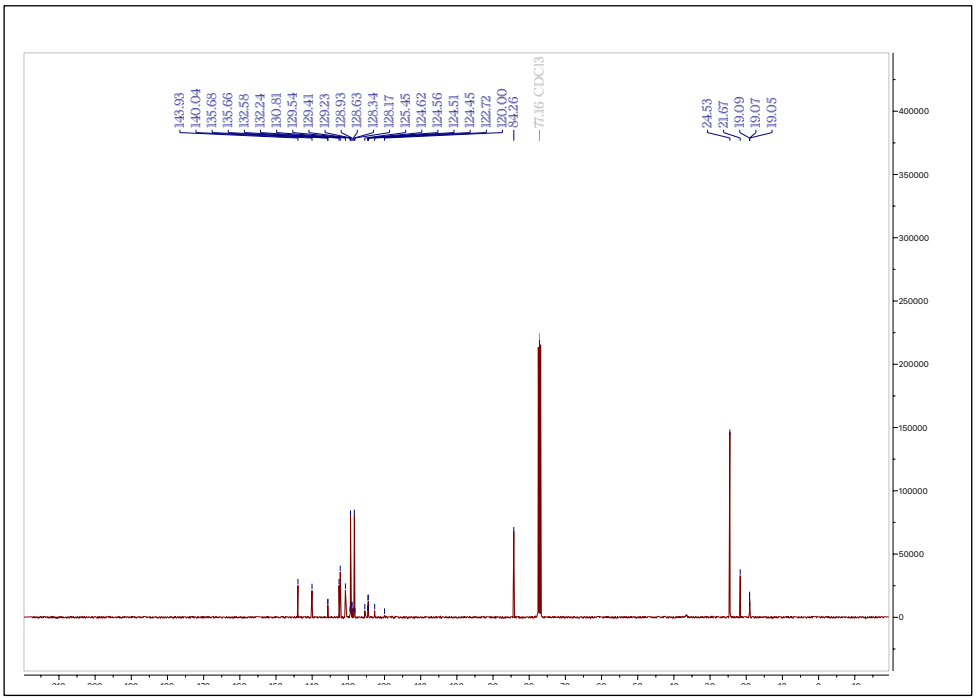
143.93
140.04
135.68
135.66
132.58
132.24
130.81
129.54
129.41
129.23
128.93
128.63
128.34
128.17
125.45
124.62
124.56
124.51
124.45
122.72
120.00
84.26
77.16 CDCl3
24.53
21.67
19.09
19.07
19.05

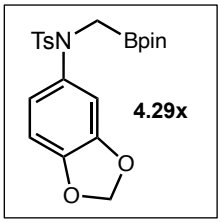
TsN
Bpin
4.29x
O
O

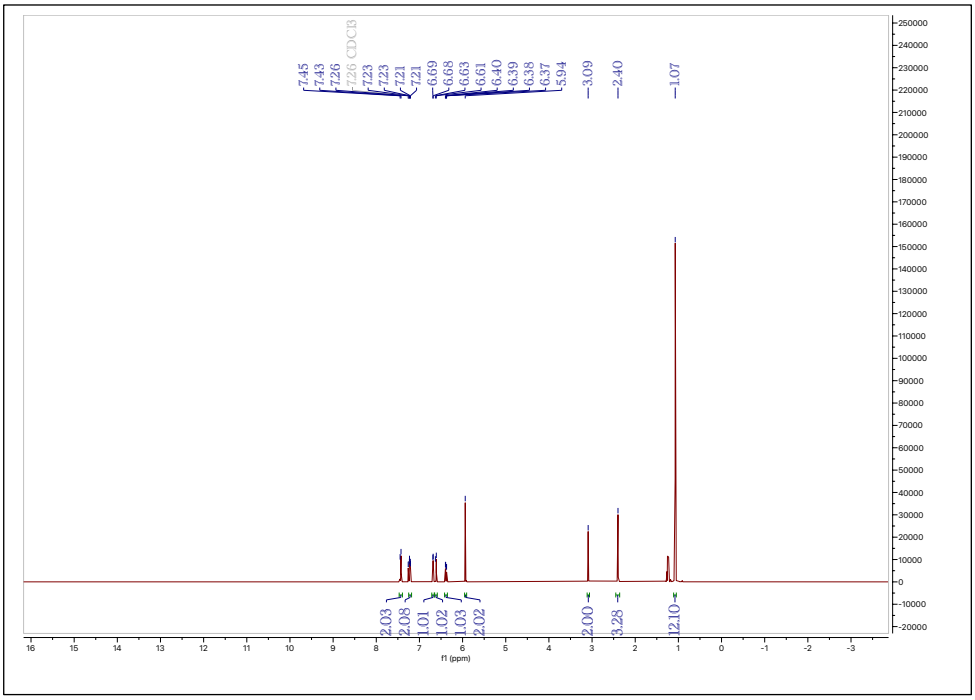
7.45
7.43
7.26
7.26 CDCl3
7.23
7.23
7.21
7.21
6.69
6.68
6.63
6.61
6.40
6.39
6.38
6.37
5.94
3.09
2.40
1.07
2.03
2.08
1.01
1.02
1.03
2.02
2.00
3.28
12.10
f1 (ppm)

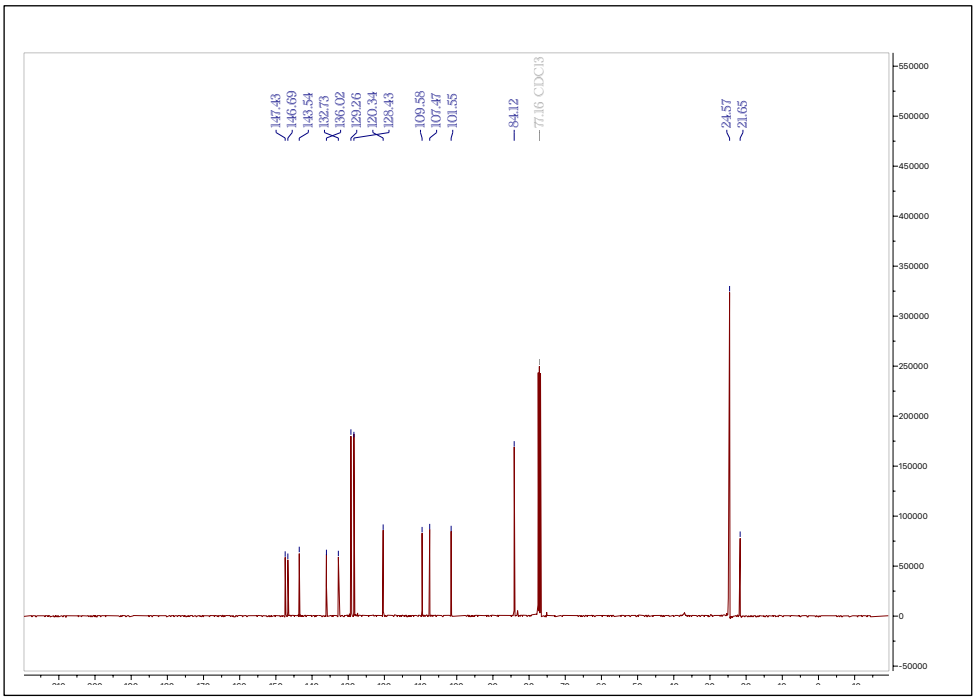
147.43
146.69
143.54
132.73
136.02
129.26
120.34
128.43
109.59
107.47
101.55
84.12
77.16 CDCl3
24.57
21.65

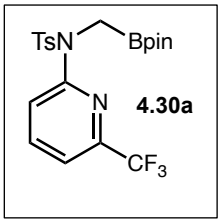
TsN
Bpin
N
4.30a
CF3

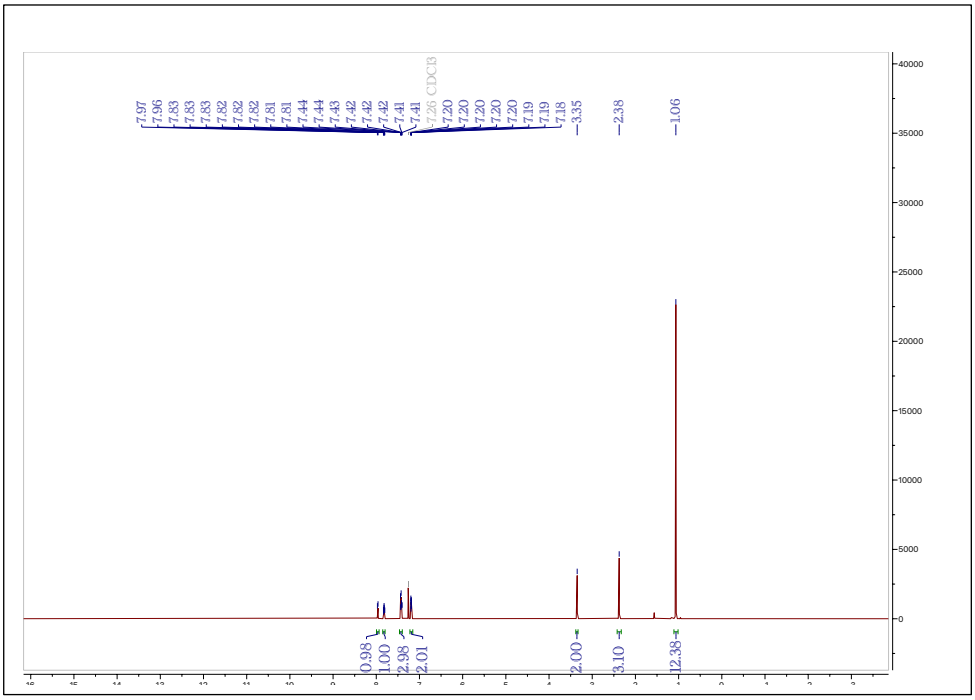
7.97
7.96
7.83
7.83
7.83
7.82
7.82
7.82
7.81
7.81
7.44
7.44
7.43
7.42
7.42
7.42
7.41
7.41
7.26 CDCl3
7.20
7.20
7.20
7.20
7.20
7.19
7.19
7.18
3.35
2.38
1.06
0.98
1.00
2.98
2.01
2.00
3.10
12.38

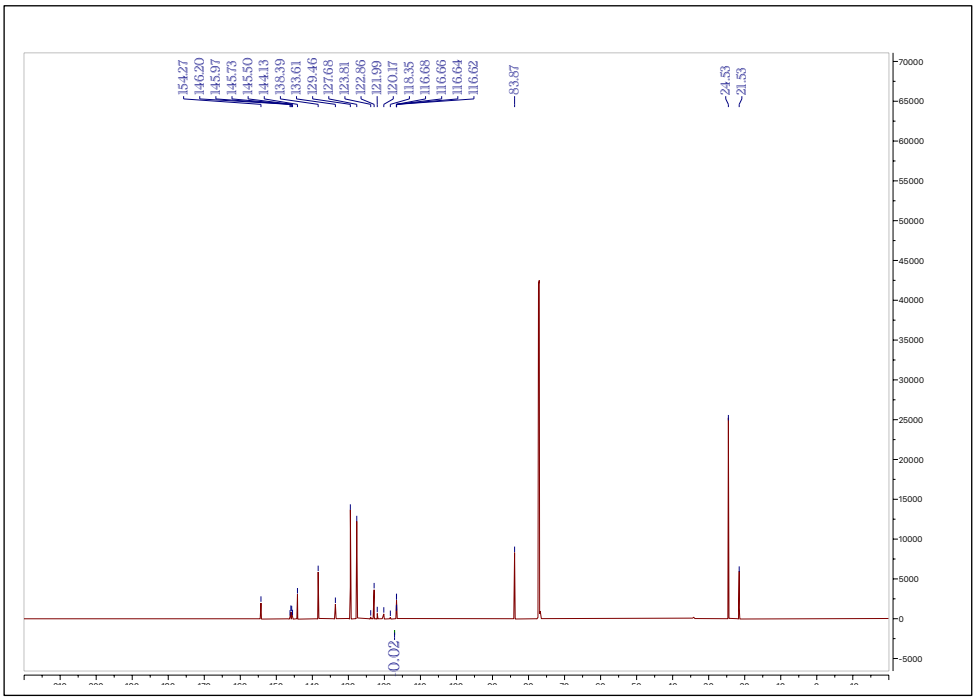
154.27
146.20
145.97
145.73
145.50
144.13
138.39
133.61
129.46
127.68
123.81
122.86
121.99
120.17
118.35
116.68
116.66
116.64
116.62
83.87
24.53
21.53
0.02

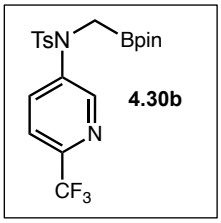
TsN
Bpin
4.30b
N
CF3

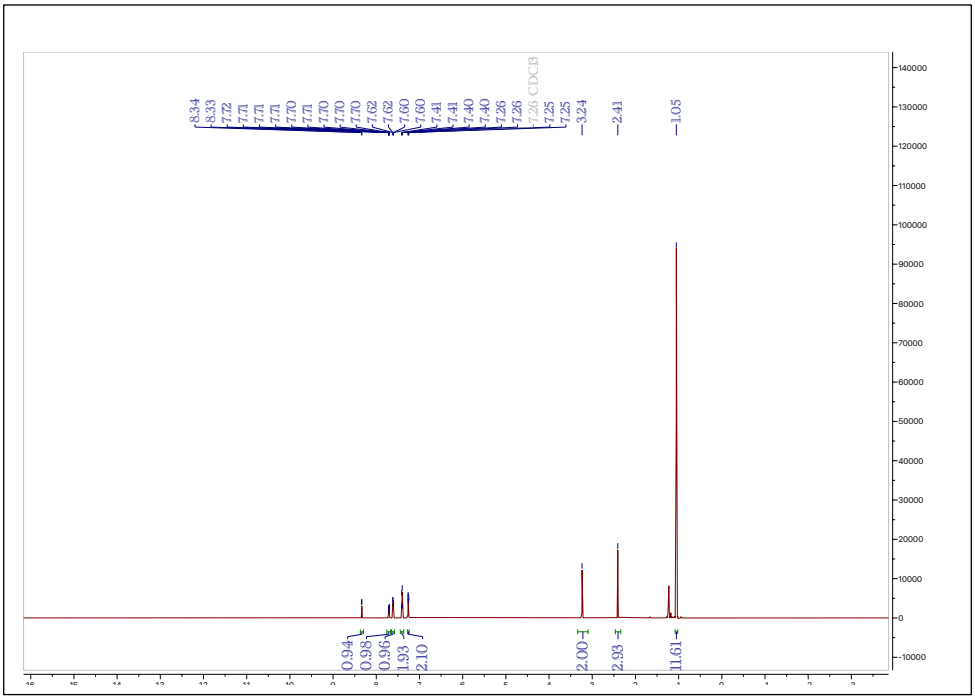
8.34
8.33
7.72
7.71
7.71
7.71
7.71
7.70
7.71
7.70
7.70
7.70
7.70
7.62
7.62
7.60
7.60
7.41
7.41
7.40
7.40
7.26
7.26
7.26 CDCl3
7.25
7.25
3.24
2.41
1.05
0.94
0.98
0.96
1.93
2.10
2.00
2.93
11.61

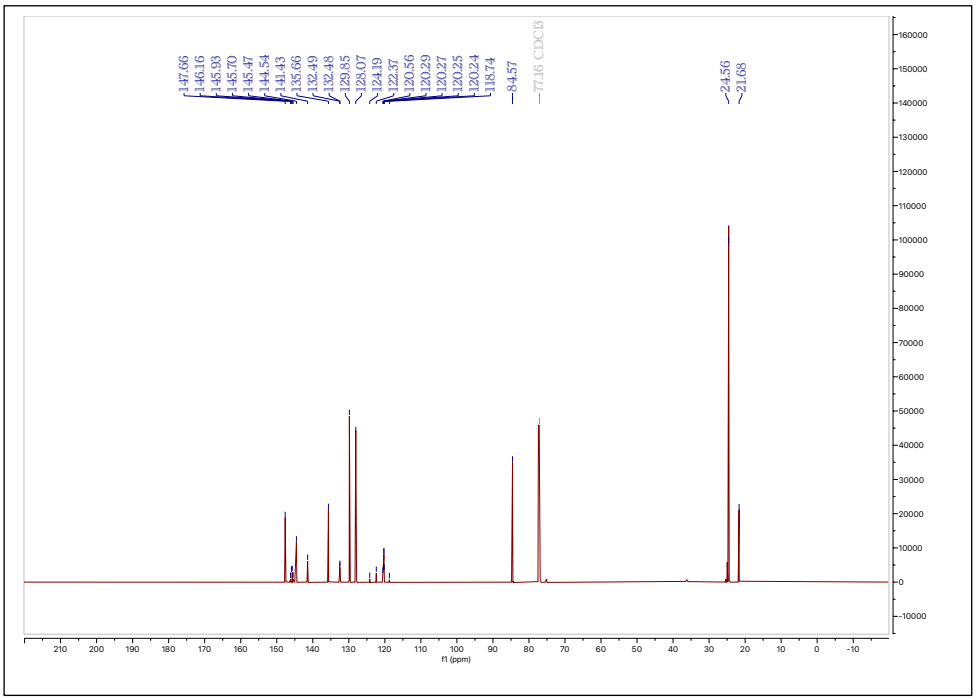
147.66
146.16
145.93
145.70
145.47
144.54
141.43
135.66
132.49
132.48
129.85
128.07
124.19
122.57
120.56
120.29
120.27
120.25
120.24
118.74
84.57
77.16 CDCl3
24.56
21.68
f1 (ppm)

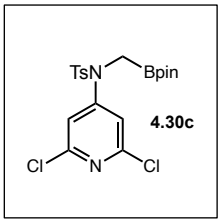
TsN
Bpin
4.30c
Cl
N
Cl

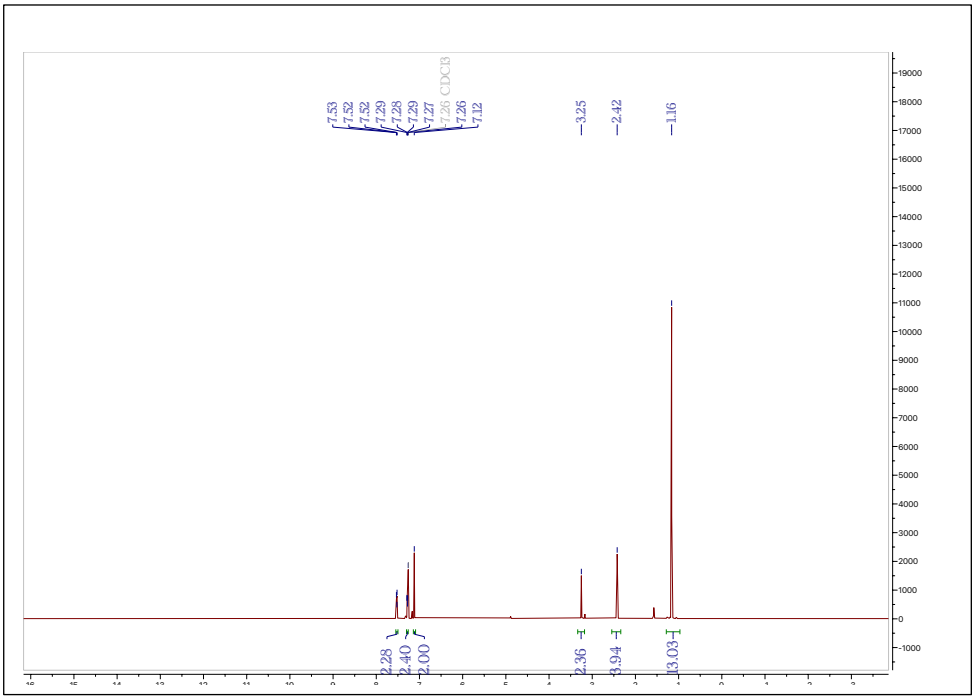
7.53
7.52
7.32
7.29
7.28
7.29
7.27
7.26 CDCl3
7.26
7.12
3.25
2.42
1.16
2.28
2.40
2.00
2.36
3.94
13.03

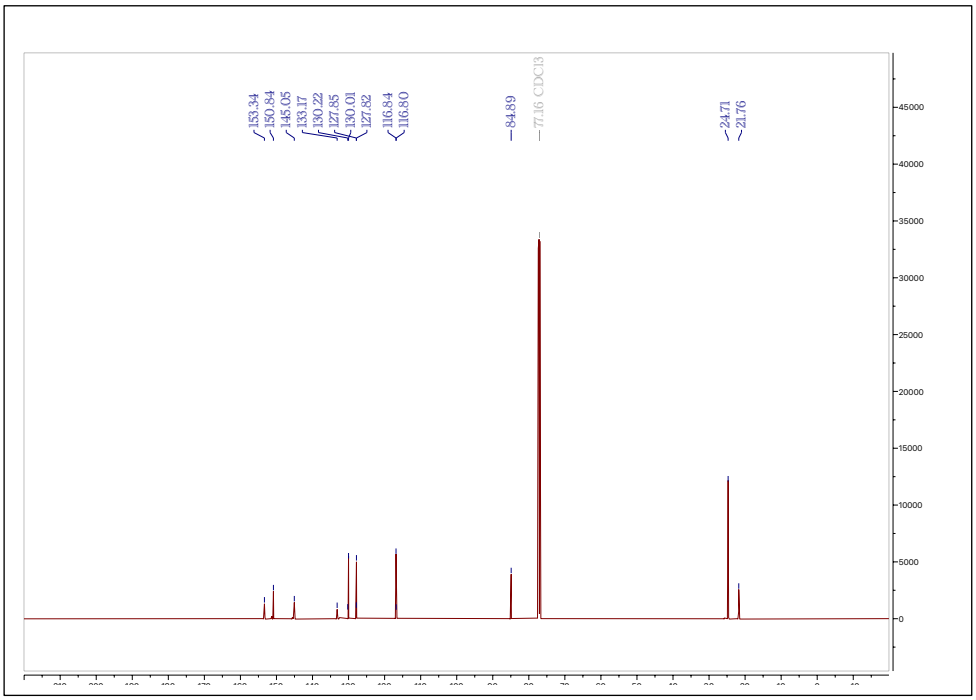
153.34
150.84
145.05
133.17
130.22
127.85
130.01
127.82
116.84
116.80
84.89
77.16 CDCl3
24.71
21.76

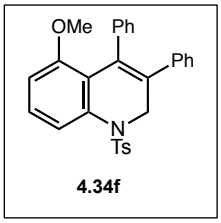

4.34f

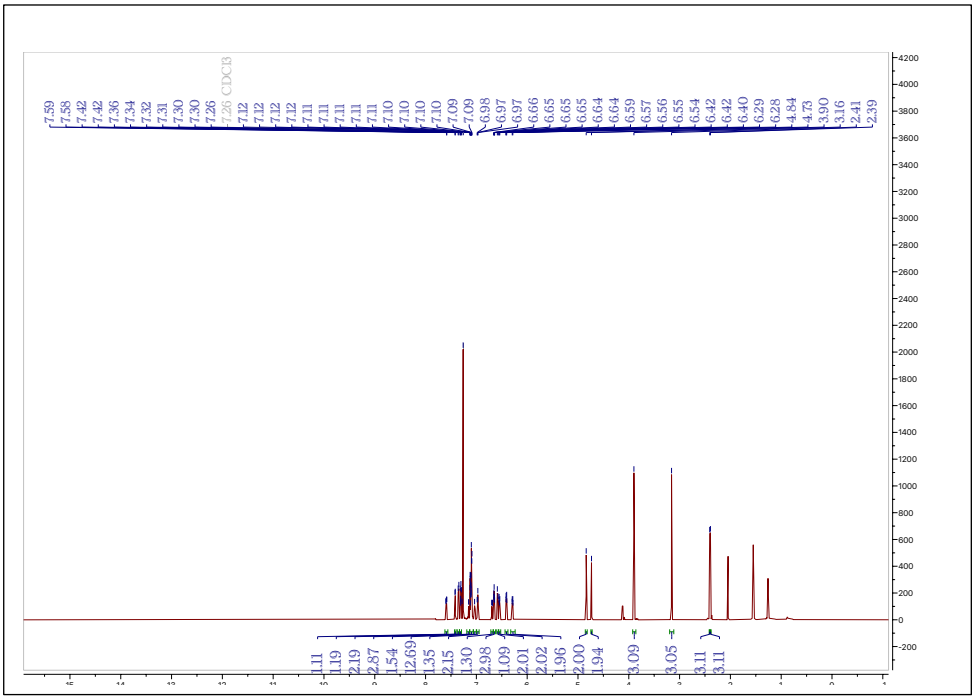

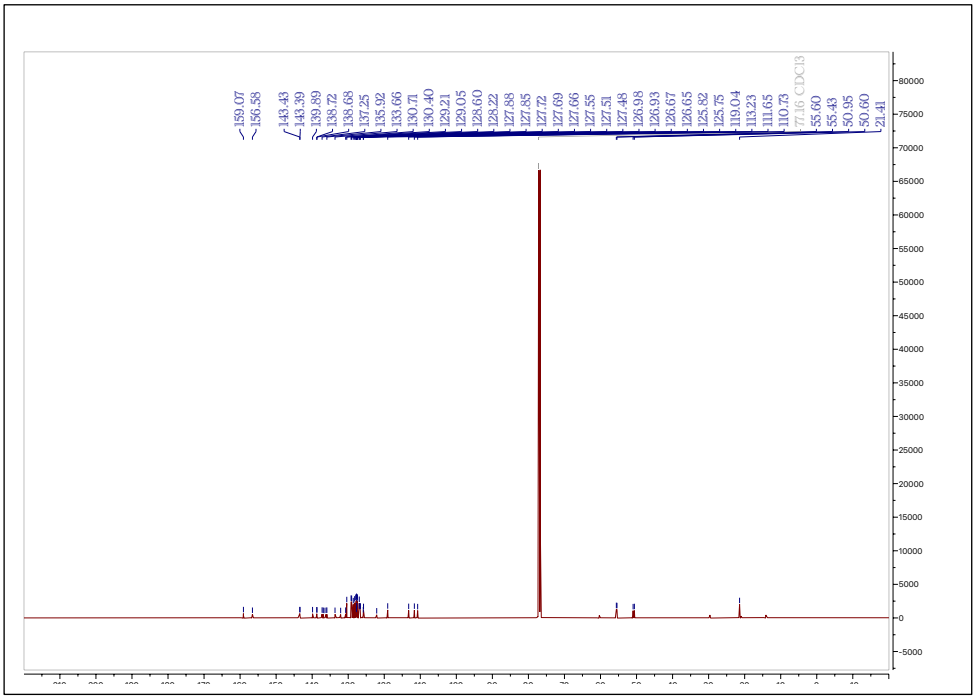

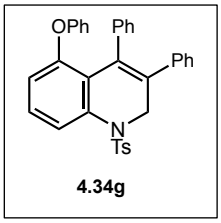

4.34g

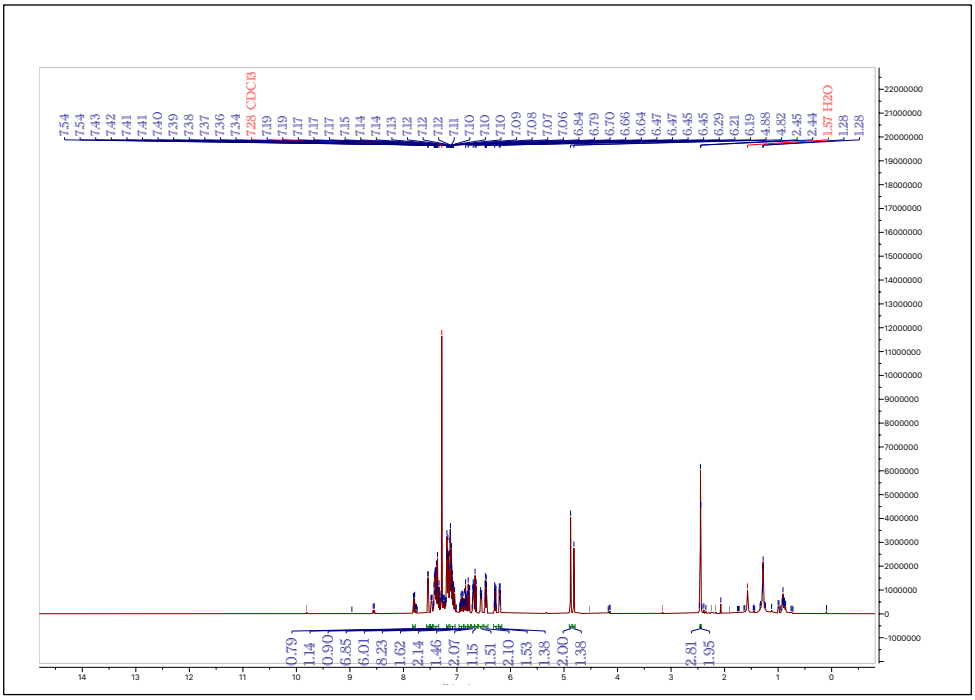

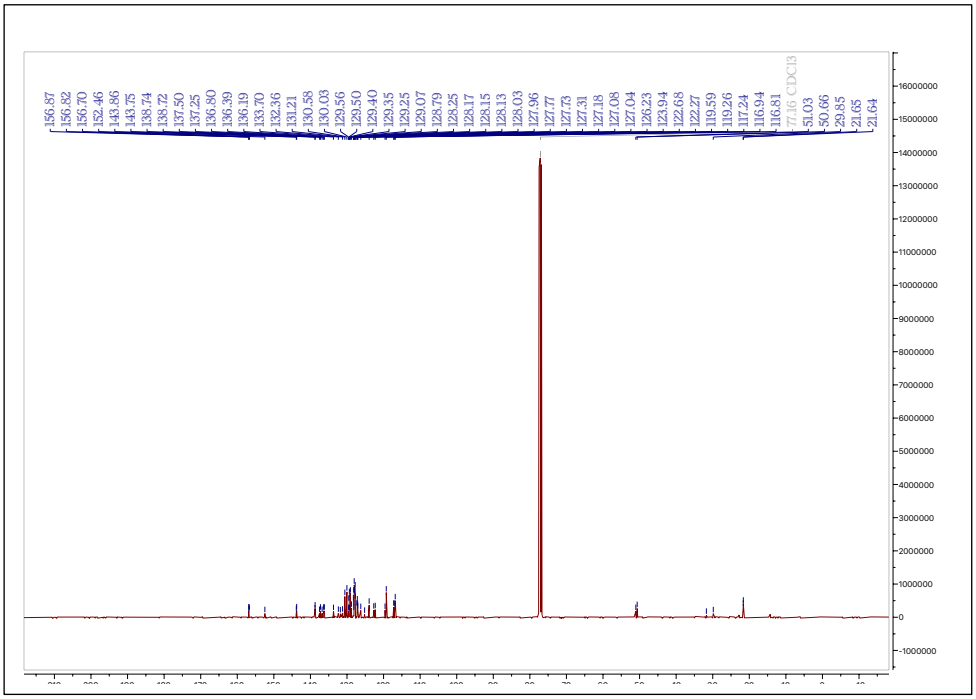

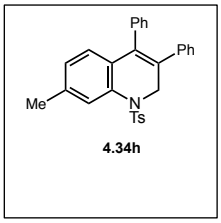
Ph
Ph
Me
N
Ts

4.34h

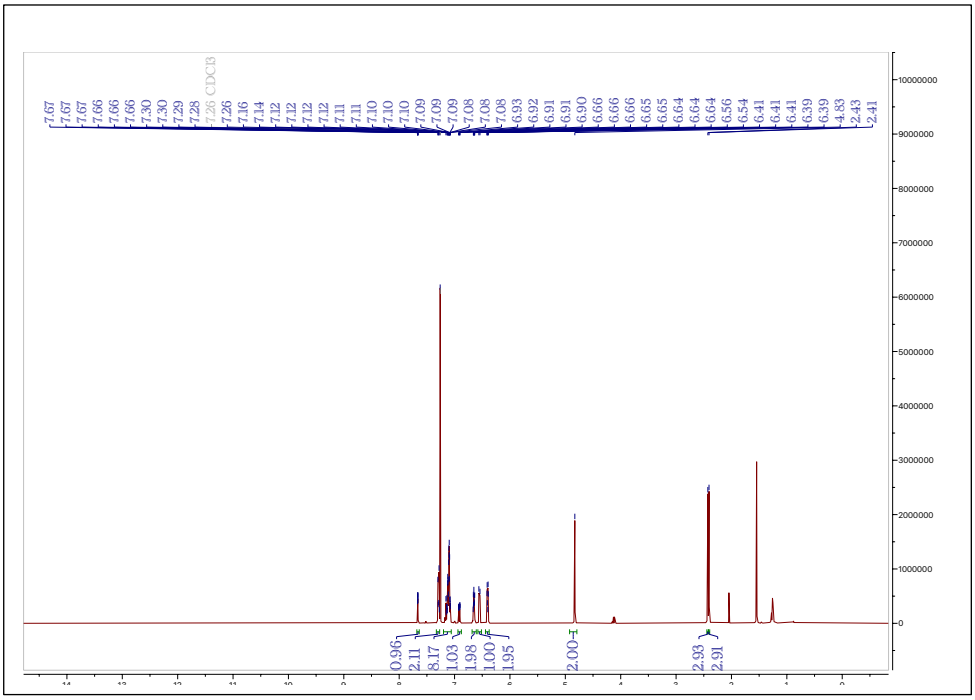
7.67
7.67
7.67
7.66
7.66
7.66
7.30
7.30
7.29
7.28
7.26 CDCl3
7.26
7.16
7.14
7.12
7.12
7.12
7.12
7.11
7.11
7.10
7.10
7.10
7.09
7.09
7.09
7.09
7.08
7.08
7.08
6.93
6.92
6.91
6.91
6.90
6.66
6.66
6.66
6.65
6.64
6.64
6.64
6.64
6.56
6.54
6.41
6.41
6.41
6.39
6.39
4.83
2.43
2.41
0.96
2.11
8.17
1.03
1.98
1.00
1.95
2.00
2.93
2.91

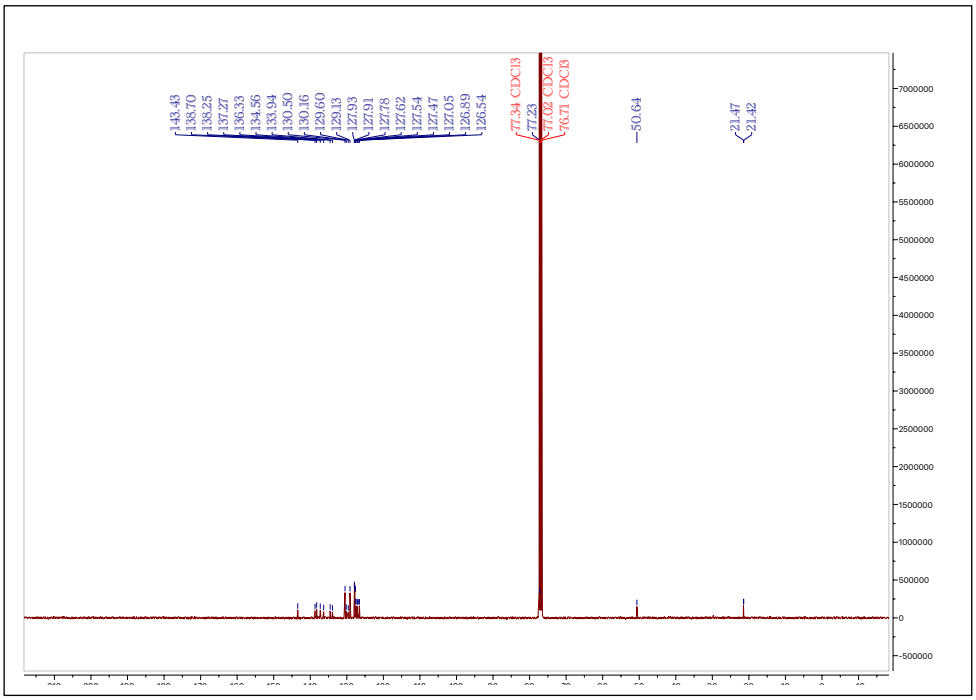
143.43
138.70
138.25
137.27
136.33
134.56
133.94
130.50
130.16
129.60
129.13
127.93
127.91
127.78
127.62
127.54
127.47
127.05
126.89
126.54
77.34 CDCl3
77.23
77.02 CDCl3
76.71 CDCl3
50.64
21.47
21.42

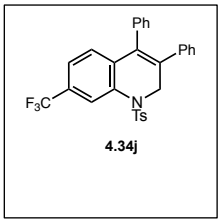
Ph
Ph
F3C
N
Ts

4.34j

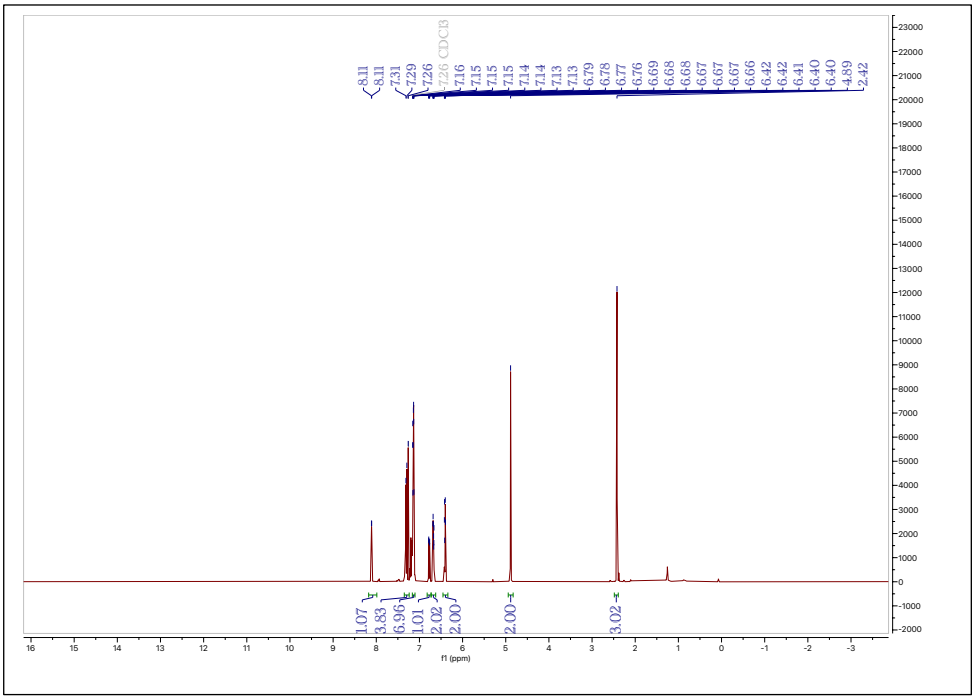
8.11
8.11
7.31
7.29
7.26
7.26 CDCl3
7.16
7.15
7.15
7.15
7.14
7.14
7.13
7.13
6.79
6.78
6.77
6.76
6.69
6.68
6.68
6.67
6.67
6.67
6.66
6.42
6.42
6.41
6.40
6.40
4.89
2.42
1.07
3.83
6.96
1.01
2.02
2.00
2.00
3.02
f1 (ppm)

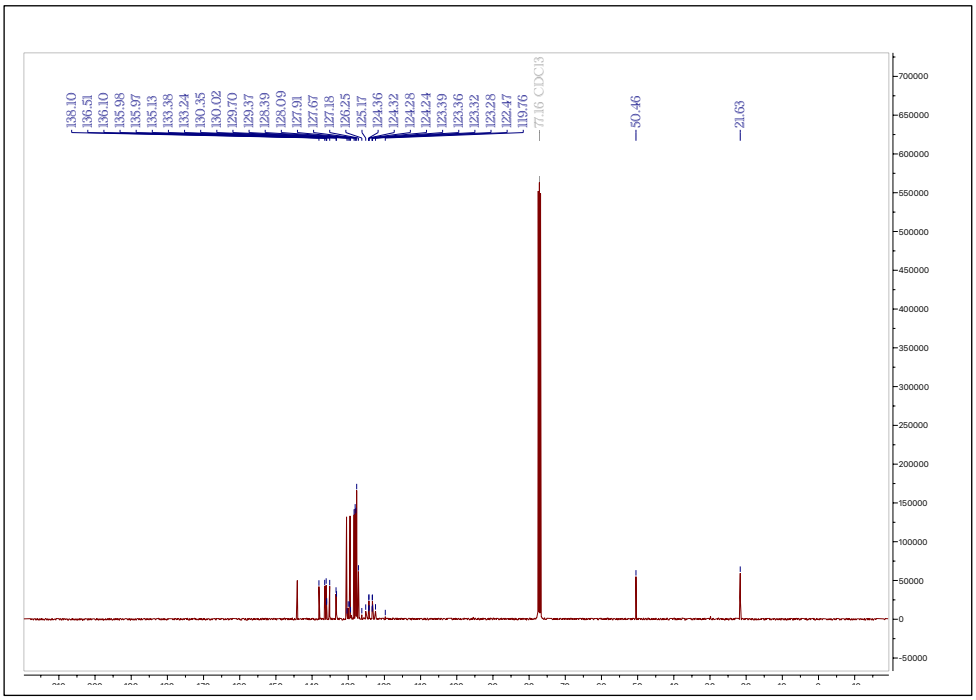
138.10
136.51
136.10
135.98
135.97
135.13
133.38
133.24
130.35
130.02
129.70
129.37
128.39
128.09
127.91
127.67
127.18
126.25
125.17
124.36
124.32
124.28
124.24
123.39
123.36
123.32
123.28
122.47
119.76
77.16 CDCl3
50.46
21.63

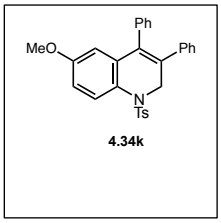
Ph
MeO
Ph
N
Ts

4.34k

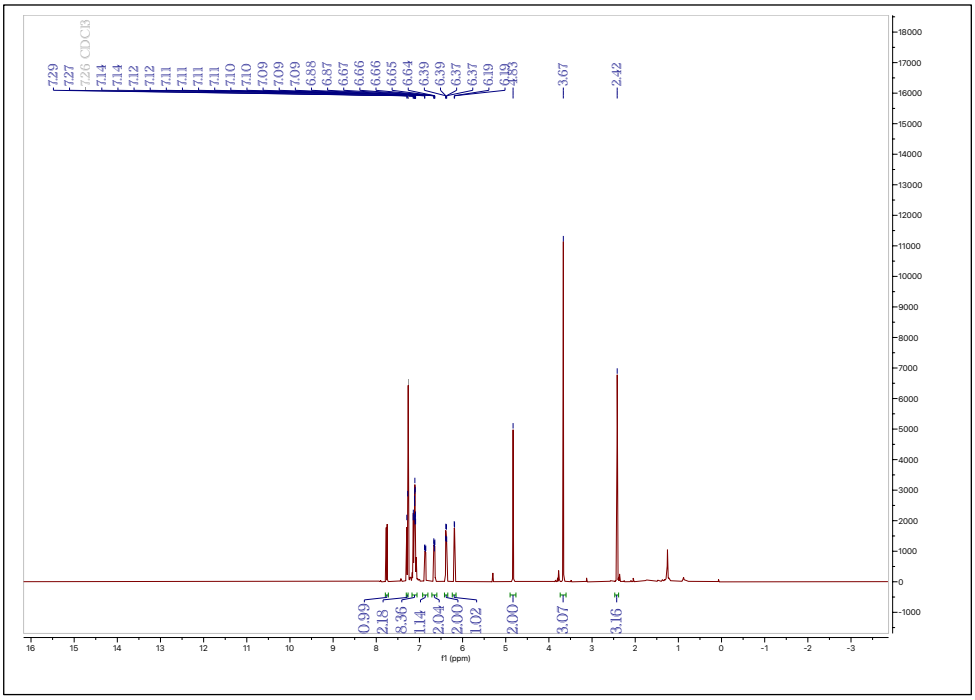
7.29
7.27
7.26 CDCl3
7.14
7.14
7.12
7.12
7.11
7.11
7.11
7.11
7.11
7.10
7.10
7.09
7.09
7.09
6.88
6.87
6.67
6.66
6.66
6.65
6.64
6.39
6.39
6.37
6.37
6.19
6.19
3.83
3.67
2.42
0.99
2.18
8.36
1.14
2.04
2.00
1.02
2.00
3.07
3.16
f1 (ppm)

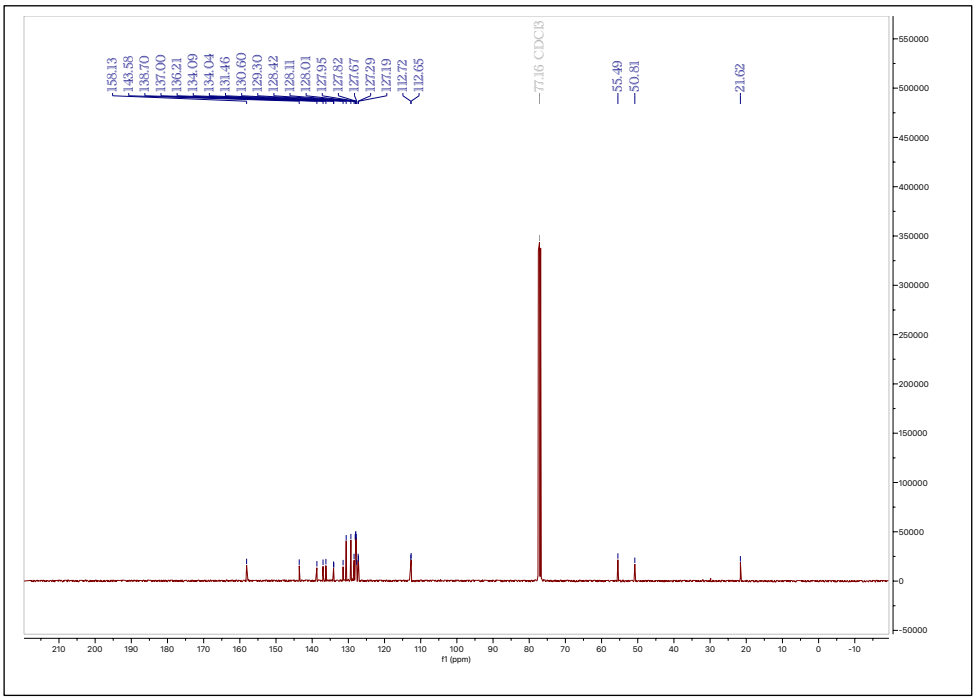
158.13
143.58
138.70
137.00
136.21
134.09
134.04
131.46
130.60
129.30
128.42
128.11
128.01
127.95
127.82
127.67
127.29
127.19
112.72
112.65
77.16 CDCl3
55.49
50.81
21.62
f1 (ppm)

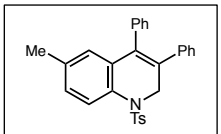
Ph
Me
Ph
N
Ts

4.27

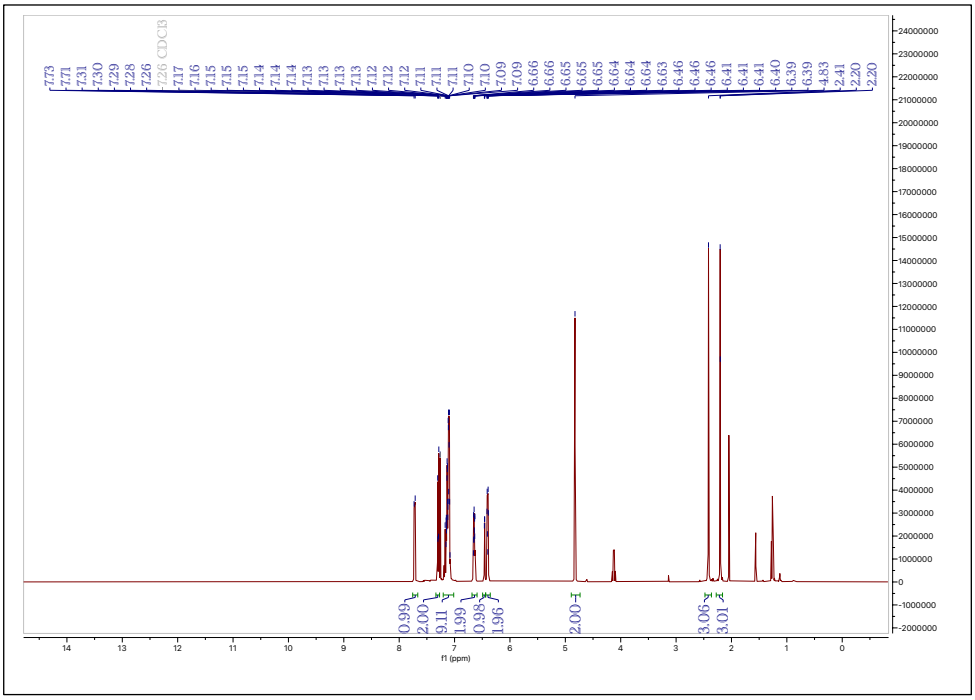
7.73
7.71
7.31
7.30
7.29
7.28
7.26
7.26 CDCl3
7.17
7.16
7.15
7.15
7.15
7.14
7.14
7.14
7.13
7.13
7.13
7.13
7.12
7.12
7.12
7.11
7.11
7.11
7.10
7.10
7.09
7.09
6.66
6.66
6.65
6.65
6.64
6.64
6.64
6.63
6.46
6.46
6.46
6.41
6.41
6.41
6.40
6.39
6.39
4.83
2.41
2.20
2.20
0.99
2.00
9.11
1.99
0.98
1.96
2.00
3.06
3.01
f1 (ppm)

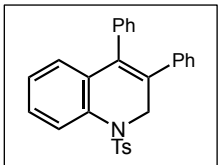
Ph
Ph
N
Ts

4.35

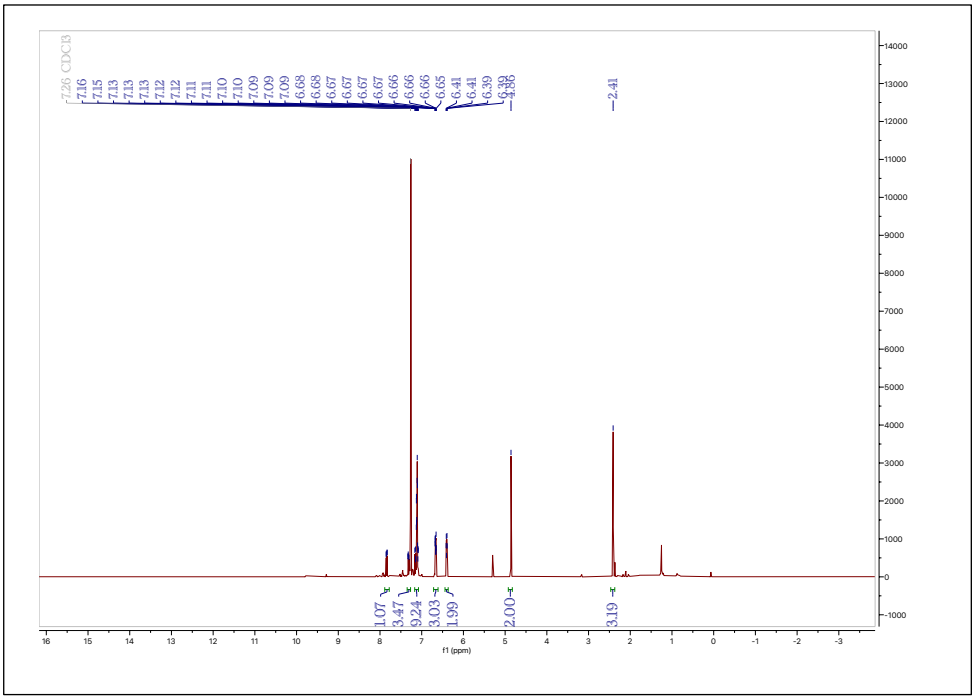
7.26 CDCl3
7.16
7.15
7.13
7.13
7.13
7.12
7.12
7.11
7.11
7.10
7.10
7.09
7.09
7.09
6.68
6.68
6.67
6.67
6.67
6.67
6.66
6.66
6.66
6.65
6.41
6.41
6.39
6.39
2.41
1.07
3.47
9.24
3.03
1.99
2.00
3.19
f1 (ppm)

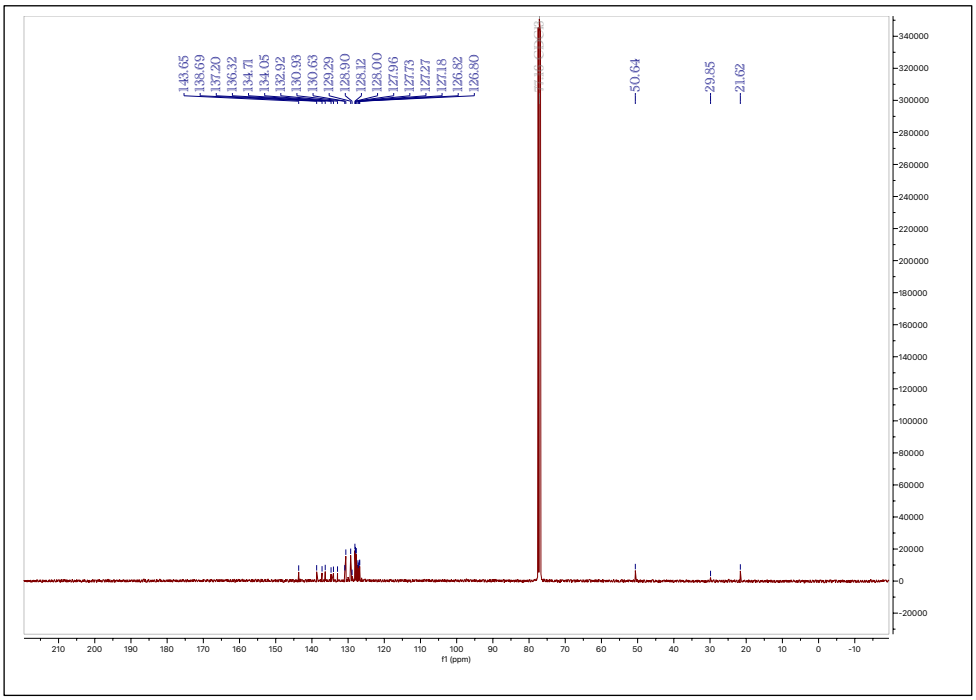
143.65
138.69
137.20
136.32
134.71
134.05
132.92
130.93
130.63
129.29
128.90
128.12
128.00
127.96
127.73
127.27
127.18
126.82
126.80
50.64
29.85
21.62
f1 (ppm)

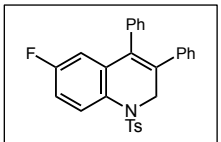
Ph
F
Ph
N
Ts

4.34l

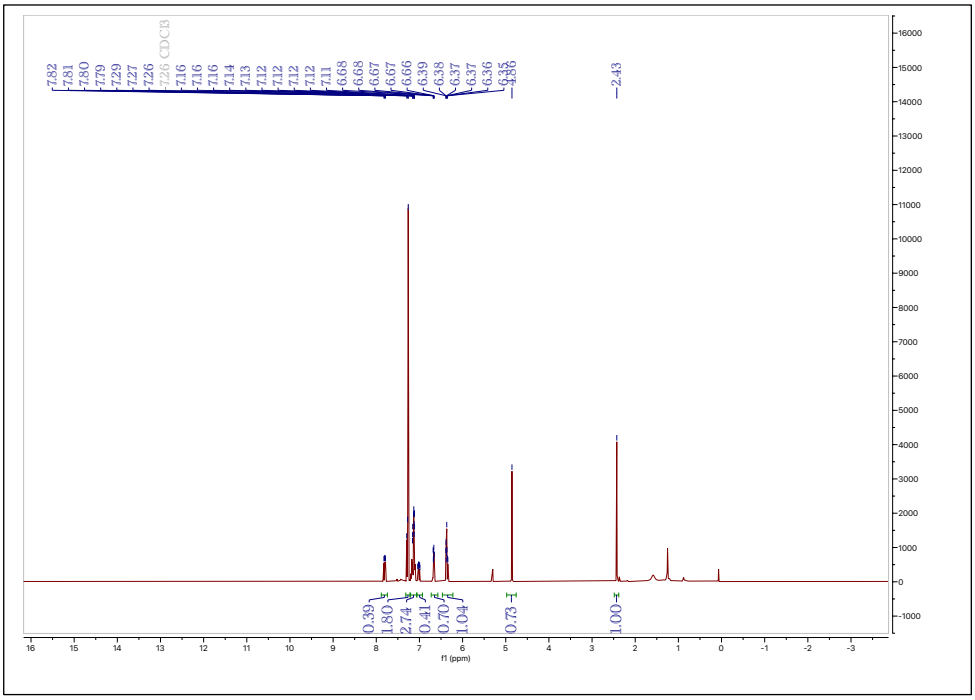
7.82
7.81
7.80
7.79
7.29
7.27
7.26
7.26 CDCl3
7.16
7.16
7.16
7.14
7.13
7.12
7.12
7.12
7.12
7.11
6.68
6.68
6.67
6.67
6.66
6.39
6.38
6.37
6.37
6.36
6.35
2.43
0.39
1.80
2.74
0.41
0.70
1.04
0.73
1.00
f1 (ppm)

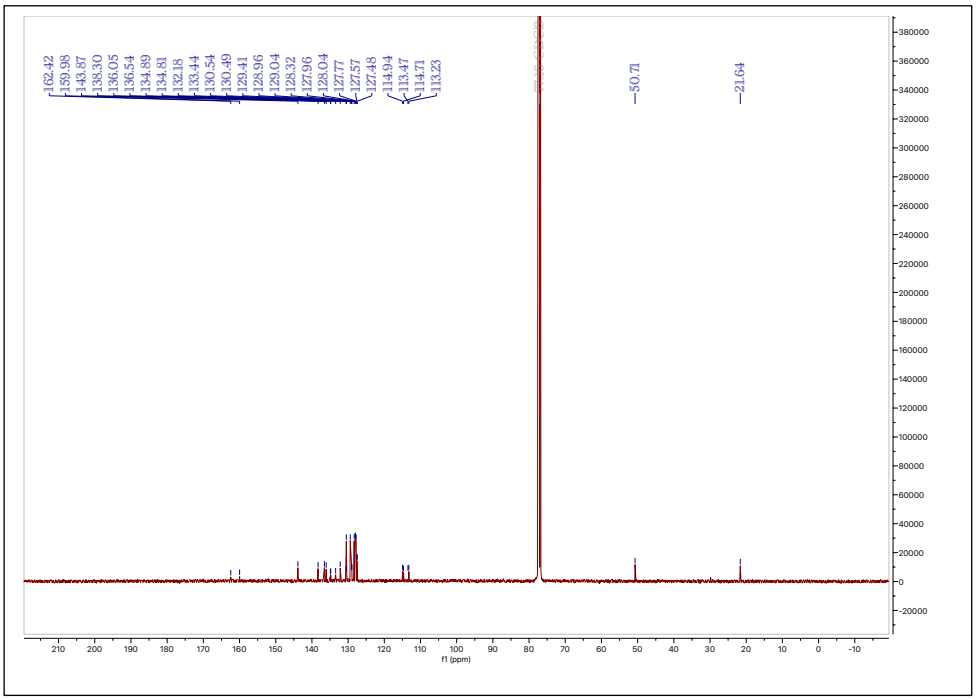
162.42
159.98
143.87
138.30
136.05
136.54
134.89
134.81
132.18
133.44
130.54
130.49
129.41
128.96
129.04
128.32
127.96
128.04
127.77
127.57
127.48
114.94
113.47
114.71
113.23
50.71
21.64
f1 (ppm)

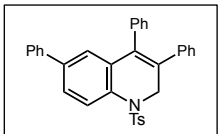
Ph
Ph
Ph
N
Ts

4.34m

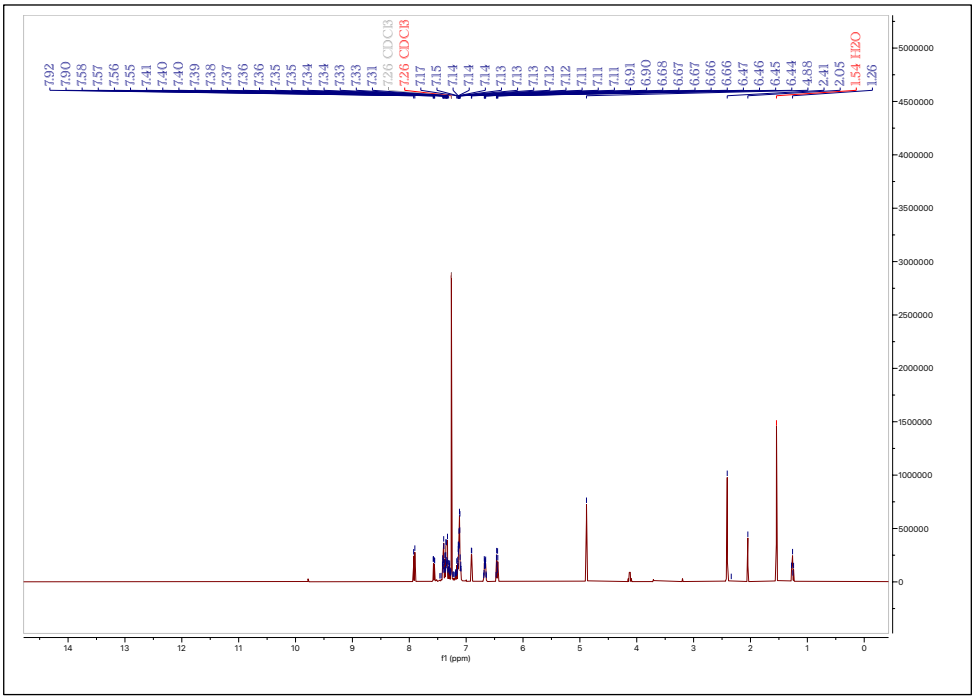
7.92
7.90
7.58
7.57
7.56
7.55
7.41
7.40
7.40
7.39
7.38
7.37
7.36
7.36
7.35
7.35
7.34
7.34
7.33
7.33
7.31
7.26 CDCl3
7.26 CDCl3
7.17
7.15
7.14
7.14
7.14
7.14
7.13
7.13
7.13
7.12
7.12
7.11
7.11
7.11
6.91
6.90
6.68
6.67
6.67
6.66
6.66
6.47
6.46
6.45
6.44
4.88
2.41
2.05
1.54 H2O
1.26
f1 (ppm)

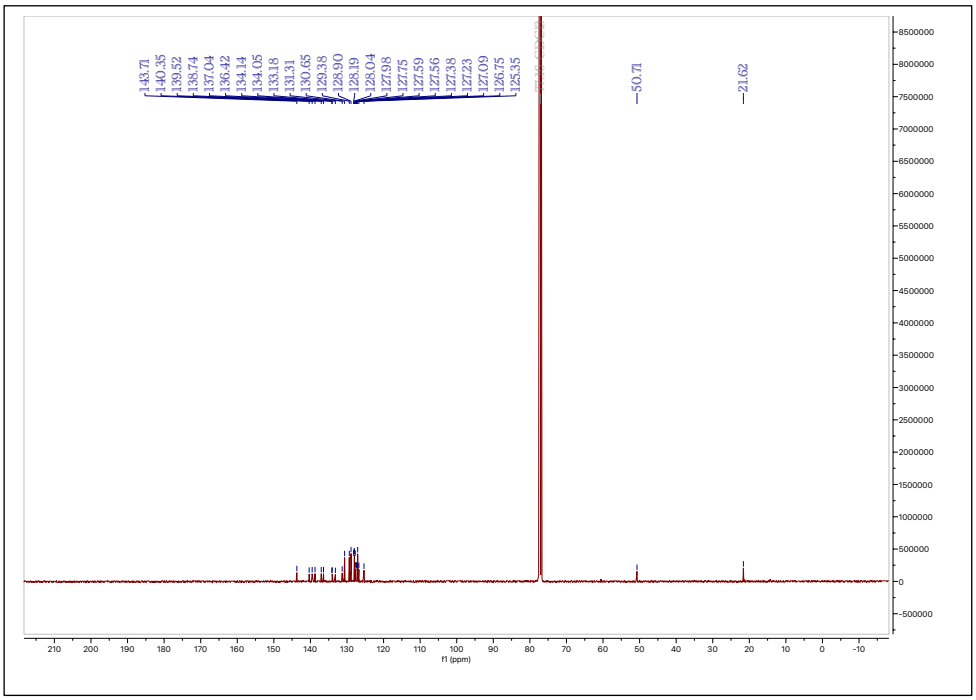
143.71
140.35
139.52
138.74
137.04
136.42
134.14
134.05
133.18
131.31
130.65
129.38
128.90
128.19
128.04
127.98
127.75
127.59
127.56
127.38
127.23
127.09
126.75
125.35
50.71
21.62
f1 (ppm)

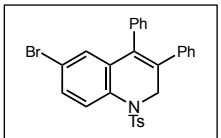
Ph
Br
Ph
N
Ts

4.34n

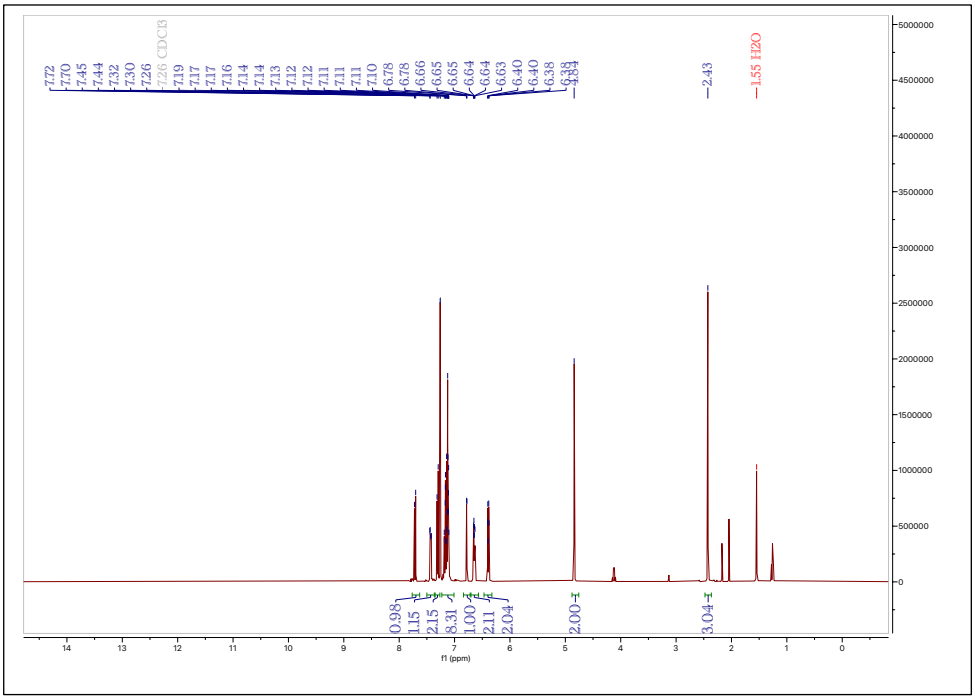
7.72
7.70
7.45
7.44
7.32
7.30
7.26
7.26 CDCl3
7.19
7.17
7.17
7.16
7.14
7.14
7.13
7.12
7.12
7.11
7.11
7.11
7.10
6.78
6.78
6.66
6.65
6.65
6.64
6.64
6.63
6.40
6.40
6.38
6.38
4.84
2.43
1.55 H2O
0.98
1.15
2.15
8.31
1.00
2.11
2.04
2.00
3.04
f1 (ppm)

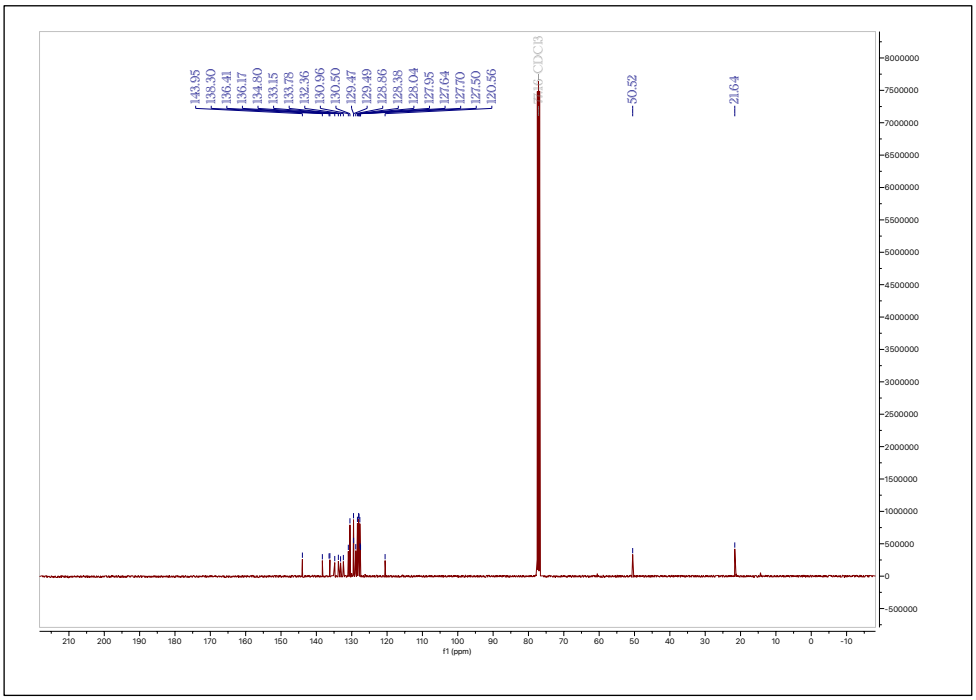
143.95
138.30
136.41
136.17
134.80
133.15
133.78
132.36
130.96
130.50
129.47
129.49
128.86
128.38
128.04
127.95
127.64
127.70
127.50
120.56
77.16 CDCl3
50.52
21.64
f1 (ppm)

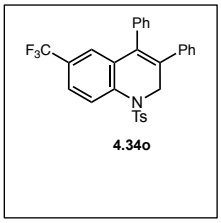
Ph
F3C
Ph
N
Ts

4.34o

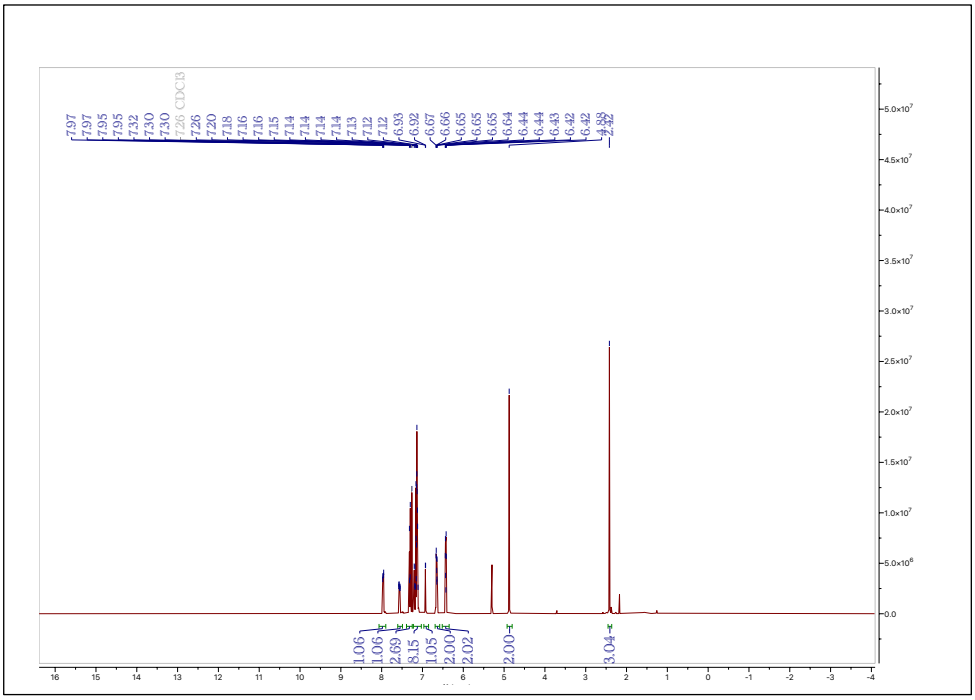
7.97
7.97
7.95
7.95
7.32
7.30
7.30
7.26 CDCl3
7.26
7.20
7.18
7.16
7.16
7.15
7.14
7.14
7.14
7.14
7.13
7.12
7.12
6.93
6.92
6.67
6.66
6.65
6.65
6.65
6.64
6.44
6.44
6.43
6.42
6.42
4.38
4.32
1.06
1.06
2.69
8.15
1.05
2.00
2.02
2.00
3.04

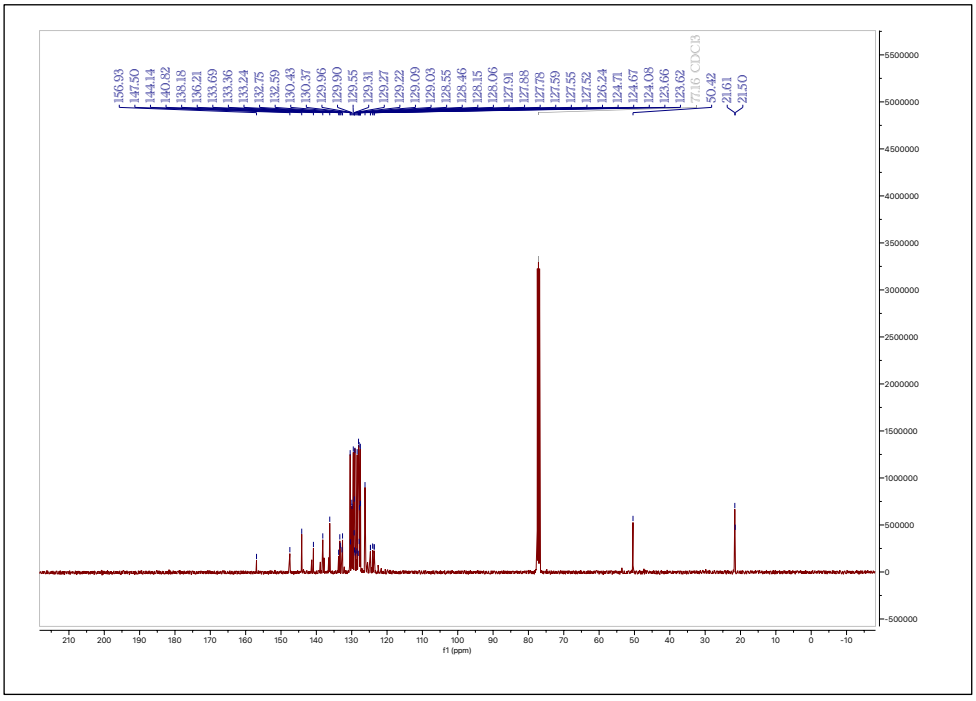
156.93
147.50
144.14
140.82
138.18
136.21
133.69
133.36
133.24
132.75
132.59
130.43
130.37
129.96
129.90
129.55
129.31
129.27
129.22
129.09
129.03
128.55
128.46
128.15
128.06
127.91
127.88
127.78
127.59
127.55
127.52
126.24
124.71
124.67
124.08
123.66
123.62
77.16 CDCl3
50.42
21.61
21.50
f1 (ppm)

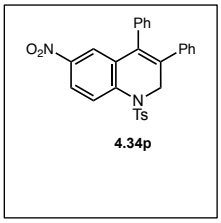
Ph
O2N
Ph
N
Ts

4.34p

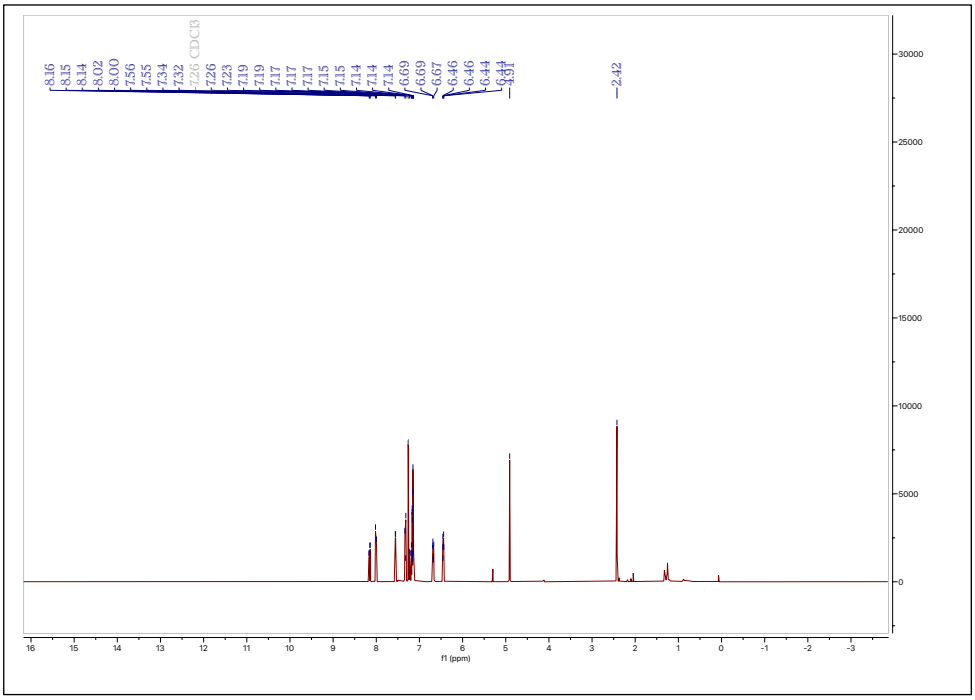
8.16
8.15
8.14
8.02
8.00
7.56
7.55
7.34
7.32
7.26 CDCl3
7.26
7.23
7.19
7.19
7.17
7.17
7.17
7.15
7.15
7.14
7.14
7.14
6.69
6.69
6.67
6.46
6.46
6.44
6.44
4.91
2.42
f1 (ppm)

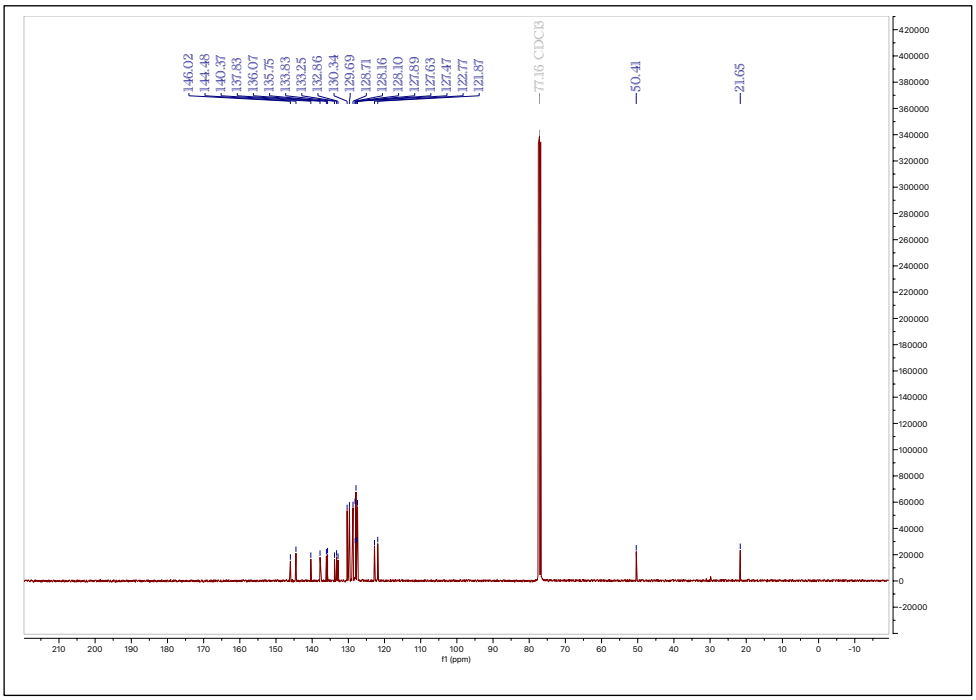
146.02
144.48
140.37
137.83
136.07
135.75
133.83
133.25
132.86
130.34
129.69
128.71
128.16
128.10
127.89
127.63
127.47
122.77
121.87
77.16 CDCl3
50.41
21.65
f1 (ppm)

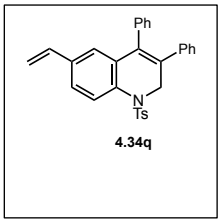
Ph
Ph
N
Ts

4.34q

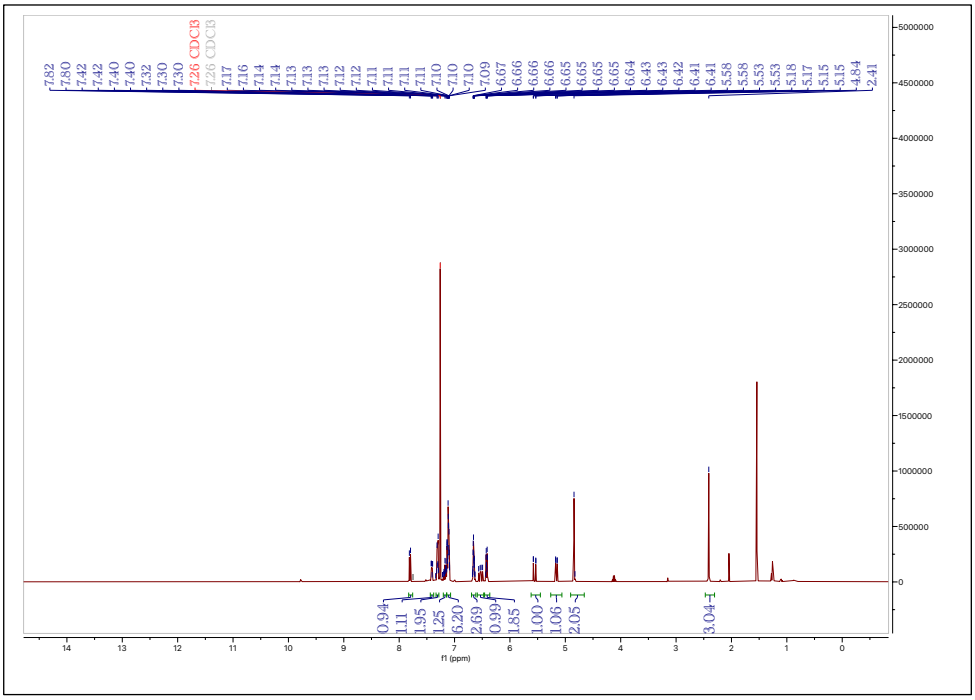
7.82
7.80
7.42
7.42
7.40
7.40
7.32
7.30
7.30
7.26 CDCl3
7.26 CDCl3
7.17
7.16
7.14
7.14
7.13
7.13
7.13
7.12
7.12
7.11
7.11
7.11
7.11
7.10
7.10
7.10
7.09
6.67
6.66
6.66
6.66
6.65
6.65
6.65
6.65
6.64
6.43
6.43
6.42
6.41
6.41
5.58
5.58
5.53
5.53
5.18
5.17
5.15
5.15
4.84
2.41
0.94
1.11
1.95
1.25
6.20
2.69
0.99
1.85
1.00
1.06
2.05
3.04
f1 (ppm)

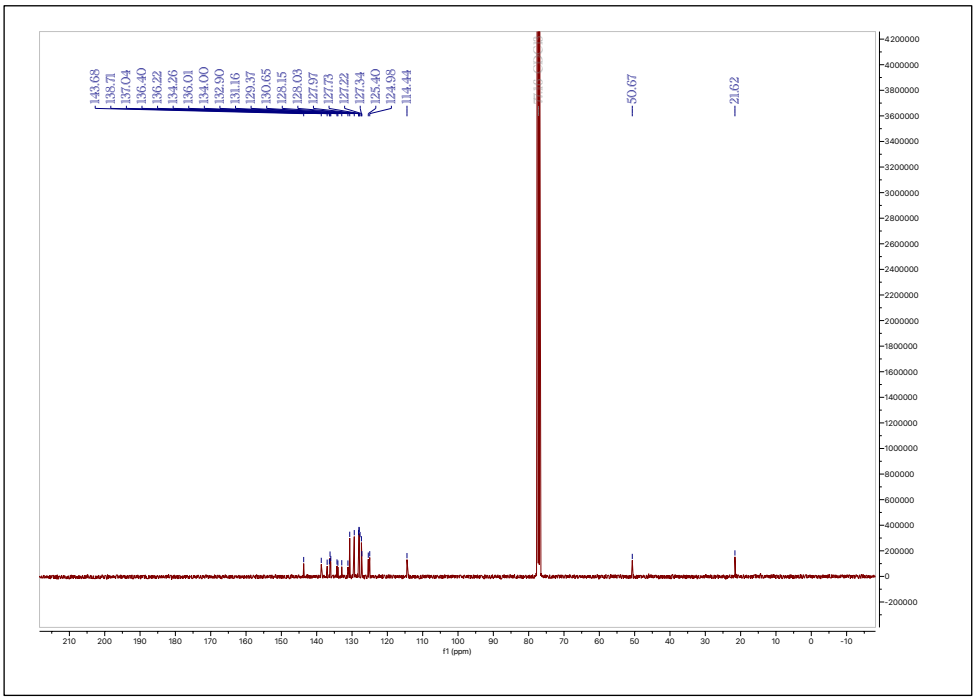
143.68
138.71
137.04
136.40
136.22
134.26
136.01
134.00
132.90
131.16
129.37
130.65
128.15
128.03
127.97
127.73
127.22
127.34
125.40
124.98
114.44
50.67
21.62
f1 (ppm)

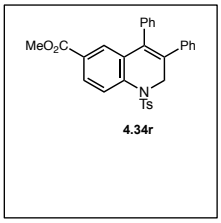
Ph
MeO2C
Ph
N
Ts

4.34r

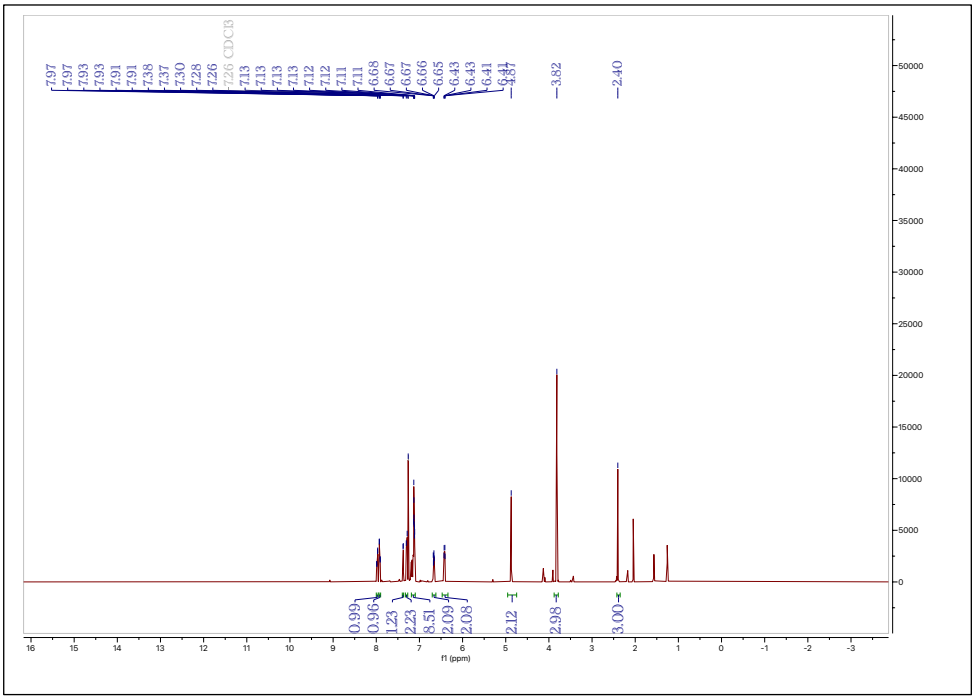
7.97
7.97
7.93
7.93
7.91
7.91
7.38
7.37
7.30
7.28
7.26
7.26 CDCl3
7.13
7.13
7.13
7.13
7.12
7.12
7.11
7.11
6.68
6.67
6.67
6.66
6.65
6.43
6.41
4.87
3.82
2.40
0.99
0.96
1.23
2.23
8.51
2.09
2.08
2.12
2.98
3.00
f1 (ppm)

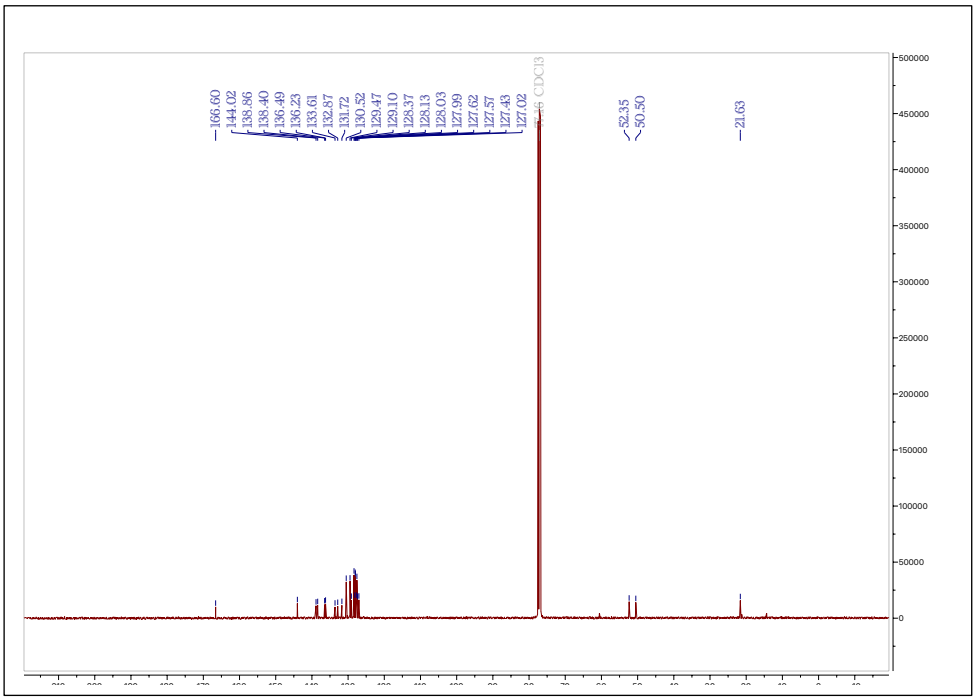
166.60
144.02
138.86
138.40
136.49
136.23
133.61
132.87
131.72
130.52
129.47
129.10
128.37
128.13
128.03
127.99
127.62
127.57
127.43
127.02
77.16 CDCl3
52.35
50.50
21.63

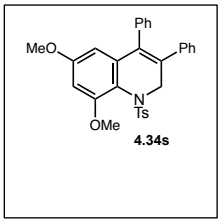
Ph
MeO
Ph
N
Ts
OMe

4.34s

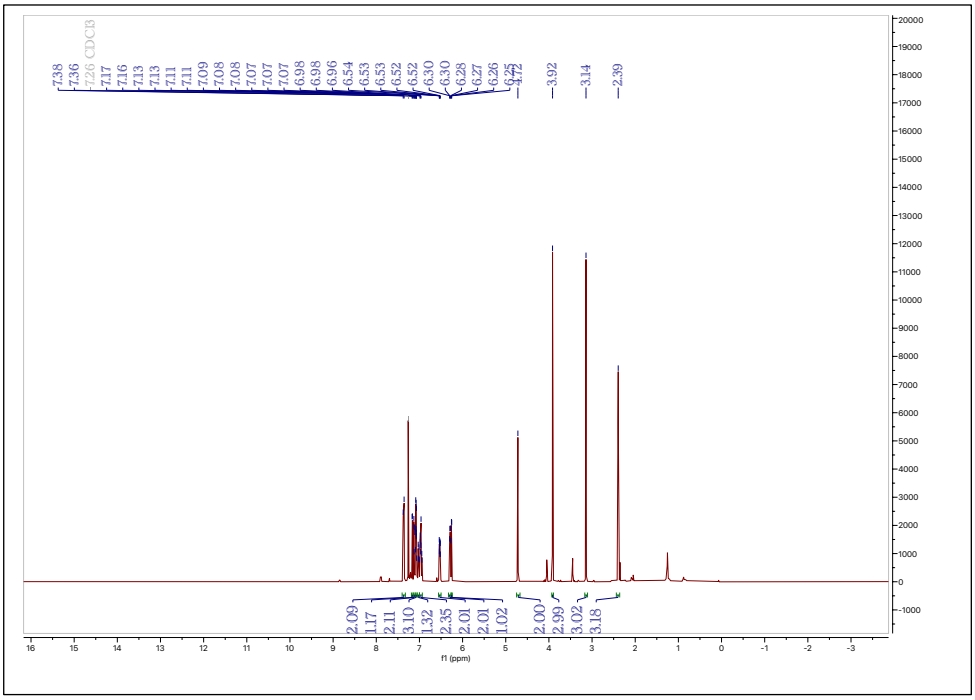
7.38
7.36
7.26 CDCl3
7.17
7.16
7.13
7.13
7.11
7.11
7.09
7.08
7.08
7.07
7.07
7.07
6.98
6.98
6.96
6.54
6.53
6.53
6.52
6.52
6.30
6.30
6.28
6.27
6.26
4.72
3.92
3.14
2.39
2.09
1.17
2.11
3.10
1.32
2.35
2.01
2.01
1.02
2.00
2.99
3.02
3.18
f1 (ppm)

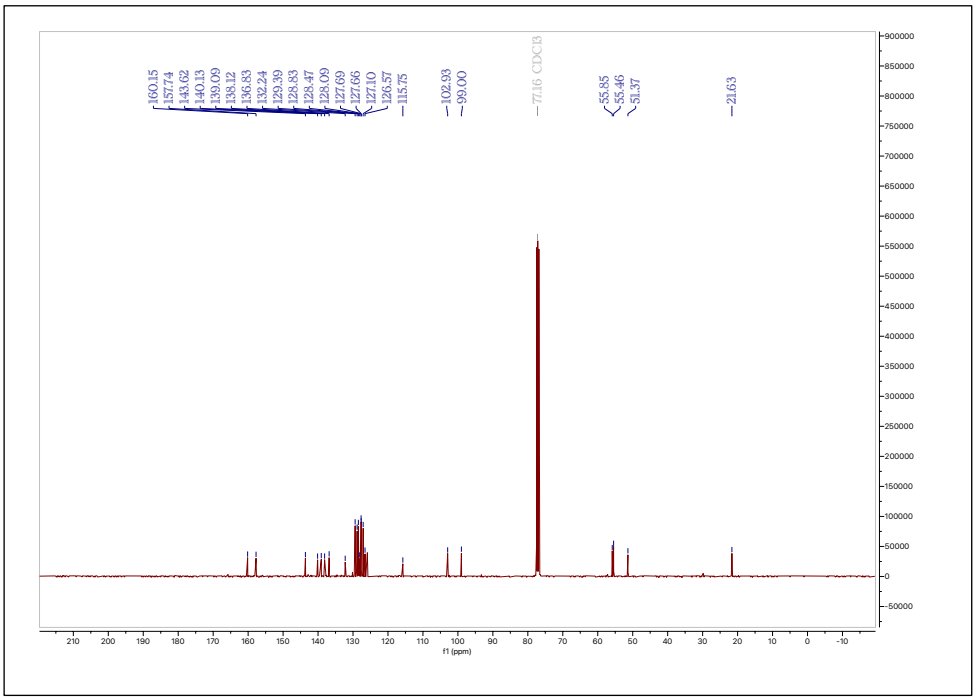
160.15
157.74
143.62
140.13
139.09
138.12
136.83
132.24
129.39
128.83
128.47
128.09
127.69
127.66
127.10
126.57
115.75
102.93
99.00
77.16 CDCl3
55.85
55.46
51.37
21.63
f1 (ppm)

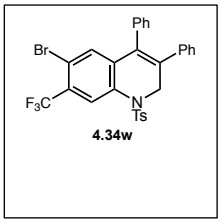
Ph
Br
Ph
F3C
N
Ts

4.34w

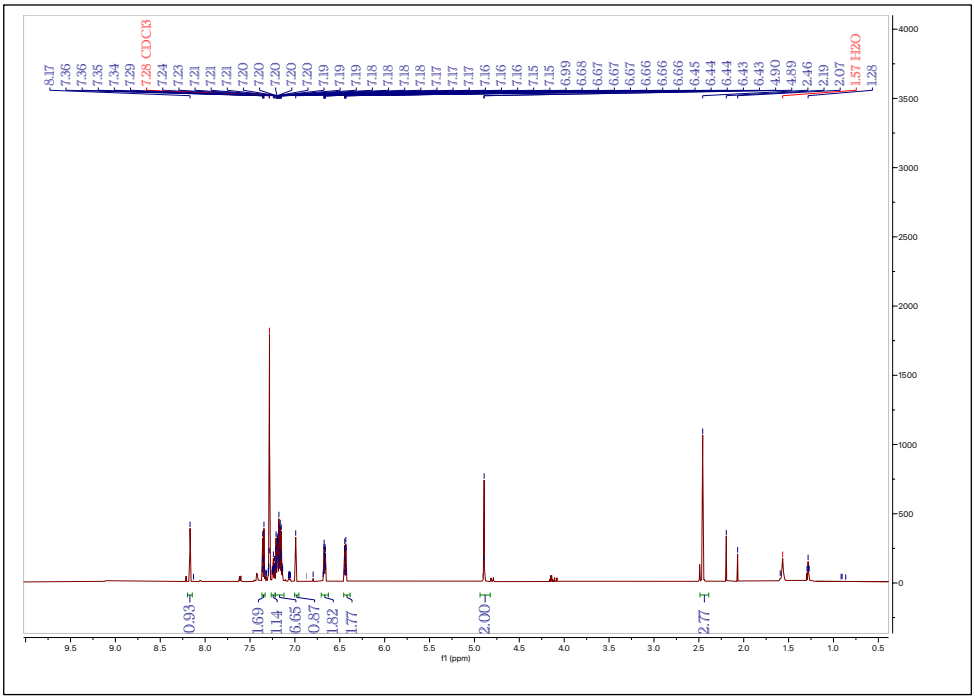
8.17
7.36
7.36
7.35
7.34
7.29
7.28 CDCl3
7.24
7.23
7.21
7.21
7.21
7.20
7.20
7.20
7.20
7.20
7.19
7.19
7.19
7.18
7.18
7.18
7.18
7.17
7.17
7.17
7.16
7.16
7.16
7.15
7.15
6.99
6.68
6.67
6.67
6.67
6.66
6.66
6.66
6.45
6.44
6.44
6.43
6.43
4.90
4.89
2.46
2.19
2.07
1.57 H2O
1.28
0.93
1.69
1.14
6.65
0.87
1.82
1.77
2.00
2.77
f1 (ppm)

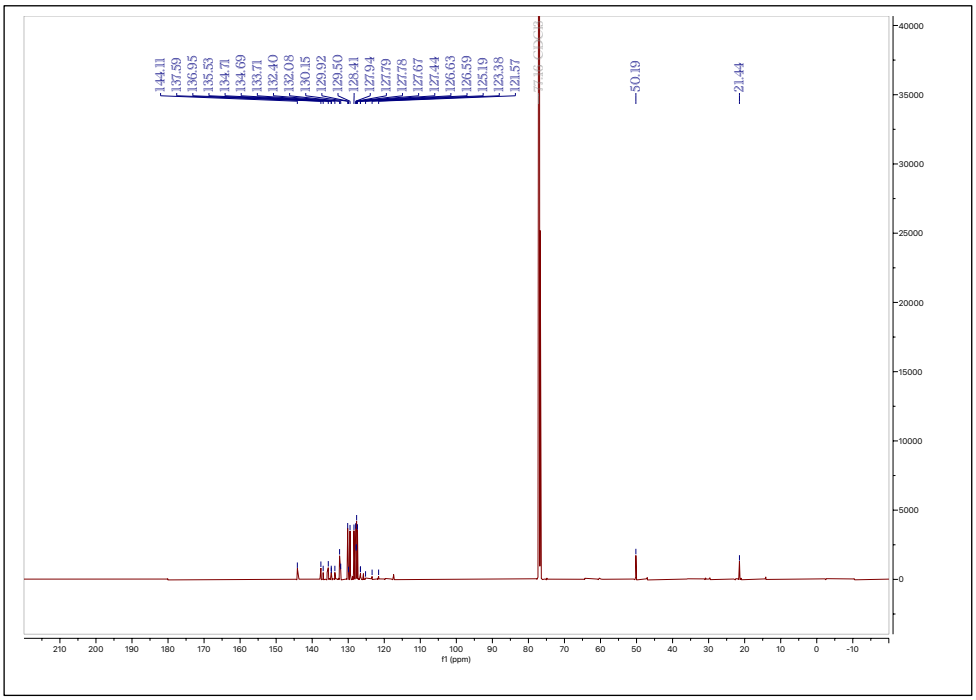
144.11
137.59
136.95
135.53
134.71
134.69
133.71
132.40
132.08
130.15
129.92
129.50
128.41
127.94
127.79
127.78
127.67
127.44
126.63
126.59
125.19
123.38
121.57
77.48 CDCl3
50.19
21.44
f1 (ppm)

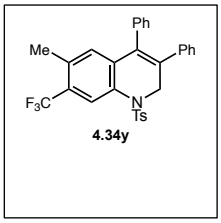

4.34y

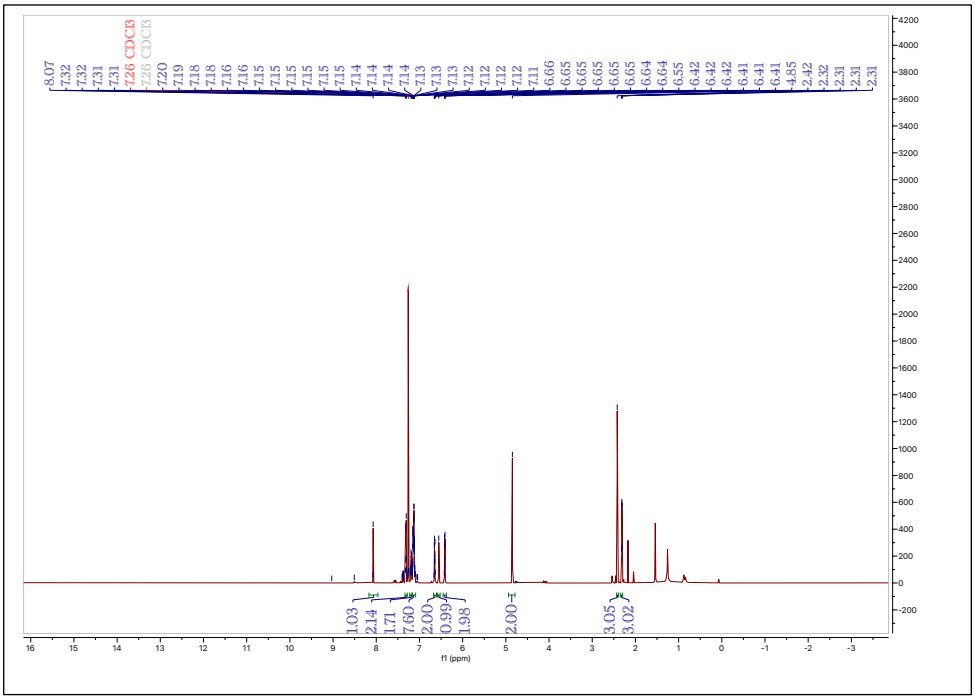

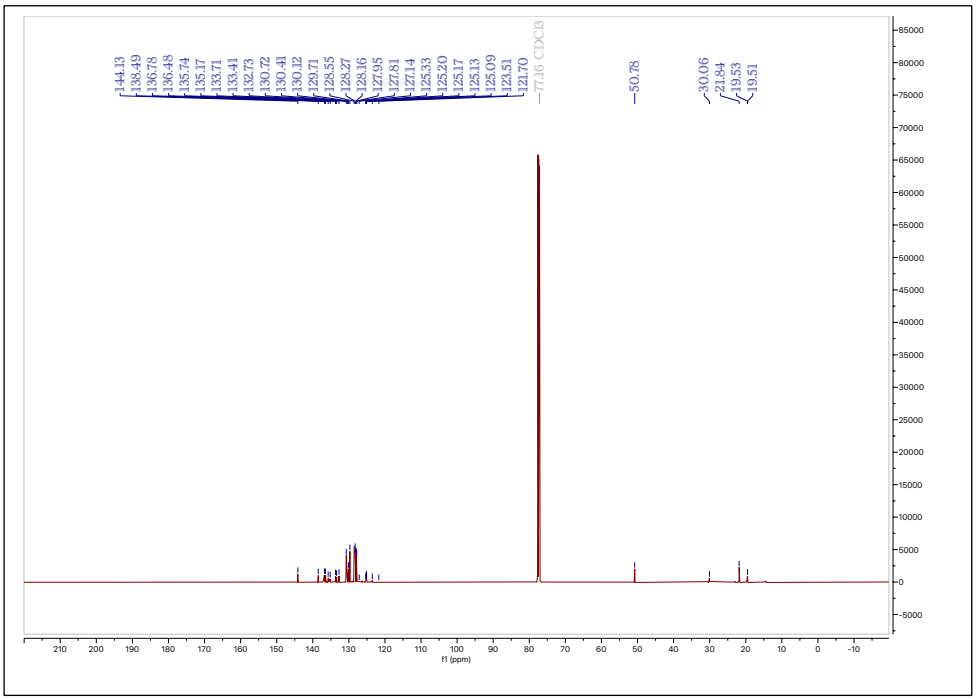

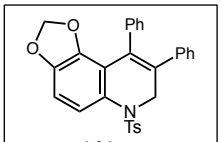
O
O
Ph
Ph
N
Ts

4.34x

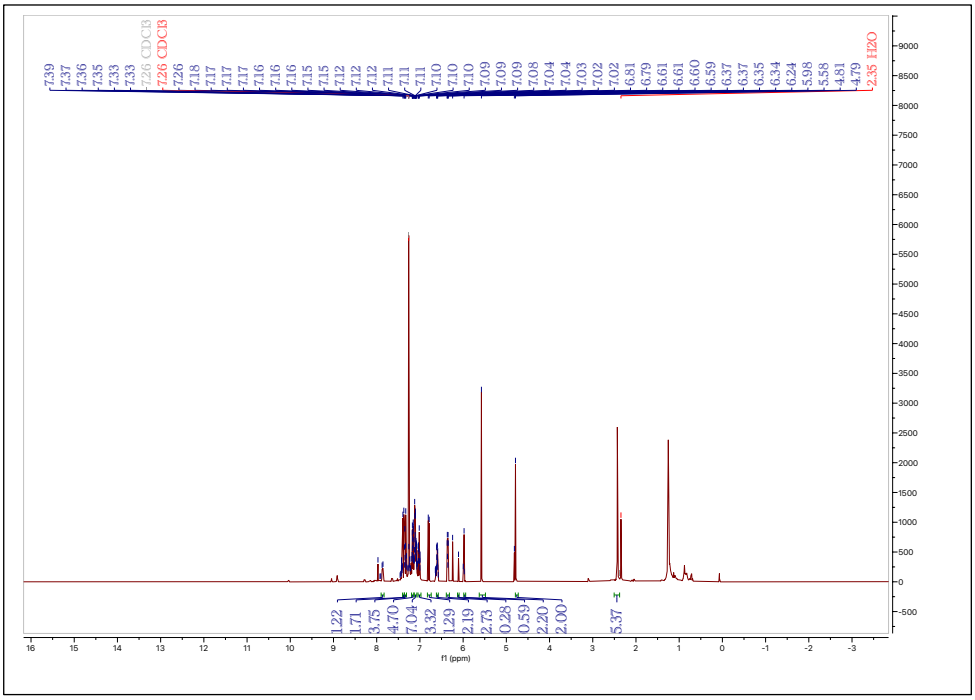
7.39
7.37
7.36
7.35
7.33
7.33
7.26 CDCl3
7.26 CDCl3
7.26
7.18
7.17
7.17
7.17
7.16
7.16
7.16
7.15
7.15
7.12
7.12
7.12
7.11
7.11
7.11
7.10
7.10
7.10
7.09
7.09
7.09
7.08
7.04
7.04
7.03
7.02
7.02
6.81
6.79
6.61
6.61
6.60
6.59
6.37
6.35
6.34
6.24
5.98
5.58
4.81
4.79
2.35 H2O
1.22
1.71
3.75
4.70
7.04
3.32
1.29
2.19
2.73
0.28
0.59
2.20
2.00
5.37
f1 (ppm)

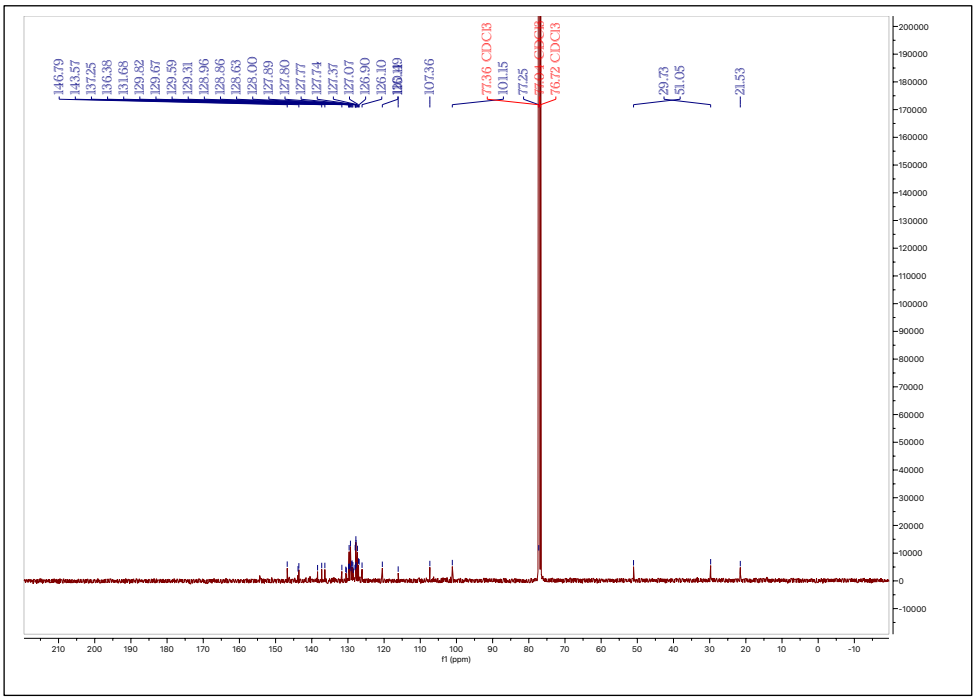
146.79
143.57
137.25
136.38
131.68
129.82
129.67
129.59
129.31
128.96
128.86
128.63
128.00
127.89
127.80
127.77
127.74
127.37
127.07
126.90
126.10
107.36
77.36 CDCl3
101.15
77.25
76.72 CDCl3
29.73
51.05
21.53
f1 (ppm)

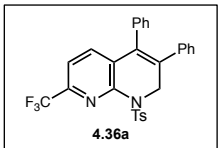
Ph
Ph
F3C
N
N
Ts

4.36a

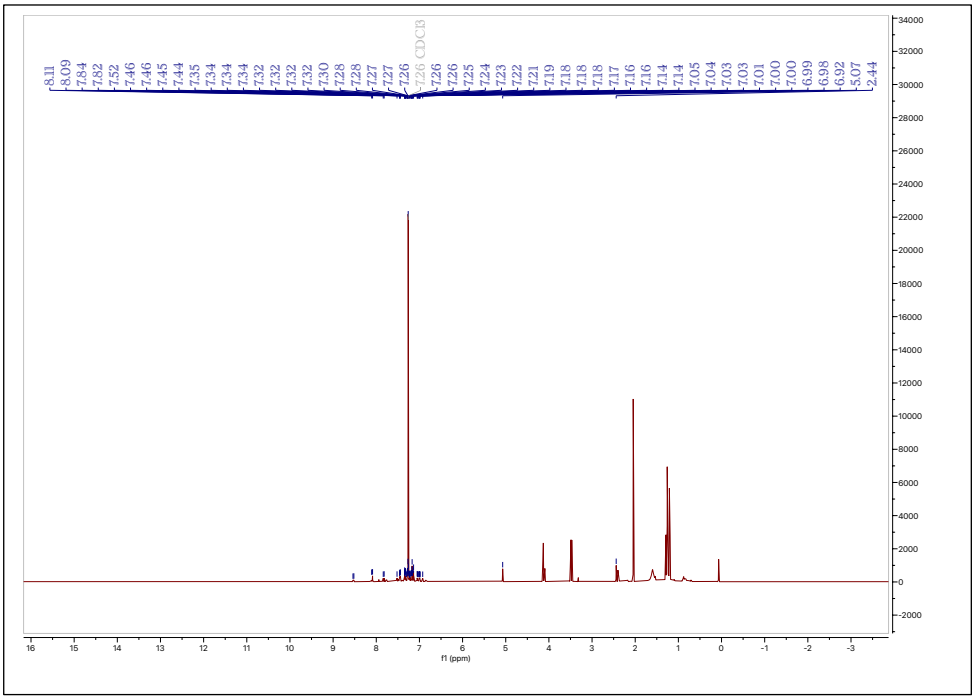
8.11
8.09
7.84
7.82
7.52
7.46
7.46
7.45
7.44
7.35
7.34
7.34
7.34
7.32
7.32
7.32
7.30
7.28
7.28
7.27
7.27
7.26
7.26 CDCl3
7.26
7.25
7.24
7.23
7.22
7.21
7.19
7.18
7.18
7.18
7.17
7.16
7.16
7.14
7.14
7.05
7.04
7.03
7.03
7.01
7.00
7.00
6.99
6.98
6.92
5.07
2.44
f1 (ppm)

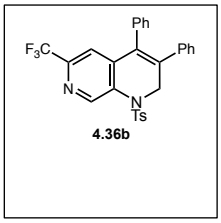
Ph
F3C
Ph
N
N
Ts

4.36b

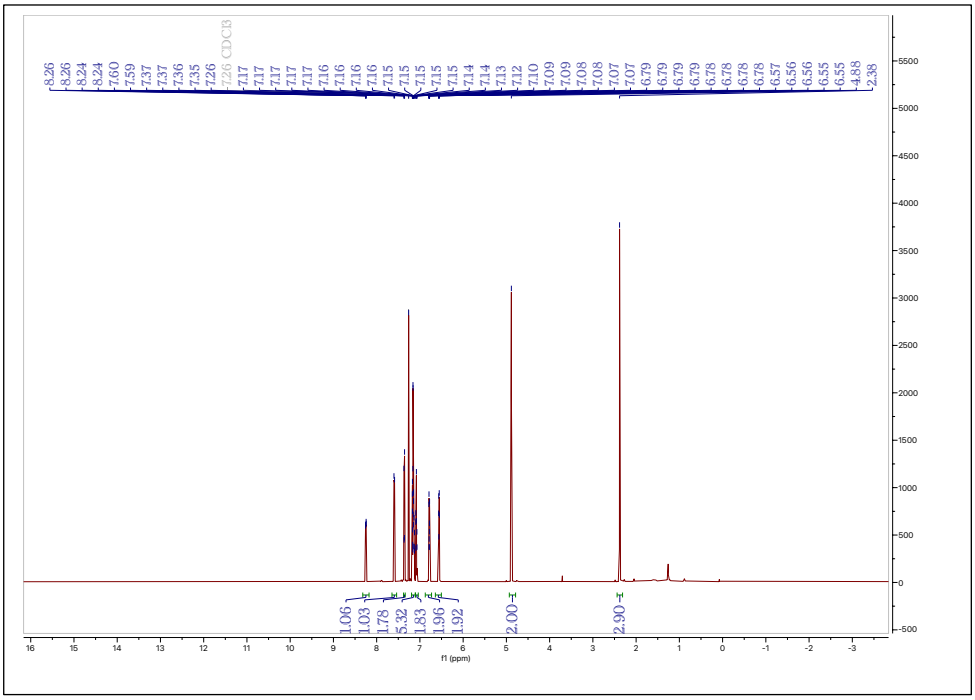
8.26
8.26
8.24
8.24
7.60
7.59
7.37
7.37
7.36
7.35
7.26
7.26 CDCl3
7.17
7.17
7.17
7.17
7.17
7.16
7.16
7.16
7.15
7.15
7.15
7.15
7.14
7.14
7.13
7.12
7.10
7.09
7.09
7.08
7.08
7.07
7.07
6.79
6.79
6.79
6.78
6.78
6.78
6.78
6.57
6.56
6.56
6.55
6.55
4.88
2.38
1.06
1.03
1.78
5.32
1.83
1.96
1.92
2.00
2.90
f1 (ppm)

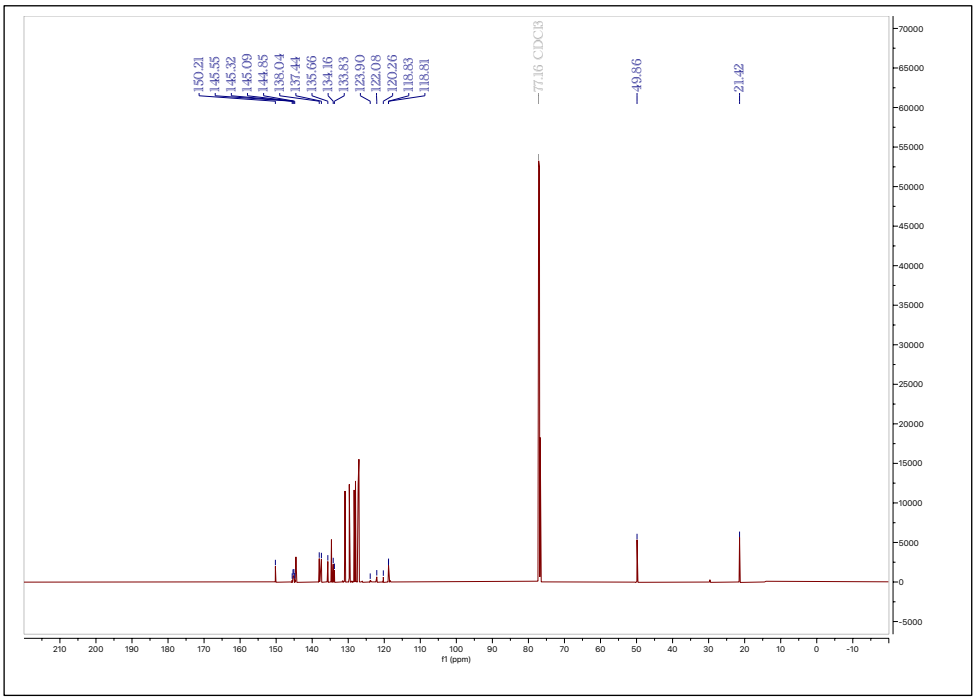
150.21
145.55
145.32
145.09
144.85
138.04
137.44
135.66
134.16
133.83
123.90
122.08
120.26
118.83
118.81
77.16 CDCl3
49.86
21.42
f1 (ppm)

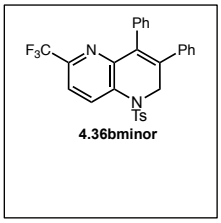
Ph
F3C
N
Ph
N
Ts

4.36bminor

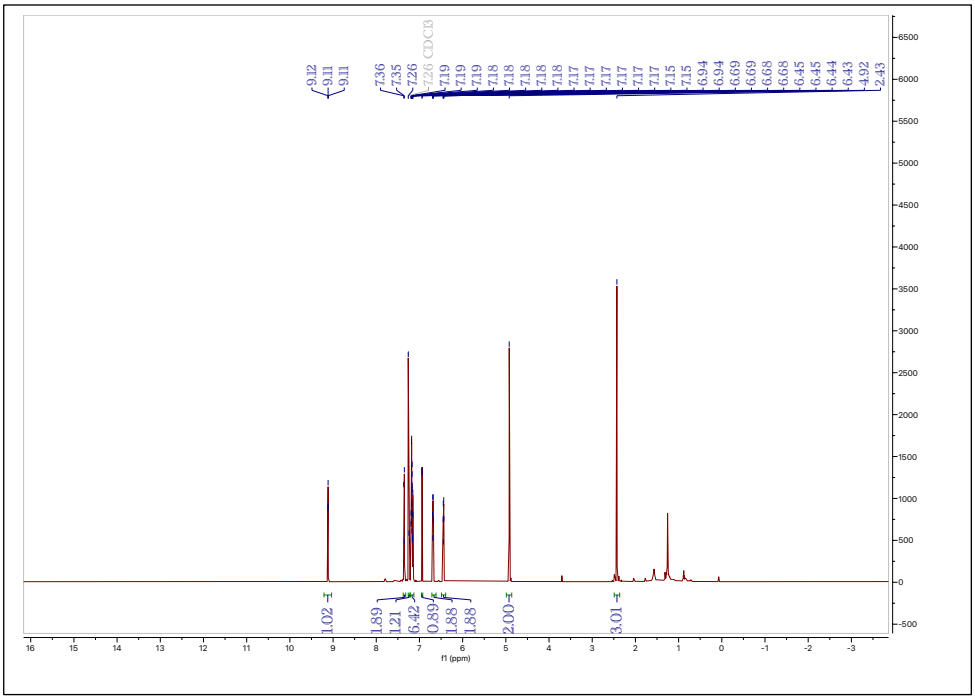
9.12
9.11
9.11
7.36
7.35
7.26
7.26 CDCl3
7.19
7.19
7.19
7.18
7.18
7.18
7.18
7.17
7.17
7.17
7.17
7.17
7.17
7.17
7.15
6.94
6.94
6.69
6.69
6.68
6.68
6.45
6.45
6.44
6.43
4.92
2.43
1.02
1.89
1.21
6.42
0.89
1.88
1.88
2.00
3.01
f1 (ppm)

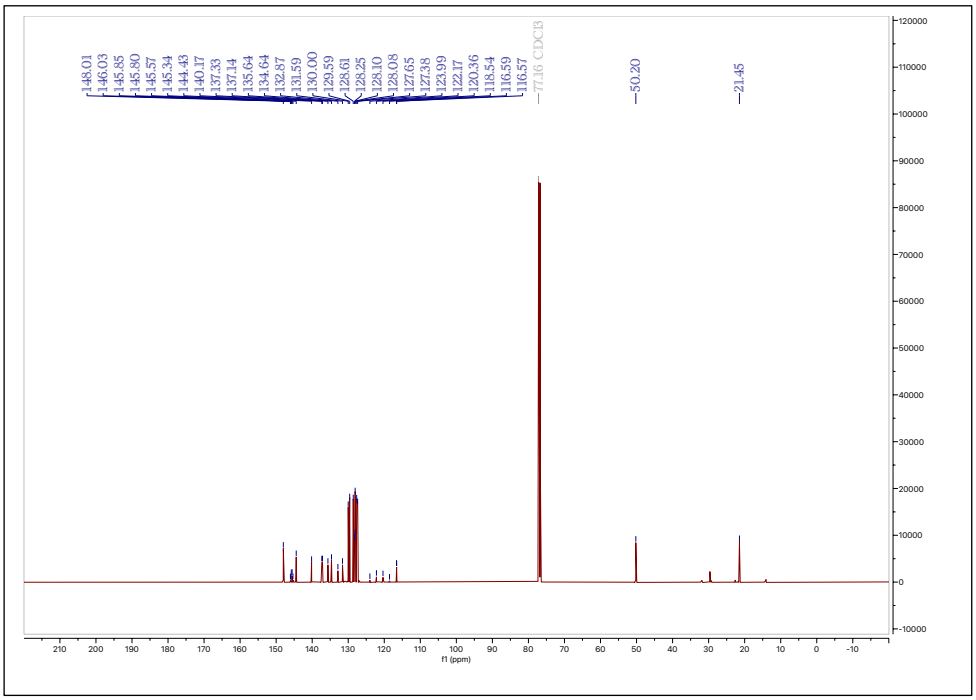
148.01
146.03
145.85
145.80
145.57
145.34
144.43
140.17
137.33
137.14
135.64
134.64
132.87
131.59
130.00
129.59
128.61
128.25
128.10
128.08
127.65
127.38
123.99
122.17
120.36
118.54
116.59
116.57
77.16 CDCl3
50.20
21.45
f1 (ppm)

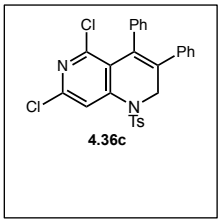
Cl
Ph
Ph
N
Cl
N
Ts

4.36c

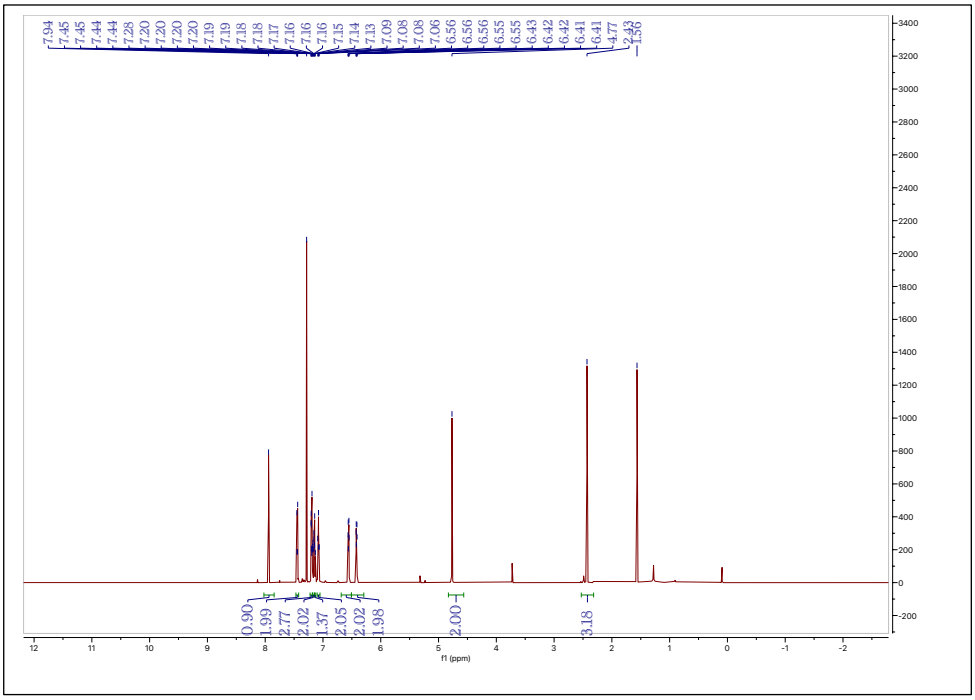
7.94
7.45
7.45
7.44
7.44
7.28
7.20
7.20
7.20
7.19
7.19
7.18
7.18
7.17
7.16
7.16
7.16
7.15
7.14
7.13
7.09
7.08
7.08
7.06
6.56
6.56
6.55
6.55
6.43
6.42
6.42
6.41
6.41
4.77
2.43
1.56
0.90
1.99
2.77
2.02
1.37
2.05
2.02
1.98
2.00
3.18
f1 (ppm)

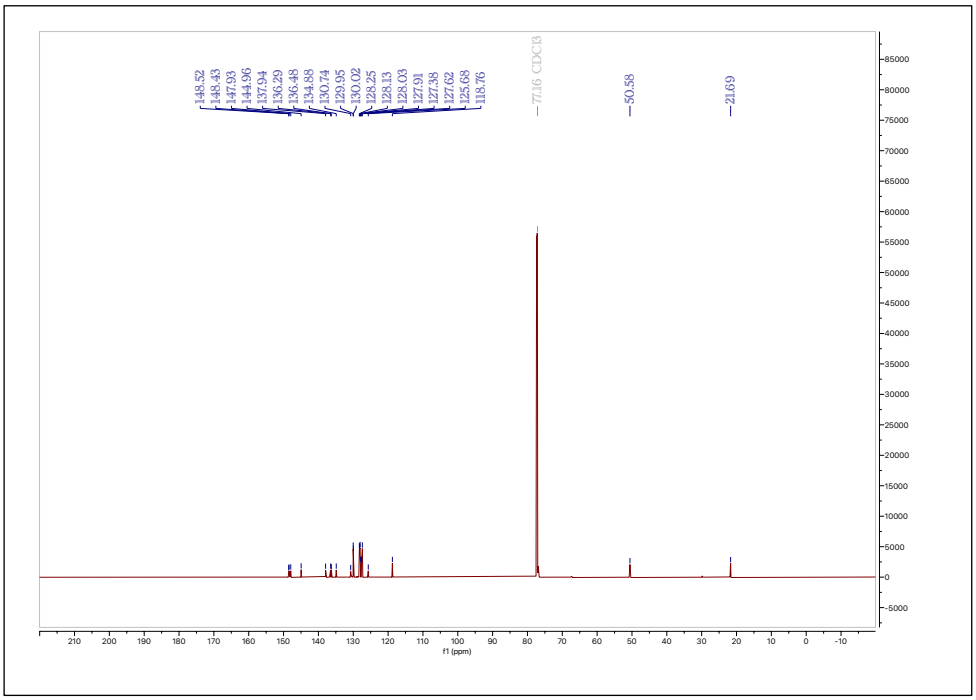
148.52
148.43
147.93
144.96
137.94
136.29
136.48
134.88
130.74
129.95
130.02
128.25
128.13
128.03
127.91
127.38
127.62
125.68
118.76
77.16 CDCl3
50.58
21.69
f1 (ppm)

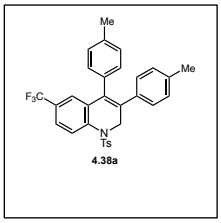
Me
Me
F3C
N
Ts

4.38a

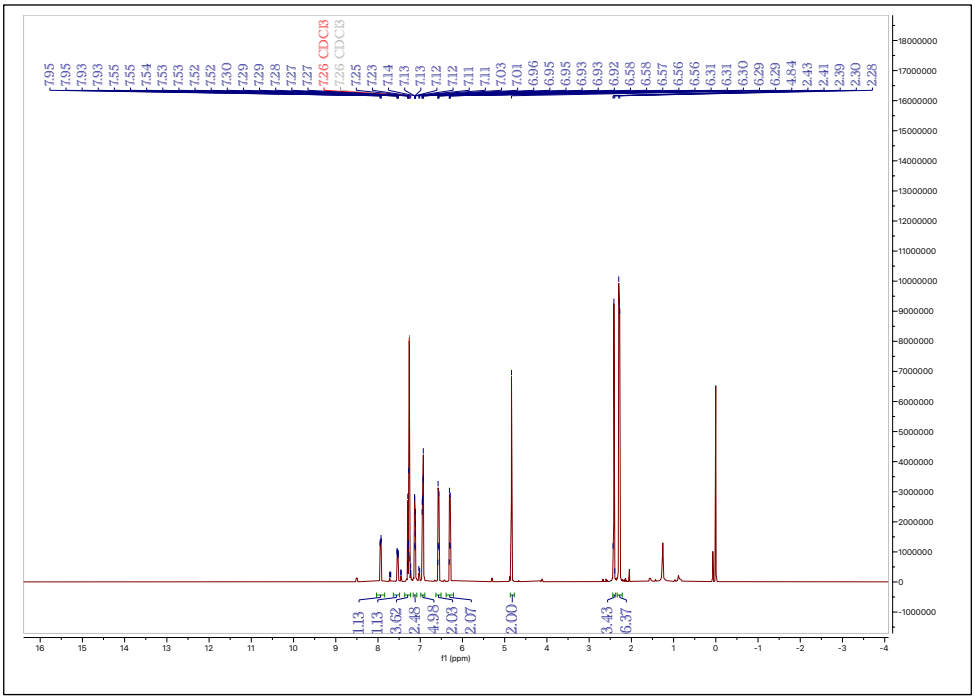
7.95
7.95
7.93
7.93
7.55
7.55
7.54
7.53
7.53
7.52
7.30
7.29
7.29
7.28
7.27
7.27
7.26 CDCl3
7.25
7.23
7.14
7.13
7.13
7.12
7.12
7.11
7.11
7.03
7.01
6.96
6.95
6.95
6.93
6.93
6.92
6.58
6.58
6.57
6.56
6.56
6.31
6.31
6.30
6.29
4.84
2.43
2.41
2.39
2.30
2.28
1.13
1.13
3.62
2.48
4.98
2.03
2.07
2.00
3.43
6.37
f1 (ppm)

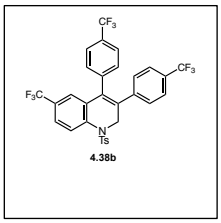
CF3
CF3
F3C
N
Ts

4.38b

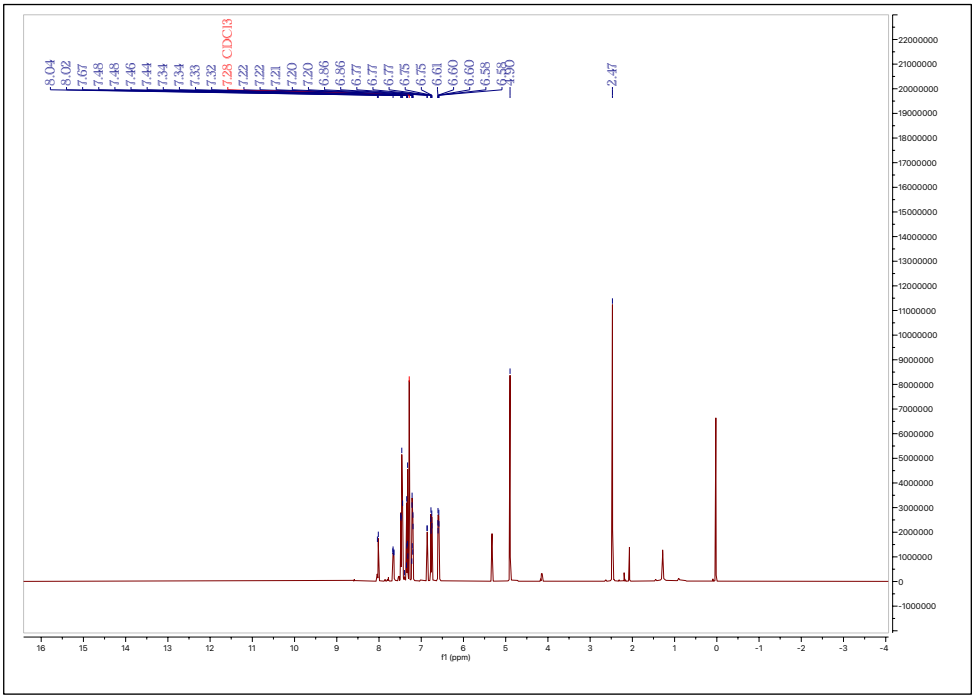
8.04
8.02
7.67
7.48
7.48
7.46
7.44
7.34
7.34
7.33
7.32
7.28 CDCl3
7.22
7.22
7.21
7.20
7.20
6.86
6.86
6.77
6.77
6.77
6.75
6.75
6.61
6.60
6.60
6.58
4.90
2.47
f1 (ppm)

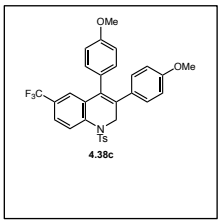
OMe
OMe
F3C
N
Ts

4.38c

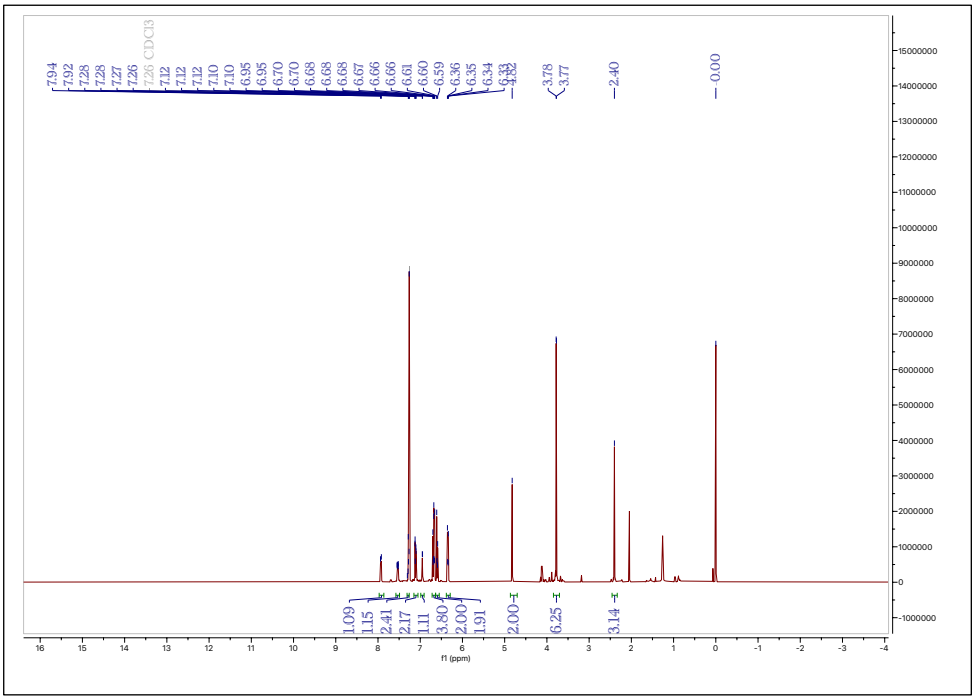
7.94
7.92
7.28
7.28
7.27
7.26
7.26 CDCl3
7.12
7.12
7.12
7.12
7.10
7.10
6.95
6.95
6.70
6.70
6.68
6.68
6.68
6.67
6.66
6.66
6.61
6.60
6.59
6.36
6.35
6.34
6.33
3.78
3.77
2.40
0.00
1.09
1.15
2.41
2.17
1.11
3.80
2.00
1.91
2.00
6.25
3.14
f1 (ppm)

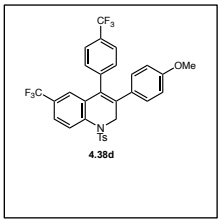
CF3
OMe
F3C
N
Ts

4.38d

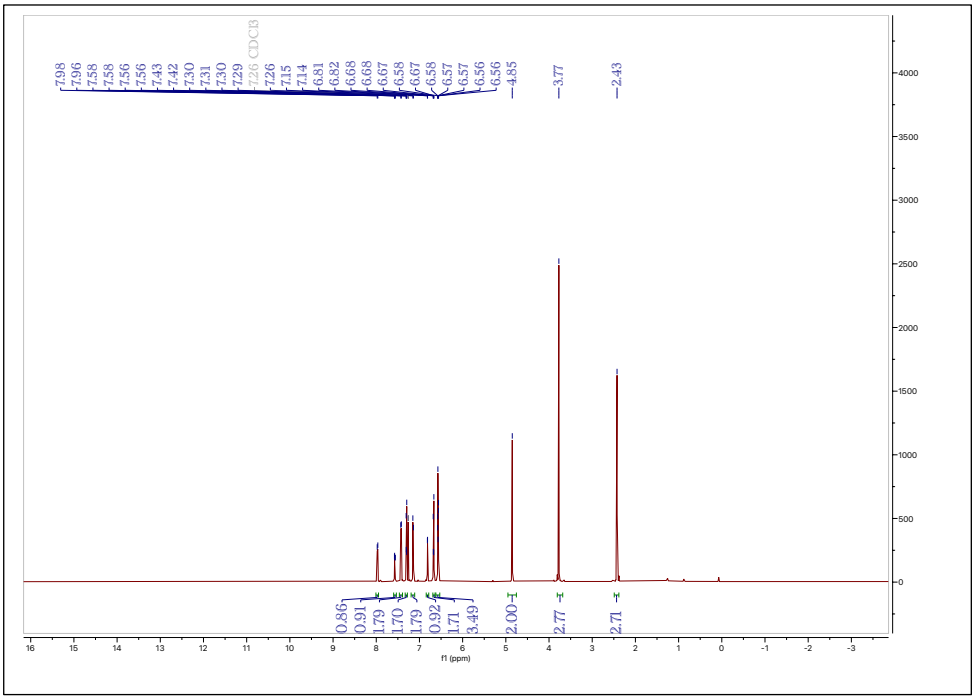
7.98
7.96
7.58
7.58
7.56
7.56
7.43
7.42
7.30
7.31
7.30
7.29
7.26 CDCl3
7.26
7.15
7.14
6.81
6.82
6.68
6.68
6.67
6.58
6.67
6.58
6.57
6.57
6.56
6.56
4.85
3.77
2.43
0.86
0.91
1.79
1.70
1.79
0.92
1.71
3.49
2.00
2.77
2.71
f1 (ppm)

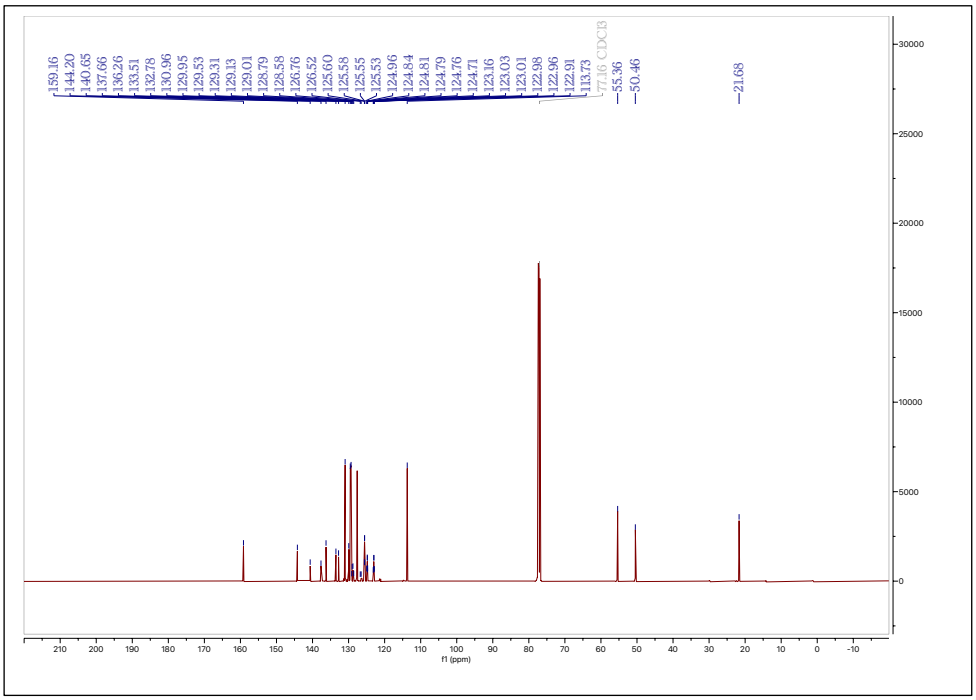
159.16
144.20
140.65
137.66
136.26
133.51
132.78
130.96
129.95
129.53
129.31
129.13
129.01
128.79
128.58
126.76
126.52
125.60
125.58
125.55
125.53
124.96
124.84
124.81
124.79
124.76
124.71
123.16
123.03
123.01
122.98
122.96
122.91
113.73
77.16 CDCl3
55.36
50.46
21.68
f1 (ppm)

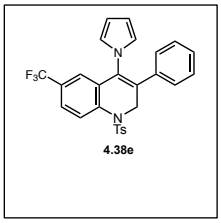
F3C
N
N
Ts

4.38e

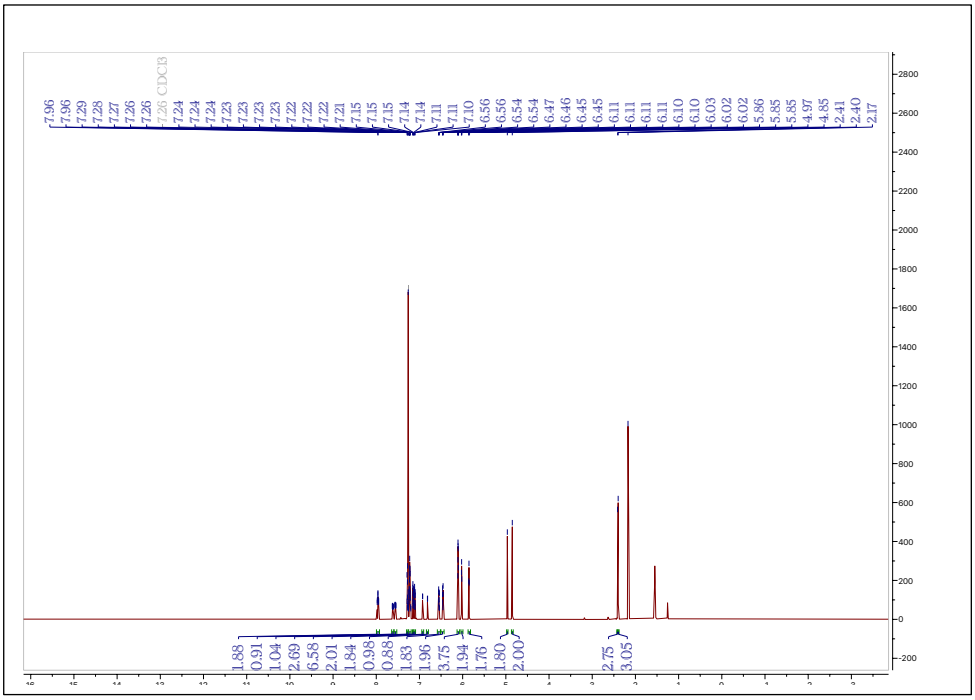
7.96
7.96
7.29
7.28
7.27
7.26
7.26
7.26 CDCl3
7.24
7.24
7.24
7.23
7.23
7.23
7.23
7.22
7.22
7.22
7.21
7.15
7.15
7.15
7.14
7.14
7.11
7.11
7.11
7.10
6.56
6.56
6.54
6.54
6.47
6.46
6.45
6.45
6.11
6.11
6.11
6.11
6.10
6.10
6.03
6.02
6.02
5.86
5.85
5.85
4.97
4.85
2.41
2.40
2.17
1.88
0.91
1.04
2.69
6.58
2.01
1.84
0.98
0.88
1.83
1.96
3.75
1.94
1.76
1.80
2.00
2.75
3.05

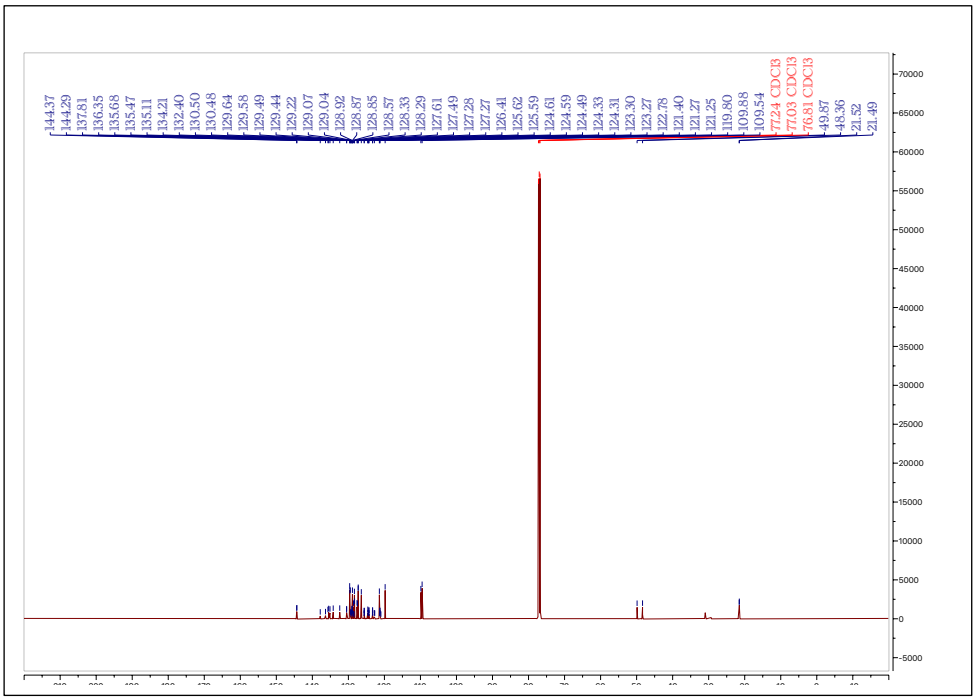
144.37
144.29
137.81
136.35
135.68
135.47
135.11
134.21
132.40
130.50
130.48
129.64
129.58
129.49
129.44
129.22
129.07
129.04
128.92
128.87
128.85
128.57
128.33
128.29
127.61
127.49
127.28
127.27
126.41
125.62
125.59
124.61
124.59
124.49
124.33
124.31
123.30
123.27
122.78
121.40
121.27
121.25
119.80
109.88
109.54
77.24 CDCl3
77.03 CDCl3
76.81 CDCl3
49.87
48.36
21.52
21.49

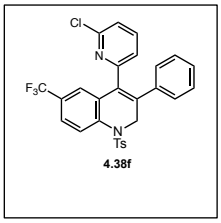
Cl
N
F3C
N
Ts

4.38f

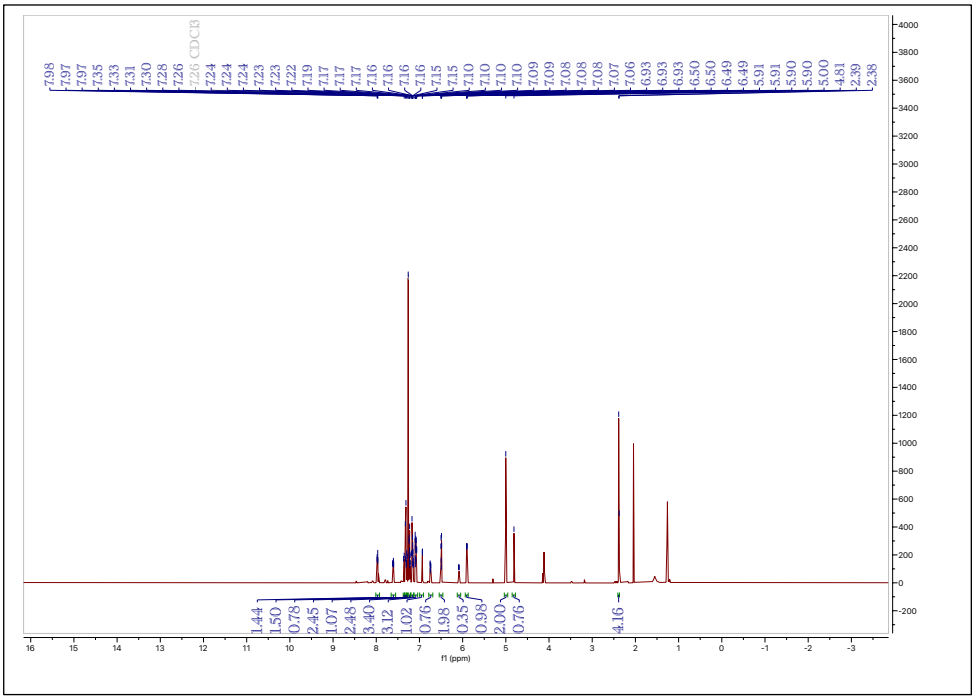
7.98 7.97 7.97 7.35 7.33 7.31 7.30 7.28 7.26 CDCl3 7.24 7.24 7.24 7.23 7.23 7.22 7.19 7.17 7.17 7.17 7.16 7.16 7.16 7.16 7.15 7.15 7.10 7.10 7.10 7.10 7.09 7.09 7.08 7.08 7.08 7.07 7.06 6.93 6.93 6.93 6.50 6.50 6.49 6.49 5.91 5.90 5.90 5.00 4.81 2.39 2.38
1.44 1.50 0.78 2.45 1.07 2.48 3.40 3.12 1.02 0.76 1.98 0.35 0.98 2.00 0.76 4.16
f1 (ppm)

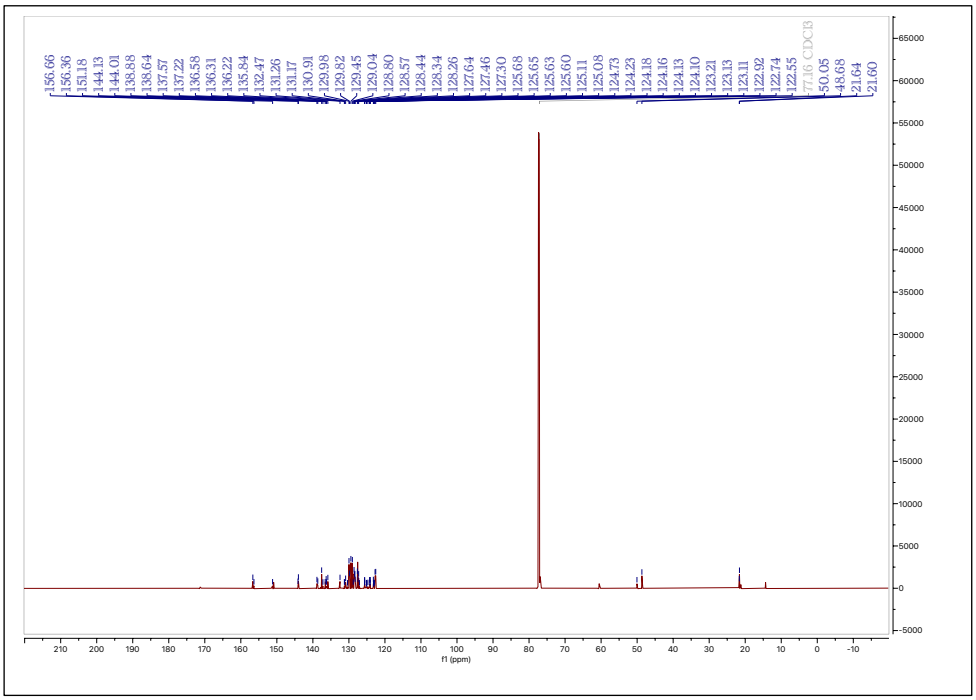
156.66 156.36 151.18 144.13 144.01 138.88 138.64 137.57 137.22 136.58 136.31 136.22 135.84 132.47 131.26 131.17 130.91 129.98 129.82 129.45 129.04 128.80 128.57 128.44 128.34 128.26 127.64 127.46 127.30 125.68 125.65 125.63 125.60 125.11 125.08 124.73 124.23 124.18 124.16 124.13 124.10 123.21 123.13 123.11 122.92 122.74 122.55 77.16 CDCl3 50.05 48.68 21.64 21.60
f1 (ppm)

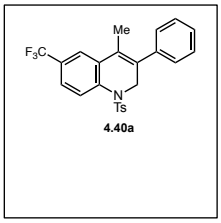
Me
F3C
N
Ts

4.40a

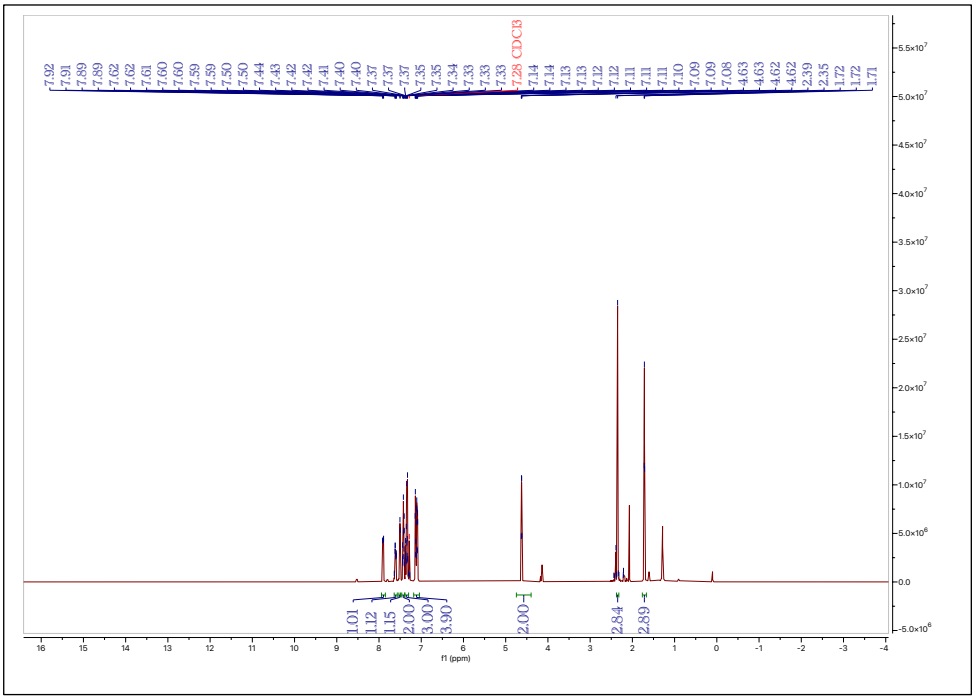
7.92
7.91
7.89
7.89
7.89
7.62
7.62
7.61
7.60
7.60
7.59
7.59
7.50
7.50
7.44
7.43
7.42
7.42
7.41
7.40
7.40
7.37
7.37
7.37
7.35
7.35
7.34
7.33
7.33
7.29 CDCl3
7.14
7.14
7.13
7.13
7.12
7.12
7.11
7.11
7.11
7.10
7.09
7.09
7.08
4.63
4.63
4.62
4.62
2.39
2.35
1.72
1.72
1.71
1.01
1.12
1.15
2.00
3.00
3.90
2.00
2.84
2.89
f1 (ppm)

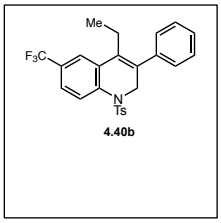
Me
F3C
N
Ts

4.40b

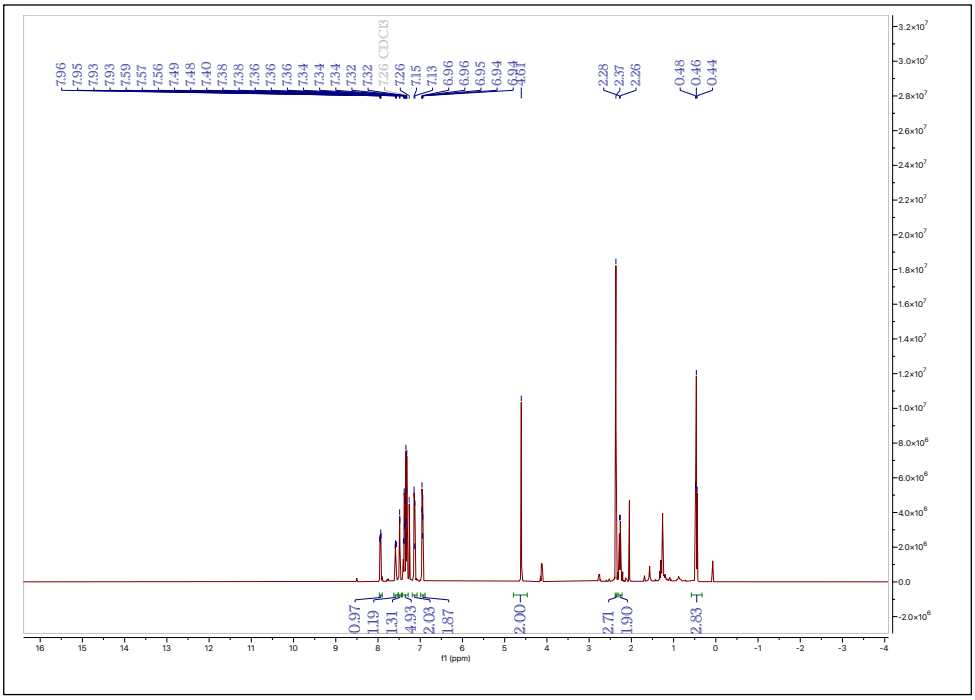
7.96
7.95
7.93
7.93
7.59
7.57
7.56
7.49
7.48
7.40
7.38
7.38
7.36
7.36
7.36
7.34
7.34
7.34
7.32
7.26 CDCl3
7.26
7.15
7.13
6.96
6.96
6.95
6.94
6.94
4.61
2.28
2.37
2.26
0.48
0.46
0.44
0.97
1.19
1.31
4.93
2.03
1.87
2.00
2.71
1.90
2.83
f1 (ppm)

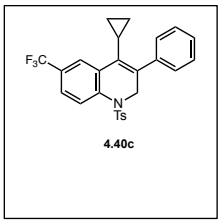
F3C
N
Ts

4.40c

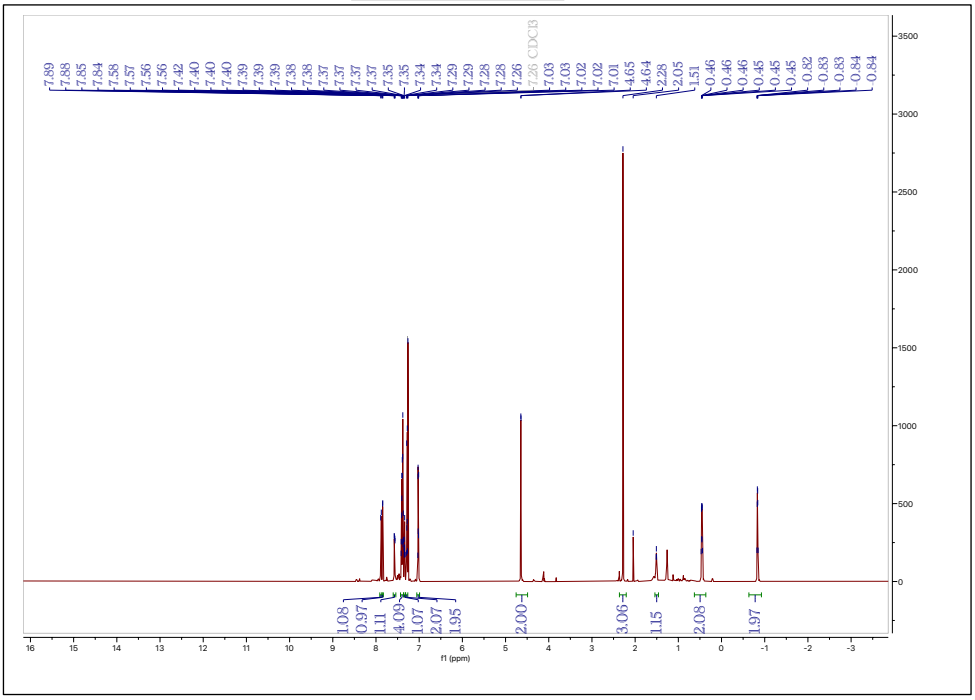
7.89
7.88
7.85
7.84
7.58
7.57
7.56
7.56
7.42
7.40
7.40
7.40
7.39
7.39
7.39
7.38
7.38
7.37
7.37
7.37
7.37
7.35
7.35
7.34
7.34
7.29
7.29
7.28
7.28
7.26
7.26 CDCl3
7.03
7.03
7.02
7.02
7.01
4.65
4.64
2.28
2.05
1.51
0.46
0.46
0.46
0.45
0.45
0.45
0.82
0.83
0.83
0.84
0.84
1.08
0.97
1.11
4.09
1.07
2.07
1.95
2.00
3.06
1.15
2.08
1.97
f1 (ppm)

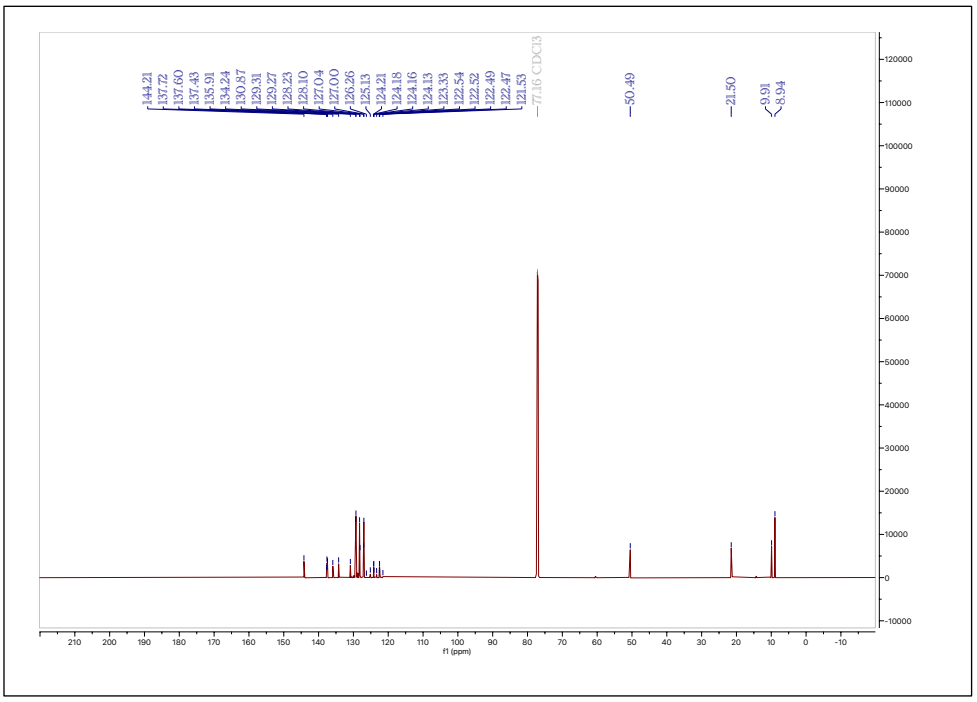
144.21
137.72
137.60
137.43
135.91
134.24
130.87
129.31
129.27
128.23
128.10
127.04
127.00
126.26
125.13
124.21
124.18
124.16
124.13
123.33
122.54
122.52
122.49
122.47
121.53
77.16 CDCl3
50.49
21.50
9.91
8.94
f1 (ppm)

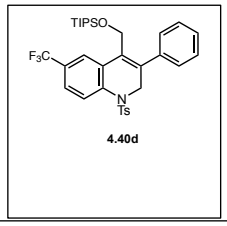
TIPSO
F3C
N
Ts

4.40d

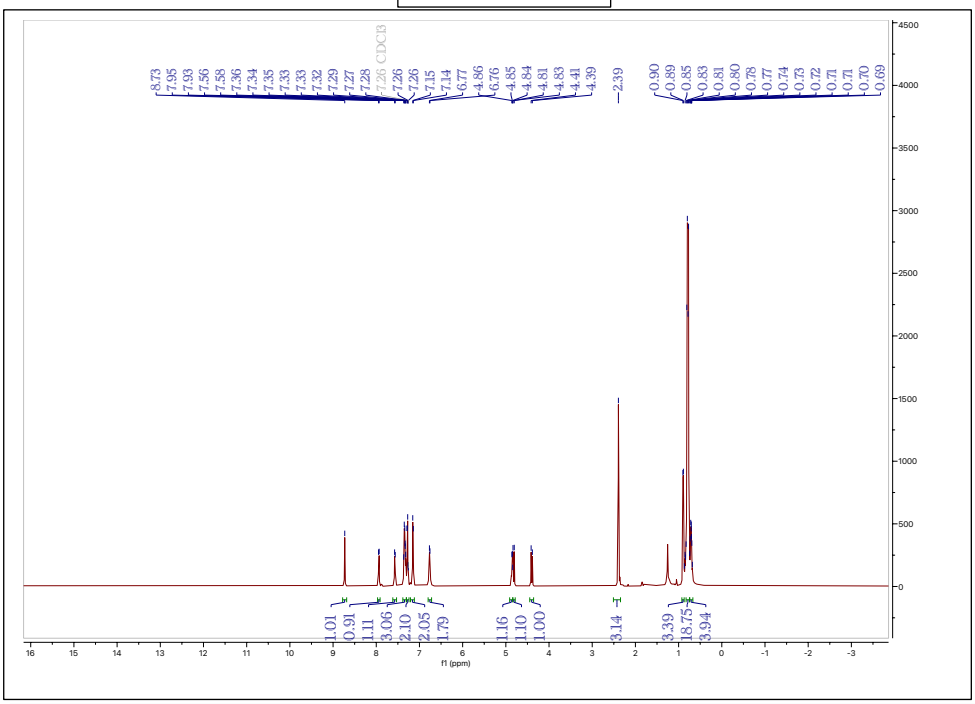
8.73
7.95
7.93
7.56
7.58
7.36
7.34
7.35
7.33
7.33
7.32
7.29
7.27
7.28
7.26 CDCl3
7.26
7.26
7.15
7.14
6.77
4.86
6.76
4.85
4.84
4.81
4.83
4.41
4.39
2.39
0.90
0.89
0.85
0.83
0.80
0.81
0.78
0.77
0.74
0.73
0.72
0.71
0.71
0.70
0.69
1.01
0.91
1.11
3.06
2.10
2.05
1.79
1.16
1.10
1.00
3.14
3.39
18.75
3.94
f1 (ppm)

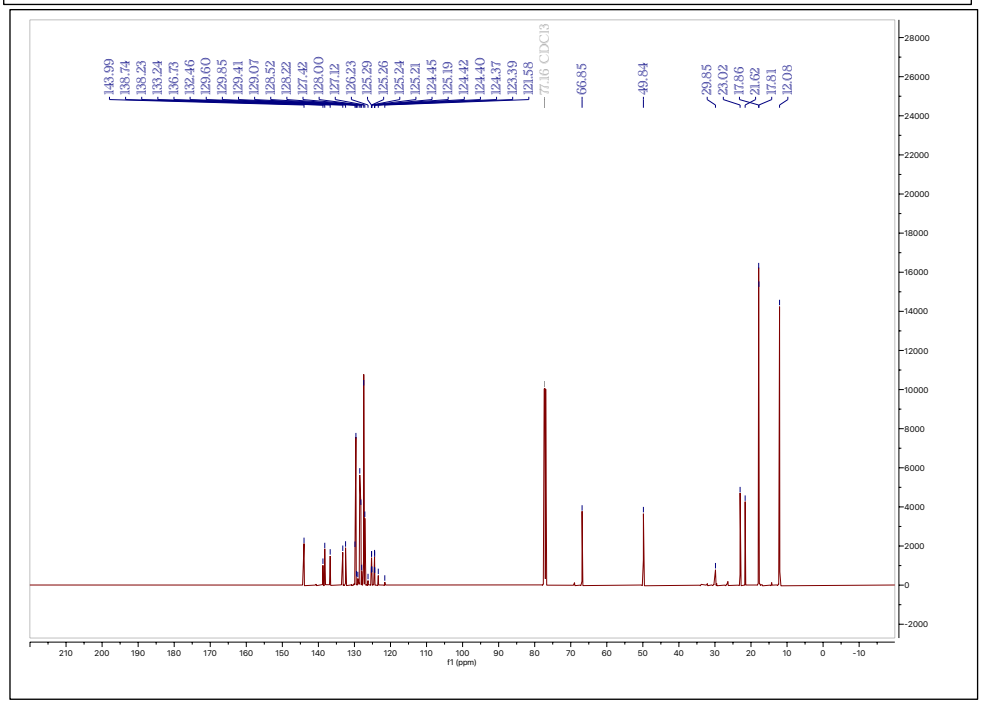
143.99
138.74
138.23
133.24
136.73
132.46
129.60
129.85
129.41
129.07
128.52
128.22
127.42
128.00
127.12
126.23
125.29
125.26
125.24
125.21
124.45
125.19
124.42
124.40
124.37
123.39
121.58
77.16 CDCl3
66.85
49.84
29.85
23.02
17.86
21.62
17.51
12.08
f1 (ppm)

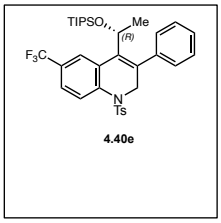

4.40e

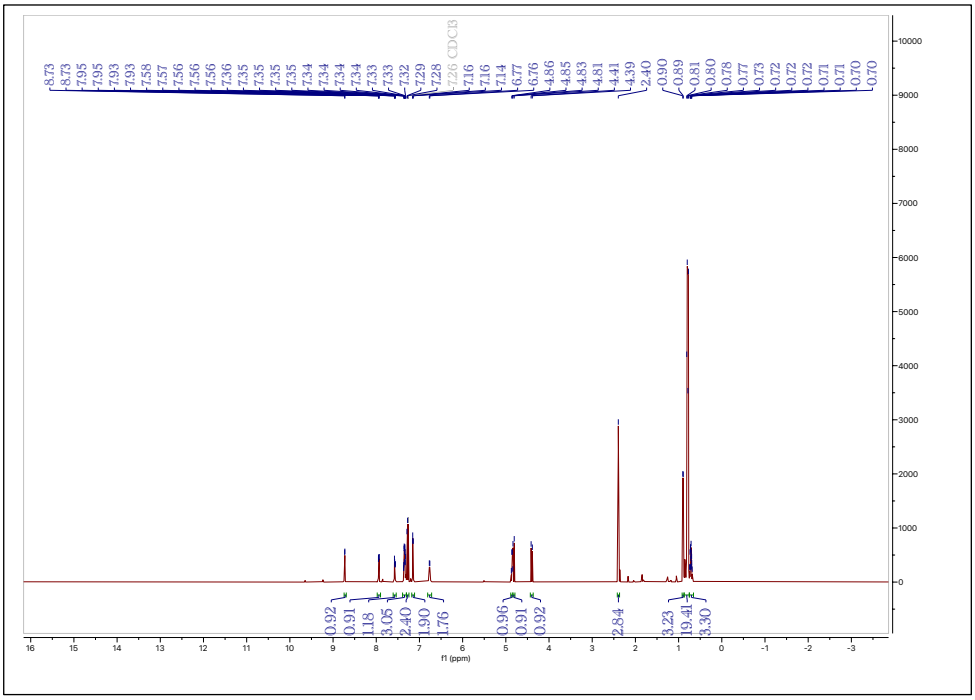

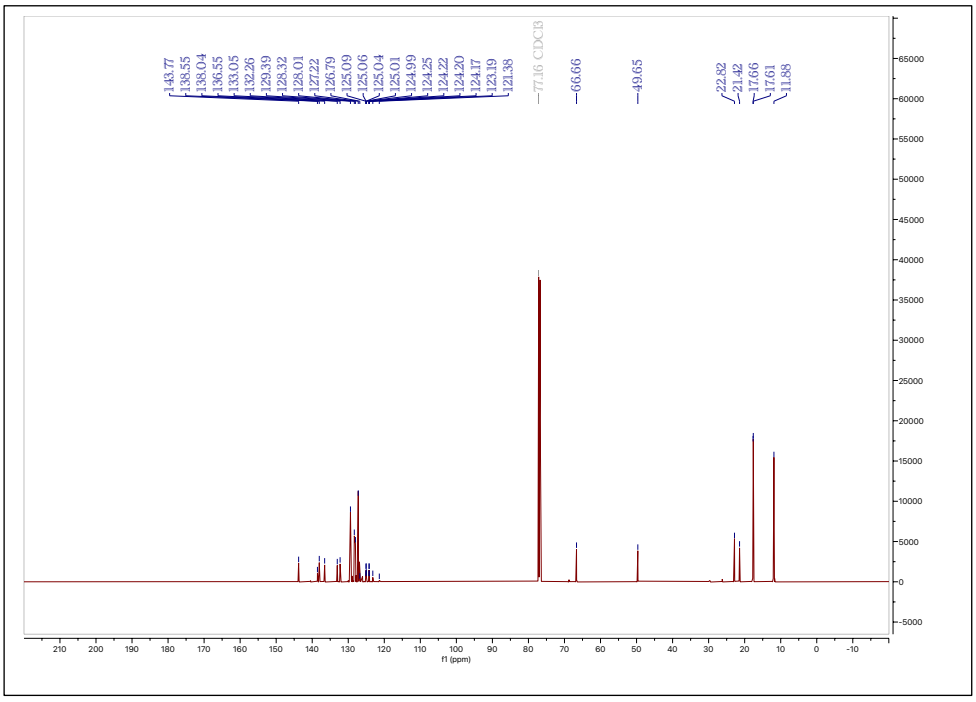

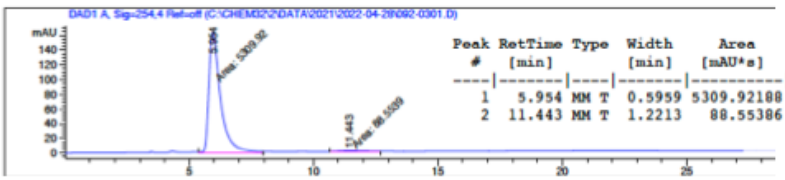

Peak #	RetTime [min]	Type	Width [min]	Area [mAU*s]	Height [mAU]	Area %
1	5.954	MM T	0.5959	5309.92188	163.07468	98.3597
2	11.443	MM T	1.2213	88.55386	1.20848	1.6403

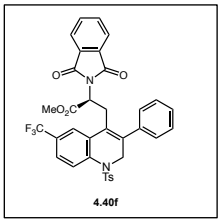
O
N
O
MeO2C
F3C
N
Ts

4.40f

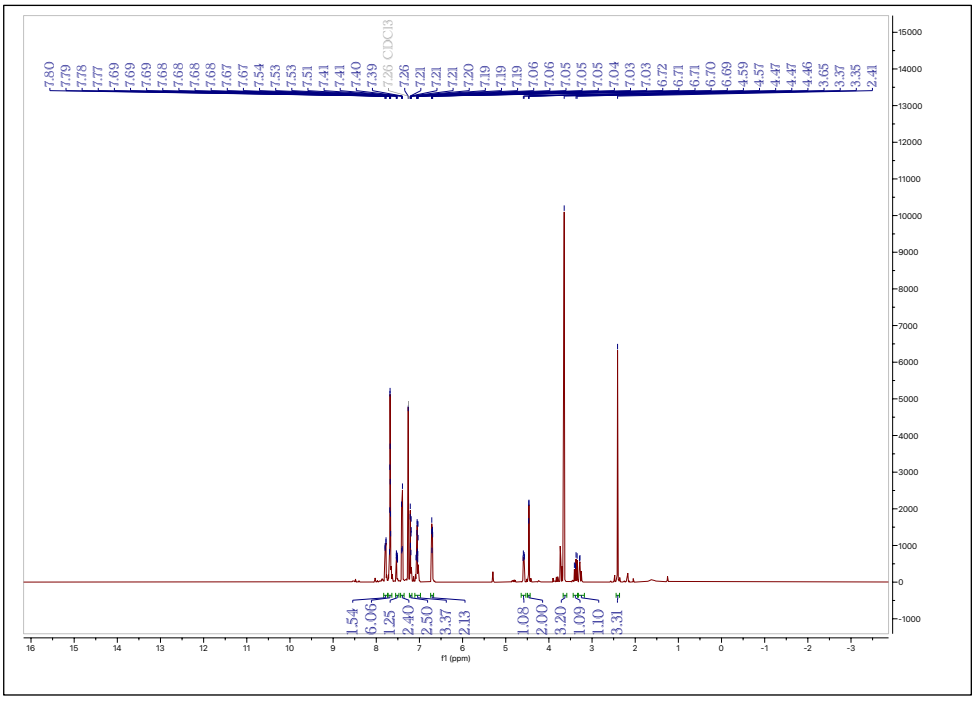
7.80
7.79
7.78
7.77
7.69
7.69
7.69
7.68
7.68
7.68
7.68
7.67
7.67
7.54
7.53
7.53
7.51
7.41
7.41
7.40
7.39
7.26 CDCl3
7.26
7.21
7.21
7.20
7.19
7.19
7.19
7.06
7.06
7.05
7.05
7.05
7.04
7.03
7.03
6.72
6.71
6.71
6.70
6.69
4.59
4.57
4.47
4.47
4.46
3.65
3.37
3.35
2.41
1.54
6.06
1.25
2.40
2.50
3.37
2.13
1.08
2.00
3.20
1.09
1.10
3.31
f1 (ppm)

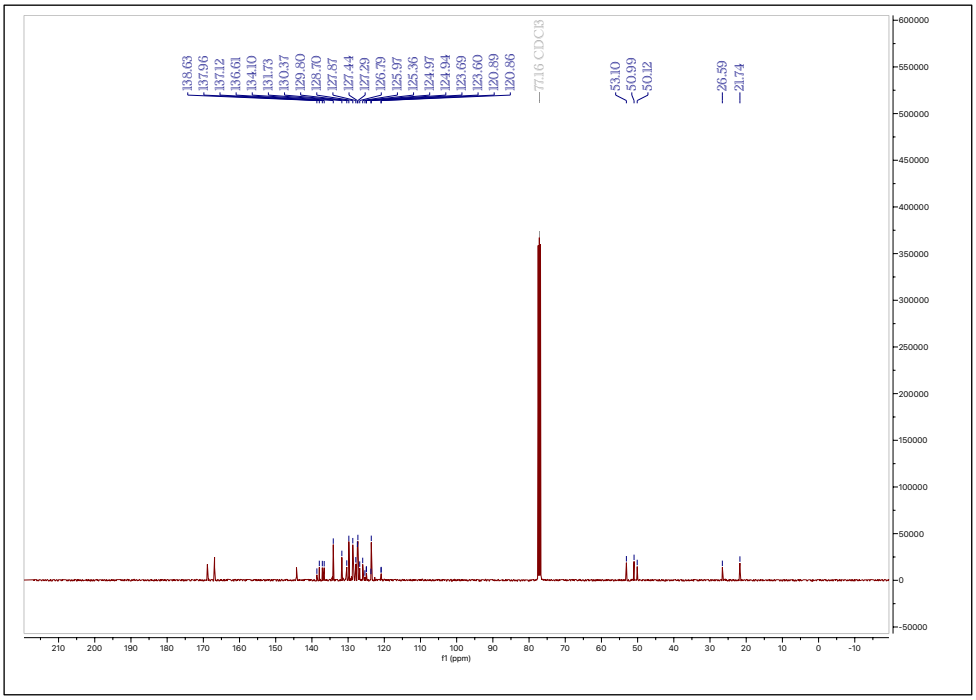
138.63
137.96
137.12
136.61
134.10
131.73
130.37
129.80
128.70
127.87
127.44
127.29
126.79
125.97
125.36
124.97
124.94
123.69
123.60
120.89
120.86
77.16 CDCl3
53.10
50.99
50.12
26.59
21.74
f1 (ppm)

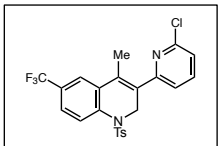
Cl
Me
N
F3C
N
Ts

4.42a

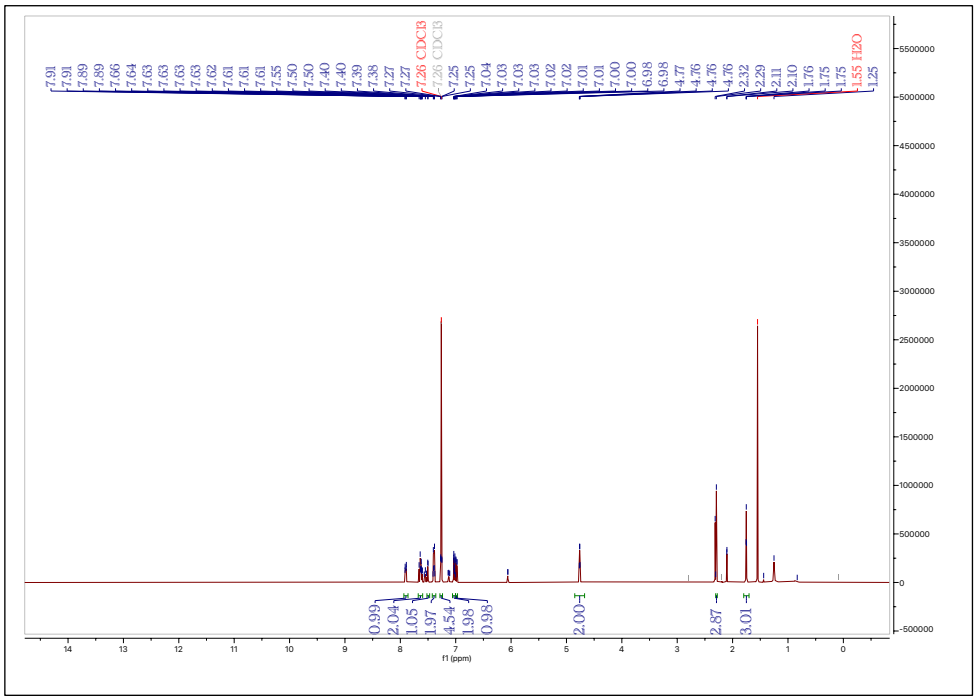
7.91
7.91
7.89
7.89
7.66
7.64
7.63
7.63
7.63
7.63
7.62
7.61
7.61
7.61
7.61
7.55
7.50
7.50
7.40
7.40
7.39
7.38
7.27
7.26 CDCl3
7.26 CDCl3
7.25
7.25
7.04
7.03
7.03
7.03
7.02
7.02
7.01
7.01
7.00
7.00
6.98
6.98
4.77
4.76
4.76
4.76
2.32
2.29
2.11
2.10
1.76
1.75
1.75
1.55 H2O
1.25
0.99
2.04
1.05
1.97
4.54
1.98
0.98
2.00
2.87
3.01
f1 (ppm)

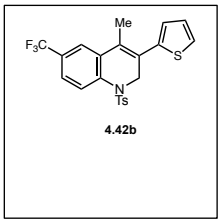
Me
F3C
S
N
Ts

4.42b

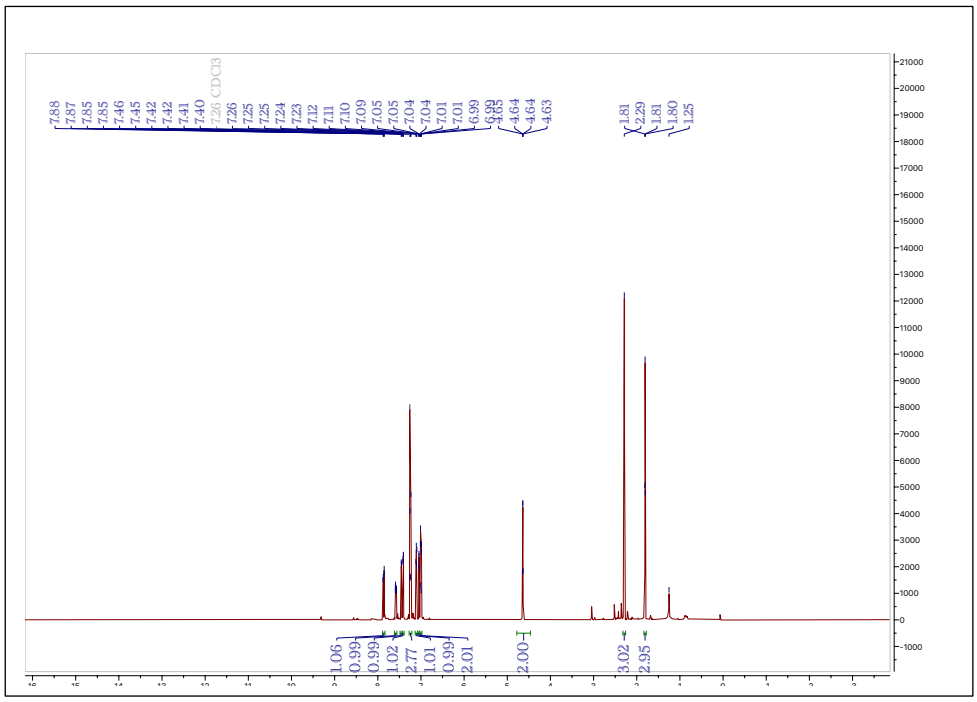
7.88
7.87
7.85
7.85
7.46
7.45
7.42
7.42
7.41
7.40
7.26 CDCl3
7.26
7.25
7.25
7.24
7.23
7.12
7.11
7.10
7.09
7.05
7.05
7.04
7.04
7.01
7.01
6.99
6.99
4.65
4.64
4.64
4.63
1.81
2.29
1.81
1.80
1.25
1.06
0.99
0.99
1.02
2.77
1.01
0.99
2.01
2.00
3.02
2.95

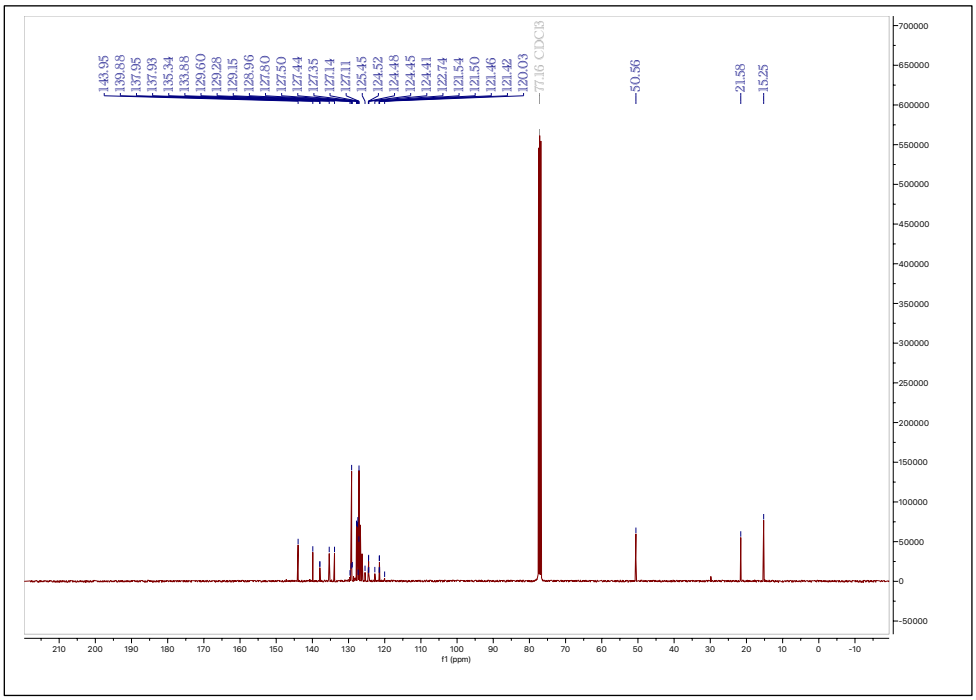
143.95
139.88
137.95
137.93
135.34
133.88
129.60
129.28
129.15
128.96
127.80
127.50
127.44
127.35
127.14
127.11
125.45
124.52
124.48
124.45
124.41
122.74
121.54
121.50
121.46
121.42
120.03
77.46 CDCl3
50.56
21.58
15.25
f1 (ppm)

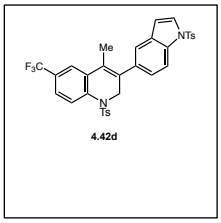
Me
NTs
F3C
N
Ts

4.42d

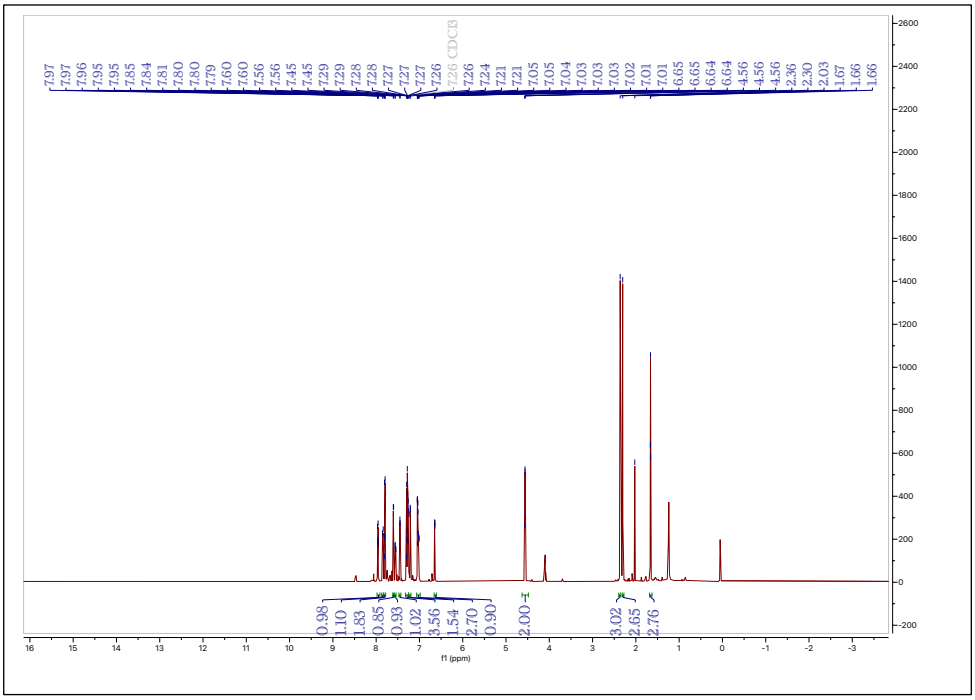
7.97 7.97 7.96 7.95 7.95 7.85 7.84 7.81 7.80 7.80 7.79 7.60 7.60 7.56 7.56 7.45 7.45 7.29 7.29 7.28 7.28 7.27 7.27 7.27 7.26 7.26 CDCl3 7.26 7.24 7.21 7.21 7.05 7.05 7.04 7.03 7.03 7.03 7.02 7.01 7.01 6.65 6.65 6.64 6.64 4.56 4.56 4.56 2.36 2.30 2.03 1.67 1.66 1.66
0.98 1.10 1.83 0.85 0.93 1.02 3.56 1.54 2.70 0.90 2.00 3.02 2.65 2.76
f1 (ppm)

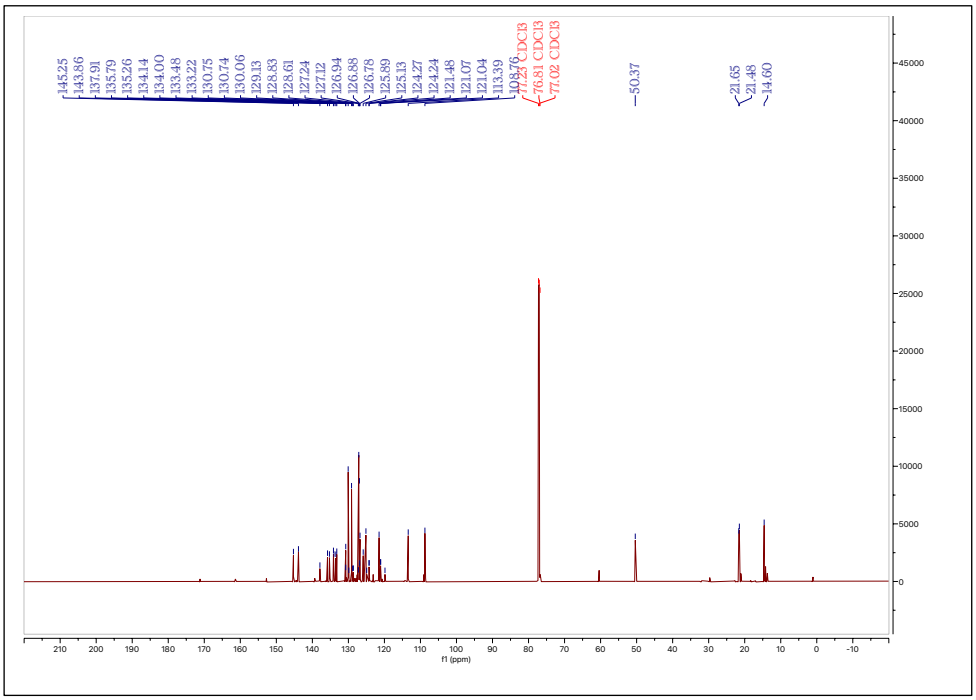
145.25 143.86 137.91 135.79 135.26 134.14 134.00 133.48 133.22 130.75 130.74 130.06 129.13 128.83 128.61 127.24 127.12 126.94 126.88 126.78 125.89 125.13 124.27 124.24 121.48 121.07 121.04 113.39 108.76 77.23 CDCl3 76.81 CDCl3 77.02 CDCl3 50.37 21.65 21.48 14.60
f1 (ppm)

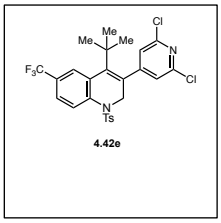
Me
Me
Me
Cl
N
Cl
F3C
N
Ts

4.42e

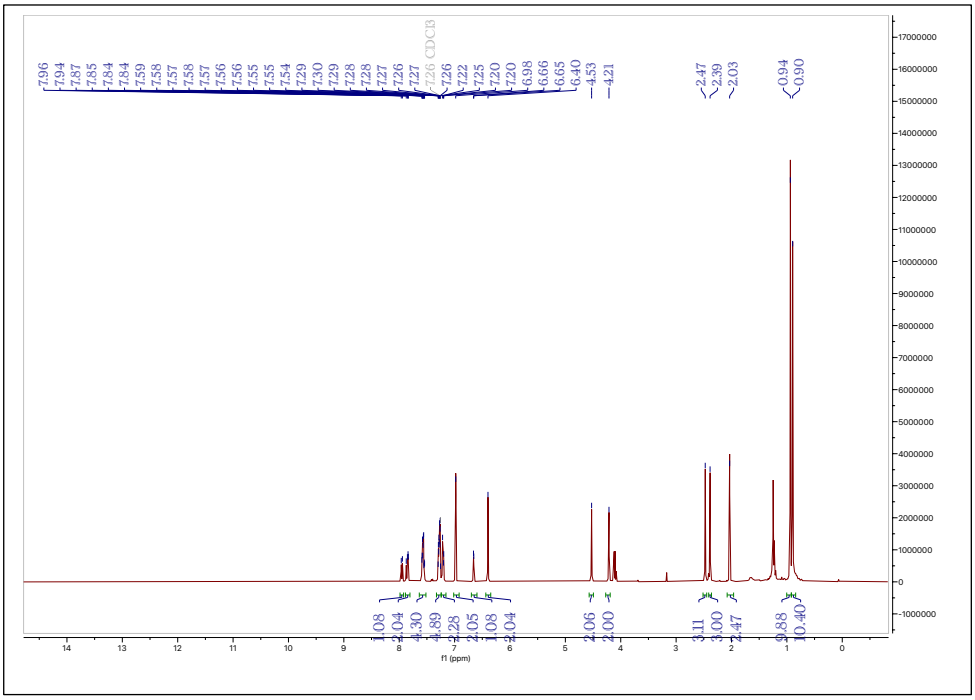
7.96
7.94
7.87
7.85
7.84
7.84
7.59
7.58
7.57
7.58
7.57
7.56
7.56
7.55
7.55
7.54
7.29
7.30
7.29
7.28
7.28
7.27
7.26
7.27
7.26 CDCl3
7.26
7.22
7.25
7.20
7.20
6.98
6.66
6.65
6.40
4.53
4.21
2.47
2.39
2.03
0.94
0.90
1.08
2.04
4.30
4.89
2.28
2.05
1.08
2.04
2.06
2.00
3.11
3.00
2.47
9.88
10.40
f1 (ppm)

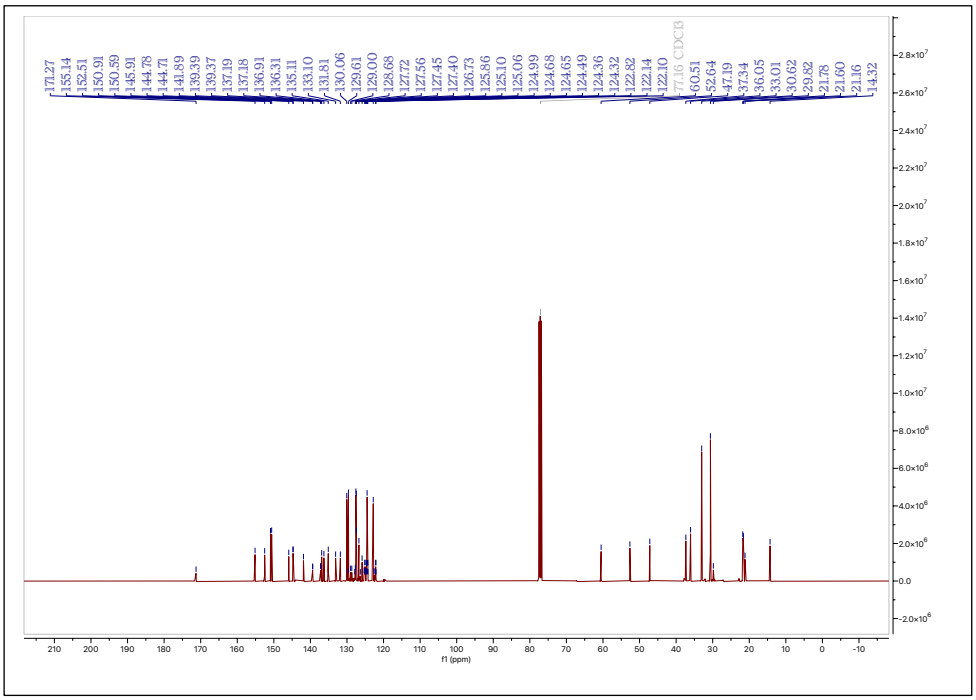
171.27
155.14
152.51
150.91
150.59
145.91
144.78
144.71
141.89
139.39
139.37
137.19
137.18
136.91
136.31
135.11
133.10
131.81
130.06
129.61
129.00
128.68
127.72
127.56
127.45
127.40
126.73
125.86
125.10
125.06
124.99
124.68
124.65
124.49
124.36
124.32
122.82
122.14
122.10
77.16 CDCl3
60.51
52.64
47.19
37.54
36.05
33.01
30.62
29.82
21.78
21.60
21.16
14.32
f1 (ppm)

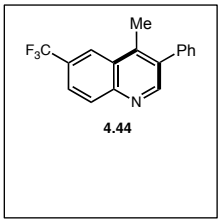
Me
F3C
Ph
N

4.44

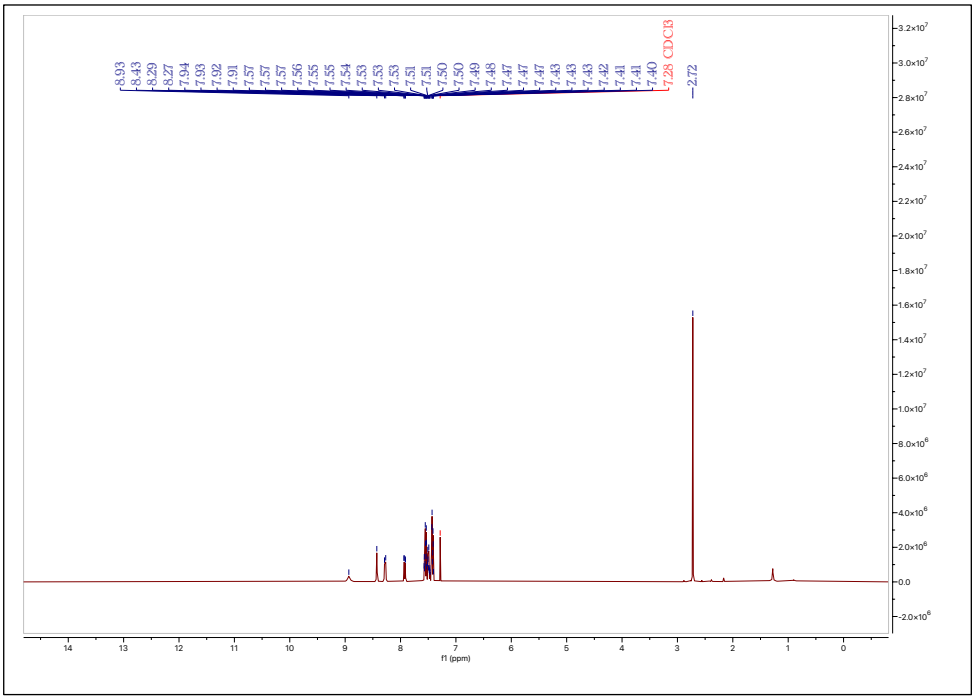
8.93
8.43
8.29
8.27
7.94
7.93
7.92
7.91
7.57
7.57
7.57
7.57
7.56
7.55
7.55
7.54
7.53
7.53
7.53
7.51
7.51
7.50
7.50
7.49
7.48
7.47
7.47
7.47
7.43
7.43
7.43
7.42
7.41
7.41
7.40
7.28 CDCl3
2.72
f1 (ppm)

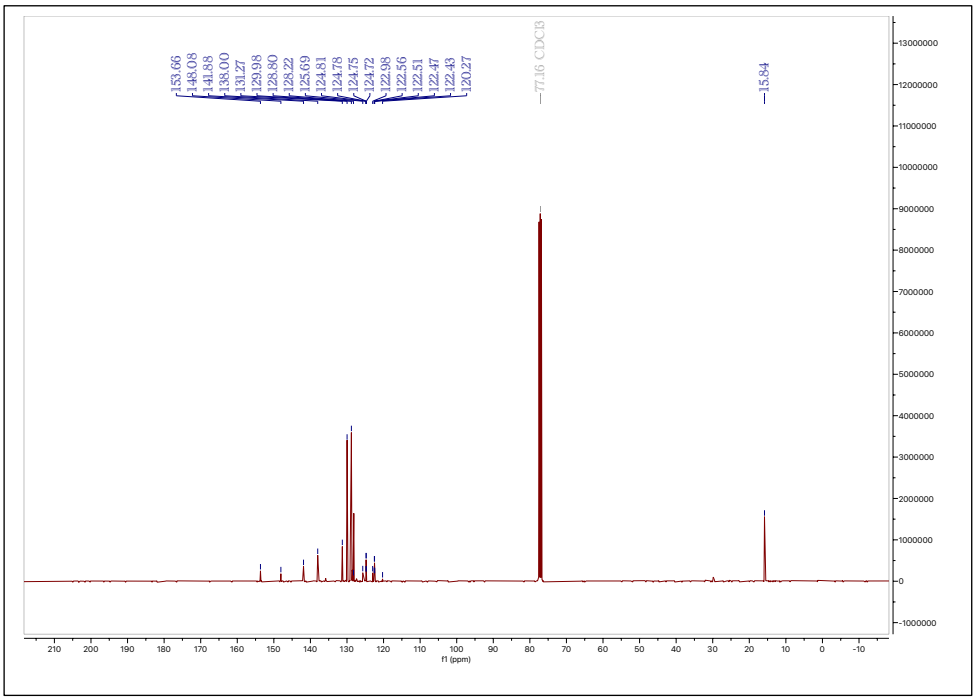
153.66
148.08
141.88
138.00
131.27
129.98
128.80
128.22
125.69
124.81
124.78
124.75
124.72
122.98
122.56
122.51
122.47
122.43
120.27
77.16 CDCl3
15.84
f1 (ppm)

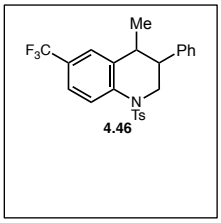
Me
F3C
Ph
N
Ts

4.46

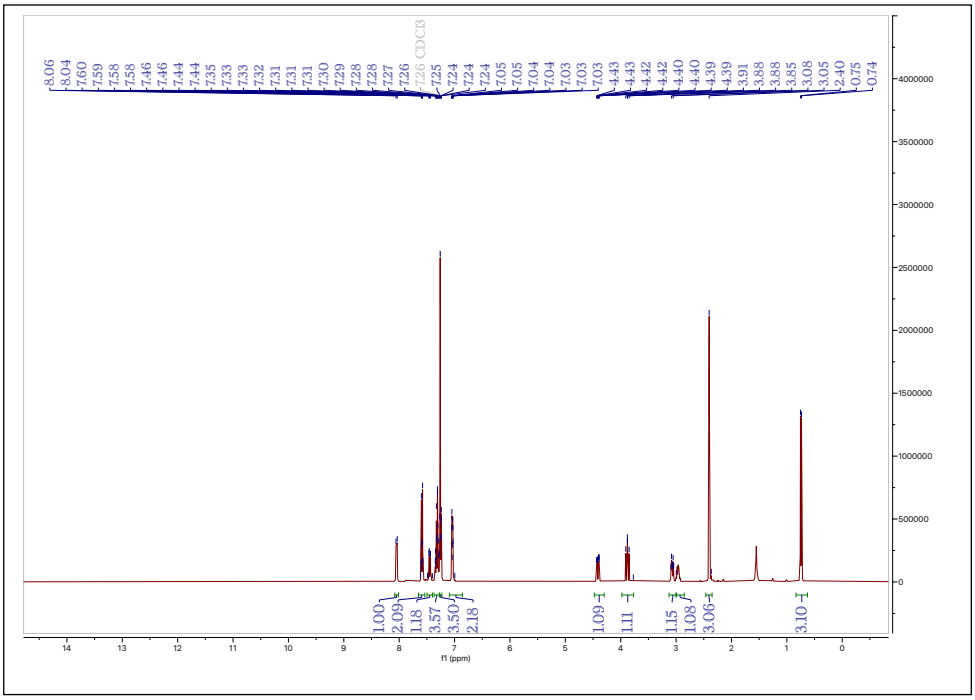
8.06
8.04
7.60
7.59
7.58
7.58
7.46
7.46
7.44
7.44
7.44
7.35
7.33
7.33
7.32
7.31
7.31
7.31
7.30
7.29
7.28
7.28
7.27
7.26
7.26 CDCl3
7.25
7.24
7.24
7.24
7.05
7.05
7.04
7.04
7.03
7.03
7.03
4.43
4.43
4.42
4.42
4.40
4.40
4.39
4.39
3.91
3.88
3.85
3.08
3.05
2.40
0.75
0.74
1.00
2.09
1.18
3.57
3.50
2.18
1.09
1.11
1.15
1.08
3.06
3.10
f1 (ppm)

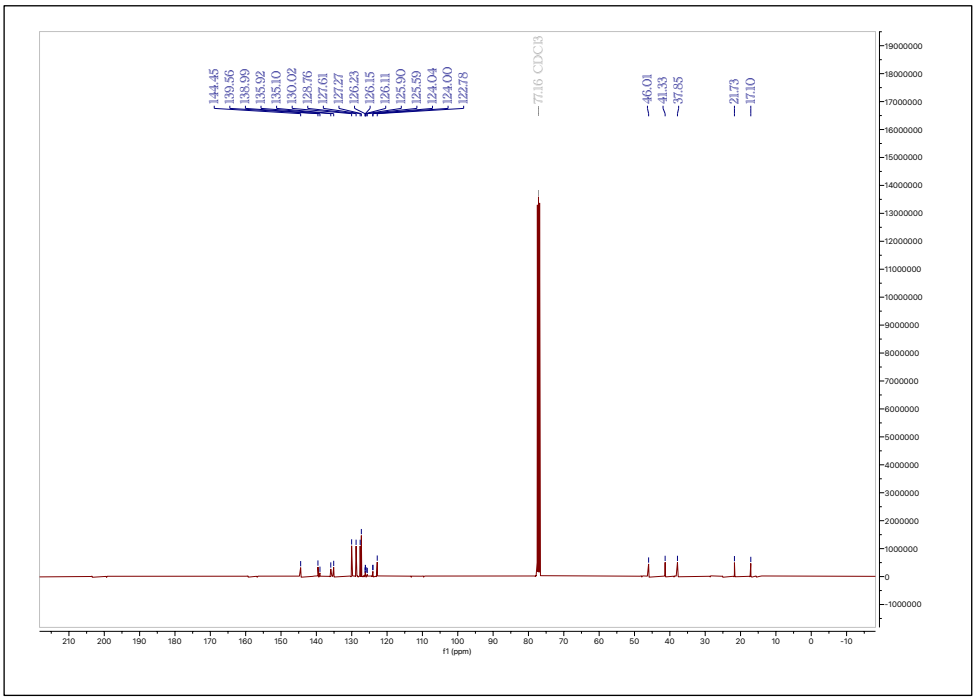
144.45
139.56
138.99
135.92
135.10
130.02
128.76
127.61
127.27
126.23
126.15
126.11
125.90
125.59
124.04
124.00
122.78
77.16 CDCl3
46.01
41.33
37.85
21.73
17.10
f1 (ppm)

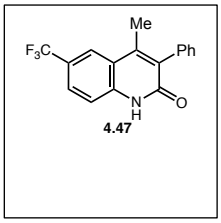
Me
F3C
Ph
N
H
O

4.47

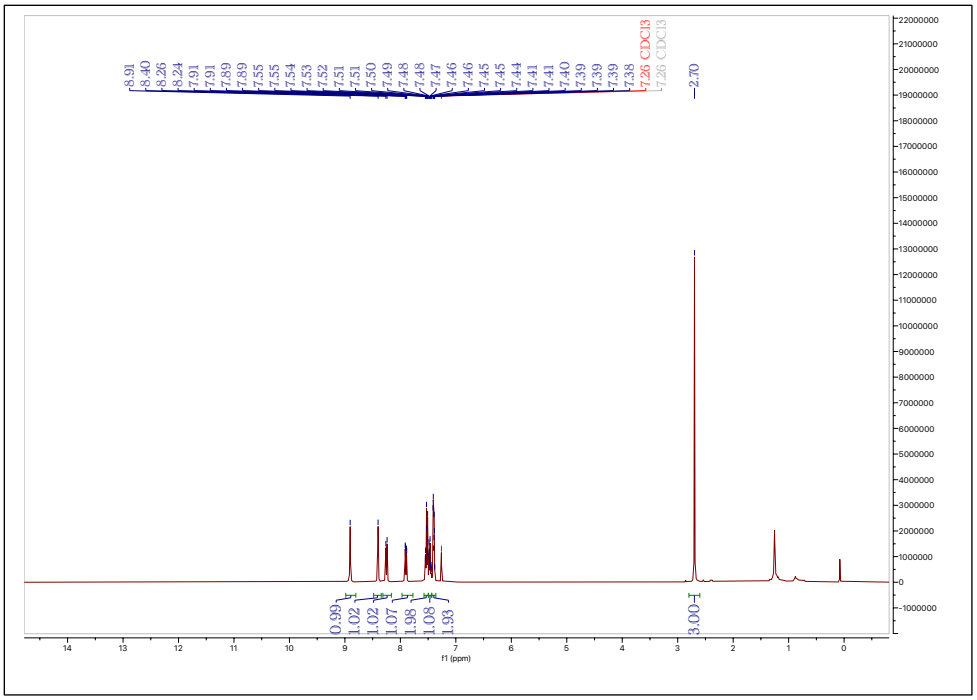
8.91
8.40
8.26
8.24
7.91
7.91
7.89
7.89
7.55
7.55
7.54
7.53
7.52
7.51
7.51
7.50
7.49
7.48
7.48
7.47
7.46
7.46
7.45
7.45
7.44
7.41
7.41
7.40
7.39
7.39
7.39
7.38
7.26 CDCl3
7.26 CDCl3
2.70
0.99
1.02
1.02
1.07
1.98
1.08
1.93
3.00
f1 (ppm)

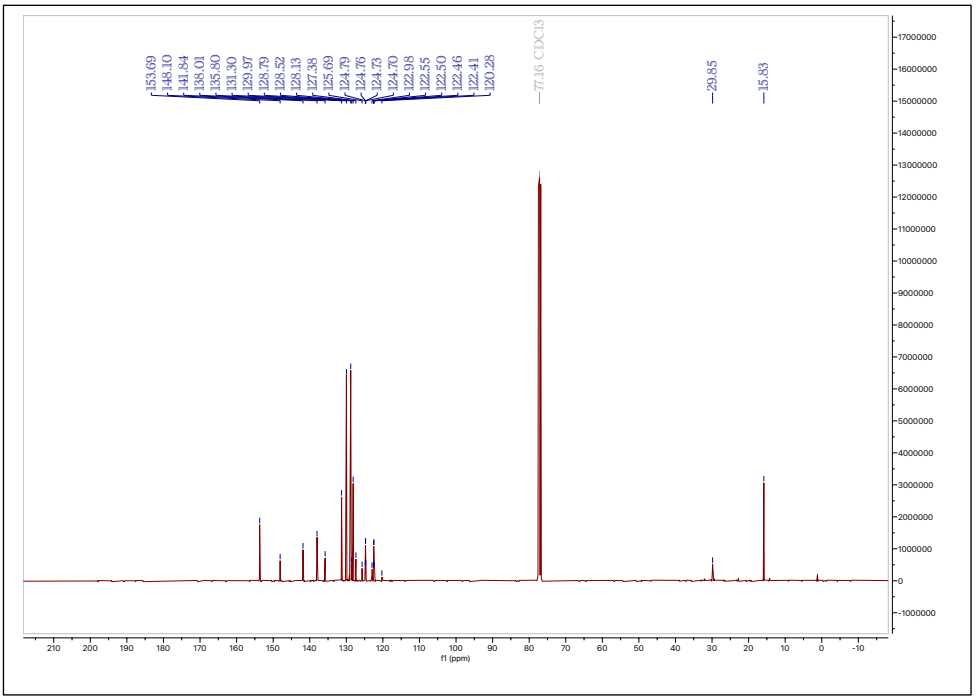
153.69
148.10
141.84
138.01
135.80
131.30
129.97
129.79
129.52
128.13
127.38
125.69
124.79
124.76
124.73
124.70
122.98
122.55
122.50
122.46
122.41
120.28
77.16 CDCl3
29.85
15.83
f1 (ppm)

EMORY UNIVERSITY | X-ray Crystallography Center

MRH_pTolTsNBpin

R_1=1.61%

Submitted by: **Michael Hollerbach,**
Blakey Lab
Solved by: **John Bacsa**

Crystal Data and Experimental

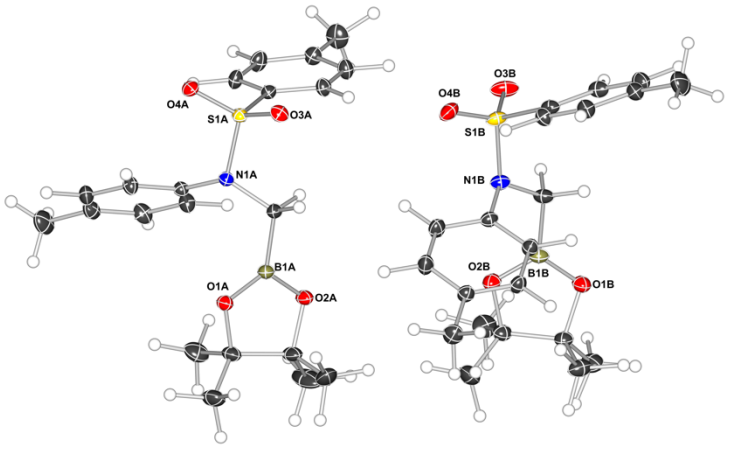

Experimental. Single colorless block crystals of **MRH_pTolTsNBpin** were crystallised from pentane and diethyl ether by solvent layering. A suitable crystal with dimensions 0.23 × 0.23 × 0.19 mm^3 was selected and mounted on a loop with paratone on a XtaLAB Synergy-S diffractometer. The crystal was kept at a steady T = 100.01(12) K during data collection. The structure was solved with the ShelXT (Sheldrick, 2015) solution program using dual methods and by using Olex2 (Dolomanov et al., 2009) as the graphical interface. The model was refined with olex2.refine 1.3-alpha (Bourhis et al., 2015) using full matrix least squares minimisation on F^2.

Crystal Data. $C_{21}H_{28}BNO_4S$, M_r = 401.351, monoclinic, $P2_1/n$ (No. 14), a = 10.80507(7) Å, b = 19.66742(11) Å, c = 20.64231(12) Å, β = 97.0721(6)°, α = γ = 90°, V = 4353.28(5) Å^3, T = 100.01(10) K, Z = 8, Z' = 2, μ(Cu K$_\alpha$) = 1.527, 68476 reflections measured, 8303 unique (R_{int} = 0.0323) which were used in all calculations. The final wR_2 was 0.0349 (all data) and R_1 was 0.0161 (I≥2 σ(I)).

Compound	**MRH_pTolTsNBpin**
Formula	$C_{21}H_{28}BNO_4S$
$D_{calc.}$/ g cm^{-3}	1.225
μ/mm^{-1}	1.527
Formula Weight	401.351
Color	colorless
Shape	block
Size/mm^3	0.23×0.23×0.19
T/K	100.01(10)
Crystal System	monoclinic
Space Group	$P2_1/n$
a/Å	10.80507(7)
b/Å	19.66742(11)
c/Å	20.64231(12)
α/°	90
β/°	97.0721(6)
γ/°	90
V/Å^3	4353.28(5)
Z	8
Z'	2
Wavelength/Å	1.54184
Radiation type	Cu K$_\alpha$
Θ_{min}/°	3.11
Θ_{max}/°	72.76
Measured Refl's.	68476
Indep't Refl's	8303
Refl's I≥2 σ(I)	7983
R_{int}	0.0323
Parameters	1010
Restraints	78
Largest Peak	0.2162
Deepest Hole	-0.1120
GooF	1.0996
wR_2 (all data)	0.0349
wR_2	0.0346
R_1 (all data)	0.0171
R_1	0.0161

Structure Quality Indicators

Reflections:	d min (Cu) 0.81	I/σ(I) 62.6	Rint 3.23%	complete 100% (IUCr) 100%
Refinement:	Shift 0.001	Max Peak 0.2	Min Peak -0.1	GooF 1.100

A colorless block-shaped crystal with dimensions 0.23 × 0.23 × 0.19 mm^3 was mounted on a loop with paratone. Data were collected using a XtaLAB Synergy, Dualflex, HyPix diffractometer equipped with an Oxford Cryosystems low-temperature device operating at T = 100.01(10) K.

Data were measured using ω scans using Cu K$_\alpha$ radiation. The diffraction pattern was indexed and the total number of runs and images was based on the strategy calculation from the program CrysAlisPro (Rigaku, V1.171.40.84a, 2020). The maximum resolution that was achieved was Θ = 72.76° (0.81 Å).

The unit cell was refined using CrysAlisPro (Rigaku, V1.171.40.84a, 2020) on 51597 reflections, 75% of the

observed reflections.

Data reduction, scaling and absorption corrections were performed using CrysAlisPro (Rigaku, V1.171.40.84a, 2020). The final completeness is 99.82 % out to 72.76° in Θ. A numerical absorption correction based on a Gaussian integration over a multifaceted crystal model absorption correction was performed using CrysAlisPro 1.171.40.79a (Rigaku Oxford Diffraction, 2020). An empirical absorption correction using spherical harmonics, implemented in SCALE3 ABSPACK scaling algorithm was also applied. The absorption coefficient μ of this material is 1.527 mm^{-1} at this wavelength (λ = 1.54184Å) and the minimum and maximum transmissions are 0.639 and 1.000.

The structure was solved and the space group $P2_1/n$ (# 14) determined by the ShelXT (Sheldrick, 2015) structure solution program using dual methods and refined by full matrix least squares minimisation on $\boldsymbol{F^2}$ using version of olex2.refine 1.3-alpha (Bourhis et al., 2015). All atoms, even hydrogen atoms, were refined anisotropically. Hydrogen atom positions were located from the electron densities and freely refined using the riding model. Hydrogen atom positions were calculated geometrically and refined using Hirshfeld scattering factors.

_refine_special_details: Refinement using NoSpherA2, an implementation of NOn-SPHERical Atom-form-factors in Olex2.Please cite:F. Kleemiss, H. Puschmann, O. Dolomanov, S.Grabowsky - to be published - 2020NoSpherA2 implementation of HAR makes use of tailor-made aspherical atomic form factors calculatedon-the-fly from a Hirshfeld-partitioned electron density (ED) - not fromspherical-atom form factors.The ED is calculated from a gaussian basis set single determinant SCFwavefunction - either Hartree-Fock or DFT using selected funtionals - for a fragment of the crystal.This fregment can be embedded in an electrostatic crystal field by employing cluster charges.The following options were used: SOFTWARE: ORCA PARTITIONING: NoSpherA2 INT ACCURACY: Normal METHOD: PBE BASIS SET: def2-SVP CHARGE: 0 MULTIPLICITY: 1 DATE: 2020-09-16_12-21-55

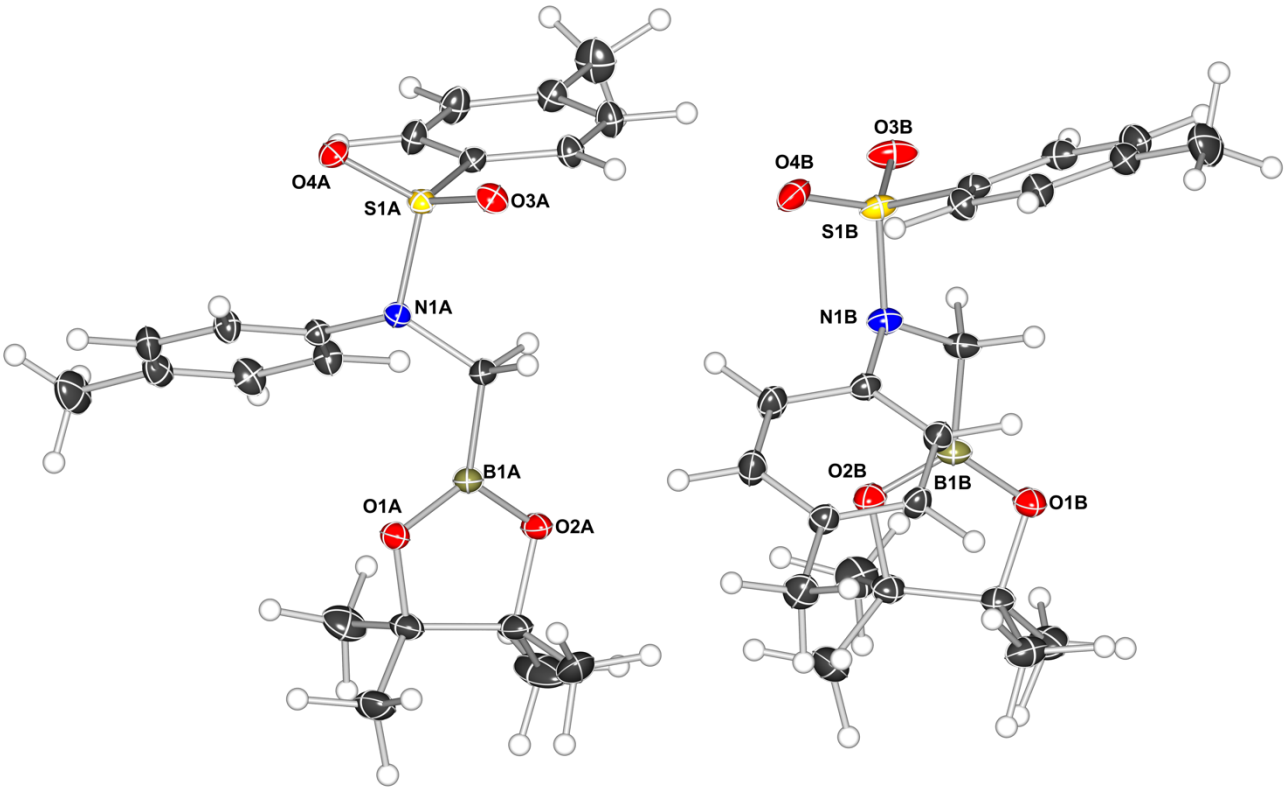

Figure 1: Thermal ellipsoid plot of the asymmetric unit. There are two molecules with the same chemical structure but very dissimilar conformations of the different groups in either molecule.

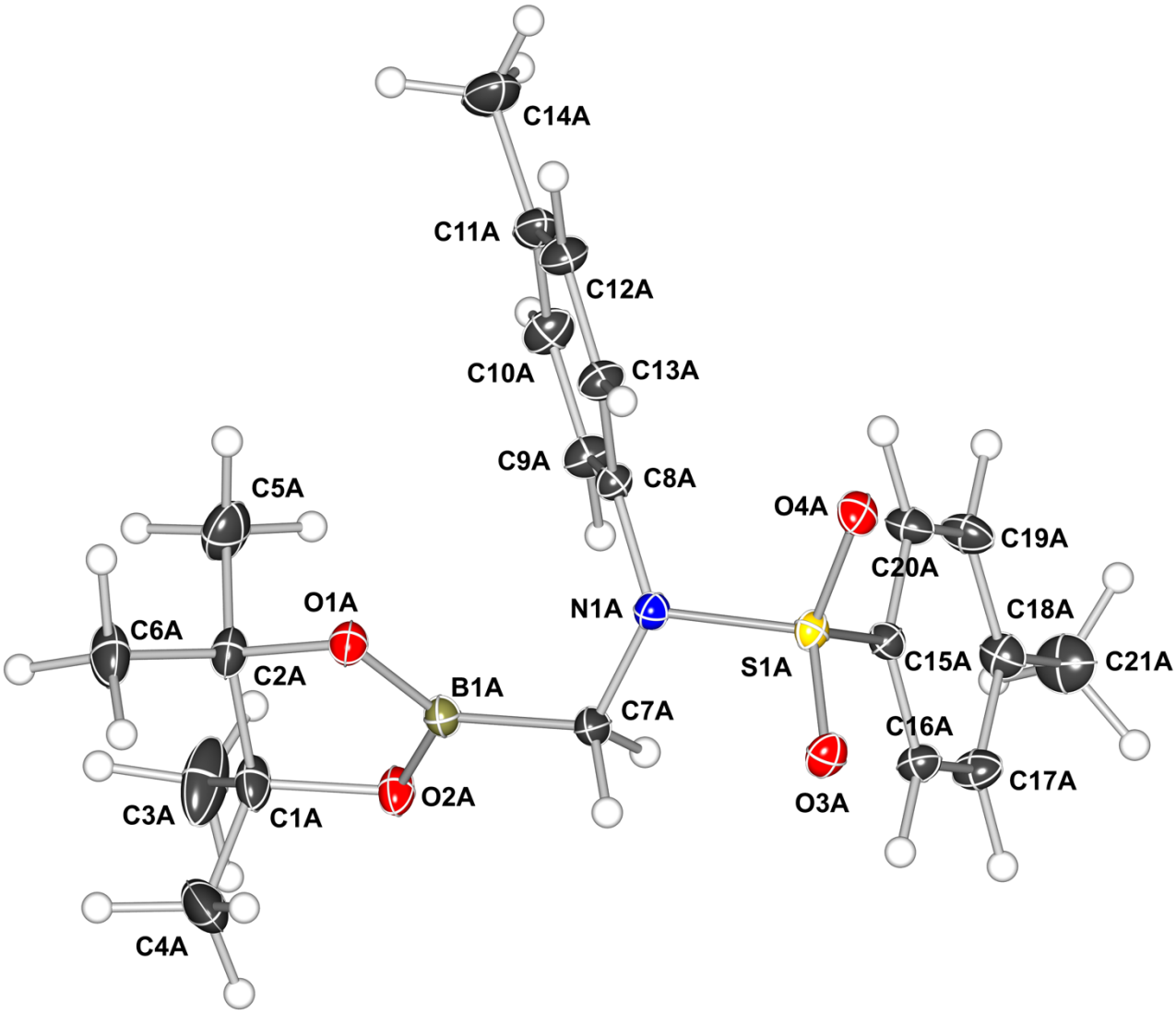

Figure 2: Thermal ellipsoid plot of one of the two molecules of the asymmetric unit.

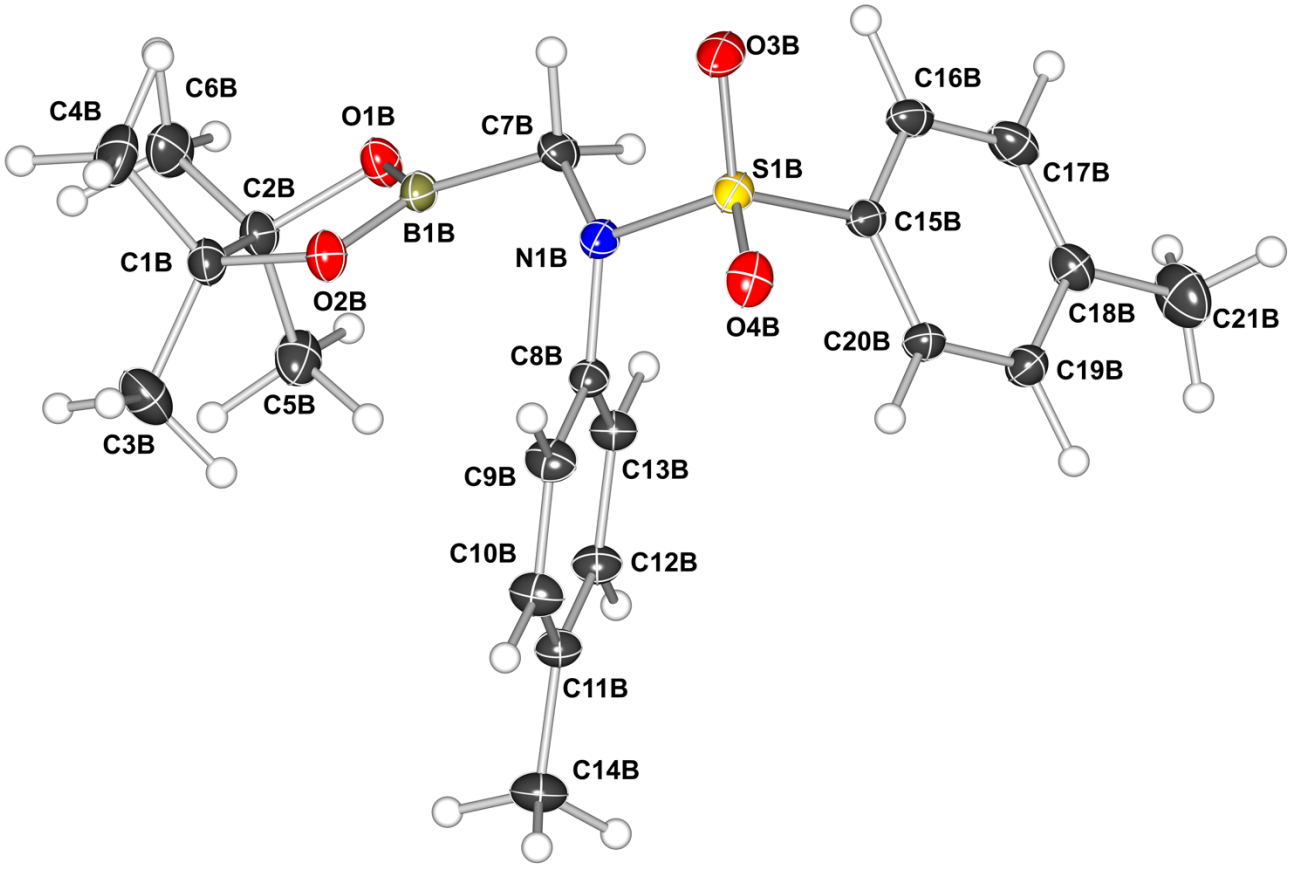

Figure 3: Thermal ellipsoid plot of one of the two molecules of the asymmetric unit.

Data Plots: Diffraction Data

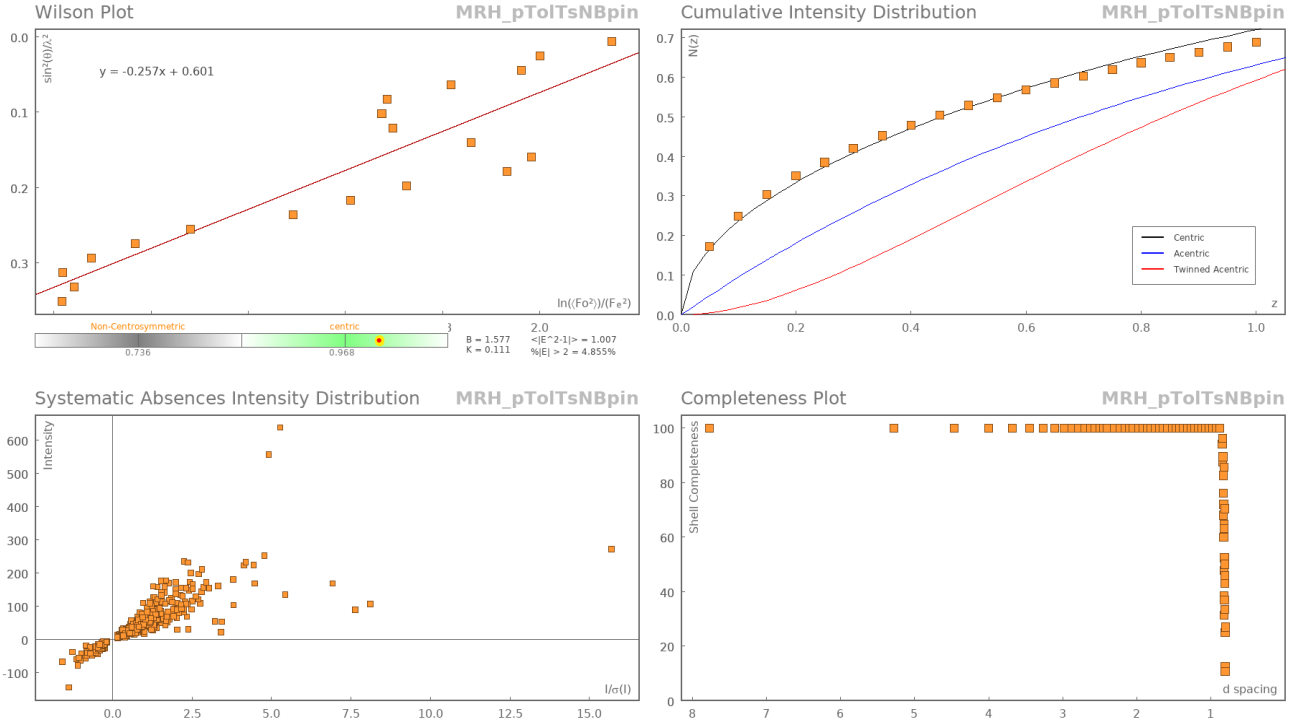

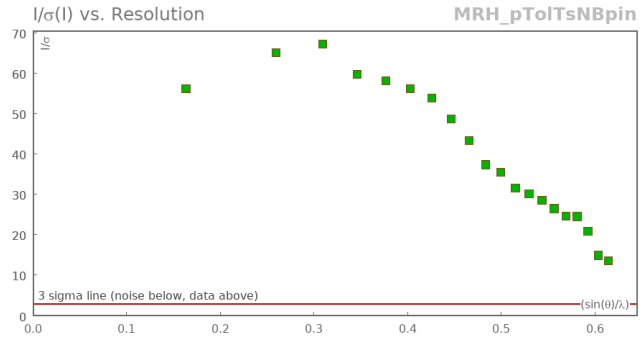

Data Plots: Refinement and Data

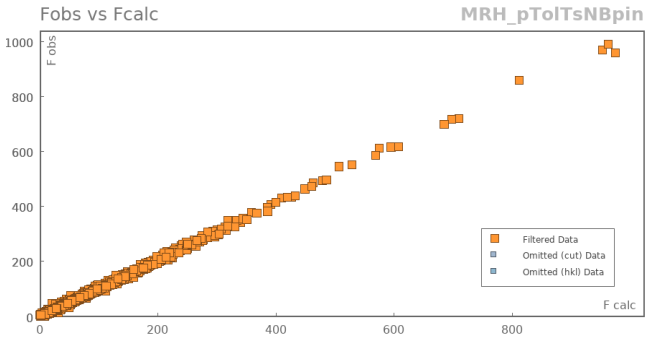

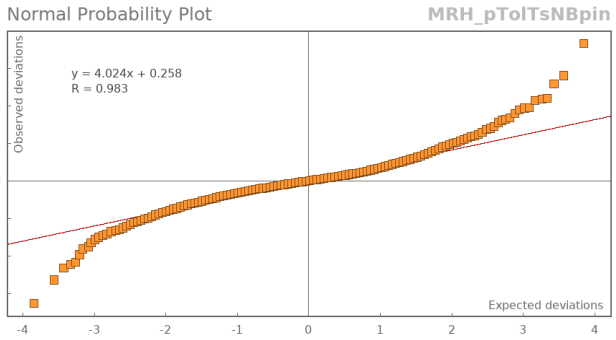

Reflection Statistics

Total reflections (after filtering)	69656	Unique reflections	8303
Completeness	0.957	Mean I/σ	40.91
hkl_{max} collected	(12, 24, 23)	hkl_{min} collected	(-13, -23, -25)
hkl_{max} used	(13, 24, 25)	hkl_{min} used	(-13, 0, 0)
Lim d_{max} collected	100.0	Lim d_{min} collected	0.77
d_{max} used	20.49	d_{min} used	0.81
Friedel pairs	9271	Friedel pairs merged	1
Inconsistent equivalents	3	R_{int}	0.0323
R_{sigma}	0.016	Intensity transformed	0
Omitted reflections	0	Omitted by user (OMIT hkl)	0
Multiplicity	(7253, 6060, 4171, 2830, 1893, 1081, 558, 337, 176, 114, 59, 26, 13, 2, 1)	Maximum multiplicity	24
Removed systematic absences	1180	Filtered off (Shel/OMIT)	0

Images of the Crystal on the Diffractometer

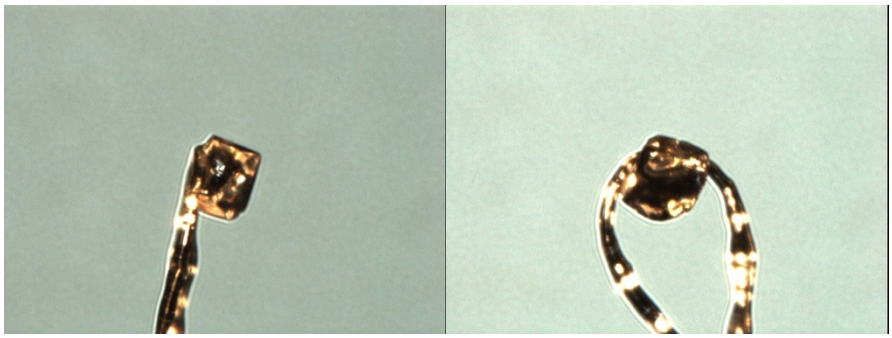

Table 1: Fractional Atomic Coordinates (×10⁴) and Equivalent Isotropic Displacement Parameters (Å²×10³) for **MRH_pTolTsNBpin**. U_{eq} is defined as 1/3 of the trace of the orthogonalised U_{ij}.

Atom	x	y	z	U_{eq}
S1A	3367.27(13)	7512.98(7)	4746.57(7)	14.17(4)
S1B	3928.20(14)	4912.83(8)	2650.57(7)	19.51(4)
O3A	2980.3(4)	7642.9(2)	4068.7(2)	19.07(9)
O4A	2740.9(4)	7851.5(2)	5228.9(2)	18.99(9)
O1A	7644.6(4)	8116.0(2)	4798.0(2)	18.63(9)
O2A	7823.9(4)	7099.5(2)	4280.2(2)	21.01(10)
O1B	8248.2(4)	3977.4(2)	2207.4(2)	23.45(10)
O2B	8151.4(4)	4732.1(2)	3039.5(2)	22.46(10)
O4B	3563.8(4)	5527.5(2)	2945.4(2)	25.43(10)
O3B	3645.2(4)	4270.4(2)	2923.6(2)	30.14(11)
N1A	4862.7(4)	7725.9(2)	4885.4(2)	14.92(10)
N1B	5464.1(5)	4939.8(3)	2658.0(2)	19.04(11)
C15A	3302.3(5)	6628.7(3)	4877.4(3)	15.18(12)
C9A	6108.2(6)	7204.7(3)	5844.4(3)	19.98(13)
C16A	3204.4(6)	6184.4(3)	4348.9(3)	18.12(12)
C20B	3090.1(6)	5555.8(3)	1519.3(3)	19.13(13)
C15B	3294.2(5)	4927.8(3)	1824.6(3)	18.02(12)
C20A	3386.0(6)	6381.2(3)	5515.4(3)	20.05(13)
C11B	6975.1(6)	6801.7(3)	2067.0(3)	19.22(13)
C12B	6860.3(6)	6245.3(3)	1645.5(3)	19.85(13)
C8A	5382.4(5)	7737.1(3)	5563.3(3)	14.72(12)
C8B	5950.2(5)	5573.5(3)	2444.0(3)	17.17(12)
C13A	5160.3(6)	8298.8(3)	5941.5(3)	18.82(12)
C16B	3028.0(6)	4325.3(3)	1480.1(3)	22.64(13)
C12A	5659.7(6)	8324.2(3)	6594.8(3)	22.49(13)
C10A	6617.3(6)	7240.8(3)	6496.2(3)	23.46(14)
C13B	6344.9(6)	5636.4(3)	1828.3(3)	19.33(13)
C19B	2615.6(6)	5579.6(3)	863.9(3)	21.29(13)
C7A	5609.9(6)	7411.4(3)	4413.2(3)	18.06(12)
C11A	6404.1(6)	7799.9(3)	6882.6(3)	22.14(13)
C18A	3234.4(6)	5230.0(3)	5095.1(3)	20.94(13)
C2A	8984.8(6)	7968.7(3)	4858.4(3)	21.77(13)
C7B	6035.3(6)	4313.6(3)	2439.7(3)	21.56(13)
C19A	3353.7(6)	5683.8(3)	5619.3(3)	22.60(13)
C17A	3166.9(6)	5488.5(3)	4462.1(3)	21.31(13)
C9B	6057.4(6)	6125.4(3)	2868.2(3)	22.30(13)
C10B	6554.2(6)	6733.7(3)	2676.4(3)	23.85(14)
C2B	9524.7(6)	4225.4(3)	2374.7(3)	20.87(13)
C18B	2348.8(6)	4983.6(3)	506.9(3)	23.27(14)
C1B	9471.6(6)	4571.1(3)	3055.5(3)	21.38(13)
C1A	9057.4(6)	7407.7(3)	4326.1(3)	24.78(14)
C17B	2553.1(6)	4358.9(3)	822.8(3)	25.67(14)
C14B	7545.9(7)	7455.6(3)	1872.6(4)	26.78(15)
C6A	9682.5(7)	8619.0(4)	4748.2(4)	31.83(16)
C6B	10418.9(7)	3629.3(4)	2381.0(4)	30.95(16)
C5B	9756.5(7)	4726.2(4)	1840.3(4)	29.48(16)
B1A	7051.9(6)	7561.1(3)	4515.1(3)	16.41(13)
C21A	3193.7(8)	4476.9(4)	5211.3(4)	33.03(17)
C14A	6970.4(8)	7838.9(4)	7583.7(3)	35.05(17)
C4A	9194.1(9)	7699.3(5)	3652.8(4)	40.03(19)
C4B	9803.1(8)	4094.7(5)	3632.8(4)	35.80(18)
C3B	10206.8(7)	5227.6(4)	3158.6(4)	34.70(17)
B1B	7511.4(6)	4345.9(3)	2565.9(3)	18.91(14)
C5A	9357.7(8)	7711.4(4)	5550.4(4)	33.64(17)
C21B	1843.3(9)	5020.6(5)	-203.7(4)	38.82(19)

Atom	x	y	z	U_{eq}
C3A	10010.1(7)	6855.6(4)	4504.5(6)	47.6(2)

Table 2: Anisotropic Displacement Parameters (×10^4) for **MRH_pTolTsNBpin**. The anisotropic displacement factor exponent takes the form: $-2\pi^2[h^2a^{*2} \times U_{11} + ... + 2hka^* \times b^* \times U_{12}]$

Atom	U_{11}	U_{22}	U_{33}	U_{23}	U_{13}	U_{12}
S1A	11.55(7)	14.53(7)	16.14(7)	1.60(5)	0.62(5)	0.07(5)
S1B	14.81(8)	23.57(8)	20.94(8)	0.96(6)	5.36(6)	7.19(6)
O3A	17.3(2)	20.1(2)	18.7(2)	1.22(17)	-2.43(17)	2.51(17)
O4A	14.8(2)	19.1(2)	23.4(2)	3.16(16)	3.61(17)	-2.99(17)
O1A	15.5(2)	17.5(2)	23.0(2)	-0.80(16)	2.70(17)	-2.99(17)
O2A	14.6(2)	19.4(2)	29.7(2)	-1.18(16)	5.08(17)	-5.94(18)
O1B	16.2(2)	24.7(2)	29.1(2)	-0.28(17)	1.45(18)	-4.72(19)
O2B	17.3(2)	28.2(2)	21.8(2)	1.50(18)	2.10(17)	-1.24(18)
O4B	21.7(2)	35.2(3)	20.7(2)	4.57(19)	7.95(18)	0.69(19)
O3B	20.6(2)	34.0(3)	36.4(3)	-2.22(19)	6.1(2)	18.2(2)
N1A	13.7(2)	15.9(2)	15.0(2)	0.14(19)	0.89(19)	-0.26(19)
N1B	15.7(3)	20.3(3)	21.3(3)	0.3(2)	3.1(2)	5.2(2)
C15A	14.4(3)	15.6(3)	15.8(3)	0.8(2)	2.8(2)	-0.1(2)
C9A	23.2(3)	16.8(3)	19.0(3)	3.7(2)	-1.3(2)	-0.2(3)
H9A	65(7)	30(5)	38(5)	21(4)	-7(5)	-17(4)
C16A	21.5(3)	17.4(3)	15.0(3)	-0.4(2)	0.6(2)	-0.0(2)
H16A	64(7)	44(5)	25(5)	0(5)	2(4)	1(4)
C20B	21.1(3)	15.1(3)	20.9(3)	0.2(2)	1.3(2)	-0.1(2)
H20B	59(6)	24(3)	44(5)	-5(2)	0(4)	-12.9(18)
C15B	14.4(3)	16.6(3)	23.5(3)	0.7(2)	4.0(2)	2.9(2)
C20A	26.9(3)	18.3(3)	15.9(3)	1.0(2)	6.3(2)	-0.8(3)
H20A	82(7)	29(5)	32(5)	2(5)	13(5)	-14(4)
C11B	21.6(3)	17.2(3)	19.5(3)	-0.9(2)	5.3(2)	1.2(2)
C12B	23.9(3)	18.7(3)	18.2(3)	-1.2(2)	7.8(3)	0.9(2)
H12B	70(7)	39(5)	38(5)	-11(5)	25(5)	3(4)
C8A	14.5(3)	14.6(3)	14.9(3)	0.5(2)	1.1(2)	-0.1(2)
C8B	16.3(3)	18.5(3)	17.1(3)	-0.0(2)	3.4(2)	3.1(2)
C13A	21.1(3)	16.2(3)	18.7(3)	2.2(2)	0.5(2)	-2.3(2)
H13A	66(7)	33(5)	50(6)	22(5)	-6(5)	-4(4)
C16B	19.1(3)	15.5(3)	34.0(4)	0.8(2)	5.9(3)	1.8(3)
H16B	59(7)	24(5)	75(7)	8(4)	8(5)	12(5)
C12A	26.1(3)	22.4(3)	18.7(3)	-1.4(3)	1.8(3)	-5.7(3)
H12A	73(7)	41(6)	48(6)	7(5)	1(5)	-20(5)
C10A	26.7(3)	21.3(3)	20.7(3)	1.1(3)	-3.9(3)	3.9(3)
H10A	76(7)	46(6)	52(6)	23(5)	-12(5)	12(5)
C13B	22.1(3)	17.4(3)	19.2(3)	-0.5(2)	5.5(2)	-0.5(3)
H13B	73(7)	30(5)	39(5)	-11(4)	23(5)	-14(4)
C19B	23.2(3)	19.5(3)	20.8(3)	0.9(2)	0.7(2)	1.7(3)
H19B	71(7)	25(5)	46(6)	1(4)	4(5)	12(4)
C7A	14.4(3)	22.7(3)	17.3(3)	-0.9(2)	2.6(2)	-2.7(2)
H7Aa	34(5)	78(7)	22(4)	13(4)	2(2)	11(3)
H7Ab	45(6)	25(3)	49(6)	-4(2)	14(4)	-6(2)
C11A	24.8(3)	25.4(3)	15.7(3)	-5.4(3)	0.2(2)	1.2(2)
C18A	24.7(3)	16.5(3)	22.0(3)	0.5(2)	4.5(3)	1.2(2)
C2A	14.5(3)	21.6(3)	28.9(3)	-2.8(2)	1.6(3)	-2.1(3)
C7B	15.3(3)	20.0(3)	29.7(4)	-2.3(2)	3.9(3)	2.6(3)
H7Ba	32(5)	36(5)	42(4)	-1(4)	-8(2)	2(2)
H7Bb	43(6)	43(5)	82(7)	0(3)	26(4)	30(3)
C19A	31.9(4)	19.8(3)	17.3(3)	0.5(3)	7.5(3)	3.0(3)
H19A	91(8)	41(6)	27(5)	-1(5)	18(5)	8(4)

Atom	U_{11}	U_{22}	U_{33}	U_{23}	U_{13}	U_{12}
C17A	28.4(3)	16.5(3)	18.7(3)	-0.8(2)	1.7(3)	-2.1(3)
H17A	92(8)	36(5)	28(5)	-7(5)	6(5)	-16(4)
C9B	27.8(3)	23.4(3)	16.7(3)	-3.5(3)	7.1(3)	0.3(3)
H9B	81(7)	46(6)	32(5)	-19(5)	21(5)	-5(4)
C10B	31.3(4)	21.7(3)	19.6(3)	-3.9(3)	7.3(3)	-3.1(3)
H10B	86(8)	48(6)	40(6)	-21(5)	20(5)	-20(5)
C2B	15.0(3)	23.4(3)	24.2(3)	0.7(2)	2.4(2)	0.3(3)
C18B	21.8(3)	24.8(3)	23.1(3)	-2.6(3)	2.6(3)	-4.1(3)
C1B	16.5(3)	25.5(3)	21.6(3)	-0.3(2)	0.3(2)	1.5(3)
C1A	13.9(3)	23.2(3)	38.2(4)	-1.4(2)	7.1(3)	-6.5(3)
C17B	24.0(3)	20.4(3)	33.0(4)	-3.0(3)	5.4(3)	-7.4(3)
H17B	72(7)	36(5)	73(7)	-15(5)	5(5)	-35(5)
C14B	31.8(4)	19.7(3)	30.0(4)	-3.9(3)	8.7(3)	1.3(3)
H14d	28(4)	46(7)	204(14)	0(2)	17(3)	38(8)
H14e	134(10)	27(5)	81(7)	-9(4)	61(6)	-17(3)
H14f	171(13)	87(9)	47(5)	-62(8)	-37(4)	35(4)
C6A	23.0(4)	25.9(4)	47.6(5)	-8.0(3)	8.3(3)	-5.2(3)
H6Aa	67(7)	42(6)	57(4)	-5(4)	-5(3)	5(2)
H6Ab	22(2)	56(7)	120(9)	-4.5(15)	15.4(18)	-10(6)
H6Ac	57(7)	53(5)	77(5)	-21(4)	28(4)	-34(3)
C6B	20.9(4)	29.1(4)	42.7(5)	5.3(3)	3.4(3)	-3.0(4)
H6Ba	46(6)	37(6)	82(8)	-4(5)	23(5)	15(6)
H6Bb	21(5)	64(7)	61(7)	21(5)	-6(5)	-2(5)
H6Bc	67(8)	73(8)	54(7)	15(6)	6(6)	-33(6)
C5B	20.9(4)	40.6(4)	27.5(4)	0.4(3)	5.5(3)	7.7(3)
H5Ba	85(8)	84(8)	27(5)	0(6)	11(5)	-19(6)
H5Bb	22(6)	81(8)	71(7)	-5(5)	11(5)	12(6)
H5Bc	25(5)	57(6)	63(7)	10(5)	13(5)	22(5)
B1A	13.3(3)	18.5(3)	17.6(3)	-0.8(3)	2.5(3)	-0.7(3)
C21A	45.4(5)	18.3(3)	35.5(4)	-0.7(3)	5.2(3)	4.2(3)
H21a	56(5)	52(7)	227(16)	17(3)	31(5)	26(9)
H21b	143(11)	39(6)	82(7)	-23(5)	-46(5)	1(4)
H21c	199(14)	55(8)	76(6)	-8(8)	79(4)	11(4)
C14A	41.1(5)	44.8(5)	17.6(3)	-9.0(4)	-3.1(3)	1.4(3)
H14a	90(5)	279(18)	63(9)	-116(4)	-15(5)	23(11)
H14b	300(20)	58(5)	57(8)	-18(6)	-57(10)	24(3)
H14c	138(12)	270(20)	48(8)	119(7)	-12(5)	-49(7)
C4A	35.1(5)	49.1(5)	40.2(5)	-14.8(4)	22.1(4)	-12.4(4)
H4Aa	74(8)	72(8)	69(7)	-25(6)	32(6)	-37(6)
H4Ab	57(7)	93(9)	81(8)	-35(6)	46(6)	-15(6)
H4Ac	69(8)	74(8)	73(8)	28(7)	34(6)	8(6)
C4B	31.3(5)	47.3(5)	26.8(4)	5.8(4)	-4.2(3)	10.2(4)
H4Ba	87(9)	105(10)	29(6)	14(7)	10(6)	-9(6)
H4Bb	22(6)	107(9)	56(7)	8(5)	-16(5)	14(6)
H4Bc	74(8)	37(6)	75(8)	-12(6)	-14(6)	12(5)
C3B	27.8(4)	35.3(4)	40.5(5)	-8.1(3)	2.0(3)	-9.6(3)
H3Ba	65(7)	44(5)	70(6)	-1(4)	-14(4)	3(3)
H3Bb	20(4)	66(7)	76(7)	-12(2)	5(2)	-13(5)
H3Bc	71(8)	77(8)	51(4)	-22(6)	15(3)	-31(3)
B1B	14.3(3)	19.4(3)	23.0(3)	0.3(3)	1.7(3)	4.3(3)
C5A	23.8(4)	40.0(5)	34.4(4)	-2.3(3)	-7.2(3)	3.4(4)
H5Aa	87(9)	73(8)	36(6)	9(6)	0(6)	-25(6)
H5Ab	22(6)	87(8)	79(8)	7(5)	-15(5)	12(6)
H5Ac	51(7)	55(7)	67(7)	-23(5)	-10(5)	26(5)
C21B	41.6(5)	48.3(5)	25.4(4)	-9.5(4)	-0.8(3)	-6.7(4)
H21d	53(3)	228(17)	69(8)	-52(2)	-6(3)	6(10)
H21e	155(15)	186(17)	63(9)	83(13)	7(9)	-47(10)
H21f	250(20)	67(9)	63(9)	-69(11)	-56(10)	27(7)

Atom	U_{11}	U_{22}	U_{33}	U_{23}	U_{13}	U_{12}
C3A	18.0(4)	32.4(4)	91.1(8)	4.9(3)	1.5(4)	-15.3(5)
H3Aa	51(7)	57(7)	105(5)	8(5)	14(3)	1(3)
H3Ab	22(3)	69(7)	216(15)	-9(2)	-5(4)	-17(8)
H3Ac	68(8)	53(6)	112(6)	1(5)	11(5)	-36(3)

Table 3: Bond Lengths in Å for **MRH_pTolTsNBpin**.

Atom	Atom	Length/Å
S1A	O3A	1.4331(4)
S1A	O4A	1.4347(4)
S1A	N1A	1.6596(5)
S1A	C15A	1.7627(6)
S1B	O4B	1.4304(5)
S1B	O3B	1.4318(5)
S1B	N1B	1.6586(5)
S1B	C15B	1.7577(6)
O1A	C2A	1.4669(7)
O1A	B1A	1.3602(8)
O2A	C1A	1.4565(7)
O2A	B1A	1.3619(8)
O1B	C2B	1.4636(7)
O1B	B1B	1.3609(8)
O2B	C1B	1.4575(7)
O2B	B1B	1.3580(8)
N1A	C8A	1.4424(7)
N1A	C7A	1.4759(7)
N1B	C8B	1.4427(7)
N1B	C7B	1.4729(8)
C15A	C16A	1.3917(8)
C15A	C20A	1.3965(8)
C9A	C8A	1.3914(8)
C9A	C10A	1.3913(9)
C16A	C17A	1.3899(9)
C20B	C15B	1.3919(8)
C20B	C19B	1.3873(9)
C15B	C16B	1.3935(9)
C20A	C19A	1.3892(9)
C11B	C12B	1.3939(9)
C11B	C10B	1.3958(9)
C11B	C14B	1.5021(9)
C12B	C13B	1.3923(9)
C8A	C13A	1.3907(8)
C8B	C13B	1.3949(8)
C8B	C9B	1.3904(9)
C13A	C12A	1.3904(9)
C16B	C17B	1.3919(10)
C12A	C11A	1.3948(9)
C10A	C11A	1.3942(9)
C19B	C18B	1.3957(9)
C7A	B1A	1.5740(9)
C11A	C14A	1.5022(9)
C18A	C19A	1.3965(9)
C18A	C17A	1.3955(9)
C18A	C21A	1.5019(9)
C2A	C1A	1.5659(9)
C2A	C6A	1.5159(9)
C2A	C5A	1.5224(10)
C7B	B1B	1.5853(9)
C9B	C10B	1.3886(9)
C2B	C1B	1.5686(9)
C2B	C6B	1.5182(9)
C2B	C5B	1.5225(9)
C18B	C17B	1.3958(9)
C18B	C21B	1.5026(10)
C1B	C4B	1.5236(9)
C1B	C3B	1.5172(9)
C1A	C4A	1.5273(11)
C1A	C3A	1.5102(10)

Table 4: Bond Angles in ° for **MRH_pTolTsNBpin**.

Atom	Atom	Atom	Angle/°
O4A	S1A	O3A	119.27(2)
N1A	S1A	O3A	106.52(2)
N1A	S1A	O4A	107.19(2)
C15A	S1A	O3A	108.25(3)
C15A	S1A	O4A	108.69(3)
C15A	S1A	N1A	106.19(3)
O3B	S1B	O4B	119.67(3)
N1B	S1B	O4B	107.25(3)
N1B	S1B	O3B	106.65(3)
C15B	S1B	O4B	107.69(3)
C15B	S1B	O3B	108.66(3)
C15B	S1B	N1B	106.17(3)
B1A	O1A	C2A	106.61(5)
B1A	O2A	C1A	107.17(5)
B1B	O1B	C2B	106.95(5)
B1B	O2B	C1B	107.77(5)
C8A	N1A	S1A	115.20(4)
C7A	N1A	S1A	112.36(4)
C7A	N1A	C8A	117.89(5)
C8B	N1B	S1B	115.24(4)
C7B	N1B	S1B	115.27(4)
C7B	N1B	C8B	116.53(5)

Atom	Atom	Atom	Angle/°
C16A	C15A	S1A	120.00(5)
C20A	C15A	S1A	119.29(5)
C20A	C15A	C16A	120.68(6)
C10A	C9A	C8A	120.02(6)
C17A	C16A	C15A	119.17(6)
C19B	C20B	C15B	119.37(6)
C20B	C15B	S1B	118.37(5)
C16B	C15B	S1B	120.80(5)
C16B	C15B	C20B	120.81(6)
C19A	C20A	C15A	119.33(6)
C10B	C11B	C12B	118.27(6)
C14B	C11B	C12B	120.88(6)
C14B	C11B	C10B	120.86(6)
C13B	C12B	C11B	120.92(6)
C9A	C8A	N1A	121.68(5)
C13A	C8A	N1A	118.90(5)
C13A	C8A	C9A	119.41(5)
C13B	C8B	N1B	121.28(5)
C9B	C8B	N1B	119.13(5)
C9B	C8B	C13B	119.56(6)
C12A	C13A	C8A	119.99(6)
C17B	C16B	C15B	119.03(6)
C11A	C12A	C13A	121.41(6)
C11A	C10A	C9A	121.33(6)
C8B	C13B	C12B	120.04(6)
C18B	C19B	C20B	120.94(6)
B1A	C7A	N1A	116.51(5)
C10A	C11A	C12A	117.82(6)
C14A	C11A	C12A	121.17(6)
C14A	C11A	C10A	121.01(6)
C17A	C18A	C19A	118.81(6)
C21A	C18A	C19A	120.55(6)
C21A	C18A	C17A	120.64(6)
C1A	C2A	O1A	102.34(5)
C6A	C2A	O1A	108.95(5)
C6A	C2A	C1A	114.86(6)

Atom	Atom	Atom	Angle/°
C5A	C2A	O1A	106.84(5)
C5A	C2A	C1A	113.20(6)
C5A	C2A	C6A	110.01(6)
B1B	C7B	N1B	111.54(5)
C18A	C19A	C20A	120.87(6)
C18A	C17A	C16A	121.13(6)
C10B	C9B	C8B	119.88(6)
C9B	C10B	C11B	121.31(6)
C1B	C2B	O1B	102.62(5)
C6B	C2B	O1B	108.96(5)
C6B	C2B	C1B	114.87(6)
C5B	C2B	O1B	106.20(5)
C5B	C2B	C1B	113.34(6)
C5B	C2B	C6B	110.15(6)
C17B	C18B	C19B	118.82(6)
C21B	C18B	C19B	120.10(7)
C21B	C18B	C17B	121.08(6)
C2B	C1B	O2B	102.56(4)
C4B	C1B	O2B	106.65(5)
C4B	C1B	C2B	113.77(6)
C3B	C1B	O2B	108.20(5)
C3B	C1B	C2B	114.73(6)
C3B	C1B	C4B	110.19(6)
C2A	C1A	O2A	102.38(5)
C4A	C1A	O2A	106.70(6)
C4A	C1A	C2A	113.13(6)
C3A	C1A	O2A	107.90(6)
C3A	C1A	C2A	115.28(6)
C3A	C1A	C4A	110.63(7)
C18B	C17B	C16B	121.02(6)
O2A	B1A	O1A	114.27(5)
C7A	B1A	O1A	127.84(6)
C7A	B1A	O2A	117.87(5)
O2B	B1B	O1B	114.15(5)
C7B	B1B	O1B	122.23(6)
C7B	B1B	O2B	123.62(6)

Table 5: Torsion Angles in ° for **MRH_pTolTsNBpin**.

Atom	Atom	Atom	Atom	Angle/°
S1A	N1A	C8A	C9A	100.87(5)
S1A	N1A	C8A	C13A	-79.81(5)
S1A	N1A	C7A	B1A	-178.05(4)
S1A	C15A	C16A	C17A	179.37(5)
S1A	C15A	C20A	C19A	-179.04(5)
S1B	N1B	C8B	C13B	-104.29(5)
S1B	N1B	C8B	C9B	77.49(5)
S1B	N1B	C7B	B1B	-171.22(4)
S1B	C15B	C20B	C19B	178.62(5)
S1B	C15B	C16B	C17B	-178.55(5)
O1A	C2A	C1A	O2A	-26.36(5)
O1A	C2A	C1A	C4A	88.07(6)
O1A	C2A	C1A	C3A	-143.22(6)
O1A	B1A	O2A	C1A	-8.34(6)
O1A	B1A	C7A	N1A	-27.55(7)
O2A	C1A	C2A	C6A	-144.25(5)

Atom	Atom	Atom	Atom	Angle/°
O2A	C1A	C2A	C5A	88.25(5)
O2A	B1A	C7A	N1A	154.62(5)
O1B	C2B	C1B	O2B	-23.77(5)
O1B	C2B	C1B	C4B	90.99(5)
O1B	C2B	C1B	C3B	-140.84(5)
O1B	B1B	O2B	C1B	-5.74(6)
O1B	B1B	C7B	N1B	-154.67(6)
O2B	C1B	C2B	C6B	-141.85(5)
O2B	C1B	C2B	C5B	90.30(5)
O2B	B1B	C7B	N1B	26.10(7)
N1A	C8A	C9A	C10A	178.52(6)
N1A	C8A	C13A	C12A	-179.47(5)
N1B	C8B	C13B	C12B	-177.21(5)
N1B	C8B	C9B	C10B	178.30(6)
C15A	C16A	C17A	C18A	-0.45(7)
C15A	C20A	C19A	C18A	-0.24(7)
C9A	C8A	C13A	C12A	-0.14(7)
C9A	C10A	C11A	C12A	0.09(8)
C9A	C10A	C11A	C14A	-179.23(6)
C16A	C17A	C18A	C19A	-0.63(7)
C16A	C17A	C18A	C21A	-179.96(6)
C20B	C15B	C16B	C17B	0.04(7)
C20B	C19B	C18B	C17B	0.78(7)
C20B	C19B	C18B	C21B	-179.60(7)
C15B	C16B	C17B	C18B	0.34(7)
C20A	C19A	C18A	C17A	0.98(8)
C20A	C19A	C18A	C21A	-179.69(7)
C11B	C12B	C13B	C8B	-0.88(7)
C11B	C10B	C9B	C8B	-1.26(8)
C12B	C13B	C8B	C9B	1.00(7)
C8A	C13A	C12A	C11A	1.08(7)
C13A	C12A	C11A	C10A	-1.04(7)
C13A	C12A	C11A	C14A	178.28(6)
C16B	C17B	C18B	C19B	-0.75(7)
C16B	C17B	C18B	C21B	179.64(7)

Table 6: Hydrogen Fractional Atomic Coordinates (×10⁴) and Equivalent Isotropic Displacement Parameters (Å²×10³) for **MRH_pTolTsNBpin**. U_{eq} is defined as 1/3 of the trace of the orthogonalised U_{ij}.

Atom	x	y	z	U_{eq}
H9A	6274(8)	6750(4)	5553(4)	46(2)
H16A	3142(8)	6387(4)	3856(4)	45(2)
H20B	3286(8)	6021(4)	1794(4)	43(2)
H20A	3471(9)	6741(4)	5920(4)	47(2)
H12B	7167(9)	6292(4)	1163(4)	48(2)
H13A	4588(9)	8714(4)	5717(4)	51(3)
H16B	3166(9)	3830(4)	1724(5)	53(3)
H12A	5481(9)	8774(4)	6886(4)	54(3)
H10A	7176(9)	6814(5)	6714(4)	59(3)
H13B	6260(9)	5207(4)	1493(4)	46(2)
H19B	2432(9)	6068(4)	627(4)	48(2)
H7Aa	5224(8)	7593(5)	3920(4)	45(2)
H7Ab	5505(8)	6849(4)	4396(4)	39(2)
H7Ba	5756(8)	4199(4)	1912(4)	38(2)
H7Bb	5717(8)	3894(4)	2733(5)	55(3)
H19A	3412(9)	5488(4)	6112(4)	52(3)

Atom	x	y	z	U_{eq}
H17A	3091(10)	5140(4)	4045(4)	52(3)
H9B	5743(9)	6072(4)	3356(4)	52(3)
H10B	6645(10)	7163(5)	3019(4)	57(3)
H17B	2329(9)	3890(4)	553(5)	61(3)
H14d	8543(9)	7427(5)	1918(7)	93(4)
H14e	7336(12)	7872(5)	2173(5)	77(4)
H14f	7224(14)	7598(6)	1374(5)	106(5)
H6Aa	9277(9)	8866(5)	4275(5)	56(3)
H6Ab	10688(8)	8514(5)	4757(6)	66(3)
H6Ac	9569(9)	8988(5)	5147(5)	61(3)
H6Ba	10143(9)	3221(5)	2691(5)	54(3)
H6Bb	11391(8)	3811(5)	2557(5)	49(3)
H6Bc	10392(10)	3422(5)	1875(5)	65(3)
H5Ba	9628(10)	4453(5)	1363(4)	65(3)
H5Bb	10704(9)	4931(5)	1919(5)	57(3)
H5Bc	9078(8)	5157(5)	1815(5)	48(3)
H21a	4098(11)	4253(6)	5227(8)	111(5)
H21b	2614(13)	4207(5)	4826(6)	93(4)
H21c	2845(15)	4348(6)	5651(6)	105(5)
H14a	7845(13)	8051(10)	7649(6)	146(6)
H14b	7090(20)	7375(7)	7822(6)	144(8)
H14c	6441(15)	8104(10)	7868(6)	153(7)
H4Aa	9084(10)	7286(6)	3293(5)	69(3)
H4Ab	10127(10)	7915(6)	3652(5)	74(3)
H4Ac	8460(11)	8099(6)	3517(5)	70(3)
H4Ba	9578(11)	4354(6)	4081(5)	74(3)
H4Bb	10802(9)	3990(6)	3697(5)	64(3)
H4Bc	9283(10)	3606(5)	3562(5)	64(3)
H3Ba	9798(10)	5613(5)	2807(5)	61(3)
H3Bb	11237(8)	5127(5)	3119(5)	54(3)
H3Bc	10123(10)	5414(5)	3661(5)	66(3)
H5Aa	9112(10)	8108(6)	5901(5)	66(3)
H5Ab	10361(9)	7616(5)	5639(5)	64(3)
H5Ac	8863(9)	7236(5)	5643(5)	59(3)
H21d	888(12)	4901(9)	-285(6)	118(6)
H21e	2236(16)	4635(9)	-483(6)	135(7)
H21f	1985(18)	5503(7)	-408(6)	132(7)
H3Aa	9818(10)	6582(6)	4932(6)	71(3)
H3Ab	10950(9)	7070(6)	4591(8)	104(5)
H3Ac	9981(10)	6476(5)	4103(6)	78(3)

Citations

CrysAlisPro (ROD), Rigaku Oxford Diffraction, Poland (?).

CrysAlisPro Software System, Rigaku Oxford Diffraction, (2020).

L.J. Bourhis and O.V. Dolomanov and R.J. Gildea and J.A.K. Howard and H. Puschmann, The Anatomy of a Comprehensive Constrained, Restrained, Refinement Program for the Modern Computing Environment - Olex2 Disected, *Acta Cryst. A*, (2015), **A71**, 59-71.

O.V. Dolomanov and L.J. Bourhis and R.J. Gildea and J.A.K. Howard and H. Puschmann, Olex2: A complete structure solution, refinement and analysis program, *J. Appl. Cryst.*, (2009), **42**, 339-341.

EMORY UNIVERSITY | X-ray Crystallography Center

R_1=5.66%

Crystal Data and Experimental

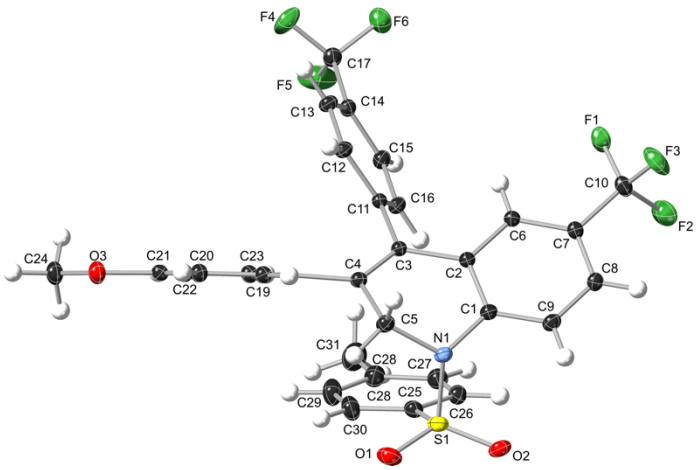

Experimental. Single colourless plate-shaped crystals of **MixedDPA_isomer2-RT** were chosen from the sample as supplied. A suitable crystal with dimensions 0.30 × 0.17 × 0.10 mm³ was selected and mounted on a loop with paratone on a XtaLAB Synergy, Dualflex, HyPix diffractometer. The crystal was kept at a steady T = 270(2) K during data collection. The structure was solved with the ShelXT 2018/2 (Sheldrick, 2018) solution program using dual methods and by using Olex2 1.5-alpha (Dolomanov et al., 2009) as the graphical interface. The model was refined with ShelXL 2018/3 (Sheldrick, 2015) using full matrix least squares minimisation on F^2.

Crystal Data. $C_{31}H_{23}F_6NO_3S$, M_r = 603.56, monoclinic, $P2_1/c$ (No. 14), a = 18.8947(4) Å, b = 10.0287(2) Å, c = 15.9095(3) Å, β = 111.722(2)°, α = γ = 90°, V = 2800.61(10) Å³, T = 270(2) K, Z = 4, Z' = 1, μ(Cu K$_\alpha$) = 1.692, 20472 reflections measured, 5370 unique (R_{int} = 0.0452) which were used in all calculations. The final wR_2 was 0.1676 (all data) and R_1 was 0.0566 (I≥2 σ(I)).

Formula	$C_{31}H_{23}F_6NO_3S$
$D_{calc.}$/ g cm^{-3}	1.431
μ/mm^{-1}	1.692
Formula Weight	603.56
Colour	colourless
Shape	plate-shaped
Size/mm³	0.30×0.17×0.10
T/K	270(2)
Crystal System	monoclinic
Space Group	$P2_1/c$
a/Å	18.8947(4)
b/Å	10.0287(2)
c/Å	15.9095(3)
α/°	90
β/°	111.722(2)
γ/°	90
V/Å³	2800.61(10)
Z	4
Z'	1
Wavelength/Å	1.54184
Radiation type	Cu K$_\alpha$
Θ_{min}/°	5.039
Θ_{max}/°	72.983
Measured Refl's.	20472
Indep't Refl's	5370
Refl's I≥2 σ(I)	4126
R_{int}	0.0452
Parameters	500
Restraints	228
Largest Peak	0.271
Deepest Hole	-0.317
GooF	1.046
wR_2 (all data)	0.1676
wR_2	0.1556
R_1 (all data)	0.0709
R_1	0.0566

Structure Quality Indicators

Reflections:	d min (Cu\a) 2Θ=146.0° 0.81	I/σ(I) 24.3	Rint 4.52%	Full 135.4° 96% to 146.0° 99.5
Refinement:	Shift -0.001	Max Peak 0.3	Min Peak -0.3	GooF 1.046

A colourless plate-shaped-shaped crystal with dimensions 0.30 × 0.17 × 0.10 mm^3 was mounted on a loop with paratone. Data were collected using a XtaLAB Synergy, Dualflex, HyPix diffractometer operating at T = 270(2) K.

Data were measured using ω scans with Cu K_α radiation. The diffraction pattern was indexed and the total number of runs and images was based on the strategy calculation from the program CrysAlisPro 1.171.41.98a (Rigaku OD, 2021). The maximum resolution that was achieved was Θ = 72.983° (0.81 Å).

The unit cell was refined using CrysAlisPro 1.171.41.98a (Rigaku OD, 2021) on 8566 reflections, 42% of the observed reflections.

Data reduction, scaling and absorption corrections were performed using CrysAlisPro 1.171.41.98a (Rigaku OD, 2021). The final completeness is 99.50 % out to 72.983° in Θ. A numerical absorption correction based on gaussian integration over a multifaceted crystal model was performed using CrysAlisPro 1.171.41.98a (Rigaku Oxford Diffraction, 2021). An empirical absorption correction using spherical harmonics, implemented in SCALE3 ABSPACK scaling algorithm was also applied. The absorption coefficient μ of this material is 1.692 mm^{-1} at this wavelength (λ = 1.54184Å) and the minimum and maximum transmissions are 0.660 and 1.000.

The structure was solved and the space group $P2_1/c$ (# 14) determined by the ShelXT 2018/2 (Sheldrick, 2018) structure solution program using using dual methods and refined by full matrix least squares minimisation on $\boldsymbol{F^2}$ using version 2018/3 of ShelXL 2018/3 (Sheldrick, 2015). All non-hydrogen atoms were refined anisotropically. Hydrogen atom positions were calculated geometrically and refined using the riding model. Hydrogen atom positions were calculated geometrically and refined using the riding model.

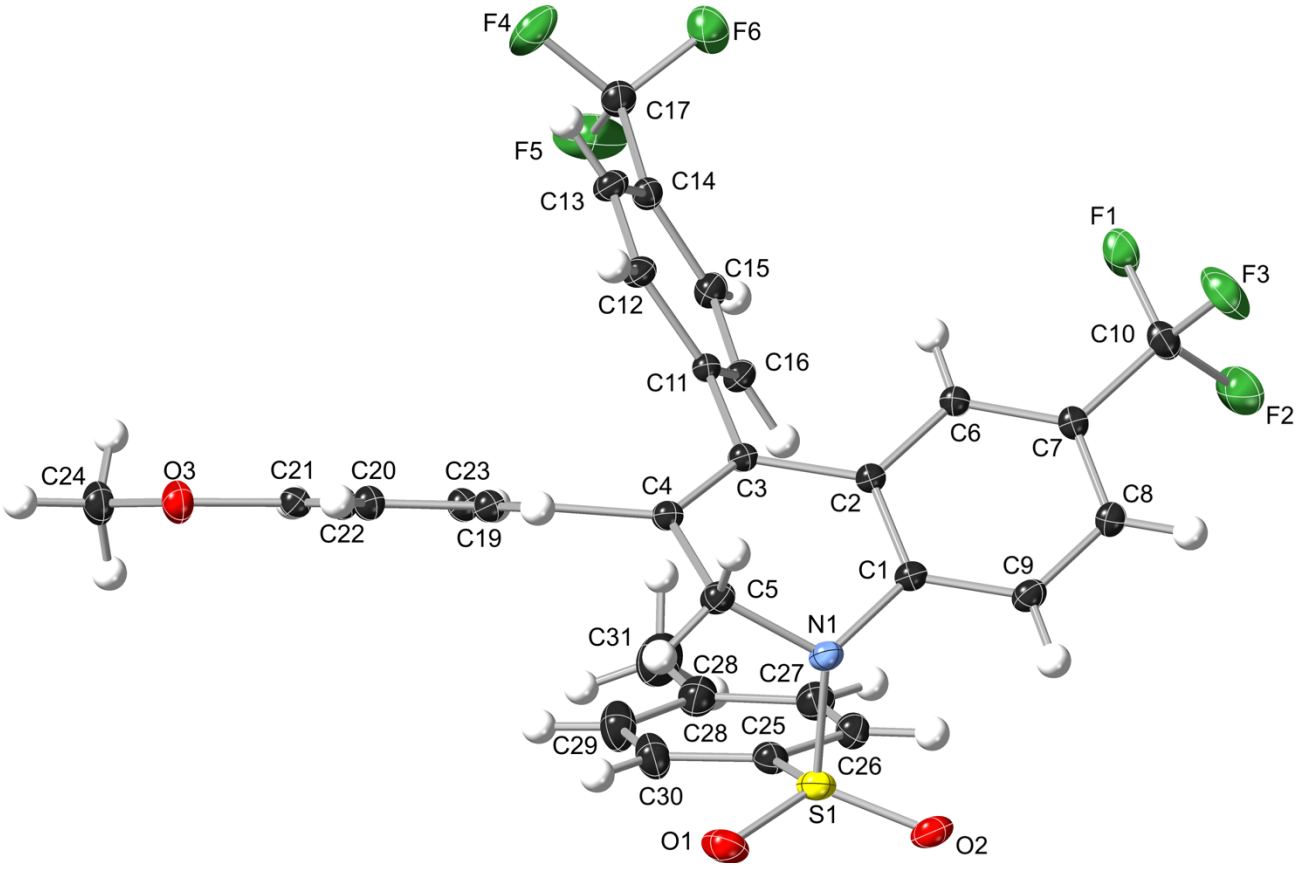

Figure 3: There is a single formula unit in the asymmetric unit, which is represented by the reported sum formula. In other words: Z is 4 and Z' is 1. However the CF3 groups and the O-Me groups are disordered. At low temperatures partial ordering of these groups occurs but resulting in a much larger supercell and too many independent molecules for reasonable refinements.

Data Plots: Diffraction Data

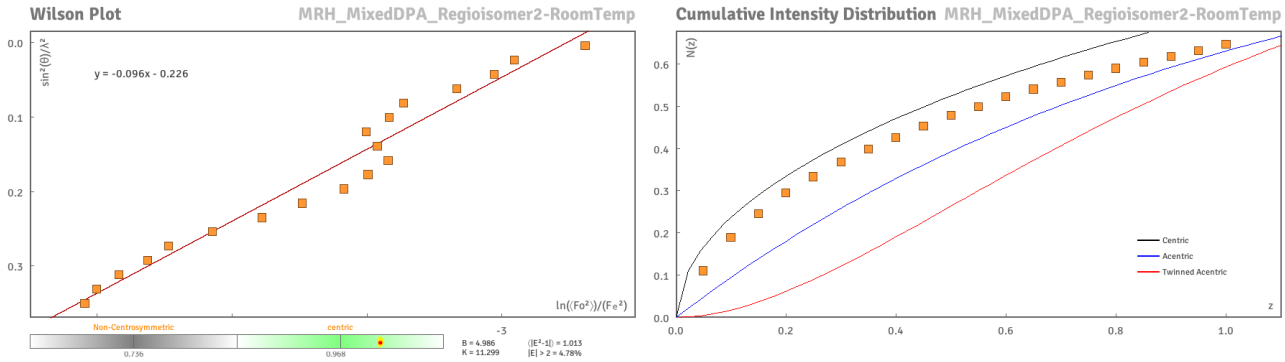

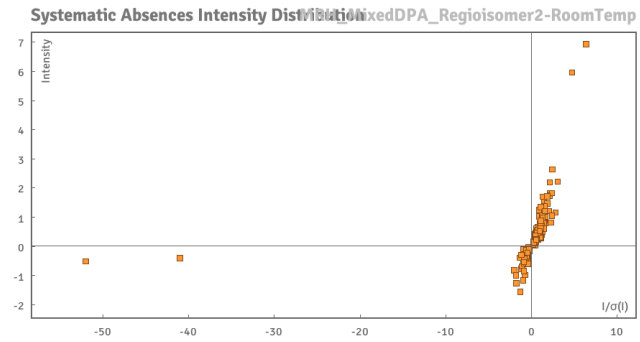

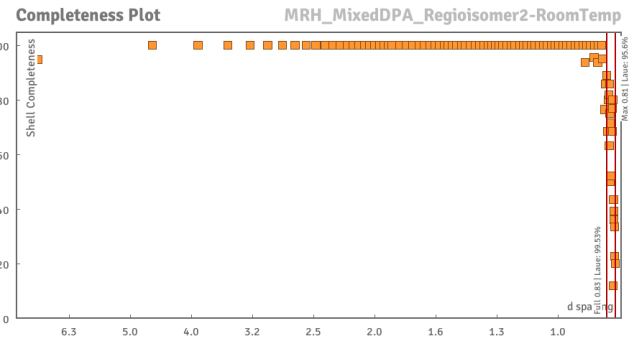

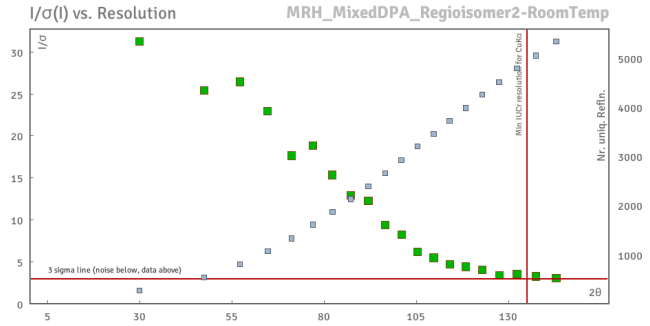

Data Plots: Refinement and Data

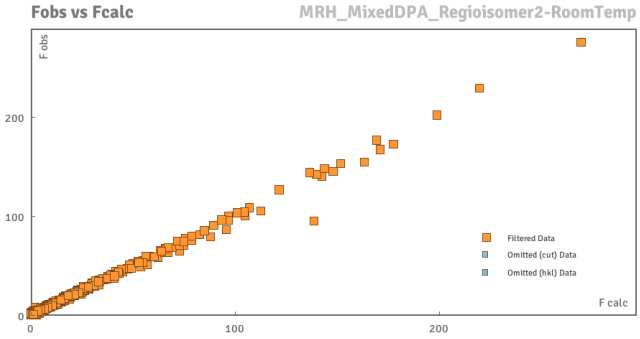

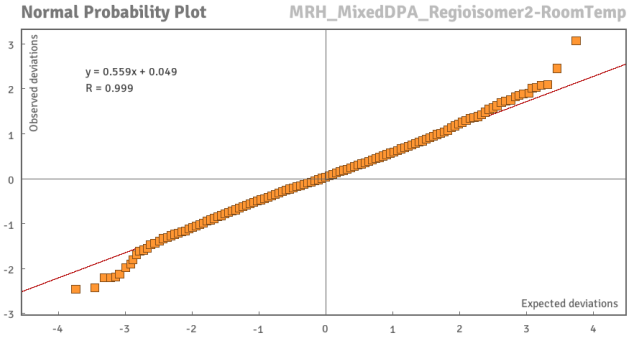

Reflection Statistics

Total reflections (after filtering)	21304	Unique reflections	5370
Completeness	0.956	Mean I/σ	12.32
hkl_{max} collected	(22, 12, 19)	hkl_{min} collected	(-23, -12, -19)
hkl_{max} used	(21, 12, 19)	hkl_{min} used	(-23, 0, 0)
Lim d_{max} collected	100.0	Lim d_{min} collected	0.77
d_{max} used	14.78	d_{min} used	0.81
Friedel pairs	3206	Friedel pairs merged	1
Inconsistent equivalents	6	R_{int}	0.0452
R_{sigma}	0.0412	Intensity transformed	0
Omitted reflections	0	Omitted by user (OMIT hkl)	0
Multiplicity	(7675, 2956, 1415, 584, 170, 43, 4)	Maximum multiplicity	13
Removed systematic absences	832	Filtered off (Shel/OMIT)	0

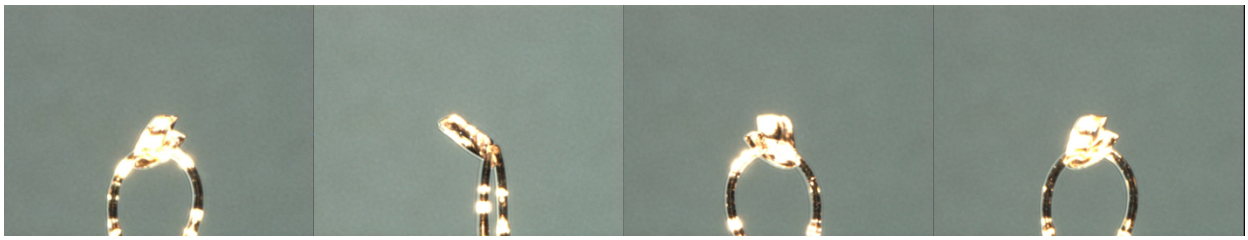

Table 7: Fractional Atomic Coordinates (×10^4) and Equivalent Isotropic Displacement Parameters (Å^2×10^3) for **MixedDPA_isomer2-RT**. U_{eq} is defined as 1/3 of the trace of the orthogonalised U_{ij}.

Atom	x	y	z	U_{eq}
S1	6412.5(4)	3428.3(7)	4966.8(5)	73.2(2)
O1	5731.8(13)	3586(2)	4186.7(15)	101.3(7)
O2	6634.2(13)	2147.5(18)	5362.9(15)	88.5(6)
N1	6294.1(11)	4375.5(18)	5760.3(14)	58.5(5)
C1	6916.0(13)	4412(2)	6617.9(15)	53.0(5)
C2	7345.2(12)	5586(2)	6861.5(14)	48.9(5)
C3	7152.9(12)	6759(2)	6244.9(14)	48.1(5)
C4	6460.1(12)	6810(2)	5574.7(15)	53.4(5)
C5	5916.2(13)	5672(2)	5494.0(18)	62.9(6)
C6	7943.6(14)	5598(2)	7700.1(15)	57.1(5)
C7	8101.4(14)	4488(2)	8260.1(14)	64.8(6)
C8	7666.5(17)	3353(3)	8008.6(18)	68.8(7)
C9	7070.0(15)	3321(2)	7187.4(18)	64.1(6)
C11	7723.4(12)	7850(2)	6444.1(14)	48.3(5)
C12	7535.7(13)	9141(2)	6605.5(16)	57.9(5)
C13	8079.2(14)	10138(2)	6837.2(18)	65.0(6)
C14	8810.5(12)	9873(2)	6906.1(16)	59.0(6)
C15	9000.3(13)	8606(2)	6719.8(17)	60.9(6)
C16	8459.2(13)	7613(2)	6492.0(16)	57.0(5)
C25	7172.4(17)	4120(3)	4741.4(17)	71.8(7)
C26	7916.6(17)	3770(3)	5271.8(19)	72.7(7)
C27	8508.7(18)	4388(3)	5134(2)	79.9(8)
C28	8391(2)	5365(3)	4479(2)	88.2(9)
C29	7650(3)	5669(4)	3947(2)	105.7(12)
C30	7047(2)	5071(4)	4072(2)	96.4(11)
C31	9055(3)	6054(5)	4360(3)	124.5(15)
O3	4892.4(15)	10678(3)	2970.6(18)	84.6(7)
C18	6101.9(18)	7885(3)	4911(2)	59.5(5)
C19	5328.7(17)	8185(4)	4729(2)	64.8(9)
C20	4950.2(17)	9132(3)	4089(2)	68.2(8)
C21	5324.3(15)	9779(3)	3603.4(19)	64.0(8)
C22	6075.5(16)	9499(3)	3769(2)	67.1(8)
C23	6454.5(18)	8551(4)	4423(2)	66.6(9)
C24	5227(2)	11355(4)	2447(3)	85.8(9)
O3B	5545(2)	10809(4)	2878(2)	84.6(7)
C18B	6234(2)	7911(4)	4899(3)	59.5(5)
C19B	6727(2)	8426(5)	4493(3)	69.7(17)
C20B	6475.7(18)	9385(4)	3822(3)	76.7(17)
C21B	5737.4(17)	9867(4)	3552(2)	69.0(14)
C22B	5253.4(18)	9395(4)	3948(3)	68.1(14)
C23B	5511(2)	8422(5)	4621(3)	65.8(15)
C24B	4822(2)	11384(6)	2597(4)	85.8(9)
F1A	8659(2)	5480(3)	9681(3)	122(2)
F2A	9389.2(18)	4937(5)	9031(3)	118(2)
F3A	8920(3)	3487(3)	9595(3)	113.8(14)
C10A	8762.5(15)	4599(3)	9136.3(17)	97.3(9)
F1B	9131.7(16)	5607(2)	9340.2(19)	155(2)

Atom	x	y	z	U_{eq}
F2B	9231.3(15)	3548(2)	9266(2)	172(2)
F3B	8492.6(15)	4355(4)	9821.6(15)	158.1(15)
C10B	8740.0(12)	4504(2)	9162.3(13)	97.3(9)
F4A	9123.8(18)	12150(2)	7091(3)	143(3)
F5A	9858.3(17)	10932(4)	6733.2(19)	168(4)
F6A	9842.9(18)	10836(4)	8027.9(15)	121.2(19)
C17A	9401.9(12)	10947(2)	7177.1(15)	75.7(7)
F4B	9334(2)	11663(4)	7870.0(19)	140(3)
F5B	9398(2)	11734(3)	6593.1(18)	110(2)
F6B	10107.8(15)	10467(4)	7573(3)	117(2)
C17B	9411.6(13)	10922(2)	7236.7(16)	75.7(7)

Table 8: Anisotropic Displacement Parameters ($\times 10^4$) for **MixedDPA_isomer2-RT**. The anisotropic displacement factor exponent takes the form: $-2\pi^2[h^2a^{*2} \times U_{11} + \ldots + 2hka^* \times b^* \times U_{12}]$

Atom	U_{11}	U_{22}	U_{33}	U_{23}	U_{13}	U_{12}
S1	73.7(4)	64.7(4)	68.2(4)	-20.5(3)	10.9(3)	-0.6(3)
O1	86.4(14)	108.4(17)	80.4(13)	-33.5(12)	-2.5(11)	-0.4(12)
O2	103.1(15)	52.6(10)	100.2(15)	-20.9(10)	26.4(12)	-1.6(10)
N1	56.0(10)	47.7(10)	64.5(11)	-9.2(9)	14.1(9)	-4.2(8)
C1	55.4(12)	47.6(11)	56.2(12)	-5.0(9)	20.7(10)	-2.2(9)
C2	52.2(11)	45.9(11)	48.3(11)	-1.3(9)	18.1(9)	0.4(9)
C3	49.5(11)	44.1(11)	48.1(11)	-2.0(9)	15.2(9)	-0.2(9)
C4	53.5(11)	48.7(11)	52.7(12)	-3.7(9)	13.4(9)	1.0(9)
C5	51.4(12)	53.3(13)	72.8(15)	-4.5(11)	9.9(11)	-0.8(10)
C6	66.1(13)	50.1(12)	49.5(12)	-0.8(9)	15.2(10)	-4.5(10)
C7	80.9(16)	57.4(14)	49.7(12)	4.7(10)	16.5(11)	1.0(12)
C8	92.4(18)	52.8(13)	59.9(14)	7.8(11)	26.6(13)	-0.8(13)
C9	76.2(15)	46.3(12)	71.6(15)	-1.9(11)	29.2(13)	-7.5(11)
C11	51.8(11)	43.6(11)	44.7(10)	0.6(8)	12.5(9)	-0.4(9)
C12	52.6(12)	48.8(12)	66.7(14)	-5.8(10)	15.6(10)	3.0(10)
C13	65.7(14)	45.1(12)	75.1(16)	-7.8(11)	15.6(12)	0.7(11)
C14	60.3(13)	49.8(12)	56.8(13)	4.0(10)	10.1(10)	-7.3(10)
C15	50.5(12)	57.8(13)	70.7(15)	4.9(11)	18.1(11)	-0.1(10)
C16	58.3(12)	45.8(11)	66.4(14)	-0.5(10)	22.6(11)	3.0(10)
C25	86.9(18)	69.9(16)	55.3(14)	-8.3(12)	22.4(13)	18.4(14)
C26	82.8(18)	66.1(16)	67.0(16)	3.5(13)	25.3(14)	13.9(14)
C27	85.4(19)	78.9(19)	79.4(19)	-1.0(15)	35.1(16)	12.7(15)
C28	120(3)	80.6(19)	83(2)	3.9(16)	61(2)	22.5(18)
C29	138(3)	113(3)	88(2)	33(2)	67(2)	48(2)
C30	112(3)	112(3)	67.0(17)	20.2(18)	35.4(18)	45(2)
C31	153(4)	115(3)	142(4)	23(3)	98(3)	12(3)
O3	81.9(12)	80.8(14)	74.3(14)	20.5(10)	9.3(11)	12.2(11)
C18	65.9(11)	50.6(11)	46.9(10)	-7.1(7)	3.3(8)	2.1(8)
C19	67.0(12)	55.6(18)	57.8(18)	-1.0(13)	6.8(10)	4.8(11)
C20	67.8(14)	60.4(17)	61.8(16)	3.0(12)	7.0(12)	6.2(13)
C21	68.3(12)	55.9(16)	51.1(15)	-4.1(11)	2.4(10)	1.4(11)
C22	69.2(13)	60.8(18)	56.2(17)	1.7(12)	5.7(12)	1.8(12)
C23	67.0(14)	62.1(19)	55.8(16)	1.7(13)	5.7(12)	2.6(12)
C24	82.6(15)	83(2)	74.6(19)	22.2(14)	9.7(13)	13.2(14)
O3B	81.9(12)	80.8(14)	74.3(14)	20.5(10)	9.3(11)	12.2(11)
C18B	65.9(11)	50.6(11)	46.9(10)	-7.1(7)	3.3(8)	2.1(8)
C19B	69.8(18)	69(4)	58(3)	8(3)	8(2)	6.9(17)
C20B	76(2)	77(3)	63(3)	15(3)	10(2)	11(2)
C21B	73(2)	59(3)	57(2)	1(2)	3.6(19)	3.7(19)
C22B	73(2)	53(3)	62(3)	0(2)	6.0(19)	5.5(19)

Atom	U_{11}	U_{22}	U_{33}	U_{23}	U_{13}	U_{12}
C23B	67.0(14)	53(3)	62(3)	0(2)	6.1(15)	4.1(17)
C24B	82.6(15)	83(2)	74.6(19)	22.2(14)	9.7(13)	13.2(14)
F1A	174(6)	96(2)	73(3)	-3(2)	21(3)	-16(3)
F2A	128(3)	118(4)	80(4)	27(3)	7(3)	-14(2)
F3A	158(3)	96(2)	68(3)	23.1(18)	20(2)	-2(2)
C10A	127(2)	84.1(18)	54.2(14)	9.7(11)	2.1(15)	-14.6(16)
F1B	171(3)	107(2)	97(2)	26.5(19)	-56(2)	-52(2)
F2B	160(3)	164(4)	112(3)	-15(2)	-43(2)	78(3)
F3B	190(3)	213(3)	53.0(14)	8.4(19)	23.4(17)	-17(3)
C10B	127(2)	84.1(18)	54.2(14)	9.7(11)	2.1(15)	-14.6(16)
F4A	102(3)	52.8(19)	218(7)	6(3)	-7(4)	-18.2(19)
F5A	162(6)	197(7)	189(7)	-80(6)	116(6)	-123(5)
F6A	100(3)	120(3)	98(3)	15(3)	-17(2)	-50(2)
C17A	74.6(16)	62.3(15)	73.5(17)	3.3(12)	7.8(14)	-16.5(13)
F4B	140(6)	142(6)	149(5)	-92(5)	66(5)	-79(5)
F5B	121(5)	85(4)	101(3)	26(3)	13(3)	-43(3)
F6B	69(2)	107(3)	134(4)	1(3)	-9(2)	-27(2)
C17B	74.6(16)	62.3(15)	73.5(17)	3.3(12)	7.8(14)	-16.5(13)

Table 9: Bond Lengths in Å for **MixedDPA_isomer2-RT**.

Atom	Atom	Length/Å
S1	O1	1.428(2)
S1	O2	1.424(2)
S1	N1	1.660(2)
S1	C25	1.747(3)
N1	C1	1.434(3)
N1	C5	1.469(3)
C1	C2	1.401(3)
C1	C9	1.381(3)
C2	C3	1.488(3)
C2	C6	1.394(3)
C3	C4	1.349(3)
C3	C11	1.486(3)
C4	C5	1.509(3)
C4	C18	1.485(3)
C4	C18B	1.489(3)
C6	C7	1.388(3)
C7	C8	1.374(4)
C7	C10A	1.492(3)
C7	C10B	1.495(3)
C8	C9	1.374(4)
C11	C12	1.391(3)
C11	C16	1.385(3)
C12	C13	1.383(3)
C13	C14	1.371(3)
C14	C15	1.381(3)
C14	C17A	1.496(3)
C14	C17B	1.494(3)
C15	C16	1.377(3)
C25	C26	1.391(4)
C25	C30	1.383(4)
C26	C27	1.366(4)
C27	C28	1.388(4)
C28	C29	1.376(5)
C28	C31	1.503(5)
C29	C30	1.366(5)
O3	C21	1.373(3)
O3	C24	1.395(4)
C18	C19	1.413(4)
C18	C23	1.370(4)
C19	C20	1.383(4)
C20	C21	1.386(4)
C21	C22	1.373(4)
C22	C23	1.396(4)
O3B	C21B	1.373(3)
O3B	C24B	1.395(4)
C18B	C19B	1.413(4)
C18B	C23B	1.370(4)
C19B	C20B	1.383(4)
C20B	C21B	1.386(4)
C21B	C22B	1.373(4)
C22B	C23B	1.396(4)
F1A	C10A	1.3029(15)
F2A	C10A	1.3012(15)
F3A	C10A	1.3053(15)
F1B	C10B	1.3029(15)
F2B	C10B	1.3012(15)
F3B	C10B	1.3054(15)
F4A	C17A	1.3029(15)
F5A	C17A	1.3013(15)
F6A	C17A	1.3054(15)
F4B	C17B	1.3029(15)
F5B	C17B	1.3012(15)
F6B	C17B	1.3054(15)

Table 10: Bond Angles in ° for **MixedDPA_isomer2-RT**.

Atom	Atom	Atom	Angle/°
O1	S1	N1	105.44(12)
O1	S1	C25	108.78(15)
O2	S1	O1	120.50(14)
O2	S1	N1	106.27(12)
O2	S1	C25	108.63(13)
N1	S1	C25	106.34(11)
C1	N1	S1	116.38(15)
C1	N1	C5	113.07(17)
C5	N1	S1	118.38(17)
C2	C1	N1	118.09(19)
C9	C1	N1	120.2(2)
C9	C1	C2	121.7(2)
C1	C2	C3	120.47(19)
C6	C2	C1	117.0(2)
C6	C2	C3	122.55(19)
C4	C3	C2	118.69(19)
C4	C3	C11	123.76(19)
C11	C3	C2	117.44(18)
C3	C4	C5	118.0(2)
C3	C4	C18	130.0(2)
C3	C4	C18B	122.3(2)
C18	C4	C5	111.8(2)
C18B	C4	C5	119.7(2)
N1	C5	C4	113.71(19)
C7	C6	C2	120.9(2)
C6	C7	C10A	116.5(2)
C6	C7	C10B	120.9(2)
C8	C7	C6	121.0(2)
C8	C7	C10A	122.5(2)
C8	C7	C10B	118.1(2)
C7	C8	C9	119.2(2)
C8	C9	C1	120.3(2)
C12	C11	C3	120.69(19)
C16	C11	C3	121.30(19)
C16	C11	C12	118.0(2)
C13	C12	C11	120.5(2)
C14	C13	C12	120.5(2)
C13	C14	C15	119.70(19)
C13	C14	C17A	120.4(2)
C13	C14	C17B	120.2(2)
C15	C14	C17A	119.9(2)
C15	C14	C17B	120.0(2)
C16	C15	C14	119.7(2)
C15	C16	C11	121.5(2)
C26	C25	S1	119.9(2)
C30	C25	S1	120.8(2)
C30	C25	C26	119.2(3)
C27	C26	C25	119.5(3)
C26	C27	C28	121.9(3)
C27	C28	C31	120.7(4)
C29	C28	C27	117.5(3)
C29	C28	C31	121.8(3)
C30	C29	C28	121.8(3)
C29	C30	C25	120.0(3)
C21	O3	C24	118.7(2)
C19	C18	C4	117.7(3)
C23	C18	C4	124.6(3)
C23	C18	C19	117.6(2)
C20	C19	C18	120.7(3)
C19	C20	C21	120.1(3)
O3	C21	C20	115.4(2)
O3	C21	C22	124.5(2)
C22	C21	C20	120.1(2)
C21	C22	C23	119.4(3)
C18	C23	C22	122.1(3)
C21B	O3B	C24B	118.7(2)
C19B	C18B	C4	122.7(3)
C23B	C18B	C4	119.7(3)
C23B	C18B	C19B	117.6(2)
C20B	C19B	C18B	120.7(3)
C19B	C20B	C21B	120.1(3)
O3B	C21B	C20B	115.4(2)
O3B	C21B	C22B	124.5(2)
C22B	C21B	C20B	120.1(2)
C21B	C22B	C23B	119.4(3)
C18B	C23B	C22B	122.1(3)
F1A	C10A	C7	113.1(3)
F1A	C10A	F3A	105.45(13)
F2A	C10A	C7	112.7(3)
F2A	C10A	F1A	106.06(13)
F2A	C10A	F3A	105.36(13)
F3A	C10A	C7	113.5(3)
F1B	C10B	C7	114.2(2)
F1B	C10B	F3B	105.44(13)
F2B	C10B	C7	113.5(2)
F2B	C10B	F1B	106.06(13)
F2B	C10B	F3B	105.36(13)
F3B	C10B	C7	111.6(2)
F4A	C17A	C14	114.1(2)
F4A	C17A	F6A	105.44(13)
F5A	C17A	C14	114.1(2)
F5A	C17A	F4A	106.06(13)
F5A	C17A	F6A	105.35(13)
F6A	C17A	C14	111.0(2)
F4B	C17B	C14	112.7(3)
F4B	C17B	F6B	105.44(13)
F5B	C17B	C14	111.9(2)
F5B	C17B	F4B	106.06(13)
F5B	C17B	F6B	105.36(13)
F6B	C17B	C14	114.7(2)

Table 11: Torsion Angles in ° for **MixedDPA_isomer2-RT**.

Atom	Atom	Atom	Atom	Angle/°
S1	N1	C1	C2	108.8(2)
S1	N1	C1	C9	-72.5(3)
S1	N1	C5	C4	-91.9(2)
S1	C25	C26	C27	-175.2(2)
S1	C25	C30	C29	175.4(3)
O1	S1	N1	C1	-178.73(18)
O1	S1	N1	C5	-38.8(2)
O1	S1	C25	C26	-161.5(2)
O1	S1	C25	C30	22.2(3)
O2	S1	N1	C1	52.3(2)
O2	S1	N1	C5	-167.80(17)
O2	S1	C25	C26	-28.6(3)
O2	S1	C25	C30	155.1(2)
N1	S1	C25	C26	85.4(2)
N1	S1	C25	C30	-90.9(3)
N1	C1	C2	C3	0.4(3)
N1	C1	C2	C6	179.65(19)
N1	C1	C9	C8	179.9(2)
C1	N1	C5	C4	49.2(3)
C1	C2	C3	C4	17.0(3)
C1	C2	C3	C11	-166.80(19)
C1	C2	C6	C7	0.2(3)
C2	C1	C9	C8	-1.5(4)
C2	C3	C4	C5	0.4(3)
C2	C3	C4	C18	175.3(3)
C2	C3	C4	C18B	-176.8(3)
C2	C3	C11	C12	-121.2(2)
C2	C3	C11	C16	57.5(3)
C2	C6	C7	C8	-0.8(4)
C2	C6	C7	C10A	179.0(2)
C2	C6	C7	C10B	-179.6(2)
C3	C2	C6	C7	179.4(2)
C3	C4	C5	N1	-33.2(3)
C3	C4	C18	C19	-137.3(3)
C3	C4	C18	C23	46.7(5)
C3	C4	C18B	C19B	42.6(6)
C3	C4	C18B	C23B	-140.3(4)
C3	C11	C12	C13	176.6(2)
C3	C11	C16	C15	-176.8(2)
C4	C3	C11	C12	54.8(3)
C4	C3	C11	C16	-126.5(2)
C4	C18	C19	C20	-177.1(3)
C4	C18	C23	C22	176.1(3)
C4	C18B	C19B	C20B	175.5(5)
C4	C18B	C23B	C22B	-175.9(5)
C5	N1	C1	C2	-33.2(3)
C5	N1	C1	C9	145.5(2)
C5	C4	C18	C19	37.9(4)
C5	C4	C18	C23	-138.1(3)
C5	C4	C18B	C19B	-134.6(4)
C5	C4	C18B	C23B	42.5(6)
C6	C2	C3	C4	-162.2(2)
C6	C2	C3	C11	14.0(3)
C6	C7	C8	C9	0.4(4)
C6	C7	C10A	F1A	65.4(3)
C6	C7	C10A	F2A	-54.9(3)
C6	C7	C10A	F3A	-174.5(3)
C6	C7	C10B	F1B	-2.4(3)

Atom	Atom	Atom	Atom	Angle/°
C6	C7	C10B	F2B	-124.1(3)
C6	C7	C10B	F3B	117.1(3)
C7	C8	C9	C1	0.8(4)
C8	C7	C10A	F1A	-114.7(3)
C8	C7	C10A	F2A	125.0(3)
C8	C7	C10A	F3A	5.3(4)
C8	C7	C10B	F1B	178.8(2)
C8	C7	C10B	F2B	57.1(3)
C8	C7	C10B	F3B	-61.7(3)
C9	C1	C2	C3	-178.3(2)
C9	C1	C2	C6	1.0(3)
C11	C3	C4	C5	-175.5(2)
C11	C3	C4	C18	-0.6(4)
C11	C3	C4	C18B	7.2(4)
C11	C12	C13	C14	0.4(4)
C12	C11	C16	C15	2.0(3)
C12	C13	C14	C15	1.7(4)
C12	C13	C14	C17A	-178.6(2)
C12	C13	C14	C17B	-174.5(2)
C13	C14	C15	C16	-1.9(4)
C13	C14	C17A	F4A	-17.8(3)
C13	C14	C17A	F5A	-140.0(3)
C13	C14	C17A	F6A	101.1(3)
C13	C14	C17B	F4B	36.4(3)
C13	C14	C17B	F5B	-83.0(3)
C13	C14	C17B	F6B	157.1(3)
C14	C15	C16	C11	0.0(4)
C15	C14	C17A	F4A	161.9(3)
C15	C14	C17A	F5A	39.7(3)
C15	C14	C17A	F6A	-79.2(3)
C15	C14	C17B	F4B	-139.7(3)
C15	C14	C17B	F5B	100.8(3)
C15	C14	C17B	F6B	-19.1(3)
C16	C11	C12	C13	-2.2(3)
C25	S1	N1	C1	-63.32(19)
C25	S1	N1	C5	76.59(19)
C25	C26	C27	C28	0.2(4)
C26	C25	C30	C29	-0.9(5)
C26	C27	C28	C29	-1.9(5)
C26	C27	C28	C31	178.3(3)
C27	C28	C29	C30	2.2(5)
C28	C29	C30	C25	-0.8(5)
C30	C25	C26	C27	1.2(4)
C31	C28	C29	C30	-178.1(3)
O3	C21	C22	C23	-179.2(3)
C18	C4	C5	N1	151.0(3)
C18	C19	C20	C21	1.3(5)
C19	C18	C23	C22	0.2(6)
C19	C20	C21	O3	178.6(3)
C19	C20	C21	C22	-1.2(5)
C20	C21	C22	C23	0.5(5)
C21	C22	C23	C18	0.0(6)
C23	C18	C19	C20	-0.8(6)
C24	O3	C21	C20	-179.1(3)
C24	O3	C21	C22	0.6(5)
O3B	C21B	C22B	C23B	179.2(5)
C18B	C4	C5	N1	144.1(3)
C18B	C19B	C20B	C21B	1.1(8)

Atom	Atom	Atom	Atom	Angle/°
C19B	C18B	C23B	C22B	1.4(8)
C19B	C20B	C21B	O3B	-179.6(5)
C19B	C20B	C21B	C22B	0.0(7)
C20B	C21B	C22B	C23B	-0.4(7)
C21B	C22B	C23B	C18B	-0.4(8)
C23B	C18B	C19B	C20B	-1.8(8)
C24B	O3B	C21B	C20B	-177.2(5)
C24B	O3B	C21B	C22B	3.1(8)
C10A	C7	C8	C9	-179.4(3)
C10B	C7	C8	C9	179.2(2)
C17A	C14	C15	C16	178.4(2)
C17B	C14	C15	C16	174.3(2)

Table 12: Hydrogen Fractional Atomic Coordinates ($\times 10^4$) and Equivalent Isotropic Displacement Parameters ($Å^2 \times 10^3$) for **MixedDPA_isomer2-RT**. U_{eq} is defined as 1/3 of the trace of the orthogonalised U_{ij}.

Atom	x	y	z	U_{eq}
H5A	5624.97	5862.88	5870	75
H5B	5560.92	5617.1	4872.14	75
H6	8241.14	6360.49	7886.96	68
H8	7774.55	2615.58	8389.72	83
H9	6768.69	2560.46	7014.36	77
H12	7040.76	9333.8	6557.24	69
H13	7947.77	10996.41	6947.12	78
H15	9491.39	8425.56	6748.14	73
H16	8590.95	6762.22	6367.42	68
H26	8010.41	3119.54	5716.82	87
H27	9004.88	4146.55	5489.69	96
H29	7556.86	6299.15	3489.86	127
H30	6551.59	5303.87	3707.53	116
H31A	9243.08	6740.7	4808.54	187
H31B	8893.15	6443.15	3767.76	187
H31C	9451.87	5417.38	4429.1	187
H19	5071.41	7741.26	5043.7	78
H20	4444.26	9335.07	3983.51	82
H22	6329.29	9936.93	3447.67	81
H23	6963.07	8366.48	4531.2	80
H24A	4862.47	11954.05	2042.09	129
H24B	5391	10723.83	2102.54	129
H24C	5658.3	11852.71	2834.53	129
H19B	7225.58	8117.92	4678.85	84
H20B	6802.57	9706	3552.9	92
H22B	4758.59	9719.9	3770.48	82
H23B	5181.25	8110.28	4888.99	79
H24D	4771.38	12034.31	2136.26	129
H24E	4753.79	11808.09	3103.34	129
H24F	4441.9	10703.9	2359.55	129

Table 13: Atomic Occupancies for all atoms that are not fully occupied in **MixedDPA_isomer2-RT**.

Atom	Occupancy	Atom	Occupancy	Atom	Occupancy	Atom	Occupancy
O3	0.645(2)	C19	0.645(2)	C20	0.645(2)	C21	0.645(2)
C18	0.645(2)	H19	0.645(2)	H20	0.645(2)	C22	0.645(2)

Atom	Occupancy
H22	0.645(2)
C23	0.645(2)
H23	0.645(2)
C24	0.645(2)
H24A	0.645(2)
H24B	0.645(2)
H24C	0.645(2)
O3B	0.355(2)
C18B	0.355(2)
C19B	0.355(2)
H19B	0.355(2)
C20B	0.355(2)
H20B	0.355(2)
C21B	0.355(2)
C22B	0.355(2)
H22B	0.355(2)
C23B	0.355(2)
H23B	0.355(2)
C24B	0.355(2)
H24D	0.355(2)
H24E	0.355(2)
H24F	0.355(2)
F1A	0.271(4)
F2A	0.271(4)
F3A	0.271(4)
C10A	0.271(4)
F1B	0.729(4)
F2B	0.729(4)
F3B	0.729(4)
C10B	0.729(4)
F4A	0.551(6)
F5A	0.551(6)
F6A	0.551(6)
C17A	0.551(6)
F4B	0.449(6)
F5B	0.449(6)
F6B	0.449(6)
C17B	0.449(6)

Citations

CrysAlisPro (Rigaku, V1.171.41.98a, 2021)

CrysAlisPro (ROD), Rigaku Oxford Diffraction, Poland (?).

O.V. Dolomanov and L.J. Bourhis and R.J. Gildea and J.A.K. Howard and H. Puschmann, Olex2: A complete structure solution, refinement and analysis program, *J. Appl. Cryst.*, (2009), **42**, 339-341.

Sheldrick, G.M., Crystal structure refinement with ShelXL, *Acta Cryst.*, (2015), **C71**, 3-8.

Sheldrick, G.M., ShelXT-Integrated space-group and crystal-structure determination, *Acta Cryst.*, (2015), **A71**, 3-8.

MRH_CuOxidant

Submitted by: **Michael Hollerbach**
Emory University
Solved by: **John Bacsa**
Sample ID: **MRH_CuOxidant**

R_1=4.48%

Crystal Data and Experimental

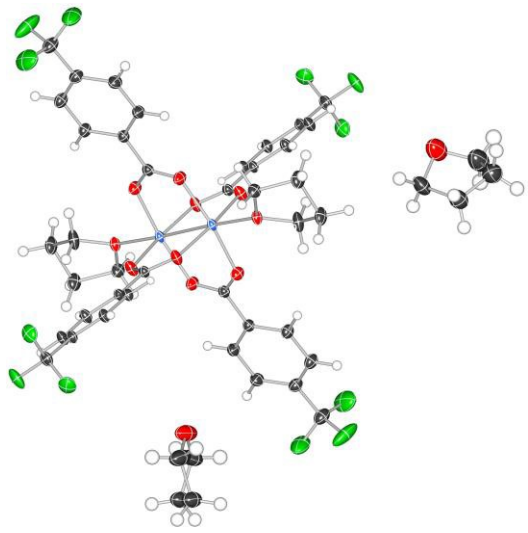

Experimental. Single greenish blue prism-shaped crystals of **MRH_CuOxidant** were The crystal was chosen from the sample as supplied.. A suitable crystal 0.34×0.33×0.21 mm³ was selected and mounted on a loop with paratone oil on an XtaLAB Synergy, Dualflex, HyPix diffractometer. The crystal was kept at a steady T = 99.98(10) K during data collection. The structure was solved with the ShelXT (Sheldrick, 2015) structure solution program using the Intrinsic Phasing solution method and by using **Olex2** (Dolomanov et al., 2009) as the graphical interface. The model was refined with version 2018/3 of ShelXL 2018/3 (Sheldrick, 2015) using Least Squares minimisation.

Crystal Data. $C_{52}H_{56}Cu_2F_{12}O_{13}$, M_r = 1244.04, monoclinic, $I2/a$ (No. 15), a = 16.2908(2) Å, b = 14.13310(10) Å, c = 24.4682(3) Å, β = 108.6720(10)°, α = γ = 90°, V = 5337.03(10) Å³, T = 99.98(10) K, Z = 4, Z' = 0.5, μ(Mo Kα) = 0.902, 82962 reflections measured, 13940 unique (R_{int} = 0.0321) which were used in all calculations. The final wR_2 was 0.1207 (all data) and R_1 was 0.0448 (I > 2(I)).

Compound	**MRH_CuOxidant**
Formula	$C_{52}H_{56}Cu_2F_{12}O_{13}$
$D_{calc.}$/ g cm^{-3}	1.548
μ/mm^{-1}	0.902
Formula Weight	1244.04
Colour	greenish blue
Shape	prism
Size/mm³	0.34×0.33×0.21
T/K	99.98(10)
Crystal System	monoclinic
Space Group	$I2/a$
a/Å	16.2908(2)
b/Å	14.13310(10)
c/Å	24.4682(3)
α/°	90
β/°	108.6720(10)
γ/°	90
V/Å³	5337.03(10)
Z	4
Z'	0.5
Wavelength/Å	0.71073
Radiation type	Mo Kα
Θ_{min}/°	1.688
Θ_{max}/°	38.084
Measured Refl.	82962
Independent Refl.	13940
Reflections with I > 2(I)	11823
R_{int}	0.0321
Parameters	377
Restraints	63
Largest Peak	1.940
Deepest Hole	-1.670
GooF	1.036
wR_2 (all data)	0.1207
wR_2	0.1158
R_1 (all data)	0.0551
R_1	Oooops!

Structure Quality Indicators

Reflections:	d min (Mo) 0.58	I/σ 46.1	Rint 3.21%	complete 100% (IUCr) 100%
Refinement:	Shift -0.002	Max Peak 1.9	Min Peak -1.7	GooF 1.036

Experimental Extended. A greenish blue prism-shaped crystal with dimensions 0.34×0.33×0.21 mm^3 was mounted on a loop with paratone oil. Data were collected using an XtaLAB Synergy, Dualflex, HyPix diffractometer equipped with an Oxford Cryosystems low-temperature device operating at T = 99.98(10) K.

Data were measured using ω scans of 0.5° per frame for 8.4/16.0 s using Mo K$_\alpha$ radiation. The total number of runs and images was based on the strategy calculation from the program CrysAlisPro (Rigaku, V1.171.40.67a, 2019) The maximum resolution that was achieved was Θ = 38.084° (0.58 Å).

The diffraction pattern was indexed The total number of runs and images was based on the strategy calculation from the program CrysAlisPro (Rigaku, V1.171.40.67a, 2019) and the unit cell was refined using CrysAlisPro (Rigaku, V1.171.40.67a, 2019) on 39069 reflections, 47% of the observed reflections.

Data reduction, scaling and absorption corrections were performed using CrysAlisPro (Rigaku, V1.171.40.67a, 2019). The final completeness is 100.00 % out to 38.084° in Θ. A gaussian absorption correction was performed using CrysAlisPro 1.171.40.67a (Rigaku Oxford Diffraction, 2019)Numerical absorption correction based on gaussian integration over a multifaceted crystal modelEmpirical absorption correction using spherical harmonicsas implemented in SCALE3 ABSPACK.. The absorption coefficient μ of this material is 0.902 mm^{-1} at this wavelength (λ = 0.711Å) and the minimum and maximum transmissions are 0.501 and 1.000.

The structure was solved and the space group *I*2/*a* (# 15) determined by the ShelXT (Sheldrick, 2015) structure solution program using Intrinsic Phasing and refined by Least Squares using version 2018/3 of ShelXL 2018/3 (Sheldrick, 2015). All non-hydrogen atoms were refined anisotropically. Hydrogen atom positions were calculated geometrically and refined using the riding model. Hydrogen atom positions were calculated geometrically and refined using the riding model.

_exptl_absorpt_process_details: CrysAlisPro 1.171.40.67a (Rigaku Oxford Diffraction, 2019)Numerical absorption correction based on gaussian integration over a multifaceted crystal modelEmpirical absorption correction using spherical harmonicsas implemented in SCALE3 ABSPACK.

Table 1: Fractional Atomic Coordinates (×10^4) and Equivalent Isotropic Displacement Parameters (Å^2×10^3) for **MRH_CuOxidant**. U_{eq} is defined as 1/3 of the trace of the orthogonalised U_{ij}.

Atom	x	y	z	U_{eq}
C1	3728.2(7)	5968.4(8)	4396.5(5)	14.92(17)
C2	2960.1(7)	6513.1(8)	4030.7(5)	14.62(17)
C3	2190.3(7)	6511.2(8)	4166.3(5)	15.34(17)
C4	1473.7(7)	7004.6(9)	3823.9(5)	17.13(19)
C5	1534.8(7)	7512.5(9)	3351.0(5)	16.60(18)
C6	2303.0(8)	7530.3(10)	3217.7(5)	19.7(2)
C7	3013.5(8)	7019.3(10)	3553.7(5)	19.4(2)
C8	750.3(8)	8027.5(10)	2983.1(6)	22.0(2)
C9	4252.5(8)	3560.3(9)	4449.7(5)	16.50(18)
C10	3749.0(8)	2762.2(9)	4095.4(5)	17.15(18)
C11	3230.4(9)	2188.5(10)	4313.1(6)	21.5(2)
C12	2727.8(9)	1481.1(10)	3974.4(6)	23.0(2)
C13	2745.9(9)	1349.6(10)	3414.3(6)	21.6(2)

Atom	x	y	z	U_{eq}
C14	3267.5(9)	1912.0(11)	3193.3(6)	23.2(2)
C15	3770.5(8)	2619.8(10)	3535.5(6)	20.2(2)
C16	2179.5(10)	609.3(12)	3039.1(7)	29.3(3)
C17	6728.0(9)	5942.2(10)	4016.5(6)	22.1(2)
C18B	6891(3)	5945(3)	3448.5(15)	27.5(4)
C19	6129.1(10)	5345.6(12)	3051.6(6)	26.8(3)
C20	5497.1(9)	5208.8(13)	3377.8(6)	27.2(3)
Cu1	5394.1(2)	5140.4(2)	4622.1(2)	13.07(4)
F1	449.0(7)	8651.8(8)	3284.6(5)	32.8(2)
F2	88.4(6)	7430.4(8)	2740.6(4)	31.5(2)
F3	898.0(6)	8500.8(9)	2551.2(5)	34.8(2)
F4	1440.1(9)	964.4(11)	2701.3(7)	58.5(4)
F5	2559.1(10)	168.8(11)	2705.3(7)	59.8(5)
F6	1960.9(11)	-68.3(10)	3347.7(6)	51.4(4)
O1	4362.7(6)	5885.0(8)	4212.0(4)	21.20(17)
O2	3677.9(6)	5629.4(7)	4861.8(4)	19.60(16)
O3	4784.0(6)	3987.8(7)	4258.8(4)	20.78(17)
O4	4094.1(7)	3754.5(7)	4909.1(4)	22.02(17)
O5	6005.6(6)	5318.7(7)	3974.9(4)	17.51(15)
C7S	1757(2)	-369.3(16)	4911.6(12)	52.8(5)
C8S	2090.3(16)	-1359.5(14)	5084.7(10)	43.5(4)
O6S	2500	213.9(15)	5000	55.2(5)
C18A	6618(2)	6212(3)	3382.8(8)	27.5(4)
C1S_2	22(5)	6209(5)	1370(3)	43.2(6)
O2S_2	-382(5)	6838(6)	880(3)	62.8(6)
C3S_2	110(30)	6440(30)	550(20)	50.5(17)
C4S_2	364(5)	5501(5)	620(4)	42.6(15)
C5S_2	641(6)	5525(7)	1234(4)	43.2(6)
C1S_1	-194.4(18)	6917(2)	1380.2(10)	62.8(6)
O2S_1	-682(3)	6665(3)	772.6(14)	62.8(6)
C3S_1	72(13)	6355(13)	574(8)	50.5(17)
C4S_1	605(2)	5743(3)	1062.5(16)	44.2(7)
C5S_1	357(2)	6071(2)	1595.5(14)	43.2(6)

Table 2: Anisotropic Displacement Parameters ($\times 10^4$) **MRH_CuOxidant**. The anisotropic displacement factor exponent takes the form: $-2\pi^2[h^2a^{*2} \times U_{11} + ... + 2hka^* \times b^* \times U_{12}]$

Atom	U_{11}	U_{22}	U_{33}	U_{23}	U_{13}	U_{12}
C1	14.6(4)	15.9(4)	14.6(4)	1.7(3)	5.1(3)	2.5(3)
C2	13.8(4)	16.1(4)	14.1(4)	2.2(3)	4.7(3)	2.1(3)
C3	13.7(4)	18.0(4)	14.3(4)	2.7(3)	4.4(3)	-0.1(3)
C4	12.8(4)	21.4(5)	16.5(4)	3.3(4)	3.8(3)	0.5(3)
C5	14.3(4)	18.9(5)	15.2(4)	2.9(3)	2.7(3)	2.2(3)
C6	19.2(5)	23.7(5)	17.5(5)	7.5(4)	7.8(4)	5.1(4)
C7	17.4(4)	23.7(5)	19.1(5)	7.1(4)	8.9(4)	5.3(4)
C8	17.1(5)	26.3(6)	20.4(5)	7.0(4)	2.9(4)	3.9(4)
C9	16.3(4)	17.1(4)	16.2(4)	1.7(3)	5.5(3)	2.2(3)
C10	17.2(4)	18.3(5)	17.2(4)	0.8(4)	7.2(4)	1.3(4)
C11	27.1(6)	20.7(5)	19.2(5)	0.5(4)	10.7(4)	-2.9(4)
C12	26.7(6)	21.0(5)	23.4(5)	0.4(4)	11.2(5)	-4.1(4)
C13	20.9(5)	21.9(5)	23.3(5)	-4.0(4)	9.1(4)	-2.1(4)
C14	22.8(5)	28.0(6)	21.7(5)	-5.6(4)	11.3(4)	-3.7(5)
C15	19.3(5)	24.0(5)	19.9(5)	-2.1(4)	9.9(4)	-1.8(4)
C16	28.0(6)	31.4(7)	30.8(7)	-9.3(5)	12.7(5)	-8.0(5)
C17	22.8(5)	24.7(6)	22.0(4)	-0.5(4)	11.6(4)	-4.5(4)
C18B	26.2(9)	37.6(9)	22.3(5)	0.5(5)	12.9(5)	-7.0(7)
C19	27.0(6)	38.9(7)	17.5(5)	0.5(4)	11.6(4)	-6.6(5)
C20	17.3(5)	49.3(9)	14.7(5)	7.5(5)	4.4(4)	0.3(5)
Cu1	12.62(6)	15.81(6)	11.97(6)	2.68(4)	5.60(4)	2.54(4)
F1	27.7(4)	31.5(5)	37.3(5)	3.4(4)	7.8(4)	14.6(4)
F2	18.1(4)	40.1(5)	28.7(4)	3.6(4)	-2.9(3)	-2.0(3)
F3	25.0(4)	46.9(6)	30.7(5)	24.1(4)	6.4(4)	8.9(4)

Atom	U_{11}	U_{22}	U_{33}	U_{23}	U_{13}	U_{12}
F4	42.6(7)	53.3(8)	57.9(8)	-11.1(7)	-14.4(6)	-6.4(6)
F5	57.8(8)	64.7(9)	72.9(10)	-48.5(8)	43.7(8)	-31.2(7)
F6	71.0(9)	40.9(6)	45.8(7)	-10.7(5)	23.4(7)	-32.4(6)
O1	17.7(4)	28.3(5)	20.8(4)	9.4(3)	10.6(3)	9.3(3)
O2	17.0(4)	27.3(4)	16.0(3)	7.6(3)	7.3(3)	6.7(3)
O3	21.5(4)	22.8(4)	21.3(4)	-2.7(3)	11.4(3)	-4.0(3)
O4	28.0(5)	22.4(4)	19.5(4)	-2.8(3)	13.1(3)	-4.6(3)
O5	15.1(3)	25.3(4)	13.4(3)	2.7(3)	6.3(3)	-0.9(3)
C7S	84.5(13)	32.2(6)	55.6(12)	7.8(7)	41.7(11)	7.5(6)
C8S	62.1(12)	29.9(6)	48.2(10)	1.5(6)	31.2(10)	1.4(6)
O6S	95.9(14)	31.0(7)	59.9(13)	0	54.8(12)	0
C18A	26.2(9)	37.6(9)	22.3(5)	0.5(5)	12.9(5)	-7.0(7)
C1S_2	47.4(15)	43.3(13)	39.8(14)	15.4(11)	15.2(11)	10.0(11)
O2S_2	82.8(12)	59.4(10)	55.2(9)	9.4(8)	34.8(9)	18.2(9)
C3S_2	58(2)	46(4)	49.5(19)	-1(2)	19.2(12)	3(2)
C4S_2	38(3)	39(3)	55(4)	-6(3)	21(3)	0(3)
C5S_2	47.4(15)	43.3(13)	39.8(14)	15.4(11)	15.2(11)	10.0(11)
C1S_1	82.8(12)	59.4(10)	55.2(9)	9.4(8)	34.8(9)	18.2(9)
O2S_1	82.8(12)	59.4(10)	55.2(9)	9.4(8)	34.8(9)	18.2(9)
C3S_1	58(2)	46(4)	49.5(19)	-1(2)	19.2(12)	3(2)
C4S_1	45.6(15)	44.3(17)	44.4(17)	6.9(13)	16.9(13)	8.8(13)
C5S_1	47.4(15)	43.3(13)	39.8(14)	15.4(11)	15.2(11)	10.0(11)

Table 3: Bond Lengths in Å for **MRH_CuOxidant**.

Atom	Atom	Length/Å
C1	C2	1.4976(15)
C1	O1	1.2588(14)
C1	O2	1.2619(14)
C2	C3	1.3962(16)
C2	C7	1.3953(16)
C3	C4	1.3874(16)
C4	C5	1.3921(16)
C5	C6	1.3908(17)
C5	C8	1.4956(17)
C6	C7	1.3883(17)
C8	F1	1.3399(18)
C8	F2	1.3480(17)
C8	F3	1.3360(16)
C9	C10	1.4971(18)
C9	O3	1.2616(15)
C9	O4	1.2617(15)
C10	C11	1.3941(18)
C10	C15	1.3961(17)
C11	C12	1.3864(19)
C12	C13	1.3927(19)
C13	C14	1.393(2)
C13	C16	1.499(2)
C14	C15	1.3906(19)
C16	F4	1.322(2)
C16	F5	1.327(2)
C16	F6	1.337(2)
C17	C18B	1.496(4)
C17	O5	1.4473(16)
C17	C18A	1.551(2)
C18B	C19	1.558(4)
C19	C20	1.504(2)
C19	C18A	1.542(2)
C20	O5	1.4386(16)
Cu1	Cu1[1]	2.5975(3)
Cu1	O1	1.9642(9)
Cu1	O2[1]	1.9600(9)
Cu1	O3	1.9661(10)
Cu1	O4[1]	1.9590(10)
Cu1	O5	2.1387(9)
C7S	C8S	1.512(3)
C7S	O6S	1.423(3)
C8S	C8S[2]	1.519(4)
C1S_2	O2S_2	1.468(5)
C1S_2	C5S_2	1.509(12)
O2S_2	C3S_2	1.421(5)
C3S_2	C4S_2	1.39(4)
C4S_2	C5S_2	1.424(11)
C1S_1	O2S_1	1.487(3)
C1S_1	C5S_1	1.487(3)
O2S_1	C3S_1	1.523(9)
C3S_1	C4S_1	1.50(2)
C4S_1	C5S_1	1.555(5)

[1]1-x,1-y,1-z; [2]1/2-x,+y,1-z

Table 4: Bond Angles in ° for **MRH_CuOxidant**.

Atom	Atom	Atom	Angle/°
O1	C1	C2	117.30(10)
O1	C1	O2	125.87(11)
O2	C1	C2	116.82(10)

Atom	Atom	Atom	Angle/°
C3	C2	C1	119.95(10)
C7	C2	C1	119.98(10)
C7	C2	C3	120.08(10)

Atom	Atom	Atom	Angle/°
C4	C3	C2	120.11(10)
C3	C4	C5	119.40(11)
C4	C5	C8	118.45(11)
C6	C5	C4	120.89(10)
C6	C5	C8	120.65(11)
C7	C6	C5	119.60(11)
C6	C7	C2	119.91(11)
F1	C8	C5	112.47(11)
F1	C8	F2	105.80(11)
F2	C8	C5	111.67(12)
F3	C8	C5	112.59(11)
F3	C8	F1	107.23(12)
F3	C8	F2	106.65(11)
O3	C9	C10	117.41(11)
O4	C9	C10	116.71(11)
O4	C9	O3	125.87(12)
C11	C10	C9	120.24(11)
C11	C10	C15	119.99(12)
C15	C10	C9	119.71(11)
C12	C11	C10	120.34(12)
C11	C12	C13	119.34(12)
C12	C13	C14	120.90(12)
C12	C13	C16	119.54(13)
C14	C13	C16	119.53(12)
C15	C14	C13	119.46(12)
C14	C15	C10	119.96(12)
F4	C16	C13	112.15(14)
F4	C16	F5	107.71(16)
F4	C16	F6	105.71(15)
F5	C16	C13	112.81(13)
F5	C16	F6	105.82(16)
F6	C16	C13	112.16(14)
O5	C17	C18B	108.56(17)
O5	C17	C18A	104.40(12)
C17	C18B	C19	103.6(2)
C20	C19	C18B	106.45(17)
C20	C19	C18A	98.60(15)
O5	C20	C19	104.80(11)
O1	Cu1	Cu1[1]	84.75(3)
O1	Cu1	O3	89.26(5)
O1	Cu1	O5	94.80(4)
O2[1]	Cu1	Cu1[1]	84.93(3)
O2[1]	Cu1	O1	169.66(4)
O2[1]	Cu1	O3	90.31(4)
O2[1]	Cu1	O5	95.53(4)
O3	Cu1	Cu1[1]	84.36(3)
O3	Cu1	O5	92.91(4)
O4[1]	Cu1	Cu1[1]	85.40(3)
O4[1]	Cu1	O1	90.35(5)
O4[1]	Cu1	O2[1]	88.24(5)
O4[1]	Cu1	O3	169.74(4)
O4[1]	Cu1	O5	97.34(4)
O5	Cu1	Cu1[1]	177.24(3)
C1	O1	Cu1	122.23(8)
C1	O2	Cu1[1]	122.18(8)
C9	O3	Cu1	122.48(8)
C9	O4	Cu1[1]	121.67(9)
C17	O5	Cu1	125.50(8)
C20	O5	C17	109.16(10)
C20	O5	Cu1	119.06(8)
O6S	C7S	C8S	106.4(2)
C7S	C8S	C8S[2]	101.06(14)
C7S[2]	O6S	C7S	109.2(2)
C19	C18A	C17	101.81(19)
O2S_2	C1S_2	C5S_2	111.4(6)
C3S_2	O2S_2	C1S_2	92(2)
C4S_2	C3S_2	O2S_2	120(3)
C3S_2	C4S_2	C5S_2	95(2)
C4S_2	C5S_2	C1S_2	103.9(6)
C5S_1	C1S_1	O2S_1	103.3(3)
C1S_1	O2S_1	C3S_1	99.2(9)
C4S_1	C3S_1	O2S_1	103.4(9)
C3S_1	C4S_1	C5S_1	104.8(3)
C1S_1	C5S_1	C4S_1	103.4(2)

[1]1-x,1-y,1-z; [2]1/2-x,+y,1-z

Table 5: Torsion Angles in ° for **MRH_CuOxidant**.

Atom	Atom	Atom	Atom	Angle/°
C1	C2	C3	C4	-179.14(11)
C1	C2	C7	C6	-179.47(12)
C2	C1	O1	Cu1	-176.95(8)
C2	C1	O2	Cu1[1]	177.75(8)
C2	C3	C4	C5	-1.05(18)
C3	C2	C7	C6	0.7(2)
C3	C4	C5	C6	0.07(19)
C3	C4	C5	C8	179.12(12)
C4	C5	C6	C7	1.3(2)
C4	C5	C8	F1	57.51(17)
C4	C5	C8	F2	-61.26(16)
C4	C5	C8	F3	178.79(12)
C5	C6	C7	C2	-1.7(2)

C6	C5	C8	F1	-123.43(14)
C6	C5	C8	F2	117.80(14)
C6	C5	C8	F3	-2.15(19)

Atom	Atom	Atom	Atom	Angle/°
C7	C2	C3	C4	0.65(18)
C8	C5	C6	C7	-177.71(13)
C9	C10	C11	C12	176.56(12)
C9	C10	C15	C14	-176.53(12)
C10	C9	O3	Cu1	172.65(8)
C10	C9	O4	Cu1[1]	-173.44(8)
C10	C11	C12	C13	0.0(2)
C11	C10	C15	C14	0.7(2)
C11	C12	C13	C14	0.6(2)
C11	C12	C13	C16	-177.79(14)
C12	C13	C14	C15	-0.6(2)
C12	C13	C16	F4	95.44(19)
C12	C13	C16	F5	-142.72(17)
C12	C13	C16	F6	-23.3(2)
C13	C14	C15	C10	-0.1(2)
C14	C13	C16	F4	-83.00(19)
C14	C13	C16	F5	38.8(2)
C14	C13	C16	F6	158.22(15)
C15	C10	C11	C12	-0.6(2)
C16	C13	C14	C15	177.83(14)
C17	C18B	C19	C20	11.0(3)
C18B	C17	O5	C20	-21.8(3)
C18B	C17	O5	Cu1	-173.3(2)
C18B	C19	C20	O5	-23.8(3)
C19	C20	O5	C17	28.27(16)
C19	C20	O5	Cu1	-178.05(10)
C20	C19	C18A	C17	42.5(2)
O1	C1	C2	C3	170.39(12)
O1	C1	C2	C7	-9.39(17)
O1	C1	O2	Cu1[1]	-1.84(19)
O2	C1	C2	C3	-9.24(17)
O2	C1	C2	C7	170.98(12)
O2	C1	O1	Cu1	2.64(19)
O3	C9	C10	C11	172.23(12)
O3	C9	C10	C15	-10.57(17)
O3	C9	O4	Cu1[1]	5.23(18)
O4	C9	C10	C11	-8.97(18)
O4	C9	C10	C15	168.23(12)
O4	C9	O3	Cu1	-6.02(18)
O5	C17	C18B	C19	5.8(3)
O5	C17	C18A	C19	-27.2(3)
C8S	C7S	O6S	C7S[2]	12.86(11)
O6S	C7S	C8S	C8S[2]	-32.8(3)
C18A	C17	O5	C20	0.1(2)
C18A	C17	O5	Cu1	-151.50(17)
C18A	C19	C20	O5	-43.8(2)
C1S_2	O2S_2	C3S_2	C4S_2	31(4)
O2S_2	C1S_2	C5S_2	C4S_2	-21.4(10)
O2S_2	C3S_2	C4S_2	C5S_2	-45(4)
C3S_2	C4S_2	C5S_2	C1S_2	34(2)
C5S_2	C1S_2	O2S_2	C3S_2	-3(2)
C1S_1	O2S_1	C3S_1	C4S_1	44.8(12)
O2S_1	C1S_1	C5S_1	C4S_1	36.2(4)

O2S_1	C3S_1	C4S_1	C5S_1	-23.0(13)
C3S_1	C4S_1	C5S_1	C1S_1	-7.5(9)
C5S_1	C1S_1	O2S_1	C3S_1	-50.3(8)

[1]1-x,1-y,1-z; [2]1/2-x,+y,1-z

Table 6: Hydrogen Fractional Atomic Coordinates (×10⁴) and Equivalent Isotropic Displacement Parameters (Å²×10³) for **MRH_CuOxidant**. U_{eq} is defined as 1/3 of the trace of the orthogonalised U_{ij}.

Atom	x	y	z	U_{eq}
H3	2157.74	6178.52	4486.67	18
H4	957.21	6996.21	3909.5	21
H6	2340.62	7882.41	2905.53	24
H7	3524.23	7014.47	3460.88	23
H11	3221.55	2280.63	4687.54	26
H12	2382.02	1098.3	4119.8	28
H14	3279.18	1815	2819.94	28
H15	4120.99	2998.08	3391.44	24
H17C	7240.03	5723.69	4317.78	27
H17D	6595.34	6577.69	4112.37	27
H17A	7274.97	5620.49	4193.04	27
H17B	6705.32	6499.77	4242.37	27
H18A	7445.49	5657.8	3481.5	33
H18B	6880.33	6583.95	3301.71	33
H19C	5854.56	5674.65	2691.37	32
H19D	6338.97	4739.2	2966.25	32
H19A	5839.6	5484.86	2647.38	32
H19B	6507.07	4803.09	3086.27	32
H20A	5039.86	5679.02	3265.12	33
H20B	5238.56	4583.79	3307.4	33
H7SA	1397.74	-354.75	4509.85	63
H7SB	1414.66	-152.48	5146.75	63
H8SA	1681.66	-1834.44	4873.26	52
H8SB	2217.75	-1462.36	5495.49	52
H18C	6280.68	6787.11	3269.75	33
H18D	7174.59	6293.35	3323.27	33
H1SA_2	-425.68	5857.36	1464.64	52
H1SB_2	332.5	6585.2	1703.3	52
H3SA_2	-216.13	6535.76	147.55	61
H3SB_2	635.5	6820.5	628.8	61
H4SA_2	832.52	5361.13	467.84	51
H4SB_2	-115.32	5068.9	458.21	51
H5SA_2	1233.63	5748.11	1387.89	52
H5SB_2	600.82	4903.11	1390.94	52
HA_1	-984.36	7205.94	555.75	75
HB_1	-1089.19	6154.44	749.25	75
H3SA_1	-130.26	5998.01	217.52	61
H3SB_1	403.25	6895.5	518.09	61
H4SA_1	1219.13	5835.71	1127.14	53
H4SB_1	466.88	5079.93	980.9	53
H5SA_1	36.97	5582.39	1719.16	52
H5SB_1	867.99	6234.27	1914.88	52

Table 7: Atomic Occupancies for all atoms that are not fully occupied in **MRH_CuOxidant**.

Atom	Occupancy	Atom	Occupancy	Atom	Occupancy	Atom	Occupancy
H17C	0.446(5)	H19B	0.554(5)	H3SB_2	0.297(3)	HB_1	0.703(3)
H17D	0.446(5)	C18A	0.554(5)	C4S_2	0.297(3)	C3S_1	0.703(3)
H17A	0.554(5)	H18C	0.554(5)	H4SA_2	0.297(3)	H3SA_1	0.703(3)
H17B	0.554(5)	H18D	0.554(5)	H4SB_2	0.297(3)	H3SB_1	0.703(3)
C18B	0.446(5)	C1S_2	0.297(3)	C5S_2	0.297(3)	C4S_1	0.703(3)
H18A	0.446(5)	H1SA_2	0.297(3)	H5SA_2	0.297(3)	H4SA_1	0.703(3)
H18B	0.446(5)	H1SB_2	0.297(3)	H5SB_2	0.297(3)	H4SB_1	0.703(3)
H19C	0.446(5)	O2S_2	0.297(3)	C1S_1	0.703(3)	C5S_1	0.703(3)
H19D	0.446(5)	C3S_2	0.297(3)	O2S_1	0.703(3)	H5SA_1	0.703(3)
H19A	0.554(5)	H3SA_2	0.297(3)	HA_1	0.703(3)	H5SB_1	0.703(3)

Citations

O.V. Dolomanov and L.J. Bourhis and R.J. Gildea and J.A.K. Howard and H. Puschmann, Olex2: A complete structure solution, refinement and analysis program, *J. Appl. Cryst.*, (2009), **42**, 339-341.

Chapter 5 Supplemental:

5.5.4 Spectra

Methyl-(S)-2-((tert-butoxycarbonyl)amino)-3-(4-

(((trifluoromethyl_sulfonyl_oxe)phenyl)proponate **(5.S1)**

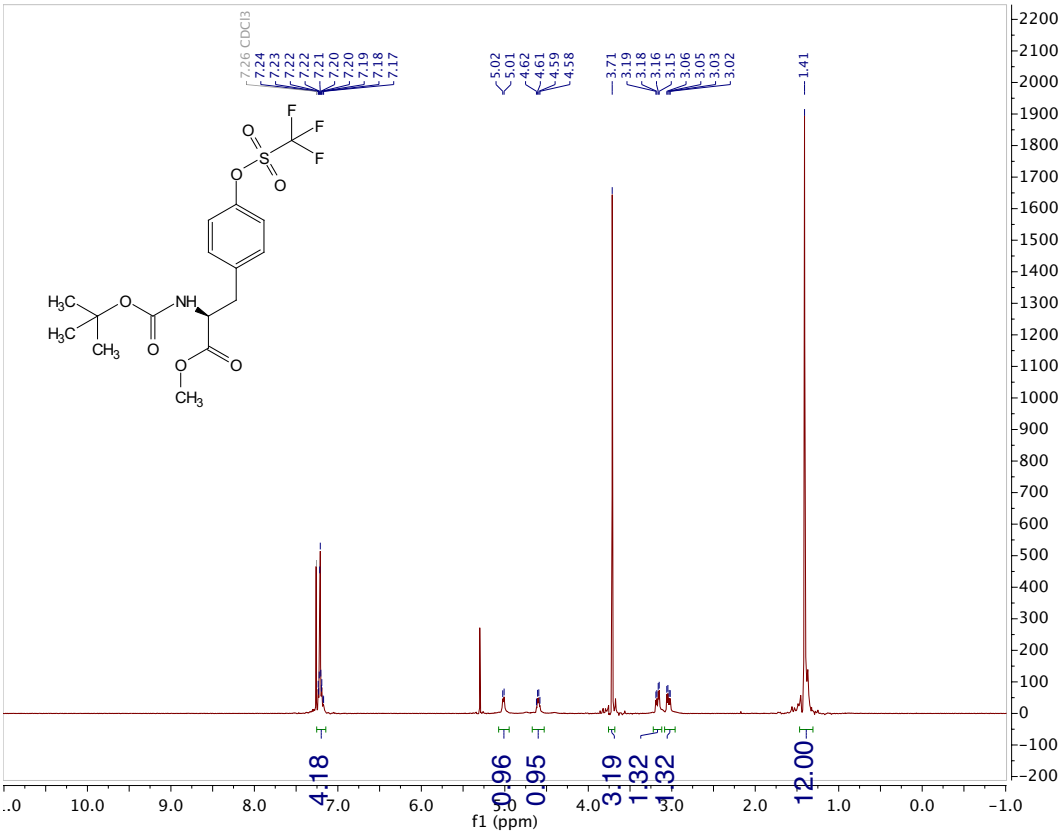

Methyl (S)-2-((tert-cutoxycarbonyl)amino)-3-(4-(4,4,5,5-tetramethyl-1,3,2-dioxaborolan-2-yl)phenyl)propanoate **(5.12)**

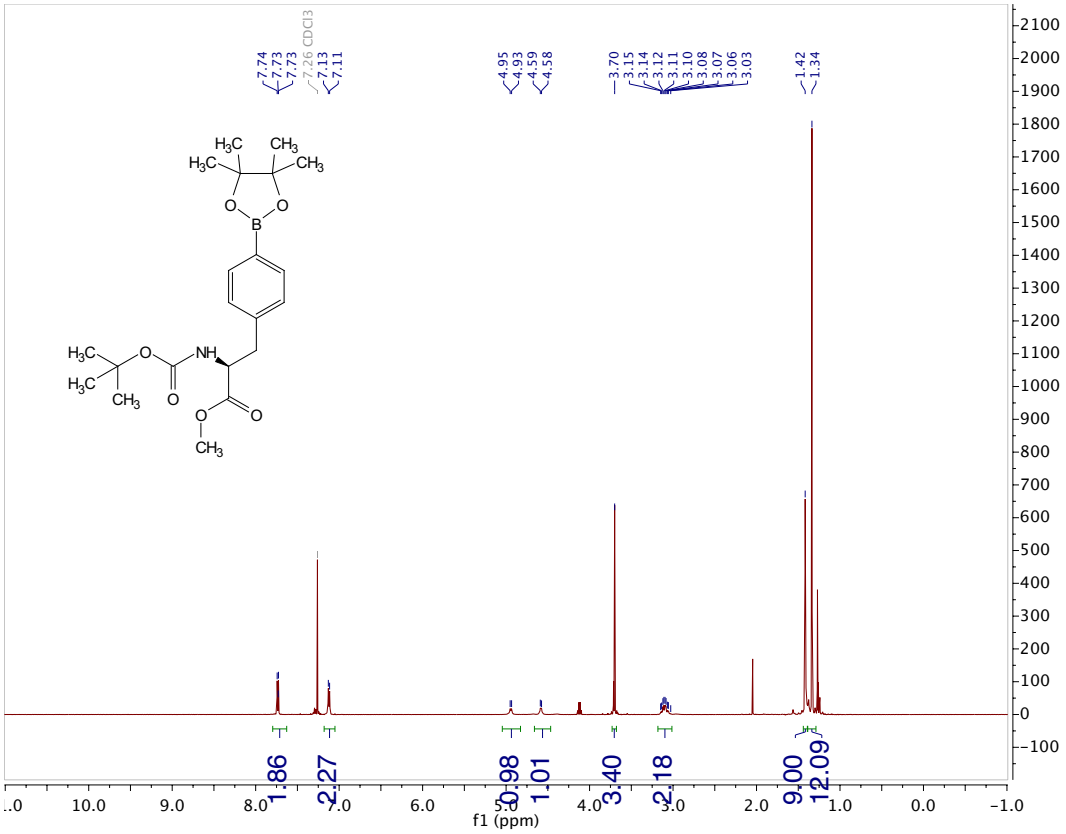

(S)-(4-(2-((tert-butoxycarbonyl)amino)-3-methoxy-3-oxopropyl)phenyl)boronic acid **(5.13)**

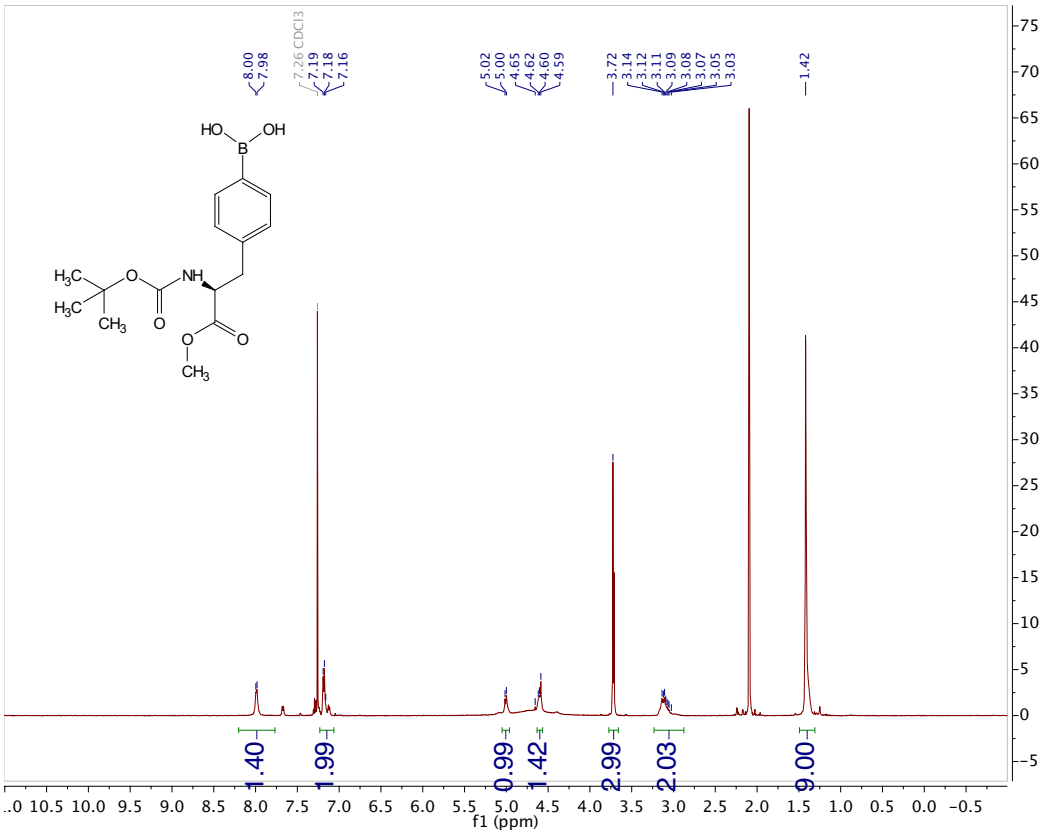

Methyl-(S)-2-((tert-butoxycarbonyl)amino)-3-(4-((1,3-dioxoisointolin-2-yl)oxy)phenyl)propanoate **(5.14)**

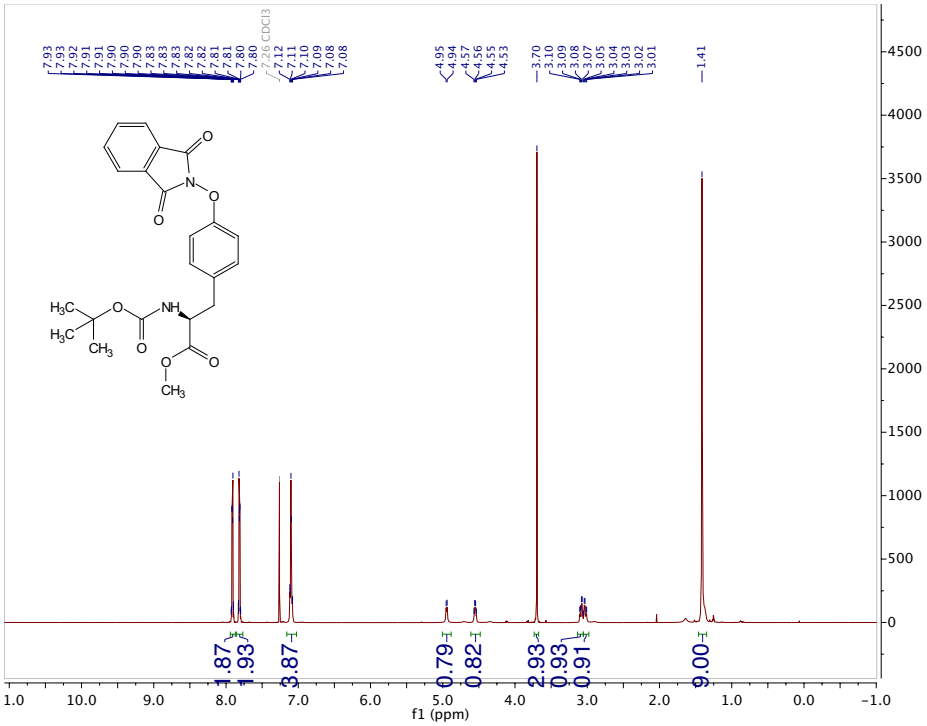

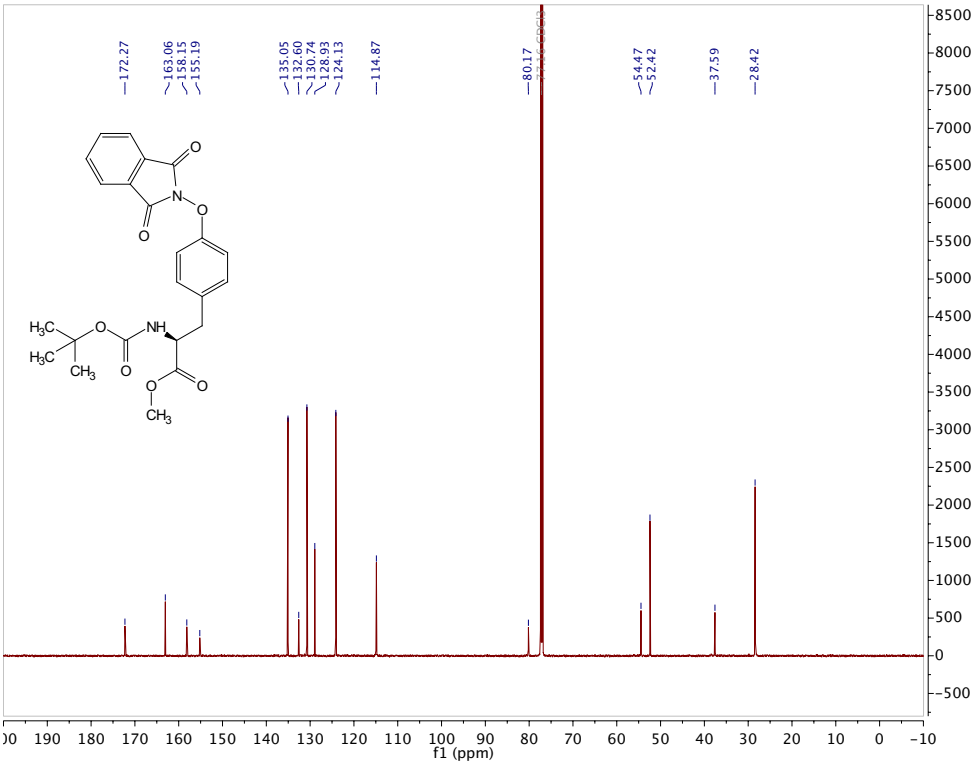

Emory EHSO Developed SOP:

Lab Name:	Blakey Lab
Chemical Process:	Heated reactions under pure or heavily enriched oxygen atmosphere.

School / Department:	Emory University / Chemistry		
SOP Preparation Date:	8/8/2022	***SOP Approval Date:***	
Principal Investigator:	Simon Blakey		
Lab Manager Name:	Michael Hollerbach		
Laboratory Phone:	(404) 727-6634	***PI Office Phone:***	(404) 727-6738
Emergency Contact:	Simon Blakey	***Emergency Contact Phone:***	404-626-9047
Laboratory locations covered by this SOP (building / room number): Atwood 612 - 641			

Type of SOP:	☒	***Process***	☐	***Hazardous Chemical***	☐ ***Hazardous Class***

Purpose

The purpose of this SOP is to describe the safety considerations and methods by which reaction methodology is undertaken when heating solvents under pure or heavily enriched oxygen atmospheres.

Physical and Chemical Properties / Definition of Chemical Group

Pure Oxygen - May cause or intensify fire; oxidizer. (SDS : https://www.airgas.com/msds/001043.pdf)

Personal Protective Equipment (PPE)

Respiratory Protection

Respiratory protection may be required if an airborne hazard is present when work is done outside of approved containment or when cleaning up a spill. Surgical masks or dust masks do not provide adequate protection.

Respirators should be used under the following circumstances:

- As a last line of defense (i.e., after engineering and administrative controls have been exhausted).
- When the exposure limit has been exceeded or when there is a possibility that the exposure limit will be exceeded.
- When recommended exposure limit (TLV, NIOSH) has been exceeded.

- An employer requires the use of a respirator.
- There is potential for harmful exposure due to an atmospheric contaminant (in the absence of an OSHA exposure limit or recommended exposure limit)
- As PPE in the event of a chemical spill clean-up process.

Lab personnel intending to use/wear a respirator must be trained and fit-tested annually. This is a regulatory requirement.
http://www.ehso.emory.edu/documents/ehs-311-respirator-protection-program.pdf

Hand Protection
Handle with gloves. Laboratory personnel must wear gloves tested and rated for use with specified hazardous chemical.

NOTE: Consult with your preferred glove manufacturer to ensure that the gloves you plan on using are compatible with specified hazardous chemical. Gloves should be chemical resistant such as Rubber Latex, Nitrile, or Butyl.
Refer to glove selection chart from the links below:
http://www.ansellpro.com/download/Ansell_8thEditionChemicalResistanceGuide.pdf
OR
http://www.showabestglove.com/site/default.aspx

Eye Protection
- Wear chemical splash goggles, safety glasses with side shields, or a face shield plus safety glasses/goggles to protect from splash hazards and chemical vapors.

Skin & Body Protection
- Lab coat
- Full-length pants/skirt
- Closed toe, closed heel shoes

Hygiene Measures
Avoid contact with skin, eyes, and clothing. Wash hands before and immediately after handling the product.

Engineering Controls

- Prior to the experiment, consider calculating the estimated heat and pressure that may be generated during the reaction (such as the adiabatic temperature (no heat transfer) or exothermic potential).
- Consult with the PI and receive approval from the PI before the initial reaction and before scaling up the reaction.
- Use small volumes for preliminary experiments with new or unfamiliar reactants.
- The use of a blast shield is required for all heated reactions bearing a pure oxygenated atmosphere.
- Balloons will be used for oxygen introduction unless previously discussed with PI or under Parr reactor conditions.
- Check equipment and wires/cables of equipment (e.g., heating mantle) for damage before each use. Do not proceed with the experiment if equipment is damaged or has frayed/damaged cords.

- Conduct the experiment in a chemical fume hood with the sash lowered.
- Do not heat above the solvent's boiling point.
- Monitor the temperature and pressure (Parr Reactor method is preferred).
- For Parr Reactors, do not reach exceed 90% of the specific unit's maximum pressure or maximum temperature listed in the user manual (Blakey Lab max is 3000 psi/ 90% is 2700psi).
- For Parr Reactors, do not overfill the vessel (no more than two-thirds; half full or less is preferred) [Parr reactor scale up or direct addition of solvent requires PI approval].

Handle in a properly functioning chemical fume hood. The CFH should have a face velocity between 80 – 120 linear feet per minute (lfm) and it must be tested annually. Verify the performance test and working condition prior to use.

First Aid Procedures

If inhaled… Move to fresh air. If the person is not breathing, give artificial respiration. DO NOT use mouth to mouth resuscitation. If emergency medical attention is required, call 911. Call Occupational Injury Management (OIM)/Employee Health at 404-686-8587; if after hours call OIM Nurse Practitioner on-call at 404-686-5500, ID# 50464. Notify your supervisor/PI immediately of the incident. Report the incident in H.O.M.E./PeopleSoft.

In case of skin contact… Remove all contaminated clothing. Immediately (within seconds) flush affected area for FIFTEEN (15) minutes. If emergency medical attention is required, call 911. Call Occupational Injury Management (OIM)/Employee Health at 404-686-8587; if after hours call OIM Nurse Practitioner on-call at 404-686-5500, ID# 50464. Notify your supervisor/PI immediately of the incident. Report the incident in H.O.M.E./PeopleSoft.

In case of eye contact… Remove any contact lenses. Use nearest emergency eyewash immediately and flush for at least FIFTEEN (15) minutes. DO NOT allow victim to rub eyes or keep eyes closed. If emergency medical attention is required, call 911. Call Occupational Injury Management (OIM)/Employee Health at 404-686-8587; if after hours call OIM Nurse Practitioner on-call at 404-686-5500, ID# 50464. Notify your supervisor/PI immediately of the incident. Report the incident in H.O.M.E./PeopleSoft.

If swallowed… DO NOT INDUCE VOMITING. Refer to the specified hazardous chemical's SDS for immediate care instructions (for example, the SDS may instruct to give large quantities of water, or milk, etc.). Never give anything by mouth to an unconscious person. If emergency medical attention is required, call 911. Call Occupational Injury Management (OIM)/Employee Health at 404-686-8587; if after hours call OIM Nurse Practitioner on-call at 404-686-5500, ID# 50464. Notify your supervisor/PI immediately of the incident. Report the incident in H.O.M.E./PeopleSoft.

Special Storage & Handling Requirements

Incompatible Materials and Environments

The use of known explosive reagents should be avoided in these reactions and will require a switch to 95%/5% N2/O2 or a different oxygenation method. These known groups are indicated in the list at the link Known Explosive Groups or in the accompanying image below.

TABLE I. Atomic Groupings That Characterize Explosive Compounds

Name	Structure
Acetylide	—C≡C—Metal
Amine oxide	
Azide	—N=N=N
Chlorate	$—ClO_3$
Diazo	—N=N—
Diazonium	$(—N{\equiv}N)^{\oplus}X^{\ominus}$
Fulminate	—O=N=C
N-Haloamine	
Hydroperoxide	—O—O—H
Hypohalite	—O—X
Nitrate	$—O—NO_2$
Nitrite	–O—NO
Nitro	$—NO_2$
Nitroso	—NO
Ozonide	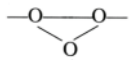
Peracid	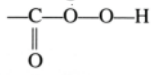
Perchlorate	$—ClO_4$
Peroxide	—O—O—

Storage

- Ensure the container is tightly closed at all times.
- Keep in a dry, well-ventilated area away from incompatible materials and environments.
- Label secondary containers with the full chemical name and GHS hazard pictograms.
- Containers which are opened must be carefully resealed and kept upright to prevent leakage.
- Dry powders must be in sealed, shatter-resistant containers during transportation. If the container is not shatter-resistant, use a secondary container.
- If the material may be flammable, reactive, or explosive, keep away from heat and open flame.

Handling

- Provide hazardous chemical and specific SOP training to personnel working with hazardous chemicals and any other personnel authorized or required to be in the laboratory or shared space during work with the agent.
- The lab where the material is being handled must have an approved/certified emergency eyewash and safety shower.
- Set up a designated area for work with hazardous chemicals.
- If weighing dry powders and the balance cannot be located in a fume hood or BSC, tare a container then add the material to the container in a hood and seal the container before returning to the balance to weigh the powder.
- If necessary and once work with hazardous chemical is complete, decontaminate the work area *(e.g., a mild detergent and water, or another solvent may be used - as long as the method is compatible with the chemical.)*
- Avoid ingestion or inhalation.
- Use only with adequate ventilation or respiratory protection.

Spill and Accident Procedure

1. **Spill** – Assess the extent of danger. Help contaminated or injured persons. Evacuate the spill area. Avoid breathing vapors. If possible, confine the spill to a small area using a spill kit or absorbent material. Keep others from entering contaminated area (e.g., use caution tape, barriers, etc.).
2. **Incidental** – If you have training, you may assist in the clean-up effort. Use appropriate personal protective equipment and clean-up material (inert absorbents and/or spill pads) for chemical spilled. Dispose of clean-up material in solid chemical waste bucket, label and request a chemical waste pick-up. *Notify your supervisor/PI immediately of the incident.*
3. **Emergency/Large Spill** – If possible and safe to do so, stop the spread of chemicals and reduce aerosol generation. Evacuate all personnel from the laboratory and restrict access to the laboratory. Call EHSO Spill Response Team at 404-727-2888 (24/7). If injuries

and emergency medical attention is required, call 911. Call Occupational Injury Management (OIM)/Employee Health at 404-686-8587; if after hours call OIM Nurse Practitioner on-call at 404-686-5500, ID# 50464. Notify your supervisor/PI immediately of the incident. Report the incident in H.O.M.E./PeopleSoft.

4. **Chemical Spill on Body or Clothes** – Remove clothing and rinse body thoroughly in emergency shower for at least FIFTEEN (15) minutes. Seek medical attention. Notify your supervisor/PI immediately of the incident. Report the incident in H.O.M.E./PeopleSoft.
5. **Chemical Splash in Eyes** – Immediately rinse eyeball and inner surface of eyelid with water from the emergency eyewash station for FIFTEEN (15) minutes by forcibly holding the eye open. Seek medical attention. Notify your supervisor/PI immediately of the incident. Report the incident in H.O.M.E./PeopleSoft.
6. **Fire** – If fire or explosion occurs, evacuate all personnel from the laboratory and restrict access to the laboratory. Adhere to normal fire safety protocol and only engage secondary fires if one can do so safely. **If fire occurs adjacent to an Oxygen tank, evacuate immediately and notify first responders of the potential danger**. If injuries and emergency medical attention is required, call 911. Notify your supervisor/PI immediately of the incident. Report the incident in H.O.M.E./PeopleSoft.

Decontamination / Waste Disposal Procedure

Liquid waste should be collected and disposed of as hazardous waste. Any consumables (gloves, plastics, etc) that come into contact with the chemical should be disposed of as solid waste.

Label waste

- Attach an EHSO Hazardous Waste label to all waste containers as soon as the first drop of waste is added to the container.
- Attach GHS pictogram(s) to define the hazard(s) associated with the chemical waste stream.
- Fill in all requested information and list all constituents on label.

Store waste

- Store laboratory waste in closed containers, in secondary containment (liquid wastes) and in a designated storage location.
- Waste must be under the control of the person/laboratory generating and disposing of it.

Dispose of waste

- Dispose of laboratory generated hazardous waste when container becomes 3/4 full.
- Request for waste removal using EHSO online Waste Collection pickup request form.
- Empty chemical stock containers should be triple rinsed using a compatible solvent and all rinsates should be disposed of as hazardous waste. Rinsates should not be mixed with incompatible waste streams.
- Contact EHSO Environmental Compliance team (ChemWaste@emory.edu) with questions.

Protocol / Procedure

Example Procedures for Preparation

Flask: All solids are added to an oven-dried round bottom with a stir bar. Close with septa. The flask is evacuated and backfilled with N2 in 3x1min cycles. The solvent is added to the flask with stirring and the reaction is allowed to homogenize. Oxygen balloons are then used to exchange the atmosphere of the flask using a vent needle with 2 party-sized balloons. The reaction is then placed under a third balloon and the heat is turned on. The reaction is left to stir for 24 hr before cooling, venting, and workup.

Parr Reactor: All solids are added to an oven-dried vial with a stir bar. Closed with lid and septa. The solvent is added to the flask with stirring and the reaction is allowed to homogenize. The glass vial is placed into the Parr reactor with a needle in the septa. The reactor is sealed, evacuated to the closed O2 tank, and backfilled with N2 in 3x1min cycles. The oxygen tank is then slowly opened to exchange the atmosphere of the reactor using the bubbler to vent. The reaction is then placed under desired pressure, sealed and the tank closed. The heat is turned on and the pressure is monitored until at temperature. The reaction is left to stir for 24 h before cooling, venting, and workup.

IMPORTANT NOTE: Any deviation from this SOP requires advance PI approval.

For Questions or Other Assistance

Please contact the laboratory's assigned EHSO Research Safety Building Liaison: Kristina Bowen (kristina.bowen@emory.edu)

Documentation of Training

- Prior to conducting any work with this material, Principal Investigator or designee must provide his/her laboratory personnel instruction on the specific hazards involved in working with this substance, work area decontamination, and emergency procedures.
- The Principal Investigator must provide his/her laboratory personnel with a copy of this SOP and a copy of the SDS provided by the manufacturer.
- The Principal Investigator must ensure that his/her laboratory personnel have attended appropriate/required laboratory safety training or refresher training within the last one year.

I have read and understand the content of this SOP.

PRINT NAME	Emory NET ID	SIGNATURE	DATE

PRINT NAME	Emory NET ID	SIGNATURE	DATE